The Ageing Brain: Exploring Corticocerebellar Network Contributions to Cognition Across the Lifespan

Matthew Stephen Danvers

Submitted in partial fulfilment of the requirements for the degree of

Doctor of Philosophy in the Department of Psychology

Royal Holloway, University of London

2023

Abstract

This thesis comprises a series of studies aimed at addressing cognitive ageing, investigating differences between age groups at the level of baseline haemodynamic responding in the brain, as well as behavioural performance, cognitive load, and event related haemodynamic responding during an instrumental learning task. In general results support the prefrontal-executive theory specifically implicating regions of the dorsolateral prefrontal cortex in age-related performance deficits. However this brain area is known to connect with cerebellar lobule HVIIa, a candidate region within an expanding literature that sees the cerebellum contributing to cognitive as well as motor function. Therefore although the prefrontal-executive theory focuses upon prefrontal structures, this thesis expanded upon existing knowledge investigating putatively connected cerebellar regions also implicated in cognition. Based upon putative reductions in grey matter density and/or reduced connectivity, corticocerebellar network impairments may contribute to age-related deficits, this investigation potentially further informing how prefrontal regions are implicated in cognitive ageing. This was investigated using a combination of cross-sectional comparisons of age groups carrying out instrumental learning whilst undergoing 3 Tesla functional magnetic resonance imaging, as well as implementing a similar but more challenging version of the same task within young adults using ultra-high field 7 Tesla functional magnetic resonance imaging. Oculomotor responses were used due to the well documented brain networks involved. Through rigorous experimental control, flexible modelling approaches, and comparisons made between both tasks, and events within tasks, more in depth conclusions were drawn regarding the role of the dlPFC and cerebellum in cognitive ageing.

Declaration of Authorship for Co-authored Work

If you are presenting partly co-authored work, please indicate below your individual contribution to the thesis.

Name of candidate: Matthew Stephen Danvers

Thesis title: The Ageing Brain: Exploring Corticocerebellar Network Contributions to Cognition Across the Lifecourse

I confirm that the thesis that I am presenting has been co-authored with: Narender Ramnani & Michael Longley

Within this partly co-authored work, I declare that the following contributions are entirely my own work:

(Here you should indicate, in précis style, the datasets that you gathered, interpreted and discussed; methods that you developed; complete first drafts that you wrote; content that is entirely your own work; etc. It is often appropriate to organise this statement by chapter)

Chapter 1: Entirely my own work, but Narender Ramnani provided feedback.

Chapter 2: Entirely my own work, but Narender Ramnani provided feedback.

Chapter 3: Development of the experimental idea and approach was a collaboration between me and Narender Ramnani. Training in SPM was provided by Narender Ramnani. Functional neuroimaging data was provided by the CamCAN group (Shafto et al., 2014; Taylor et al., 2017). The chapter was written by me, neuroimaging data was pre-processed and quality checked by me (partially based on scripts provided by Narender Ramnani, but modified by me), all other scripts aside from those acquired from within the SPM software were written by me, and all analyses, interpretation, and simulations were carried out by me. Narender Ramnani provided feedback on written work and helped with ethical review.

Chapter 4: Development of the experimental idea and approach was a collaboration between me and Narender Ramnani. Functional neuroimaging data was provided by the
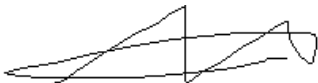
CamCAN group (Shafto et al., 2014; Taylor et al., 2017). The chapter was written by me, neuroimaging data was pre-processed and quality checked by me (partially based on scripts provided by Narender Ramnani, but modified by me), all other scripts aside from those acquired from within the SPM software were written by me, and all analyses and interpretation was carried out by me. Narender Ramnani provided feedback on written work and helped with ethical review.

Chapter 5: Advertising, recruitment, screening, creation of the experiment using Experiment Builder, and collection of neuroimaging data were carried out by me, however assistance was received from two research assistants (Vrishni Kanhye and Chelsea Shepherd) who created advertising materials and compiled a database of interested participants. Development of the experimental idea/approach, ethical review, and technical piloting was a collaboration between me, Michael Longley, and Narender Ramnani. Michael Longley assisted with some neuroimaging sessions and provided a Spike2 script used in piloting and when recording event times, and Ari Lingeswaran operated the MRI scanner. Data was pre-processed, quality checked, analysed, interpreted, and written up by me. Narender Ramnani provided feedback on all written work. All scripts aside from those acquired from within the SPM software and the aforementioned Spike script were written by me, and the frontal lobe mask was created by me.

Chapter 6: Advertising, recruitment, screening, creation of the experiment using Experiment Builder, and collection of neuroimaging data were carried out by me, with assistance from the FMRIB Department at the John Radcliffe Hospital. Development of the experimental idea/approach, ethical review, and technical piloting was a collaboration between me, Michael Longley, and Narender Ramnani. Michael Longley provided a Spike script used in piloting and when recording event times. Data was pre-processed, quality checked, analysed, interpreted, and written up by me. Narender Ramnani provided

feedback on written work. All scripts aside from those acquired from within the SPM software and the aforementioned Spike script were written by me, and the frontal lobe mask was created by me.

Chapter 7: Entirely my own work, but Narender Ramnani provided feedback.

Signed: Date: 12/04/2023

(Candidate)

Signed: Date: 17/04/2023

(Supervisor)

This form should be signed by the candidate and the candidate's supervisor and returned to the Doctoral School when the electronic copy of the thesis is submitted Student Administration, Royal Holloway, Egham, Surrey TW20 0EX with the copies of the thesis.

Acknowledgements

I would like to express my gratitude firstly to my wonderful wife Viktorija for believing in me, sitting in my corner, motivating me, and for putting up with my carrying out this PhD across two full pregnancies, whilst living in a one bed flat. I would also like to thank my parents Sarah and Brian for their support, care, help, and love over the last 35 years, and for allowing me to work remotely from their spare room once my wife decided that she would prefer not to witness my carrying out this PhD, across two full pregnancies, whilst living in a one bed flat. It is a great regret of mine that my father passed away shortly before this thesis was submitted, and will never see me graduate, but I take solace in knowing he was proud of me whatever the outcome. Furthermore, I wish to thank my two sons Severus and Darius for providing the motivation to get this done, and my sister Ruth for setting the bar high.

In terms of contributions to the thesis itself, I offer my thanks to Narender Ramnani for my appointment and his assistance throughout, and also Szonya Durant for her help at times when I was struggling. Michael Longley also deserves to be here, as he assisted me in terms of piloting work, theoretical understanding, data collection, figuring out software problems, and served as a friend within the lab. Additionally Iqra Arshad helped by discussing neuroimaging problems, alongside lending a sympathetic ear. Further assistance was offered by John Ashburner who helped with methodological issues, Rik Henson who critiqued my approach, both Ayan Sengupta and Ari Lingeswaran who facilitated both the procurement and handling of MRI data, and Vrishni Kanhye and Chelsea Shepherd who assisted with recruitment. I also thank the Biotechnology and Biological Sciences Research Council who funded research costs. Finally my father deserves to be here again, as someone who showed a genuine interest in my topic and against whom I could bounce ideas, whilst providing genuinely helpful insights consistent with his own sharp intellect.

Table of Contents

Table of Tables

Table of Figures

the conditions of interest, green highlights the Fourier basis set regressors pertaining to the conditions of interest, and blue highlights head-motion regressors.	
Figure 11. 2nd-level design matrix from chapter 5, including experimental and control conditions across two age groups, using a three-function flexible basis set, totalling 12 conditions. One covariate regressor is included for each basis function (the final three columns), here denoting gender.	**30**
Chapter 3 (starts on page 24 of thesis)	
Figure 1. Estimated haemodynamic responses from analyses using all three mHRFs plotted within each ROI; with peak latency (PL) and FWHM also specified within each legend. Vertical lines denote the peak.	**20**
Figure 2. Distributions of peak latency and FWHM as estimated by each flexible model, for PBRs (+) and NBRs (-) independently. Coloured lines denote medians, with the black lines denoting each timing property as assumed by the HRFc model.	**22**
Figure 3. Histograms showing the distributions of difference scores (Fourier minus HRFtd) across both PBRs and NBRs, for both peak latency and FWHM. Black vertical lines denote medians.	**23**
Figure 4. Distribution of peak latency and FWHM across GM, derived from the Fourier analysis. These are overlaid upon the MNI152 brain.	**24**
Figure 5. The best fitting linearly combined estimate of each of the five simulations using the HRFtd model (left, in orange) and Fourier set (right, in yellow). The artificially created signals are in blue, with timing properties increasing from the top-most to the bottom-most. For each a scatter plot is included, showing the line of best fit with the artificial "*BOLD*" signal on the Y axis and the estimated HRF on the X axis.	**27**
Chapter 4 (starts on page 25 of thesis)	
Figure 1. The mean haemodynamic response function for each age group, plotted separately for each flexible model, and showing magnitude changes over peri-stimulus time. The y axis is normalised (left) and showing percentage signal change (right).	**17**

effect of condition across age groups are in red, and those pertaining to the age x condition interaction (not surviving correction) are in green. Activations from chapter 6 pertaining to the main effect of condition are in blue.	
Figure 5. Activations surviving FWE correction within the striatum from chapters 5 and 6 overlayed upon the MNI brain. Activations from chapter 5 pertaining to the conjunction effect of condition across age groups are in red. Activations from chapter 6 pertaining to the main effect of condition are in blue, and event x condition interactions are in green.	**20**
Figure 6. Effects of condition (chapter 5 in red, chapter 6 in blue), age x condition interactions from chapter 5 (green), event x condition interactions from chapter 6 (light blue) and error-status x condition interactions in chapter 6 (yellow). Cross-hairs indicate location of peak MNI coordinates regarding prefronto-cerebellar connectivity, as per O'Reilly et al. (2010).	**22**

Chapter 1
General Introduction

Matthew Danvers

Word count: 16,802 excluding references

1.1. Introductory Overview

"Could the young but realize how soon they will become mere walking bundles of habits,

they would give more heed to their conduct while in the plastic state" – James (1890, p. 85).

Humanity is currently experiencing an ageing population with the number of people

over 60 expected to double between 2015 and 2050 (World Health Organisation, 2018). This

raises concerns as ageing occurs alongside reductions in myriad functions such as processing

speed, reasoning, and memory, impacting day-to-day functioning, quality of life, and

independence (Park & Schwarz, 1999, p.7; Salthouse, 2004). This not only extends to

individuals but also those tasked with caring for them. According to Salthouse (2004) the key

questions are *what* age-related effects exist (such as deficits in reasoning), *when* across the

life-course are they seen (evidence of deficits starting in 20-30 year-olds), *why* do they occur

(a result of grey and/or white matter degradation?), *where* in the nervous system can this be

traced to (is this seen in the cerebellum or regions of the prefrontal cortex?), and *how* does

this affect cognition (does degradation of white matter tracts reduce processing speed?).

There are many theories about cognitive ageing, and there are likely to be multiple causes

varying across tasks, contexts, and individuals, which are herein discussed. To better

understand what differences exist between young and elderly adults, as well as where these

can be traced to anatomically, comparisons both of behavioural data and functional task-

related brain activity were made between age groups. Functional magnetic resonance

imaging (fMRI) was therefore employed as a non-invasive (albeit indirect) measure of task-

related neural activity, based upon haemodynamic changes in the brain. However to

meaningfully interpret these results methodological issues were first investigated. This

helped establish the ways in which commonly used modelling methods differ when

estimating haemodynamic activity in the brain, expanded upon in chapter 3. Leading on

from this was the issue of whether different modelling methods biased results to any one

age group, crucial as this could form a confound in the experimental design. The outcomes

of this investigation are presented in chapter 4.

Once the methodology had been decided upon it was applied to chapter 5,

investigating whether functional brain activity supported the contribution of cerebellar and

prefrontal regions to cognition (Balsters & Ramnani, 2008, 2011; Balsters et al, 2013 ; Bunge,

2004; Mansouri et al., 2020; Sakai et al., 2002) using instrumental trial-and-error learning.

This behavioural model involved the arbitrary association between sensory (visual) cues and

goals (the goal being a visuo-spatially defined oculomotor action; a saccade), and was

selected due to its wide application in the literature and the consequent high level of

theoretical, behavioural, and anatomical understanding. The model can also be referred to

as conditional visuo-oculomotor learning, conditional discrimination, or arbitrary visuo-

oculomotor mapping. One aim was to shed light on whether activity identified within

candidate regions of the prefrontal cortex (PFC) and cerebellar cortex reflect the expected

exchange of information within the corticocerebellar system (Balsters et al., 2014; Buckner

et al., 2011; Kelly & Strick, 2003; Ramnani, 2006, 2014; Schmahmann & Pandya, 1995, 1997),

but a second fundamental question asked whether there were functional differences within

this putative network driven by age (in accordance with Woodruff-Pak et al., 2010). The

behavioural model was further suited to this enterprise due to a high level of experimental

control over learning, the ability to separate events in order to control for confounds, and a

pre-existing knowledge of the circuitry within non-human primates (see Passingham & Wise,

2012). However fMRI at 3T has limits in terms of the signal-to-noise ratio and spatial

resolution, limiting the scope to identify subtle effects and localise these to specific areas of

the brain (Duyn, 2012; Francis & Panchuelo, 2014). To address this chapter 6 utilised ultra-

high field 7-Tesla fMRI to further elucidate the mechanisms underlying instrumental

learning. This broke the behavioural model down into its three constituent phases,

presentation of the cue (context), execution of the response, and receipt of appropriate

feedback. In this final study correct and incorrect trials were contrasted, looking for changes occurring once a rule is learnt.

Within the field of cognitive ageing this thesis at least partly addresses the question of **what** age-related effects exist, specifically asking whether conditional visuo-oculomotor learning is affected by age in humans. It also investigates **where** this can be localised to, establishing whether differences are attributable to candidate regions in the cerebellum and PFC. Finally the thesis considers **how** differences in functional activation of candidate regions may contribute to age-related behavioural impairment. It is important to state at the outset that any contributions identified are unlikely to act in isolation, with it predicted that the prefronto-cerebellar component of the corticocerebellar system plays a part within a much greater story. As alluded to above, understanding cognitive ageing forms a core foundation of this thesis, however evidence of a cerebellar role in cognition also expands upon a growing literature which views this structure as contributing to more than just motor errors (Budisavljevic & Ramnani, 2012; Dow, 1942a; Ramnani, 2006). Additionally the investigations into modelling methods have relevance beyond this thesis, applying both to the functional study of ageing using neuroimaging techniques, and to the neuroimaging literature in general. That responses were recorded using an eye-tracker also facilitated a practical test of eye-tracking methods in both a 3T and a 7T scanner, alongside use of an effector with a well-documented network likely to include the caudally located eye fields and oculomotor vermis (OMV) (Amiez & Petrides, 2009; Kojima & Soetedjo, 2018; Lefevre et al., 1998; Quaia et al., 1999). Within this introduction firstly the research-area is evaluated in sections **1.2**-**1.12**, followed by a summary, then the predictions within the thesis.

1.2. Methodological Issues: fMRI

In keeping with the order of experimental chapters, this evaluation opens by discussing practical concerns when running fMRI studies, also considering how these can be applied to comparisons of age groups. There are multiple methods available when

establishing where in the brain task-related neural activity occurs, with a trade-off between directness of measurement and degree of invasiveness. For example, electrophysiological studies directly measure neural activity but are highly invasive, meaning they are rarely carried out in human cohorts. A non-invasive but indirect alternative with good spatial resolution is fMRI, estimating neural activity from changes in the ratio of oxygenated (HbO) to deoxygenated (HbR) haemoglobin, which forms the blood oxygen level dependent (BOLD) signal (Bandettini, 2020, pp. 1-6; Ogawa et al., 1990; Poldrack et al., 2011, pp. 1-2). When neural activity occurs although there is a metabolic cost vasodilation increases cerebral blood flow (CBF) and volume (CBV), increasing HbO levels in excess of HbR. This can be depicted as a positive peak in the BOLD signal followed by an undershoot before returning to baseline (Bandettini, 2002; Boynton et al., 1996; Buxton et al., 2004; Csipo et al., 2019; D'Esposito et al., 2003; Francis & Panchuelo, 2014; Takano et al., 2006; Tarantini et al., 2017). Near-infrared techniques have estimated that oxygen delivery begins 200-400ms after neural activity onset, with cerebral blood flow increasing 200-400ms later, leading to a substantial rise in HbO less than 1000ms later (Frostig et al., 1990). This response to neural activity, measured using the BOLD signal, forms what is known as the haemodynamic response function (HRF).

In order for event-related fMRI analyses to be effective they are reliant upon a model which accurately estimates the HRF. A common approach is to use a single 'canonical' function comprised of two gamma functions (Friston et al., 1998a; Lindquist et al., 2009; Worsley et al., 2002), referred to as the HRFc model. When this model is applied to analysis of the BOLD signal using a general linear model (GLM) approach (discussed further in chapter 2) a β weighting is produced which acts as a proxy for the magnitude of the estimated HRF. However aspects of the HRFc model's time-course sit as fixed parameters, these including time to onset of the initial rise, rise duration, latency to primary peak (peak latency), dispersion of primary peak, time to undershoot, and the ratio between primary

peak and undershoot amplitude. This inflexibility raises concerns due to evidence that peak latency and dispersion are commonly lower than the HRFc model assumes (Ramnani & Henson, 2005; West et al., 2019). Variability is also found between both participants and brain regions (Aguirre et al., 1998; Handwerker et al., 2004; Taylor et al., 2018), as well as preliminary evidence of the HRFc model underestimating relative undershoot amplitude (Ramnani & Henson, 2005). Of direct relevance to this thesis, there is evidence that peak latency also increases with age (Richter & Richter, 2003; Stefanova et al., 2013; Taoka et al., 1998; West et al., 2019), which may mean assumptions made about the time-course of the haemodynamic response form a confound whereby modelling is better suited to one age group over another. If so, the HRFc model may both fail to reflect the true time course of the estimated HRF, and lead to false conclusions about putative differences between age groups in terms of magnitude.

1.3. Flexible Modelling, a Solution?

This modelling dilemna can potentially be addressed using flexible approaches, one example being the addition of temporal and/or dispersion derivatives (HRFtd) to the HRFc model (Friston et al., 1998a; Poldrack et al., 2011, pp. 76-78; Ramnani & Henson, 2005), see Figure 1. Each of the three functions are convolved with event onset times, and entered as a separate regressor in the GLM, resulting in three β values. These are however associated with one another, as the regressors are tested for optimal fit when linearly combined, so once the β values are known a representation of the estimated HRF can be made by multiplying each function by its β, then summing. Generally a positively weighted temporal derivative serves to reduce the peak latency of the estimated HRF (a negative weighting increasing peak latency) and dispersion derivative β weightings have the same effect but upon dispersion of the primary peak. That this extension to the HRFc model gives it the ability to vary properties of it's time-course may explain why it has been found to outperform the canonical model (Henson et al., 2001; Lindquist et al., 2009). It is important

however to clarify that the β values cannot be reliably interpreted as proxies for magnitude, peak latency, and dispersion respectively, as they are not independent of one another. For example, an increased weighting of the temporal derivative could artificially decrease the weighting of the canonical function (Lindquist & Wager, 2007; Lindquist et al., 2009), meaning that if change in magnitude were a crucial variable of interest, any differences found between the canonical function could also be attributable to change in peak latency and/or dispersion (and vice versa). However, the HRFc model does not offer any improvement on this, as not accommodating these variable timing properties doesn't prevent them from affecting signal estimation (and so the β value). Instead it could be argued that the HRFc model oversimplifies the task, entirely ignoring these interactive effects when making critical comparisons, with an additional increased risk of missing meaningful signal due to its inflexibility. In terms of age comparisons, differences in timing properties will still evoke differences between β values. However there will be less bias in terms of how well any one age group is modelled, and what drives the difference can be more readily discerned by plotting the estimated HRF.
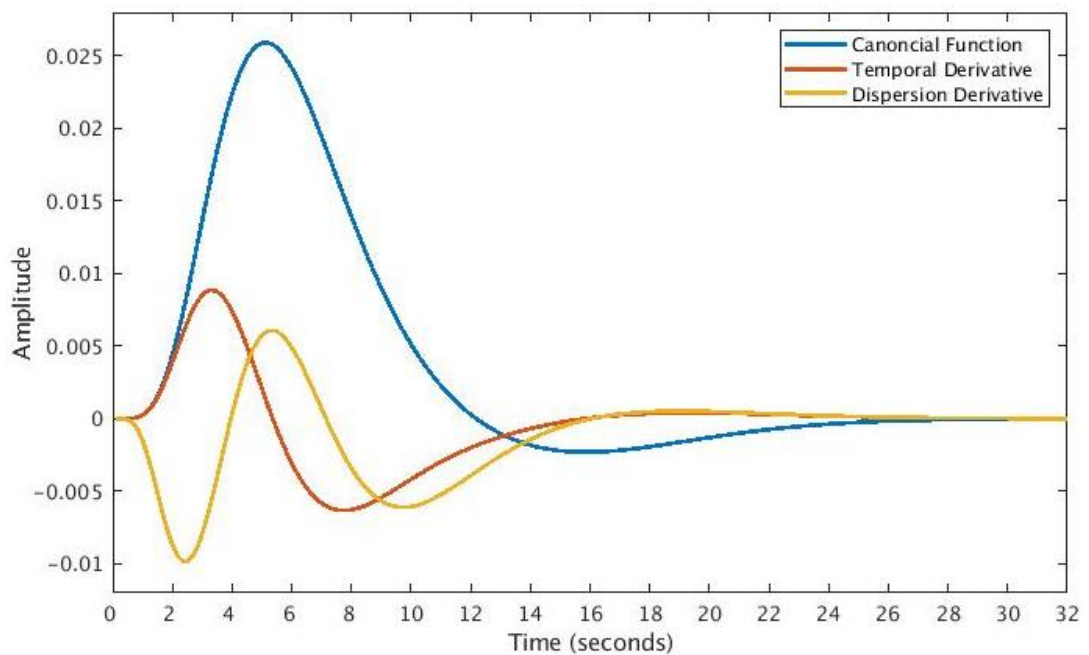
Figure 1. The canonical with derivatives basis set.

6

There are increasingly flexible options available as well, an example being the Fourier basis set (see Figure 2) which uses a selection of sinusoidal functions which are weighted then summed to best represent the signal being modelled. Like the HRFtd model, the combination of this relatively small number of functions facilitates modelling of a huge range of time-courses, however the Fourier model makes even fewer assumptions about the shape of the haemodynamic response (D'esposito et al., 1999; Ramnani & Miall, 2003), and so may be more likely to catch signal with atypical timing properties. This relates to the bias-variance trade-off, as although the Fourier set is less biased by the shape of a given HRF, there will be an increased risk of variability in its estimates which could negatively impact signal detection (Poldrack et al., 2011, pp. 76-77). Importantly, it has been demonstrated that this approach also captures more signal than the HRFc model (Liu et al., 2017), and can capture signal missed when using the HRFtd model (Ramnani & Henson, 2005). However, it remains plausible that the Fourier set will also capture greater noise, and so may rely more upon firm predictions about where activity is expected to be found, and strong experimental designs controlling for confounds. A further issue is that although the Fourier set has the capacity to model very complex signal patterns, in fMRI research the available degrees of freedom are reduced with the addition of regressors at the 1st-level of analysis. Therefore a trade-off is required, whereby the number of regressors is reduced to preserve degrees of freedom, but this theoretically reduces the amount of variance captured by the model. Finally there is the criticism that a Fourier set results in difficulties interpreting results (Aguirre et al., 1998), as differences could be occurring at any of the functions, and the contribution of that function to the final model is not always clear. However, in a well-controlled design the primary question remains 'is there a difference between experimental and control conditions?', and so it could be argued that further interpretability goes beyond the remit of fMRI. Furthermore, more simple models are also affected in many subtle ways, but with even less capacity to elucidate what is causing the difference. The Fourier set, like

the HRFtd model, can at least be subjectively investigated by summing the weighted

functions of each condition, plotting them, and observing what differences appear. It cannot

be said that the differences are necessarily what caused the significant effect, but it provides

greater insight than fixed modelling.
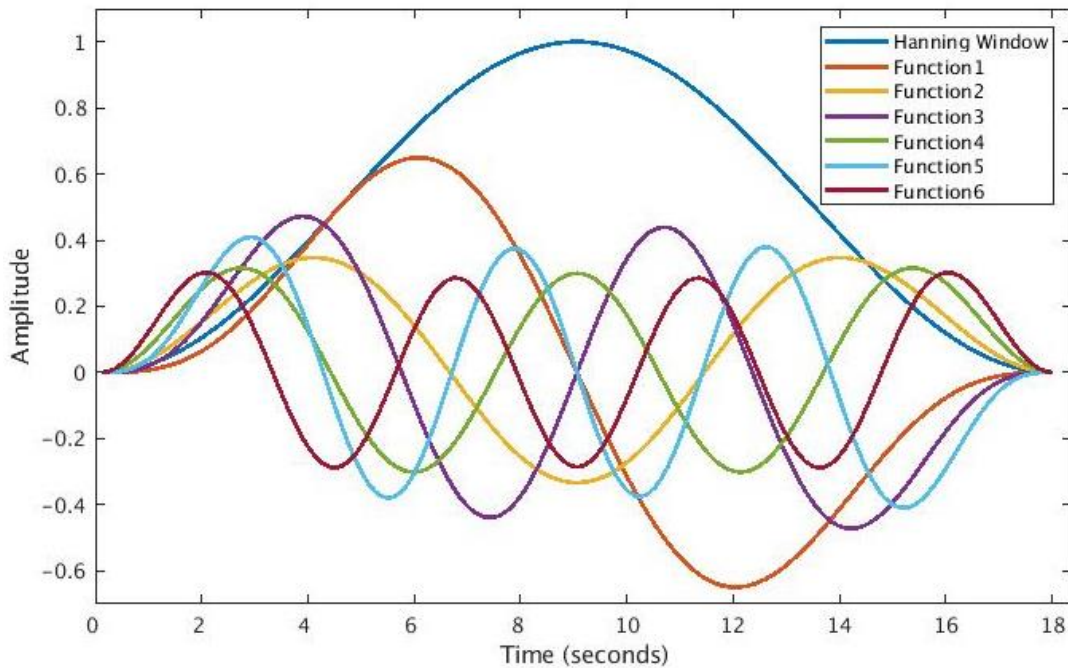
Figure 2. A third order Fourier set with Hanning Window.

1.4. Methodological Issues: Behavioural

Beyond modelling of the BOLD response, there are also a range of general

considerations when designing a study comparing age groups. Although these are applied in

the experimental chapters, some detail is provided here for clarity. For example, there is

evidence of age-related differences in circadian rhythms, meaning one must consider a

participant's preferred time of day. The elderly generally demonstrate a bias towards

mornings (Mecacci et al., 1986) with rates as high as 75% (compared to only 3% showing a

preference towards evenings). Conversely ~40% of young adults show a bias towards

evenings, with only ~10% being biased towards mornings (Park & Schwarz, 1999, p. 153).

Given evidence that testing at non-optimal times of day can affect performance on cognitive

tasks (Intons-Peterson et al., 1998; Park & Schwarz, 1999, p. 154), it is important to establish

a means of measuring preferred time of day, otherwise there is a risk of this becoming a confound. Fortunately there are options available, such as the MESSi (morningness-eveningness stability scale improved; Faßl et al., 2019) or the MEQ (morninginess-eveningness questionnaire; Horne & Östberg, 1976), the latter applied in chapter 5.

When considering the literature on cognitive ageing there is also a potential issue regarding longitudinal datasets, in that retesting participants may introduce test experience effects, posited as being responsible for initial improvements found in early adulthood. Quasi-longitudinal tests generally find a decline with increasing age even in early adulthood (not necessarily picked up by longitudinal datasets) seen in memory and reasoning domains (with an accelerating decline), the speed domain (with a linear decline), and the spatial domain, but not vocabulary, supporting improvements during the early years being introduced by familiarity with testing (Salthouse, 2016, 2019). Alternatively cross-sectional comparisons can be used, however these may allow confounding group differences to drive effects (such as dietary/cultural differences, or years of education), and are deemed a less reliable measure (Hofer et al., 2002). An example of this is that cross sectional and longitudinal designs find similar results when looking at age-related change in the PFC, but with cross-sectional designs underestimating shrinkage in the cerebellum (Raz & Lindenberger, 2011). Despite this, the design of studies in this thesis have had to utilise a cross-sectional design due to both data-availability and time limitations. As a result it must be accepted that measurements of cognitive function may be complicated by a variable range of trajectories. For example, past studies have identified that some elderly participants show maintenance even in their 70s, whilst others show major decline, predicted by variables such as exercise, smoking, level of education, and even ninth-grade literacy (Yaffe et al., 2009). Additionally there is a risk that elderly participants will experience stereotype-threat, whereby common beliefs about cognitive performance deficits in the elderly lead to a 'self-fulfilling prophecy', potentially reducing performance in line with the stereotype (Barber, 2017, 2020; Lamont et

al., 2015). As a result controls were put in place within chapter 5, to reduce the risk that the elderly would expect to fail the task.

1.5. Cognitive Ageing

As a core focus of this thesis, an overview is here provided of some theories within the literature which attempt to explain the effects of age upon cognition, with consideration given to how these link back to the instrumental behavioural model applied. One such example is the processing-speed theory (Salthouse, 1993, 1996) suggesting a reduction in processing speed is responsible for general cognitive slowing, supported by high covariance between cognitive tasks regarding performance. It was posited that when slowing occurs there is less time for successful processing of information held in working memory (termed 'limited time'). This means that when more abstract processing takes place (reliant upon the convergence of multiple pieces of information) there is less available information to act upon (termed 'simultaneity') increasing error rates and/or requiring repetition. In the case of instrumental learning for example, information is held in the brain pertaining to the perceived visual cue, previous associated feedback, and feedback-target pairings, all of which need to be available for the more abstract process of goal formation in the current context. This theory is fairly consistent with the 'common cause' hypothesis which finds that basic sensory functioning (such as visual or auditory acuity) is predictive of cognitive function and mediates variance accounted for by processing speed (Lindenberger & Baltes, 1994; Park & Schwarz, 1999, p. 17). However, there is recent contradictory evidence suggesting that there are independent roles of processing speed and executive dysfunction with increasing age (Baudouin et al., 2019), suggesting that the picture of cognitive ageing is likely to be both context-dependent and complicated (see below for further elaboration).

Researchers have also suggested a degenerative core biological process underpinning age-related cognitive deficits (Deary et al., 2009; Rabbitt & Lowe, 2000). This would be consistent and may even be a causal factor in a general reduction in processing-

10

speed or sensory function. Supporting evidence is found within aged cats which show slower conduction speed within pyramidal tract neurons of the motor cortex (Xi et al., 1999). This can also be seen in elderly humans, with delayed neural activity in the visual cortex associated with reduced white matter density, as well as a cumulative delay (with no effect upon onset time, but an increasing effect upon later components of the response) within the auditory cortex associated with reduced grey matter density (Price et al., 2017). Dickstein et al. (2007) supported this further with evidence of reduced synaptic density and soma size. If connectivity is generally impaired within the elderly it could affect processing which is reliant upon a network of brain regions. This is relevant to cognition due to proposed hierarchical structuring of the PFC (with rostral regions helping mediate activity in more caudal areas) and evidence of myriad connectivity with other brain regions (Amiez & Petrides, 2009; Mansouri et al., 2020; Petrides & Pandya, 1999; Petrides, 2005; Ramnani, 2006, 2014; Sundermann & Pfleiderer, 2012; Uddin, 2021). This range of theoretical and empirical evidence suggests that a core biological process may underpin cognitive ageing, the impact potentially dependent upon the function in question, and its reliance upon neural networks.

Therefore, it is important to consider the components of cognition and how these relate to both brain structure and age-effects. This triangle of factors is referred to as ABC; age, brain structure, and cognition (Raz & Lindenberger, 2011). In order to understand cognitive ageing intelligence is further considered, albeit this being something of an umbrella term. Intelligence can be split into two forms, fluid and crystallized. The former refers to facets such as processing speed, working memory, attention, and problem solving, the latter to knowledge, or more colloquially, wisdom (Zaval et al., 2015). Between the age of approximately 20 to 90 years, measures of fluid intelligence generally decline (seen for reasoning, spatial visualization, memory, and speed, as well as protocols such as the Wisconsin Card Sorting Task, and the n-back Task), but crystallized intelligence (vocabulary knowledge) tends to increase until plateauing after ~60 years of age (Gajewski et al., 2018;

Park & Schwarz, 1999, pp. 43-54; Salthouse, 2010). Further complicating matters and allowing for a more in-depth look at cognition, fluid intelligence is associated with executive functions (Diamond, 2013; Roca et al., 2010). These are specific functions which serve to control/coordinate more general cognitive functioning, and are primarily comprised of inhibition, working memory, and cognitive flexibility as a means of top-down control (Diamond, 2013). However these three do not necessarily show the same profiles of change with increasing age (Ferguson et al., 2021). This suggests that an age-related decline in cognition may vary dependent upon multiple different executive functions, all of which may depend upon brain structures and networks to differing degrees, with the potential for some facets to not be impaired at all.

As an example of the above, working memory does show an age-related impairment, the elderly demonstrating less improvement with practise in working memory tasks which could not be fully accounted for by differences in initial performance (Rhodes & Katz, 2017). This was supported by Ferguson et al. (2021) who conducted an extensive (N = 354) cross-sectional study from age 10 to 86 years, based upon a community sample and looking at age as a continuous variable, addressing the Age and Cognition components of the ABC triangle. It was found that when IQ and socioeconomic status are controlled for inhibition and working memory show quadratic trends, initially improving, then decreasing (peaking at 35 and 30 years respectively). The trajectories were not significantly different, consistent with ideas that the two rely upon each other (Diamond, 2013). However cognitive flexibility was also measured, asking participants to repeatedly switch task-set during a task, and measuring the 'cost'. On some trials participants had to report the shape shown and on others they had to report the colour of said shape, the task determined by positioning of the shape. The cost was measured by comparing reaction times between trials in which the task-set matched the previous trial, and trials in which the task-set differed from the previous trial, with it expected that participants would be slower on the latter. Interestingly, there

was a linear improvement with age, suggesting that the elderly were better able to switch

mid-task. However, the overall cost of this switching task was also checked, comparing

performance on trials in which there was no switch against an alternative where the task-set

only changed between blocks. It was found that here the cost increased with age, and the

cost within the switching task was negatively associated with the cost between tasks (when

partialling out age). The authors suggested younger participants struggle to switch within-

task due to increased task-based attention (decreased task-attention in the elderly meaning

the switch-cost is lessened), but the elderly demonstrate a general struggle to maintain

information when faced with multiple tasks, affecting both the switch and non-switch trials.

Planning was also tested using the Tower of Hanoi task, showing a cubic trend improving

from 10-30 years, decreasing until 70 years, but with a small but variable improvement from

70 years. It is recognised that this study is discussed in detail, but it highlights how age

comparisons can lack subtlety, especially when dealing with multiple executive functions,

many of which show independent ageing effects which are not necessarily linear.

Focusing upon one of the aforementioned facets of cognition is Inhibition Theory,

whereby inhibition of task-irrelevant information occurs at three stages. Firstly there is

'access', limiting attention to goal-relevant data (e.g. blocking out distractors), then

'deletion', removing any data held in mind that is not now relevant, and finally 'restraint',

suppressing goal-inappropriate responses (Campbell et al., 2020). This may apply to the

behavioural model in this thesis as subjects learnt a number of rules in the same study, and

therefore had to inhibit responses associated with all other rules in order to focus on specific

associations with the current rule. When considering the ABC triangle, there is evidence that

elderly participants are less able to cope with interference from goal-irrelevant information,

associated with reduced fronto-posterior effective and structural connectivity. Critically

elderly participants seem to recruit more frontal regions such as bilateral inferior frontal

gyrus (IFG), left dorsolateral PFC (dlPFC; specifically areas 8 and 9), and right anterior

cingulate cortex (ACC) when dealing with interference, which associates with improved

performance within the elderly cohort, implying it is compensatory (Hinault et al., 2019).

That fronto-posterior networks (such as prefronto-parietal) are associated with both

working memory and selective attention remains consistent with ideas that there remains

some overlap between facets of cognitive function (Diamond, 2013; Ferguson et al., 2021).

This suggests that the PFC contributes to inhibition of irrelevant information, and

the operation of selective attention. This localisation is consistent with the prefrontal-

executive theory, otherwise known as the frontal lobe hypothesis. Under this it was

suggested that the PFC (and therefore executive functioning) is more susceptible to age-

related decline than other brain regions, based on earlier and greater age-related

impairment of putatively PFC-dependent tasks (West, 1996, 2000). This was anatomically

supported in humans with evidence that although overall brain volume drops by ~6% by the

age of 80 years (Haug & Eggers, 1991) this is highest within the PFC, more so than for

example temporal and parietal regions (Haug & Eggers, 1991; Raz et al., 1997). The effect

appeared to be driven by a drop in neuron size rather than number (Haug & Eggers, 1991),

and was further supported more specifically by reduced MFG synaptic density in the elderly

(Huttenlocher, 1979). This is consistent with evidence of differentiation within the PFC,

greater reduction evidenced within dorsolateral area 6 than the orbitofrontal cortex (OFC;

Haug & Eggers, 1991), as well as a greater age-related performance decline in tasks

dependent upon the dlPFC relative to the vmPFC (MacPherson et al., 2002). The

contribution of this localised impairment specific to executive functions has been compared

to that of the more global processing speed theory, with it identified that there is shared

variance between the two (Albinet et al., 2012). However although much variance between

age and executive functions was accounted for by processing speed, there was still a unique

effect of age relating to executive functions. There was also a unique contribution of age

regarding processing speed (independent contributions consistent with Baudouin et al.,

2019), with this greater than that specific to executive function, the results suggesting both contribute individually, but with overlap.

The frontal lobe hypothesis originally pertained specifically to inhibition, however West (1996) extended this, segmenting prefrontal functions into the following. Firstly there is retrospective memory which associates events with past experiences, mediated by outputs from the dlPFC to temporal and parietal regions where representations are held. Next is prospective memory which utilises this information when preparing to respond accordingly, and then inhibition of prepotent responses whereby a dominant general response is inhibited in favour of a contextually appropriate one. For example if a rightward saccade had been repeatedly rewarded for cue A, but then cue B is shown instructing the subject to saccade left, the subject should inhibit the rightward saccade in favour of a new contextually appropriate response. These were all deemed to be dlPFC dependent, although the author suggests prospective memory tends to be more impaired than retrospective, potentially due to a lesser dependence upon the parietal and temporal cortices. Finally there is interference control which serves to remove task-irrelevant information, and is deemed mediated by the OFC, an area seemingly less affected by ageing (Haug & Eggers, 1991). Therefore under this theory it may be expected that regions within the dlPFC will show age related differences regarding functional brain activity during an instrumental task requiring both retrospective and prospective memory, and inhibition of prepotent responses.

It Is also relevant to consider indirect factors which may contribute to cognitive impairment. One such area is 'useful field of view', which refers to the area of visual field from which information can be attained whilst both the head and eyes remain stationary. This has been found to decline with increasing age (Dunterman et al., 2019; Edwards et al., 2006; Sekuler et al., 2000) which could be interpreted as a cognitive deficit, a visual deficit, or both. When controlling for ocular disorders and elementary visual functions (such as acuity, crowding, and contrast sensitivity) only measures of selective attention showed a

decline with increasing age, implying a non-visual cause. However tests putatively measuring

processing speed and divided attention found no age association (Woutersen et al., 2018). It

should however be noted that the authors reported the test of processing speed lacked

power, and tests of both processing speed and divided attention suffered from floor effects.

This same literature applies to driving performance, accuracy reducing with age within a

sample of able drivers aged over 70 years (Willstrand et al., 2017). Attention related errors

to road signs, lines, and traffic lights was the third most frequent error made, and the

selective attention component of the useful field of view test correlated both with on-road

attention-related performance and age. A meta-analysis by Woutersen et al. (2017) tested

the contribution of multiple factors to the useful field of view, finding that all subtest scores

correlated with attention, visual speed/contrast/acuity, executive functioning, general

cognition, and memory, these associations strongest for putative tests of divided and

selective attention. Critically there was no interaction, implying the relative contribution of

factors did not differ across subtests, however the test of divided attention had additional

correlations with spatial ability and visual closure. This suggests each subtest receives

contributions from myriad visual and cognitive domains (consistent with cognitive tasks

being reliant upon network-based processing in the brain) and is not limited to the function

it was designed to test (e.g. divided attention as measured by subtest two). Consequently,

when designing studies it should be considered that older participants may be less able to

perceive peripheral stimuli due to either/both visual and/or cognitive decline, the causal

relation between the two remaining unclear.

1.6. Rules and Associative Learning: Introduction

As the thesis employs an instrumental learning behavioural model, this is discussed

in more detail. This phenomenon has been well examined, dating back to Thorndike's Law of

Effect which posited that actions preceding desirable outcomes are 'stamped in', and those

preceding undesirable outcomes are 'stamped out' (Walker 1987, pp. 118-121). Passingham

& Wise (2012) have written extensively about this behaviour, theorising that as early anthropoids began foraging for fruits and tender leaves within the 'fine branch niche' the visual environment became increasingly complex, with resource volatility necessitating a broader range over which food is sought. These environmental pressures are thought to have driven development of the granular prefrontal cortex (areas 8, 11, 13, 14, and 46) as well as additional posterior parietal and temporal cortical regions. It is postulated that the inferior temporal cortex (ITC) encodes perceptual/object details (Muhammad et al., 2006), whereas the posterior parietal cortex (PPC) handles metric data (e.g. number, distance, and location; Burr et al., 2010; Merritt et al., 2010). This is then processed by regions of the PFC in such a way as to allow for interactions between streams of information. For example, when foraging an arboreal anthropoid may have to make a choice as to which cluster of berries to approach first. Object details will inform them whether the berries are a suitable food source, with details such as numerosity and position suggesting the largest/closest cluster as the optimal target. These networks may underpin problem solving in modern humans via the generation of goals (a cognitive task), at a basic level this being a simple movement (forming a behavioural outcome).

The requirement for successful foraging is thought to have been put under greater pressure in early human evolution by the increased risk of predation when traversing greater ranges to procure food (Passingham & Wise, 2012). Classical associative learning by repeated trial-and-error is of little benefit when errors may result in serious injury or death, therefore it is suggested that the granular PFC facilitates contextualised learning from single events. Additionally there is what is termed 'fast learning' whereby a previously acquired learning set can be applied to future novel problems (Passingham & Lau, 2022). Learning from single events should rely far less upon costly errors and so offers a clear evolutionary advantage (Genovesio et al., 2014; Passingham & Wise, 2012). To demonstrate this difference, in a typical classical eyeblink conditioning task the participant will gradually

adjust the onset of their blink until it precedes the airpuff, using the associated conditioned

stimulus (CS; such as an auditory tone) to guide their learning. Eventually the blink will occur

early enough to protect their eye from the air entirely (Gormezano et al., 1962; Ramnani et

al., 2000). However in an instrumental task a participant may be tasked with blinking when

they hear a specific tone, with feedback given to determine whether they were correct. If

after hearing the tone they blink and get 'correct' feedback, it is reasonable to assume that

the next time the tone plays they will blink again, demonstrating a learned response from a

single piece of feedback, rather than a gradual shift. Also, after a period of practise the

response may become 'second nature', meaning it can be performed even in the face of

distraction (Balsters & Ramnani, 2011).

When considering cognitive ageing, it is plausible that impairments in associative

learning may be attributed to an inability to retain 'learned' correct responses (forgetting)

and a tendency to repeatedly provide incorrect responses (perseveration), with repetition

within a learning task found to be of less benefit in the elderly (Salthouse, 1993, Salthouse &

Kersten, 1993). Considering localisation, lesions in the human caudal dlPFC (areas 8 and

rostral 6) result in conditional associative learning impairments, with a healthy elderly

cohort showing a milder version of the same deficit (Levine et al., 1997). The healthy elderly

cohort differed from the young cohort in terms of overall performance, a tendency to match

responses to the previous trial (despite a change of cue), and increased perseveration,

attributed to impairments in response inhibition. There is also evidence of different learning

strategies with age (Walford, 2011) the elderly tending towards elemental learning,

summing the associative strength of a compound stimulus consistent with the Rescorla-

Wagner model. The young tend towards a configural model, considering not just the

generalised strength of a compound stimulus, but also each component. Furthermore when

presented with two strategies (scanning through options, or memorising for later recall) the

elderly are more likely to utilise visual scanning (Rogers et al., 2000). This is important as

memorisers generally responded faster than scanners (more pronounced in older adults) and despite evidence that participants initially scan but shift to a memorisation technique, this shift was more pronounced in the young. Reaction time performance in elderly memorisers was similar to young scanners, and recall better in elderly memorisers than elderly scanners, accounting for much of the difference found in learning performance. In total it was found that elderly adults recalled less after learning, had shallower learning curves, and took longer to reach criterion. All this demonstrates how there are likely baseline differences between age groups, but there are also differences in strategy. Critically, it is not always clear whether it is strategy affecting performance, or whether diminished performance has necessitated a compensatory new strategy. In summary, the evidence discussed is deemed sufficient to justify investigation of cognitive ageing using an associative learning task.

1.7. Rules and Associative Learning: Role of the PFC

Before considering how prefrontal and cerebellar regions contribute as a network to the learning of rules it is important to first discuss each of these regions individually, starting with the role of various subdivisions of the PFC. Previous cytoarchitectonic studies were used to better differentiate the frontal lobe (Petrides & Pandya, 1999; Petrides, 2005; Petrides et al., 2012). Starting on the lateral surface at the central sulcus there is agranular area 4 in the precentral gyrus, the rostral region of which is agranular area 6. Rostral to this is area 8Av which sits in the caudal middle frontal gyrus (MFG) ventral to the middle frontal sulcus (MFS) and has a better developed granular layer IV than 8Ad which extends from the caudal MFG (dorsal to the MFS) into the caudal superior frontal sulcus (SFS). 8Ad however has a better developed granular layer IV than dysgranular 8B which is in the caudal superior frontal gyrus (SFG) occupying both medial and lateral walls. Rostral to this is area 9 within the SFG (medial and lateral walls) which is also dysgranular, but can be differentiated

cytoarchitectonically as 8B has a better defined layer IV (although 8B and 9 share a similarly well-developed layer V relative to layer III).

Ventral to area 9 is area 9/46d in the caudal mid-section of the MFG above the MFS (with a well-developed layer IV unlike area 9, but a dense population of large pyramidal cells in layer III comparable to area 9). Area 9/46v sits below the MFS and also has a well-developed layer IV and large pyramidal cells in layer III, however layer IV is broader and layer III pyramidal cells are less dense than 9/46d. Rostral to this in the rostral mid-section of the MFG is area 46, which sits in the MFS extending both dorsally and ventrally into the gyri, and bordered ventrally and dorsally by areas 9/46v and 9/46d. It has a well-developed layer IV like 9/46d and 9/46v, but sparse small to medium sized pyramidal cells in layers III, V and VI). It is worth noting that Walker's definition of area 46 (Walker, 1940) included what is now thought to be area 9/46, the two comparable in terms of them both having a well-developed granular layer IV but differentiated by 9/46 having large pyramidal cells in layer III. At the rostral-most point of the PFC is area 10 (extending onto the medial wall), which has a well-developed layer IV (but less so than area 9/46d, 46, and 9/46v) and a less well developed layer V than area 9. In the ventral frontal lobe rostral to area 6 is dysgranular area 44 (within pars opercularis) with a poorly developed layer IV, but large pyramidal cells in lower layer III and layer V. Rostral to this is area 45 (within pars triangularis) which can be differentiated from the dorsally located 9/46v as it has very large pyramidal cells in layer IIIc, and relative to the dorsally located 8A as it has smaller layer V neurons (and unlike in 8A micro-stimulation does not elicit saccades). Both areas 44 and 45 have been functionally associated with controlled memory retrieval rather than oculomotor function. Finally rostroventral to area 45 and sitting caudal to area 10 is area 47/12 (area 47 sitting within pars orbitalis) which has a less well-developed layer IV and smaller pyramidal cells in layer IIIc relative to area 45. Considering the dlPFC specifically, this is functionally defined as encompassing part

of frontopolar area 10, and working back caudally includes areas 46, 9/46, 9, 8 and rostral area 6, across both the middle and superior frontal gyri (Petrides, 2000). See Figure 3.
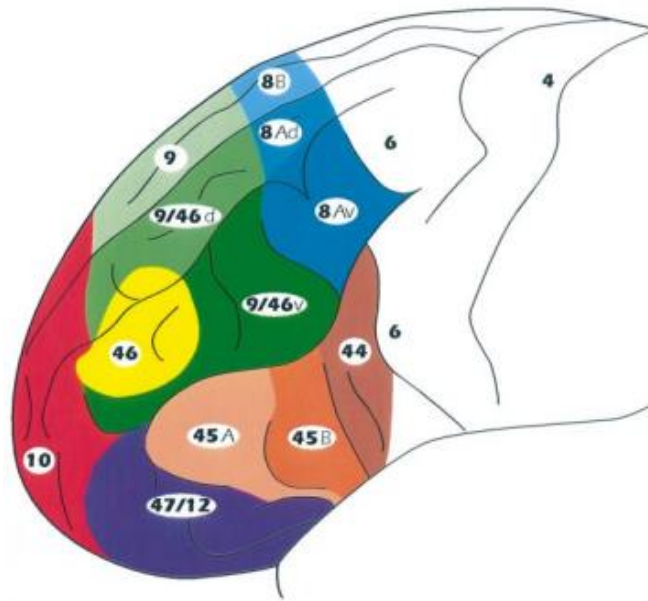
Figure 3. Sub-divisions of the frontal lobe, copied from Petrides & Pandya (1999) with permission.

With sub-divisions of the PFC determined, this brain area is considered in relation to learning. Passingham & Lau (2022) suggest the PFC is specifically involved in transforming inputs into the targets of action, whether that target is defined as an object or a spatial position. Broadly speaking caudal, dorsolateral, or ventral prefrontal regions may determine what the goal of an action is (e.g. which target to select), delegating action preparation to connected premotor or oculomotor regions. The PFC is also thought to hold relevant information in working memory, a process that involves both storage and manipulation of information (Boschin & Buckley, 2015; Christophel et al., 2017; Mansouri et al., 2015). As working memory has a finite capacity plasticity is required, supported by adaptation within individual PFC neurons (Cromer et al., 2010; Mansouri et al., 2020). Looking at sub-regions, Mansouri et al. (2020) nominated the dlPFC as being key to working memory, specifically in

non-human primate (NHP) principal and arcuate sulci. This is supported by lesions in NHP dorsolateral areas 46, 9/46, 8, and 9 (extending into 10, 6, and 12) resulting in impairments to rule learning and memory, tested using a delayed non-matching to sample task (Moore et al., 2012). Rainer et al. (1998) found further evidence that the lateral PFC encodes identity and position of visual objects, consistent with evidence of connectivity between prefrontal areas and parietal and inferotemporal cortices (Petrides & Pandya, 2002; Petrides, 2005; Petrides et al., 2012). Rainer et al. (1998) also demonstrated that target stimuli captured the visual attention of monkeys, measured via time spent fixating the target. This is important as not only is the attended information held in working memory, but what is held in working memory can guide what is attended to, suggesting the lateral PFC may guide attention. The authors suggest that outputs from the lateral PFC also bias activity in posterior regions responsible for attention, such as the parietal and inferior temporal cortices. Interestingly neurons within dorsolateral area 46 and dorsomedial PFC (areas 8, 9 and rostral 6) also show activity coding for specific strategies during trial-and-error learning of abstract rules (Genovesio et al., 2005). This was irrespective of requirement for selective attention, motor/sensory/spatial factors, task difficulty, or reward expectation. Furthermore, Genovesio, Tsujimoto & Wise (2006) found activity in these regions demonstrated a phasic increase with increasing delay duration, not associated with the actual timing of the saccade, the stimulus shown, foveal location, oculomotor response executed, or the probability of reward. Within dorsolateral area 46, and dorsal areas 8, 9, and rostral 6 evidence has also been identified that neurons represent either past or future goals (Genovesio, Brasted & Wise, 2006), important as distinguishing between these helps reduce errors such as perseveration.

Considering connected regions, Muhammad et al. (2006) also looked at the lateral PFC in monkeys, finding that rule and response information was primarily encoded in the premotor cortex (PMC), followed by activity in the lateral PFC, then the striatum. Perceptual

information (relating to stimulus identity and match/non-match rule status) was encoded in the ITC followed by activity in the lateral PFC. They noted that not only was this consistent with known connectivity (such as the ITC projecting to the PFC), but that the lateral PFC was the only region active at all stages of learning. It was potentially expected that when encoding the rule the lateral PFC would project to the PMC, however the authors note that subjects had over a year's familiarity with the learned rule. Given evidence that prefrontal involvement is primarily associated with new rules and diminishes with familiarity (Jenkins et al., 1994; Jueptner et al., 1997; Passingham, 1996; Raichle et al., 1994), it is plausible the direction of activation may shift in a novel task. Adding to this NHP literature, Passingham & Wise (2012, pp. 157-194) state that the mid-lateral PFC (pertaining to area 46), shows connectivity with the PPC, the upper bank of the superior temporal sulcus (STS), perirhinal cortex, somatosensory areas, premotor cortex (PMC), preSMA, the rostral cingulate motor area, the ACC, retrosplenial cortex, and OFC. The authors call this a unique pattern, supporting a role in processing information from the dorsal visual stream as well as directly receiving information regarding objects (not just indirectly via the more ventral prefrontal regions). They also suggest a potential role in action valuation and resultant action selection based upon experience. Damage across area 46 and the more caudal 9/46 has a subtle effect on oculomotor delayed response tasks (likely due to the visuo-spatial component). But damage specific to area 46 has a devastating impact upon the classical motor variant of the task. It is suggested by the authors that this difference may be methodological, as in the classical variant errors are coded categorically (a partial error is not possible) whereas in the oculomotor variant partial errors are recorded. Additionally the authors note that lesions of the caudal PFC are generally evidenced as impacting conditional visuo-motor/oculomotor tasks, but lesions to area 46 have a specific effect upon tasks with a delay period. Consequently, it is suggested that mid-lateral activity during delay may represent encoding of the spatial goal (termed prospective encoding), supporting the relevance of sustained

activity when a delay is present. This would be consistent with the evidence discussed above, as to prospectively encode a goal requires both visual attention and working memory, manipulating perceptual information for transformation into a spatial goal, informing a subsequent suitable action.

The dlPFC therefore forms a candidate region within this thesis (based both upon evidence of its role in prospective encoding, and it being a core site of age-related decline). However it would be too reductive to talk about this area without further considering other prefrontal regions. For example, Mansouri et al. (2020) cited evidence that the OFC, ventrolateral PFC (vlPFC) and dlPFC (principal and arcuate sulci) are all involved in the learning of concrete rules. Due to its connectivity with limbic regions the OFC is considered to have a role in generating expectations to guide behaviours (Schoenbaum et al., 1998, 2003; Schoenbaum & Roesch, 2005) and so activity is generally considered in relation to feedback. Passingham & Wise (2012, pp. 157-194) also suggest that both the OFC and area 46 have a role in generating a goal based on a cue, with damage to these areas resulting in goals being based on the average of past cues rather than the specific trial. This is linked to the risk of trial-to-trial interference and pre-potent responses, whereby the subject must base their selected action on the current trial's cue, not previous cues. The authors surmise that the OFC learns associations between choices and outcomes, which informs prospective encoding of the spatial goal in area 46 (working against trial-to-trial interference) and visuo-spatial information generally contributing across areas 9/46 and 46. That both dorsolateral areas such as 8, 9, and 46, and ventrolateral areas such as 47/12, 44, and 45 can receive the relevant information is further supported by evidence of projections from visual, auditory, and somatosensory cortices (Petrides & Pandya, 2002; Petrides, 2005; Petrides et al., 2012). As Rao et al. (1997) found evidence that 'what' information from the ITC, and 'where' information from the PPC converges in both the dlPFC (areas 46 and 9) and vlPFC (area 12), it is plausible that these structures are both crucial when processing rules. However not only

does mid dorsolateral area 46 have the capacity to receive and process information relevant to prospective encoding of goals, but it also alters motor outputs via projections to the supplementary motor area (SMA), preSMA, rostral cingulate, PMC, cerebellum, superior colliculus, and area 8, as well as the basal ganglia (Miller & Cohen, 2001).

Considering the underlying executive functions involved, prospective encoding of spatial goals requires working memory. Of relevance, the role of sustained activity in mid dorsolateral area 46 has been evidenced during the delay period in a visuospatial learning task, performed in the face of distraction (Sakai et al., 2002). Between area 46, area 8, and the intraparietal sulcus (IPS) only area 46 was sustained during correct but not incorrect trials (the others sustained on both). Also, although activity in area 46 did not correlate with that of the IPS or area 8, the correlation between these two more caudal regions was tighter when area 46 was active. This supports an active maintenance role whereby connections to both regions may have assisted memory in the face of distraction. This role in maintaining spatial memory over delay was further evidenced in NHP studies via ablation of the principal sulcus (Goldman & Rosvold, 1970). Of interest, lesion studies targeting the vlPFC found no direct impact upon working memory and object discrimination (Bussey et al., 2001). Conversely however, transection of pathways between ITC and the ventral prefrontal cortex have been shown to result in a 2.3 fold increase in the number of errors made (Bloedel et al., 1996, pp. 266-275), supported by Browning & Gaffan (2008) and Gaffan & Wilson (2008). This is not surprising, as without this connection the PFC is less able to receive object-relevant information. Additionally, it is not just the mid-section of the dlPFC that is important, with evidence of more caudal lesions of the arcuate sulcus in monkeys also resulting in impaired conditional associative motor learning, however this was in non-spatial tasks (Petrides, 1982, 1985), and could have been due to impairment of the delivery of the response rather than the encoding of the goal. In total the evidence provided suggests that

in an associative learning task the dlPFC is reliant upon facets of working/spatial memory when prospectively encoding goals.

1.8. Rules and Associative Learning: Role of the Cerebellum

The cerebellum is next considered as the second candidate region. This brain structure has been implicated as contributing to the initial selection of an appropriate action over a series of trial-and-error attempts within motor-oriented tasks (Medina & Lisberger, 2008), with a role in motor memory (Ramnani, 2006). However there is a suggestion that it also contributes to cognition, potentially helping reinforce or even bypass the relevant frontal or prefrontal regions required in attending to and processing stimuli, and so essentially automating the learning process (Ito, 2005; Ramnani, 2006, 2014). Support for this can be found, with evidence that cerebellar damage (either by pathology or lesions) impacts associative learning as tested in a visuo-motor task (Drepper et al., 1999). This impact was attributable to neither memory (Bracke-Tolkmitt et al., 1989; Canavan et al., 1994) nor motor deficits (Timmann et al., 2002) and exceeded that seen in those suffering from Parkinson's Disease (Tucker et al., 1996). Furthermore inactivation of cerebellar lobules CRUS I and CRUS II in NHPs using muscimol impaired only new conditional visuo-motor learning (not seen with overtrained associations) with no impact upon the subject's ability to use effectors such as the hand or eyes (Sendhilnathan & Goldberg, 2020). The role of the cerebellum within this cognitive network was addressed by Luria (translated by Budisavljevic & Ramnani, 2012) who suggested that cerebellar damage induced 'pseudo-frontal' symptoms due to corticocerebellar connectivity. This is supported by evidence of cerebellar inputs from numerous brain regions via the pre-cerebellar pontine nucleus (Evarts & Thach, 1969; Glickstein et al., 1985). In NHPs there were strong connections with the primary motor cortex (M1), primary somatosensory cortex (S1), PPC, PMC, and frontal operculum, alongside some association with the occipital and temporal lobes (Dow, 1942b). Of specific interest to the prospective encoding of goals was evidence of connectivity between the PFC

and lateral cerebellar lobule HVIIa (Buckner et al., 2011; Kelly & Strick, 2003; Ramnani, 2006).

When considering how the PFC may fit into the corticocerebellar system, comparisons can be made to a suggested hierarchical motor network (Ramnani, 2006, 2014). Within this model regions such as the PMC output to M1, which outputs via the corticospinal tract to the relevant musculature. If borrowing terminology from control theory, the PMC acts as a controller, outputting to a plant (e.g. M1) which is itself a controller when outputting to another plant (e.g. the corticospinal tract). The cerebellar cortex fits in as a forward dynamic model, receiving efference copies of motor commands via collaterals from controller outputs, with the capacity to then activate a forward output model, here defined as the deep cerebellar nuclei (DCN). In this example, efference copies are relayed via the pontine nucleus to cerebellar lobules HIV-HVI (Kelly & Strick, 2003). This allows the cerebellum to make predictions about sensory consequences of actions, which are then compared to sensory feedback delivered through climbing fibers which originate in the inferior olive (here acting as a comparator). If there is a mismatch between expected and actual feedback, cerebellar outputs via the dorsal dentate nucleus then feed back to the originating controller via the thalamus, and/or to plants downstream in this processing hierarchy via the red nucleus. The idea is that over the course of learning the forward model increasingly inhibits feedback from the inferior olive making the context-specific motor response increasingly resistant to feedback, and so automating the process by lowering the processing load (Ramnani, 2006, 2014).

This begs the question, is there support for prefrontal structures fitting into a similar prefronto-cerebellar system, facilitating the more cognitive components of conditional visuo-motor/oculomotor learning such as the prospective encoding of goals. Work using anterograde tracers in rhesus monkeys found PFC efferents projecting to the basilar pons (a bridge between cerebrum and cerebellum) from dorsolateral areas 46, 8A, 9 and 10, medial

areas 8B, 9 and 10, as well as areas 32 and 45B (Schmahmann & Pandya, 1995, 1997), these

regions consistent with this area of cognition (Genovesio et al., 2005; Genovesio, Brasted &

Wise, 2006; Goldman & Rosvold, 1970; Mansouri et al., 2020; Moore et al., 2012;

Muhammad et al., 2006; Passingham & Wise, 2012, pp. 157-194; Rainer et al., 1998; Sakai et

al., 2002). This was later supported by evidence of closed loops between Walker's area 46

(including area 9/46) and lobule HVIIa (strongest in CRUS II, which outputs via the ventral

dentate nucleus) using retrograde and anterograde tracers in Cebus monkeys (Kelly & Strick,

2003). This connectivity further justified the choice of the dlPFC as a candidate region in this

thesis, and suggested cerebellar lobule HVIIa as a second region. Ramnani (2006, 2014)

suggested that prefrontal regions such as area 46 act as a controller, sitting before the PMC

(plant) within the aforementioned hierarchy. In this setup area 46 may encode the goal

(transforming the contextual cue data into a suitable goal-oriented response), informing

action preparation in premotor regions, with resultant execution in primary motor regions.

Critically this hierarchy could mean that each controller-plant pairing has its own forward

model. If so, a forward model generated between area 46 and the PMC could encode a goal

irrespective of the effector through which the goal is to be achieved, provided it is an

effector governed by the PMC. This is supported by evidence in NHPs that spiking in the

lateral cerebellum was independent of the limb used to achieve the goal (Greger et al.,

2004).

When comparing to the hierarchical motor network described above, it is not

definitive that connectivity between the PFC and cerebellum stems specifically from

collaterals of outputs to the premotor cortex, but crucially the prefronto-cerebellar

connectivity has been evidenced. This could explain the huge expansion of human cerebellar

lobule VII/HVII (Balsters et al., 2010; Diedrichsen et al., 2009) and the cerebral peduncle

predominately carrying fibers from the PFC in humans, but predominately from motor

cortices in macaques. Additionally, connections between cerebellar cortex and the dentate

nucleus are mainly from non-motor lobule HVIIa in humans (from motor lobules in NHPs),

and project to the inferolateral dentate with the relative minority of motor-originating

connections projecting to the superior dentate (Steele et al., 2017). This is consistent with

the ventral:dorsal dentate volume ratio being greater in humans relative to other great apes

(Matano, 2001). For clarity, these claims remain reliant on the assumption that

interconnected regions expand concurrently as per the mosaic hypothesis. Importantly it is

also seen that both the inferior olive and ventral tegmental area (VTA) provide feedback to

lobule HVIIa, meaning the putative forward model within a prefronto-cerebellar network

could receive information about both sensory *and* reward consequences of actions

(Ramnani, 2014; Yang et al., 2003).

This model of cerebellar function has been used to explain subtle modulation of

motor action, a good example of which is the vestibulo-ocular reflex. Here movement of the

head is accompanied by an equal but opposite movement of the eyes, in order to maintain

fixation during motion. This does not require conscious thought, resulting instead from

feedforward information about head movement triggering appropriate compensatory

responses within the extraocular musculature (Ito et al., 1974). Analogously,

corticocerebellar connections suggest potential modulation of cognitive function, allowing

application of cognitive processes within a recognised context without effortful conscious

deliberation or reliance upon feedback. As mentioned above, this could be interpreted as

automation of processing. Automation is defined as the ability to conduct a simultaneous

task without disrupting primary task performance, due to a lessened dependence upon finite

attentional and working memory resources. Using dual-system theory (Kahneman, 2011) the

PFC can be classified as 'system 2', which is slow, conscious, and employed in novel

circumstances. In short, not automatic. However the cerebellum acting as a forward model

could be classified as 'system 1' which is fast, context dependent, and so automatic. The idea

is system 1 is employed to reduce pressure on system 2, as conscious effortful processing is not always practical when facing the cognitive demands of everyday life (Ramnani, 2014).

If automation is occurring it may be expected that over time as a task becomes familiar prefrontal activity would be reduced in magnitude, or potentially maintained in some select neurons but less distributed. Supporting this, numerous studies have identified PFC and ACC reductions in task-related activity with increasing practise (Jenkins et al., 1994; Jueptner et al., 1997; Passingham,1996; Raichle et al., 1994). Reductions in task-related activity have also been associated with increases in automation (Jueptner et al., 1997; Passingham, 1996). Considering the role of the cerebellum, fMRI studies in humans have identified activity specific to lobule HVIIa, time-locked to symbolic cue presentation in a conditional visuo-motor learning task when that cue carries rule-related information (Balsters & Ramnani, 2008). This was seen even when the cue does not directly specify an action (Balsters et al., 2013), with activity levels changing in a manner consistent with degree of automation (Balsters & Ramnani, 2011). Interestingly Sendhilnathan & Goldberg (2020) identified that the cerebellum was not critical in visuo-motor performance of overlearned responses, potentially suggesting that it is involved only in initial learning. However although it remains possible that the cerebellum does have a fundamental role in initial learning, it may still have a more subtle role in overlearned responses, perhaps pertaining specifically to performance under distraction. Although this lends support to a prefronto-cerebellar network, it is not possible to assert that reductions in prefrontal firing rates are caused by the cerebellum. For example, change over time in the cerebellum could also be influenced by reductions in the firing rates of prefrontal regions which project to this structure, with prefrontal reductions potentially mediated by other brain areas. However, it remains true that these findings are consistent with the idea of a cerebellar internal model (either forward or inverse, see below) which over time renders the controller feedback-resistant within a learned context. To expand upon this, Ito (2005) considered how the association

cortex may also form internal loops whereby there is a bidirectional connection between, for example, the PFC (executive cortex) and posterior regions such as the temporoparietal cortex (an internal environment). Within the internal environment it was suggested that there is a mental model acted upon by the executive cortex, just like in motor learning the PMC acts on M1. This way a cerebellar forward model may copy the process of 'thinking' in the executive cortex, with the mental model acting as a plant in the coordination of perception (Ito, 2008). This prefronto-posterior connectivity would be consistent with evidence above suggesting the same connections support spatial attention and working memory (Rainer et al., 1998; Sakai et al., 2002). Ito (2005) go further still, suggesting that incorporation of a theoretical inverse model (whereby the internal model outputs directly to the plant, bypassing the controller) alongside the existing forward model may result in regions such as the cerebellum taking over the whole process of 'thinking'.

1.9. Rules and Associative Learning: Cerebellar Mechanism

This leads to the critical question of how learning occurs in the cerebellum. This thesis is not directly tasked with understanding the mechanism at a cellular level, but when investigating via fMRI comprehension of the possible mechanisms is important for setting informed hypotheses pertaining to expected changes in the BOLD signal. As a starting point both Marr and Albus developed a theory of cerebellar motor learning via plasticity at the parallel fiber-Purkinje cell synapse, modulated by simultaneous parallel fiber and climbing fiber activation, their ideas informed by the writings of Ito. They agreed that parallel fiber inputs to Purkinje cells result from mossy, granule, and Golgi cell firing patterns, forming the subsequent Marr-Albus (or Marr-Albus-Ito) hypothesis (Albus, 1971, 1989, pp. 578-581; Marr, 1969). This further predicted that specific olivary neurons are paired with Purkinje cells, and when both spatially and temporally associated with certain patterns of mossy fiber activation the Purkinje cell output is altered, subsequently persisting even when there is no climbing fiber input. Here the mossy-granule-parallel fiber pathway is thought to serve as a

pattern separator differentiating mossy fiber inputs. This putative mechanism could potentially facilitate learning related to a huge number of cortical inputs for every climbing fiber connection, with an estimated 7000 mossy fibers synapsing with a single Purkinje cell (Marr, 1969). Supporting this, there is evidence that a Purkinje cell can respond to pontine nucleus elicited activation by at least two different sensory modalities (Rasmussen et al., 2015), potentially due to this huge number of mossy fiber connections. There were however crucial differences between Albus and Marr regarding how the mechanism can lead to learning.

Marr (1969) suggested that specific patterns of active mossy fiber subsets (termed codons) synapsing upon the Purkinje cell represented the input (codon representation). This was based upon synaptic facilitation/long term potentiation (LTP), whereby climbing and parallel fibers provide an excitatory input to Purkinje cells. Concurrent firing (within the same 50-100ms window) then strengthens the parallel fiber-Purkinje cell synapse to achieve learning of correct behaviours/actions via Hebbian plasticity (Hebb, 1949) whereby neurons which fire together form stronger synaptic connectivity. Due to the Purkinje cell's inhibitory effect upon the DCN Marr suggested that the Purkinje cell's role in learning was training the organism what to ignore. This may facilitate environmental adaptation and potentially free up the cerebrum to deal with new tasks. Conversely, Albus (1971) hypothesised a variant of this mechanism, whereby excitatory parallel fiber synapses with inhibitory stellate and basket cells (molecular layer interneurons; MLIs) cause inhibition of the Purkinje cell. Golgi cells were suggested as parallel fiber moderators, setting the granule cell threshold; if lower mossy/parallel fiber activation of Golgi cells then the threshold is set lower via reduced inhibition, if more mossy/parallel fiber activation the threshold is increased, controlling the gain. Crucially this determines which parallel fibers fire, keeping the total number low thus reducing complexity whilst increasing the information processing capacity of the system. The model also utilised the climbing fibers net inhibitory impact upon Purkinje cells (rather than

the excitatory effect Marr described) as when firing at 2Hz although Purkinje cell

depolarisation occurred alongside a complex burst in Purkinje cell dendrites, there followed

a pause lasting approximately 15-30ms. During this window Albus posited that parallel fibers

could not elicit Purkinje cell excitation, taking 100-300ms to restore to a baseline firing rate.

An error is registered when the Purkinje cell receives excitatory input from a parallel fiber

during the time window between depolarised and polarised states, therefore synchronised

with the climbing fiber input, with later comparable parallel fiber activations able to elicit

this Purkinje cell pause. This effect of synaptic weakening may be more consistent with

learning typified by improvement until asymptote, at which point the learned response

should be stable. However, if reliant upon synaptic strengthening (as per Marr's suggestion)

saturation may follow asymptote, leading to a decline in the learned response.

This theory has been evidenced in vivo by Demer et al. (1985), who found simple

spikes in Purkinje cells of the feline flocculus (with a baseline of approximately 37Hz) were

silenced by climbing fiber elicited complex spikes once a median complex frequency of 5Hz

was achieved (baseline is approximately 0.5-1Hz; Crepel et al., 1996). In this way olivary

projections can silence Purkinje cells, indirectly eliciting excitation of the DCN. This

mechanism was explained via long term depression (LTD), otherwise known as a lasting

reduced efficacy of the parallel fiber-Purkinje synapse, specifically associated with the

Purkinje cell being stimulated simultaneously by both parallel and climbing fibers,

supporting the Marr-Albus hypothesis (Albus, 1989 p. 579; Crepel et al,. 1996; Ito et al.,

2014). If the excitatory parallel fiber-Purkinje synapse is weakened via LTD, then the

inhibitory effects of MLIs upon the Purkinje cell could lead to the Purkinje cell pause

(Johansson, 2019). The means by which LTD may occur is summarised by Ito et al. (2014)

whereby climbing and parallel fiber co-activation produces calcium ions, calcium production

increasing significantly with concurrent firing. This increase activates both protein Kinase C

(which attaches phosphoryl groups to Purkinje cell AMPA glutamate receptors) and cytosolic

phospholipase A2α, which induces LTD via prostaglandin D2 and E2. These chemical

reactions result in endocytosis of Purkinje cell dendritic AMPA receptors, thus reducing the

excitatory post-synaptic potential/current at the parallel fiber-Purkinje synapse.

Compensatory dephosphorylation also occurs via calcium calmodulin kinase II, reducing

phosphodiesterase 1 and resulting in production of protein kinase G which inhibits

phosphates PP1 and PP2A via phosphorylation, causing AMPA exocytosis. LTP also

contributes via nitric oxide elicited exocytosis, caused by repeated parallel fiber stimulation

at a frequency of 1Hz, which may increase Purkinje cell firing in the absence of climbing fiber

innervation. This is consistent with what is termed the reverse BCM rule whereby small

intracellular calcium increases result in Purkinje cell LTP with larger increases resulting in

Purkinje cell LTD (Hirano, 2018). Crucially this suggests the parallel fiber-Purkinje synapse is

weakened via endocytosis (due to concurrent climbing-parallel fiber activation) and

strengthened by exocytosis, the net outcome dependent upon the relation between inputs.

This is just one explanation of the mechanism by which parallel and climbing fiber

inputs can modify Purkinje cell firing, but has support. In practise the effect is commonly

examined in the context of classical conditioning within non-primate mammals, parallel fiber

excitation relating to the CS, and climbing fiber excitation to the unconditioned stimulus

(US), the Purkinje cell pause then freeing the DCN to elicit the conditioned response (CR).

For example, the Purkinje cell pause is considered to reduce error in the blink response

during eyeblink conditioning (Jirenhed & Hesslow, 2016). This is supported by experimental

suppression of spontaneous Purkinje cell firing affecting movement kinematics (Heiney et

al., 2014) as well as inter-stimulus intervals (ISIs) affecting Purkinje cell pause timing, and

pauses emerging over acquisition then disappearing with extinction (Johansson et al., 2014).

Considering parallel fiber-Purkinje LTD, it has been questioned whether this mechanism is

able to achieve the required temporal accuracy. A time-varying mechanism has been

suggested whereby multiple clusters of granule cells are activated sequentially during the CS

presentation (potentially mediated by Golgi cell inhibition), those most closely associated

temporally with the US showing modification at the parallel fiber-Purkinje synapse

(Johansson et al., 2016). This mechanism relies upon a net inhibitory effect upon the

Purkinje cell via parallel fiber-Purkinje LTD, parallel fiber-MLI LTP, and MLI-Purkinje inhibition

(Albus, 1971; Hirano, 2018) as well as temporal coding via time-varying signals from granule

cells. There is however evidence inconsistent with this theory. Firstly direct parallel fiber

stimulation can be used, bypassing putative temporal coding at the granule cells (Jirenhed et

al., 2007; Johansson et al., 2018) with antidromic signalling deemed unlikely (Johansson,

2019). Secondly the Purkinje cell pause persists even when the GABA$_A$ antagonist gabazine

was administered, which disrupts MLI inhibition of the Purkinje cell (Johansson et al., 2014).

Thirdly CRs were still generated both when AMPA endocytosis (the putative mechanism of

LTD) was blocked both via T-588 (Schonewille et al., 2011; Welsh et al., 2005), and within

mutant mice bred with AMPA endocytosis impairments (Schonewille et al., 2011). Finally

there is a core dilemma in that LTD of the parallel fiber-Purkinje synapse takes just minutes

to induce but the resultant Purkinje cell pause can take hours (Johansson, 2019).

An alternative suggestion is hyperpolarization of the Purkinje cell via intrinsic

changes in membrane excitability, termed intrinsic plasticity (Johansson, 2019), as opposed

to the above synaptic plasticity. A candidate mechanism may involve the metabotropic

glutamate receptor mGluR7 found on the Purkinje cell. When mGluR7 antagonists are

administered in decerebrate ferrets, acquired Purkinje cell pauses ceased to occur (no effect

seen with mGluR1 antagonists; Johansson et al., 2015). Regarding the biochemical cascade

which links mGluR7 receptor activation to the pause, activation of G-protein-coupled

inwardly-rectifying potassium channels (GIRK) may play a role (Johansson & Hesslow, 2020).

These channels become permeable to potassium when activated, hyperpolarizing the cell.

The authors identified that when a GIRK antagonist was introduced the pause was weakened

(the spontaneous firing of the cell remaining unaffected), with no such effect specific to the

Purkinje cell found when a non-specific potassium channel antagonist was used. At present it is inconclusive whether GIRK channels are linked to an mGluR7 initiated cascade, or form a separate mechanism. Unsurprisingly there is contradictory evidence within the literature arguing both for and against the roles of intrinsic plasticity, LTD, and LTP. For example Boele et al. (2018) found that in mutant mice with both parallel fiber-Purkinje LTD and MLI-Purkinje inhibition impairment, CR acquisition and amplitude were reduced, but with either seeming to compensate for the other when just one was impaired. Timing remained intact, but this was also true when GIRK antagonists were administered (Johansson & Hesslow, 2020).

At this stage it remains plausible that synaptic and intrinsic plasticity are both involved (Boele et al., 2018; Johansson, 2019), and that parallel fiber-Purkinje LTD is unlikely to be the sole mechanism underlying motor learning (Schonewille et al., 2011) potentially also having other roles, such as preventing excitotoxic cell death (Welsh et al., 2005). That there is a role of the Purkinje cell pause in motor learning is however supported by Medina & Lisberger (2008) in vivo, who identified that whilst complex spike probability was less than three times baseline, learning was associated with an increase of Purkinje cell simple spike firing rates. But when complex spike probability exceeded three times baseline simple spike firing rates were depressed. The authors themselves suggested this is evidence of multiple mechanisms of plasticity within the cerebellum, which may be consistent with an alternative and more complex model put forward by D'Angelo (2014) which involves LTD and LTP at multiple synapses, as well as both intrinsic factors (such as local biochemical changes) and extrinsic factors (such as the impact of neuromodulators).

This information can now be considered in relation to hypothesised changes in BOLD signal. As outlined above, it is plausible there would be LTP at the parallel fiber-MLI synapse. If this develops over the course of learning it may increase the BOLD signal magnitude as a consequence of greater MLI firing, assuming parallel fiber activation remained fairly

consistent (based on a consistent CS). Additionally it is plausible that over the course of learning parallel fiber activity will generally result in an increased BOLD signal. In the absence of errors, this would align with a subsequent increase in Purkinje cell simple spike firing (Medina & Lisberger, 2008). However over time there may also be reductions in Purkinje cell firing from various sources. These include parallel fiber-Purkinje LTD and subsequent inhibition of the purkine cell, reduced inputs from prefrontal regions reducing parallel fiber (and consequently Purkinje cell) activity, and reduced climbing fiber activity attributed to the DCN inhibiting the inferior olive (Ramnani, 2006, 2014). These have the potential to lower recruitment of oxygenated haemoglobin due to depression of firing rates, reducing the BOLD signal magnitude in the relevant cerebellar lobule, consistent with work by both Balsters & Ramnani (2011) and Imamizu et al. (2000).

In summary Medina & Lisberger (2008) suggest suppression results specifically from errors, whereas Balsters & Ramnani (2011) suggest suppression as a result of increasing automation. The difference may be linked to the former using a smooth pursuit motor task with error measured on a continuous scale, whereas the second used a visuo-motor task with error categorically defined. However in theory if the mechanism is that an error on trial n results in a Purkinje cell pause on trial n+1 (Medina & Lisbrger, 2008), this could be applied to either task. More likely, the difference may be a result of the differing methods of measurement, electrophysiology (Medina & Lisberger, 2008) versus fMRI (Balsters & Ramnani, 2011). Imamizu et al. (2000) suggested that the cerebellum holds multiple possible internal models, all of which receive the error signal (hence much BOLD activity in early trials). They suggest the relevant internal models undergo learning, performance improves, and the resultant error signal reduces across the cerebellum, consistent with reduced BOLD activity in later learning. The relevant internal models should still be active, but as their activity is the sum of multiple inputs, a reduction is still seen due to the absence of error, climbing fiber elicited error signals deemed a large contributor to the BOLD response. Based

on this, predictions made in chapter 5-6 assume a net positive BOLD signal within the cerebellar cortex indicating the presence of inputs to the cerebellum which are timed to the cognitive components of learning. It will also be investigated whether there are practise-modulated reductions in magnitude (as in Balsters & Ramnani, 2011), and differences between error and correct trials, which may indicate the advancement of learning via the formation of internal models.

1.10. Rules and Associative Learning: Reward

As it is suggested that cerebellar internal models also contribute to higher-level cognitive functions (Ramnani, 2014), it is important to consider the role of reward feedback in this mechanism. When looking at sensory feedback such as that seen in eyeblink conditioning the story is well established. The CS (tone) coincides with a US (air-puff) which elicits an unconditioned response (UR), in this case a blink. Onset of the blink is slowly conditioned to occur earlier in time based upon error feedback delivered by climbing fibers when the air hits the eye, the system working to reduce error. This should result in a complex spike which when coinciding with the simple spike activity of parallel fibers (caused by the tone) results in a Purkinje cell pause, disinhibiting the DCN. Outputs feed back to relevant circuitry, modifying the blink until the error is removed (the air puff is predicted and countered via closure of the eye). However when considering reward-related feedback things are less clear. It is important to first confirm connectivity between lobule HVII and the inferior olive, and between the inferior olive and relevant reward-processing regions. It has been shown that neocortical stimulation can elicit climbing fiber activity in Rhesus monkeys (Sasaki et al., 1977), medial prelimbic PFC stimulation in rats also resulting in complex spikes within lobule VII (Watson et al., 2009). Tracer studies have further supported connectivity in rats between infralimbic/prelimbic/orbital regions and the inferior olive (Swenson et al., 1989) with human homologues corresponding to orbital and insula cortices (Wise, 2008), as well as dorsal ACC (BA32) and subgenual cingulate cortex (BA25). Additionally connections

have been found between CRUS II and the inferior olive, and between vermal lobule VII and both the retrosplenial and orbital cortices (Suzuki et al., 2012). That the OFC shows connectivity is relevant, as there is evidence it processes reward-related feedback and so may affect goal-related behaviours (Burke et al., 2008; Frank & Claus, 2006; Groman et al., 2019; Murray & Rudebeck, 2013; Takahashi et al., 2009). Therefore feedback from regions such as the OFC should be able to reach lobule VII/HVIIa via the inferior olive, potentially acting as a teaching signal (Ramnani, 2014). There is also evidence that with repeated reward climbing fiber activity reduces (Kostadinov et al., 2019), with further work in mice demonstrating that climbing fiber inputs to lobule CRUS II were associated with reward-prediction errors, again reducing as learning progressed (Hoang et al., 2023). This is consistent with learning theory in that as something is learnt it becomes more predictable, and so learning as an active process should diminish.

This suggests that prefrontal regions may carry reward-relevant information to the cerebellum via the inferior olive. Next it is considered how dopamine neurons in the midbrain respond to rewards, potentially acting upon the cerebellum via the VTA. The VTA is known to influence regions associated with outcomes, such as the cingulate cortex, OFC, and striatum (Chowdhury et al., 2013; Ramnani, 2014), receiving glutamatergic inputs from the PFC (including ACC), superior colliculus and hypothalamus (Geisler & Wise, 2008), and striatum (Loopuijt & Van der Kooy, 1985). There is evidence in rats that the VTA connects directly with lobule HVII, sending collateral projections to the PFC (such as prelimbic ACC and piriform entorhinal areas), with cerebellar terminations seen in the granular and pyramidal layers, dopaminergic outputs specifically to the cortex, non-dopaminergic to the DCN (Ikai et al., 1992, 1994). This lends support to the idea that the VTA may also act as a pre-cerebellar nucleus, directly influencing change in Purkinje cell firing rates. There is however also connectivity between the VTA and the inferior olive (Oades & Halliday, 1987) alongside other dopaminergic inputs to the inferior olive (Sladek & Bowman, 1975; Toonen

et al., 1998), suggesting the VTA indirectly impacting upon the cerebellum. That the VTA also shows connectivity with areas such as the OFC (Takahashi et al., 2009) supports a contribution to reward related OFC activity. This may form another pathway through which the VTA indirectly communicates with the cerebellum due to aforementioned orbitofronto-olivary connectivity. Additionally in mice it has been shown that Purkinje cells can moderate dopamine release in the medial PFC, mainly attributed to VTA-medial PFC connectivity modulated by glutamate (Mittleman et al., 2008; Rogers et al., 2011). It has also been argued that the cerebellum has the capacity to inhibit the VTA, which would support the cerebellum becoming increasingly resistant to feedback as learning progresses, as is seen via inhibition of the inferior olive (Ramnani, 2006, 2014).

Considering the precise role of striatal dopamine cells there is evidence of activation in the presence of an unexpected reward, and depression with the unexpected omission of reward (Schultz, 2013). If the mechanism here is comparable with teaching via sensory consequences, then complex spikes should be elicited when outcomes are unexpected (for example on trial n when the participant got 'incorrect' feedback), which then modifies firing on trial n+1 (Medina & Lisberger, 2008). Theoretically, dopaminergic depression when reward is unexpectedly omitted may signal errors and consequently produce complex spikes believed to alter intrinsic and/or synaptic plasticity at the Purkinje cell. Kostadinov et al. (2019) further investigated how reward can influence complex spiking in the climbing fiber-Purkinje synapse within mice. It was identified that there are functional microzones in the cerebellum (clusters of olivary-Purkinje cell pairings which fire synchronously), which can differ in terms of their firing characteristics. Using two-photon microscopy it was evidenced that when rewards were delivered some microzones predictably showed increased complex spike activity, and others predictably showed reduced complex spike activity. However both showed increased complex spike activity when a reward was omitted, especially in instances where reward was expected, consistent with the proposed striatal error signal. Although this

does not explain the precise mechanism by which dopaminergic neurons can influence complex spiking in the climbing fiber-Purkinje synapse, it does suggest that complex spikes can be present in the omission of reward, and that their presence is perhaps more generally associated with a violation of expectation.

Another problem to consider is how a feedback-driven complex spike separated potentially by seconds from parallel fiber induced simple spiking (elicited by a cue) could result in a Purkinje cell pause. That this is possible is supported by evidence of climbing fiber activity in the presence of cues which reliably predict rewards (Hull, 2020) implying a shift to the time of the conditional cue, bridging the discontiguity between cue and feedback events. As an analogy, when considering classical associative learning using a trace procedure, there is a gap between the CS and the US. Typically hippocampal activity is seen specific to this behavioural model (rather than in delay conditioning where the US is delivered during the CS), possibly using memory processes to bridge the gap (Thompson & Kim, 1996). Interestingly, cerebellar activity (mainly lobule HVI) is seen in both models of classical conditioning. In order to bridge this gap between events during an instrumental behavioural model there are a few possible theories. Firstly, complex spike activity identified by Hull (2020) may be driven by dopaminergic projections to the cerebellum as per Schultz (2013) and Kostadinov et al. (2019). Secondly, structures such as the hippocampus may play a similar role in instrumental behavioural models such as conditional visuo-oculomotor learning as they do in the aforementioned classical models, potentially via interactions with prefrontal structures (Petrides, 2005). Thirdly, the frontopolar cortical area 10 (FPC) has been suggested as having a role monitoring/evaluating decisions in relation to feedback, and so may re-represent cues/goals at the time of feedback/reward, potentially facilitating cue or goal-feedback pairing (Tsujimoto et al., 2010, 2011, 2012). In this way it is plausible that a connection can be formed across the temporal gap separating cues from their subsequent reward. A full investigation of this mechanism goes beyond the reasonable boundaries of

this thesis, however it does form both an important consideration when interpreting results, and a key area of future research.

1.11. The Eye Fields

Moving away from the cerebellar mechanism and the cognitive component of learning, next the effector used in chapters 5-6 is considered. As conditional visuo-oculomotor learning is employed using saccadic eye movements to select a target it is necessary to discuss the eye fields. These were defined by Amiez & Petrides (2009) as divided into four regions; the frontal eye fields (FEF) located in the ventral branch of the superior precentral sulcus (sPCS), the supplementary eye fields (SEF) located rostral to the medial precentral sulcus at the junction of the medial and lateral cortical surface, the cingulate eye fields (CEF) located in the vertical branch of the cingulate sulcus, and the premotor eye fields (PrEF) in the dorsal branch of the inferior precentral sulcus. This was based on both inter-species comparisons (using gross anatomy and functional classification) and an fMRI study in humans in which saccadic movement was compared against ocular fixation, with good preservation seen between these regions as defined in the human brain, and homologous regions in the monkey brain. However there remains some discrepancy in humans, with electrical cortical stimulation studies generally placing the FEFs more rostrally, in the caudal MFG, extending into both the fundus of the precentral sulcus and caudal end of the superior frontal sulcus, but fMRI studies placing the FEFs more caudally into the precentral gyrus (Blanke et al., 2000, Blanke & Seeck, 2003).

Control of saccades via the FEFs is discussed by Purves et al. (2008, pp. 460-507), with the key points reported below. Saccadic control is achieved by projections to the paramedian pontine reticular formation (PPRF) which can be either direct or indirect via the ipsilateral superior colliculus (Jerde et al., 2012; Segraves & Goldberg, 1987). There are two gaze-center targets, the PPRF being one (controlling horizontal eye movements) and the rostral interstitial nucleus being the other (controlling vertical eye movements). Both

lateralisation of activity and ratio between the two gaze-centers determine the resultant eye

movement, with FEFs and the superior colliculi containing topographic maps of upper motor

neurons sensitive to direction. The amplitude of the saccade is controlled by duration of

lower motor neuron activity in the oculomotor nuclei, and correlations found with the burst

duration of the abducens nucleus. Critically both the FEFs and superior colliculus are thought

to also contain sensory neurons, with evidence of retinal axons terminating in the superior

colliculus as well as dorsal visuo-spatial pathway projections, meaning sensory activity can

be mapped to consequent motor outputs. Interestingly the striatum also outputs to upper

motor neurons of the superior colliculus via the substantia nigra pars reticulata (SNPR) which

tonically inhibits the superior colliculus during fixation, eliciting saccades via GABAergic

medium spiny neurons originating in the caudate inhibiting the SNPR and thus disinhibiting

the superior colliculus. Connectivity between the FEFs and areas such as the superior

colliculus, cerebellum, pretectum, striatum, and pontine reticular formation is made possible

by the thalamus, specifically the intralaminar and ventrolateral thalamic nuclei (Shaikh &

Wang, 2021).

Further regarding functionality, there is evidence that both the sPCS and IPS show

persistent activation when preparing to saccade (Curtis & Connolly, 2008), this same

persistent activity seen across covert attention, working memory, and planning tasks (Jerde

et al., 2012). Jerde et al. (2012) suggest this implicates spatial prioritisation rather than

coding of task or goal type, consistent with priority map theory whereby locations in the

visual field are ranked by importance, based upon both endogenous and exogenous factors

(Jerde et al., 2012). However, there is also evidence of a role in the deployment of spatial

attention rather than solely the execution of saccades. For example, activity in Rhesus

monkeys predicted target detection on a change blindness task based upon persistent firing

during the delay period, irrespective of whether a saccade was executed (Armstrong et al.,

2009). It is relevant that the PPC is also implicated in shifting visual attention, and is

interconnected with both the FEFs and superior colliculus (Rivaud et al., 1994). In humans (with treatment resistant epilepsy) electrical cortical stimulation of the dorsolateral frontal cortex (including the FEFs) has been shown to elicit eye movements (saccades and smooth pursuit) predominately to the contralateral hemifield, with the angle of movement dependent upon the starting eye position (Blanke et al., 1999; Blanke & Seeck, 2003). Further information comes from human lesion studies, implicating the FEFs in target disengagement, contralateral saccades, saccade prediction, and control of smooth pursuit, suggesting FEF cells silence superior colliculus cells which control fixation, indirectly eliciting a saccade (Rivaud et al., 1994). Work in rhesus monkeys (whereby FEF corticotectal neurons were antidromically stimulated from the superior colliculus) also implicated the FEF in both visual and memory guided saccades, alongside reward-based processes due to activity post-trial but pre-reward (Segraves & Goldberg, 1987). It can therefore be concluded that the FEFs may have a varied role, carrying target information, fixation maintenance/release, express saccades, spatial selection, saccade preparation, analysing visual stimuli, and spatial working memory (Armstrong et al., 2009; Blanke et al., 1999; Curtis & Connolly, 2008; Rivaud et al., 1994; Segraves & Goldberg, 1987), with modulation also seen in relation to reward value (Bourgeois et al., 2021).

Given the aforementioned role of the superior colliculus, it is relevant that this structure, the FEFs and the SEFs project to the pontine nuclei (Huerta & Harting, 1984; Shook et al., 1990; Stanton et al., 1988; Voogd et al., 2012), and that the superior colliculus shows indirect connectivity with the OMV (vermal lobules VI-VIII) via the pontine nucleus and the inferior olive (Brodal & Brodal, 1981; Frankfurter et al., 1976; Yamada & Noda, 1987), as well as projections back to the FEFs (Sommer & Wurtz, 2004). Both the FEFs and the SEFs also show evidence of connections to the OMV specifically via the nucleus reticularis tegmenti pontis (Voogd et al., 2012). This could mean that these structures (superior colliculus, FEFs, and SEFs) send efference copies of their outputs to the OMV,

which may then facilitate adaptation of saccadic eye movements (Kojima & Soetedjo, 2018; Lefevre et al., 1998; Quaia et al., 1999). Importantly the cerebellum also has outputs reaching back to these regions, the posterior dentate nucleus of the Cebus monkey shown to project back to the FEFs via the thalamus (Lynch et al., 1994), with work in cats demonstrating projections from the DCN to deep layers of the contralateral superior colliculus (Roldán & Reinoso-Suárez, 1981). Additionally functional connectivity studies in humans have suggested connectivity between the FEFs and the dlPFC, specifically area 9/46 (Hutchison et al., 2012). It is therefore possible that, consistent with ideas put forward by Ramnani (2014), more rostral prefrontal regions which carry out higher order processing may have a controller-plant relationship with the FEFs, whilst sending efference copies to cerebellar lobule HVIIa allowing for adaptation of more cognitive components of a task. This may then also be seen between FEFs and the superior colliculus, and between the superior colliculus and oculomotor nuclei for lower order processes, sending efference copies to regions such as the OMV where internal models can be formed for oculomotor responses.

Of interest, is has been found that removal/ablation of the FEFs does not impair conditional motor learning in monkeys (Halsband & Passingham, 1982), providing the cue and response locations were spatially contiguous (Passingham, 1985). Impairments when cue and response locations differed were attributed to neglect of visual stimuli residing in the periphery of the visual field, a result of reduced attention. However these tasks used a form of visuo-motor learning whereby the effector through which the subject responds is traditionally a limb, supporting the FEFs having a role specific to formation of oculomotor preparation and responding. There is evidence that in a visuo-visual behavioural model FEF lesions do in fact impair performance, but during a visuo-oculomotor behavioural model with saccadic responding activity in the SEFs correlates with performance (but is not associated with the saccade itself) some cells increasingly active as an association is learned, others responding to novel cues and diminishing over learning (Bloedel et al., 1996, pp. 266-

275; Chen & Wise, 1995a; Petrides, 2019, pp. 91-108). The SEFs and FEFs do show

connectivity (Hutchison et al., 2012; Schall et al., 1993) but also differ in that the FEFs

coordinate saccades based on retinal position, but the SEFs coordinate based on the position

of the eye in space (Schall et al., 1993). This implies that the SEFs may locate targets and

feed the necessary retinotopic coordinates to the FEFs, consistent with evidence that they

are not critical for gross saccade execution (Abzug & Sommer, 2017), and have reciprocal

connectivity with the dlPFC (principal and arcuate sulci; Huerta & Kaas, 1990). That said, the

SEFs do still project to the superior colliculus (Shook et al., 1990) and so may also play a

direct role in execution. Finally the role of the CEFs remains relatively vague, but the

cingulate motor areas connect with both frontal and supplementary eye fields (Amiez &

Petrides, 2009). Furthermore, in the presence of conditional visual cues the cingulate cortex

can elicit saccades (Paus et al., 1993), and so activity found in this region will still be

considered in the context of the instrumental behavioural model.

1.12. Additional Structures

Finally, beyond core structures investigated within the thesis and the expected

contribution of the eye fields, when considering the neural correlates of cognition other

regions have relevance. Firstly the basal ganglia is considered (specifically the striatum),

which has some similarities to the cerebellum (see below). Purves et al. (2008, pp. 460-474)

describes the striatum as comprised of two substructures, namely the caudate and the

putamen. These receive cortical inputs via pyramidal cells, caught by the large dendritic

trees of their medium spiny neurons. Inputs include collaterals from cortical, thalamic, and

brainstem regions, potentially comparable with the cerebellum receiving inputs from across

the brain via parallel and climbing fibers (Albus, 1971; Marr, 1969). Striatal structures output

via inhibition of the globus pallidus and the substantia nigra pars reticulata (SNPR), which

themselves inhibit regions such as the thalamus and superior colliculus (respectively). Thus

striatal activation can disinhibit the superior colliculus by inhibition of the SNPR. This is

perhaps comparable to disinhibition of the DCN via LTD at the parallel fiber-Purkinje synapse (Albus, 1971; Marr, 1969). Interestingly, structures such as the SNPR also project back to the dendrites of medium spiny neurons, and so can modulate their own inhibition, potentially akin to the DCN inhibiting inferior olive activity (Ramnani, 2006, 2014). Therefore the striatum has the connectivity necessary to control eye movements, connects with the putative pre-cerebellar VTA (Loopuijt & Van der Kooy, 1985), and is implicated in processing rule/response information (Muhammad et al., 2006). Secondly, it has been demonstrated that regions involved in conditional motor learning include the hippocampus and its outputs via the fornix. The hippocampus is also discussed above as a potential means of bridging the gap between cues and subsequent feedback, and so its contribution is deemed plausible. Supporting this, fornix transection resulted in a 2.7 fold increase in number of errors (Rupniak & Gaffan, 1987). It is however worth considering that although hippocampal damage is associated with slower learning, learning typically still progresses, the impairment less consistent and not as absolute as when there is damage to the dorsal premotor cortex or thalamic outputs from the basal ganglia (Bloedel et al., 1996, pp. 266-275). This is not surprising as damage to a peripheral node in a complicated network may be less likely to be terminal than damage to a core node, an example being the dorsal PMC in a traditional conditional visuo-motor learning task, which is thought to be critical in converting goal information into action via the limbs (Wise & Murray, 2000).

1.13. Summary and Predictions

An initial general prediction is that there is a hierarchically organised corticocerebellar network including prefrontal regions (Ramnani, 2006, 2014), supported by lobule HVIIa showing cue-related activity during conditional visuo-motor learning in humans (Balsters & Ramnani, 2008, 2011; Balsters et al., 2013), HVIIa resting state activity correlating with prefrontal and parietal cortices (Bernard et al., 2012; Buckner et al., 2011; Orr et al., 2019), HVIIa having reciprocal connections to dorsolateral areas 46 and 9/46 via the dentate

nucleus in NHPs (Kelly & Strick, 2003), and lobule VII/HVII accounting for approximately half of human cerebellar grey matter (Balsters et al., 2010; Diedrichsen et al., 2009) implying co-evolution with the PFC. The second prediction is that healthy elderly adults will show impairment relative to young adults. As this thesis utilised fMRI and a cross-sectional design to compare age groups, it is unfortunately unable to definitively infer whether age differences *caused* impairments. However this can be theoretically considered in order to check compatibility with results. That age-related performance differences can be attributable to regions within the dlPFC has been evidenced above, but has been further demonstrated using conditional visuo-motor learning in rats presented with three conditions, one in which responses were given during visual stimulus presentation, compared to a five and a fifteen second delay. It was found that young rats outperformed elderly, this difference increasing with delay, implying learning was impaired at baseline but with an additional impact driven by retention (Winocur, 1992). The authors attribute the baseline deficit to age related differences in the PFC, consistent with findings that using the same behavioural model, rats with dorsolateral and dorsomedial PFC lesions showed impaired performance (but no effect of delay). Conversely the deficit due to delay was attributed to the hippocampus, as hippocampal lesions left baseline performance unimpaired yet introduced an effect of delay (Winocur, 1991). This is consistent with the aforementioned evidence that in humans conditional associative learning performance in the elderly was found to be impaired in a manner similar to those with lesions of dorsolateral areas 8 and rostral 6 (Levine et al., 1997).

In the cerebellum, a meta-analysis by Gellersen et al. (2021) identified significant age-related grey matter loss in bilateral CRUS I, CRUS II and HVI, vermal VI, and left lateralised HVIIb and HVIII, these regions associated with working memory and attention as well as visual, affective, and language processing via default mode, frontoparietal, and attention networks. It may be reasonable to suggest that this contributes to impairments in

cerebellar dependent functions such as classical eyeblink conditioning, with evidence of both

reduced conditioned response frequency and discriminative learning in elderly humans

(Bellebaum & Daum, 2004). Therefore any role the cerebellum may have in cognitive

processes such as prospective encoding of rules (Balsters & Ramnani, 2008, 2011; Balsters et

al., 2013; Ramnani, 2006, 2014) may be similarly impaired. This would be consistent with the

cognitive ageing literature, as conditional visuo-motor/oculomotor learning requires facets

of fluid intelligence such as working memory (manipulating learned information so that

upon recall it can inform subsequent action) alongside the need to inhibit incorrect

responses. It is therefore plausible that in conditional visuo-motor learning tasks where

dlPFC and cerebellar contributions have been evidenced (Balsters & Ramnani, 2008, 2011;

Balsters et al., 2013; Levine et al., 1997; Winocur, 1991, 1992) impairments within this

purported network (whether due to impaired connectivity or grey matter loss; Budisavljevic

& Ramnani, 2012; Dickstein et al., 2007; Price et al., 2017) may be evidenced in terms of

reduced performance and measurable differences in functional activity.

For the reasons outlined above, chapter 3 of this thesis has been dedicated to a

systematic investigation of flexible modelling in event related fMRI, whereby the HRFc

model, the HRFtd model, and the Fourier basis set are compared within a number of brain

regions, and across grey matter. This utilised a large sample of 558 participants from the

CamCAN dataset (Shafto et al., 2014; Taylor et al., 2017). Manipulation of the 1st-level

design matrices facilitated a further look into whether each flexible model captured variance

missed by the other (following the work of Ramnani & Henson, 2005), and simulations were

applied to help make sense of the results. It was determined that an investigation into the

pros and cons of each of these commonly used approaches would be informative for the

literature, whilst commenting on regional differences to aid researchers in tailoring their

approach dependent upon the target brain areas. In chapter 4 this dataset was further

utilised to investigate age-related differences in peak latency, dispersion, and the amplitude

of the undershoot relative to primary peak. Also the two flexible models were compared to the HRFc model in terms of the number of voxels captured within each age group. This was intended to shed further light upon aged-related differences in HRF time-courses, whilst examining how these differences may bias the capacity of the model to capture variance across the adult lifespan. It was predicted that there would be greater signal captured by flexible modelling, with the most signal captured when using the Fourier set, due to it having fewer assumptions (chapter 3). It was also predicted that the elderly would show HRF time-courses increasingly similar to that of the HRFc model due to peak latency and dispersion gradually increasing, and so the HRFc model would be more effective with increasing age (chapter 4).

In chapter 5 the findings from these studies were applied to the modelling approach when comparing young (18-35 years old) and elderly (65+ years old) adults carrying out conditional visuo-oculomotor learning in a 3T MRI scanner. It was predicted that there would be evidence of better performance and faster learning in the young, alongside greater automaticity measured using pupillometry, reaction times, reducing prefrontal BOLD activity (specifically within dorsolateral prefrontal regions such as areas 46 and 9/46) and corresponding reductions in cerebellar BOLD activity (specifically within lobule HVIIa). In general it was anticipated that the dlPFC, the eye fields, and cerebellar lobule HVIIa would be active in the task, the dlPFC acting as a controller projecting to the eye fields which prepare and initiate the required oculomotor response, and collaterals to the cerebellar forward model serving to reduce error in this process. It was also expected that there would be impaired learning/automaticity in the elderly, resulting in estimated HRFs with a greater magnitude due to increased error signalling in the cerebellum, and an increased reliance upon dlPFC structures. Finally chapter 6 utilised ultra-high field MRI to further investigate learning in the cerebellum, also considering the contributions of prefrontal structures, and the role of both the eye fields and OMV in saccade execution. This used an altered but

comparable conditional visuo-oculomotor learning model, but directly compared correct and incorrect trial types to better understand the progression of learning (predicting greater magnitude estimated HRFs during error trials). Additionally both cue and feedback events were investigated to determine which brain regions show activity at either one, the other, or both, with predictions based on the existing literature.

Chapter 2
General Methods

Matthew Danvers
In preparation for publication

Word count: 7963 excluding references

This chapter comprises three sub-sections; behavioural methods, functional

magnetic resonance imaging (fMRI) methods, and statistical methods. Behavioural methods

cover eye-tracking in theory and application, discussing how timings of presented stimuli

and oculomotor events were recorded and checked. This was crucial in identifying brain

activity time-locked to specific events. Screening protocols and their justification are also

included. fMRI methods discusses biophysics, covering the blood-oxygen-level-dependent

(BOLD) response, its measurement, and how this relates to neural activity. Although

introduced in chapter 1, this is reiterated and expounded upon as the BOLD response was

the fundamental means of estimating neural activity across experimental chapters. The

section includes a review of ultra-high-field techniques as applied in chapter 6. Finally

statistical methods covers pre-processing, quality assurance, and application of the general

linear model (GLM) at first and 2nd-levels of analysis. This focus is due to all experimental

chapters being concerned with analysing fMRI data.

2.1. Behavioural Methods

2.1.1. Eye-Tracking: Overview

Eye-tracking provided measures of fixations, saccades between fixations, and pupil

size. Visual information travels down the optic nerve to the central nervous system, and via

the thalamus to the occipital cortex where perception commences (Carter & Luke, 2020).

The Eye-mind hypothesis/link assumes no appreciable lag between what is fixated and what

is processed, hence fixation being used as a proxy of processing. Fixations last ~180-330ms

dependent upon the type of visual processing (Rayner, 2009), relying upon the fovea

centralis of the retina which is dense with light-sensitive photoreceptors called cones. With a

diameter approximately 1.5mm this covers only 1-2 degrees of visual angle (approximately a

thumbnail at arms length), therefore saccadic eye movements are fundamental for

gathering information about a scene (Carter & Luke, 2020). However visual information is

not processed mid-saccade, with evidence the gap is retrospectively filled using information

from the next fixation. Chronostasis (the stopped-clock illusion) demonstrates this, a clock's

second hand perceived as remaining static for too long (Yarrow, 2010, pp. 163-176). Saccade

duration is ~32-48ms for distances of 3-8.5 degrees of visual angle, saccadic velocity

increasing with saccade distance (Abrams et al., 1989). The figures discussed suggest

saccades/fixations occur 2.6-4.7 times per second, requiring a high sampling rate to monitor.

In this thesis sampling was achieved using an Eyelink 1000 Plus provided by SR Research,

sampling at 1000hz. To monitor eye position near infrared light is shone onto the eye where

it is reflected off the cornea, resulting in a 'glint'. Based on pupil position (where infra-red

light is absorbed) and estimates of distances (eye-to-camera and eye-to-screen) gaze

direction is calculated, the pupil moving but the glint remaining stationary (Carter & Luke,

2020; SR Research Ltd., 2022a).

The eye-tracker setup includes a high-speed camera, with information processed by

a Host PC (via Ethernet cable) with an approximate 3ms delay (SR Research Ltd., 2022b).

Experiment Builder software is run on a Stimulus PC (connecting to the Host via an ethernet

cable) with the screen image projected. Output data was saved to the Stimulus PC, viewed

using Dataviewer software. Although eye movements were sampled at 1000hz, stimuli were

constrained by the monitor/projector's refresh rate. For example, a refresh rate of 60hz

meant screen updates every 16.667ms. Therefore stimuli presented post-refresh would be

delayed by up to 16.667ms. All events in chapters 5-6 were timed relative to the trial's start,

minimising risk of cumulative error. Trials only started when a TTL pulse denoted onset of a

scan from the MRI scanner, ensuring temporal jittering (discussed below) remained

accurate. During pilots a TTL pulse was generated, replicating the scanner repetition time

(TR, duration of a single scan) via Spike2 software (version 9.07). A PC running Spike2 sent

the TTL pulse to a CED1401, and on to the Stimulus PC running experiment builder (via 1401

DAC output to a parallel port). The experimental design also included a TTL output for

onset/offset of visual stimuli, fed from Stimulus PC to 1401 ADC input (via the parallel port) and on to the Spike2 PC, registered as categorical signal change.

2.1.2. Eye-Tracking: Piloting

To confirm event timings (three events per trial; cue, targets, and feedback) were accurate a block of 18 experimental trials were scrutinised. The maximum error between programmed and actual presentation time was 20.05ms, varying by up to 16.73ms (approximately one refresh), measured by Spike2. This was consistent with the 3ms delay (SR Research Ltd., 2022b) and 60hz refresh rate (~3ms + 16.667ms = ~20ms). There was also a presentation duration error varying categorically by +/-16.67ms. This was plausible as actual duration will be divisible by the refresh duration, due to actual onsets/offsets occurring upon refresh. If the programmed onset is triggered just after a refresh actual onset will occur upon the next refresh (with duration up to 16.67ms shorter than intended). If the programmed onset and offset occur just before a refresh duration should be accurate (whilst divisible by refresh duration). Finally, if the programmed offset occurs just after a refresh actual offset will occur upon the next refresh (with duration up to 16.67ms longer than intended).

Critically, recorded event onset/offset times denoted when stimuli were drawn to/from the screen, not when they were scheduled. This was confirmed using a photodiode (recording via CED1401), meaning timings are consistent with actual onsets/offsets, ensuring event times used in analyses were accurate. It was therefore deemed unnecessary to replace monitors with options providing faster refresh rates. Further tests were run on cathode-ray tube (CRT) and liquid-crystal display (LCD) screens (see Figure 1). There was a difference between screen-type, relating to measurement of stimuli presentations using a photodiode (sampling at 5000hz). With either screen, presentations matched TTL signals, however the CRT screen had a low signal-to-noise ratio (SNR), attributed to the phosphors declining in brightness over each refresh. Conversely the LCD screen had a higher SNR, but a

3

more gradual reduction to baseline (attributed to independent control of pixels). As screen types with comparable refresh rates had little effect upon onset/offset times either was sufficient. Consequently data reported above/in piloting used an LCD screen deemed more comparable to the setup in the MRI unit.
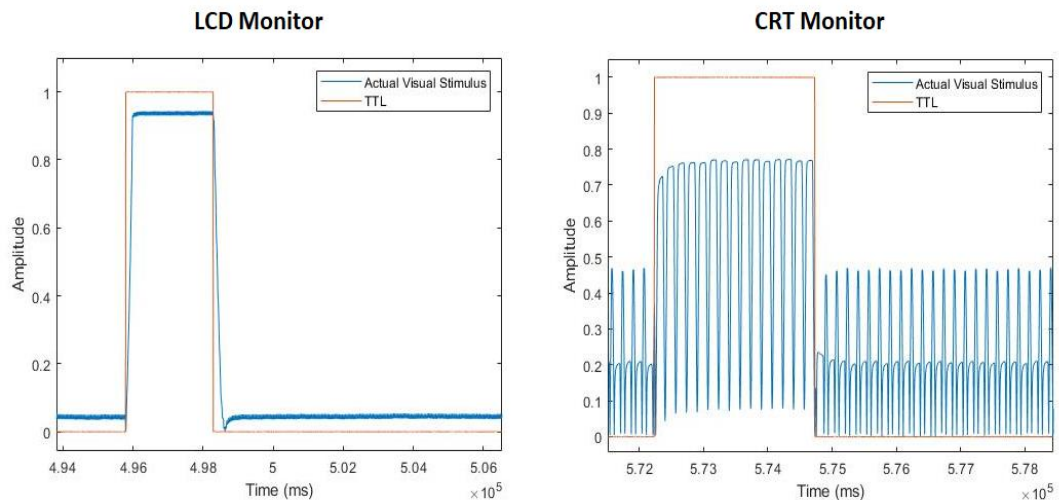
Figure 1. Comparison of LCD and CRT monitors using a photodiode to record event onsets, offsets, and durations.

The primary purpose of eye-tracking in chapters 5-6 was to register fixation of targets, informing delivery of feedback. A fixation trigger was used, requiring a fixation of 200ms within specified regions-of-interest (tROI) before a target was 'selected'. Choice of minimum fixation duration required a trade-off, as high thresholds may cause missed trials due to a tendency to saccade. Conversely low thresholds may increase errors due to erroneous selection of unintended targets. SR Research suggest 250-350ms (SR Research Experiment Builder 2.1.140, 2017), however pilot runs worked well using 200ms. With target presentation lasting 1250ms and a 200ms fixation threshold, theoretically fixations had to begin within 1050ms. Piloting identified that fixation onsets within the first 1010ms were successful, but from 1048ms after target onset, the trial was missed. This was consistent with a reported 35ms delay in live feedback (SR Research Experiment Builder 2.1.140, 2017). Consequently it was confirmed that fixations occurring within the first 1010ms would be

registered. During technical development a saccade trigger was considered, registering a saccade of pre-specified amplitude ending within a tROI. This was deemed suboptimal as saccades landing near a tROI may require a corrective micro-saccade, potentially not exceeding threshold. This approach may also increase risk of incorrect feedback, if participants erroneously saccaded to a target but instantly corrected to another. The fixation trigger fed back only on clear fixations, hopefully more consistent with conscious intentions. This allowed for a change-of-mind when the first fixation did not exceed 200ms, deemed important for the paradigms used in chapters 5-6.

All piloting to develop experimental designs for chapters 5-6 took place in a mock MRI scanner. This was of comparable bore-size to the 3T Siemens TIM Trio used in chapter 5, with scanner sounds played through speakers at approximately 65dB (see Figure 2). This included a decommissioned scanner bed and head coil, with a mirror so participants could see an LCD screen at the head of the bore. This setup piloted the task in a manner comparable to the real scanner, meaning performance reductions attributed to the scanner environment (a phenomenon evidenced by Gutchess & Park, 2006) should also present. Figure 3 contains diagrams of the eye-tracker setup in chapters 5-6.

Figure 2. Mock MRI scanner used for piloting studies.
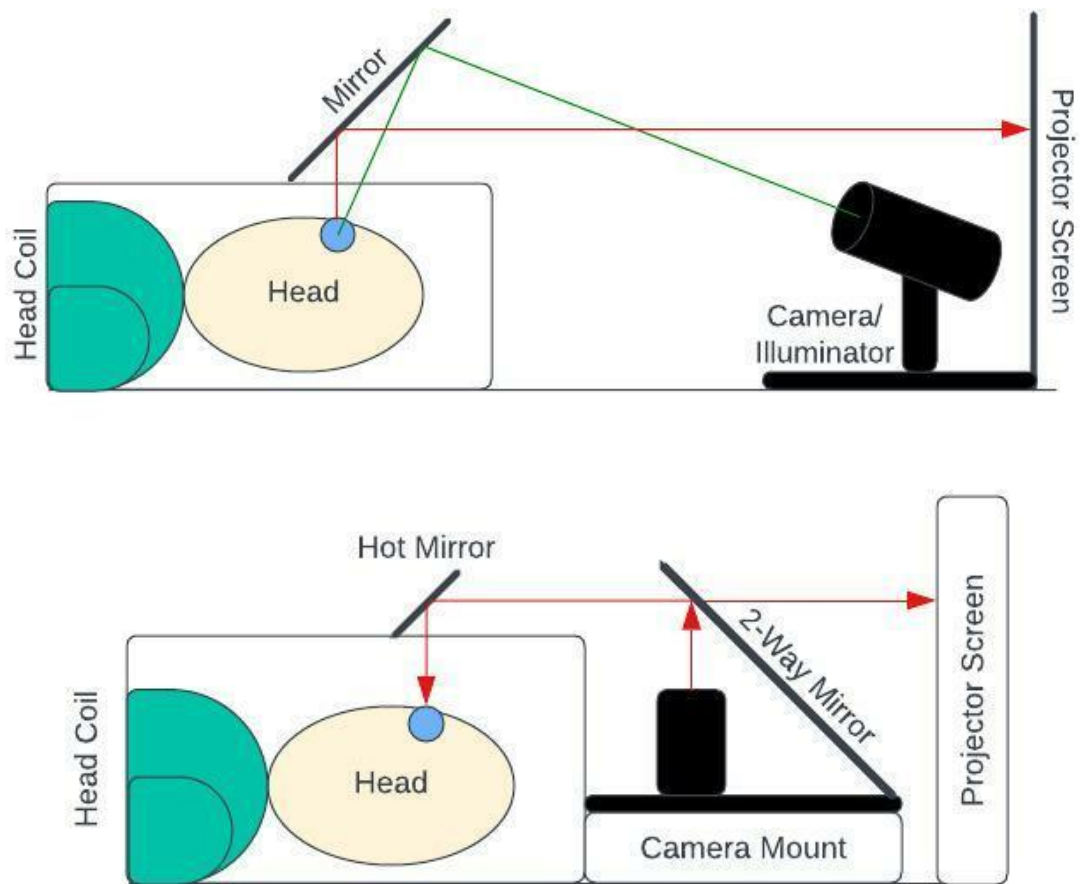
Figure 3. Diagrams of the eye-tracker setup in both the three Tesla (top) and seven Tesla (bottom) scanners used in chapters 5 and 6 respectively.

2.1.3. Eye-Tracking: Pupillometry

Eye-tracking also collects pupillometry data, suggested as a proxy for cognitive load. Cognitive Load Theory is described as learning-related mental activity imposed upon working memory, varying according to characteristics of the learner, task, and environment. Changes in load relating to task difficulty (interacting with expertise) are termed 'intrinsic', if relating to task presentation (e.g. degree of clarity) this is 'extraneous', and if relating to content processing (e.g. degree of automation) this is 'germane' (Huh et al., 2019). This can be measured subjectively (e.g. introspection/rating scales), by performance (e.g. accuracy), or using physiological proxies. An example of the latter is the 'task-evoked pupillary response'

(Gavas et al, 2017), with pupil dilation believed to positively associate with mental effort/task difficulty/cognitive load (Alnæs et al., 2014; Beatty & Kahneman, 1966; Bradshaw, 1967; Hosseini et al., 2017; Hess & Polt, 1964; Huh et al., 2019; Kahneman & Beatty, 1966, 1967; Kahneman & Peavler, 1969). Despite this plethora of evidence and confirmation that pupil dilation associates with error rates (Kahneman & Beatty, 1967), there is disagreement. Zagermann et al. (2018) found evidence that although dilation denotes task onset, increased frequency of fixations and saccades were a more reliable measure of cognitive load. Gavas et al. (2017) also found that a metric based on both frequency and magnitude of dilations was more accurate than percentage change in diameter (relative to baseline) when comparing high and low load tasks. This was supported by a negative association with intelligence scores. There is also cognitive 'overload', evidenced using a digit-span recall task. When cognitive load was manageable (5 digits) dilation occurred. However when difficulty was set at or just above processing capacity (9 digits) there was little change, and when the system was overloaded (13 digits) constriction occurred (Granholm et al., 1996). Therefore dilation as a proxy for cognitive load may not be a strictly linear change, but is generally supported.

Pupil dilation is governed by the sympathetic branch of the autonomic nervous system, occurring when the system is under stress, with a response time of ~two seconds and pupil diameters ranging from 1.5mm-9mm (Gao et al., 2007; Gavas et al., 2017). There are sources of noise, for example effects of accommodation, Hess & Polt (1964) finding changes in distance-to-stimulus (from 99cm to 314cm) led to a 2.1% increase in mean pupil size. However, the authors identified that experimental changes based on task difficulty ranged between 10.8-21.6%, exceeding variability introduced by noise. Kahneman & Beatty (1966) identified that in a digit-recall task the pupil dilated with each digit presented (peak dilation positively associating with number of digits/difficulty), constricting with each digit recalled. The peak occurred in the pause between presentation and recall, except when a

more difficult 'digit transformation' task was carried out. Here the peak occurred in the early stages of recall, these trajectories supported by similar work (Hess & Polt, 1964; Beatty & Kahneman, 1966). There is evidence that the right superior parietal lobule (SPL) responds to visuo-motor cognitive load, activity associating positively with pupil diameter and performance, and generalising across different methods of altering task difficulty (Hosseini et al., 2017). The SPL also receives dense inputs from the locus coeruleus (Benarroch, 2009), a brainstem nucleus operating as a noradrenergic modulatory system contributing to pupil diameter change (Alnæs et al., 2014; Murphy et al., 2014).

Regarding application of the task-evoked pupillary response (chapter 5) it was deemed reasonable to use peak values over a set time-window, however averages have previously been used (Alnæs et al., 2014). The chosen value is then compared to a control condition, accounting for baseline changes over the course of the study due to extraneous factors such as anxiety (Kahneman & Beatty, 1966; Peavler, 1974). Of relevance there is evidence of pupil size being reduced in the elderly, and so it was considered whether this measure may be biased when comparing age groups, but importantly constriction is found to be unaffected when considered proportionally to baseline (Birren et al., 1950; Daneault et al., 2012). Consequently, an indirect but justified measure of cognitive load can be taken, using data already collected whilst eye-tracking.

2.1.4. Screening

Within this thesis one aim was to identify age-related differences in cognitive functioning within a healthy cohort. It was therefore important that participants with symptoms of dementia were excluded. There are multiple tests available to screen for dementia and mild cognitive impairment (MCI), MCI not being clinically defined but involving cognitive decline despite the ability to proceed with daily life (Steenland et al., 2008). The mini-mental state exam (MMSE, implemented in secondary data used for chapters 3-4) is often reported as the most common (Carson et al., 2018; Steenland et al., 2008) but the

Montreal Cognitive Assessment (MoCA) is gaining traction in the field (Carson et al., 2018).

One potential downside of the MMSE is that it is not available for free, however the MoCA

also now asks users to partake in training (requiring payment) within one year of

downloading materials. However, the MoCA offers alternative methods for testing (such as

over the phone) which show sufficient sensitivity (true positive rate, few false negatives) and

specificity (true negative rate, few false positives) (Katz et al., 2021). Considering

performance, the MoCA is believed to have better sensitivity than the MMSE when

detecting MCI and mild Alzheimer's disease (Nasreddin et al., 2005) but is to be run by a

trained neuropsychologist (Bottiroli et al., 2017) taking approximately 10 minutes to

complete (Carson et al., 2018).

A faster and less demanding option is the mini-cog, designed to separate demented

from non-demented elderly adults. The benefits include that it is free, takes approximately

three minutes to administer, has either comparable or higher

sensitivity/specificity/classification rates relative to the MMSE, is not influenced by

education level or linguistic factors, and requires little training, naïve testers showing good

agreement with researchers (Borson et al., 2000, 2003, 2005; Brodaty et al., 2006; Yang et

al., 2016). There is evidence of marginal mini-cog underperformance relative to MMSE when

both are combined with the functional activities questionnaire (FAQ, requiring an informant)

to classify dementia specifically (Steenland et al., 2008). But still the mini-cog-FAQ

combination outperformed MMSE-FAQ when classifying MCI. The mini-cog has also been

compared to the cognitive disorders examination (Codex) concluding that for dementia both

were sufficient (with a slight Codex advantage for specificity) but for MCI the mini-cog was

superior (Larner, 2020). Although tests of this nature are primarily concerned with

identifying dementia and MCI (traditionally associated with the elderly) there are incidences

of them being run on participants from the age of 20 (Gluhm et al., 2013, specifically the

MMSE and MoCA). This is relevant as in chapter 5 the mini-cog was run on both young and

elderly participants, to keep experiences comparable. There were also considerations of participant care, with it being important not to antagonise respondents with tasks potentially perceived as difficult. Jha et al. (2001) identified that most dementia patients report back positively on screening, Borson et al. (2000) also reporting positive feedback on the mini-cog from patients and their families, alongside good engagement. Conversely the same study found that the MMSE caused distress when participants failed items early on. Therefore, although the mini-cog cannot substitute for a full diagnostic evaluation (Borson et al., 2000) it was applied to screen participants for cognitive impairment on the basis that is has good sensitivity (good true positive and few false negative, so rarely classifies people as fine when they display cognitive impairment), is less likely to cause distress, is fast to administer, and can be implemented by non-medical researchers.

Participants were also screened across chapters 5-6 for diagnoses of psychiatric, developmental, neurological or sensory disorders, specific learning difficulties such as dyslexia, dyspraxia, and ADHD, and any history of epilepsy or seizures. This was to reduce the risk that group comparisons would be biased by any unbalanced prevalence of these conditions, with it possible that disorders/conditions of this nature may introduce noise in the data, either due to medication taken (D'esposito et al., 2003; Linke et al., 2017), damage to the brain (D'esposito et al., 2003; Kumar et al., 2009), or differing functional activity/structural anatomy (D'Mello & Gabrieli, 2018; Eden et al., 1996; Nutt & Malizia, 2004). The latter two checks (pertaining to epilepsy and seizures) were also in place to reduce the risk of participants having an adverse reaction to visual stimuli presented, sometimes in quick succession.

2.2. Functional Magnetic Resonance Imaging Methods

Functional Magnetic Resonance Imaging was used across all chapters to estimate which regions of the brain showed consistent changes in neural activity at the time of specified events of interest. This estimate is carried out across three-dimensional space, via

the blood oxygen level dependent (BOLD) response (Ogawa et al., 1990), and is plotted as a

haemodynamic response function (HRF). This is touched upon in chapters 1, 3, and 4, but

reiterated here regarding the methodological approach.

2.2.1. Biophysics

The approach relies upon haemoglobin bound to oxygen (HbO) weakly repelling a

magnetic field (diamagnetism), with unbound haemoglobin (HbR) distorting a magnetic field,

an example of magnetic susceptibility contrast. An MRI scanner produces a strong static

magnetic field, spin precession of protons occurring in this plane. Radio-frequency pulses

cause the spin to precess in the transverse plane, and measures are taken of the time taken

for dephasing to occur as the spin succumbs to the static field. There are different methods,

for example T2 (time taken for protons to dephase) uses a spin-echo pulse sequence,

whereas T2* (effective measure of time taken for protons to dephase) uses a gradient-echo

pulse sequence, which is more sensitive. Critically, the greater the HbO:HbR ratio the longer

it takes for dephasing to occur (due to diamagnetic properties of HbO) meaning oxygenation

levels can be estimated (Bandettini, 2020, pp. 54-61) via the BOLD response. It is important

to clarify that oxygenation is an indirect measure of neural activity, the BOLD response an

indirect measure of oxygenation, and fMRI analysis estimates the BOLD response through

partial sampling, meaning this is a thrice removed indirect measure of neural activity.

However, there is evidence of correlations between BOLD activity and local field potentials

(Logothetis et al., 2001) and between BOLD percentage-signal-change and evoked-potential

amplitude (Arthurs & Boniface, 2003), mediated by astrocyte cells (Petzold & Murthy, 2011).

It is therefore generally accepted that fMRI provides an appropriate estimate of neural

activity, without resorting to invasive means.

Fortunately even brief instances of neural activity result in a vasodilation-mediated

increase in cerebral blood flow (CBF) and cerebral blood volume (CBV). This exceeds that of

oxygen metabolism ($CMRO_2$), with the HbO:HbR ratio further amplified by 'washing out' of

existing HbR, resulting in a relatively clear BOLD response (Bandettini, 2002; Boynton et al., 1996; Buxton et al., 2004; Csipo et al., 2019; D'esposito et al., 2003; Francis & Panchuelo, 2014; Takano et al., 2006; Tarantini et al., 2017). Typically a post-stimulus undershoot follows a primary peak before the signal returns to baseline (Buxton et al., 2004; Friston et al., 1998a; Logothetis, 2003), albeit with some oscillations termed ringing (Ress et al., 2009). One key assumption is that the BOLD response demonstrates linear time invariance. Time invariance pertains to the response being time-locked to the neural event so that a delay in neural activity evokes an equal delay in the BOLD response. Linearity pertains to scaling of the response being proportional to the magnitude of neural activity. This includes an assumption of additivity whereby two neural events occurring close in time would produce a BOLD response that is the sum of the two events where they overlap. There are exceptions, but for the most part these assumptions are upheld (Poldrack et al., 2011, pp. 72-74).

2.2.2. Ultra-High Field MRI

As elaborated upon by Duyn (2012) and Francis & Panchuelo (2014), the benefits of ultra-high field neuroimaging include improved sensitivity, specificity, and spatial resolution (the degree to which space is parcellated). Additionally, magnetic susceptibility contrast is increased, improving the ability to contrast magnetic susceptibility between tissue types, such as oxygenated and deoxygenated haemoglobin. This is fundamental when measuring the BOLD response during functional scans, and when separating tissue types during anatomical scans. Generally within fMRI the effect size (referred to as contrast) is relatively small, change in signal sometimes less than 1% and rising only to 2-3%. As spatial resolution is increased the SNR (contrasting signal with noise) and contrast to noise ratio (CNR, the contrast between tissue types through noise) are reduced. Therefore to increase spatial resolution without losing signal the field strength needs to be increased, van der Zwaag (2009) finding that the ratio between the relaxation rates of active versus inactive voxels (determining BOLD contrast) increased with field strength. Increases in field strength also

lead to signal from capillary beds increasing to a greater degree than from large draining veins (draining veins deemed a source of noise).

This approach is not without problems, as smaller voxel sizes result in a greater susceptibility to head motion artifacts, extending even to effects of brain pulsation when the head remains still. Additionally, higher radio frequency fields can interact with both objects and the environment to create noise, and can increase the degree to which tissue heating occurs. As a result the specific absorption rate must be more carefully considered. The increase in magnetic susceptibility contrast also means there may be an issue of magnetic susceptibility artifacts which can blur the image. Despite this it is recognised that ultra-high field does result in net increases in SNR, allowing for increased spatial resolution. This in turn reduces the impact of partial volume effects, more prevalent with larger voxel sizes wherein more tissue types are present, meaning the intensity value at that voxel is less specific to the contrast of interest. Therefore the movement to ultra-high field opens up new applications for neuroimaging techniques such as imaging of cortical columns and laminar differentiation within the human brain (Harel, 2012; Uğurbil, 2012), alongside interpretation of single-subject fixed-effects analyses (Viessmann & Polimeni, 2021; Vu et al., 2017). For images of the eye-tracker setup within an ultrahigh field 7 Tesla MRI scanner, see Figure 4.
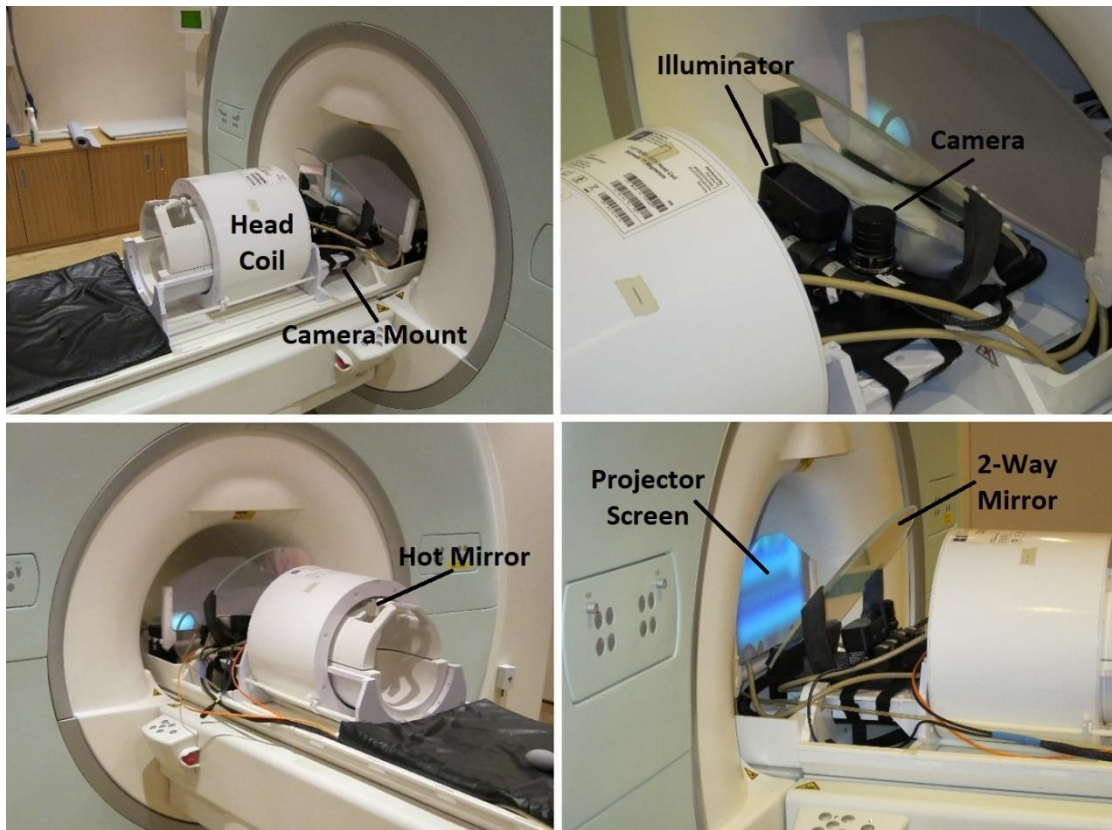
Figure 4. Eyelink 1000 eye-tracker setup in the 7T magnet at the FMRIB unit of the John Radcliffe Hospital (see Figure 3).

2.3. Statistical Methods

2.3.1. Pre-Processing fMRI Data

Functional imaging datasets typically comprise a set of echo-planar imaging (EPI) images (the functional scans measuring the BOLD response), an anatomical image (a relatively high-resolution image with structural detail), and field maps. Prior to analysis data is pre-processed, there being some differences in how this can be approached. One of the first concerns to address relates to magnet susceptibility effects, specifically signal displacement caused by inhomogeneity in the static magnetic field (B0), generally more pronounced around the sinuses. Field maps can restore displaced signal, achieved by running a gradient echo sequence with two different echo times. The differences in phase can then be calculated (producing a single difference image), and should equal the difference between the two echo times plus inhomogeneity (B0). If there is no

inhomogeneity then there should be no difference in phase beyond that introduced by echo times, and so the difference is divided by the difference in echo times, the resultant figure used to approximate and correct for inhomogeneity via a voxel displacement map (Acquiring and Using Field Maps — LCNI, n.d.). Next head motion is considered, with 'bulk motion' artefacts deemed especially problematic at the edge of the image. This is where motion may result in an out-of-brain voxel suddenly containing signal from within the brain (Poldrack et al., 2011, p.43). This can be corrected by realigning to a reference such as the mean EPI image, using affine registration whereby the source image is rotated on two axes to best fit the reference. The realignment procedure provides a set of parameters (see Figure 5), a quantitative estimation of head movement which can be included as regressors within the 1st-level design matrix, regressing out effects highly correlated with head motion.
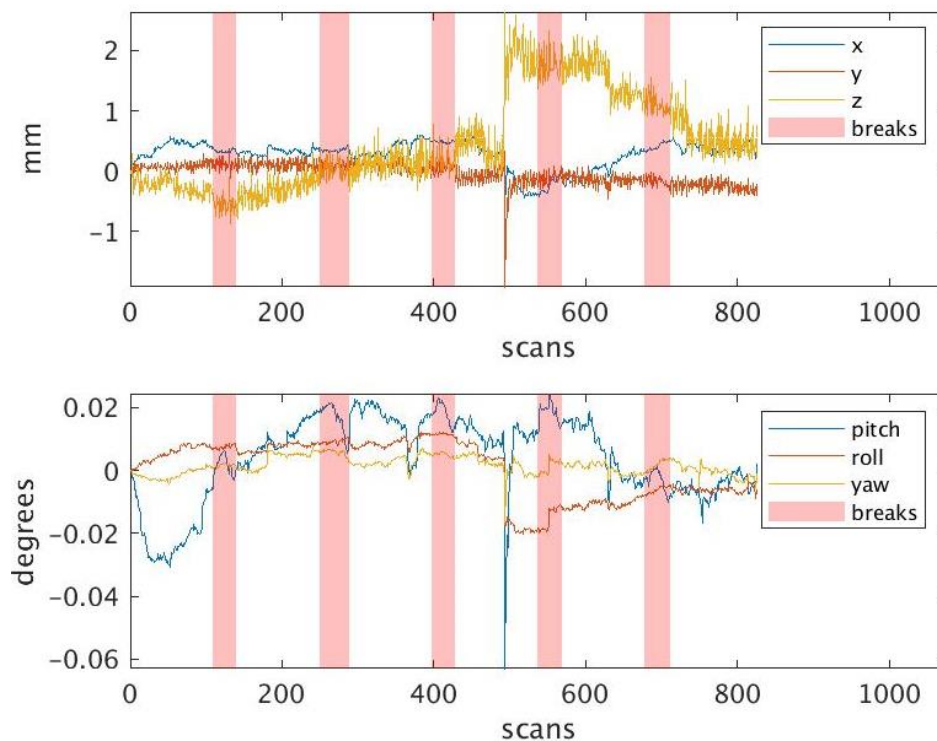
Figure 5. Realignment parameters pertaining also to Figure 7. Translational head movements (top) and rotational head movements (bottom). Red shaded sections correspond to break periods in the study.

There is a second consequence of head-motion that realignment cannot control for, known as spin history artifacts. These primarily pertain to head motion moving through acquired slices within the brain, affecting signal due to complex interactions with the magnetic field. For example, when the head moves protons within a specific region of the brain may shift from one slice to the next, resulting in unexpected levels of excitation. When running an interleaved acquisition this should be visible as alternating dark/light stripes across slices (Poldrack et al., 2011, pp. 43-44). Not only does this impact signal within that scan, but the spin history of previous scans also contributes. Spin excitation is based upon a complicated interaction between the magnetic field at a particular position, and a Fourier transform of the slice-selective pulse. Therefore effects are seen which relate to saturation of the magnetization of a protons spin, associated with positioning in previous scans (Friston et al., 1996). Within-slice movement is typically less of an issue, but through-slice movement is a concern. Additionally the relation between T1 (time taken for protons to revert to normal precession) and TR also matters, as historical effects are a problem primarily when the next set of slices are acquired before signal returns to baseline. Friston et al. (1996) demonstrated these effects using a 64 year-old patient suffering from paranoid psychosis, with excessive head motion. In total, 89.04% of the signal variance was attributable to within-scan head-motion, 3.98% to previous-scan head-motion, leaving just 6.98%. Although an extreme example, this demonstrates that even after realignment spin history can impact the data.

Once displaced signal is relocated and EPI images realigned, each participant's anatomical scan (source) was co-registered to their mean EPI image (reference). The anatomical scan differs from EPI images in that it is not a time-series but is instead a T1 or T2 weighted high resolution image. Within this, structures can be seen and grey matter/white matter/cerebrospinal fluid can be estimated. SPM co-registration affine registers one image to another, either with or without re-slicing (re-writing the source to equal the reference

image regarding voxel number/size, creating a voxel-to-voxel match). The next process is segmentation, whereby the coregistered anatomical image is segmented into grey and white matter images (isolating the two different tissue types) based upon the tissue probability map (TPM) provided by SPM (with additional tissue types available, such as cerebrospinal fluid). This may not be necessary if looking at an individual subject via a 1st-level fixed-effects analysis, as effects found within the functional scans can be overlaid upon the subject's own anatomical image. However, if looking at group-level effects it is necessary for EPI images to be standardised three-dimensionally into a common space. This is achieved using normalisation, accounting for differences not just in head position, but in head size and within-brain structures, discussed below.

In discussing normalisation the MNI (Montreal Neurological Institute) brain is relevant, this being the average of 305 aligned brain images, using affine registration across nine parameters (Evans et al., 1993; Poldrack et al., 2011, p.55). This not only provides a TPM for segmentation, but also means studies can discuss findings in standardised space. Normalisation involves stretching and warping EPI images so they are comparable in space. In this thesis there were different protocols used, Dartel normalisation employed in chapters 3-4 as it is evidenced as being superior to standard non-linear SPM normalisation (Klein et al., 2009). However EPI images with isotropic voxels (as in chapters 5-6) can utilise a contemporary geodesic shooting procedure via the Shoot toolbox, thought to be an improvement upon the Dartel method in terms of accuracy, however no published comparisons were found to support this claim. Both approaches utilise the same logic whereby a mean of all grey and white matter images (via segmentation) form a template, then deviations between the template and the images determines a set of inverse deformations to be applied back to the images to normalise them into the same space. This is repeated iteratively to improve homogeneity between participants, at the end of which these deformations are applied to the EPI images, normalising them to this averaged group

space. It is for this reason that co-registration is crucial, as grey/white matter and EPI images

must be well aligned. During this procedure the normalised EPI images are affine registered

to the MNI brain. It is argued that the warping process should match the MNI brain, as it is

itself a group average (Ashburner & Friston, 2011; Ashburner et al., 2020). Finally the data is

smoothed in order to improve detectability of meaningful effects, chapters 3-5 using a

smoothing kernel of 8mm as recommended by Mikl et al. (2008) for 3mm voxels (chapters 3-

4 using 3x3x4, chapter 5 using 3x3x3), and chapter 6 reducing this kernel proportionally with

reduction in voxel size (1.5x1.5x1.5) to 4mm, close to suggestions of a kernel twice the voxel

size (Poldrack et al., 2011, pp. 51-52). A flowchart of pre-processing steps is available in

Figure 6.
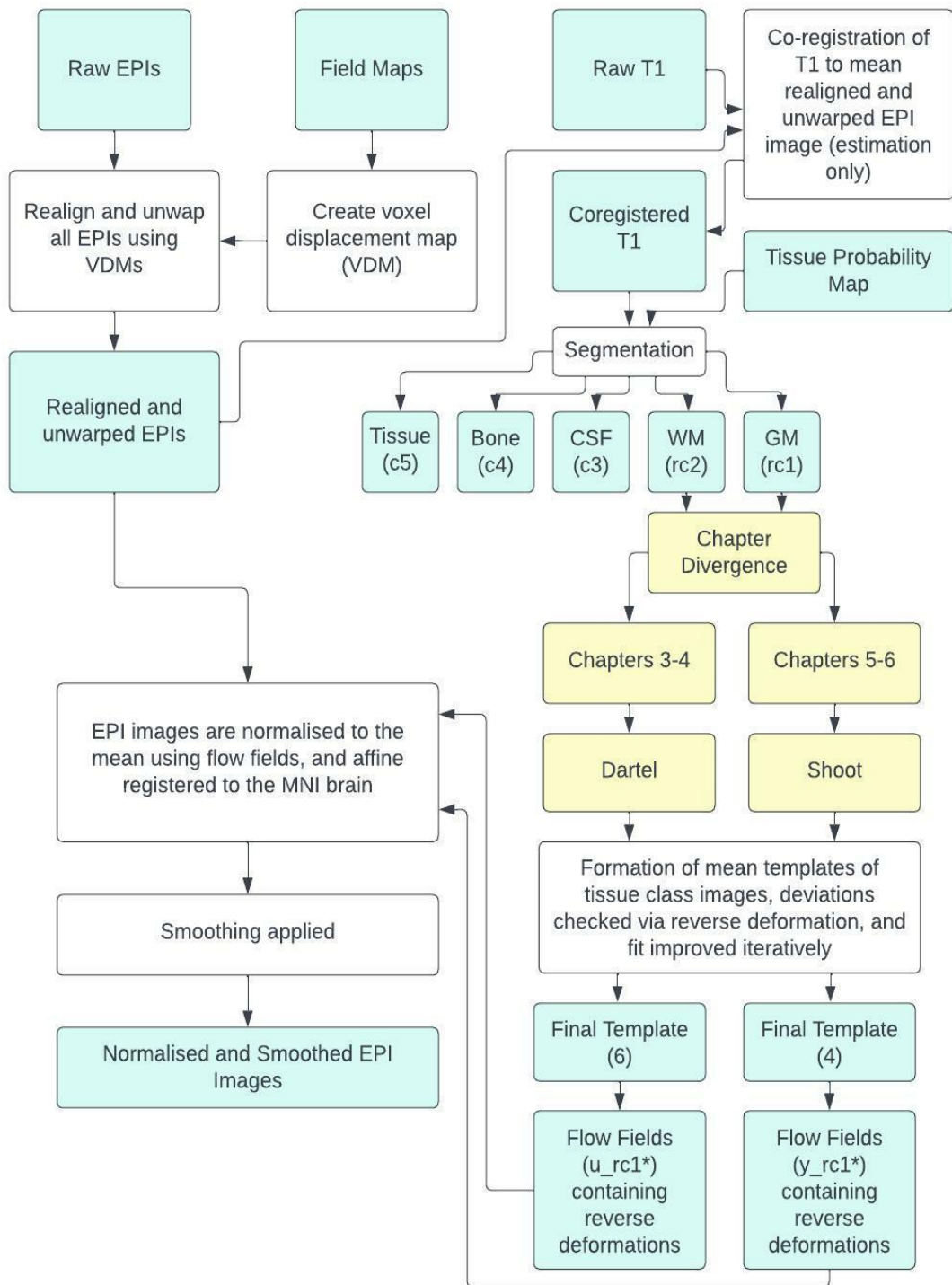
Figure 6. Flowchart specifying pre-processing steps across chapters 3-6.

2.3.2. Quality Assurance

Quality assurance covers both the raw data, and pre-processing steps. Visual checks were made of raw EPI images using SPM's check-reg and display functions. Within chapters 3-5 EPI signal was plotted post-unwarping/realignment, facilitating subjective checks that these steps had improved the data in line with expectations, looking for unexplained, spiking or periodic signal. This was carried out both in the raw data and the smoothed realigned data within chapter 6. To accomplish this the mean intra-slice signal (MIS) was calculated within each scan and plotted in two dimensions, scans on the x axis and slices across the brain on the y axis (see the top plot in Figure 7). A second plot showed the same data normalised to the mean of each slice, better visually representing variability over time (see the middle plot in Figure 7). Finally a fast fourier transform (FFT) was applied to the normalised data, checking for periodicity in the frequency domain (see the bottom plot in Figure 7). The example in Figure 7 demonstrates head-motion just before the 500th scan, more obvious when looking at the normalised plot. This was supported by a graphical depiction of head motion regressors (see Figure 5). This information was quantitatively and subjectively analysed for chapters 5-6, but sample size rendered subjective analysis impractical in chapters 3-4.
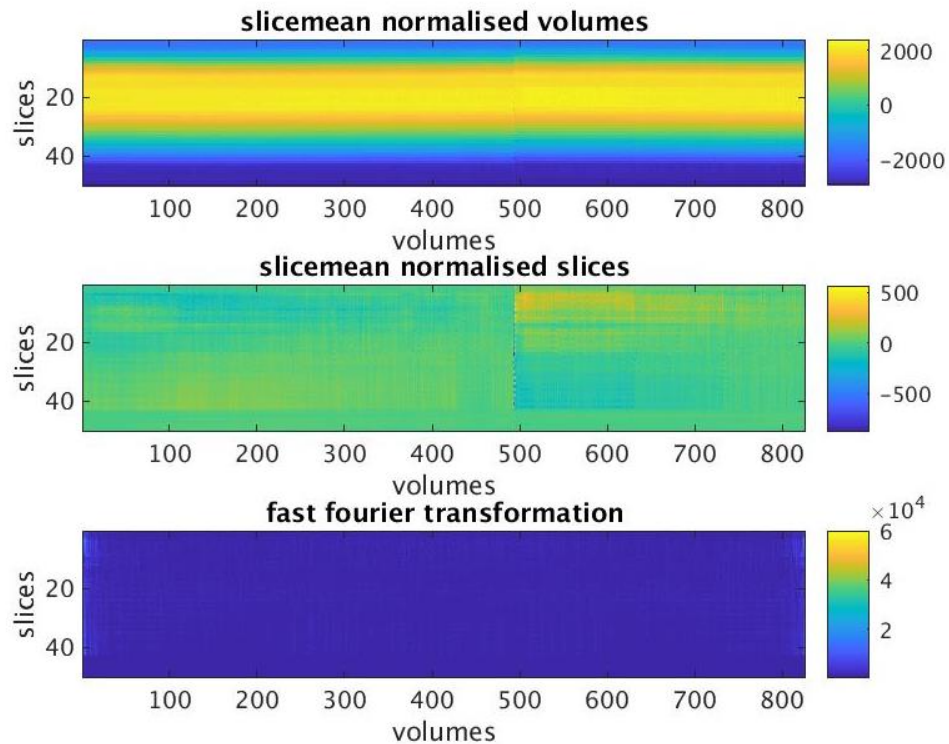
Figure 7. Mean intra-slice signal normalised across slices within each volume (top), across volumes within each slice (middle) and a FFT of the normalised slices (bottom). Volumes on the x axis refer to scans.

Quantitative analyses looked at the range in signal amplitude calculated across scans within each slice (temporal range, change over time), and across slices within each scan (spatial range, change over space), identifying high **absolute** variability in signal. This was repeated for individual shifts, calculating the maximum single 'temporal shift' over two consecutive scans within a slice, and 'spatial shift' over two consecutive slices within a scan, highlighting **sudden** signal change over time and space. High **relative** signal variability was also calculated via coefficients of variation (COV), the standard deviation (SD) of all scans divided by the mean of all scans within each slice (temporal COV) then selecting the maximum. This was repeated examining variability across slices within each scan (spatial COV). Objective checks of shifts and relative signal variability were applied to all chapters, however absolute variability was only checked in chapters 3-4 (included due to the large sample requiring greater reliance upon objective checks). Accuracy was checked in chapter

21

3-4, participants with outlying values (identified using z scores) randomised among a randomly selected equal number of non-outlier participants. The experimenter remained blind to outlier classification examining the graphical outputs (including but not limited to the data in Figure 7), rating participants on a 1-4 scale (1 = very good, 2 = good, 3 = poor, 4 = very poor). This resulted in 86.765% agreement with the objective method, errors only occurring with less confident ratings 2-3, but never on confident ratings 1 and 4.

Post realignment quality assurance also investigated estimates of head-motion to identify participants with excessive movement. Across each of the six head-motion measures shifts between each pair of consecutive scans, and the total range across scans were examined. Different thresholds were used dependent predominately upon sample size and when motion occurred. In chapters 3-4 a more conservative objective threshold was applied using voxel size, as the large sample meant removal of head motion artefacts could be prioritised over retaining participants. Conversely in chapters 5-6 smaller samples meant a greater emphasis on only removing those who showed clear departure from group norms. Additionally, within these latter studies there were break periods, change occurring during breaks deemed less likely to negatively impact the data.

Quality assurance of co-registration was carried out subjectively by checking registration between each participant's anatomical and mean EPI image using SPM's check-reg function (chapters 3-4). For chapters 5-6 checks were made of outputs mid co-registration. Normalisation also required quality assurance, again carried out subjectively by looking at each participant's EPI images relative to the MNI brain (using SPM's check-reg function). A quantitative investigation was also run for chapters 3-5, omitted in chapter 6 due to the small sample size. Once the 1st-level of analysis had been carried out masks were produced for each participant, denoting voxels containing signal. Firstly the total was calculated for each participant, z-scores identifying outliers. Secondly a group mask was created by summing the mask values (zero denoting no signal, one denoting signal) within

each voxel across all participants, then dividing by the number of participants. If the

resulting value was >=0.5 it was allocated the value of one, if <0.5 it was allocated the value

of zero, essentially calculating the mode to represent the group. Each participant's mask was

then compared to the group mask, ascertaining how many voxels did not match, z-scores

identifying outliers (see Figure 8a). Once removed the process was re-run, results seen in

Figure 8b.
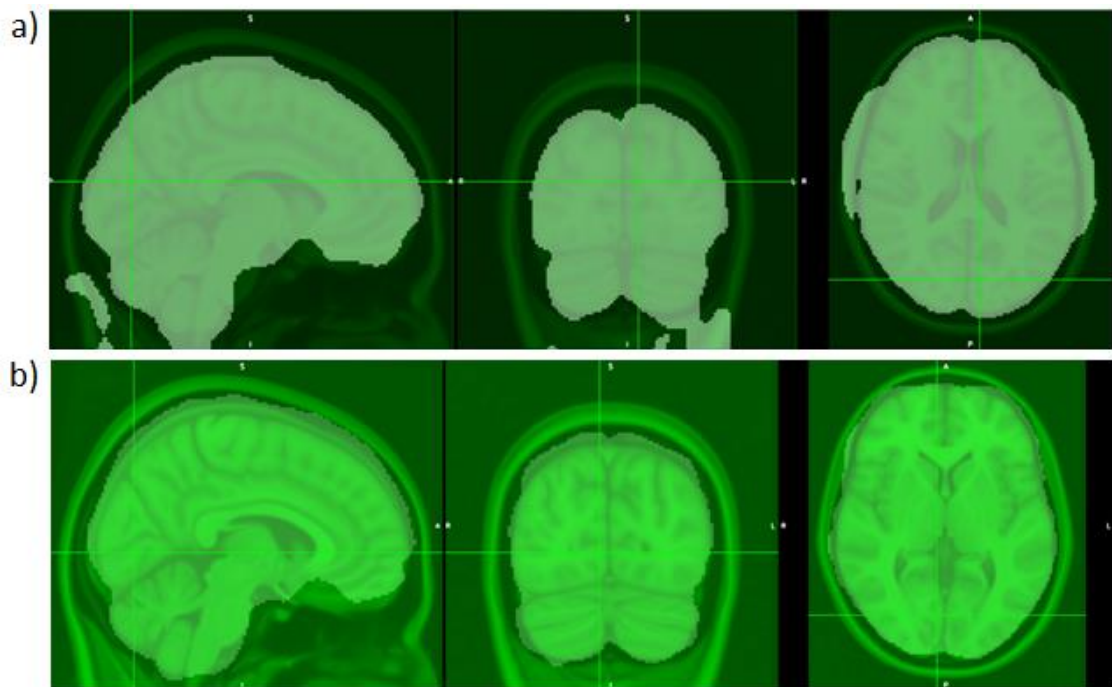
Figure 8. Masks generated in chapter 3, overlaid upon the MNI brain; a) A randomly selected
mask outlier, b) The worst fitting mask after the first round of outliers were removed.

2.3.3. General Linear Model Principles for fMRI

For analysis a general linear model (GLM) approach can be taken. In every voxel

regressors formed via convolution of estimated HRFs with known event onset times are

tested for their fit to the BOLD signal. Here regressors form independent variables and the

BOLD signal a dependent variable within a regression analysis. Where a good fit is found it is

assumed the region is showing activity time-locked to the event of interest. Output beta (β)

values serve as a proxy for the scaling of the model (e.g. a larger BOLD response resulting in

a larger beta), and residual error values denote the fit. This uses the following model in which Y represents the estimated BOLD response, X represents the regressor of predicted haemodynamic responses, β represents the gradient of the association between the two, n represents the number of regressors, and *e* represents residual error:

$$Y = X_1\beta_1 + X_n\beta_n + e$$

A well-estimated predicted HRF is therefore required (Lu et al., 2007), with a canonical model (HRFc) employed to approximate the typical BOLD response. This is comprised of gamma functions modelling both a primary peak and a post-stimulus undershoot (Friston et al., 1998b). Improvements have subsequently been made, such as a canonical model with temporal and dispersion derivatives, specifically aimed at accommodating variability in timing properties such as latency to and dispersion within the primary peak (Poldrack et al., 2011, p.77-78; Ramnani & Henson, 2005). Another example is the Fourier basis set, employing a chosen number of Fourier functions to model variable signal shapes (D'esposito et al., 1999; Liu et al., 2017; Ramnani & Henson, 2005). Both models reduce available degrees of freedom relative to HRFc as they are comprised of multiple functions, each entered as a separate regressor in the GLM. However, the trade-off is an increased flexibility to pick up BOLD responses with poor conformity to presumed timing properties. This is especially important when dealing with inter-regional analyses or comparisons of age groups, between which BOLD signals can vary in their timing properties (Aguirre et al., 1998; Handwerker et al., 2004; Miezin et al., 2000; Richter & Richter, 2003; Taoka et al., 1998; Taylor et al., 2018; West et al., 2019).

To sample the BOLD signal effectively temporal jittering was also employed. For example, assuming an HRF has a duration of 30 seconds (including rise-to-peak, fall-to-baseline, and subsequent undershoot), and events occur every 20 seconds, the number of sampling points during the 30s time-window is dependent upon the TR. With a TR of two seconds, there would be only 15 sampling points. This is a worst-case scenario as the inter-

stimulus-interval (ISI) is perfectly divisible by the TR, meaning for each event the same 15 points of the HRF are sampled. Within this specific example improved sampling can be achieved using a shorter TR, however there are limitations regarding what can be implemented within fMRI. To reduce the TR further multi-band factors need to be increased (potentially reducing SNR) or the number of slices need to be decreased (excluding brain regions or reducing spatial resolution, both limiting the scope of potential inferences). A more practical course of action is to ensure that the same points are not being sampled with each presentation of the event by jittering onset times. Randomisation is one option, meaning the ISI is variable and so will not be clearly divisible by the TR. However sampling can be further optimised by uniformly distributing the onset times of events over the duration of the TR (applied to chapters 5-6). This was deemed optimal as a random distribution can result in sampling points clustering together by chance, or even overlapping. For example, in a study with just 16 events and a TR of 2000ms a uniform spread of onsets across the TR can be calculated by dividing 2000 by 16 (equalling 125ms) and using this to evenly distribute event onset times. Consequently only one event will occur 125ms into the TR, only one will occur 250ms into the TR and so on, meaning the greatest possible spread of sampling points is achieved, see Figure 9 for a simulation of the above example.
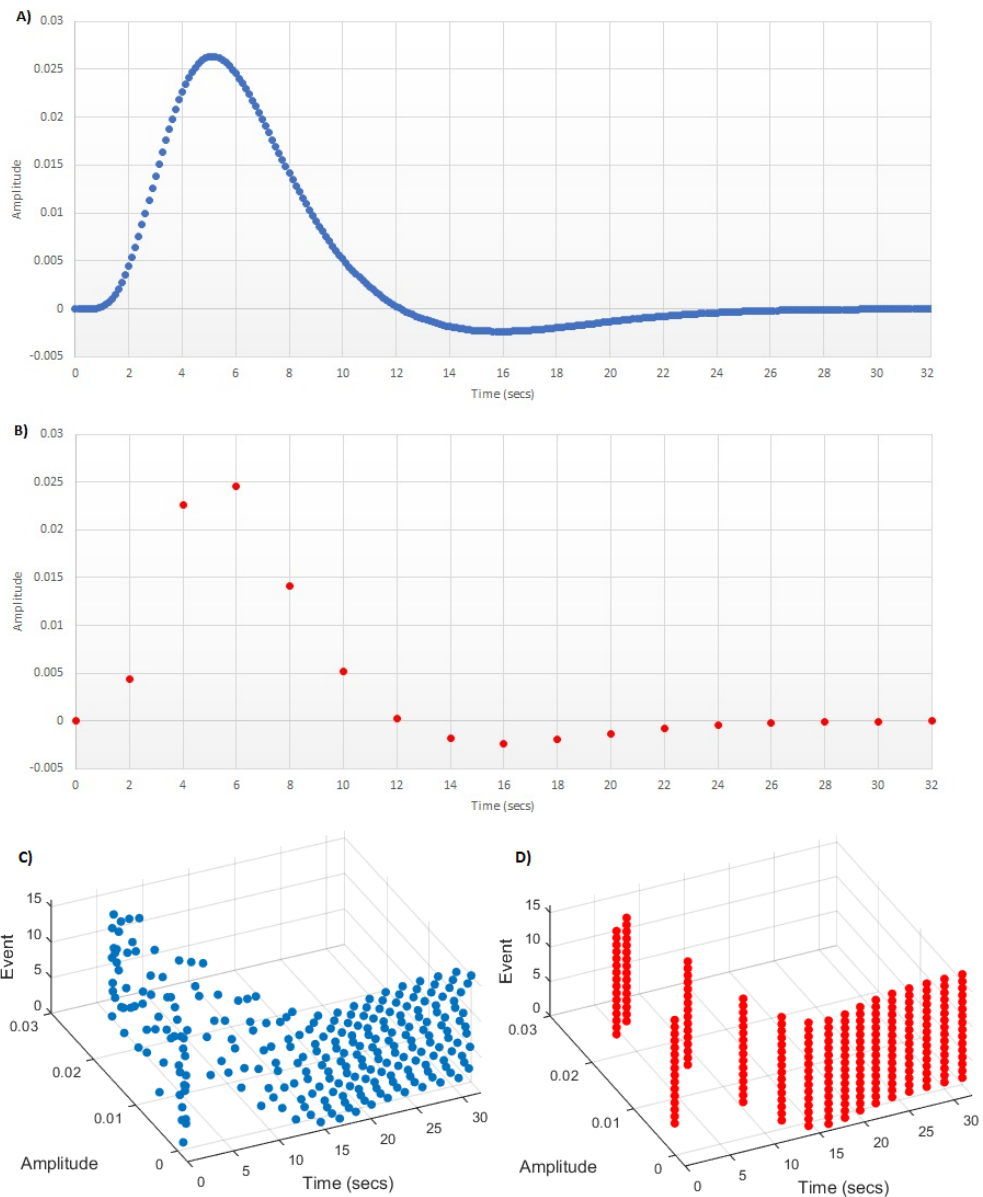
Figure 9. A) Simulated sampling of the canonical haemodynamic response function with 16 events uniformly jittered over a 2000ms TR, B) The same simulation when events occur with a fixed ISI divisible by the TR (a worst-case scenario). Three dimensional plots demonstrating how sampling is distributed over each TR are included for, C) the jittered timings, and D) the non-jittered timings.

1st-level fixed-effects analyses establish where there is significant event-related activity within each participant, but only taking within-subject variability into consideration (residual error) meaning results cannot be ascribed to the population. When running a 1st-level analysis microtime resolution (denoting the number of time-windows to divide the TR

into) and microtime onset (denoting which time-window the data is re-sampled to) are required, the latter generally set to a central point resulting in groups of slices acquired over the TR being aligned to a common time-window (Ashburner et al., 2020). This is relevant as with a two second TR the last slice will be acquired two seconds after the first, so aligning to a common time-window serves a function analogous to mean-centering. An example 1st-level design matrix (from chapter 3) can be seen in Figure 10, with a column for each condition x basis function pairing. Red highlights the three regressors pertaining to a sequence of events in the condition of interest, convolved with the canonical function, temporal derivative, and dispersion derivative accordingly. Green highlights the seven Fourier functions convolved with the same events, and blue highlights the six head-motion parameters. At this stage all recorded events are included to account for as much variance as possible. This can be considered in terms of forced entry multiple regression, with regressors formed for each independent variable on the x axis and running the length of the number of scans on the y axis. The aim is to form the best fitting model for the BOLD signal, based on predictions of HRF shape and the timing of the BOLD response. Where signal is shared between any two regressors it will effectively cancel out, reflected by a change in the beta value within the regression model, hence inclusion of regressors modelling estimates of head motion. For each regressor a beta value is produced at every voxel, and converted into con images.
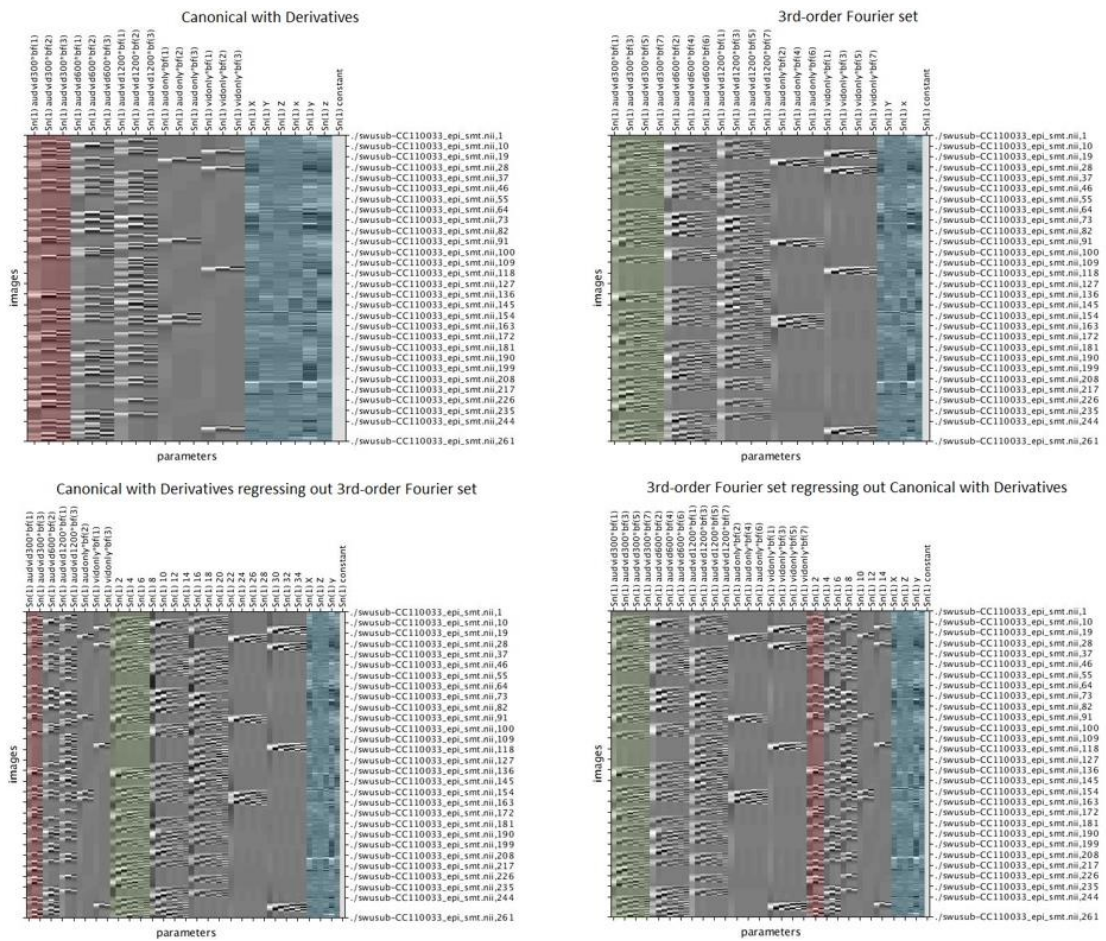
Figure 10. 1st-level design matrices from chapter 3 including all five conditions. Red highlights canonical-with-derivatives regressors pertaining to the conditions of interest, green highlights the Fourier basis set regressors pertaining to the conditions of interest, and blue highlights head-motion regressors.

2nd-level random-effects analyses involve selection of the con images (parameter estimates) pertaining to conditions of interest. This was set up as a full factorial analysis, selecting factors such as age (chapter 5) and levels of those factors (e.g. young versus elderly). At each voxel a mean value is calculated across participants and compared to the null hypothesis that it will be zero (Penny et al., 2011, p. 29). This takes into consideration variability between-subjects within coordinates with an available parameter estimate for all participants, highlighting coordinates with a consistent non-zero value across the group. When using basis sets each weighted function was linearly combined, testing for significant change in any one or any combination of the three regressors. An example design matrix is

available in Figure 11, the x axis comprised of columns (one for each level/condition being tested), the y axis comprised of rows (one for each batch of participants pertaining to the respective condition) containing contrast weights. This summary statistic approach to random-effects analysis was introduced within SPM so that inference could extend beyond the individual to the population, and is deemed formally equivalent to a multilevel hierarchical analysis/a mixed-effect analysis, balancing contributions of both within and between-subject variability, however design matrices at the 1st-level must be "sufficiently similar" (Penny et al., 2011, p. 7, p. 29-30). The summary statistic approach uses sample means for each participant drawn from the true population effect to estimate a population mean and its variance, comparable to the use of maximum-likelihood estimates (partial data informing estimation of parameters relating to an assumed probability distribution). Penny & Holmes (2007) found that when design matrices are not balanced at the 1st-level of analysis (e.g. when the number of events is not under the control of the experimenter, as in chapters 5-6) the equivalence of summary statistic and maximum likelihood procedures is no longer formally supported. However the authors also report that in practical terms the summary statistic approach still functioned as expected. When carried out in SPM unequal variance was assumed within each factor and if levels of a factor are derived from the same participants they were deemed not independent, violating assumptions of sphericity. In both cases estimates of covariance were produced using Restricted Maximum Likelihood to adjust the degrees of freedom (Ashburner, 2020). The benefit of the summary statistic approach is that it reduces computational cost, bringing forward only a parameter estimate for each participant to the 2nd-level (rather than incorporating all scans), also meaning multiple conditions can be contrasted (Penny & Holmes, 2007).
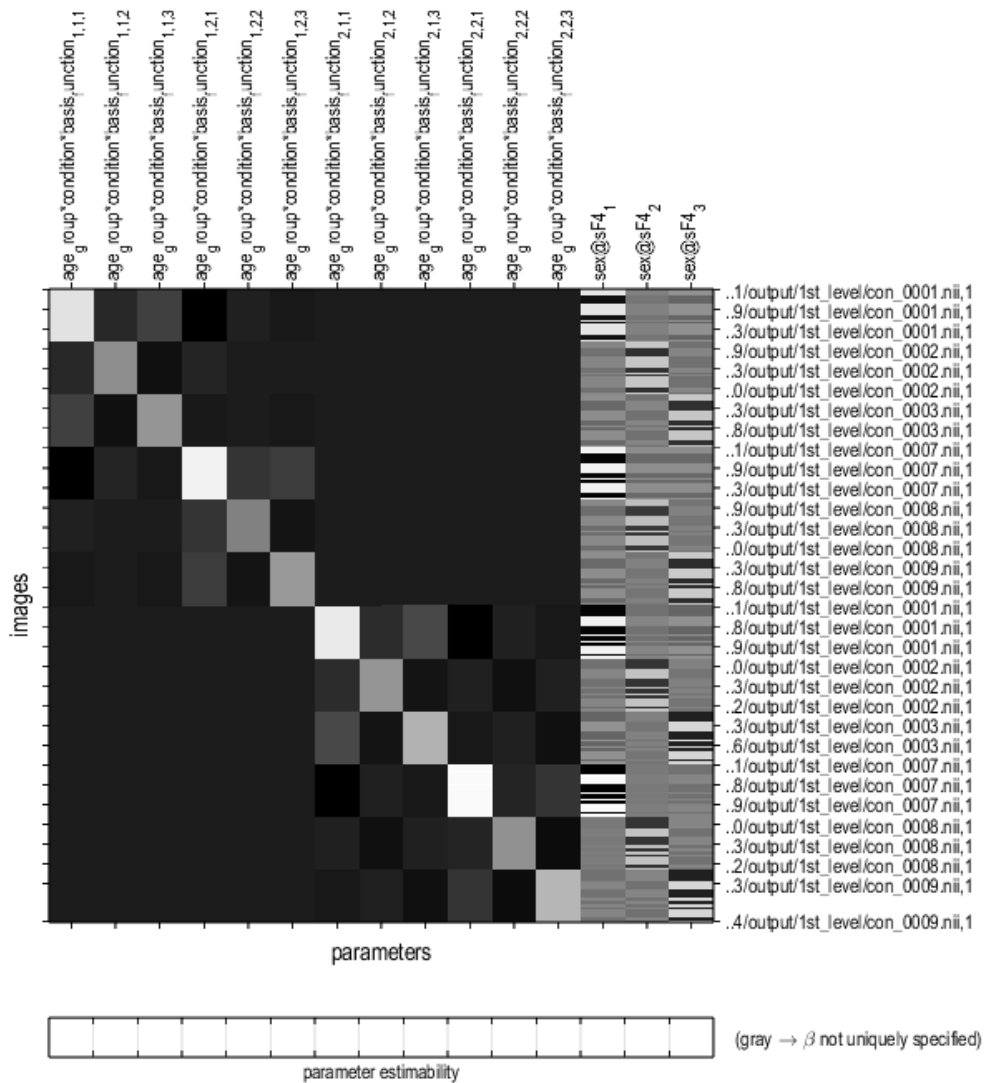
Figure 11. 2nd-level design matrix from chapter 5, including experimental and control conditions across two age groups, using a three-function flexible basis set, totalling 12 conditions. One covariate regressor is included for each basis function (the final three columns), here denoting gender.

The GLM approach was applied to various analyses throughout the thesis. Within chapter 3, three different modelling techniques were employed, providing information on

the typical timing properties of the HRF, how different modelling approaches dealt with variability in these properties, and with some evidence of inter-regional variability. As can be seen in Figure 10, regressors of events convolved with the Fourier basis set were also added to the canonical-with-derivatives design matrix, and vice versa. This meant estimates could be made of how much additional variance was captured by each. Chapter 4 investigated how timing properties of the HRF differed between age groups, utilising the same three modelling approaches to establish which best handled this variation. Chapters 5 and 6 utilised the canonical-with-derivatives model to estimate where event-related activity was occurring in the brain during an instrumental learning model, the model chosen based on the results of chapters 3 and 4. This was especially important for chapter 5 when comparing age groups, with baseline age-differences found in chapter 4.

2.3.4. Interpreting the HRF

When plotting an estimated HRF pertaining to a significant effect it is important to consider what the magnitude is measured in. This is thoroughly discussed in MarsBaR FAQ — MarsBaR 0.45 documentation, (n.d.). In SPM, signal within the brain is scaled to have a mean of 100, meaning the magnitude of BOLD signal estimates is the percentage signal change relative to the mean signal over the entire brain (a change of 1 unit being 1% of the overall mean). As the mean signal could change systematically across brain regions and tissue types (for instance grey matter tending towards higher signal than the whole-brain average), this measure of percentage signal change may not be meaningful for any one haemodynamic response, and reduces comparability between studies. To address this, percentage signal change can be calculated relative to the mean of a selected region, with the final column of the 1st-level design matrix/the final beta value denoting the mean signal at each voxel within a participant. Within this thesis percentage signal change was always calculated relative to the mean of the voxel in question rather than a broader region of interest, which required dividing signal by the voxel's final beta value, then multiplying by

100. However, as all analyses were carried out at the 2nd-level this required an estimate of the voxel's mean signal across participants. Where comparisons were run between groups means were calculated within each group. To achieve this a 2nd-level analysis was run on contrast images derived from each participant's final column at the 1st-level of analysis, generating a mean baseline across participants. This was checked in a sub-sample, comparing to 1000 random coordinates (identified as significant in the 2nd-level analysis) calculating a mean baseline across participants for each coordinate manually, using the final column beta values. There was no difference exceeding 0.0001% confirming the process was accurate.

2.4. Methods Summary

Eye-tracking was specific to chapters 5-6, with pupillometry analyses only applied in chapter 5. Screening as discussed was only relevant to chapters 5-6 (as chapters 3-4 used secondary data with its own screening protocols) and some aspects of screening were specific to chapter 5 due to the ageing component. fMRI methods were applied across chapters 3-6, including quality assurance (with some minor divergence in application, discussed above), and a standard pre-processing pipeline (with two different normalisation procedures used, see Figure 6). Application of the GLM was fairly consistent across chapters, as was use of flexible BASIS sets. Finally ultra-high field scanning was expounded upon, predominately relevant to chapter 6 but covering topics which pertain to neuroimaging generally.

Chapter 3
A Systematic Investigation into Flexible Modelling of the Haemodynamic Response Function

Matthew Danvers
Michael Longley
Narender Ramnani
In preparation for publication

Word count: 10,314 excluding references

Abstract

In functional MRI the Blood Oxygen Level Dependent (BOLD) response is a secondary marker of neural activity, often modelled using assumptions about its time-course. Many studies have employed a "canonical" model which assumes invariant timing properties, however the BOLD time-course is known to vary across brain regions, tasks and people. Analyses are reported based upon a simple sensorimotor task undertaken by 558 participants. Comparisons were made between the canonical model, a canonical model incorporating temporal and dispersion derivatives that provide some flexibility, and a Fourier basis set with even greater flexibility. All models found plausible activations in primary motor, auditory and visual cortices, the cerebellum and the prefrontal cortex. The flexible models revealed evidence of large variability in the estimated BOLD time-course across the brain, and explained experimental variance in more voxels than the canonical model in all areas except the primary auditory cortex. Furthermore, the canonical model-with-derivatives captured additional experimental variance in more voxels than the Fourier basis set within regions where peak latency and dispersion were typically below that predicted by the canonical model. However, the Fourier basis set was more consistent in its ability to model variance across simulated haemodynamic responses with varying timing properties, capturing more additional variance within regions with typically later peaks and wider dispersions.

3.1. Introduction

Functional magnetic resonance imaging (fMRI) uses the BOLD response to estimate neural activity (Ogawa et al., 1990). This is the ratio between oxygenated (HbO) relative to deoxygenated (HbR) haemoglobin, plotted as a haemodynamic response function (HRF). Increases in the HbO/HbR ratio are attributed to astrocyte-driven vasodilation-mediated increased cerebral blood flow (CBF) and cerebral blood volume (CBV) exceeding oxygen metabolism ($CMRO_2$), amplified by 'washing out' of existing HbR, resulting in a positive primary peak in the BOLD signal (Bandettini, 2002; Boynton et al., 1996; Buxton et al., 2004; Csipo et al., 2019; D'esposito et al., 2003; Takano et al., 2006; Tarantini et al., 2017). A post-stimulus undershoot follows before return-to-baseline (Buxton et al., 2004; Friston et al., 1998a; Logothetis, 2003), barring some continued oscillation termed ringing (Ress et al., 2009). Data collected using an event-related design is often analysed using a general linear model (GLM) approach. Here, a model haemodynamic response function (mHRF) is convolved with stimulus-onset times across the experiment, resulting in predicted time-courses that serve as GLM regressors. The approach tests for the goodness of fit between the time-course of the acquired data and linear combinations across these regressors (Friston et al., 1995; Poldrack et al., 2011, p. 70-76, 191-200; Worsley & Friston, 1995). Considering the shape of the primary peak, key parameters include peak amplitude, peak duration (dispersion) and peak latency (time from stimulus to peak; Lindquist & Wager, 2007). A suitable and accurate mHRF is therefore required to reliably ascertain if signal is stimulus-related whilst avoiding type two errors (Lu et al., 2007).

Gamma density functions have been used to model the HRF, Friston et al. (1994) forming a Poisson function from a single gamma density, derived from autocorrelations (a means of locating periodic patterns) in physiological data. These have been applied in various ways, including linear combinations of different gamma density functions to accommodate variation in the HRF form (Aguirre et al., 1998; Boynton et al., 1996; Friston et

al., 1998a). This lead to the canonical mHRF (HRFc) which linearly combines two gamma functions in order to represent the primary peak and post-stimulus undershoot typically seen (Friston et al., 1998b; Lindquist et al., 2009; Worsley et al., 2002). The HRFc assumes that the HRF predominately varies in peak amplitude (biasing results towards HRFs which confirm to its assumed time-course; Lu et al., 2007), however evidence suggests a trend of peak latency and dispersion being lower than assumed by the HRFc model (Ramnani & Henson, 2005; West et al., 2019), potentially better modelled by more flexible basis sets. This was attempted by adding a temporal derivative (accommodating peak latency variation; Friston et al., 1998b; Poldrack et al., 2011, p. 77-78) and dispersion derivative (accommodating dispersion variation; Poldrack et al., 2011, p.77-78; Ramnani & Henson, 2005) forming the HRFtd model. This was found to increase the variance captured relative to HRFc (Henson et al., 2001; Lindquist et al., 2009), as did inclusion of even the temporal derivative on it's own (Lindquist et al., 2009; Lindquist & Wager, 2007). For example, Steffener et al. (2010) found this approach accommodated a peak latency variability of 4-5s in cortical visual areas and 5-6s in non-visual areas. However with this increase in flexibility comes a potential drop in interpretability. When using a single function (e.g. HRFc) a comparison between two conditions is simply a contrast of two parameter estimates, with one potentially greater than the other. However when handling a linear combination of three functions it is not as simple to interpret, as change in one estimate is not necessarily independent of change in another. For example dispersion increases can be underestimated and cause overestimation of peak latency and amplitude (Lindquist et al., 2009; Lindquist & Wager, 2007).

It could be argued that modelling approaches should use as few assumptions about the time-course as possible. Fourier basis sets could be an effective way of doing so (Friston et al., 1998b; Josephs et al., 1997) as applied by D'esposito et al. (1999). This approach is more flexible than the HRFtd model, and so might lead to increased detection of

voxels/improved characterization of HRF shape. This has been evidenced relative to HRFc (Liu et al., 2017), and with better capture of signal than the HRFtd model (Ramnani & Henson, 2005). However the use of Fourier functions is not without it's problems. For example Henson et al. (2001) has challenged the view that it provides greater optimisation than the HRFtd model. Also, although it may operate with fewer assumptions about the shape of the BOLD response, the increasing flexibility offered by greater numbers of functions may introduce greater variability within each parameter estimate at the 2nd-level of analysis, relative to that seen when a single parameter estimate is used, referred to as the bias-variance trade-off (Poldrack et al., 2011, p. 76). A further criticism of the Fourier set is reduced strength of inference due to change over numerous parameters (Aguirre et al., 1998). In contrast the HRFc model has a single parameter estimate for each level of a condition, and so comparisons can be made clearly. This benefit is however traded against the fact that it cannot be disambiguated whether a change in the resulting parameter estimate is due to a difference in peak amplitude, peak latency, dispersion, or any combination thereof (Lindquist & Wager, 2007).

An additional concern relates to power, since each function entered into the model reduces the available degrees of freedom (df) in 1st-level analyses. This can be ameliorated by reducing the number of functions, for example a first order Fourier basis set employs only three. However this in turn reduces the mHRFs flexibility and so increases it's bias towards capturing haemodynamic responses that map well to the time-courses it can model via linear combination of its functions. Systematic comparisons between flexible mHRFs are critical to ascertain the best compromise and to determine how the functions contribute to modelling. This informs not only future work but potentially assists comprehension of previous work. There may be no one-model-fits-all solution, therefore consideration of the causes and extent of HRF heterogeneity are also crucial.

The literature suggests that peak latency can range from 2.5-6.5s (compared with HRFc = ~5.17s) across participants and regions (Aguirre et al., 1998; Handwerker et al., 2004), with lower intra-participant intra-regional variability of 50-100ms (Aguirre et al., 1998). However this variability may have neurovascular (Ramnani & Henson, 2005; Tarantini et al., 2017) as well as task-dependent, or analysis-dependent origins. One such example of a task-driven difference is saturation via longer stimulus durations/shorter inter-trial-intervals (or inter-stimulus-intervals, dependent upon the task) which can cause plateauing (Fabiani et al., 2014; Hillman, 2014). This demonstrates non-linearity, whereby haemodynamic responses that overlap in time may not show the assumed additive increase in magnitude, essentially suggesting a ceiling effect (Poldrack et al., 2011, p.72). Complicating things further, inter-regional variability (Handwerker et al., 2004; Miezin et al., 2000; Taylor et al., 2018) could be partially attributable to cross-modal variation in stimulus intensity. For example when varying the brightness of an auditory stimulus one can make objective judgements (e.g. 100dB is twice 50dB). But there is no conclusive objective means of matching a 50dB auditory stimulus to a visual stimulus (measured in lumens) of equivalent intensity. As intensity is thought to affect scaling of the HRF (Poldrack et al., 2011, p.72) if one stimulus type is of a higher intensity it could lead to differential rates of plateauing. This could then lead to differential alteration of timing properties of the response, meaning it is problematic to objectively compare HRF shapes across regions. Alternatively, inter-regional variation could be due to mechanisms of neurovascular coupling (controlling how the neurovascular system responds to neural activity) varying across brain regions within-subject (Sloan et al., 2010). Variability between-subjects is also evidenced attributed to factors such as age (Fabiani et al., 2014; Hutchison et al. (2013); Ward et al., 2015).

A good example of analysis driven differences are slice-timing effects. GLM-based approaches typically assume signal from all slices is acquired at the same time (e.g. upon scan onset; Poldrack et al., 2011, pp. 41-42). This leads to artificial variability by up to the

repetition time (TR). For example, with a two second TR the final slice is not acquired until approximately two seconds after the first, and so the estimated peak latency would artificially be two seconds shorter. Assuming a consistent HRF this can result in a systematic change in peak latency with each slice. This can be accounted for by flexible modelling or ameliorated using slice-timing correction via interpolation (Henson et al., 1999), interpolation found to be more effective than addition of the temporal derivative (Sladky et al., 2011). However, flexible modelling may accommodate *both* slice-timing and non-slice-timing related variability, with potential further improvements from increasingly flexible basis sets (Fourier deemed most resistant to slice-timing effects; Josephs & Henson, 1999; Ramnani & Henson, 2005). There is also an additional benefit in that interpolation carries risks such as interacting with head-motion and aliasing effects (Henson et al., 1999; Poldrack et al., 2011, p. 41-42; Sladky et al., 2011).

That the HRF is not a single consistent shape is therefore supported via estimations across multiple studies (Henson et al., 1999, 2001; Lindquist et al., 2009; Lindquist & Wager, 2007; Liu et al., 2017; Ramnani & Henson, 2005; Steffener et al., 2010), alongside evidence that flexible models (such as Fourier and HRFtd) capture more variance than HRFc (Henson et al., 2001; Lindquist et al., 2009; Ramnani & Henson, 2005). However, the question remains as to the relative effectiveness of HRFtd or Fourier models in identifying signal in human fMRI studies, and the reasons for this. Here, hypotheses were made about the effectiveness of HRFc, HRFtd, and Fourier models, in 500+ participants from the CamCAN dataset (Taylor et al., 2017). All executed the same sensorimotor task (visual, auditory, motor, and cognitive demands) in an event-related design. This dataset was optimised for testing such questions as it covers the typical adult age-range, included only healthy participants, and used timings optimised for estimating the HRF (with stimulus onset asynchrony varying between 2-26s; Shafto et al., 2014). With the number of papers using fMRI continually increasing (current annual publication rate of ~5000; Bandettini, 2020) and

representing a significant investment of time and money, effective fMRI analysis is of the utmost importance.

Hypothesis 1: As a baseline measure to ensure regions of interest (ROI) were adequately selected, it was predicted there would be significant activations in the anterior prefrontal cortex (aPFC) due to the task requiring some level of cognition, primary cortical regions M1 (due to the motor response), A1 (due to the auditory tone played), and V1 (due to the visual stimuli presented), as well as the cerebellum (due to the motor response), using the HRFc, HRFtd and Fourier basis sets.

Hypothesis 2: It was predicted that within given ROIs, the HRFtd model would produce a greater percentage of significant voxels, relative to the HRFc model.

Hypothesis 3: It was predicted that within given ROIs, there would be voxels where the Fourier basis set would explain experimental variance over and above the HRFtd model .

Hypothesis 4: It was predicted that the number of voxels in which variance explained by the Fourier basis set over and above that explained by the HRFtd model, would exceed the number of voxels where there was additional variance explained by the HRFtd model.

3.2. Methods

All scripts are available on https://github.com/mdanve01/Project1.

3.2.1. Participants

Participants were randomly selected from the Cambridge City area using listings from the Primary Care Trust, excluding those residing at the University during term-time only, or deemed unsuitable by their general practitioner (GP). Six-hundred and fifty-six (aged 18-87 years) were cleared by their GP for MRI scanning, and gave informed consent. Exclusions were based upon MRI contraindications, serious medical/psychiatric conditions, current or historical drug abuse, inability to walk 10 metres, inability to hear a 35db tone at 1000Hz in either ear, not a native English speaker, corrected vision below 20/100, or cognitive impairment (Mini-Mental State Examination score below 25). Handedness was

assessed using the Edinburgh Handedness Inventory. Recruitment aimed to achieve an approximately uniform age distribution and an equal sex split within each decade. Five hundred and fifty-eight participants were included, with 11 removed due to missing/unreadable files, and 87 removed due to artefact/head motion. More detail on participant removal can be found in the 'Pre-Processing Methods' below.

Data collection and sharing for this project was provided by the Cambridge Centre for Ageing and Neuroscience (CamCAN). CamCAN funding was provided by the UK Biotechnology and Biological Sciences Research Council (grant number BB/H008217/1), together with support from the UK Medical Research Council and University of Cambridge, UK. All raw data in the study was collected by the Cam-CAN project and made available from their repository. The text below summarises their approach to recruitment and data collection, however pre-processing, quality analysis, and data analysis was carried out by the author. The data and further details can be found at www.mrc-cbu.cam.ac.uk/datasets/camcan/ (Shafto et al., 2014; Taylor et al., 2017). Ethical approval was provided by the Cambridgeshire 2 Research Ethics Committee (ref: 10/H0308/50) and Royal Holloway Ethics Committee (ref: Full-Review-2246-2023-01-05-10-18-UPJT002).

3.2.2. Behavioural Methods

Data was acquired using the sensorimotor task (T2* weighted) performed by participants in the camCAN study. This ran for approximately nine minutes, following 25 minutes of structural scanning, nine minutes of resting state fMRI acquisition, and eight minutes of movie watching fMRI acquisition. For this study data was taken from the sensorimotor task. The task had 129 trials (including one practise trial), in which either both visual and auditory stimuli were presented (120 trials), just auditory (4 trials) or just visual (4 trials). The visual stimulus was a pair of checkerboards presented either side of a centralised fixation cross for 34ms. The auditory stimulus was a 300ms binaural tone varying in frequency pseudorandomly (300, 600, and 1200Hz, 40 trials of each). During bimodal trials

auditory and visual onsets occurred simultaneously. Participants were instructed to press a button with their right index finger upon seeing or hearing a stimulus. An event-related design was employed in order to estimate the shape of task-specific HRFs. To maximise the effectiveness of this approach event onsets were maximally uncorrelated using an m-sequence (length = 255; m = 2; stimulus onset asynchrony ranging between two and 26 seconds) and stimulus onset jittered across 0.1-0.3 seconds (Buracas & Boynton, 2002; Shafto et al., 2014).

3.2.3. MRI Data Acquisition

Scanning was carried out using a 3T Siemens TIM Trio with 32-channel head coil, located at the MRC-CBSU with memory foam cushions positioned either side of the head to minimise movement. A custom button-box recorded motor responses, auditory stimuli were presented through MR compatible etymotics headphones, and visual stimuli were projected onto a screen viewable through a head-coil mounted mirror. Structural images were acquired using a Magnetization Prepared Rapid Gradient Echo sequence, with a repetition time (TR) of 2250ms, echo time (TE) of 2.99ms, field of view (FOV) of 256 x 240 x 192mm and total duration of 272secs. Resolution = 1mm, GRAPPA acceleration factor = 2, inversion time (TI) = 900ms and flip angle = 9 degrees. Functional scans were T2* weighted with a Gradient-Echo Echo-Planar Imaging sequence, a TR of 1970ms, TE of 30ms, FOV of 192 x 192mm, total duration of 520 secs, flip angle of 78° and voxel size of 3 x 3 x 4.44mm. There were 261 volumes comprised of 32 descending axial slices (thickness = 3.7mm; interslice gap = 20%) covering the whole brain inclusive of the cerebellum.

3.2.4. Pre-Processing Methods

EPI images were realigned to the mean and unwarped using field maps. The anatomical (T1) image was co-registered to the mean unwarped EPI image using estimation only (Ashburner et al., 2020). The T1 image was then segmented using the MNI tissue probability map (TPM) and Dartel imported tissue class images were formed for grey matter

9

(GM) and white matter (WM). Realigned and unwarped EPI images were affine-registered to MNI space, normalised, and smoothed with an 8mm full-width half-maximum (FWHM) gaussian kernel. Pre-processing was carried out using the SPM batch editor and Dartel normalisation was used (Klein et al., 2009). Slice timing correction was omitted due to a risk of aliasing and interactions with head motion (Henson et al., 1999; Poldrack et al., 2011, p. 41-42; Sladky et al., 2011).

For quality assurance, T1, mean unwarped/coregistered EPI, and pre-unwarped 1st EPI images were compared using the 'check-reg' function in SPM12. Outliers were subjectively identified if images were co-registered incorrectly, were distorted, or had slices missing (totalling 33). Cases in which there was excessive head motion (movement beyond 2.5mm/1 degree, or movement between consecutive scans exceeding 1.5mm/0.5 degrees) were also classified as outliers. Thresholds were deemed appropriate as they are below the voxel size (Ashburner et al., 2020, p. 259; Wylie et al., 2014) with those in excess of one degree deemed large (Ashburner et al., 2020, p. 35). Eighteen outliers were identified, four of which were excluded in the previous step.

EPI signal was quantitatively investigated within each individual participant, based upon mean intra-slice signal (MISS) within each scan (32 slices x 261 scans). Post-segmentation/pre-normalisation the signal amplitude range was calculated across scans within each slice (temporal range), and across slices within each scan (spatial range), the maximum value was selected for each measure, for each participant. This was repeated for individual 'shifts', calculating the maximum change over two consecutive scans within a slice (checking for sudden change over time; temporal shift), and over two consecutive slices within a scan (checking for sudden change over space; spatial shift). Coefficients of variation (COV) were also used as a measure of variability. Checking for change over time the standard deviation (SD) across scans was divided by the mean of all scans, for each slice then the maximum value selected (temporal COV). This was repeated examining variability across

slices within each scan (spatial COV). Outliers were defined as scores beyond 2.5 SDs above the group mean. A total of 34 outliers were identified, 18 of which were already identified by realignment parameter/co-registration checks.

After normalisation, a randomly selected normalised scan from each participant was displayed alongside the MNI template brain using the SPM12 'check reg' function, and manually checked for correspondence. Nine cases were found to have excessive signal drop-out, distortion, and mis-alignment. Two further cases were identified during statistical analysis (see below) as having no significant voxels. The 1st-level analyses were then run using the HRFc model, generating masks. The number of voxels containing signal were calculated for each participant, identifying two outliers with no signal (as expected based upon the above) and these were immediately removed. Next each participant's mask was compared to a group-level standardised mask, created as the mode of all participant's binary masks at each coordinate (meaning if the majority of participants had signal at coordinate x,y,z then a one was assigned, if not a zero was assigned). This found 15 outliers with a number of coordinates which did not match the standardised mask exceeding 2.5SDs. Good registration between the image with the fewest mismatched coordinates (and therefore the most representative of the standardised mask) and the MNI brain was confirmed. A new Dartel template was created and normalisation carried out, the worst fit deemed acceptable subjectively. This resulted in 558 usable participants.

3.2.5. Design

In order to test the different modelling approaches (hypotheses 1 and 2) separate design matrices were created for each of the three models under investigation (HRFc, HRFtd, and Fourier). In order to test hypotheses 3 and 4 design matrices were created for both HRFtd and the Fourier set, both of which included derivatives from the other model as regressors of no interest. Finally, in order to better understand factors driving model

differences simulations were run on signals with artificially manipulated timing properties. These are explained below.

fMRI 1st-level Experimental Design: The general linear model (GLM) was employed using a full factorial analysis. The within-participant 'stimulus' independent variable (IV) had five levels. Three of these were bimodal events (auditory tone and visual stimulus presented) each with 40 trials, and split by the tone played (300Hz, 600Hz and 1200Hz). The final two comprised the visual only condition (4 events) and auditory only condition (4 events). Microtime resolution = 16, microtime onset = 8, with a 128 second high-pass filter applied. An event-related design was employed, using the HRFc (one function), HRFtd (three functions) and a 3rd order Fourier(Hanning) set (seven functions). The Fourier set modelling strategy was determined by a set of pilots run, aiming to minimise multicollinearity but maintain window-length. As a result the HRFc GLM totalled 11 regressors, the HRFtd GLM 21 regressors, and the Fourier GLM 41 regressors (plus intercept). In order to ascertain where the Fourier set captured additional variance beyond HRFtd, the 15 derivatives from the HRFtd analysis (each denoting convolution of a function with events across the 261 scans, within each stimulus condition, totalling five conditions x three functions) were then included as regressors of no interest in a 2nd Fourier analysis; Fourier(HRFtd). The 35 derivatives from the Fourier analysis were also included as regressors of no interest in a second HRFtd analysis, to establish where this model captured additional variance beyond the Fourier set; HRFtd(Fourier). This method regressed out variance picked up by the opposing mHRF, and kept the total 1st-level degrees of freedom equivalent between analyses, allowing identification of significant variance within one model (over and above the other) and comparisons between models. The six head-motion parameters were included as regressors and con images were generated for each function across all conditions. Sampling over the peri-stimulus time period was checked to ensure the temporal jitter had been effective, and was subjectively deemed to be sufficient.

fMRI 2nd-level Experimental Design: A full factorial design matrix was formed combining all participants across age groups, with a single variable of function, applied across the five models (a 1 x 1 design for HRFc, 1 x 3 for HRFtd and HRFtd(Fourier), and 1 x 7 for Fourier and Fourier(HRFtd)). For HRFtd, Fourier, HRFtd(Fourier) and Fourier(HRFtd) independence was not assumed and variance was left as default (unequal). For HRFc both were left as default. Only the bimodal 300hz condition was examined as, **a)** effect of auditory pitch was not a variable of interest, **b)** processing limitations precluded a full analysis of multiple stimulus conditions, **c)** age-related hearing loss (presbycusis) begins in the higher frequencies meaning 300Hz should be least affected (Huang & Tang, 2010), and **d)** there were a sufficient number of trials. All analyses were corrected for multiple comparisons using the family-wise-error rate (FWE), $\alpha = 0.05$. F contrasts were then run, and for HRFtd and Fourier analyses each function was linearly combined. The gross anatomical location of each peak voxel was established using Duvenoy's and Schmahmann's atlases (Duvernoy, 1999; Schmahmann et al., 2000).

Simulations: Five artificial HRF signals were created based on the canonical HRF. Firstly, the canonical HRF served as the control, with two reduced versions, one where all timing properties (including peak latency and FWHM) were halved, another replicating this response but resetting peak latency to its canonical value. Next there were two increased versions, one where all timing properties (including peak latency and FWHM) were multiplied by 1.5, and another multiplied by two. The Fourier and HRFtd basis sets were then tested on how they modelled degrees of deviation from canonicality using multiple regression (forced entry), which provided measures of fit and beta values by which to weight the regressors. This was run on a single event to eliminate effects of events overlapping in an additive fashion (with multiple events there was a risk of the results varying dependent upon factors such as the inter-stimulus-interval). This meant the findings could be applied more broadly and were not specific to this one study. There was a concern that the HRFtd

model may do better in the reduced timing property simulations, as it had a longer window length allowing a well-fitted, flat, post-peak baseline. To control for this a vector of zeros was added to the Fourier functions until each had a length of 260 units (comparable with fMRI where a single vector of baseline values is convolved with multiple events), rendering the models comparable. Additionally adjusted R^2 values were reported to control for the increased number of predictor variables in the Fourier set. Finally, consistency with the dataset used was confirmed by convolving both the basis functions and the manipulated signals with zero-value baseline vectors at the time of each of the 40 events as used in the study, and then forced entry regression run.

3.2.6. Statistical Analysis

In order to check the number of significant voxels within key regions of interest ROI masks were created in SPM's anatomy toolbox version 2.2b, based upon cytoarchitectonic maps. The motor ROI included unilateral left areas 4a and 4p (Geyer et al., 1996) and is referred to as M1, included due to the motor component of the task. The composite auditory ROI included bilateral TE 1.0, TE 1.1, and TE 1.2 (Morosan et al., 2001) and is referred to as A1, included due to the auditory tones played during the task. The composite visual ROI included bilateral hOC1 (Amunts et al., 2000) and is referred to as V1, included due to the visual stimuli presented during the task. The composite cerebellar ROI was comprised of bilateral lobules I-X including vermal regions VI-X (Diedrichsen et al., 2009), included due to it having an evidenced role in both motor action and cognition. The composite aPFC ROI was comprised of bilateral Fp1 in the frontopolar gyrus, included due to both its functional role in cognition and perception, and its clear cytoarchitectonic definition, with Fp2 excluded due to activity being more closely association with social cognition (Bludau et al., 2014). All were saved in MNI space as per the anatomy toolbox. When looking across tissue types the TPM was used to ascertain whether a voxel had greater than 0.5 probability of being GM, WM or other.

In order to check characteristics of the HRF these were estimated then plotted by multiplying each basis function in the 1st-level analysis by it's corresponding 2nd-level beta value. In cases where multiple basis functions were used the resulting functions were summed to form a single function, reflecting a response that was representative of the group mHRF. This was then divided by the mean baseline within the group at that voxel, and multiplied by 100 (to create percentage signal change). Only voxels significant in the HRFc analysis were included, potentially increasing type two error rates as extreme non-canonicality was less likely to be found. However this approach has the advantage of allowing differentiation between positive BOLD responses (PBRs) and negative BOLD responses (NBRs) in a consistent manner. If the HRFc beta value was negative the mHRF was classed as an NBR, and vice versa, with this positive/negative allocation extended to flexible mHRFs within the same coordinates. Although this approach could be applied to voxels in which flexible models found significance and HRFc did not (as HRFc beta values were still available), these were found to provide a poor classification.

For responses derived from flexible models peaks with a prominence at least 25% of their magnitude was ascertained using the 'findpeaks' Matlab command. For PBRs the primary peak was determined to be the greatest magnitude positive peak, for NBRs this was the lowest magnitude negative-going peak. This method agreed with a simple max() or min() function, but additionally returned data on bimodality. For FWHM the 'findpeaks' function was set to use 'halfheight', therefore determining the half height position between 0 and peak rather than between e.g. minimum and peak. This was chosen as it should remove any influence of the undershoot amplitude upon the FWHM. FWHM values were truly continuous but peak latency was comprised of discrete time-points. The HRFtd model had a 32.0125 second window divided into 260 discrete time-points, the Fourier set had an 18 second window divided into 147 time-points, introducing minor binning differences. Finally analysis was carried out using Matlab 2019a, SPM12, and FSLstats (using the command "-V"

to identify the volumes of voxels), run on a Red Hat Enterprise Linux Server version 7.9 (Maipo), and IBM SPSS version 25.

3.2.7. Declaration

It was realised post-analysis that the EPI readout time (ERT) used when unwarping via field maps was set to 32.1303ms which corresponds to the FSL definition; (number of echoes-1) x effective echo spacing, instead of the SPM definition; number of echos x effective echo spacing, which results in 32.6403ms. It was decided that this is a marginal difference (1.59% increase from FSL to SPM) which is unlikely to negatively impact the unwarping process, but to check this 40 random participants (median age = 48.5, ranging from 18-77) were selected and unwarping carried out using both the SPM and FSL defined ERTs. The mean unwarped image was then loaded for each ERT definition, the difference in signal calculated at each coordinate and where there was a difference the absolute difference value and maximum absolute signal value (whichever was higher between SPM and FSL ERT derived unwarped images) were saved. For each participant the median difference value across the brain was divided by the median signal value across the brain and multiplied by 100 to ascertain percentage amplitude differences relative to signal. Across participants the median percentage difference value was 0.29%, ranging from 0.05% to 0.80%. There was no significant correlation with age; $r(38) = -.126$, $p = .439$, or brain volume; $r(38) = .162$, $p = .318$. As the ERTs were only marginally different, differences in the resulting unwarped images were relatively small, and unwarping (not a mandatory process) still restored signal that was distorted, it was decided that the FSL defined ERT was suitable.

3.3. Results

3.3.1. Regional Analysis 1 (RA1)

In order to address the hypotheses it was ascertained how many significant voxels there were as a proportion of each ROI's volume. It was generally found that all three models captured significance (pertaining to hypothesis 1), however flexible modelling

approaches captured more significant voxels than fixed (except in A1). This was the case even with just the addition of derivatives to the canonical model (pertaining to hypothesis 2). When extending this across the whole brain, the HRFtd model identified 0.41% more significant voxels than Fourier and 49.17% more than HRFc. The total volume of significant voxels restricted to GM was highest using the HRFtd model (587458mm^3) relative to the Fourier set (585739mm^3) and HRFc (439378mm^3). This tentatively suggests the additional signal captured by flexible models is less likely to be false positives. Regarding the combined analyses (pertaining to hypotheses 3 and 4), across the whole brain the HRFtd(Fourier) analysis identified 23.39% more than the Fourier(HRFtd) analysis, with a 59.55% increase within GM. Specific to the ROIs, HRFtd(Fourier) versus Fourier(HRFtd) increases were 27.29% (M1), 17.53% (A1), 26.03% (V1) and 65.94% (cerebellum). The aPFC was the only ROI to show no variance captured by HRFtd(Fourier), but with the Fourier set capturing variance beyond the HRFtd model in 1.01% of the aPFC. These results are summarised in Table 1. All ROIs showed a strong tendency towards PBRs, the aPFC being the only exception (NBRs comprising 100% of responses).

Table 1. Percentage volume of significant voxels across ROIs, the whole brain, and different tissue types, looking at each of the five analyses.

Region	ROI volume	Percentage of ROI volume in which significance was found				
	(mm³)	HRFc	HRFtd	Fourier	Fourier(HRFtd)	HRFtd(Fourier)
M1	10040	60.94	94.33	94.33	58.39	74.32
A1	7059	98.73	98.73	98.73	84.00	98.73
V1	32662	76.63	77.10	77.10	56.68	71.43
Cerebellum	180343	35.72	45.49	45.83	10.24	16.99
aPFC	28001	15.56	18.13	18.18	1.01	0.00
		Volume (mm³) of significant voxels				
Whole Brain	-	891594	1329993	1324603	488474	602735
		Percentage of significant voxels found within each cellular region				
GM	-	49.28	44.17	44.22	35.97	46.51
WM	-	30.55	34.59	34.56	36.76	33.07
Other	-	20.18	21.24	21.22	27.27	20.42

The HRFtd(Fourier) and Fourier(HRFtd) analyses were further investigated. Where at least one analysis was significant, within A1, M1, V1, and the cerebellum a large proportion of voxels were actually significant in both analyses. Observations suggested that within these shared coordinates median F values were typically higher in the HRFtd(Fourier) analysis. Additionally it was confirmed that within all regions except the aPFC there were more coordinates where only the HRFtd(Fourier) analysis was significant, relative to those where only the Fourier(HRFtd) analysis was significant.

3.3.2. Regional Analysis 2 (RA2)

In order to explore the shape of the HRF as estimated by each model, peak voxel coordinates within each ROI were identified from the HRFc analysis (M1, left precentral gyrus, -36, -21, 52.5; A1, left transverse temporal gyrus, -51, -21, 7.5; V1, right lingual gyrus, 12, -88.5, 1.5; cerebellum, right lobule HVI, 24, -54, -21; aPFC, left superior frontopolar gyrus, -3, 64.5, 13.5). All coordinates were highly significant across mHRFs and estimated HRFs were plotted in Figure 1 (derived from 2nd-level analysis beta values). When looking at timing properties of the HRF (specifically peak latency and FWHM), there was a general trend of these being lower than predicted by the HRFc model. This was most extreme when using the HRFtd model. The aPFC instead showed higher timing properties than predicted by the HRFc model, most extreme using the Fourier set.
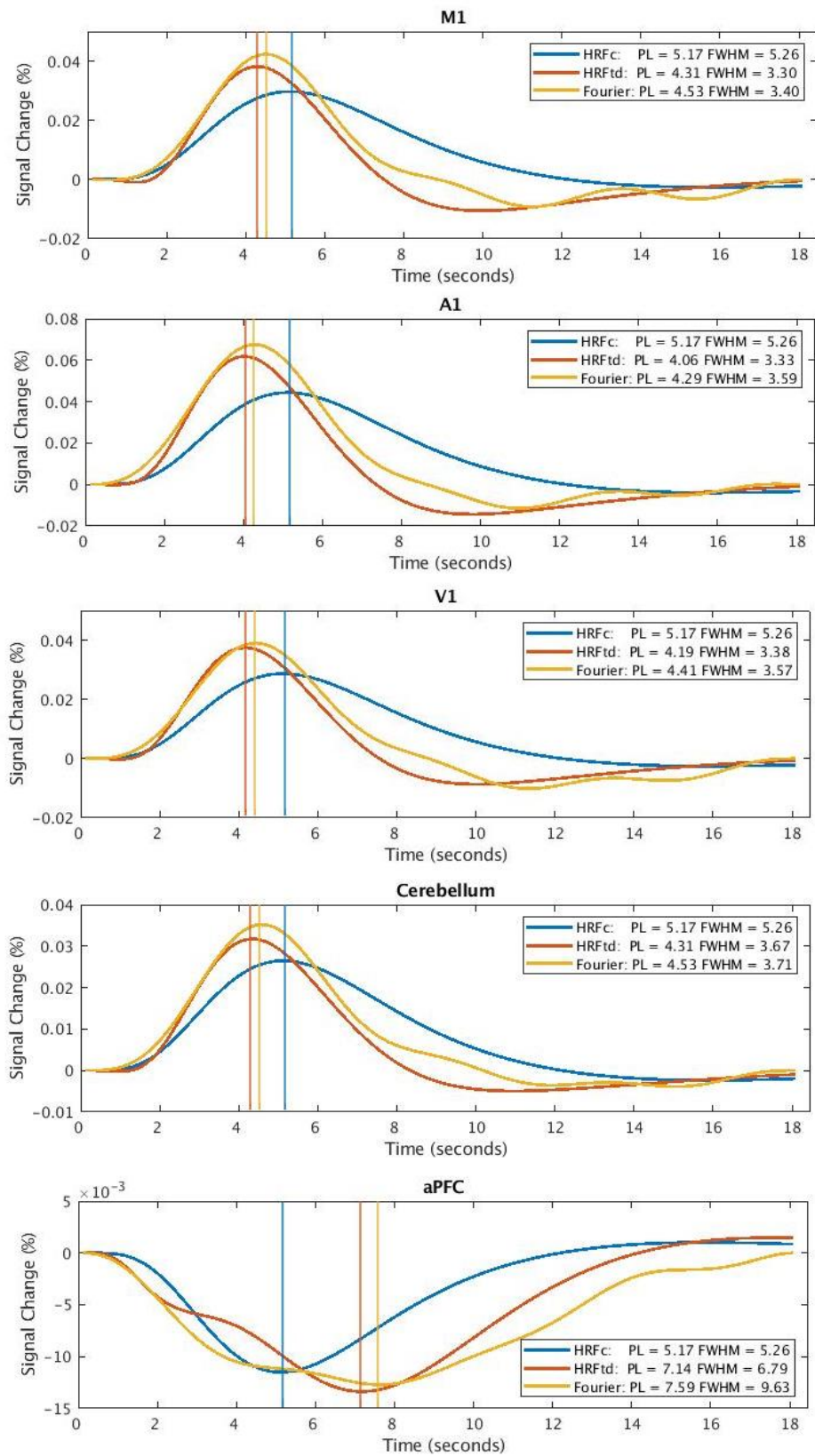
Figure 1. Estimated haemodynamic responses from analyses using all three mHRFs plotted within each ROI; with peak latency (PL) and FWHM also specified within each legend. Vertical lines denote the peak.

20

Next an exploratory analysis was carried out, whereby peak latency and FWHM were estimated specifically using the Fourier set. This enabled a comparison between ROIs, to determine whether there were inter-regional differences in these timing properties. This investigation was still limited to voxels significant for both Fourier and HRFc approaches, as HRFc beta values were used to differentiate PBRs from NBRs. Due to skew in the data and unequal sample sizes two Kruskal-Wallis tests were run (Monte-Carlo method, 10000 samples). There was a significant effect of peak latency (aPFC > cerebellum > M1 > V1 > A1; $H(4)=10361.014$, $p<.001$), and of FWHM (aPFC > A1 > cerebellum > V1 > M1; $H(4)=7446.663$, $p<.001$). When exploring these main effects, differences between individual ROIs were significant with a Bonferroni corrected threshold ($\alpha = 0.00625$). Crucially, Mann-Whitney U tests confirmed that the cerebellum had lower peak latency than the aPFC, and A1 had lower FWHM than the aPFC (both of which being the ROI with the next-highest peak latency/FWHM respectively).

3.3.3. Whole GM Analysis

To establish whether the trends seen in ROIs generalised across the rest of cortical GM, every flexibly-modelled significant voxel was selected, looking at the HRFtd model and Fourier set independently. If residing within GM (with a probabilistic threshold of 0.5) and significant in the HRFc analysis, peak latency and FWHM were calculated for each of the two modelling approaches. Histograms in Figure 2 show evidence of bimodality within each timing property for each flexible model. This can be summarised as the presence of a peak both lower than and higher than the timing properties assumed by the HRFc model. To explore this two independent binary logistic regressions (using Fourier-derived data) indicated that peak latency significantly predicted whether the HRF was positive or negative with 91.4% accuracy (Nagelkerke $R^2=.612$; $\beta=-1.434$, SE$=.009$; wald$=25400.229$, $p<.001$; $\chi^2(1)=72798.263$, $p<.001$). FWHM was similarly predictive, with 97.8% accuracy (Nagelkerke $R^2=.922$; $\beta=-5.203$, SE$=.052$; wald$=10183.665$, $p<.001$; $\chi^2(1)=134894.325$,

p<.001). Higher value timing properties were generally associated with NBRs. However for

each analysis the assumption of linearity was violated, as for peak latency approximately

5.724% of standardized residuals were beyond +/-2.58. For FWHM this was also seen but to

a lesser degree (1.251%). This threshold was justified by Field (2009, p. 293) suggesting that

only 5% of studentized residuals should be beyond +/-1.96, and 1% beyond +/-2.58. Despite

this, it seemed that PBR and NBR allocation contributed to bimodality, and so analyses were

carried out in each independently. Consequently eight two-tailed Wilcoxon Matched Pairs

Signed Ranks (WMPSR) tests were run to compare each flexible model's median peak

latency and FWHM to HRFc. Due to binning differences the canonical timing properties being

compared to varied slightly (peak latency=5.17 and FWHM=5.26 for HRFtd, peak

latency=5.14 and FWHM=5.23 for Fourier). Relative to the HRFc model, peak latency and

FWHM estimates were significantly lower within PBRs, and significantly higher within NBRs.

This was true for both flexible mHRFs (see Figure 2), with all differences having a large effect

size (r > 0.60).
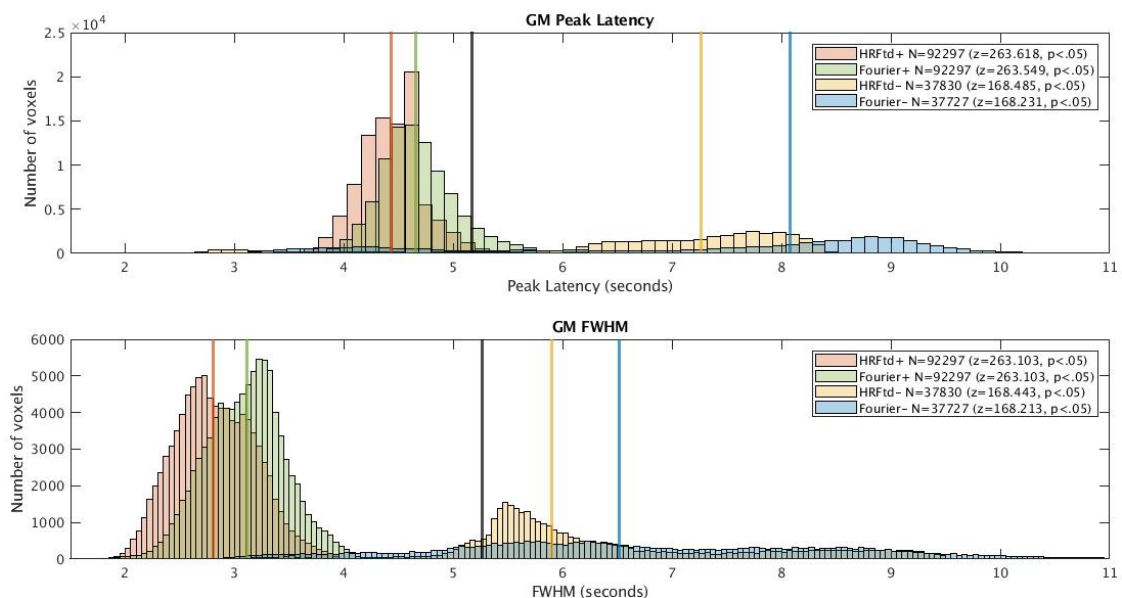
Figure 2. Distributions of peak latency and FWHM as estimated by each flexible model, for

PBRs (+) and NBRs (-) independently. Coloured lines denote medians, with the black lines

denoting each timing property as assumed by the HRFc model.

Next the two flexible models were directly compared across defined GM voxels in which all three models achieved significance. Four two-tailed WMPSR tests compared HRFtd to Fourier for peak latency and FWHM, within PBRs and NBRs independently. The Fourier set consistently estimated a significantly later peak latency and greater FWHM, with large effect sizes in PBRs (r > 0.60), a medium effect size for peak latency in NBRS (r = 0.30), and a small effect size for FWHM in NBRs (r = 0.26), see Figure 3. In total 12 tests were run surviving a Bonferroni corrected threshold (α=0.0042).
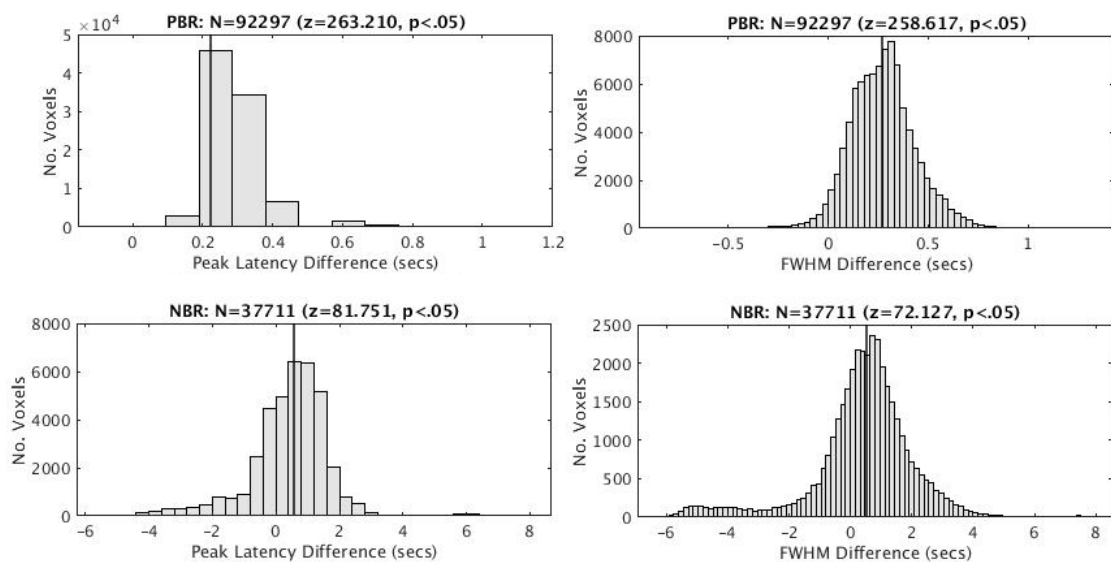
Figure 3. Histograms showing the distributions of difference scores (Fourier minus HRFtd) across both PBRs and NBRs, for both peak latency and FWHM. Black vertical lines denote medians.

Finally, in order to visualise regional differences in peak latency and FWHM across the brain, timing properties as estimated via the Fourier analysis were overlaid upon the MNI brain, see Figure 4. These were not formally investigated further as a lack of slice-timing correction adds complexity to such an approach. However it was tentatively confirmed that dorsal and rostral portions of the prefrontal cortex (frontal pole, superior frontal gyrus and dorsal regions of the middle frontal gyrus) as well as the more ventral inferior frontal gyrus demonstrated increased FWHM. However for peak latency the superior frontal gyrus

typically had lower values than the middle frontal gyrus, and ventrally increases were more

limited to the inferior frontal sulcus. In the cerebellum there was also a larger variability in

timing properties, which was consistent with variability evidenced within the regional

analyses.
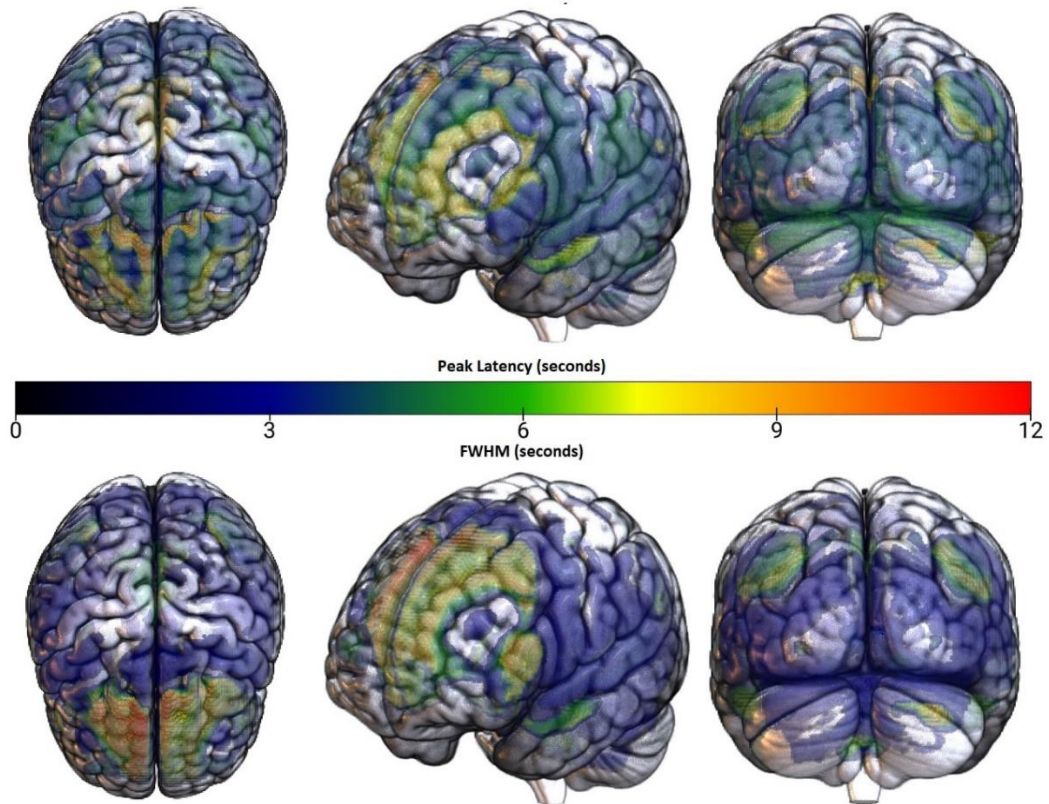
Figure 4. Distribution of peak latency and FWHM across GM, derived from the Fourier

analysis. These are overlaid upon the MNI152 brain.

3.3.4. Simulation

In order to better understand how the HRFtd model and Fourier set model signal which

deviates from that assumed by the HRFc model, simulations were run. These tested the

flexible approaches capacity to model a set of systematically manipulated artificial HRFs

using linear regression, see **3.2.5. Design > Simulations** above for details. When timing

properties were half that of the HRFc model, the HRFtd model was better able to capture

variance in the signal than when timing properties were double that assumed by the HRFc model (determined by R^2 values). There was also evidence of a reduced relative weighting of the canonical function at either extreme. This was expected as it demonstrated that the model became less reliant upon the canonical function, and more so upon its derivatives. By comparison the Fourier set showed greater consistency in its capacity to capture variance across the five artificial signals. There was however a trend of R^2 values being higher when timing properties were increased, with the model capturing more variance when timing properties were doubled, than when they were halved. This was the opposite of that seen with the HRFtd model.

In relation to the parameter estimates themselves (the beta values used to weight the functions) it was noted that for the HRFtd model there was a general trend of derivatives being positively weighted when their respective timing property was low (e.g. if FWHM was low the dispersion derivative would be positive), and negatively weighted when their respective timing property was high. However of interest, when both peak latency and dispersion were low the dispersion derivative was negatively weighted. This implies that parameter estimates are not always reliable as proxies for the timing property they approximate. Parameter estimates for the Fourier set also somewhat represent timing properties, as the model increasingly relied upon its higher frequency functions when timing properties were low, and its initial lower frequency functions when timing properties were high. In general both flexible sets tended to underestimate extremes, with both delayed peak latency/increased FWHM estimates in the reduced timing property models, and reduced peak latency/FWHM estimates in the increased timing property models. This was important as it confirmed that neither was prone to erroneous exaggeration of either extreme, and that if anything the deviations reported in the study may be underestimated. See Table 2 and Figure 5.

Table 2. Simulated parameter estimates (β) and measures of fit (R^2) for each flexible model across the five simulated signals. The absolute highest weighted β values are highlighted in blue. PL = peak latency. 'Diff' refers to the difference between the signal and estimated model (e.g. peak latency of estimated model minus peak latency of simulated signal).

	0.5 x timings	0.5 x timings (1 x PL)	Canonical	1.5 x timings	2 x timings
HRFtd					
Adjusted R^2	.925	.932	1	.898	.540
F	1068.370	1191.953	4.792E+13	759.420	102.480
dfm,dfr	3,256	3,256	3,256	3,256	3,256
p value	< .001	< .001	< .001	< .001	< .001
Constant	.008	.025	0	.046	.213
β_1	11.016	22.375	38.593	33.366	12.944
β_2	59.671	4.686	0	-71.269	-77.457
β_3	-37.135	35.842	0	-37.642	-45.145
PL/diff	2.95 / + .37	5.17 / 0	5.17 / 0	7.51 / - .25	8.25 / - 2.09
FWHM/diff	2.61 / - .02	3.43 / + .80	5.26 / 0	5.69 / -2.20	5.29 / -5.23
Fourier					
Adjusted R^2	.905	.971	.996	.995	.911
F	354.732	1251.787	9065.922	7945.301	382.065
dfm,dfr	7,252	7,252	7,252	7,252	7,252
p value	< .001	< .001	< .001	< .001	< .001
Constant	-.001	.006	-.024	-.054	.048
β_1	.051	.210	.542	.992	.935
β_2	.190	.588	.793	.247	-.390
β_3	.760	.565	.537	.031	.136
β_4	.525	.132	.335	-.073	-.323
β_5	.677	-.485	-.102	-.001	.172
β_6	.498	-.298	.073	-.061	-.231
β_7	.333	-.191	-.112	.047	.141
PL/diff	3.06 / + .49	5.39 / + .24	5.02 / -.12	7.47 / - .24	10.29 / 0
FWHM/diff	2.77 / + .16	3.04 / + .42	5.17 / -.06	7.72 / - .13	9.91 / - .55
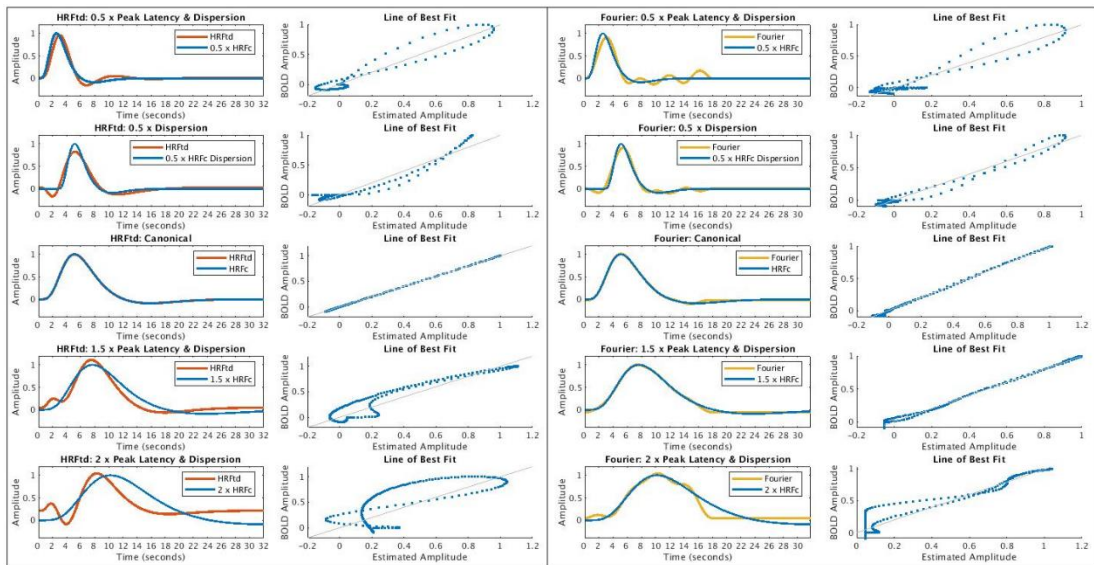
Figure 5. The best fitting linearly combined estimate of each of the five simulations using the HRFtd model (left, in orange) and Fourier set (right, in yellow). The artificially created signals are in blue, with timing properties increasing from the top-most to the bottom-most. For each a scatter plot is included, showing the line of best fit with the artificial "*BOLD*" signal on the Y axis and the estimated HRF on the X axis.

3.4. Discussion

3.4.1. Hypotheses

The primary purpose of the study was to compare two commonly used flexible modelling approaches, to establish whether it was the case that the Fourier set captured additional variance over and above the HRFtd model, across a range of ROIs. In order to do this it was first checked whether the three modelling approaches captured significant signal within the ROIs selected, and whether the addition of derivatives to the HRFc model increased capture. This was confirmed, with all models finding significant plausible activation within ROIs, and the HRFtd model identifying more significant voxels than HRFc in all but A1. Therefore the 1st and 2nd null hypotheses can be rejected for remaining ROIs, confirming ROIs were appropriately selected and that addition of derivatives improved modelling, consistent with previous work (Henson et al., 1999, 2001; Lindquist et al., 2009; Lindquist & Wager, 2007; Ramnani & Henson, 2005; Steffener et al., 2010). Next significant

voxels were identified in all ROIs using the Fourier(HRFtd) analysis. This lead to rejection of the 3rd null hypothesis, as the Fourier set did indeed appear to model variance beyond that captured by the HRFtd model. However it was recognised that the two models may capture much shared variance, but just because the Fourier set captures signal missed by the HRFtd model, this does not mean that the HRFtd model does not also capture signal missed by the Fourier set. Therefore hypothesis 4 ran the opposite analysis, to check whether the HRFtd model also captured additional variance. Against the prediction, more significant voxels were identified in the HRFtd(Fourier) analysis within all ROIs barring the aPFC, further supported by F values being typically higher in this analysis. Therefore the null hypothesis could only be rejected within the aPFC, but failed rejection in A1, M1, V1, and the cerebellum.

3.4.2. Overview

Across the brain the HRFtd(Fourier) analysis captured ~23% more significant voxels relative to Fourier(HRFtd). This was unlikely to be attributable to noise (such as modelling non-neural signal as a result of over-fitting) as the HRFtd model is more constrained than the Fourier set. Visual examination further supported the idea that the Fourier set was more likely to over-fit the data, with the Fourier(HRFtd) analysis more likely to find activity in non-neural regions such as the ventricles. However, under 50% of active voxels were found within the population of voxels with greater than 0.5 probability of being GM, highlighting how increased power from the large dataset may lead to modelling of noise and exaggeration of effect sizes (stressing the necessity of well-sampled control conditions). Additionally, although flexible models found more significant GM voxels than inflexible modelling using fixed parameters, these represented a smaller proportion of total significant voxels, implying increased proportional noise with the flexible approach. Furthermore exaggeration of effects as a result of the large sample size may account for HRFtd and Fourier sets finding significance within nearly 100% of A1 voxels. Fortunately there were

differences between the HRFtd(Fourier) and Fourier(HRFtd) analyses, enabling comparisons within this ROI. However that these differences exist implied a ceiling effect in the standard analyses.

As HRFtd(Fourier) and Fourier(HRFtd) analyses had equivalent degrees of freedom at the 1st-level of analysis, and equivalent relative degrees of freedom at the second (residual degrees of freedom always increased proportionally to model degrees of freedom), the number of functions could not account for the differences between them. Such differences are likely to be attributed to the HRFtd model capturing more experimental variance, potentially due to it being less biased than the HRFc model, and with less variability in parameter estimates than the Fourier set. In short it may strike an appropriate balance in the bias-variance trade-off. It could be described as unbiased enough to capture variable signal, but with parameter estimates that do not vary hugely across participants (supported using simulations). It is suggested that the Fourier set suffers from over-fitting at the individual level, meaning parameters estimates vary widely across the cohort due to individual differences in HRF shape, meaning poor signal-to-noise at the 2nd-level of analysis. It could also be argued that the HRFtd model benefits from relative simplicity/interpretability (Aguirre et al., 1998) as the Fourier set has a range of functions none of which are linked to any one timing property (e.g. dispersion). However although the three functions of the HRFtd model loosely relate to peak amplitude, peak latency, and dispersion, they do not independently represent them, and so interpretation remains problematic (Lindquist et al., 2009; Lindquist & Wager, 2007).

Considering how flexible mHRFs model the BOLD response, ROI and whole brain GM estimates of PBRs identified low peak latency and FWHM, consistent with previous work (Ramnani & Henson, 2005; West et al., 2019). As microtime onset was set to a central slice there was an expected peak latency error of approximately +/- one second, but crucially neither timing property decreased systematically in the dorsoventral plane (see Figure 4).

Instead inter-regional variability (potentially due to differences within the vasculature; Ramnani & Henson, 2005) was suggested, supported by significant inter-ROI differences. This is to be interpreted cautiously, as uncontrolled factors such as stimulus/response strength/duration may have contributed (Boynton et al., 1996; Fabiani et al., 2014). Fundamentally, across GM the Fourier set estimated a significantly longer peak latency and FWHM than the HRFtd model (exceeding the previously mentioned measurement differences introduced by binning). Assuming reductions in peak latency and FWHM are unlikely to be erroneously exaggerated (supported using simulations) it is suggested the HRFtd model may be less prone to underestimation of HRFs with low timing properties due to it being better suited to modelling these signal types. It is relevant therefore that low timing properties were typical of PBRs across GM, as well as ROIs such as A1, M1, V1, and the cerebellum, with these being regions where the HRFtd model captured additional variance over and above the Fourier set.

NBRs were also investigated, occurring in 29.10% of significant GM voxels (measured using the valence of the HRFc model's beta value as a proxy). This was plausible, being consistent with a 27% prevalence reported by Taylor et al. (2018). The lack of categorical distinction between an NBR and a small PBR with large undershoot was considered, however both would present the same challenges regarding modelling, reducing relevance of this ambiguity. When investigating the timing properties of NBRs the flexible modelling approaches typically produced an HRF estimate with peak latency and FWHM that exceeded that assumed by the HRFc model. Interestingly, opposite to that seen in PBRs, the HRFtd model seemed to underestimate these properties. Therefore as simulations again suggested that increased timing properties such as peak latency tend not to be overestimated, alongside findings that the Fourier set captured additional variance over and above that of the HRFtd model in the aPFC (where HRFs were typically negative with larger peak latency

and dispersion), it is reasonable to suggest that estimates using the Fourier set may better represent true signal.

Interestingly, previous work has found PBRs and NBRs tend to share comparable timing properties within the visual cortex (Shmuel et al., 2002), and that HRFs in the aPFC tend to demonstrate increased timing properties even within PBRs (Schacter et al., 1997). Therefore the association between increased timing properties and NBRs may be coincidental. However, in the analysis classification into PBR and NBR served as a fairly reliable proxy of timing properties, allowing for a split in analyses between PBRs and NBRs, breaking down bimodal distributions into more manageable unimodal ones. That this proxy is imperfect would however explain the prevalence of cases with large standardised residuals in the logistic regression analysis, likely driven by NBRs with low peak latency (29.3% of NBRs misclassified versus .02% of PBRs) or FWHM (7.1% of NBRs misclassified versus .03% of PBRs).

That the Fourier set may better model HRFs with increased timing properties (such as peak latency) was supported by the aPFC being the only ROI in which the Fourier(HRFtd) analysis outperformed HRFtd(Fourier). All significant coordinates within the region typically demonstrated high timing properties and/or bimodality. Additionally, the cerebellar and aPFC ROIs had a larger percentage of significant voxels in the standard Fourier analysis relative to the HRFtd analysis. This was consistent with evidence of greater occurrence of high timing property HRFs/NBRs in these regions. This was less clear in the cerebellum as HRFs were highly varied regarding timing properties, however when isolating specific coordinates where only the Fourier set captured significance there is a trend of increased timing properties such as peak latency and dispersion. Further confirming the conclusion that the Fourier set may better model HRFs with delayed properties, the HRFtd model showed a far clearer trend of reduced fit as timing properties increased, within the simulations run.

Overall it was unexpected that the HRFtd approach would model additional variance in more voxels than the highly flexible Fourier set, but does make sense retrospectively in terms of the HRFtd model representing a better balance in the bias-variance trade-off. Additionally, as the Fourier set seemed to rely on its high frequency functions to model reduced peak latency and FWHM, this may increase oscillations within the signal at the 1st-level of analysis. In short, a high frequency function may be called to model an HRF with early peak and low dispersion, but in calling a function with multiple peaks, the latter end of the estimated HRF is liable to erroneous oscillation. This is visually demonstrated in the simulations with reduced temporal parameters, and supported by the simulated Fourier mHRF being maximally weighted by the 3rd and 5th, and 2nd and 3rd functions (later functions increasing in oscillation frequency) when modelling HRFs with reduced timing properties (see Figure 5). In contrast, beta weights were greater for the 1st and 2nd functions (with low frequency oscillation) when modelling simulated HRFs with increased timing properties. Considering the HRFtd approach it is deemed likely that the model is too biased towards modelling HRFs with timing properties that typically align with or are lesser than that assumed by the HRFc model. As a result this approach may be less capable of accurately capturing signal in which peak latency and dispersion are increased. Additionally, when looking to simulations in Figure 5 and Table 2, in the bottom-most example (when peak latency and dispersion were doubled) both derivatives were negatively weighted. As a result what would be called an "undershoot" (following the primary peak) instead forms a delayed positive primary peak. This may contribute to an increased risk of erroneous bimodality, supported by HRFtd modelled bimodality only occurring within the typically high timing property NBRs. Conversely, when the HRF signal has low timing properties (top-most example in Figure 5) this appears to suit the existing shape of the HRFtd's derivatives. Regarding interpretability, as expected increasingly positive temporal derivative beta weightings represented low peak latency, negative weightings representing high (Steffener

et al., 2010). The dispersion derivative showed the same trend when FWHM was reduced

but peak latency was not (second simulation, Figure 5). However when low peak latency and

FWHM coincided (top-most simulation, Figure 5) the dispersion derivative's beta weighting

was negative, rendering this a misleading representation of dispersion (Lindquist et al.,

2009; Lindquist & Wager, 2007).

3.4.3. Limitations

A limitation of this work was that HRF shape estimation took place at the 2nd-level

analysis using a summary statistic approach, but was deemed acceptable as evidence has

shown it produces accurate results (Penny & Holmes, 2007) and the computing power for a

single stage hierarchical approach (accounting directly for both within and between subject

variance) was unavailable. That 2nd-level data was examined also meant that when

examining estimates of peak latency and FWHM, inferential statistics were run on data

pertaining to voxels rather than participants. This was despite voxels not necessarily being

completely independent of one another (due to smoothing and the potential for shared

contributions to BOLD signal), and so increases the risk of false positives. This compromise

was accepted as it allowed for a voxel-wide investigation at the group level, the results were

consistent with findings via simulations and regional investigations looking at the number of

significant voxels (neither of which were affected by this compromise), and even without

inferential statistics the distributions themselves demonstrate a clear trend. Omission of

slice-timing-correction may have also biased results in favour of the more flexible Fourier

set, but this would not explain the HRFtd model capturing additional variance, and was not

the case in simulations which supported the data.

There was also no guarantee that signal represented meaningful haemodynamic

activity, with it possible that some proportion of additional signal may be attributed to

noise. This could be a result of inflated effect size, or of flexible models picking up on non-

neural signals. For this reason using 'number of significant voxels' as a measure is imperfect,

hence examination of F values to confirm the trends, alongside use of simulations and the

GM analyses to establish potential causes of modelling differences. Simulations themselves

were run over a single event to ensure there was no impact of overlapping event-related

haemodynamic activity (linear addition). However an alternative was run whereby each of

the five HRF shapes and the relevant basis set functions were convolved with the 40 event

timings as used in the study. Forced entry linear regression was run and the same trends

were seen. The simulation analyses also applied to the 1st-level of analysis where residual

error in the fit of the model is considered, but the core analyses were run at the 2nd-level

using a summary statistic approach (looking at variability between subjects in the parameter

estimates; Mumford & Nichols, 2006). Theoretically within this approach the 2nd-level

parameter estimates still implicitly represent 1st-level variability (hence why it is deemed

comparable to a hierarchical approach) meaning insights regarding fit at the 1st-level were

still deemed relevant (Penny & Holmes, 2007). Critically, these conclusions pertain to this

specific sample/task/analysis (except for the simulations which were sample and task

independent). This means it is important that future research replicates this work in

separate datasets, and looks at different sets of parameters defining the Fourier set. For

example, when a Fourier set without a Hanning window was used the variance explained by

the model increased when modelling simulated HRFs with timing properties that were

extremely low or high (as in the first and last simulation). It could also be telling to vary the

window length alongside the number of functions, to determine the optimum trade-off.

Beyond this there are additional modelling techniques now available such as the inverse

logit (IL) function (putatively capturing more variance than HRFc and HRFc with temporal

derivative; Lindquist & Wager, 2007) and FLOBs (which restricts its three functions to be

physiologically plausible; Woolrich et al., 2004), which could warrant further investigation.

The current study focussed upon classical models and their strengths and weaknesses at the

group level, whilst highlighting the risks of assumed validity of the HRFc, and the large variability seen across the brain.

3.4.4. Conclusion

In conclusion, across GM the HRFc was rarely representative of flexibly modelled HRFs, with this being to a degree that went beyond slice-timing correction. In this large dataset HRFc still captured variance in a lot of voxels despite a poor fit at the 1st-level, which could be used as evidence of its versatility, however in typically powered studies the risk of missing signal which does not conform to the canonical model may increase. It remains unclear whether applying slice-timing correction would have made a substantial improvement to the HRFc model's capacity to capture signal, to a greater degree than it would for flexible models. However it is likely that this would be the case to some degree, as flexible models naturally correct for slice-timing differences, putting the HRFc model at a disadvantage here. However the primary focus was to compare the two flexible models, not to draw conclusions about the benefits of flexible modelling over interpolation. It is however noted that deviations from peak latency and FWHM assumed by the HRFc model varied by region in a way not explained by slice-timing, and far exceeded the +/- one second variability expected from slice-timing effects. Ergo it is deemed unlikely that omitting slice-timing correction contributed much to flexible basis sets finding more significant voxels. Consequently this effect goes beyond variability induced by slice-timing, with it also recognised that deviations in additional properties such as rise time, fall time, rise onset, and relative undershoot amplitude are likely to have contributed.

Considering the differences between flexible approaches, the HRFtd model found marginally fewer intra-ROI voxels than the Fourier set. Yet it captured additional variance in more voxels, within ROIs which typically demonstrated HRFs with low timing properties. Conversely, the Fourier set captured more variance within ROIs which typically demonstrated HRFs with increased timing properties. It is unclear exactly what the HRFtd

models beyond the Fourier set (and vice versa) within the same voxel. However it is plausible that in some cases the Fourier set captures additional signal due to it being less biased towards any one HRF shape (supported by simulations). On the other hand, the HRFtd model may be biased towards a certain HRF profile, but it is a profile that was more typically seen in this study. It is important again to stress that there will be contributions from other timing properties however peak latency and FWHM did differ between flexible models, and are arguably core features of the haemodynamic response. Therefore when the expected profile of the HRF is approximately in line with the HRFc model, or demonstrates reduced peak latency and FWHM, the HRFtd model may be the better solution. When a HRF with delayed timing properties is expected, or timing properties are unknown, the Fourier set may provide a better compromise.

3.5. References

Aguirre, G. K., Zarahn, E., & D'Esposito, M. (1998). The variability of human, BOLD

hemodynamic responses. *Neuroimage*, *8*(4), 360-369.

https://doi.org/10.1006/nimg.1998.0369

Amunts, K., Malikovic, A., Mohlberg, H., Schormann, T., & Zilles, K. (2000). Brodmann's areas

17 and 18 brought into stereotaxic space—where and how

variable?. *Neuroimage*, *11*(1), 66-84. https://doi.org/10.1006/nimg.1999.0516

Ashburner, J., Barnes, G., Chen, C., Daunizeau, J., Flandin, G., Friston, K., ... & Phillips, C.

(2020). SPM12 manual. *Wellcome Centre for Human Neuroimaging, London, UK*.

https://www.fil.ion.ucl.ac.uk/spm/

Bandettini, P. A. (2002). *Neuropsychopharmacology – 5ᵗʰ Generation of Progress*: *The spatial,

temporal, and interpretive limits of functional MRI.* Lippincott Williams and Wilkins.

Bandettini, P. A. (2020). *fMRI.* MIT Press.

Bludau, S., Eickhoff, S. B., Mohlberg, H., Caspers, S., Laird, A. R., Fox, P. T., ... & Amunts, K.

(2014). Cytoarchitecture, probability maps and functions of the human frontal

pole. *Neuroimage*, *93*(2), 260-275.

https://doi.org/10.1016/j.neuroimage.2013.05.052

Boynton, G. M., Engel, S. A., Glover, G. H., & Heeger, D. J. (1996). Linear systems analysis of

functional magnetic resonance imaging in human V1. *Journal of

Neuroscience*, *16*(13), 4207-4221. https://doi.org/10.1523/JNEUROSCI.16-13-

04207.1996

Buracas, G. T., & Boynton, G. M. (2002). Efficient design of event-related fMRI experiments

using M-sequences. *Neuroimage*, *16*(3), 801-813.

https://doi.org/10.1006/nimg.2002.1116

Buxton, R. B., Uludağ, K., Dubowitz, D. J., & Liu, T. T. (2004). Modeling the hemodynamic

response to brain activation. *Neuroimage*, *23*, S220-S233.

https://doi.org/10.1016/j.neuroimage.2004.07.013

Csipo, T., Mukli, P., Lipecz, A., Tarantini, S., Bahadli, D., Abdulhussein, O., ... & Hand, R. A.

(2019). Assessment of age-related decline of neurovascular coupling responses by

functional near-infrared spectroscopy (fNIRS) in humans. *Geroscience*, *41*(5), 495-

509. https://doi.org/10.1007/s11357-019-00122-x

D'esposito, M., Zarahn, E., Aguirre, G. K., & Rypma, B. (1999). The effect of normal aging on

the coupling of neural activity to the bold hemodynamic

response. *Neuroimage*, *10*(1), 6-14. https://doi.org/10.1006/nimg.1999.0444

D'esposito, M., Deouell, L. Y., & Gazzaley, A. (2003). Alterations in the BOLD fMRI signal with

ageing and disease: a challenge for neuroimaging. *Nature Reviews

Neuroscience*, *4*(11), 863-872. https://doi.org/10.1038/nrn1246

Diedrichsen, J., Balsters, J. H., Flavell, J., Cussans, E., & Ramnani, N. (2009). A probabilistic

MR atlas of the human cerebellum. *neuroimage*, *46*(1), 39-46.

https://doi.org/10.1016/j.neuroimage.2009.01.045

Duvernoy, H. M. (1999). *The human brain: surface, three-dimensional sectional anatomy

with MRI, and blood supply*. Springer Science & Business Media.

Fabiani, M., Gordon, B. A., Maclin, E. L., Pearson, M. A., Brumback-Peltz, C. R., Low, K. A., ...

& Gratton, G. (2014). Neurovascular coupling in normal aging: a combined optical,

ERP and fMRI study. *Neuroimage*, *85*(1), 592-607.

https://dx.doi.org/10.1016/j.neuroimage.2013.04.113

Field, A. (2009). *Discovering statistics using IBM SPSS statistics*. Sage.

Friston, K. J., Jezzard, P., & Turner, R. (1994). Analysis of functional MRI time-series. *Human

brain mapping*, *1*(2), 153-171. https://doi.org/10.1002/hbm.460010207

Friston, K. J., Frith, C. D., Turner, R., & Frackowiak, R. S. (1995). Characterizing evoked

hemodynamics with fMRI. *Neuroimage*, *2*(2), 157-165.

https://doi.org/10.1006/nimg.1995.1018

Friston, K. J., Josephs, O., Rees, G., & Turner, R. (1998a). Nonlinear event-related responses

in fMRI. *Magnetic resonance in medicine*, *39*(1), 41-52.

https://doi.org/10.1002/mrm.1910390109

Friston, K. J., Fletcher, P., Josephs, O., Holmes, A., Rugg, M. D., & Turner, R. (1998b). Event-

related fMRI: characterizing differential responses. *Neuroimage*, *7*(1), 30-40.

https://doi.org/10.1006/nimg.1997.0306

Geyer, S., Ledberg, A., Schleicher, A., Kinomura, S., Schormann, T., Bürgel, U., ... & Roland, P.

E. (1996). Two different areas within the primary motor cortex of

man. *Nature*, *382*(6594), 805-807. https://doi.org/10.1038/382805a0

Handwerker, D. A., Ollinger, J. M., & D'Esposito, M. (2004). Variation of BOLD hemodynamic

responses across participants and brain regions and their effects on statistical

analyses. *Neuroimage*, *21*(4), 1639-1651.

https://doi.org/10.1016/j.neuroimage.2003.11.029

Henson, R., Büchel, C., Josephs, O., & Friston, K. (1999). The slice-timing problem in event-

related fMRI. *NeuroImage*, *9*, 125. https://www.mrc-

cbu.cam.ac.uk/personal/rik.henson/personal/HensonEtAl_HBM_Abstract_99.pdf

Henson, R., Rugg, M. D., & Friston, K. J. (2001). The choice of basis functions in event-related

fMRI. *NeuroImage*, *13*(6), 149. https://doi.org/10.1016/S1053-8119(01)91492-2

Hillman, E. M. (2014). Coupling mechanism and significance of the BOLD signal: a status

report. *Annual review of neuroscience*, *37*, 161-181.

https://doi.org/10.1146/annurev-neuro-071013-014111

Huang, Q., & Tang, J. (2010). Age-related hearing loss or presbycusis. *European Archives of Oto-rhino-laryngology*, *267*(8), 1179-1191. https://doi.org/10.1007/s00405-010-1270-7

Hutchison, J. L., Lu, H., & Rypma, B. (2013). Neural mechanisms of age-related slowing: the ΔCBF/ΔCMRO2 ratio mediates age-differences in BOLD signal and human performance. *Cerebral Cortex*, *23*(10), 2337-2346. https://doi.org/10.1093/cercor/bhs233

Josephs, O., Turner, R., & Friston, K. (1997). Event-related f MRI. *Human brain mapping*, *5*(4), 243-248. https://doi.org/10.1002/(SICI)1097-0193(1997)5:4%3C243::AID-HBM7%3E3.0.CO;2-3

Josephs, O., & Henson, R. N. (1999). Event-related functional magnetic resonance imaging: modelling, inference and optimization. *Philosophical transactions of the royal society of london. series b: biological sciences*, *354*(1387), 1215-1228. https://doi.org/10.1098/rstb.1999.0475

Klein, A., Andersson, J., Ardekani, B. A., Ashburner, J., Avants, B., Chiang, M. C., ... & Song, J. H. (2009). Evaluation of 14 nonlinear deformation algorithms applied to human brain MRI registration. *Neuroimage*, *46*(3), 786-802. https://doi.org/10.1016/j.neuroimage.2008.12.037

Lindquist, M. A., & Wager, T. D. (2007). Validity and power in hemodynamic response modeling: a comparison study and a new approach. *Human brain mapping*, *28*(8), 764-784. https://doi.org/10.1002/hbm.20310

Lindquist, M. A., Loh, J. M., Atlas, L. Y., & Wager, T. D. (2009). Modeling the hemodynamic response function in fMRI: efficiency, bias and mis-modeling. *Neuroimage*, *45*(1), 187-198. https://doi.org/10.1016/j.neuroimage.2008.10.065

Liu, J., Duffy, B. A., Bernal-Casas, D., Fang, Z., & Lee, J. H. (2017). Comparison of fMRI analysis methods for heterogeneous BOLD responses in block design

studies. *Neuroimage*, *147*, 390-408.

https://doi.org/10.1016/j.neuroimage.2016.12.045

Logothetis, N. K. (2003). The underpinnings of the BOLD functional magnetic resonance

imaging signal. *Journal of Neuroscience*, *23*(10), 3963-3971.

https://doi.org/10.1523/JNEUROSCI.23-10-03963.2003

Lu, Y., Grova, C., Kobayashi, E., Dubeau, F., & Gotman, J. (2007). Using voxel-specific

hemodynamic response function in EEG-fMRI data analysis: An estimation and

detection model. *Neuroimage*, *34*(1), 195-203.

https://doi.org/10.1016/j.neuroimage.2006.08.023

Miezin, F. M., Maccotta, L., Ollinger, J. M., Petersen, S. E., & Buckner, R. L. (2000).

Characterizing the hemodynamic response: effects of presentation rate, sampling

procedure, and the possibility of ordering brain activity based on relative

timing. *Neuroimage*, *11*(6), 735-759. https://doi.org/10.1006/nimg.2000.0568

Morosan, P., Rademacher, J., Schleicher, A., Amunts, K., Schormann, T., & Zilles, K. (2001).

Human primary auditory cortex: cytoarchitectonic subdivisions and mapping into a

spatial reference system. *Neuroimage*, *13*(4), 684-701.

https://doi.org/10.1006/nimg.2000.0715

Mumford, J. A., & Nichols, T. (2006). Modeling and inference of multisubject fMRI data. *IEEE*

Engineering in Medicine and Biology Magazine, *25*(2), 42-51.

https://doi.org/10.1109/MEMB.2006.1607668

Ogawa, S., Lee, T. M., Kay, A. R., & Tank, D. W. (1990). Brain magnetic resonance imaging

with contrast dependent on blood oxygenation. *Proceedings of the National*

Academy of Sciences, *87*(24), 9868-9872. https://doi.org/10.1073/pnas.87.24.9868

Penny, W., & Holmes, A. (2007). Random effects analysis. *Statistical parametric mapping:*

The analysis of functional brain images, *156*, 165-186.

https://citeseerx.ist.psu.edu/document?repid=rep1&type=pdf&doi=6ed105062770d089d86e9bcc7827f54487a22017

Poldrack, R. A., Mumford, J. A., & Nichols, T. E. (2011). *Handbook of functional MRI data analysis*. Cambridge University Press.

Ramnani, N., & Henson, R. (2005). "Modelling the BOLD impulse response: Insufficiency of canonical basis functions", Abstracts of the 11th Annual Meeting of the Organization for Human Brain Mapping (2005), *NeuroImage*, Volume 26, Supplement 1, Abstract No. 622.

Ress, D., Thompson, J. K., Rokers, B., Khan, R., & Huk, A. C. (2009). A model for transient oxygen delivery in cerebral cortex. *Frontiers in neuroenergetics*, *1*(3), 1-12. https://doi.org/10.3389/neuro.14.003.2009

Schacter, D. L., Buckner, R. L., Koutstaal, W., Dale, A. M., & Rosen, B. R. (1997). Late onset of anterior prefrontal activity during true and false recognition: an event-related fMRI study. *Neuroimage*, *6*(4), 259-269. https://doi.org/10.1006/nimg.1997.0305

Schmahmann, J. D., Doyon, J., Petrides, M., Evans, A. C., & Toga, A. W. (2000). *MRI atlas of the human cerebellum*. Academic Press.

Shafto, M. A., Tyler, L. K., Dixon, M., Taylor, J. R., Rowe, J. B., Cusack, R., ... & Henson, R. N. (2014). The Cambridge Centre for Ageing and Neuroscience (Cam-CAN) study protocol: a cross-sectional, lifespan, multidisciplinary examination of healthy cognitive ageing. *BMC neurology*, *14*(204), 1-25. https://doi.org/10.1186/s12883-014-0204-1

Shmuel, A., Yacoub, E., Pfeuffer, J., Van de Moortele, P. F., Adriany, G., Hu, X., & Ugurbil, K. (2002). Sustained negative BOLD, blood flow and oxygen consumption response and its coupling to the positive response in the human brain. *Neuron*, *36*(6), 1195-1210. https://doi.org/10.1016/S0896-6273(02)01061-9

Sladky, R., Friston, K. J., Tröstl, J., Cunnington, R., Moser, E., & Windischberger, C. (2011). Slice-timing effects and their correction in functional MRI. *Neuroimage*, *58*(2), 588-594. https://doi.org/10.1016/j.neuroimage.2011.06.078

Sloan, H. L., Austin, V. C., Blamire, A. M., Schnupp, J. W., Lowe, A. S., Allers, K. A., ... & Sibson, N. R. (2010). Regional differences in neurovascular coupling in rat brain as determined by fMRI and electrophysiology. *Neuroimage*, *53*(2), 399-411. https://doi.org/10.1016/j.neuroimage.2010.07.014

Steffener, J., Tabert, M., Reuben, A., & Stern, Y. (2010). Investigating hemodynamic response variability at the group level using basis functions. *Neuroimage*, *49*(3), 2113-2122. https://doi.org/10.1016/j.neuroimage.2009.11.014

Takano, T., Tian, G. F., Peng, W., Lou, N., Libionka, W., Han, X., & Nedergaard, M. (2006). Astrocyte-mediated control of cerebral blood flow. *Nature neuroscience*, *9*(2), 260-267. https://doi.org/10.1038/nn1623

Tarantini, S., Tran, C. H. T., Gordon, G. R., Ungvari, Z., & Csiszar, A. (2017). Impaired neurovascular coupling in aging and Alzheimer's disease: contribution of astrocyte dysfunction and endothelial impairment to cognitive decline. *Experimental gerontology*, *94*, 52-58. https://doi.org/10.1016/j.exger.2016.11.004

Taylor, A. J., Kim, J. H., & Ress, D. (2018). Characterization of the hemodynamic response function across the majority of human cerebral cortex. *NeuroImage*, *173*, 322-331. https://doi.org/10.1016/j.neuroimage.2018.02.061

Taylor, J. R., Williams, N., Cusack, R., Auer, T., Shafto, M. A., Dixon, M., ... & Henson, R. N. (2017). The Cambridge Centre for Ageing and Neuroscience (Cam-CAN) data repository: structural and functional MRI, MEG, and cognitive data from a cross-sectional adult lifespan sample. *Neuroimage*, *144*, 262-269. https://dx.doi.org/10.1016/j.neuroimage.2015.09.018

Ward, L. M., Aitchison, R. T., Tawse, M., Simmers, A. J., & Shahani, U. (2015). Reduced Haemodynamic Response in the Ageing Visual Cortex Measured by Absolute fNIRS. *PLoS ONE*, *10*(4), e0125012. https://doi.org/10.1371/journal.pone.0125012

West, K. L., Zuppichini, M. D., Turner, M. P., Sivakolundu, D. K., Zhao, Y., Abdelkarim, D., ... & Rypma, B. (2019). BOLD hemodynamic response function changes significantly with healthy aging. *Neuroimage*, *188*, 198-207. https://doi.org/10.1016/j.neuroimage.2018.12.012

Woolrich, M. W., Behrens, T. E., & Smith, S. M. (2004). Constrained linear basis sets for HRF modelling using Variational Bayes. *NeuroImage*, *21*(4), 1748-1761. https://doi.org/10.1016/j.neuroimage.2003.12.024

Worsley, K. J., & Friston, K. J. (1995). Analysis of fMRI time-series revisited—again. *Neuroimage*, *2*(3), 173-181. https://doi.org/10.1006/nimg.1995.1023

Worsley, K. J., Liao, C. H., Aston, J., Petre, V., Duncan, G. H., Morales, F., & Evans, A. C. (2002). A general statistical analysis for fMRI data. *Neuroimage*, *15*(1), 1-15. http://www.math.mcgill.ca/keith

Wylie, G. R., Genova, H., DeLuca, J., Chiaravalloti, N., & Sumowski, J. F. (2014). Functional magnetic resonance imaging movers and shakers: Does participant-movement cause sampling bias?. *Human brain mapping*, *35*(1), 1-13. https://doi.org/10.1002/hbm.22150

Chapter 4
Comparing Estimations of the Haemodynamic Response Function in the Ageing Brain

Matthew Danvers
Michael Longley
Narender Ramnani
In preparation for publication

Word count: 9,326 excluding references

Abstract

In fMRI studies the haemodynamic response function is estimated via the blood oxygen level dependent (BOLD) response, acting as a proxy for neuronal activity, and measured via non-intrusive means. It has been evidenced that peak amplitude reduces with increasing age, however this is accommodated as even the inflexible canonical function can vary across this parameter. Evidence into variation of timing properties is less well founded, such as change in latency to primary peak, or dispersion of primary peak. Analyses were run on a sample of 558 participants from the Cam-CAN dataset across the adult lifespan, who partook in a sensori-motor event-related fMRI task. We present evidence that peak latency and dispersion systematically increase with age, which may bias fixed-modelling results in favour of elderly participants who presented with a more typically canonical response. However when flexible modelling is introduced the haemodynamic responses of younger adults (with typically lower peak latency and dispersion) appear to be accommodated, resulting in more significant voxels found within this group. Furthermore, the post-stimulus undershoot was generally larger than assumed by the canonical model, and showed differential age-effects across the two flexible basis sets. These results should facilitate informed decisions about analysis strategy, specifically the choice of basis set.

4.1. Introduction

In the current ageing population the number of people over 60 is predicted to double between 2015 and 2050 (World Health Organisation, 2018). Consequently, there are many reasons for research to apply itself to the investigation of ageing, one such example being dementia research and the identification of biomarkers for those at risk for cognitive decline (Soch et al., 2021), which has the potential to improve quality of life and reduce strain on public services. One means of investigating different age groups is functional magnetic resonance imaging (fMRI), which has the benefit of being non-invasive, requires neither radiation exposure nor use of contrast agents, and in terms of dementia research can provide information about how brain networks associated with memory may differ at a functional level (Sperling, 2011). However there are various considerations that need to be addressed before looking at age group comparisons, especially when using fMRI. Critically, the blood oxygen level dependent (BOLD) response is used as an estimate of neural activity (Ogawa et al., 1990), formed of the ratio between oxygenated (HbO) and deoxygenated (HbR) haemoglobin, and plotted as a haemodynamic response function (HRF). Increases in the ratio can be attributed to increased cerebral blood flow (CBF) and volume (CBV) due to vasodilation as triggered by astrocyte cells, which further reduces levels of HbR as it is 'washed out' (Bandettini, 2002; Boynton et al., 1996; Buxton et al., 2004; Csipo et al., 2019; D'esposito et al., 2003; Takano et al., 2006; Tarantini et al., 2017). When using fMRI to elucidate neuronal effects, it is desirous to attribute changes in BOLD signal to differential neural activity, rather than to confounding differences in neurovascular coupling (the neurometabolic response to neuronal activity). However both have the capacity to affect the BOLD signal.

There is indeed evidence of age-related differences in neural activity. Price et al. (2017) identified that older human participants demonstrated delays in electrical activity within the visual cortex, with a similar but cumulative delay found within the auditory cortex. This was attributed to differences in grey matter (GM) and white matter (WM) volume, with it implied that slower transmission of information was taking place in the elderly. This has the capacity to affect the BOLD signal, as a delay in signal transmission is likely to affect the onset of vasodilation. However there is also evidence that neurovascular coupling changes over the lifespan (Csipo et al., 2019), contradicting the 'age-equivalence assumption', and presenting a potentially systematic confound. Further supporting this, within rodents age-related reductions in CBF have been identified (Balbi et al., 2015) which if not accompanied by a proportional drop in neuronal activity can result in a lower magnitude BOLD signal as HbR levels increase relative to HbO. This is consistent with findings in humans whereby BOLD magnitude reduces as age increases (Ances et al., 2009; Morsheddost al., 2015; Ross et al., 1997; Tekes et al., 2005; West et al., 2019). There are myriad possible causes and effects, from both physiological changes, and external influences. A review by D'esposito et al. (2003) highlighted the potential impact from common medications (e.g. aspirin, inhibiting vasodilators such as arachidonic acid), sub-clinical vascular pathology (e.g. leukoariosis, reducing CBF and the response to hypercapnia), sclerosis, tortuosity of capillaries, reduced resting cerebral metabolic rate of oxygen ($CMRO_2$), and vein occlusion via collagenosis (evidenced in 65% of participants over 60). All of these could alter the BOLD signal independently of neural activity, with further cross-species support from Desjardins (2015).

There are also contradictory reports of non-significant age-related differences in neurovascular coupling (Rosengarten et al., 2003) and BOLD peak amplitude (Grinband et al.,

2017), however non-significant results may sometimes be due to low sample sizes. For example, it was suggested by West et al. (2019) that to investigate this area an N of 60 per age group was required (a difficult sample size to attain in fMRI research), however there is still no agreed-upon minimum N. Region-of-interest (ROI) selection also matters, Aizenstein et al. (2004) finding an increased prevalence of negative BOLD responses (NBRs) within visual but not motor cortices of elderly participants. This can result in a somewhat artificial reduction in magnitude at the group level, but not the single-subject level. Reduced signal to noise in the elderly has also been identified (supported by D'esposito et al., 2003 and Aizenstein et al., 2004) as well as a reduced number of significant voxels, even at the single-subject level and when using a flexible Fourier basis set (D'esposito et al., 1999). Consequently, if analysing age-related change many factors suggest the age-equivalence assumption is not supported. However it also remains possible that a neurovascular atypicality may be reflective of processing and performance differences (D'esposito et al., 2003; Sorond et al., 2013), white matter integrity (Sorond et al., 2013), or cerebro-microvascular pathology (Tarantini et al., 2017) meaning these effects should not be automatically discarded as irrelevant noise in fMRI analyses. Turner et al. (2019) supported this, finding that multiple sclerosis (MS) patients had a reduced peak amplitude and increased peak latency (relative to age-matched controls), prefrontal (BA9) peak latency positively correlating with reaction time, specifically in MS patients. These effects could not be attributed to medication nor age, leading the authors to conclude that low peak latency was indicative of normal cognitive function (specifically processing speed), driven by effective communication between neurons, astrocytes and the vascular system.

It is an ongoing endeavour to uncover precisely how the BOLD signal represents underlying neuronal activity, however there are other factors to be considered when using

4

fMRI to study age effects. It is clear from the evidence presented that the BOLD signal is liable to vary between age groups, however when constructing general linear models (GLMs) to analyse an fMRI dataset, assumptions are typically made as to the shape of the HRF. This is most likely true of approaches such as the inflexible canonical model (HRFc) which makes fixed assumptions as to the time-course of the HRF. However even with more flexible approaches which can accommodate these changes, there are differing degrees of flexibility. Therefore choosing the appropriate modelling approach is fundamental, as an incorrect choice may bias results in favour of one age group over the other. The focus of this paper is upon how commonly used model haemodynamic response functions (mHRFs) may bias results for or against age-effects within fMRI analyses. As HRF magnitude is allowed to vary even in the HRFc model, this is not a crucial variable of interest, however any systematic age-related change in the latency to HRF peak or the dispersion of the HRF peak may affect modelling efficiency and therefore alter results (Lu et al., 2007). In a previous study by Danvers et al. (2021) it was found that across GM most responses demonstrated a peak latency and dispersion that were significantly lower than predicted by the HRFc model. Furthermore, when pairing the canonical model with its temporal and dispersion derivatives (HRFtd) the approach demonstrated a greater aptitude in modelling HRFs with low peak latency and reduced dispersion, measured using full-width-half-maximum (FWHM). This was compared to a 3rd order Fourier set with 18 second window, which demonstrated a greater aptitude in modelling HRFs with high peak latency and FWHM (typical within the anterior prefrontal cortex; Schacter et al., 1997). For this reason these are the three models that will be investigated.

Critically, increases in peak latency over the life-course are documented (Richter & Richter, 2003; Taoka et al., 1998; West et al., 2019) alongside increased weighting of the

temporal derivative in younger participants (implying reduced peak latency; Stefanova et al., 2013). There are also non-significant results (Grinband et al., 2017) as well as contradictory evidence of the opposite effect (specifically within the calcarine cortex; Huettel et al., 2001), but these are potentially attributable to small sample sizes (West et al., 2019). Performance differences may also account for some of this latency variation, for example grip force has been associated with peak latency and magnitude of the BOLD signal (Peck et al., 2001; Sulzer et al., 2011) and beyond 40 years grip strength decreases with advancing age (Kallman et al., 1990). Therefore it must be remembered that age-related changes in timing parameters such as peak latency may be at least partially attributed to group differences in the behavioural, rather than the neurovascular response. Changes in dispersion of the HRF primary peak are less clear, West et al. (2019) finding none that survived correction, and Stefanova et al. (2013) finding dispersion derivative weightings which increased with age, implying reductions in dispersion. However, when linearly combining the functions comprising the HRFtd model the beta weightings are dependent upon one another, and so are not necessarily a reliable proxy for timing properties. For example, previous work by Danvers et al. (2021) has shown that a reduction in dispersion is indeed associated with positive weighting of the dispersion derivative. However when both peak latency and dispersion are low the dispersion derivative shows a negative weighting. Therefore conclusions cannot be clearly drawn from these parameter estimates alone, and it is surmised that if peak latency is shown to vary it remains plausible that this will be accompanied by changes in dispersion.

To summarise, any systematic age-related changes in timing properties such as peak latency or FWHM have the potential to produce results that vary dependent upon the modelling approach. For example there is evidence that peak latency increases with age but

is lower than that modelled using the HRFc model (Richter & Richter, 2003; Taoka et al., 1998; West et al., 2019). As the peak latency of the HRF increasingly conforms to the assumptions of the HRFc model, this inflexible modelling approach may provide a better fit with increasing age, artificially biasing results in favour of elderly participants. Therefore application of flexible models should result in a relative increase in the number of significant voxels within young relative to elderly age groups. As Danvers et al. (2021) found that the HRFtd approach better modelled HRFs with low peak latency and FWHM, this effect may be stronger using the HRFtd model relative to the Fourier set. Testing these modelling approaches in a systematic manner may help the field in interpreting data and making informed comparisons between studies using different approaches. Therefore results could inform prospectively in terms of study design, as well as retrospectively when examining the literature. The investigation below is not designed to pass comment upon whether age-effects provide any meaningful insight into performance or neuronal activity, but to ascertain how best to model existing variability in the signal, the causes of which remain open to debate.

Here, we used the CamCAN dataset (Taylor et al., 2017) with 500+ participants, all of whom executed the same sensorimotor task (visual, auditory, motor, and cognitive demands) in an event-related design. This dataset was optimised for testing such questions as it covers the typical adult age-range, included only healthy participants, and used timings optimised for estimating the HRF (with stimulus onset asynchrony varying between 2-26s; Shafto et al., 2014).

Hypothesis 1: Across GM there will be a significant increase in peak latency with increasing age when using both the HRFtd and the Fourier basis set. There will be a

significant age x mHRF interaction driven by the effect being stronger using the HRFtd model, due to it being better to able to model HRFs with low timing properties.

Hypothesis 2: There will be an effect of age upon FWHM. If found, there will be a significant age x mHRF interaction driven by the effect being strongest using the HRFtd set. This was justified based upon FWHM generally being lower than assumed by the HRFc model which was better modelled using the HRFtd approach (Danvers et al., 2021).

Hypothesis 3: If significant age effects are identified, it is predicted the ratio between the youngest three age groups (N = 232) and oldest three age groups (N = 237) regarding total number of significant voxels within GM, will be smallest using the HRFc model, and greatest using the HRFtd model. This is based upon the HRFc model (and the Fourier set to a lesser degree) being less able to model lower peak latency typical within younger participants.

4.2. Methods

All scripts are available on https://github.com/mdanve01/Project2.

4.2.1. Participants

Participants were randomly selected from the Cambridge City area using listings from the Primary Care Trust, excluding those residing at the University during term-time only, or deemed unsuitable by their general practitioner (GP). Six-hundred and fifty-six (aged 18-87 years) were cleared by their GP for MRI scanning, and gave informed consent. Exclusions were based upon MRI contraindications, serious medical/psychiatric conditions, current or historical drug abuse, inability to walk 10 metres, inability to hear a 35db tone at 1000Hz in either ear, not a native English speaker, corrected vision below 20/100, or cognitive impairment (Mini-Mental State Examination score below 25). Handedness was

8

assessed using the Edinburgh Handedness Inventory. Recruitment aimed to achieve an approximately uniform age distribution and an equal sex split within each decade. Five hundred and fifty-eight participants were included, with 11 removed due to missing/unreadable files, and 87 removed due to artefact/head motion. Those aged 18-27 had an N of 44 (24 female), 28-37 had an N of 96 (51 female), 38-47 had an N of 92 (47 female), 48-57 had an N of 89 (46 female), 58-67 had an N of 87 (47 female), 68-77 had an N of 78 (41 female), and 78-88 had an N of 72 (40 female). More detail on participant removal can be found in the 'Pre-Processing Methods' below.

Data collection and sharing for this project was provided by the Cambridge Centre for Ageing and Neuroscience (CamCAN). CamCAN funding was provided by the UK Biotechnology and Biological Sciences Research Council (grant number BB/H008217/1), together with support from the UK Medical Research Council and University of Cambridge, UK. All raw data in the study was collected by the Cam-CAN project and made available from their repository. The text below summarises their approach to recruitment and data collection, however pre-processing, quality analysis and data analysis was carried out by the author. The data and further details can be found at www.mrc-cbu.cam.ac.uk/datasets/camcan/ (Shafto et al., 2014; Taylor et al., 2017). Ethical approval was provided by the Cambridgeshire 2 Research Ethics Committee (ref: 10/H0308/50) and Royal Holloway Ethics Committee (ref: Full-Review-2246-2023-01-05-10-18-UPJT002).

4.2.2. Behavioural Task

Data was acquired using the sensorimotor task (T2* weighted) performed by participants in the camCAN study. This ran for approximately nine minutes, following 25 minutes of structural scanning, nine minutes of resting state fMRI acquisition, and eight minutes of movie watching fMRI acquisition. For this study we used data from the

sensoroimotor task. The task had 129 trials (including one practise trial), in which either both visual and auditory stimuli were presented (120 trials), just auditory (4 trials) or just visual (4 trials). The visual stimulus was a pair of checkerboards presented either side of a centralised fixation cross for 34ms. The auditory stimulus was a 300ms binaural tone varying in frequency pseudorandomly (300, 600 and 1200Hz, 40 trials of each). During bimodal trials auditory and visual onsets occurred simultaneously. Participants were instructed to press a button with their right index finger upon seeing or hearing a stimulus. An event-related design was employed in order to estimate the shape of task-specific HRFs. To maximise the effectiveness of this approach event onsets were maximally uncorrelated using an m-sequence (length = 255; m = 2; stimulus onset asynchrony ranging between two and 26 seconds) and stimulus onset jittered across 0.1-0.3 seconds (Buracas & Boynton, 2002; Shafto et al., 2014).

4.2.3. MRI Data Acquisition

Scanning was carried out using a 3T Siemens TIM Trio with 32-channel head coil, located at the MRC-CBSU with memory foam cushions positioned either side of the head to minimise movement. A custom button-box recorded motor responses, auditory stimuli were presented through MR compatible etymotics headphones, and visual stimuli were projected onto a screen viewable through a head-coil mounted mirror. Structural images were acquired using a Magnetization Prepared Rapid Gradient Echo sequence, with a repetition time (TR) of 2250ms, echo time (TE) of 2.99ms, field of view (FOV) of 256 x 240 x 192mm and total duration of 272secs. Resolution = 1mm, GRAPPA acceleration factor = 2, inversion time (TI) = 900ms and flip angle = 9 degrees. Functional scans were T2* weighted with a Gradient-Echo Echo-Planar Imaging sequence, a TR of 1970ms, TE of 30ms, FOV of 192 x 192mm, total duration of 520 secs, flip angle of 78° and voxel size of 3 x 3 x 4.44mm. There were 261

volumes comprised of 32 descending axial slices (thickness = 3.7mm; interslice gap = 20%)

covering the whole brain inclusive of the cerebellum.

4.2.4. Pre-Processing Methods

EPI images were realigned to the mean and unwarped using field maps. The

anatomical (T1) image was co-registered to the mean unwarped EPI image using estimation

only (Ashburner et al., 2020). The T1 image was then segmented using the MNI tissue

probability map (TPM) and Dartel imported tissue class images were formed for grey matter

(GM) and white matter (WM). Realigned and unwarped EPI images were affine-registered to

MNI space, normalised, and smoothed with an 8mm full-width half-maximum (FWHM)

gaussian kernel. Pre-processing was carried out using the SPM batch editor and Dartel

normalisation was used as it is thought to be more effective than standard non-linear SPM

normalisation (Klein et al., 2009).

For quality assurance, T1, mean unwarped/coregistered EPI and pre-unwarped 1st

EPI images were compared using the 'check-reg' function in SPM12. Outliers were

subjectively identified if images were co-registered incorrectly, were distorted, or had slices

missing (totalling 33). Cases in which there was excessive head motion (movement beyond

2.5mm/1 degree, or movement between consecutive scans exceeding 1.5mm/0.5 degrees)

were also classified as outliers. Thresholds were deemed appropriate as they are below the

voxel size (Ashburner et al., 2020, p. 259; Wylie et al., 2014) with those in excess of one

degree deemed large (Ashburner et al., 2020, p. 35). Eighteen outliers were identified, four

of which were excluded in the previous step.

EPI signal was quantitatively investigated within each individual participant, based

upon mean intra-slice signal (MISS) within each scan (32 slices x 261 scans). Post-

segmentation/pre-normalisation the signal amplitude range was calculated across scans

within each slice (temporal range), and across slices within each scan (spatial range), the maximum value was selected for each measure, for each participant. This was repeated for individual 'shifts', calculating the maximum change over two consecutive scans within a slice (checking for sudden change over time – temporal shift), and over two consecutive slices within a scan (checking for sudden change over space – spatial shift). Coefficients of variation (COV) were also used as a measure of variability. Checking for change over time the standard deviation (SD) across scans was divided by the mean of all scans, for each slice then the maximum value selected (temporal COV). This was repeated examining variability across slices within each scan (spatial COV). Outliers were defined as scores beyond 2.5 SDs above the group mean. A total of 34 outliers were identified, 18 of which were already identified by realignment parameter/co-registration checks.

After normalisation, a randomly selected normalised scan from each participant was displayed alongside the MNI template brain using the SPM12 'check reg' function, and manually checked for correspondence. Nine cases were found to have excessive signal drop-out, distortion, and mis-alignment. Two further cases were identified during statistical analysis (see below) as having no significant voxels. The 1st-level analyses were then run using the HRFc model, generating masks. The number of voxels containing signal were calculated for each participant, identifying two outliers with no signal (as expected based upon the above) and these were immediately removed. Next each participant's mask was compared to a group-level standardised mask, created as the mode of all participant's binary masks at each coordinate (meaning if the majority of participants had signal at coordinate x,y,z then a one was assigned, if not a zero was assigned). This found 15 outliers with a number of coordinates which did not match the standardised mask exceeding 2.5SDs. Good registration between the image with the fewest mismatched coordinates (and therefore the

most representative of the standardised mask) and the MNI brain was confirmed. A new Dartel template was created and normalisation carried out, the worst fit deemed acceptable subjectively. This resulted in 558 usable participants.

4.2.5. Design

fMRI 1st-level Experimental Design: In order to identify coordinates in which significance was found within individuals the general linear model (GLM) was employed using a full factorial analysis. The within-participant 'stimulus' independent variable (IV) had five levels. Three of these were bimodal events (auditory tone and visual stimulus presented) each with 40 trials, and split by the tone played (300Hz, 600Hz and 1200Hz). The final two comprised the visual only condition (4 events) and auditory only condition (4 events). Microtime resolution = 16, microtime onset = 8, with a 128 second high-pass filter applied. The same dataset was analysed using three event-related GLMs; the HRFc (1 function), HRFtd (3 functions) and a 3rd order Fourier(Hanning) set (7 functions). The Fourier set modelling strategy was determined by a set of pilots run, aiming to minimise multicollinearity whilst maintaining an adequate window-length. The six head-motion parameters were included as regressors and con images were generated for each function across all conditions. As a result the HRFc GLM totalled 11 regressors, the HRFtd GLM 21 regressors, and the Fourier GLM 41 regressors (plus intercept). Sampling over the peri-stimulus time period was checked to ensure the temporal jitter had been effective, and was subjectively deemed to be sufficient.

fMRI 2nd-level Experimental Design: In order to establish consistent activations across the sample at which the HRF could be investigated (hypotheses 1 and 2), and to determine the number of significant voxels with each modelling approach (hypothesis 3), three 2nd-level analyses were conducted. In each, a full factorial age group (7) x number-of-

functions (one for HRFc, three for HRFtd set, seven for Fourier set) design matrix was created using contrast images from the 300hz bimodal condition, levels of the age IV being 18-27, 28-37, 38-47, 48-57, 58-67, 68-77, and 78-88 years. Only the bimodal 300hz condition was examined as, **a)** effect of auditory pitch was not a variable of interest, **b)** processing limitations precluded a full analysis of multiple stimulus conditions, **c)** age-related hearing loss (presbycusis) begins in the higher frequencies meaning 300Hz should be least affected (Huang & Tang, 2010), and **d)** there were a sufficient number of trials. Sphericity was not assumed (variance = unequal) for all IVs, and only the age IV was classed as independent. All analyses were corrected for multiple comparisons using the family-wise-error rate (FWE), α = 0.05. F contrasts were then run across groups of basis functions for conditions of interest, within each age group, to test for effects explained by linear combinations of basis functions.

4.2.6. Statistical Analysis

In order to address hypotheses 1 and 2 characteristics of the HRF were estimated then plotted by multiplying each basis function in the 1st-level analysis by it's corresponding 2nd-level beta value. The resulting functions were then summed to form a single function, reflecting a response that was representative of each age-group's mHRF. This was then divided by the mean baseline within each respective age group at that voxel, and multiplied by 100 (to create percentage signal change). Only voxels significant in the HRFc analysis were included, potentially increasing type two error rates as extreme non-canonicality was less likely to be found. However this approach has the advantage of allowing differentiation between PBRs and NBRs in a consistent manner. If the HRFc beta value was negative the mHRF was classed as an NBR, and vice versa, with this positive/negative allocation extended to flexible mHRFs within the same coordinates. Although this approach could be applied to

voxels in which flexible models found significance and HRFc did not (as HRFc beta values were still available), these were found to provide a poor classification.

For responses derived from flexible models peaks with a prominence at least 25% of their magnitude were ascertained using the 'findpeaks' Matlab command. For PBRs the primary peak was determined to be the greatest magnitude positive peak, for NBRs this was the lowest magnitude negative-going peak. This method agreed with a simple max() or min() function, but additionally returned data on bimodality. For FWHM the 'findpeaks' function was set to use 'halfheight', therefore determining the half height position between 0 and peak rather than between e.g. minimum and peak. This was chosen as it should remove any influence of the undershoot amplitude upon the FWHM. FWHM values were truly continuous but peak latency was comprised of discrete time-points. The HRFtd set had a 32.0125 second window divided into 260 discrete time-points, the Fourier set had an 18 second window divided into 147 time-points, introducing minor binning differences.

Comparisons of timing properties between age groups looked only at voxels significant across all age groups and all mHRFs. This was due to the risk that voxel position (via slice-timing or inter-regional variability) may artificially introduce variability in parameters of interest, incorrectly attributed to age. Analysis was carried out using Matlab 2019a, SPM12, and FSL run on a Red Hat Enterprise Linux Server version 7.9 (Maipo), and IBM SPSS version 25.

4.2.7. Declaration

It was realised post-analysis that the EPI readout time (ERT) used when unwarping via field maps was set to 32.1303ms which corresponds to the FSL definition; (number of echoes-1) x effective echo spacing, instead of the SPM definition; number of echos x effective echo spacing, which results in 32.6403ms. It was decided that this is a marginal

difference (1.59% increase from FSL to SPM) which is unlikely to negatively impact the unwarping process, but to check this 40 random participants (median age = 48.5, ranging from 18-77) were selected and unwarping carried out using both the SPM and FSL defined ERTs. The mean unwarped image was then loaded for each ERT definition, the difference in signal calculated at each coordinate and where there was a difference the absolute difference value and maximum absolute signal value (whichever was higher between SPM and FSL ERT derived unwarped images) were saved. For each participant the median difference value across the brain was divided by the median signal value across the brain and multiplied by 100 to ascertain percentage peak amplitude differences relative to signal. Across participants the median percentage difference value was 0.29%, ranging from 0.05% to 0.80%. There was no significant correlation with age; $r(38) = -.126$, $p = .439$, or brain volume; $r(38) = .162$, $p = .318$. As the ERTs were only marginally different, differences in the resulting unwarped images were relatively small, and unwarping (not a mandatory process) still restored signal that was distorted, it was decided that the FSL defined ERT was suitable.

4.3. Results

Every voxel across the brain with greater than 0.5 probability of being GM as per the tissue probability map (and in which all three modelling approaches identified significance within every age group) was selected (N = 23841 voxels). All of these were deemed to be positive HRFs. This included areas such as the inferior parietal lobule, postcentral gyrus, calcarine sulcus, lingual gyrus, cingulate gyrus, superior frontal gyrus, lateral sulcus, superior temporal sulcus, and cerebellar lobules I-VI, see Figures 2 and 3. The mean HRF across all activated voxels from every participant was calculated for each age group, see Figure 1.
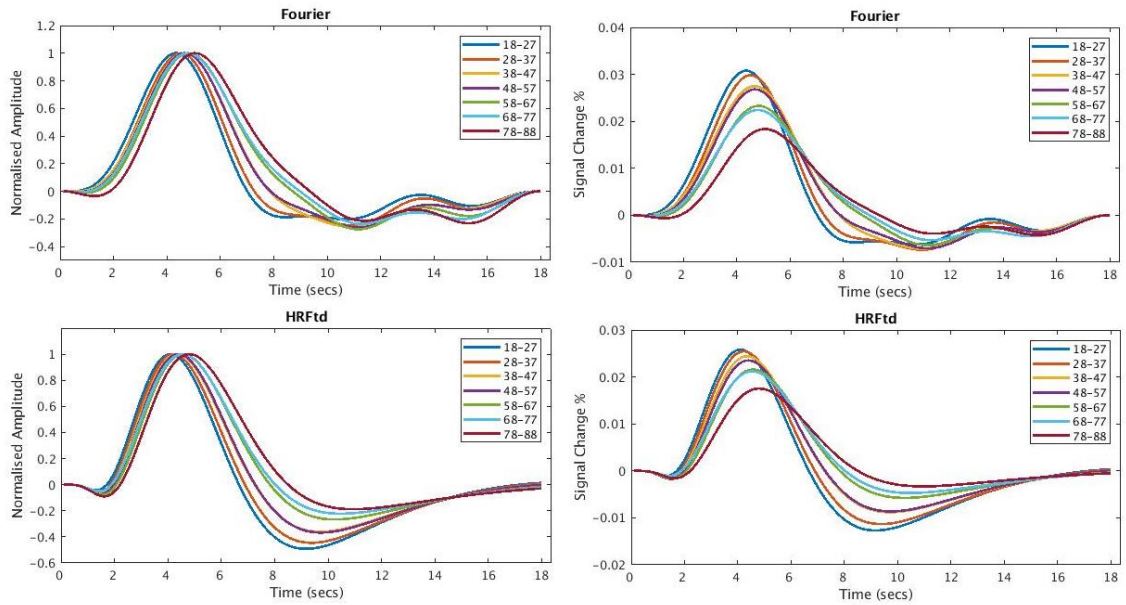
Figure 1. The mean haemodynamic response function for each age group, plotted separately for each flexible model, and showing magnitude changes over peri-stimulus time. The y axis is normalised (left) and showing percentage signal change (right).

4.3.1. Peak Latency

Peak latencies were calculated from each activated voxel, and an age x flexible mHRF (7x2) mixed ANOVA was conducted. This found a significant main effect of mHRF driven by greater peak latency in the Fourier relative to the HRFtd condition, $F(1,166880) = 1491124.538$, $p<.001$, with a large effect size (partial $\eta^2 = 0.899$). There was also a significant main effect of age (homogeneity of variance not assumed) generally driven by greater peak latency with increasing age, $F(6,166880) = 13990.807$, $p<.001$, with a large effect size (partial $\eta^2 = 0.335$), and a significant age x mHRF interaction, $F(6,166880) = 3337.394$, $p<.001$, with a moderate effect size (partial $\eta^2 = 0.107$). An independent one-way ANOVA (homogeneity of variance not assumed) for the Fourier condition found the main effect of age to be significant, $F(6,166880) = 12710.258$, $p<.001$ ($\eta^2 = 0.314$), as did a second for the HRFtd condition, $F(6,166880) = 14966.557$, $p<.001$ ($\eta^2 = 0.350$). All age-group differences

17

were found to be significant with a Bonferroni correction. See Figure 2 for activations

overlaid onto the MNI brain, Figure 4a for the plotted means, and Table 1 for descriptive

statistics. Peak latency was greater in age group seven than age group one in 99.72% (HRFtd)

and 99.56% (Fourier) of significant coordinates, with instances where this was not the case

generally seen in the visual cortex and deep in the horizontal fissure. Further checks were

run with paired t-tests comparing mHRFs in each age group, with effect sizes generally

decreasing with age, see Table 2. These remained significant with a Bonferroni corrected

threshold (α = .007). Analyses were re-run with outliers removed (scores beyond +/-3SDs)

totalling 1050 (0.63%), meaning voxels analysed were not entirely consistent across age

groups. There was no change in the trend of significant main effects or interactions,

therefore the original data was used.
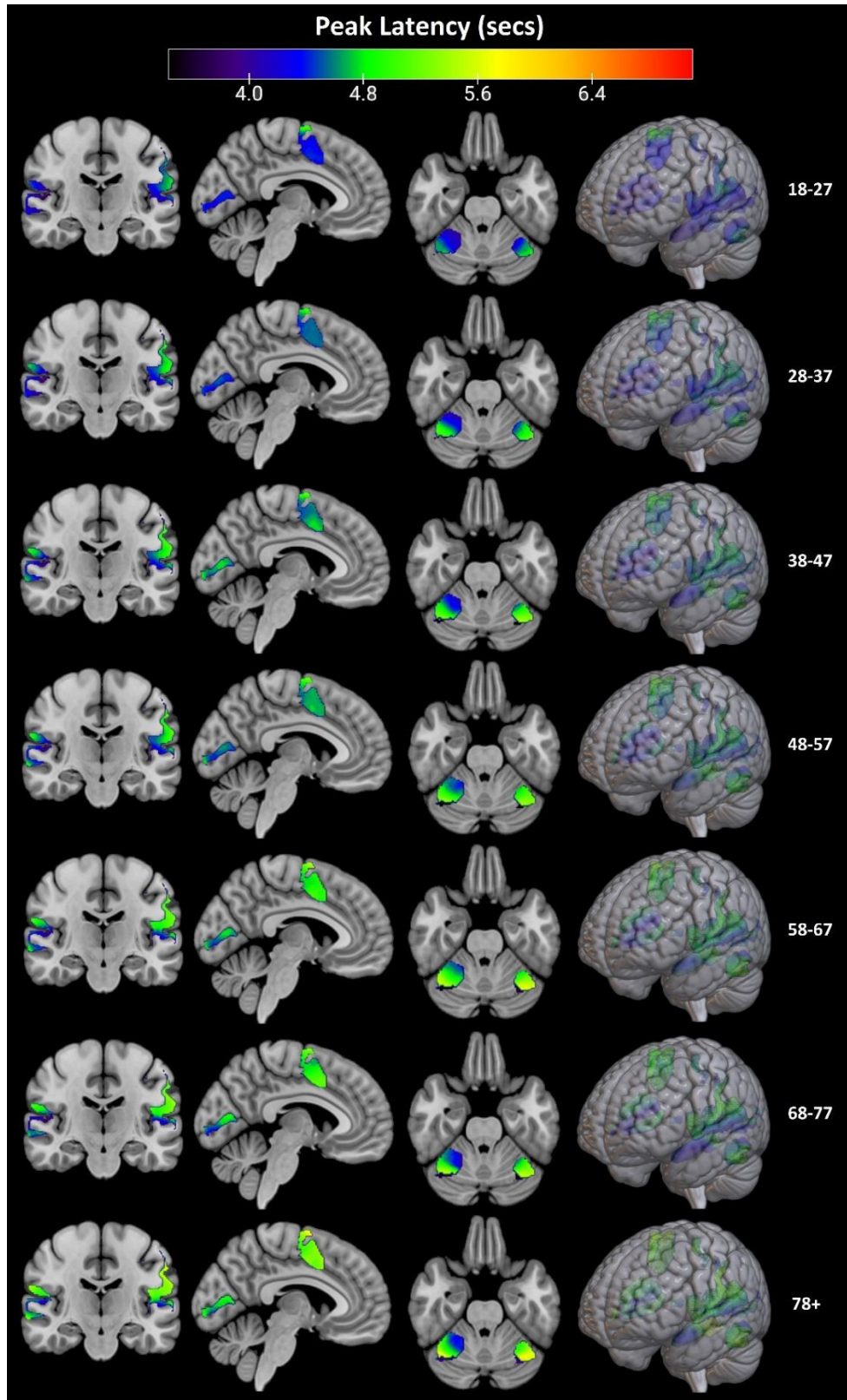
Figure 2. Peak latency for all selected coordinates overlaid upon the MNI brain, within each age group. Measures were taken using the Fourier basis set.

4.3.2. FWHM

An age x flexible mHRF (7x2) mixed ANOVA found a significant main effect of mHRF driven by greater FWHM in the Fourier relative to the HRFtd condition, $F(1,166880) = 257964.425$, p<.001, with a large effect size (partial $\eta^2 = 0.607$). There was also a significant main effect of age (homogeneity of variance not assumed) generally driven by greater FWHM with increasing age, $F(6,166880) = 11512.781$, p<.001, with a large effect size (partial $\eta^2 = 0.293$), and a significant age x mHRF interaction, $F(6,166880) = 2386.762$, p<.001, with a moderate effect size (partial $\eta^2 = 0.079$). An independent one-way ANOVA (homogeneity of variance not assumed) for the Fourier condition found a main effect of age, $F(6,166880) = 8823.53$, p<.001 ($\eta^2 = 0.241$), as did a second for the HRFtd condition, $F(6,166880) = 13956.255$, p<.001 ($\eta^2 = 0.334$). All age-group differences were significant with a Bonferroni correction. See Figure 3 for activations overlaid onto the MNI brain, Figure 4b for the plotted means, and Table 1 for descriptive statistics. FWHM was greater in age group seven than age group one in 96.33% (HRFtd) and 85.78% (Fourier) of significant coordinates, with instances where this was not the case generally seen in the visual cortex, IFG, and paracingulate gyrus. Further checks were run with paired t-tests comparing mHRFs in each age group, with effect sizes generally decreasing with age, see Table 2. These remained significant with a Bonferroni corrected threshold ($\alpha = .007$). Analyses were re-run with outliers removed (scores beyond +/-3SDs) totalling 2120 (1.27%). There was no change in the trend of significant main effects or interactions, therefore the original data was used.
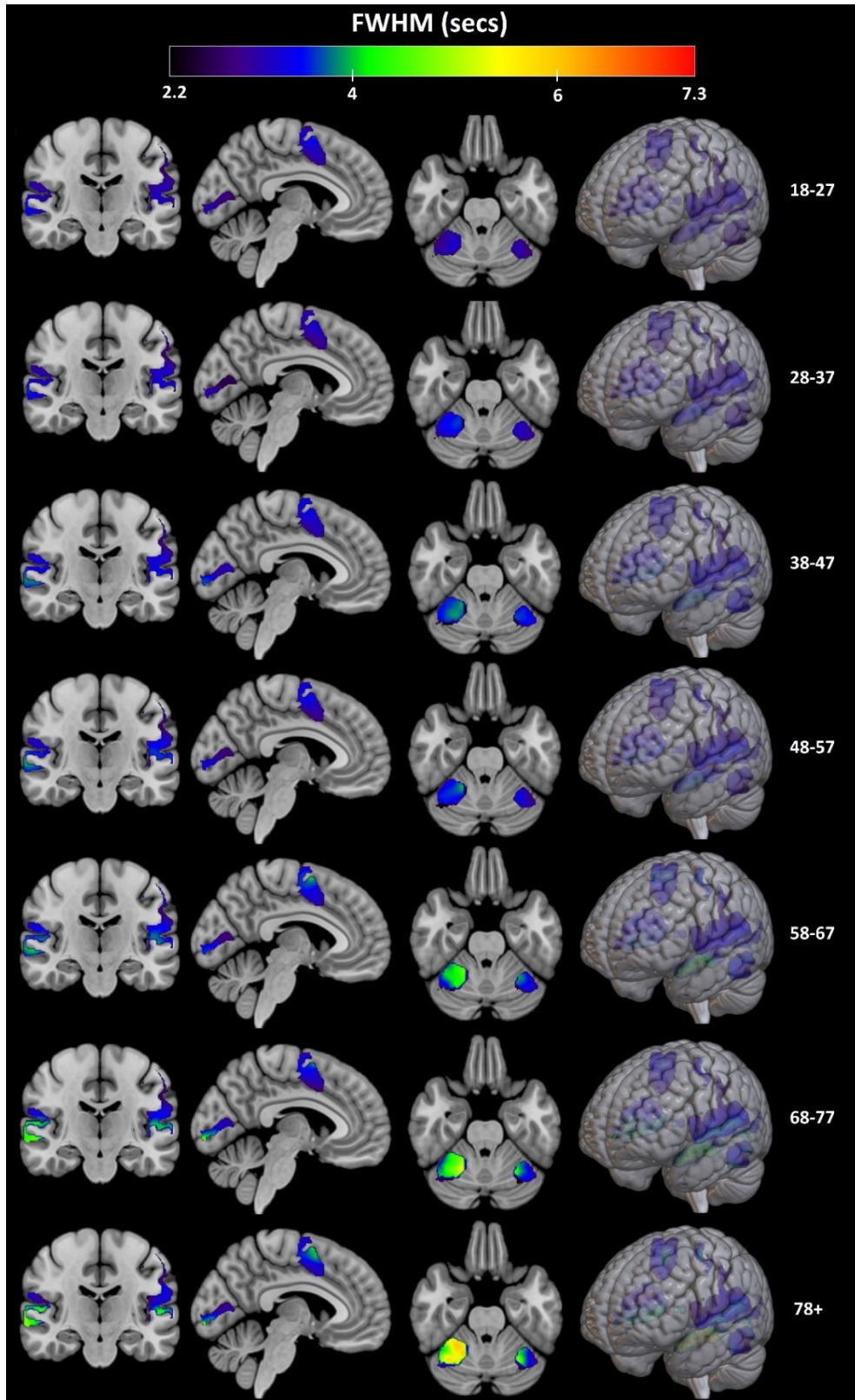
Figure 3. FWHM for all selected coordinates overlaid upon the MNI brain, within each age group. Measures were taken using the Fourier basis set.

4.3.3. Undershoot Amplitude

Following on from the data in Figure 1 the undershoot amplitude was calculated as a percentage of the peak amplitude. This was defined as the minimum value (after the primary peak) below zero on the y axis (the 'findpeaks' MATLAB function was not used as bimodality was not investigated). Twenty-one GM voxels failed to show an undershoot crossing zero into a negative value, and so were removed across models and age-groups.

An age x flexible mHRF (7x2) mixed ANOVA found a significant main effect of mHRF driven by greater undershoot amplitude in the HRFtd relative to the Fourier condition, $F(1,166712) = 151105.948$, p<.001, with a large effect size (partial $\eta^2 = 0.475$). There was also a significant main effect of age (homogeneity of variance not assumed) driven by reduced undershoot amplitude with increasing age, $F(6,166712) = 4411.232$, p<.001, with a moderate effect size (partial $\eta^2 = 0.137$). Finally a significant age x mHRF interaction was found, $F(6,166712) = 41628.797$, p<.001, with a large effect size (partial $\eta^2 = 0.600$), driven by the HRFtd condition having a greater relative amplitude in younger participants. An independent one-way ANOVA (homogeneity of variance not assumed) for the Fourier condition found a main effect of age whereby amplitude generally increased with age (barring a slight plateau and drop from 58 years onwards), $F(6,166712) = 358.309$, p<.001, but with a small effect size ($\eta^2 = 0.013$). Another was run for the HRFtd condition (homogeneity of variance not assumed) finding amplitude generally decreased with increasing age, $F(6,166712) = 15635.033$, p<.001 ($\eta^2 = 0.360$). All age-group differences (within each model) were significant with a Bonferroni correction barring 28-37 versus 38-47 in the Fourier condition, see Figure 4c and Table 1. Crucially all mean amplitudes were higher than predicted by HRFc, which assumed an undershoot amplitude 8.89% of the primary peak. This was further checked with paired t-tests comparing mHRFs in each age group, with effect sizes generally

22

decreasing with age, see Table 2. These were significant in all age groups except the 58-68 year olds, and survived a Bonferroni corrected threshold (α = .007). Analyses were re-run with outliers removed (scores beyond +/-3SDs) totalling 2408 (1.44%). There was no change in the trend of significant main effects or interactions, therefore the original data was used.
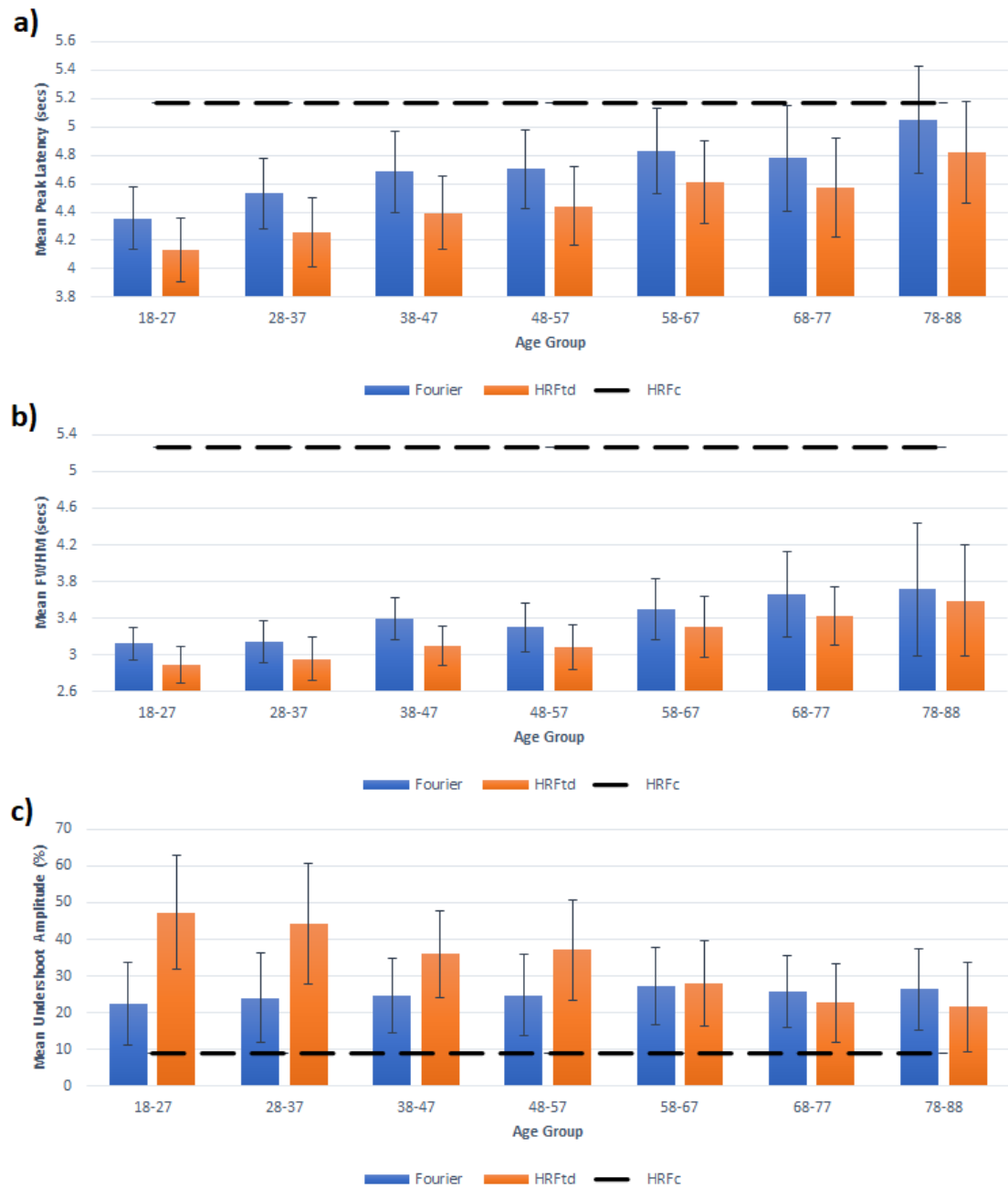
Figure 4. Bar charts showing effects of both age and choice of flexible model upon **a)** peak latency, **b)** FWHM, and **c)** undershoot amplitude (expressed as a percentage of primary peak

amplitude). Error bars denote 1SD. Dotted black lines represent the assumed value of each

measure as per the HRFc model.

Table 1. Descriptive statistics across mHRFs, parameters of interest, and age-groups.

Age	Fourier						HRFtd					
	PL (secs)		FWHM (secs)		US amplitude (%)		PL (secs)		FWHM (secs)		US amplitude (%)	
	Mean	SD	Mean	SD	Mean	SD	Mean	SD	Mean	SD	Mean	SD
18-27	4.36	0.22	3.13	0.18	24.68	12.04	4.13	0.23	2.89	0.2	51.47	16.46
28-37	4.53	0.25	3.14	0.23	26.15	13.05	4.26	0.25	2.96	0.23	47.54	17.91
38-47	4.69	0.29	3.4	0.23	26.28	10.67	4.4	0.26	3.11	0.21	37.86	12.36
48-57	4.7	0.28	3.3	0.26	26.61	11.65	4.44	0.27	3.09	0.24	39.26	14.57
58-67	4.83	0.3	3.5	0.33	29.13	11.11	4.61	0.29	3.31	0.34	29.13	12.24
68-77	4.78	0.37	3.66	0.47	27.22	10.35	4.57	0.35	3.43	0.32	23.74	10.93
78-88	5.05	0.38	3.72	0.72	27.87	11.46	4.82	0.36	3.59	0.61	22.15	12.38

Table 2. T Statistics and Associated Effect sizes (Cohen's *d*) for all mHRF Pairwise

Comparisons.

Age	PL			FWHM			US amplitude		
	t	p	*d*	t	p	*d*	t	p	*d*
18-27	557.439	<.001	3.61	342.901	<.001	2.221	535.06	<.001	3.467
28-37	637.948	<.001	4.132	314.491	<.001	2.037	369.194	<.001	2.392
38-47	609.534	<.001	3.948	397.094	<.001	2.572	219.238	<.001	1.421
48-57	604.635	<.001	3.916	256.19	<.001	1.659	194.333	<.001	1.259
58-67	480.565	<.001	3.112	197.463	<.001	1.279	0.073	.942	0
58-77	342.572	<.001	2.219	151.751	<.001	0.983	48.167	<.001	0.312
78-88	296.031	<.001	1.917	72.386	<.001	0.469	83.882	<.001	0.544

4.3.4. Investigation into the Prevalence of NBRs in Different Age Groups

In Danvers et al. (2021) there was some indication that NBRs may have timing

properties which are typically greater (increased peak latency and FWHM). It is important to

clarify there was also support for this being incidental. However there is evidence of NBRs

being more common with increasing age (Aizenstein et al., 2004), and so it was deemed

prudent to check whether this held true for individuals within the voxels included in the

analysis. If so, this could have introduced a systematic distortion in the shape of the HRF at

the group level as age increased. For each participant the percentage of NBRs was calculated

across all 23841 coordinates, at the 1st-level of analysis, ascertained using the valence of the

HRFc parameter estimates. There was no significant correlation with age, $r(556) = 0.009$, $p =$

.824, suggesting no age-related increase in the prevalence of NBRs within these particular

coordinates.

4.3.5. Undershoot Investigation

Next an investigation was run into why the HRFtd and Fourier basis sets showed

opposing age-related trends in the undershoot amplitude analysis. Generally the HRFtd

model found a negative association with age, the Fourier set finding a positive association. It

was considered that the less flexible HRFtd model may be erroneously exaggerating the

undershoot amplitude. This was tentatively illustrated when looking at peristimulus time

histograms regarding the peak voxel of a randomly chosen single subject from the 18-27

group and another from the 78-88 group. As seen in Figure 5a, the HRFtd model appeared to

overestimate undershoot amplitude in the young participant, but underestimate it in the

elderly. Conversely when using the Fourier set the modelled undershoot amplitude was

approximately correct. The data in Figure 4 clearly demonstrated that with increasing age

peak latency and FWHM increased, sitting closer to the values assumed by the HRFc model.

If with increasing age the canonical function (which forms one of the HRFtd model's three

functions) shows greater relative weighting in order to model HRFs with timing properties

more similar to those assumed by the HRFc model, then it is plausible the undershoot

amplitude will be underestimated in the elderly. This is because the undershoot amplitude of the HRFc model is relatively low (8.89% of the primary peak). It would also imply that younger participants rely more upon the derivatives, which have the capacity to exaggerate undershoot amplitude due to them having fairly high magnitude negative and positive peaks.

Therefore the HRFtd model's reliance upon the canonical function was tested across the same coordinates as in Figure 4. This was done by summing the absolute beta values for the three functions comprising the HRFtd model, then calculating the percentage contribution of the canonical function's absolute beta value; (canonical beta / (canonical beta + temporal derivative beta + dispersion derivative beta)) x 100. There was a significant increase with increasing age, $F(6,166718) = 22511.696$, $p<.001$, and a large effect size ($\eta^2 = 0.448$). Every age group showed a Bonferroni corrected significant difference except 38-47 versus 48-57, see Figure 5b. Homogeneity of variance could not be assumed, and 626 datapoints (0.38%) exceeded 3SDs, a re-run with outliers removed finding the same effects.
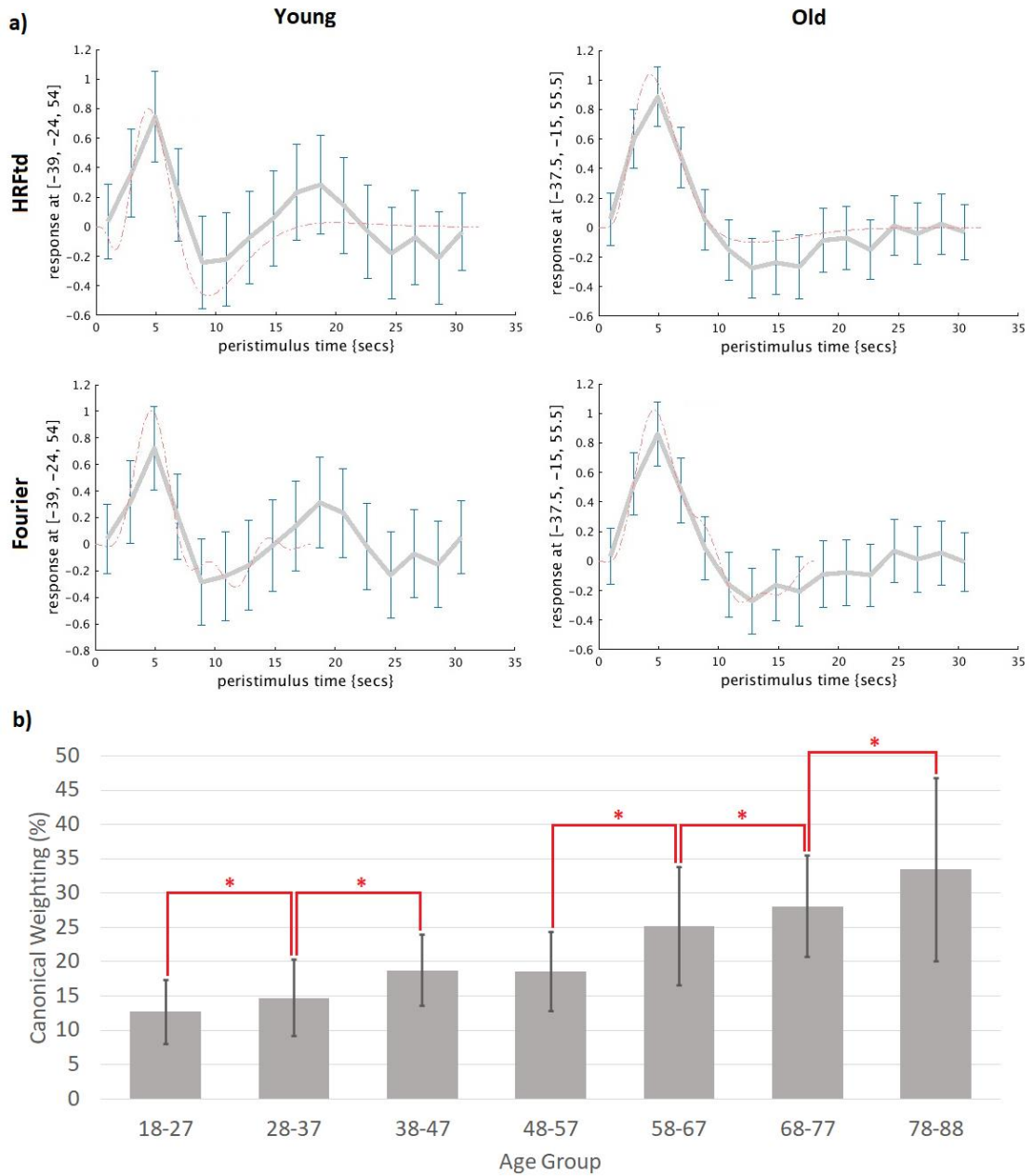
Figure 5. a) Peristimulus time histograms showing the peak voxel of a randomly selected 18-27 participant, and a randomly selected 78-88 participant. The dotted red line denotes signal as estimated using both the HRFtd and Fourier basis sets. b) Bar chart showing the average percentage canonical function weighting across each age group. Error bars denote 1SD, asterisks denote a significant difference.

4.3.6. Number of Voxels Analysis

The number of significant voxels within GM (probability > 0.5) was investigated for each mHRF. This was run to check whether age groups differed regarding the number of significant voxels (D'esposito et al., 1999). It was recognised that a comparison of age groups was fraught with complication, just one example being differing sample sizes. Hence the focus was on checking how the ratio between age groups differed across modelling approaches, thus keeping extraneous factors consistent. Overall there was a trend of more significant voxels being found within flexible models relative to the HRFc approach, and more within the HRFtd model relative to the Fourier set, across age groups, see Table 3. Interestingly, when the three youngest and three oldest age groups were summed, the HRFc model was the only approach which found more significant voxels in 58-88 year olds relative to 18-47 year olds. Flexible mHRFs found the opposite effect, but with the Fourier set having a marginally larger ratio relative to the HRFtd model. Additionally the ratio between fixed and flexible models calculated within each age group generally increased across age groups, suggesting that flexible modelling was less beneficial with increasing age.

Table 3. The number of significant voxels residing within grey matter for each age group, alongside the summed number of significant voxels identified by young groups (18-47) relative to elderly groups (58-88), the relation expressed as a ratio. Additionally the ratios across models were included within each age group, as was the sample size.

Age	HRFc	HRFtd	Fourier	HRFC:HRFtd	HRFc:Fourier	HRFtd:Fourier	N
18-27	28607	109476	96468	0.261	0.297	1.135	44
28-37	62928	143907	133283	0.437	0.472	1.080	96
38-47	68026	132986	125380	0.512	0.543	1.061	92
48-57	68260	141705	125779	0.482	0.543	1.127	89
58-67	82582	146219	137267	0.565	0.602	1.065	87
68-77	69573	114533	106249	0.607	0.655	1.078	78
78-88	56150	84327	70546	0.666	0.796	1.195	72
Age18-47	159561	386369	355131	NA	NA	NA	232
Age58-88	208305	345079	314062	NA	NA	NA	237
Ratio (y:o)	0.766	1.120	1.131	NA	NA	NA	0.979

4.4. Discussion

4.4.1. Hypotheses

In summary, participants demonstrated a trend of increased peak latency and FWHM with increasing age, yet these parameters remained predominately below those assumed by the HRFc model (in keeping with Richter & Richter, 2003; Stefanova et al., 2013; Taoka et al 1998; West et al., 2019). There was also a main effect of mHRF, the Fourier basis set consistently finding greater peak latency and FWHM, consistent with previous work by this paper's author. Age interacted with the modelling approach for both peak latency and FWHM, follow up one-way ANOVAs finding a stronger effect of age using the HRFtd model relative to the Fourier set (measured via F and η^2 values). This was confirmed when looking

at model comparisons within each age group, the effect diminishing within older groups (measured via t and *d* values). Assuming models are unlikely to underestimate timing properties such as peak latency and dispersion, this implied the Fourier set may be less successful when modelling HRFs in which these properties are reduced. Therefore for Hypotheses 1 and 2 the null hypothesis can be rejected, with the HRFtd approach appearing to better model the range of signal across age groups, potentially attributed to an increased ability to model HRFs in which timing properties are low. It was further identified that when using the HRFc approach, older participants actually demonstrated more significant voxels relative to young, which was attributed to the timing of HRFs being more closely matched with that of the HRFc model. However when using flexible models more significant voxels were identified in younger relative to older participants (as identified by D'Esposito et al., 1999), this relative difference marginally higher using the Fourier set. Therefore the null hypothesis for Hypothesis 3 can be rejected regarding flexible vs inflexible differences, but this being highest using the Fourier set was not predicted. It is cautiously suggested though that this difference is so small and inconsistent across age as to be fairly inconsequential.

4.4.2. Overview

Due to the data in Figure 1 the undershoot amplitude was examined post-hoc, with it noted that even the lowest group-level amplitude (22.15%) exceeded that assumed by the HRFc model (8.89%), consistent with Ramnani & Henson (2005). However flexible modelling identified significant age effects and a strong interaction with choice of mHRF (the HRFtd condition steeply decreasing with increasing age, the Fourier condition generally increasing). It is important to understand how the HRFtd set works, a simple explanation being that positive derivative weighting should model a reduction in the relevant parameter, with negative weighting modelling an increase. However in practise the weighting of one function

is always contingent upon the weighting of the other two. The principle behind this approach is that reductions and increases in e.g. peak latency can be accommodated using just one function/regressor. This is an advantage as it maximises available degrees of freedom at the 1st-level of analysis. However reliance upon inversion of the function means each derivative has both positive and negative peaks. Consequently, when modelling HRFs with low peak latency and/or dispersion, increased reliance upon derivatives (and a consequent reduction in reliance upon the canonical function) may exaggerate the undershoot amplitude relative to the primary peak.

This is consistent with the evidence presented of both undershoot exaggeration and a reduced relative weighting of the canonical function in younger participants (the opposite seen for elderly). In order to consider both directions of effect, it is possible systematic change in undershoot amplitude artificially affected estimates of peak latency and FWHM. However as the undershoot reduction was the only age-effect not corroborated using the Fourier set, it is most likely an artefact of the HRFtd model. This suggests that when the HRFtd model is forced to compromise between accurately modelling the primary peak or the undershoot, the primary peak (which presumably carries more signal) is prioritised. Consequently the HRFtd approach appeared to do a better job of modelling HRFs with low peak latency and dispersion (more typical of younger participants). However the Fourier set may have some advantage within this age-group as the undershoot amplitude seemed to be less influenced by timing properties of the primary peak.

As already stated, it is beyond the scope of this study to make inferences about how representative the BOLD signal is of underlying neuronal activity. However as BOLD signal is tied to neurovascular dynamics, evidence of generally increased peak latency and FWHM with increasing age potentially implies a neurovascular origin. Considering the literature,

age-related reductions in primary peak amplitude have been attributed to a lesser reduction in HbR within elderly participants, meaning the high ratio of HbO levels relative to HbR levels (which the fMRI signal is derived from) diminishes with increasing age (Fabiani et al., 2014; Ward et al., 2015). This high ratio is the result of the volume of HbO exceeding the rate of conversion into HbR, assisted by washing-out of HbR via increased cerebral blood flow. Hutchison et al. (2013) found that with increasing age there was increased metabolism of HbO with no corresponding increase in blood flow. This suggested the age-related reduced ratio was driven by increased neural activity (consistent with findings of firing rates increasing with age; Dickstein et al., 2007) without adequate compensatory vasodilation, despite evidence of the baseline metabolism being lower in the elderly (De Vis et al., 2015).

Increased neuronal activity without corresponding increases in blood flow is consistent with reduced peak amplitude of the BOLD signal, but whether it would result in a more dispersed HRF with a delayed peak remains unclear. However, using MEG data from the CamCAN dataset Price et al. (2017) identified age-related delays in electrical activity within the visual cortex, attributed to slowing of information transfer and associating with WM volume (potentially delaying peak latency). Additionally delays were evidenced within the auditory cortex which accumulated over the response and associated with GM volume (which may increase both peak latency and dispersion). These effects could trigger a delayed and/or prolonged period of vasodilation, which could theoretically have a later and/or more dispersed primary peak. It remains unclear however, whether the degree of the delay at the neuronal level could be expected to result in the relatively large delay in the BOLD response, and so requires further empirical investigation. Given that the delays found using the BOLD signal are likely to exceed that of the neural response, it is probable that the assumption of time-invariance is not met (a delay in neural should equal a delay in BOLD; Poldrack et al.,

2011, pp. 72-73) and so the age-equivalence assumption cannot be supported. For the purposes of this paper it is interesting but arguably not necessary to discover why the HRF of the elderly demonstrates different timing properties to that of the young. The focus instead is upon how and to what degree this difference presents, and how different modelling approaches can be employed to prevent false conclusions when handling datasets from different age groups.

4.4.3. Limitations

A practical limitation of this study is that more elderly subjects were removed (due to head motion and artefacts) than younger subjects, alongside the existing reduced N of the 18-27 age group. Bootstrapping was considered, however with such a large N the computational cost rendered this impractical. It was decided to proceed despite this, as leaving outliers in the analysis meant with increasing age there would be increasingly noisy data, which was deemed a less controlled source of variation than the more easily quantified change in sample size. This was unlikely to explain the effects found, which generally changed over age rather than in line with group sizes. A good example of this was variability of peak latency and FWHM was actually lowest in the youngest age group, which also had the smallest N. Also when comparing the number of significant voxels the three youngest and three eldest age-groups were summed in such a way as to approximately balance out the differences in sample sizes. Furthermore, between-model ratios calculated within age groups showed trends across age that were inconsistent with sample sizes.

When investigating peak latency and FWHM across age groups there was inhomogeneity of variance. Both timing properties demonstrated more variability across the brain within elderly participants, meaning results must be interpreted cautiously. This suggested that some brain regions showed age related increases in peak latency and FWHM,

but others did not. It was checked how many instances there were of the opposite trend (the eldest group having equal to or lower peak latency/FWHM than the youngest) with this found in 0.28-14.22% of coordinates (analysis dependent). It is also possible that this heteroscedasticity could be related to findings of increased inter-subject variability within elderly cohorts at the neuropsychological level (Woodruff-Pak, 1997, pp. 27). However this would hinge upon the assumption that a 'youthful' haemodynamic response associates with preserved performance, and so would need further investigation. It would also be a poor explanation of regional variability, more likely to instead result in a coordinate not being significant at the 2nd-level of analysis. That inferential statistics were run on data pertaining to voxels rather than participants (despite voxels not necessarily being completely independent of one another due to smoothing and the potential for shared contributions to BOLD signal) was another compromise made (increasing the chance of false positives). This was accepted as it allowed for a voxel-wide investigation at the group level, the results were approximately consistent with the number-of-voxels analysis which did not share in this compromise, and even without inferential statistics there were clear trends in the data. Additionally, both the sample size (pertaining to number of voxels) and the location of those voxels were equal between models and age groups. Therefore any differences in effect size when comparing models across age groups utilised the same N and so controlled for any inflation in the number of coordinates included in the analysis, as well as any effect of non-independence.

The HRFs investigated were constrained, both by use of the HRFc model to differentiate positive and negative HRFs, and by the task itself, however this still produced a large spread of activity across multiple core regions. Slice-timing correction was also not applied, which theoretically would negatively affect the canonical model's ability to detect

signal more than it would flexible models. As the primary focus was on flexible modelling

this was deemed acceptable, especially as comparisons were made between age groups at

the same coordinates and so should be fairly unaffected by slice-timing effects. Additionally,

in the number-of-voxels investigation comparisons were made between age groups within

each model, with no evidence to suggest that age groups would be differentially affected by

slice-timing. Finally a summary statistic approach was used (Mumford & Nichols, 2006),

deemed acceptable as evidence has shown it produces accurate results (Penny & Holmes,

2007) and the computing power for a single stage hierarchical approach was unavailable.

Future work could extend this analysis to different tasks, perhaps targeting specific

regions or varying factors such as stimulus intensity/duration to investigate the modelled

BOLD response. Furthermore checks could be run as to whether assumptions such as

temporal additivity interact with age, which could help inform future task design beyond just

the modelling approach. The study investigated just the two flexible models due to

limitations in time, storage space, and a desire to look closely at two commonly used models

and make direct comparisons. It was also considered that the focus upon just GM may miss

more subtle regional effects, the overall differences seen potentially driven by a few specific

areas. However when looking at Figures 2 and 3 it was clear that trends were seen across

multiple brain areas. Future studies would benefit both from applying this investigation to

the range of alternative mHRFs available, and using these findings to help develop new

means of modelling the haemodynamic response with increasing accuracy. This could

maximise both the power and interpretability of fMRI studies when elucidating age-effects.

4.4.4. Conclusion

Consequently it can be concluded that the type of model biases whether HRFs

typically seen in younger or elderly participants are better modelled, a crucial consideration

when looking at age-effects in the brain. As flexible models allow for variability in HRFs they should more accurately represent the actual age-effect. Conversely the HRFc model has the potential to introduce erroneous conclusions when investigating matters such as brain activity supposedly specific to elderly participants, such as hemispheric asymmetry reduction (Cabeza, 2002; Reuter-Lorenz et al., 2000). Additionally by utilising a flexible basis set the estimated HRF can be plotted and more accurately interpreted relative to the HRFc model in which change is only ever expressed in terms of magnitude. As the HRFtd model generally captured greater variability in timing properties such as peak latency and FWHM across age groups, it would appear to be the better choice when running age comparisons. This hinges upon the assumption that flexible models are unlikely to overestimate reductions in e.g. peak latency, which is supported by previous work (Danvers et al., 2021). An additional benefit of the HRFtd model is an increase in the available degrees of freedom in 1st-level GLMs (by virtue of fewer regressors in design matrices) relative to the Fourier set. This may at least partly explain why across grey matter it captured the greatest number of significant voxels (see Table 3). Despite offering the best trade-off, it is important to reiterate that the HRFtd model remains imperfect. An example of this was the reduced number of functions resulting in the undershoot amplitude of the estimated HRF being exaggerated when peak latency/FWHM were low, not seen when using the Fourier set.

4.4.5. Acknowledgements

4.5. References

Aizenstein, H. J., Clark, K. A., Butters, M. A., Cochran, J., Stenger, V. A., Meltzer, C. C., ... &
Carter, C. S. (2004). The BOLD hemodynamic response in healthy aging. *Journal of
cognitive neuroscience*, *16*(5), 786-793. https://doi.org/10.1162/089892904970681

Ances, B. M., Liang, C. L., Leontiev, O., Perthen, J. E., Fleisher, A. S., Lansing, A. E., & Buxton,
R. B. (2009). Effects of aging on cerebral blood flow, oxygen metabolism, and blood
oxygenation level dependent responses to visual stimulation. *Human brain
mapping*, *30*(4), 1120-1132. https://doi.org/10.1002/hbm.20574

Ashburner, J., Barnes, G., Chen, C., Daunizeau, J., Flandin, G., Friston, K., ... & Phillips, C.
(2020). SPM12 manual. *Wellcome Centre for Human Neuroimaging, London, UK*.
https://www.fil.ion.ucl.ac.uk/spm/

Balbi, M., Ghosh, M., Longden, T. A., Vega, M. J., Gesierich, B., Hellal, F., ... & Plesnila, N.
(2015). Dysfunction of mouse cerebral arteries during early aging. *Journal of
Cerebral Blood Flow & Metabolism*, *35*(9), 1445-1453.
https://doi.org/10.1038/jcbfm.2015.107

Bandettini, P. A. (2002). *Neuropsychopharmacology – 5th Generation of Progress*: *The spatial,
temporal, and interpretive limits of functional MRI.* Lippincott Williams and Wilkins.

Boynton, G. M., Engel, S. A., Glover, G. H., & Heeger, D. J. (1996). Linear systems analysis of
functional magnetic resonance imaging in human V1. *Journal of
Neuroscience*, *16*(13), 4207-4221. https://doi.org/10.1523/JNEUROSCI.16-13-
04207.1996

Buracas, G. T., & Boynton, G. M. (2002). Efficient design of event-related fMRI experiments

using M-sequences. *Neuroimage*, *16*(3), 801-813.

https://doi.org/10.1006/nimg.2002.1116

Buxton, R. B., Uludağ, K., Dubowitz, D. J., & Liu, T. T. (2004). Modeling the hemodynamic

response to brain activation. *Neuroimage*, *23*, S220-S233.

https://doi.org/10.1016/j.neuroimage.2004.07.013

Cabeza, R. (2002). Hemispheric asymmetry reduction in older adults: the HAROLD

model. *Psychology and aging*, *17*(1), 85-100. https://doi.org/10.1037//0882-

7974.17.1.85

Csipo, T., Mukli, P., Lipecz, A., Tarantini, S., Bahadli, D., Abdulhussein, O., ... & Hand, R. A.

(2019). Assessment of age-related decline of neurovascular coupling responses by

functional near-infrared spectroscopy (fNIRS) in humans. *Geroscience*, *41*(5), 495-

509. https://doi.org/10.1007/s11357-019-00122-x

Danvers, M., Longley, M., & Ramnani. (2021, November 8-11). *Modelling the BOLD response:*

On the insufficiency of conventional modelling approaches. [Poster Presentation].

SFN 2021, virtual.

Daselaar, S. M., Fleck, M. S., Dobbins, I. G., Madden, D. J., & Cabeza, R. (2006). Effects of

healthy aging on hippocampal and rhinal memory functions: an event-related fMRI

study. *Cerebral cortex*, *16*(12), 1771-1782. https://doi.org/10.1093/cercor/bhj112

Dennis, N. A., Kim, H., & Cabeza, R. (2007). Effects of aging on true and false memory

formation: An fMRI study. *Neuropsychologia*, *45*(14), 3157-3166.

https://doi.org/10.1016/j.neuropsychologia.2007.07.003

Dennis, N. A., Daselaar, S., & Cabeza, R. (2007). Effects of aging on transient and sustained

    successful memory encoding activity. *Neurobiology of Aging*, *28*(11), 1749-1758.

    https://doi.org/10.1016/j.neurobiolaging.2006.07.006

Desjardins, M. (2015). Vascular correlates of aging in the brain: Evidence from imaging

    data. *IRBM*, *36*(3), 158-165. https://doi.org/10.1016/j.irbm.2015.01.016

D'esposito, M., Zarahn, E., Aguirre, G. K., & Rypma, B. (1999). The effect of normal aging on

    the coupling of neural activity to the bold hemodynamic

    response. *Neuroimage*, *10*(1), 6-14. https://doi.org/10.1006/nimg.1999.0444

D'esposito, M., Deouell, L. Y., & Gazzaley, A. (2003). Alterations in the BOLD fMRI signal with

    ageing and disease: a challenge for neuroimaging. *Nature Reviews

    Neuroscience*, *4*(11), 863-872. https://doi.org/10.1038/nrn1246

De Vis, J. B., Hendrikse, J., Bhogal, A., Adams, A., Kappelle, L. J., & Petersen, E. T. (2015). Age-

    related changes in brain hemodynamics; A calibrated MRI study. *Human brain

    mapping*, *36*(10), 3973-3987. https://doi.org/10.1002/hbm.22891

Dickstein, D. L., Kabaso, D., Rocher, A. B., Luebke, J. I., Wearne, S. L., & Hof, P. R. (2007).

    Changes in the structural complexity of the aged brain. *Aging cell*, *6*(3), 275-284.

    https://doi.org/10.1111/j.1474-9726.2007.00289.x

Fabiani, M., Gordon, B. A., Maclin, E. L., Pearson, M. A., Brumback-Peltz, C. R., Low, K. A., ...

    & Gratton, G. (2014). Neurovascular coupling in normal aging: a combined optical,

    ERP and fMRI study. *Neuroimage*, *85*(1), 592-607.

    https://dx.doi.org/10.1016/j.neuroimage.2013.04.113

Grinband, J., Steffener, J., Razlighi, Q. R., & Stern, Y. (2017). BOLD neurovascular coupling

    does not change significantly with normal aging. *Human brain mapping*, *38*(7), 3538-

    3551. https://doi.org/10.1002/hbm.23608

Huang, Q., & Tang, J. (2010). Age-related hearing loss or presbycusis. *European Archives of*

    Oto-rhino-laryngology, *267*(8), 1179-1191. https://doi.org/10.1007/s00405-010-

    1270-7

Huettel, S. A., Singerman, J. D., & McCarthy, G. (2001). The effects of aging upon the

    hemodynamic response measured by functional MRI. *Neuroimage*, *13*(1), 161-175.

    https://doi.org/10.1006/nimg.2000.0675

Hutchison, J. L., Lu, H., & Rypma, B. (2013). Neural mechanisms of age-related slowing: the

    ΔCBF/ΔCMRO2 ratio mediates age-differences in BOLD signal and human

    performance. *Cerebral Cortex*, *23*(10), 2337-2346.

    https://doi.org/10.1093/cercor/bhs233

Kallman, D. A., Plato, C. C., & Tobin, J. D. (1990). The role of muscle loss in the age-related

    decline of grip strength: cross-sectional and longitudinal perspectives. *Journal of*

    gerontology, *45*(3), 82-88. https://doi.org/10.1093/geronj/45.3.M82

Klein, A., Andersson, J., Ardekani, B. A., Ashburner, J., Avants, B., Chiang, M. C., ... & Song, J.

    H. (2009). Evaluation of 14 nonlinear deformation algorithms applied to human

    brain MRI registration. *Neuroimage*, *46*(3), 786-802.

    https://doi.org/10.1016/j.neuroimage.2008.12.037

Lu, Y., Grova, C., Kobayashi, E., Dubeau, F., & Gotman, J. (2007). Using voxel-specific

    hemodynamic response function in EEG-fMRI data analysis: An estimation and

detection model. *Neuroimage*, *34*(1), 195-203.

https://doi.org/10.1016/j.neuroimage.2006.08.023

Morsheddost, H., Asemani, D., & Shalchy, M. A. (2015). Evaluation of hemodynamic

response function in vision and motor brain regions for the young and elderly

adults. *Basic and Clinical Neuroscience*, *6*(1), 58-68.

https://www.ncbi.nlm.nih.gov/pmc/articles/PMC4741271/

Mumford, J. A., & Nichols, T. (2006). Modeling and inference of multisubject fMRI data. *IEEE*

Engineering in Medicine and Biology Magazine, *25*(2), 42-51.

https://doi.org/10.1109/MEMB.2006.1607668

Ogawa, S., Lee, T. M., Kay, A. R., & Tank, D. W. (1990). Brain magnetic resonance imaging

with contrast dependent on blood oxygenation. *proceedings of the National*

Academy of Sciences, *87*(24), 9868-9872. https://doi.org/10.1073/pnas.87.24.9868

Peck, K. K., Sunderland, A., Peters, A. M., Butterworth, S., Clark, P., & Gowland, P. A. (2001).

Cerebral activation during a simple force production task: changes in the time

course of the haemodynamic response. *Neuroreport*, *12*(13), 2813-2816.

https://doi.org/10.1097/00001756-200109170-00012

Penny, W., & Holmes, A. (2007). Random effects analysis. *Statistical parametric mapping:*

The analysis of functional brain images, *156*, 165-186.

https://citeseerx.ist.psu.edu/document?repid=rep1&type=pdf&doi=6ed105062770d

089d86e9bcc7827f54487a22017

Piefke, M., Onur, Ö. A., & Fink, G. R. (2012). Aging-related changes of neural mechanisms

underlying visual-spatial working memory. *Neurobiology of aging*, *33*(7), 1284-1297.

https://doi.org/10.1016/j.neurobiolaging.2010.10.014

Price, D., Tyler, L. K., Henriques, R. N., Campbell, K. L., Williams, N., Treder, M. S., ... & Henson, R. N. A. (2017). Age-related delay in visual and auditory evoked responses is mediated by white-and grey-matter differences. *Nature communications*, *8*(1), 1-12. https://doi.org/10.1038/ncomms15671

Ramnani, N., & Henson, R. (2005). "Modelling the BOLD impulse response: Insufficiency of canonical basis functions", Abstracts of the 11th Annual Meeting of the Organization for Human Brain Mapping (2005), *NeuroImage*, Volume 26, Supplement 1, Abstract No. 622.

Reuter-Lorenz, P. A., Jonides, J., Smith, E. E., Hartley, A., Miller, A., Marshuetz, C., & Koeppe, R. A. (2000). Age differences in the frontal lateralization of verbal and spatial working memory revealed by PET. *Journal of cognitive neuroscience*, *12*(1), 174-187. https://doi.org/10.1162/089892900561814

Richter, W., & Richter, M. (2003). The shape of the fMRI BOLD response in children and adults changes systematically with age. *NeuroImage*, *20*(2), 1122-1131. https://doi.org/10.1016/S1053-8119(03)00347-1

Rosengarten, B., Aldinger, C., Spiller, A., & Kaps, M. (2003). Neurovascular coupling remains unaffected during normal aging. *Journal of Neuroimaging*, *13*(1), 43-47. https://doi.org/10.1111/j.1552-6569.2003.tb00155.x

Ross, M. H., Yurgelun-Todd, D. A., Renshaw, P. F., Maas, L. C., Mendelson, J. H., Mello, N. K., ... & Levin, J. M. (1997). Age-related reduction in functional MRI response to photic stimulation. *Neurology*, *48*(1), 173-176. https://doi.org/10.1212/WNL.48.1.173

Schacter, D. L., Buckner, R. L., Koutstaal, W., Dale, A. M., & Rosen, B. R. (1997). Late onset of

anterior prefrontal activity during true and false recognition: an event-related fMRI

study. *Neuroimage*, *6*(4), 259-269. https://doi.org/10.1006/nimg.1997.0305

Shafto, M. A., Tyler, L. K., Dixon, M., Taylor, J. R., Rowe, J. B., Cusack, R., ... & Henson, R. N.

(2014). The Cambridge Centre for Ageing and Neuroscience (Cam-CAN) study

protocol: a cross-sectional, lifespan, multidisciplinary examination of healthy

cognitive ageing. *BMC neurology*, *14*(204), 1-25. https://doi.org/10.1186/s12883-

014-0204-1

Soch, J., Richter, A., Schütze, H., Kizilirmak, J. M., Assmann, A., Behnisch, G., ... & Schott, B. H.

(2021). A comprehensive score reflecting memory-related fMRI activations and

deactivations as potential biomarker for neurocognitive aging. *Human brain

mapping*, *42*(14), 4478-4496. https://doi.org/10.1002/hbm.25559

Sorond, F. A., Hurwitz, S., Salat, D. H., Greve, D. N., & Fisher, N. D. (2013). Neurovascular

coupling, cerebral white matter integrity, and response to cocoa in older

people. *Neurology*, *81*(10), 904-909.

https://doi.org/10.1212/WNL.0b013e3182a351aa

Sperling, R. (2011). The potential of functional MRI as a biomarker in early Alzheimer's

disease. *Neurobiology of aging*, *32*, S37-S43.

https://doi.org/10.1016/j.neurobiolaging.2011.09.009

Stefanova, I., Stephan, T., Becker-Bense, S., Dera, T., Brandt, T., & Dieterich, M. (2013). Age-

related changes of blood-oxygen-level–dependent signal dynamics during

optokinetic stimulation. *Neurobiology of aging*, *34*(10), 2277-2286.

https://doi.org/10.1016/j.neurobiolaging.2013.03.031

Sulzer, J. S., Chib, V. S., Hepp-Reymond, M. C., Kollias, S., & Gassert, R. (2011, September). BOLD correlations to force in precision grip: an event-related study. In *2011 Annual International Conference of the IEEE Engineering in Medicine and Biology Society* (pp. 2342-2346). IEEE. https://doi.org/10.1109/IEMBS.2011.6090655

Takano, T., Tian, G. F., Peng, W., Lou, N., Libionka, W., Han, X., & Nedergaard, M. (2006). Astrocyte-mediated control of cerebral blood flow. *Nature neuroscience*, *9*(2), 260-267. https://doi.org/10.1038/nn1623

Taoka, T., Iwasaki, S., Uchida, H., Fukusumi, A., Nakagawa, H., Kichikawa, K., ... & Ohishi, H. (1998). Age correlation of the time peak latency in signal change on EPI-fMRI. *Journal of computer assisted tomography*, *22*(4), 514-517. https://doi.org/10.1097/00004728-199807000-00002

Tarantini, S., Tran, C. H. T., Gordon, G. R., Ungvari, Z., & Csiszar, A. (2017). Impaired neurovascular coupling in aging and Alzheimer's disease: contribution of astrocyte dysfunction and endothelial impairment to cognitive decline. *Experimental gerontology*, *94*, 52-58. https://doi.org/10.1016/j.exger.2016.11.004

Taylor, J. R., Williams, N., Cusack, R., Auer, T., Shafto, M. A., Dixon, M., ... & Henson, R. N. (2017). The Cambridge Centre for Ageing and Neuroscience (Cam-CAN) data repository: structural and functional MRI, MEG, and cognitive data from a cross-sectional adult lifespan sample. *Neuroimage*, *144*, 262-269. https://dx.doi.org/10.1016/j.neuroimage.2015.09.018

Tekes, A., Mohamed, M. A., Browner, N. M., Calhoun, V. D., & Yousem, D. M. (2005). Effect of age on visuomotor functional MR imaging1. *Academic radiology*, *12*(6), 739-745. https://doi.org/10.1016/j.acra.2004.08.015

Turner, M. P., Hubbard, N. A., Sivakolundu, D. K., Himes, L. M., Hutchison, J. L., Hart Jr, J., ...

    & Rypma, B. (2019). Preserved canonicality of the BOLD hemodynamic response

    reflects healthy cognition: insights into the healthy brain through the window of

    multiple sclerosis. *NeuroImage*, *190*, 46-55.

    https://doi.org/10.1016/j.neuroimage.2017.12.081

Ward, L. M., Aitchison, R. T., Tawse, M., Simmers, A. J., & Shahani, U. (2015). Reduced

    Haemodynamic Response in the Ageing Visual Cortex Measured by Absolute

    fNIRS. *PLoS ONE*, *10*(4), e0125012. https://doi.org/10.1371/journal.pone.0125012

West, K. L., Zuppichini, M. D., Turner, M. P., Sivakolundu, D. K., Zhao, Y., Abdelkarim, D., ... &

    Rypma, B. (2019). BOLD hemodynamic response function changes significantly with

    healthy aging. *Neuroimage*, *188*, 198-207.

    https://doi.org/10.1016/j.neuroimage.2018.12.012

Woodruff-Pak, D. S. (1997). *The neuropsychology of aging*. Blackwell Publishing.

World Health Organization. (2018). *Integrated care for older people: realigning primary*

    health care to respond to population ageing (No. WHO/HIS/SDS/2018.44). World

    Health Organization.

Wylie, G. R., Genova, H., DeLuca, J., Chiaravalloti, N., & Sumowski, J. F. (2014). Functional

    magnetic resonance imaging movers and shakers: Does participant-movement cause

    sampling bias?. *Human brain mapping*, *35*(1), 1-13.

    https://doi.org/10.1002/hbm.22150

Chapter 5
Rule Learning Across the Life-Course, a Prefronto-Cerebellar Deficit?

Matthew Danvers
Michael Longley
Narender Ramnani
In preparation for publication

Word count: 17,394 excluding references

Abstract

There is evidence of a rostro-caudal axis of activation in the dorsolateral prefrontal cortex pertaining to cognition. These regions show connectivity with cerebellar lobules also implicated in cognitive processes. This network of areas was investigated in twenty-four 18-30 year-olds, and twenty-four 65-80 year-olds, whilst partaking in a conditional visuo-oculomotor learning task. Behaviourally, younger participants demonstrated evidence of increasingly automated responses as learning progressed, as well as greater accuracy over learning. Functional imaging demonstrated that regions such as area 46, 9/46, 9, 8, and 6 contribute to this learning task, as well as cerebellar lobule CRUS I. Findings support the role of a prefronto-cerebellar network in learning, but with further evidence of interactions between experimental condition and age group within area 9/46, 9, and 8. It was considered that this may be attributable to the elderly cohort showing compensatory prefrontal activity. In conclusion, there was insufficient evidence of cerebellar impairment in the healthy elderly sample, but there was reduced performance despite an increased recruitment of prefrontal regions.

5.1. Introduction

The topic of cognitive ageing is critical at present due to ageing populations and evidence of age-related impairment of cognitive function, which may contribute to trends of reduced quality of life and independence (Salthouse, 2004; Park & Schwarz, 1999, pp.7; World Health Organisation, 2018). The following study sought to shed light on how activation of nodes within a network of frontal, prefrontal, and cerebellar regions may differ between age groups. This was investigated within an associative conditional learning task using functional magnetic resonance imaging (fMRI). How these regions may be implicated in cognitive ageing is discussed in more detail below, but first the concept of learning is considered. As described by Passingham & Wise (2012) the formation of learned associations require that a decision be made based upon perceptual/contextual information. This informs the selection of an appropriate goal, after which a relevant action will be initiated and a subsequent outcome produced. For example, an animal looking for food may see various options, but uses contextual information to determine which to select (becoming the goal) and then executes an action to obtain said item. This form of associative learning is an example of flexible, intelligent behaviour (Wise & Murray, 2000). A more familiar everyday scenario for humans could be presentation of a red traffic light (instrumental cue) in response to which a person generates a goal (apply the brakes) and executes an action to achieve this goal (extend right foot). However this motor event is likely preceded by an oculomotor response, which is presumably learnt via a similar conditioning process. For example, when approaching a junction (instrumental cue) one must generate a goal (look at the traffic lights) and execute an action to achieve this goal (saccade to lights). For the purpose of this paper goal generation is deemed to be the association formed between instrumental cues and subsequent targets of action/the action itself, based upon

past consequences of these (or similar) pairings. This falls into the realm of instrumental/operant conditioning, relying less upon costly errors than the relatively inflexible behavioural modification via classical reinforcement learning. As a result it is deemed reasonable to suggest that there is a clear evolutionary advantage to this learning mechanism (Genovesio et al., 2014; Passingham & Wise, 2012), with a wealth of literature suggesting goal generation depends upon current contextual information processed in the prefrontal cortex (PFC) (Christophel et al., 2017; Cromer et al., 2010; Mansouri et al., 2020; Passingham & Wise, 2012; Ramnani, 2014; Tsujimoto et al., 2010).

To test the learning of concrete associations the study described below presented an arbitrary non-spatial visual instrumental cue. Participants then had to form a spatially defined goal (selecting one of three identical but spatially differentiated targets) which informed a subsequent oculomotor response (saccade to target location). Feedback as to whether the correct target had been selected was given, with this informing future goals. The behavioural task falls within the realms of conditional visuo-oculomotor learning, as targets were visually identical and consistently spatially differentiated. Therefore the goal is intrinsically aligned with the motor response. The analysis isolated the onset of the instrumental cue from both target/saccade and feedback events. This was because the cue does not directly specify the subsequent action, and it was the generation of goals based upon both symbolic cues and past feedback that was of interest (Balsters & Ramnani, 2008).

Regarding the circuitry involved there is evidence that the inferior temporal cortex (ITC) encodes object information (Muhammad et al., 2006) and sends this on to the ventral prefrontal cortex (vPFC) (Bloedel et al., 1996, pp. 266-275), supported by transection of the uncinate fascicle (disconnecting PFC from ITC) resulting in impaired conditional discrimination especially when processing serial visual information (Browning & Gaffan,

2008; Gaffan & Wilson, 2008). Here it is suspected object information converges with visuo-spatial information in the dorsolateral prefrontal cortex (dlPFC, functionally defined as areas 46, 9, 9/46, 8, overlapping into rostral 6 and 10; Petrides, 2000) received from the posterior parietal cortex (PPC) (Rao et al., 1997). The mid dlPFC (areas 46 and 9/46, corresponding to Walker's area 46; Walker, 1940) is thought to maintain a memory trace between cue and response, prospectively encoding spatially defined goals by recoding multimodal information from parietal and temporal cortices to inform action (Bunge, 2004; Mansouri et al., 2020; Passingham & Wise, 2012, pp. 157-194; Petrides, 2005; Sakai et al., 2002). The dlPFC then outputs to regions such as area 8, the basal ganglia, pre supplementary motor area (preSMA), and the premotor cortex (PMC) (Miller & Cohen, 2001). These connections are relevant, as when the hand is used as an effector the PMC is evidenced as preparing actions to be carried out via M1 (Balsters & Ramnani, 2008; Balsters et al., 2013) with an analogous network suggested using the supplementary (SEF) and frontal eye fields (FEF) when preparing and executing an oculomotor response (Amiez & Petrides, 2009; Bloedel et al., 1996, pp. 266-275; Chen & Wise, 1995a, 1995b).

5.1.1. Corticocerebellar Network

Beyond the network discussed above, it is considered that the cerebellum may also contribute to prospective encoding within the mid dlPFC. One of the early claims that the cerebellum contributes to functions generally attributed to the frontal lobe was made by Luria (1964; translated by Budisavljevic & Ramnani, 2012) who observed that cerebellar damage induced 'pseudo-frontal' symptoms. This was consistent with evidence of connectivity and shared evolutionary expansion between prefrontal regions and the cerebellum, with a specific connection between the mid dlPFC and cerebellar lobule HVIIa (comprising CRUS I and CRUS II; Balsters et al., 2010, 2014; Buckner et al., 2011; Diedrichsen

et al., 2009; Kelly & Strick, 2003; Matano, 2001; O'Reilly et al., 2010; Schmahmann & Pandya, 1995, 1997; Steele et al., 2017). Pertaining specifically to conditional visuo-motor learning, there is evidence in NHPs that inactivation of cerebellar CRUS I and CRUS II specifically impairs new but not overlearned associations, with no impact upon the subject's ability to carry out the necessary response, such as a hand movement or saccade (Sendhilnathan & Goldberg, 2020). This suggested a specific role in the process of learning and was further supported by neuroimaging work in humans finding activity in lobule HVIIa at the time of cue presentation which diminished as a rule was learnt and automaticity increased (Balsters & Ramnani, 2008, 2011). Cue locked activity was also apparent even when not directly specifying an action (Balsters et al., 2013).

That cerebellar activity diminished over learning is consistent with the same being seen in the PFC and anterior cingulate cortex (ACC; Jenkins et al., 1994; Jueptner et al., 1997; Passingham,1996; Raichle et al., 1994), alongside associations with automaticity (Jueptner et al., 1997; Passingham, 1996). Automaticity is thought to indicate that learning is entrenched, often denoted by the ability to maintain performance whilst carrying out a concurrent task. This can also be measured using pupil size (the task evoked pupillary response) thought to be a physiological proxy of cognitive load (based upon Cognitive Load Theory) whereby load reduces with increasing automation, demonstrated by a reduction in pupil size (Alnæs et al., 2014; Beatty & Kahneman, 1966; Bradshaw, 1967; Gavas et al, 2017; Hess & Polt, 1964; Hosseini et al., 2017; Huh et al., 2019; Kahneman & Beatty, 1966, 1967; Kahneman & Peavler, 1969). Ramnani (2014) considered that the cerebellum may be contributing to the automation of prefrontal functions, however it should also be considered that if activity in connected regions such as the dlPFC reduces with practise due to automation via other structures (such as the basal ganglia; Arsalidou et al., 2013; van Schouwenburg et al., 2010)

this could also cause reductions in cerebellar activity. Therefore it is not possible to definitively state to what degree reductions in the cerebellar blood oxygen level dependent (BOLD) signal is attributable to automation, as there may be a purely correlational contribution too.

Considering how the cerebellum contributes to prefrontal function, using a concept borrowed from control theory Ramnani (2014) theorised that regions such as the mid dlPFC may act as 'controllers' projecting to 'plants' such as area 6 (or in the case of this study the SEFs; Chen & Wise, 1995a, 1995b), with collaterals projecting to a cerebellar 'forward model' which acts to reduce error (already evidenced as its role in eyeblink conditioning; Bracha et al., 2000; Chapman et al., 1988; Ito et al., 2014; Jirenhed & Hesslow, 2016; Ramnani et al., 2000; Woodruff-Pak et al., 1996). It is theorised that these inputs reach the cerebellar cortex via parallel fibers, influencing Purkinje cells which inhibit cerebellar outputs via the deep cerebellar nuclei (Marr, 1969). However, it is proposed that a teaching signal received via precerebellar nuclei such as the ventral tegmental area (VTA) and inferior olive (Ikai et al., 1992; Sasaki et al., 1977; Suzuki et al., 2012; Swenson et al., 1989; Watson et al., 2009) convey error signals, which potentially silence the Purkinje cell via long term depression (LTD) of the parallel fiber-Purkinje synapse (Albus, 1971; Hirano, 2018; Ito et al., 2014) this learned pause seen on trials following errors (Medina & Lisberger, 2008). In the case of classical eyeblink conditioning this disinhibits the deep cerebellar nuclei, reducing error in the conditioned response (Heiney et al., 2014; Jirenhed & Hesslow, 2016; Johansson et al., 2014). In instrumental learning tasks it is unclear whether mid dlPFC-HVIIa connections stem from collaterals of mid dlPFC projections to the eye fields, but if so errors may also silence Purkinje cells, allowing the deep cerebellar nuclei to initiate mid dlPFC activity or even bypass this region to act directly upon the plant (Ito, 2005), in this case the eye fields.

6

Therefore when a familiar cue is presented there may be changes in Purkinje cell firing based upon feedback associated with that cue (consistent with the Marr-Albus hypothesis; Albus, 1971, 1989; Marr, 1969). As the cerebellum can also inhibit these teaching signals (Mittleman et al., 2008; Ramnani, 2006, 2014; Rogers et al., 2011) over the course of learning the internal model has the capacity to become feedback-resistant, and so essentially automated. Via this mechanism the cerebellum could be reducing the PFC load both by streamlining activity to task-relevant regions and reducing reliance upon feedback.

5.1.2. Ageing

It has been suggested that faculties pertaining to fluid intelligence such as processing speed, working memory, inhibition of irrelevant information, planning, attention, and problem solving tend to decline with age, however those requiring crystallized intelligence such as vocabulary tend to increase until plateauing at approximately 60 years (Campbell et al., 2020; Ferguson et al., 2021; Gajewski et al., 2018; Hedden & Gabrieli, 2004; Park & Schwarz, 1999, pp. 43-54; Rhodes & Katz, 2017; Salthouse, 2010). It is perhaps not surprising then that the cognitive ageing literature shows learning is affected. In humans this detrimental effect of age on associative learning has been linked to a general reduction in processing speed, meaning information is encoded less efficiently (Salthouse, 1993, 1994). However, there is also evidence that the frontal lobe is disproportionately affected, termed the frontal lobe hypothesis, or prefrontal-executive theory (West, 1996, 2000). This is supported by evidence of age-differential activity in brain regions such as the dlPFC (approximately area 9/46; de Chastelaine et al., 2015) and reduced neuron size and synaptic density in the dlPFC (Haug & Eggers, 1991; Huttenlocher, 1979; Raz et al., 1997). Behaviourally healthy elderly participants also show similar associative learning deficits as patients with dlPFC lesions (areas 8 and rostral 6; Levine et al., 1997), and generally tasks

deemed reliant upon the dlPFC show greater age-related decline (MacPherson et al., 2002). This has also been demonstrated in rats performing a visuo-motor learning task (Winocur, 1991, 1992), the baseline age-related deficit comparable to rats with lesions of the dlPFC and dorsomedial PFC (dmPFC).

Although not an instrumental form of associative learning, cerebellar-dependent classical associative learning has also shown age-effects upon performance (Bellebaum & Daum, 2004; Woodruff-Pak et al., 2010) with evidence of LTD impairment in elderly mice (Woodruff-Pak et al., 2010). This suggests that if a similar cerebellar mechanism were applied to visuo-oculomotor learning it may contribute to age differences found. Learning deficits seen in the elderly could then be in part driven by age-related atrophy in the lateral PFC, striatum, and cerebellar lobules VI, HVI, and HVIIa, areas which could impact both the executive control and reward components of the proposed prefronto-cerebellar circuit (Gellersen et al., 2021). If the cerebellum serves to automate the process (Balsters & Ramnani, 2011) within elderly participants there may be less focused/more dispersed prefrontal activity, with reduced evidence of cerebellar control. If elderly participants have to rely more upon costly but flexible processing strategies (led by the PFC) this may also explain why so many executive functions decline over age, but cognitive flexibility can persist in some contexts (Ferguson et al., 2021).

5.1.3. Hypotheses

1. Young adults will show higher accuracy and faster learning compared with older adults.
2. Young adults will show greater evidence of automaticity based on reductions in reaction times and pupil size over learning.

3. Effects of condition identified across both age cohorts will be investigated within cerebellar lobule HVIIa, and frontal regions such as area 46, 9/46, and the eye fields.

4. Effects of condition which differ between age cohorts will be investigated within cerebellar lobule HVIIa, and frontal regions such as area 46, 9/46, and the eye fields.

5. Effects of practise identified across both age cohorts will be investigated within cerebellar lobule HVIIa, and frontal regions such as area 46, 9/46, and the eye fields, with reductions in BOLD response magnitude specific to the experimental condition expected, implying learning/automation.

6. Effects of practise which differ between age cohorts will be investigated within cerebellar lobule HVIIa, and frontal regions such as area 46, 9/46, and the eye fields, with reductions in BOLD response magnitude specific to the experimental condition expected to be more pronounced in the younger group.

All fMRI analyses looked specifically at BOLD activity time-locked to the symbolic cue to identify processes such as prospective encoding whilst regressing out BOLD responses associated with saccade execution or receipt of feedback. Only correct trials which were not directly preceded by an incorrect trial within the same rule were included. This was for three reasons; 1) it removed the risk of contamination via error trials, during which cerebellar learning theory would predict large plasticity related changes in cerebellar firing rate, specifically seen in the next trial (Medina & Lisberger, 2008); 2) time limitations meant not enough incorrect trials were collected to be modelled independently; 3) it kept this work comparable with previous studies (Balsters & Ramnani, 2008, 2011; Balsters et al, 2013). All predictions relating to fMRI analyses were focused upon the cerebellum (specifically lobule HVIIa) and the frontal lobe (specifically areas 9/46, 46, and the eye fields). This was due to the expected cascade of information whereby areas 46 and 9/46 prospectively encode the spatially defined goal (Passingham & Wise, 2012, pp. 157-194) outputting to the eye fields

(Hutchison et al., 2012) responsible for execution of saccadic eye movements (Amiez & Petrides, 2009). Cerebellar lobule HVIIa was then expected to form internal models relating to activity in the reciprocally connected mid dlPFC (Balsters et al., 2014; Kelly & Strick, 2003; Schmahmann & Pandya, 1995, 1997). As opportunity sampling was used, to check for disparity between age groups measures of IQ were taken and built into the analysis where necessary. To ensure our samples could be considered cognitively healthy all underwent screening for dementia or cognitive impairment using a tool called the Mini-Cog.

5.2. Methods

All scripts are available on https://github.com/mdanve01/Project3.

5.2.1. Participants

Two independent age groups were formed, the first comprised of young adults aged 18-30 (N = 24, M = 21.5 years, SD = 3.28 years, 54.17% female). Twenty-seven participants were originally scanned with two removed due to excessive head motion (beyond 10mm) and one due to abnormal normalisation. The second group was comprised of elderly adults aged 65-80 (N = 24, M = 70.17 years, SD = 4.90 years, 37.5% female). Thirty participants were originally scanned with six removed, two due to a failure to understand the task, and four due to eye-tracking failures. Recruitment was carried out within the local community and the university campus. Participants were offered a £50 Amazon voucher, an image of their brain, and reasonable travel expenses. All participants were right-handed, spoke English as their first language, had a UK-based General Practitioner, had normal or corrected to normal vision, reported no diagnosis of a psychiatric, developmental, neurological or sensory disorder, or any specific learning difficulties such as dyslexia, dyspraxia or ADHD, and had no history of seizures or epilepsy. Ethical approval was provided by the Royal Holloway Ethics Committee.

Participants were initially contacted either by email or phone to discuss the study, and if interested were emailed an information pack including screening forms to check for MRI contraindications. A face-to-face meeting was then arranged, and when mandated by the department a Covid screening call was made prior. Participants were taken to a private room where they completed the relevant Covid screening forms and the task was explained in detail. If happy to proceed, participants filled out the consent forms and the MRI safety screening forms. Participants then completed the morningness-eveningness questionnaire (MEQ), Mini-Cog, and British National Adult Reading Test (NART), in that order. The MEQ (Horne & Östberg, 1976) established the best time of day for testing. If showing a preference for morning (scores > 58) participants were booked in before midday, for evening (scores < 42) bookings were made for after 14.00, and if intermediate (42-58) bookings were made between 10.00 and 14.00. This was included as previous work showed elderly participants have a preference for morning and young adults for evening, with testing at non-optimal times affecting performance (Intons-Peterson et al., 1998; Mecacci et al., 1986; Park & Schwarz, pp. 153-154) potentially attributable to associations between MEQ scores and circadian rhythms (Roveda et al., 2017). The Mini-Cog was used to test for signs of dementia or mild cognitive impairment (participants excluded if scoring below 3) and was administered in-person (Borson et al., 2000, 2003, 2005; Brodaty et al., 2006; Larner, 2020; Yang et al., 2016). Participants were aware that Mini-Cog scores were not diagnostic, researchers were not clinicians, and that if results suggested risk of dementia their GP would be informed and would contact them if necessary. Finally the NART (Nelson & Willison, 1982) was used to estimate WAIS-IV full scale IQ scores via the following equation (which accounted for 53% of the variance in IQ; Bright & van der Linde, 2020):

$$141.126 - (1.26 \times number\ of\ NART\ errors) - (.236 \times age)$$

The test was presented to the participant on an A4 sheet of paper, the words organised into two columns, font = Calibri(body), size 22. Participants were later informed by email as to whether or not they were eligible for the study and if so, a scan date was arranged.

5.2.2. Apparatus

An MRI compatible Eyelink 1000 eyetracker (SR Research) was used to sample movements of the right eye at 1Khz. Custom calibration points were used due to a limited field of view within the scanner, the horizontal distance from the center of the screen being reduced by 20%, and the vertical distance from center by 25%. A 50mm MRI compatible lens and an MRI compatible illuminator were affixed to a screen mount in the rear of the scanner. The distance from center of screen to mirror was approximately 750mm, and the distance from mirror to eye was approximately 100mm (variability introduced due to participant-specific adjustments). Stimulus presentation and logging of responses were controlled using Experiment Builder (resolution = 1024 x 768, projected image size on screen = 500mm x 390mm). The experiment was presented using an NEC PA653UL projector; refresh rate = 60Hz, resolution = 1920x1200. To maintain control over event timings, TTL pulses marking onset times of each TR were sent to a custom parallel port connected to a 'stimulus' PC running Experiment Builder. Each trial was triggered by a TTL pulse. All TTL pulses and stimulus onsets and durations were sampled at 5KHz using a CED1401 (for verification, timings of all events were also sampled at 1KHz using Dataviewer). The timings were used to construct 1st-level design matrices in SPM12 (see below). All pre-processing and statistical analyses were run on a Red Hat Enterprise Linux Server version 7.9 (Maipo) using Matlab 2019. Once complete the 2nd-level design matrices were exported to an HP Pavilion Desktop with AMD Ryzen 7 5700G processor where the results were explored using

Matlab 2022a. Analysis of behavioural data was carried out using IBM SPSS statistics version 25.

5.2.3. Behavioural Task

Experimental Design: The conditional visuo-oculomotor task involved learning a set of associations (which remained constant over the study) whereby four different shapes (cues) were each arbitrarily paired with one of three spatially defined targets. Therefore the rule might be "if shown a square, look at the top target", see Figure 1.
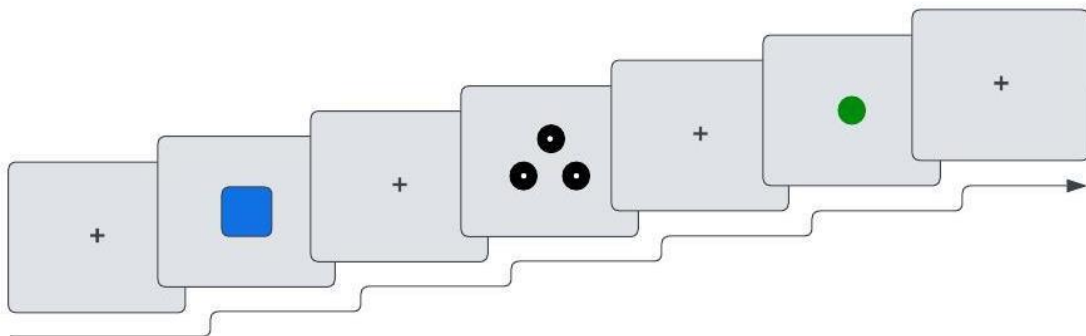
Figure 1. A full experimental trial including cue (blue square), targets (three black circles), and feedback presentation (green circle denoting a correct response).

The number of cues exceeded the number of targets to ensure that any target could be associated with more than one cue, preventing participants using information about one rule to inform deductions about another. After making their selection feedback was given. Participants were aware of the task-structure, but acquired cue-target pairings via trial and error. Consequently there were a total of three event types (cue onset, target onset, and feedback onset) across two conditions (experimental and control). Hypothesis 1 was devoted to experimental trials only, examining performance. However Hypotheses 3-6 were concerned with comparing the experimental condition with the control condition, specifically at the time of the cue. For this reason control trials involved presentation of a single target randomly positioned within one of the three target locations. Control cue-

target pairings changed pseudorandomly over the course of the study, each cue paired with each target an equal number of times, but never having the same association more than twice in a row. This meant control and experimental conditions were matched in terms of a cue being presented, followed by a target and consequent saccade, followed by feedback presentation, but differed in that no association could be learnt in the control condition. This also controlled for potential baseline differences between age-groups in their evoked haemodynamic response. In total there were 48 experimental and 24 control trials, with the study split into six blocks of 12 (8 experimental and 4 control). Fewer control trials were included to keep total scanning time down, and because more experimental trials were needed to allow for incorrect responses.

Trial Structure: When stimuli were not on the screen a centrally positioned fixation cross was presented to keep participant gaze centered. Within a trial there was a variable delay after which a cue was presented. If blue (colour code 0,0,255,255) this indicated an experimental trial, if black (colour code 0,0,0,255) this indicated a control trial. Post cue offset there was a variable delay followed by target presentation (these were positioned in a triangular formation, one-above-two-below, equidistant to the fixation cross). Presentation of targets acted as a 'GO' signal, indicating the participant was to select one by fixating it. Selection was registered when participants fixated within an area of interest for at least 200ms. Due to minor processing delays in Experiment Builder and a 1250ms target presentation time, participant fixation onsets had to occur within approximately 1010ms of target onset. Post target offset there was another variable delay followed by presentation of feedback. This was either green (colour code 0,204,0,255) if correct, red (colour code 255,0,0,255) if incorrect, or yellow (colour code 255,255,0,255) if no fixation was detected (see Figure 2). As only correct experimental trials were analysed, and within the control

14

condition there was no incorrect response, all control trials provided green feedback unless

a fixation was not detected (in which case yellow feedback was given). Due to the 60Hz

refresh rate of the projector actual event durations had a fluctuating +/-~16.67ms error (as

presentation or removal of a stimulus from the screen had to wait for a refresh).
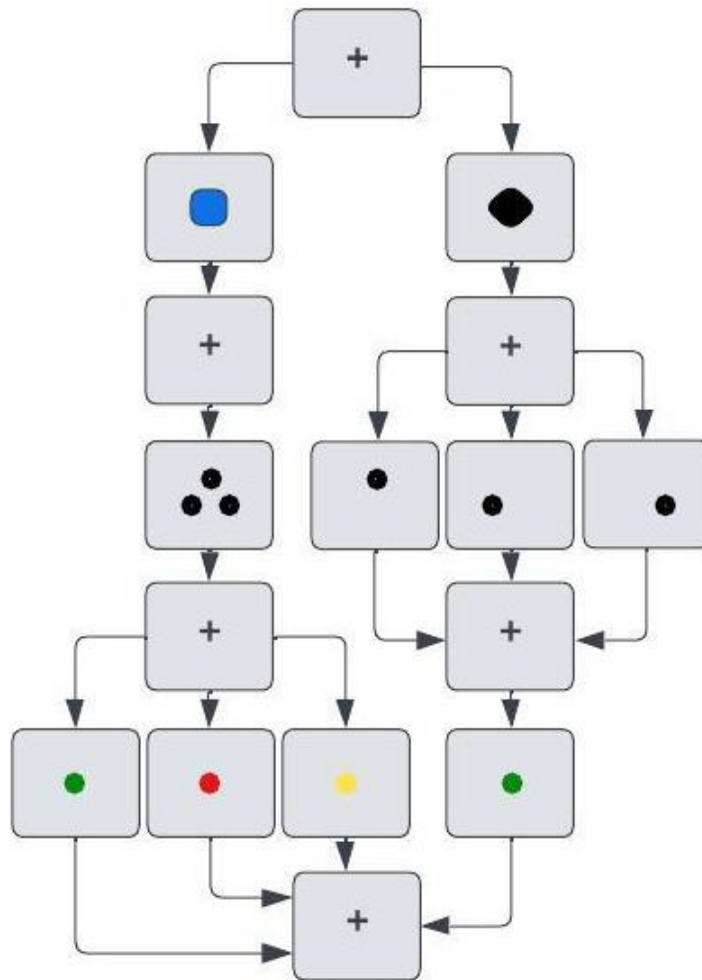
Figure 2. Schematic of task structure showing branches for the experimental (blue square)
and control (black rhombus) conditions on the left and right respectively. The sequence of
events was cue presentation, followed by targets, followed by feedback.

Timings: Within a trial the cue was presented for 250ms (uniformly jittered between

0 and 5750ms from trial start), the targets presented for 1250ms (uniformly jittered

between 6000 and 10750ms), and feedback presented for 250ms (uniformly jittered

between 12000 and 17000ms), see Figure 3. Total trial length was 18 seconds and there was

always at least 700ms between offset of feedback and trial end, allowing the system time to

prepare the next trial.
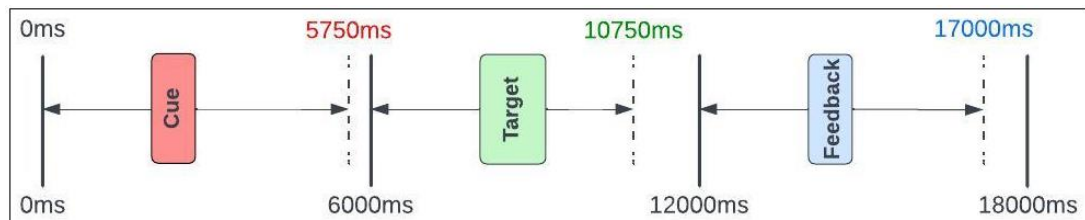
Figure 3. Event timings with temporal jitter. Solid black lines separate the six second blocks

(comprising three scans) within which each event was jittered.

As the onset of each event occurred across approximately three scans (each with a

repetition time (TR) of 2000ms) the jitter was manipulated to prevent overlap regarding

onset times within the 2000ms peristimulus period, ensuring maximal sampling (see Figure

4).
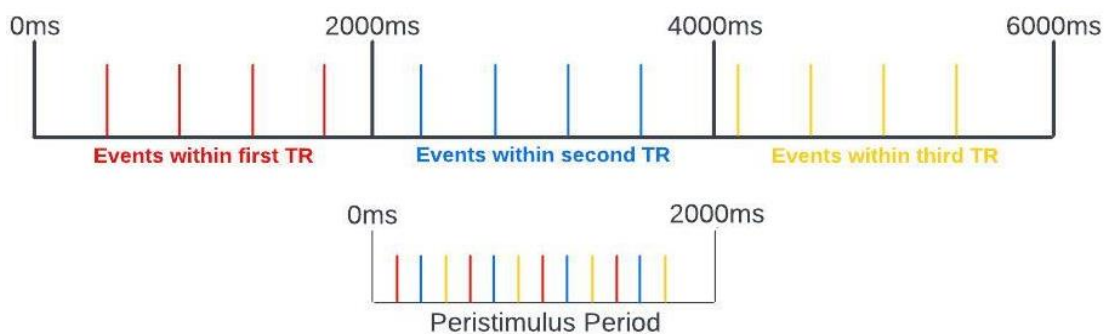
Figure 4. A visual representation of how events were uniformly spread across a six second

time window.

The jittered onset times for each event were then randomised iteratively to reduce

the correlation across event types (run separately within each condition) to minimise

multicollinearity in the design matrix. Once a set of trial timings had been decided upon a

faux design matrix was created and correlation coefficients between regressors were iteratively checked until the design matrix had sufficiently low multicollinearity (see section **5.2.7. GLM Design** below).

Procedure: On the day of the scan the task and procedure was again explained in detail to the participant, and it was made clear that they could end the experiment at any time. Participants lay on the scanner bed, with ear plugs inserted and cushions either side of their head (minimising movement, attenuating noise, and securing ear plugs). Next the eye-tracker was focused and calibrated, and participants completed eight practise trials. These comprised six experimental and two controls, within which one experimental cue-type was repeated four times to facilitate learning of at least one rule. If learning was not achieved the experimenter would discuss the task with the participant, and if necessary the practise trials were repeated. The main task used a different set of cues to ensure there was no carry-over effect from the practise trials. If participants were happy to proceed the eye-tracker was recalibrated and validated whilst localizer scans were run, followed by the EPI sequence which triggered the main task. At the end of each block there was a 30 second rest period, followed by re-calibration/validation of the eye-tracker to minimise drift, ensuring accurate target selection. Upon task completion field maps and anatomical scans were collected (see **5.2.5. MRI Data Acquisition** below), followed by debriefing. In order to reduce the risk of stereotype-threat words such as learning and memory were avoided prior to or during testing, replaced with terms such as 'figuring out the rule'. For the same reason, participants were not told until after task completion that age comparisons were being carried out.

5.2.4. Behavioural Data Acquisition

A CED 1401 collected data on the timings of all events within the study, and these were classified into the relevant conditions based on outputs from Experiment Builder and Dataviewer. This provided all data required to construct 1st-level fMRI regressors.

5.2.5. MRI Data Acquisition

Scanning was carried out using 3T Siemens Magnetom TIM Trio scanner located in the CUBIC unit at Royal Holloway University of London, with a 32-channel head array coil. Localizers used a voxel size of 1.1x1.0x7.0mm, and lasted ~29 seconds, TR = 8.6ms, TE = 4ms. The EPI sequence used isotropic 3x3x3mm voxels, phase encoding direction = A>>P, TR = 2000ms, TE = 30ms, multi-band acceleration factor = 2, slices = 50, slice thickness = 3mm, interleaved acquisition, FoV = 192x192x150mm, flip angle = 78 degrees, and EPI factor = 64. Field mapping lasted 106 seconds, voxel size = 3x3x3mm, phase encoding direction = A>>P, TR = 400ms, TE1 = 5.19ms, TE2 = 7.65ms, and flip angle = 60 degrees. Anatomical T1 weighted scans lasted 5.06 minutes, voxel size = 1x1x1mm, phase encoding direction = A>>P, TR = 1900ms, TE = 3.03ms, flip angle = 11 degrees, PAT mode = GRAPPA, Accelerating factor PE = 2, ascending series, and FoV read = 256mm.

5.2.6. Pre-Processing Methods

DICOM Conversion, Field Mapping, and Realignment: EPI scans were converted from DICOM to nifti in SPM12. Voxel displacement maps (VDM) were created using phase and magnitude information (TE = [5.19 7.65]; blip direction = -1; EPI readout time = 44.16ms). EPI images were then realigned to the mean and unwarped using the VDM. Outputs during this process allowed for a manual check that unwarping of EPI images functioned as expected.

Co-registration and Segmentation: The anatomical image was co-registered to the mean EPI image (estimation only). Finally, the anatomical image was segmented using MNI tissue probability maps. Outputs during this process allowed for a manual check that co-registration was accurate between mean EPI and anatomical images. Slice timing correction was not carried out due to a risk of aliasing and interactions with head motion (Henson et al., 1999; Poldrack et al., 2011, pp. 41-42; Sladky et al., 2011).

Quality Control: At this stage checks were made for abnormal signal variation across both slices of the brain, and scans, as well as evidence of periodicity across scans. Head motion was also examined, looking for instances of abnormally high variability across participants.

Normalisation and Smoothing: A Shoot template was created using Dartel imported grey and white matter tissue class images. Each participant's realigned and unwarped EPI images were then normalised using the Shoot template, with an 8mm full-width-half-maximum gaussian smoothing kernel (accuracy checked using SPM's check-reg function). 1st-level analyses were then run (see below for details), with con images produced for each regressor alongside a mask denoting voxels containing signal for each participant. Next was another round of quality checks which resulted in one young participant being removed.

5.2.7. GLM Design

fMRI 1st-level Experimental Design: The canonical model with temporal and dispersion derivatives was employed as an additional means of accounting for potential age-related variability in the shape of the haemodynamic response function (HRF), based upon previous work by the authors. At the 1st-level analysis a general linear model (GLM) was constructed with the following event-related regressors (see Table 1 and Figure 5), with con images derived for each.

Table 1. Event-related regressors for the 1st-level GLM with summary statistics regarding the number of trials within each.

Regressor	Explanation	Median	Range
1-3	Experimental Correct Cue Event (not preceded by an incorrect trial within the same rule)	36	8-45
4-6	Parametric Modulation (Experimental Correct Cue Event)	36	8-45
7-9	Control Correct Cue Event	24	13-24
10-12	Parametric Modulation (Control Correct Cue Event)	24	13-24
13-15	Junk (incorrect cue/correct cue preceded by incorrect trial within the same rule/missed events)	18.5	3-100
16-18	Target Event (target 1 selected)	22	18-28
19-21	Target Event (target 2 selected)	27	10-33
22-24	Target Event (target 3 selected)	21	12-30
25-27	Feedback Event (target 1 selected)	22	18-28
28-30	Feedback Event (target 2 selected)	27	10-33
31-33	Feedback Event (target 3 selected)	21	12-30
34-36	Rest/Calibration (block design)	N/A	N/A
37-42	Head Motion Parameters	N/A	N/A

In regressors 4-6 and 10-12 practise was included as a continuous factor (addressing Hypotheses 5 and 6). Practise was represented as a sequential linearly increasing weighting applied to each correct trial (within each rule) within the experimental and control conditions independently.
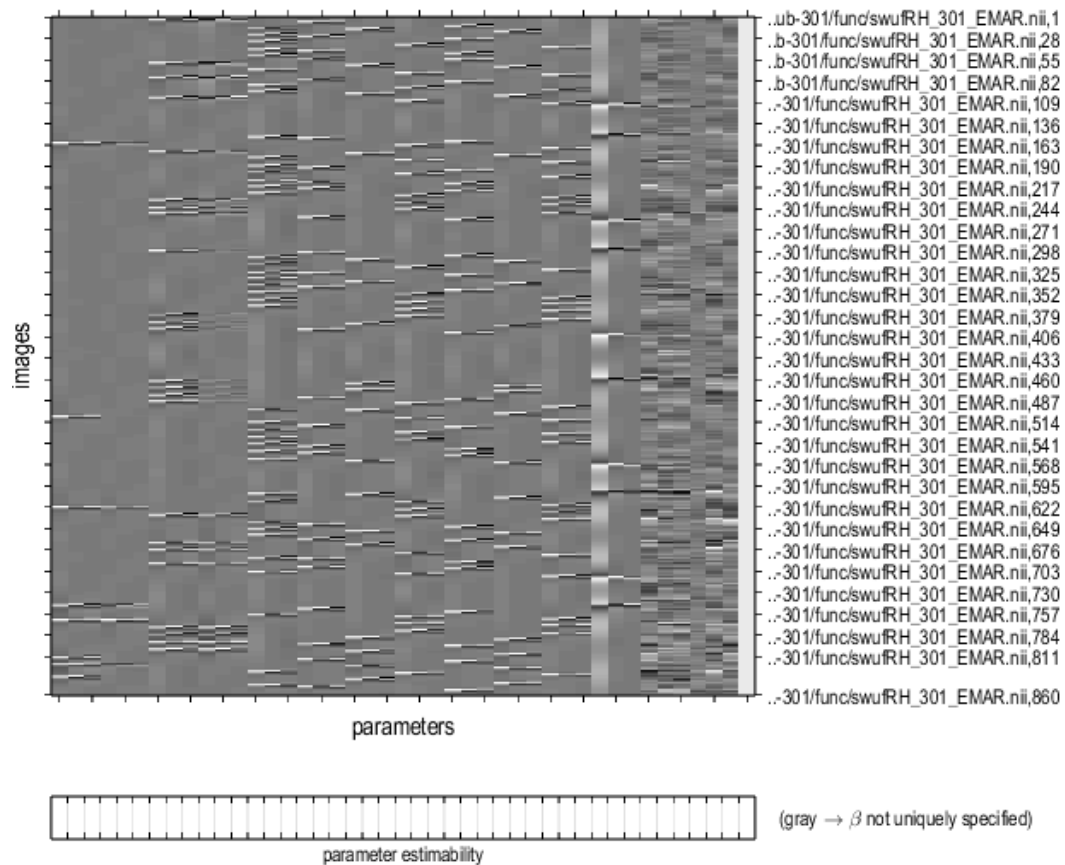
Figure 5. The 1st-level design matrix for a randomly chosen participant.

fMRI 2nd-level Experimental Design: At the 2nd-level analysis correct cue events

(regressors 1-3 and 7-9) were first examined in an unmodulated design matrix. A full

factorial analysis was run with three categorical factors (see Figure 6); age (two levels of

young and elderly, independent), condition (two levels of experimental and control, not

independent), and basis function (three levels of canonical, temporal and dispersion, not

independent), totalling 12 regressors. A second design matrix was created using con images

from the parametrically modulated 1st-level regressors (regressors 4-6 and 10-12). This

followed the same structure as the unmodulated analysis described above (age x condition x

basis function). Any effect of condition would therefore be an interaction between condition

and practise, suggesting an experience-modulated learning-related difference.
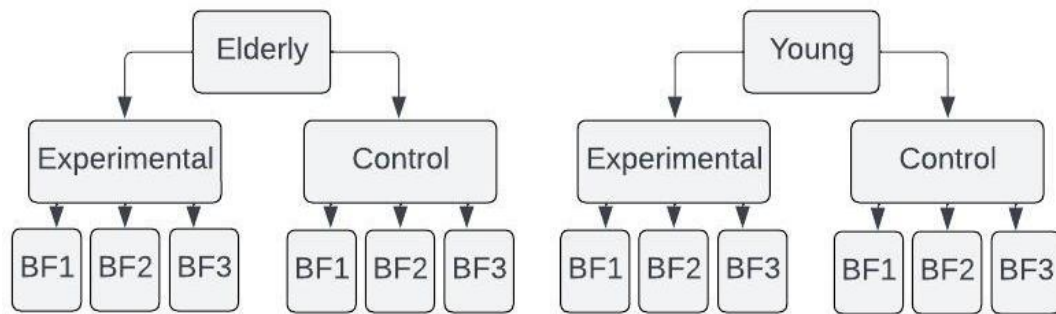
Figure 6. A schematic of the experimental design, denoting factors representing age, condition, and basis function (BF).

Covariates: IQ and participant gender (self-reported) were considered as potential confounding covariates. Both were included for each of the two 2nd-level design matrices and tested for significant effects of the covariate upon output data. Only IQ had no significant effect on output data specifically within the unmodulated design matrix, and so was removed from that analysis. As a result, for the unmodulated design matrix model degrees of freedom (dfm) = 15 and residual degrees of freedom (dfr) = 273, and for the parametrically modulated design matrix dfm = 18 and dfr = 270. The analyses reported in the results section are based on these two GLMs. The average number of included trials per cue learned was also considered as a confounding covariate, as differences may be seen based purely upon progression through learning but with a separate causal factor. There was a significant effect on output data in both design matrices. As progression, performance, and impairment are likely to be related, this was not included as a covariate in the main analysis, but where significance was found it was checked whether this was still the case when accounting for this variable. If a coordinate remained significance with this covariate included it would suggest that there may not be a simple linear relationship between performance and the output data.

To address Hypothesis 3 a conjunction analysis was run looking for an effect of condition in both age groups. The three basis functions were linearly combined for the correct experimental cue events (+1) and compared to a linear combination of correct control cue events (-1), see Figure 7. The same was applied to the condition x practise interaction, only the parametrically modulated GLM was used, to address Hypothesis 5.

Elderly		Young	
Experimental	Control	Experimental	Control

Figure 7. Weightings applied to contrast images when investigating a conjunction regarding the effect of condition using the 2nd-level design matrix.

To address Hypothesis 4 a condition x age interaction was run, linearly combining across the three basis functions for the correct experimental cue events within elderly (+1) and young (-1) groups. Weightings were flipped for linear combinations within the correct control cue events for elderly (-1) and young (+1) groups, see Figure 8. The same was applied to the condition x practise x age interaction, only the parametrically modulated GLM was used, to address Hypothesis 6.

Elderly		Young	
Experimental	Control	Experimental	Control

Figure 8. Weightings applied to contrast images when investigating an age x condition interaction using the 2nd-level design matrix.

5.2.8. Statistical Analysis

To understand the results, at each significant coordinate of interest independent tests were run to establish whether there was a main effect of condition, an age x condition interaction, an age x condition x practise interaction, and an effect of condition and/or a condition x practise interaction within either age group. It was also checked whether there was an effect of age and an age x practise interaction within each condition, as well as whether there were any simple effects e.g. a positive BOLD response in the young experimental condition. The estimated haemodynamic response function was calculated by multiplying each basis function by its respective beta value and summing across the three. This was then divided by the mean baseline within each respective age group at that voxel, and multiplied by 100 (to create percentage signal change; as per MarsBaR FAQ — MarsBaR 0.45 documentation, n.d.). It was checked whether this altered the relative magnitudes of BOLD responses between age groups by comparing to the original signal, with good consistency found. Determination of positive from negative HRFs was based on the percentage weighting of the canonical regressor's absolute beta value (relative to the sum of all three function's absolute betas).

In order to apply small volume corrections a cerebellar mask was generated using SPM's anatomy toolbox version 2.2b, containing bilateral lobules I-X (including vermal regions VI-X). A binary bilateral grey matter mask of the frontal lobe (central sulcus to frontal pole) was also constructed. During analyses the α threshold was set to .001, and then a small volume correction was applied using the relevant mask (α = .05). Finally cytoarchitectonic probabilities were established using SPM's anatomy toolbox version 3.0.

Pupillometry analyses used Data Viewer to produce estimates of pupil size for each participant within each trial, to address Hypothesis 2. This was the maximum pupil area over

the period from cue onset to target onset, measured in arbitrary units. The values for all correct experimental trials (isolated to estimate the stamping in of the learned rule in isolation from the learning curve) and all successful control trials were selected. Each was split into three blocks, due to missing values when split into six. For each block the median of the maximum pupil sizes was calculated and an age x block x condition mixed ANOVA run. Based upon previous studies it was deemed reasonable to use the peak value and compare this to the control condition to account for both baseline pupil size and the potential for general reductions over the course of the study, potentially due to practise effects (Kahneman & Beatty, 1966; Peavler, 1974).

Reaction Times (RTs) reported are the difference between target presentation and onset of gaze fixation upon target, with previous work using visuo-motor learning finding a reduction in RT over time (Balsters & Ramnani, 2011). These were analysed in the same way as the pupillometry data, splitting into three blocks and calculating a median reaction time for each, in order to address Hypothesis 2. The only difference was that anticipatory movements presenting with negative RTs were removed.

Accuracy was measured as the percentage of correct experimental trials across the entire experimental run, relative to the total number of experimental trials in which a target was successfully fixated. This was to address Hypothesis 1. As missed trials could represent either a failure to choose a target in time (performance relevant) or a system failure (performance irrelevant) these were removed from the analysis. When missed trials were investigated they were subjectively deemed to be correct responses 67.03% of the time (young; M = 70.61, SD = 39.63, elderly; M = 64.22, SD = 34.30).

Errors were calculated and summed across rules both before and after the first correct response, to establish if this differed between age groups, and whether positive

feedback reduced error numbers. In order to measure perseveration the number of errors

on which a target was selected despite previously having received red feedback within the

same rule were also calculated. A separate pair of analyses investigated the idea that a

reinforced response on trial n biased the response on trial n + 1. Firstly cases were identified

where a correct trial was directly followed by an incorrect experimental trial, to check

whether the incorrect target selection matched the previous positively reinforced target

selection (whether control or experimental), which if so would suggest bias. See Figure 9.

Figure 9. Schematic demonstrating an example of a correct trial preceding an incorrect
experimental trial, here showing the same target selection.

Secondly cases were identified where the next experimental trial (after a correct

experimental trial) was incorrect, again checking for evidence of the previous trial's target

selection biasing the subsequent selection, but removing control trials from the equation.

See Figure 10.

Figure 10. Schematic demonstrating an example of a correct experimental trial, wherein the
subsequent experimental trial is incorrect (irrespective of the control trials separating them).

For both, the percentage where target selection on the incorrect trial matched the

previous correct trial was calculated, with this expected to occur on approximately 33% of

cases.

Processing Speed was also investigated in a manner decided upon post-hoc using the median reaction time across control trials as a proxy. The aim was to establish whether processing speed accounted for age differences in performance. As age contained two categorical groups ANCOVA was used rather than linear regression, as was employed by Salthouse (1994).

Analyses looking at interactions in behavioural data always utilised parametric tests due to there being no non-parametric alternative available, but checked for consistency of results when outliers were removed. In cases where assumptions were not met, when carrying out initial/follow up univariate ANOVA, or follow up t-tests, bootstrapping was employed (this not being an option for repeated measures ANOVA). For stand-alone comparisons of just two levels of a variable (when not following up on an interaction) a choice was made between parametric (t-test) and non-parametric approaches (Mann Whitney U and Wilcoxon Matched Pairs Signed Ranks), as recommended by Field (2009, p. 540).

5.2.9. Anatomical Classification

The anatomical locations of all significant peak coordinates were superimposed on the MNI152 brain and their anatomical locations were verified using the atlas of Duvernoy (1999) for the frontal lobe, and Schmahmann et al. (2000) for the cerebellum. The eye fields were defined based upon the work of Amiez & Petrides (2009) who split these into four regions responsible for voluntary saccadic eye movement; the FEFs located in the ventral branch of the superior precentral sulcus, the SEFs located rostral to the medial precentral sulcus at the junction of the medial and lateral cortical surface, the cingulate eye fields (CEF) located in the vertical branch of the cingulate sulcus, and the premotor eye fields (PrEF) in the dorsal branch of the inferior precentral sulcus. It should be noted that Amiez & Petrides

(2009) warn the PrEF may overlap with a region within area 6 involved in blinking, and so serves as a potentially less reliable candidate for saccadic control. This was based on both inter-species comparisons (using gross anatomy and functional classification) and an fMRI study in humans in which saccadic movement was compared against ocular fixation. Previous cytoarchitectonic studies were used to differentiate regions within the frontal lobe (Petrides & Pandya, 1999; Petrides, 2005; Petrides et al., 2012).

5.3. Results

5.3.1. Behavioural Analysis

5.3.1.1. Age Comparisons of Performance

Percentage Accuracy: To address Hypothesis 1 a mixed 2x6 ANOVA was run with age as the between-subject factor (two levels; younger vs elderly), block as the within-subject factor (six levels), and accuracy as the dependent variable (see Figure 11). Mauchly's test of sphericity was significant; $W = .256$, $p<.001$, and as the Greenhouse-Geisser estimate was less than 0.75 (.687) this correction was applied. Levene's test was also significant for blocks four to six meaning homogeneity of variance could not be assumed, and there were two participants with scores +/- three SDs from the mean, as well as evidence of negative skew in later blocks. However as sample sizes were equal ANOVA is thought to be resilient to violations of normality and homogeneity of variance (Field, 2009, pp. 360) and was deemed the best option for analysing the data (bootstrapping was not available for this analysis). There was a significant main effect of block, $F(5,230) = 75.843$, $p<.001$, with a large effect size (partial $\eta^2 = .622$) and Bonferroni corrected pairwise comparisons run. These identified that block one had lower accuracy than all subsequent blocks, as did block two, however block three only differed from block six. A significant main effect of age was also found, $F(1,46) = 14.858$, $p<.001$, with a large effect size (partial $\eta^2 = .244$) driven by accuracy being

lower in the elderly group (M = 67.14, SE = 3.247) than the young group (M = 84.842, SE =

3.247). Finally a significant interaction was evidenced, $F_{(5,230)} = 2.868$, $p<.05$, with a small

effect size (partial $\eta^2 = .059$) investigated by a series of independent one-tailed t-tests

comparing age groups at each block. These found significant differences in every block

(younger higher accuracy than elderly) but with only blocks two, three, four, and five

surviving Bonferroni correction. Simple bootstrapping was employed when running t-tests,

confirming effects in blocks two and three.
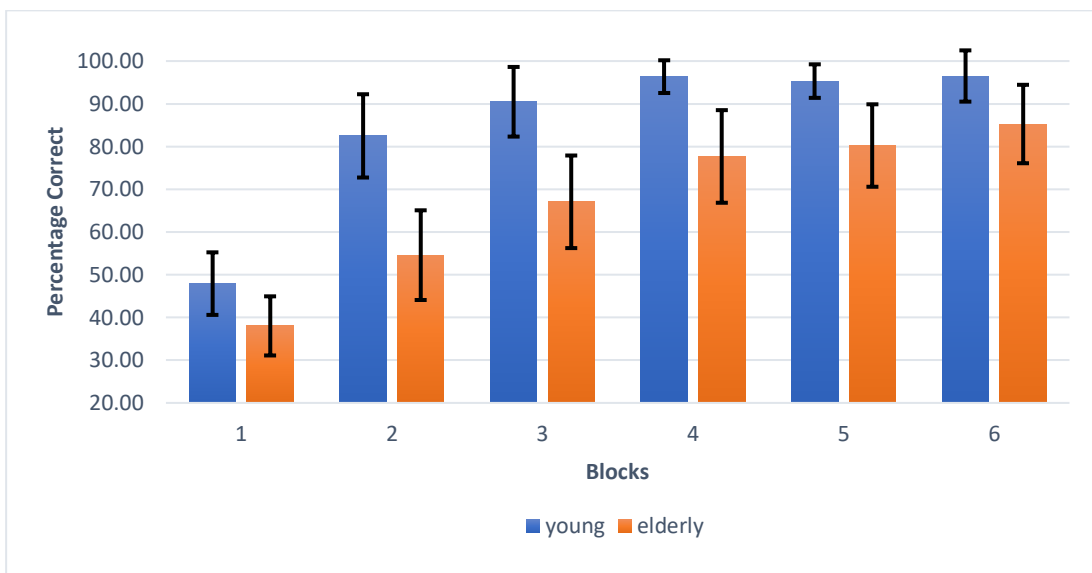
Figure 11. Percentage accuracy plotted across blocks and age groups. Error bars denote two

standard errors.

In order to check learning rate a repeated measures 1x6 ANOVA was run looking at

performance over blocks within elderly and young cohorts independently. Both the elderly

cohort; $F_{(5,115)} = 28.732$, $p<.001$ (Greenhouse Geisser corrected) with a large effect size

(partial $\eta^2 = .555$), and young cohort; $F_{(5,115)} = 59.274$, $p<.001$ (Greenhouse Geisser

corrected) with a large effect size (partial $\eta^2 = .720$), showed significant main effects.

Bonferroni corrected pairwise comparisons demonstrated that the first block to not differ

significantly from any subsequent blocks was block three for the young cohort, and block

four for the elderly (this was subsequently deemed the point at which asymptote was reached).

Reaction Times: To address Hypothesis 2 a 2x3x2 mixed ANOVA (age group x block x condition) was run on the blocked reaction time data. Sphericity was assumed (W = .901- .991, p = .096-.814) but there was evidence of both positive and negative skew, however as group sizes were equal the analysis was deemed appropriate (bootstrapping was unavailable). There was no significant 3-way interaction; $F(2,92) = .974$, $p = .381$ (ns, observed power = .215) and removal of one participant with z scores beyond +/- three SDs did not change the trend.

Pupillometry: Further investigating Hypothesis 2, a 2x3x2 mixed ANOVA (age group x block x condition) was run on the blocked pupillometry data. Sphericity could not be assumed for the block factor (W = .787, $p < .01$) and as the Greenhouse Geisser estimate exceeded .75 (.824) the Huynh-Feldt correction was applied. Sphericity was assumed for the condition x block interaction (W = .888, $p = .069$). There was evidence of positive skew however as group sizes were equal the analysis was deemed appropriate (bootstrapping was unavailable). A significant 3-way interaction was found; $F(2,92) = 5.521$, $p<.01$ with a medium effect size (partial $\eta^2 = .107$). The only other significant effects were that of condition (experimental > control); $F(1,46) = 7.016$, $p<.05$, and age group (young > elderly); $F(1,46) = 4.955$, $p<.05$ (homogeneity of variance could not be assumed), both with medium effect sizes (partial $\eta^2 = .132$ and .097 respectively), see Figure 12.
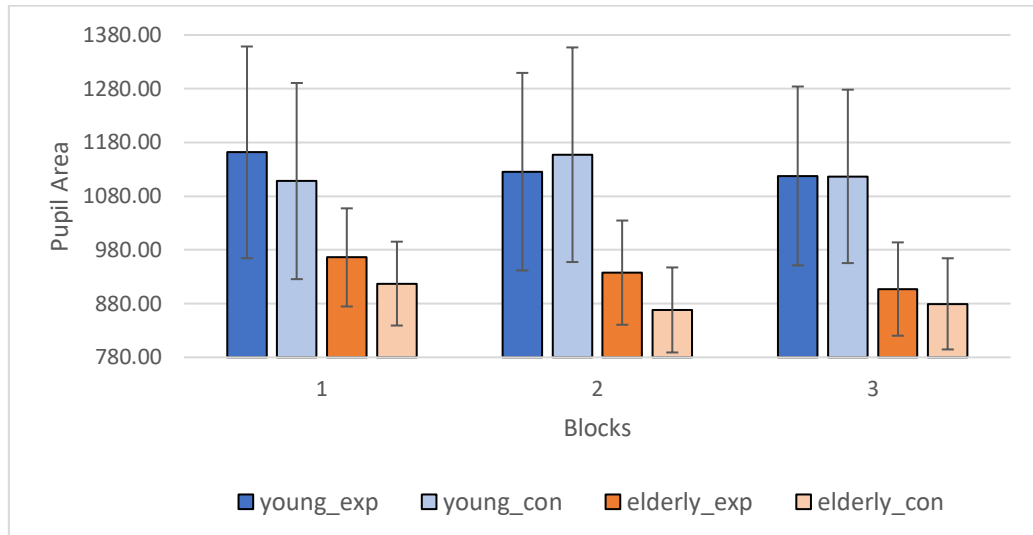
Figure 12. Bar graph demonstrating pupil area over blocks, showing differences between conditions across age groups. Error bars denote two standard errors.

To investigate the interaction a 2x3 mixed ANOVA (condition x block) was run for each age group independently. Within the young cohort sphericity was assumed for block (W = .855, p =.178) and the block x condition interaction (W = .793, p = .078). Both main effects were not significant, but there was a significant block x condition interaction; $F_{(2,46)}$ = 4.794, p<.05 with a large effect size (partial η^2 = .172). This was investigated by running three paired t-tests comparing experimental and control conditions at each level of block. There was a significantly greater pupil area in the experimental condition (M = 1161.583, SE = 98.531) relative to control (M = 1108.167, SE = 91.293) within the first block; t(23) = 3.487, p<.005 (two-tailed). This survived Bonferroni correction and had a medium effect size (cohen's *d* = .712), but no significant differences were identified in the other two blocks.

Within the elderly cohort sphericity could not be assumed for block (W = .396, p<.001) and the Greenhouse Geisser correction was employed (estimate = .623), but could be assumed for the block x condition interaction (W = .927, p=.435). There was a significant main effect of condition; $F_{(1,23)}$ = 7.392, p<.05 with a large effect size (partial η^2 = .243)

31

driven by pupil size being larger in the experimental trials, a main effect of block; $F_{(2,46)} =$ 5.507, p<.05 with a large effect size (partial $\eta^2 = .193$) driven by pupil size reducing over blocks (Bonferroni corrected pairwise comparisons finding a significant difference between blocks one and two; p<.05), but no block x condition interaction (observed power = .545).

5.3.1.2. Extraneous Variables and Follow Up

Number of Trials: The number of trials brought forward into the fMRI analysis differed significantly between age groups with young participants having more trials (young Mdn = 39, range = 34) than elderly (elderly Mdn = 24.5, range = 31). This was confirmed with a Mann Whitney U exact test; U = 87.5, Z = -4.14, p<.001 (two-tailed) with a large effect size (r = .60). As there were four rules being learnt, in order to interpret appropriately it was important to establish whether any group differences found were due to elderly participants generally learning rules to a lesser degree, or learning a smaller number of rules to a level similar to the younger cohort. Within each participant the proportion of included trials per rule was calculated and the maximum selected. This was significantly higher within elderly (Mdn = .40, range = .46) relative to young (Mdn = .30, range = .28) participants, confirmed using a Mann-Whitney U exact test; U = 93, Z = -4.03, p<.001 (two-tailed) with a large effect size (r = .58). This implied that elderly participants performed relatively better in some rules than others, with younger participants being more consistent across rules. To check whether the elderly still learnt less effectively even within a smaller number of rules, the mean number of included trials was calculated across rules with at least one included trial, excluding those with no evidence of learning (this value used as a covariate in the secondary fMRI analysis). This was still significantly lower in the elderly (Mdn = 6.88, range = 7.08) relative to young (Mdn = 9.75, range = 8.5) participants, confirmed using a Mann-Whitney U exact test; U = 92, Z = -4.05, p<.001 (two-tailed) with a large effect size (r = .58). Additionally

looking at the descriptive statistics identified that despite the elderly learning some rules better than others, the maximum actual number of correct rules within any one cue was still lower in the elderly cohort (Mdn = 10) relative to the young cohort (Mdn = 12). As a result the differences in number of trials was not just a reduction in the number of rules learnt, but that learning was generally less progressed within the elderly cohort.

Finally each of the trials directly investigated in the fMRI analysis (correct trials not preceded by an incorrect trial) were examined to check for reaction times less than or equal to zero (as these implied anticipatory saccades). As there was negative skew a Mann Whitney U exact test was run to check for differences in the proportion of trials in which reaction times were greater than zero. There was no significant difference between young (Mdn = 1, range = 0.133) and elderly (Mdn = 1, range = 0.385) cohorts; U = 246, Z = .967, p = .340 (two-tailed).

Missed Trials: There was no significant difference between young (Mdn = 0, range = 18.75) and elderly cohorts (Mdn = 2.08, range = 33.33) regarding the percentage of trials in which a response was not detected, tested using a Mann-Whitney U exact test; U = 229.5, Z = -1.288, p = .203 (two-tailed).

Order of Testing: A univariate ANOVA was run with age group as the independent variable, total accuracy over blocks as the dependent variable, and order of testing (mean centered) as a covariate. Homogeneity of variance could not be assumed and there was significant negative skew in the young cohort (d = .249, p<.001). Consequently simple bootstrapping was employed. There was only a significant main effect of age group, the young (M = 84.764, SE = 2.580) having greater accuracy than the elderly (M = 66.978, SE = 3.742); F(1,44) = 14.512, p<.001. Critically there was no significant interaction between

order of testing and age group; $F_{(1,44)} = .004$, $p = .949$, implying that performance was not modulated by order of testing in any way that varied between age groups, see Figure 13.
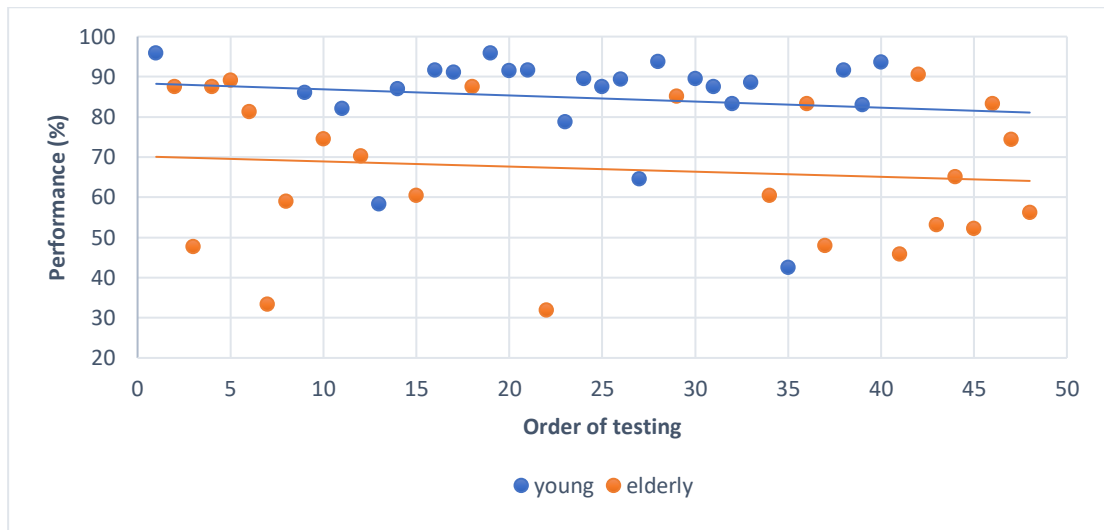
Figure 13. Scatter plot demonstrating association between Order of Testing and Accuracy, with lines of best fit for each age group (linear).

Processing Speed: This used the same effect of age group upon performance reported above, and with no covariates included the effect of age was significant; $F_{(1,46)} = 15.315$, $p<.001$ with a large effect size (partial $\eta^2 = .250$). Median reaction time across control trials (mean centered) was then included as a covariate to represent processing speed, resulting in only a negligible drop in power; $F_{(1,44)} = 14.061$, $p<.002$, partial $\eta^2 = .242$. Critically there was also no significant effect of processing speed; $F_{(1,44)} = .938$, $p = .338$ (homogeneity of slopes assumed as there was no significant processing speed x age group interaction). See Figure 14. When a single young participant with a z score beyond -3 was removed there was no appreciable change in this trend. Reaction time did not differ between age groups; $U = 266.5$, $z = .443$, $p = .664$ (two-tailed), nor did it correlate with performance; $r_{(46)} = -.205$, $p = .163$ (two-tailed).
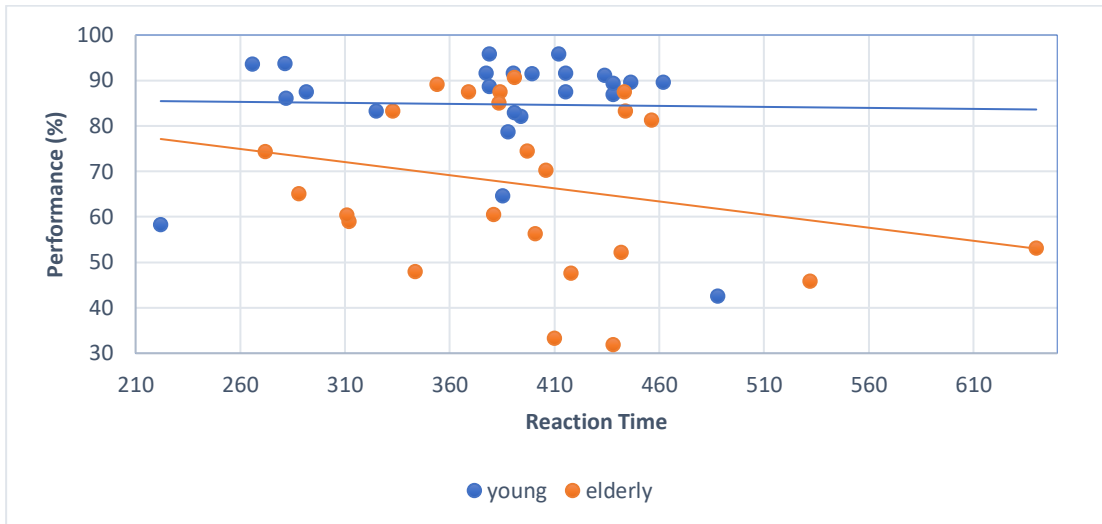
Figure 14. Scatter plot demonstrating association between Reaction Time and Performance, with lines of best fit for each age group (linear).

Time of Day: Optimal time of day for scanning had the potential to introduce a confound between age groups and so was controlled for using MEQ scores. Data was not normally distributed in the elderly cohort (d = .191-.197, p<.05) and so simple bootstrapping was employed. Minutes were divided by 60 to form ratio data, e.g. 12.30 became 12.50. As expected a univariate ANOVA (homogeneity assumed) found a significant main effect of age upon time tested; $F(1,46) = 13.166$, p<.002, with a large effect size (partial η^2 = .223). This was driven by elderly participants being tested earlier (M = 11.15, SE = .301) than younger participants (M = 12.69, SE = .297). However when MEQ score (mean centered) was included as a covariate this effect disappeared; $F(1,44) = 1.651$, p = .206. As anticipated MEQ was a significant predictor; $F(1,44) = 26.596$, p<.001, with a large effect size (partial η^2 = .377), lower MEQ scores being associated with later testing. Crucially there was no significant interaction between age group and MEQ score; $F(1,44) = .335$, p = .566, implying that the effect of MEQ upon time tested did not differ meaningfully between age groups (see Figure 15).
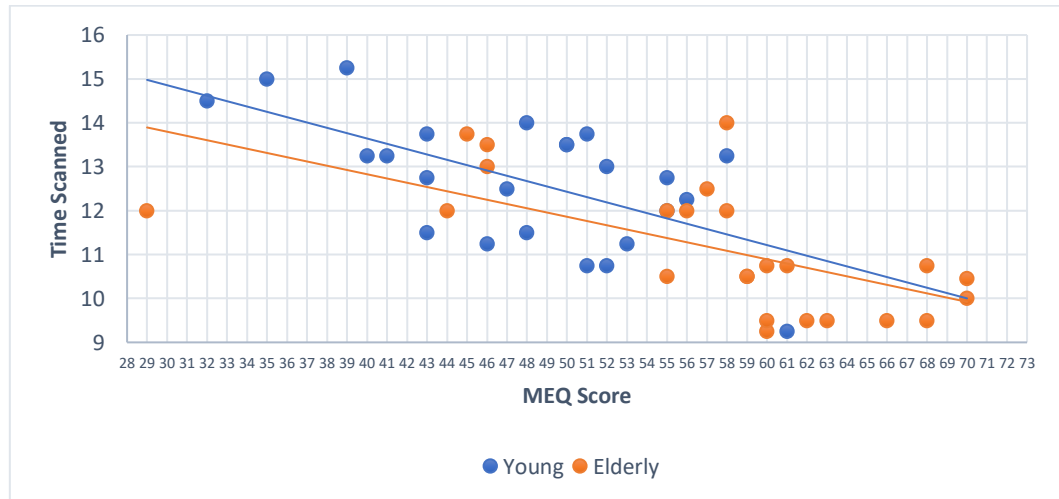
Figure 15. Scatter plot demonstrating association between MEQ score and Time Scanned, with lines of best fit for each age group (linear).

IQ: A Mann-Whitney U exact test found no significant effect of age group upon IQ; younger cohort (Mdn = 117.5, range = 30), elderly cohort (Mdn = 117, range = 23), U = 268.5, Z = -.403, p = .693 (two-tailed).

Mini-Cog: Despite all participants being subthreshold regarding early signs of dementia/mild cognitive impairment Mini-Cog scores were compared using a Mann Whitney U exact test, finding that the young cohort had a significantly higher score (Mdn = 5, range = 1) than the elderly cohort (Mdn = 4.5, range = 2); U = 177, z = 2.827, p<.01 (two-tailed) with a medium effect size (r = .408).

Multicollinearity: There were differences between age groups regarding the maximum correlation coefficients between GLM regressors in the SPM design matrices. Looking between conditions of interest and all regressors excluding head motion the elderly cohort had significantly lower coefficients in the unmodulated experimental condition, and significantly higher coefficients in the parametrically modulated experimental condition. When looking specifically at correlations between conditions of interest and head motion regressors the parametrically modulated experimental and control conditions demonstrated

significantly lower maximum coefficients in the elderly. Despite this, as the unmodulated results demonstrated ample evidence of comparable activity across age groups within plausible predicted regions, it was concluded that any age-differences in multicollinearity was not impacting the results in a meaningful way.

Errors: Firstly the number of errors before and after the first correct response was investigated. The data was not normally distributed in the 'after' condition (d = .208-.327, p<.05) and homogeneity could not be assumed, however as sample sizes were equal and interactions were of interest a mixed 2x2 ANOVA was run, see Figure 16. This looked at two independent variables, age (younger versus elderly) and error-position (before versus after). Only a significant main effect of age was found; $F_{(1,46)} = 13.245$, $p<.002$, with a large effect size (partial η^2 = .224), driven by elderly participants making more errors (mean difference = 3.875, SE = 1.065) irrespective of whether this occurred before or after the first correct response.
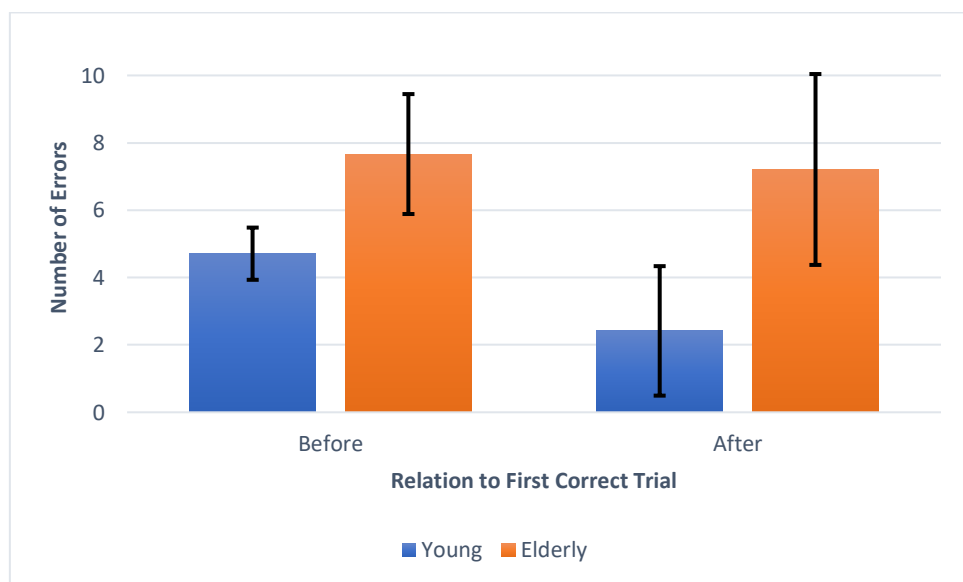
Figure 16. Number of errors before and after the first correct trial, error bars denote two standard errors.

Next the number of repeated errors (perseveration) was examined in the same way (see Figure 17). Again data was not normally distributed in three of the four conditions (d = .278-.375, p<.05) and homogeneity of variance could not be assumed. There was only a main effect of age; $F(1,46) = 13.536$, p<.002, with a large effect size (partial $\eta^2 = .227$), driven by more repeated errors in the elderly (mean difference = 3.188, SE = .866). There was one young participant with a z score greater than three in both error and repeated error analyses, however removal did not change the trend of each analysis. This confirmed elderly participants made more errors and more repeated errors, and that this was seen both before and after receiving 'correct' feedback within a rule.
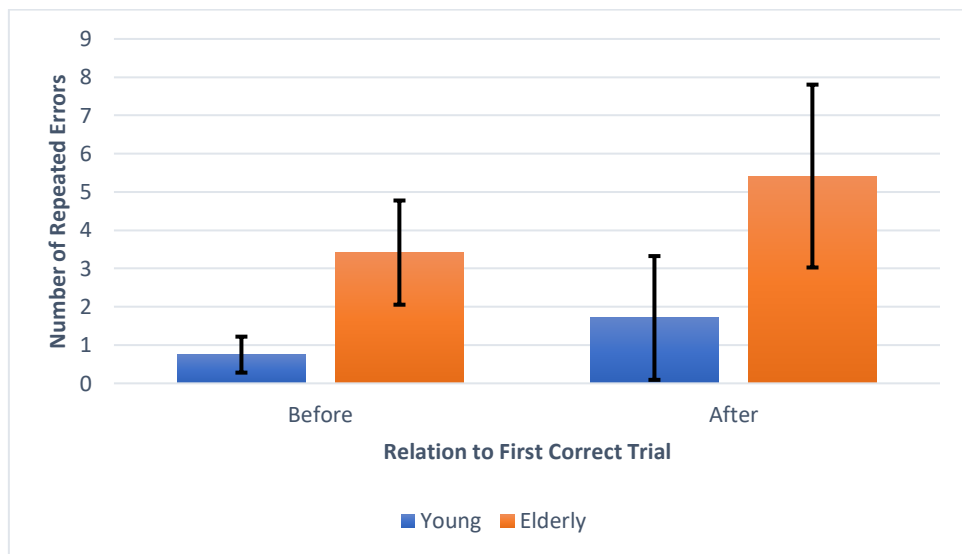
Figure 17. Number of repeated errors before and after the first correct trial, error bars denote two standard errors.

Finally instances where a correct trial was followed by an error were examined, looking at the percentage of these in which the error trial matched the correct trial in terms of target selection. Firstly when looking at data pertaining to any preceding correct trial (experimental or control) an independent t-test found no significant difference between age groups in the prevalence of correct trials biasing choices on the subsequent trial; t(46) =

.051, p=.960. When running the same analysis but with control trials removed data was not normally distributed (d = .192-.352, p<.05) and a Mann Whitney U exact test was run, finding no significant difference between age groups; U = 215, z = 1.564, p = .120 (two-tailed).

5.3.2. fMRI Analysis

5.3.2.1. Effects of Condition (Conjunction Analysis): To address Hypothesis 3 a conjunction analysis was run looking for main effects of condition (experimental versus control) across both age cohorts (elderly versus young).

Cerebellum: There was a single significant peak in left CRUS I, the cluster extending into lobule HVI. Follow up analyses found a main effect of condition potentially driven by positive BOLD responses in the experimental condition exceeding those in the control condition. See Table 2 and Figure 18.

Table 2. Coordinates with significant effects of condition across both age groups, within the cerebellar analysis.

Gross Anatomical Region	Cytoarchitectonic Region	Prob.	Coordinates	Peak F/Z	Peak P (FWE)	Cluster P (FWE)	K
L CRUS I/HVI	N/A	N/A	-37.5, -58.5, -30	12.49/5.18	<.001	<.01	789

Effect	Explanation
Simple effect (elderly experimental)	+
Simple effect (elderly control)	+
Simple effect (young experimental)	+
Simple effect (young control)	+
Main effect of condition	Experimental > Control

Figure 18. Coordinate with a significant effect of condition across both age groups, within cerebellar CRUS I. Plots show estimated BOLD responses for each level of condition and age group.

Frontal Lobe: There were five clusters in the frontal lobe with significant peak coordinates. For the first of these the primary peak was located in the left paracingulate gyrus but extended bilaterally (see Figure 19 A). The peak coordinate showed a main effect of condition potentially driven by greater magnitude BOLD responses in the experimental condition. Sub-peaks were located medially within the left medial superior frontal gyrus (SFG), potentially within the SEFs (Table 3 B, Figure 19 B), left paracingulate gyrus (Table 3 O, Figure 19 C), and right cingulate sulcus (Table 3 I, Figure 19 D).
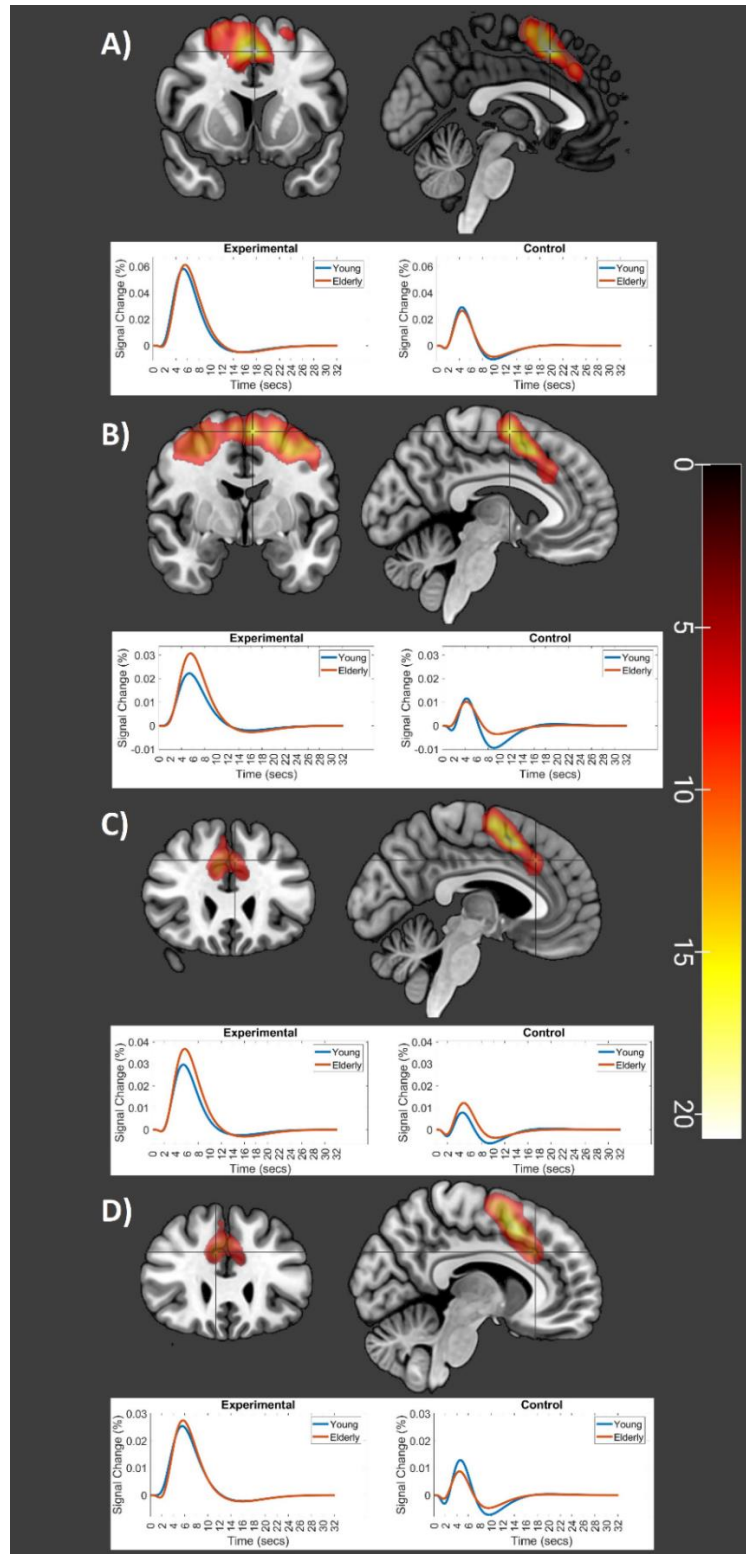
Figure 19. Coordinates with a significant effect of condition across both age groups, upon the medial wall. Plots show estimated BOLD responses for each level of condition and age group. Colour-bar denotes F values.

There was also a collection of sub-peaks thought to correspond to the FEFs (based upon the work of Amiez & Petrides, 2009). In the left hemisphere three sub-peaks sat within the ventral branch of the superior precentral sulcus (vsPCS; Table 3 C-E, Figure 20 A-C), with a further coordinate in the caudal SFG, just rostral to the top of the vsPCS (Table 3 A, Figure 20 D).
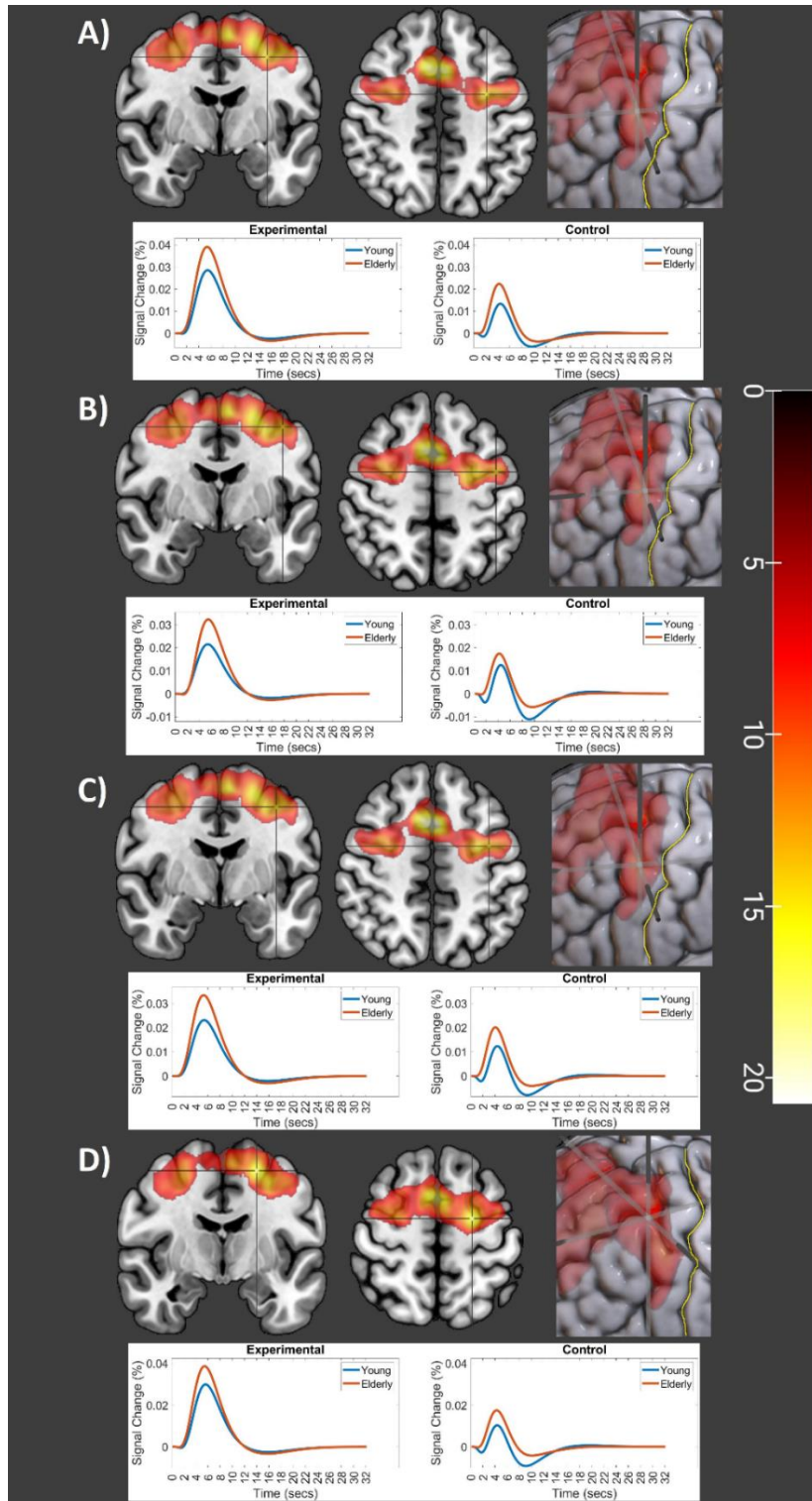
Figure 20. Coordinates with a significant effect of condition across both age groups, within the left lateralised precentral sulcus (central sulcus highlighted in yellow). Plots show estimated BOLD responses for each level of condition and age group. Colour-bar denotes F values.

43

In the right hemisphere there were also three sub-peaks within the vsPCS (Table 3 G, H, and M, Figure 21 A-C) as well as two sub-peaks nearby, the first in the right caudal SFG dorso-rostral to the vsPCS (Table 3 J, Figure 22 A) and the second in the right precentral gyrus ventro-caudal to the vsPCS (Table 3 L, Figure 22 B).
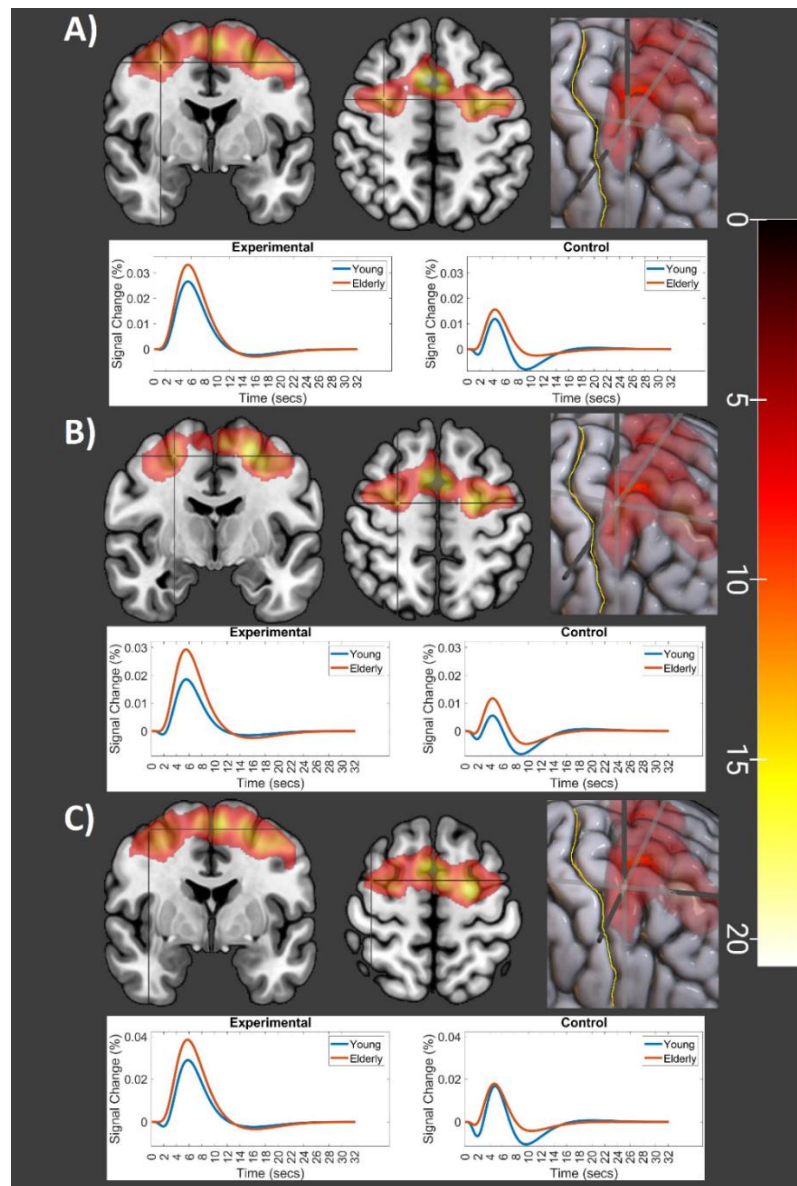
Figure 21. Coordinates with a significant effect of condition across both age groups, within the right lateralised precentral sulcus (central sulcus highlighted in yellow). Plots show estimated BOLD responses for each level of condition and age group. Colour-bar denotes F values.
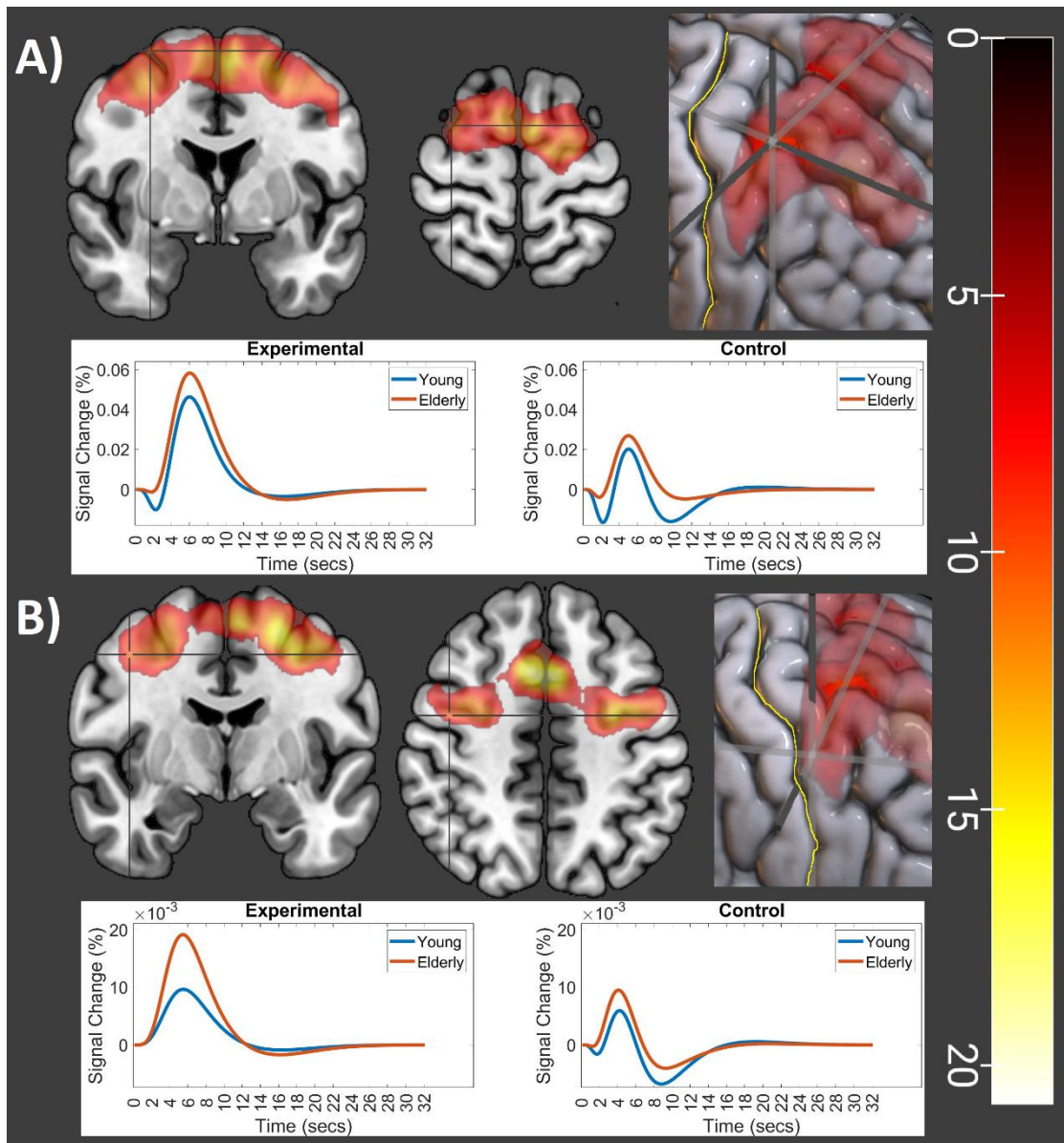
Figure 22. Coordinates with a significant effect of condition across both age groups, near the right lateralised precentral sulcus (central sulcus highlighted in yellow). Plots show estimated BOLD responses for each level of condition and age group. Colour-bar denotes F values.

There were then three sub-peaks within the caudal SFG deemed to be the dorsal aspect of area 6, two right lateralised (Table 3 K, and N, Figure 23 A-B) and one left lateralised (Table 3 F, Figure 23 C).
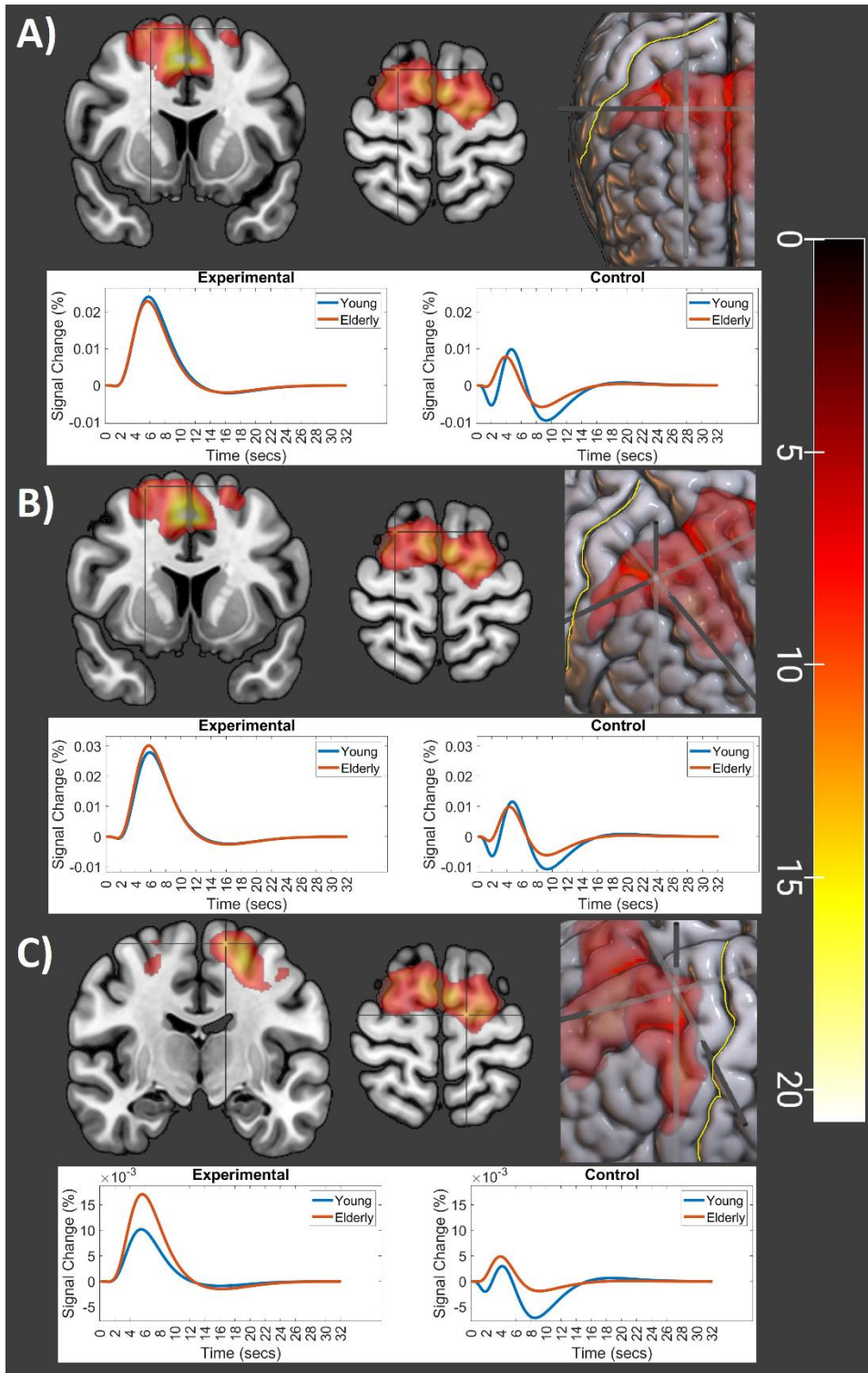
Figure 23. Coordinates with a significant effect of condition across both age groups, within the SFG (central sulcus highlighted in yellow). Plots show estimated BOLD responses for each level of condition and age group. Colour-bar denotes F values.

Table 3. Coordinates with significant effects of condition across both age groups, within the frontal lobe analysis. Data pertains only to the first cluster.

Gross Anatomical Region	Cytoarchitectonic Region	Prob.	Coordinates	Peak F/Z	Peak P (FWE)	Cluster P (FWE)	K
Bilateral Paracingulate Gyrus	N/A	N/A	-1.5, 10.5, 49.5	21.09/6.90	<.001	<.001	16488
Effect				Explanation			
Simple effect (elderly experimental)				+			
Simple effect (elderly control)				+			
Simple effect (young experimental)				+			
Simple effect (young control)				+			
Main effect of condition				Experimental > Control			
Sub-Peaks							
A) L Caudal SFG	6d1	.356	-22.5, -7.5, 57	17.36/6.23	<.001	N/A	N/A
B) L Medial SFG	6mc / SMA	.326	-6, -3, 61.5	16.46/6.05	<.001	N/A	N/A
C) L Precentral Sulcus	6d2	.074	-31.5, -4.5, 48	15.24/5.80	<.001	N/A	N/A
D) L Precentral Gyrus	N/A	N/A	-42, -4.5, 52.5	14.22/5.58	<.001	N/A	N/A
E) L Precentral Gyrus	N/A	N/A	-37.5, -4.5, 49.5	14.21/5.57	<.001	N/A	N/A
F) L Caudal SFG	6d1	.537	-13.5, -12, 66	12.94/5.29	<.002	N/A	N/A
G) R Caudal MFG	6d3	.048	31.5, -1.5, 51	12.68/5.22	<.002	N/A	N/A
H) R Precentral Gyrus	6d3	.562	25.5, -7.5, 54	12.61/5.21	<.002	N/A	N/A
I) R Cingulate Sulcus	N/A	N/A	7.5, 27, 31.5	11.54/4.94	<.005	N/A	N/A
J) R Caudal SFG	6d1	.128	30, 0, 66	11.01/4.81	<.01	N/A	N/A
K) R Caudal SFG	6d2	.364	19.5, 10.5, 66	10.57/4.69	<.02	N/A	N/A
L) R Precentral Gyrus	4a	.231	42, -6, 48	10.44/4.66	<.02	N/A	N/A
M) R Precentral Gyrus	N/A	N/A	39, -1.5, 58.5	10.43/4.66	<.02	N/A	N/A
N) R Caudal SFG	6d2	.243	24, 9, 66	10.35/4.63	<.02	N/A	N/A
O) Paracingulate Gyrus	N/A	N/A	-4.5, 25.5, 37.5	10.20/4.59	<.02	N/A	N/A

The first cluster was next checked for how well it corresponded with the eye fields as described by Amiez & Petrides (2009), see Figure 24. There was clear evidence of the bilateral FEFs being active (consistent with sub-peaks in Table 3), but additional evidence that the SEFs and CEFs were active bilaterally, alongside the PrEFs in the left hemisphere.
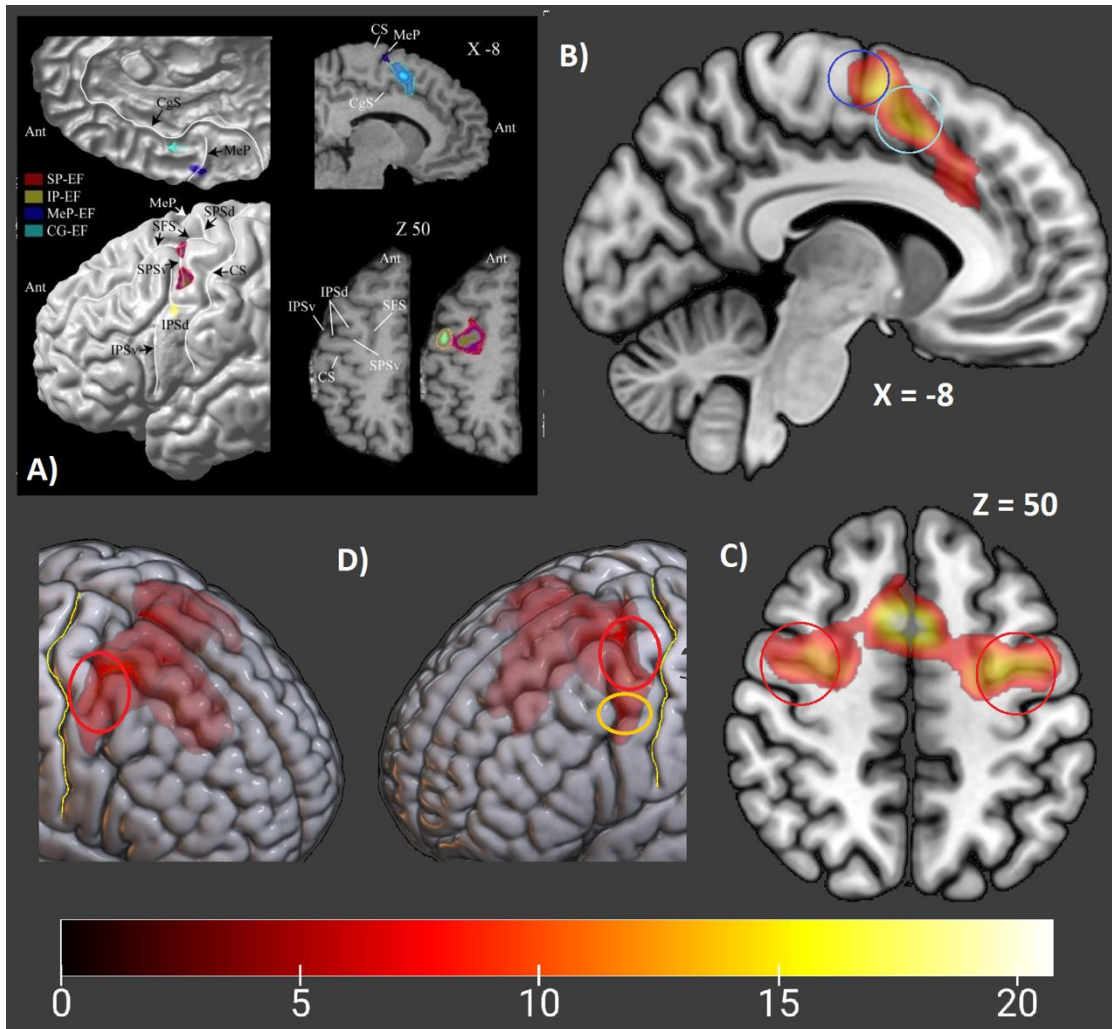
Figure 24. A) Locations of the human eye-fields as per Amiez & Petrides (2009), copied with permission. Sections B-E show evidence of eye-field activity in the conjunction analysis, all within the cluster peaking at x = -1.5, y = 10.5, z = 49.5. B) Sagittal slice (MNI coordinate X = -8) showing evidence of both SEF (dark blue, MeP-EF) and CEF (light blue, CG-EF). C) Axial slice (MNI coordinate Z = 50) showing evidence of FEF activity (red, SP-EF). D) the lateral frontal lobe showing evidence of both FEF (red) and PrEF activity (yellow, IP-EF). MeP-EF = medial precentral sulcus eye field; CG-EF = cingulate sulcus eye field; SP-EF = superior precentral sulcus eye field; IP-EF = inferior precentral sulcus eye field. Colour bar denotes F values and the central sulcus is highlighted in yellow.

The second cluster peaked within the right frontal operculum (Table 4 A, Figure 25 A), with a sub-peak within the right lateral fissure (Figure 25 B), bordering both the lateral orbital and insular cortices. This cluster extended into the inferior frontal gyrus (IFG)

48

including pars triangularis and opercularis (with evidence of cytoarchitectonic areas 44 and 45 active).
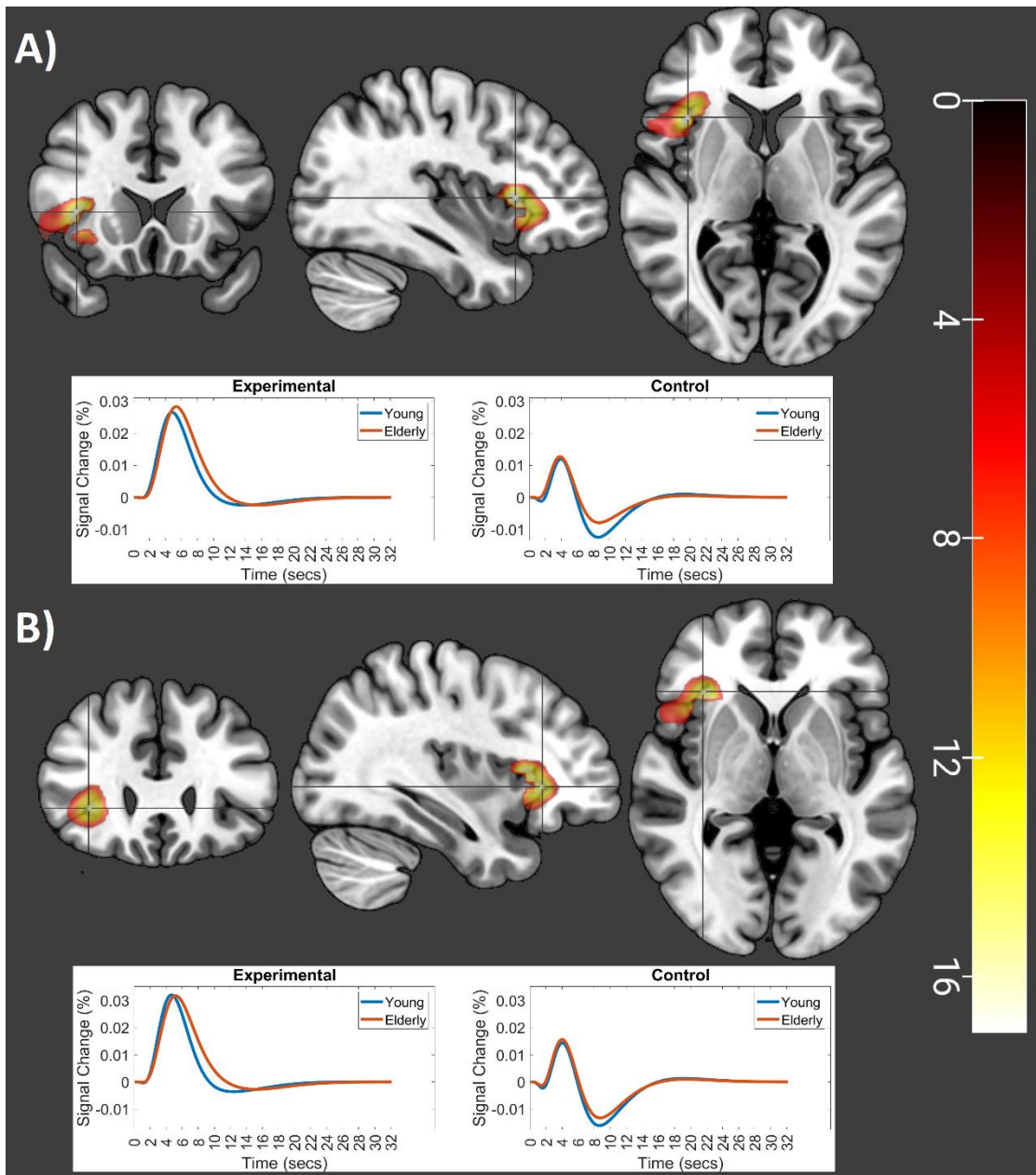
Figure 25. Coordinates with a significant effect of condition across both age groups, within the right frontal operculum. Plots show estimated BOLD responses for each level of condition and age group. Colour-bar denotes F values.

The third peaked in the left frontal operculum (Table 4 B, Figure 26 A), with sub-peaks in the orbital and insular cortices overlapping marginally into the putamen (Figure 26

49

B-E). This cluster also extended into the IFG (pars triangularis) with some evidence of cytoarchitectonic areas 44 and 45 being active, but to a lesser degree than the right hemisphere.
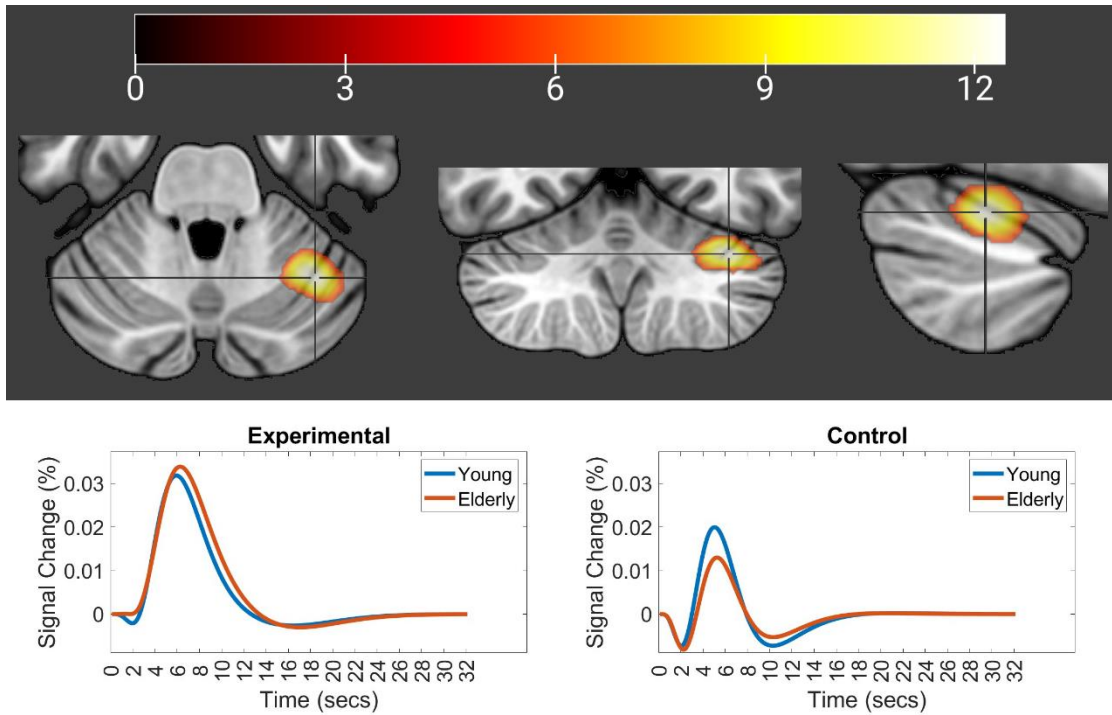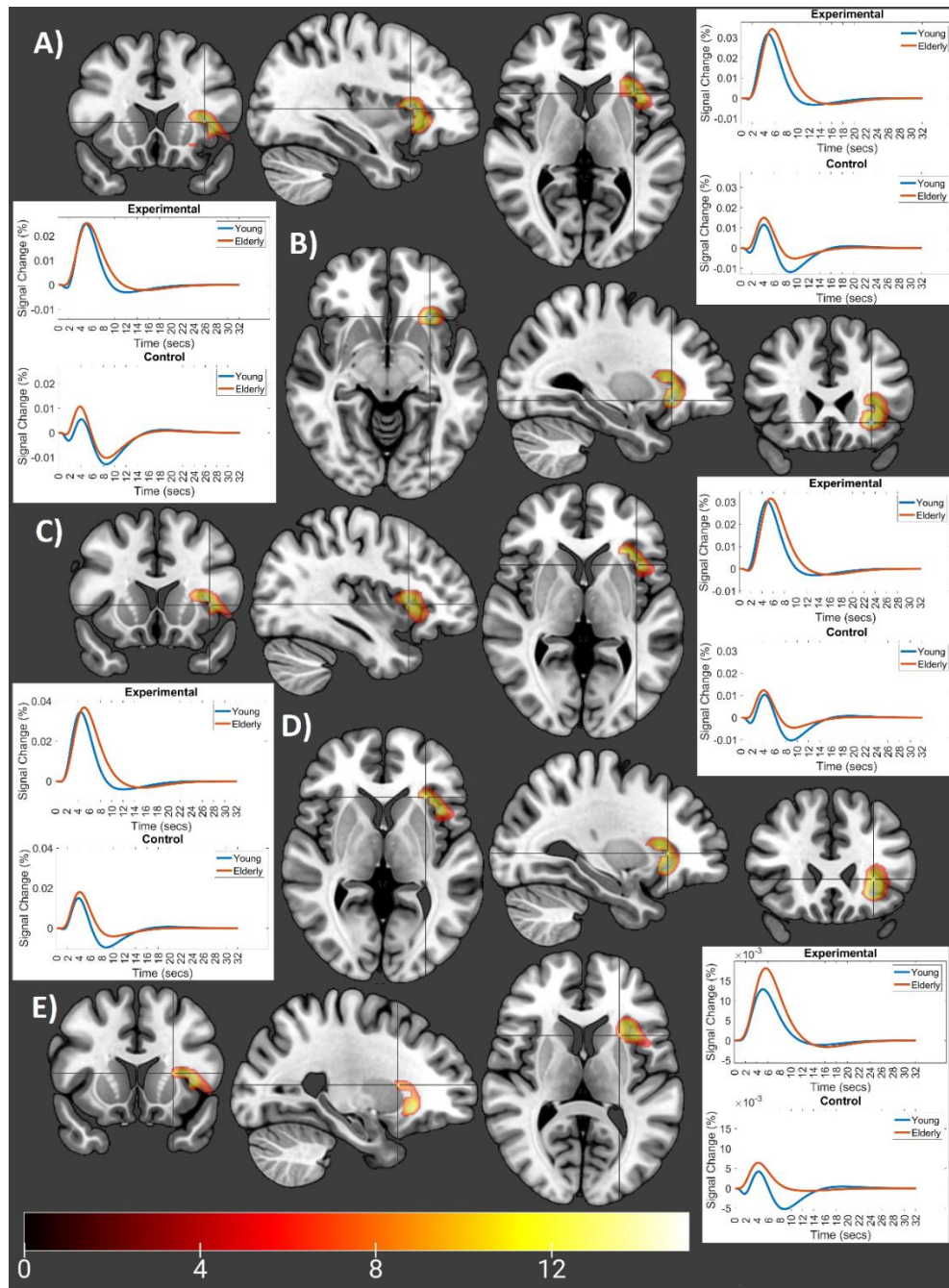

Figure 26. Coordinates with a significant effect of condition across both age groups, within the left frontal operculum. Plots show estimated BOLD responses for each level of condition and age group. Colour-bar denotes F values.

The fourth peaked within the right middle frontal sulcus (MFS), a region deemed to be area 46 based on the work of Petrides & Pandya (1999), see Table 4 C and Figure 27 B. The sub-peaks sat ventral to the MFS, but still within the middle frontal gyrus (MFG; Figure 27 C-D). The cluster extended into regions potentially including 9/46d and 9/46v.
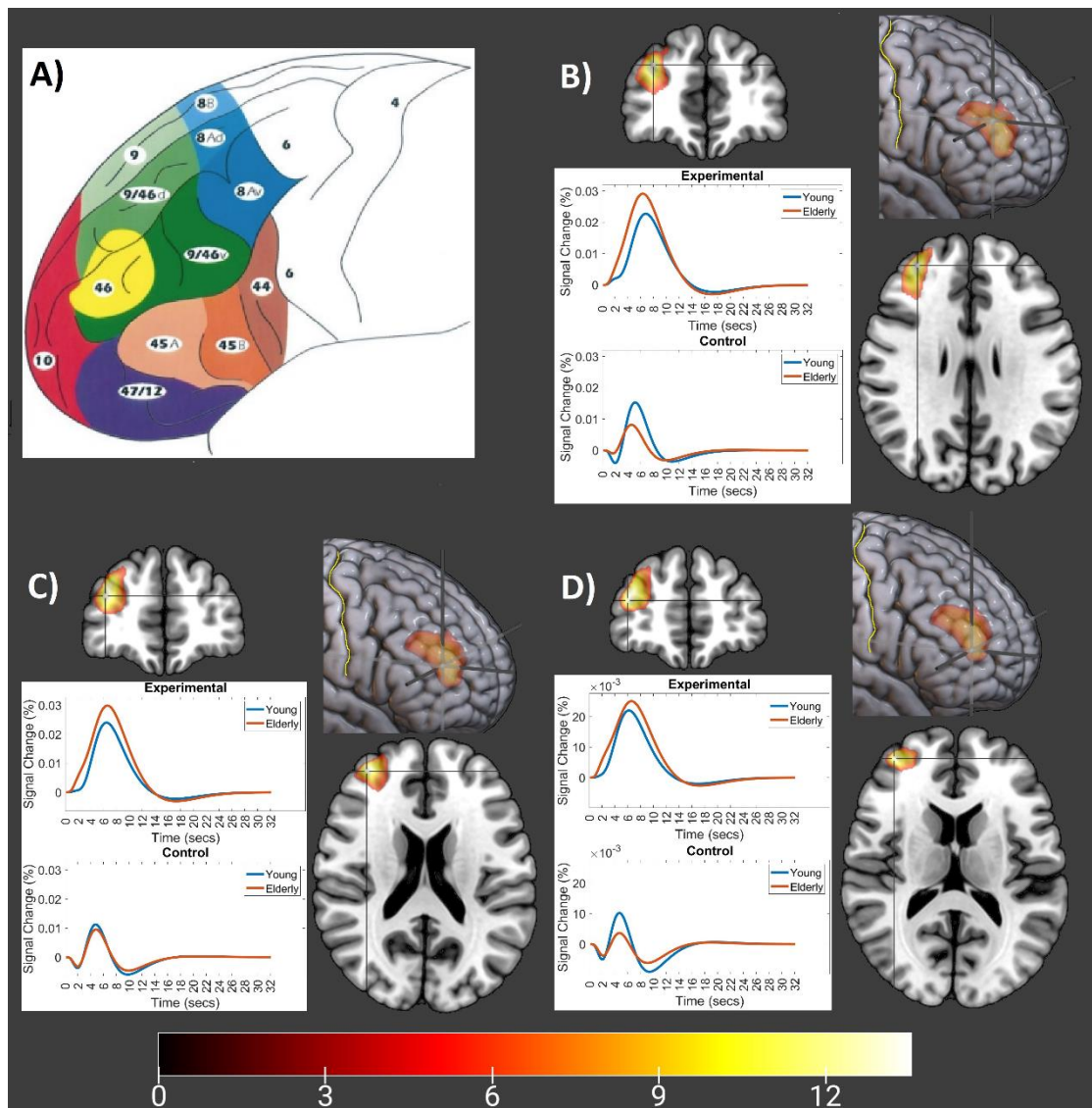
Figure 27. Coordinates with a significant effect of condition across both age groups, within the right MFG. Section A is copied from Petrides & Pandya (1999) with permission. Plots B-D show estimated BOLD responses for each level of condition and age group. Colour-bar denotes F values.

The fifth peaked within the left MFG ventral to the MFS (Table 4 D, Figure 28 B), again deemed to be area 46, with a sub-peak within a region deemed to be area 9/46v (Figure 28 C). All peaks showed main effects of condition, potentially driven by greater magnitude BOLD responses in the experimental condition.
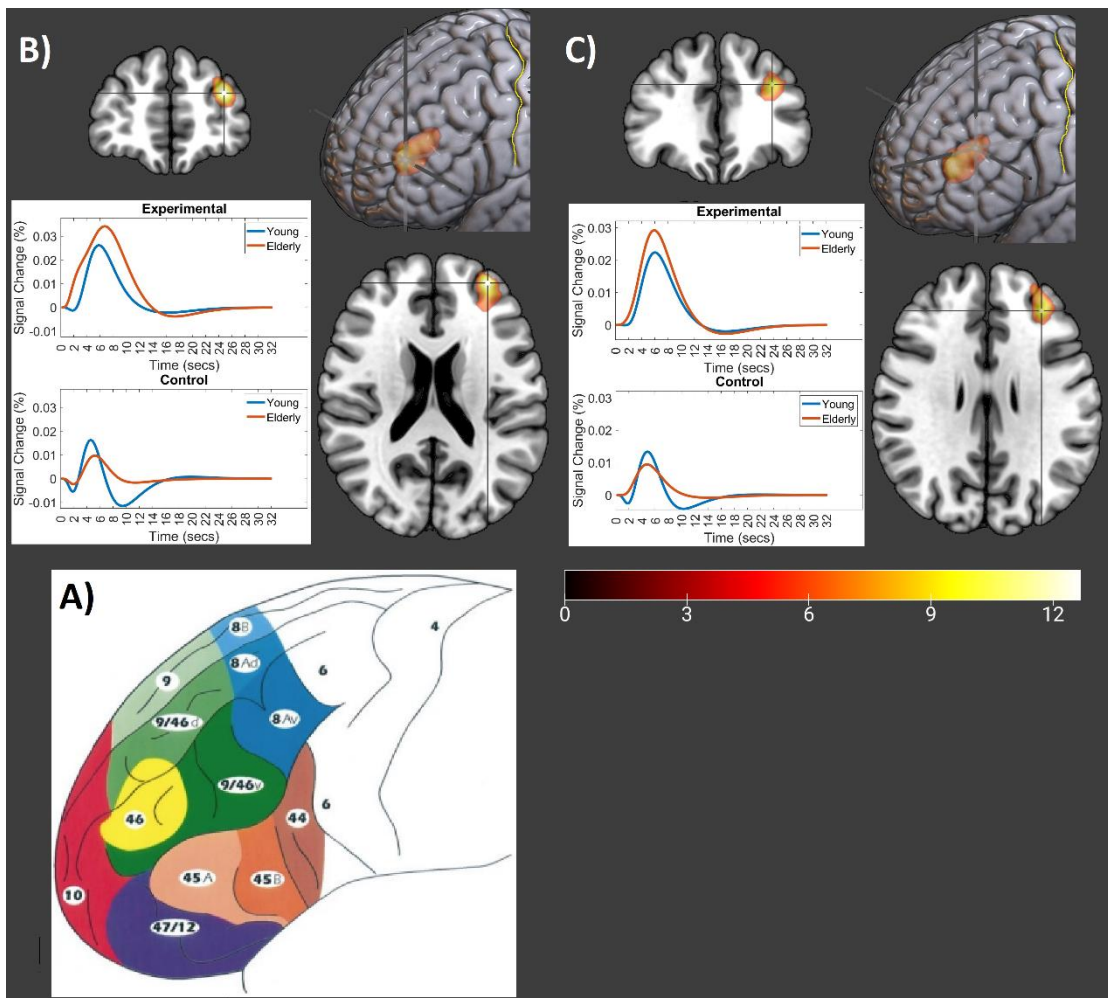
Figure 28. Coordinates with a significant effect of condition across both age groups, within the left MFG. Section A is copied from Petrides & Pandya (1999) with permission. Plots B-D show estimated BOLD responses for each level of condition and age group. Colour-bar denotes F values.

Table 4. Coordinates with significant effects of condition across both age groups, within the frontal lobe analysis. Data pertains to the second-fifth clusters.

Gross Anatomical Region	Cytoarchitectonic Region	Prob.	Coordinates	Peak F/Z	Peak P (FWE)	Cluster P (FWE)	K
A) R Frontal Operculum	OP8	.388	37.5 ,18, 6	17.26/6.21	<.001	<.001	2164
Effect				Explanation			
Simple effect (elderly experimental)				+			
Simple effect (elderly control)				+			
Simple effect (young experimental)				+			
Simple effect (young control)				-			
Main effect of condition				Experimental > Control			
Sub-Peaks							
R Lateral Fissure	Id7	.715	34.5, 27, 0	15.32/5.81	<.001	N/A	N/A
B) L Frontal Operculum	Id6	.582	-34.5, 16.5, 6	15.36/5.82	<.001	<.001	1925
Effect				Explanation			
Simple effect (elderly experimental)				+			
Simple effect (elderly control)				+			
Simple effect (young experimental)				+			
Simple effect (young control)				-			
Main effect of condition				Experimental > Control			
Sub-Peaks							
A) L Frontal Orbital Cortex	N/A	N/A	-30, 22.5, -7.5	15.12/5.77	<.001	N/A	N/A
B) L Insular Cortex	Id6	.751	-37.5, 15, 3	14.43/5.62	<.001	N/A	N/A
L Insular Cortex	Id7	.924	-30, 24, 3	12.74/5.24	<.002	N/A	N/A
L Putamen	N/A	N/A	-25.5, 13.5, 9	9.34/4.35	<.05	N/A	N/A
C) R Frontopolar Gyrus	N/A	N/A	33, 46.5, 28.5	13.71/5.47	<.001	<.001	2538
Effect				Explanation			
Simple effect (elderly experimental)				+			
Simple effect (young experimental)				+			
Simple effect (young control)				+			
Main effect of condition				Experimental > Control			
Sub-Peaks							
R Frontopolar Gyrus	N/A	N/A	36, 49.5, 19.5	13.57/5.43	<.001	N/A	N/A
R Frontopolar Gyrus	N/A	N/A	37.5, 52.5, 13.5	13.01/5.3	<.002	N/A	N/A
D) L Frontopolar Gyrus	N/A	N/A	-33, 52.5, 19.5	12.73/5.24	<.002	<.002	1492

Effect							
Simple effect (elderly experimental)				+			
Simple effect (young experimental)				+			
Simple effect (young control)				+			
Main effect of condition				Experimental > Control			
Sub-Peaks							
L Frontopolar Gyrus	N/A	N/A	-33, 37.5, 28.5	10.68/4.72	<.02	N/A	N/A

5.3.2.2. Age x Condition: To address hypothesis 4 an interaction analysis was run looking for effects of condition which differed between age groups.

Cerebellum: There were no significant peaks in the cerebellum surviving FWE correction, but there were two which were significant when uncorrected. In order to explore this trend for the cerebellar interaction uncorrected results (α = .001) are reported. In a cluster across left lobule HV-HVI only the elderly showed a significant effect of condition, with a significant positive BOLD response in the experimental condition, and significant negative BOLD response in the control condition (Table 5 A, Figure 29 A). In right CRUS I there was a similar effect, with only the elderly showing an effect of condition potentially driven by only the experimental condition being significant (Table 5 B, Figure 29 B).

54
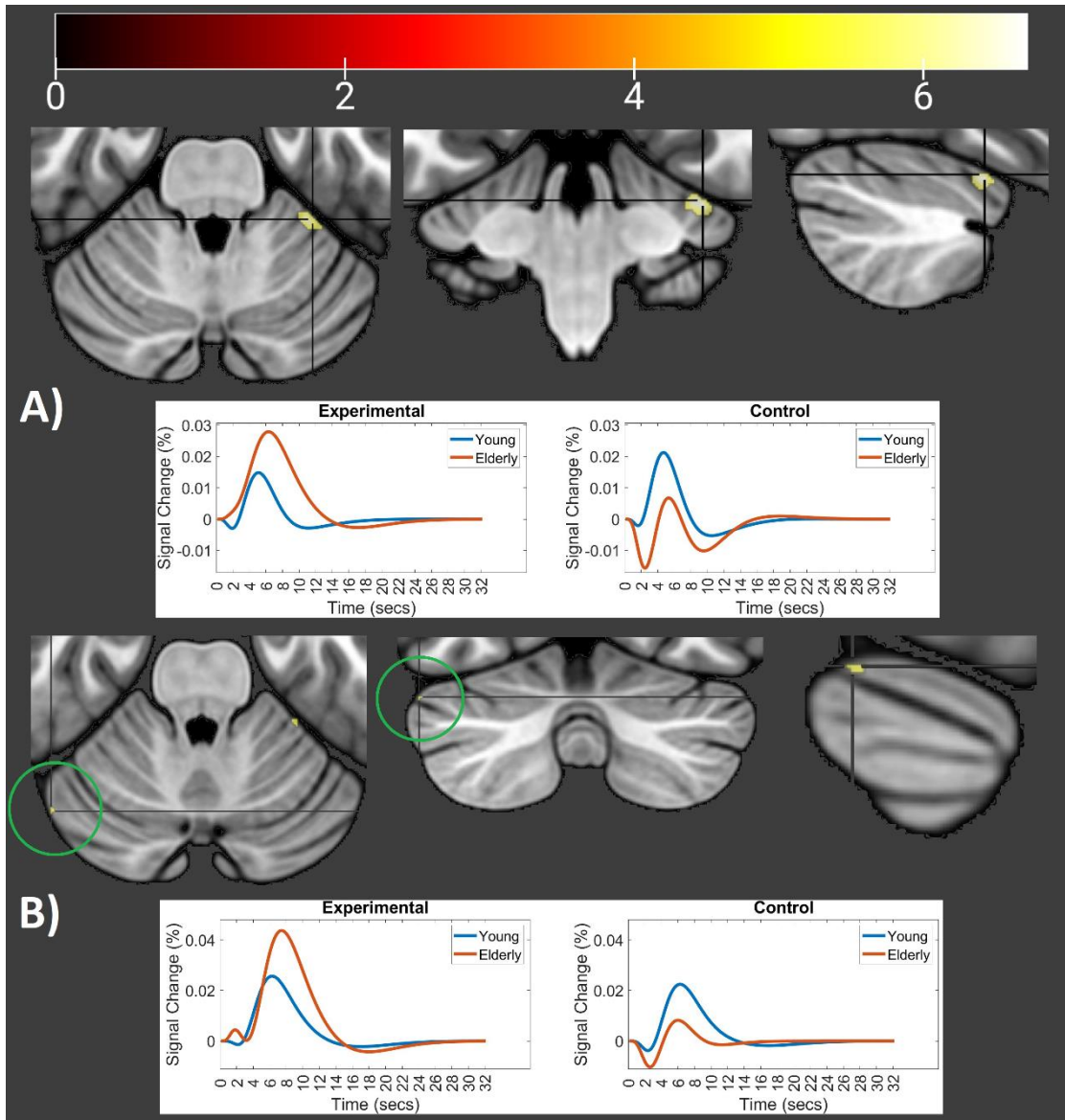
Figure 29. Coordinates with a significant age x condition interaction, within the cerebellar analysis. Plots show estimated BOLD responses for each level of condition and age group. Colour-bar denotes F values.

Table 5. Coordinates with a significant age x condition interaction when uncorrected (p<.001), within the cerebellar analysis.

Gross Anatomical Region	Cytoarchitectonic Region	Prob.	Coordinates	Peak F/Z	Peak P (FWE)	Cluster P (FWE)	K
A) L HV-HVI	N/A	N/A	-33,-39,-28.5	6.81/3.55	.277	.430	42
Effect				Explanation			
Simple effect (elderly experimental)				+			
Simple effect (elderly control)				-			
Simple effect (young experimental)				+			
Simple effect (young control)				+			
Effect of condition (elderly)				Experimental (+) > Control (-)			
Main effect of condition				Experimental > Control			
B) R CRUS I	N/A	N/A	49.5,-69,-27	6.5/3.44	.366	.674	2
Effect				Explanation			
Simple effect (elderly experimental)				+			
Simple effect (young experimental)				+			
Simple effect (young control)				+			
Effect of condition (elderly)				Experimental (+)			

Frontal lobe: There were two clusters with significant peaks surviving small volume FWE correction. The first peaked within a region of the left MFG which was deemed to border between 9/46d and area 8Ad (Table 6 A, Figure 30 A). The cluster extended into the left SFG and frontopolar gyrus, including regions deemed to be areas 9/46d, 9, and areas 8Av, Ad, and B. The effect was potentially driven by there only being an effect of condition in the elderly cohort, which only showed a significant positive BOLD response in the experimental condition. The second peaked in the right SFG (Table 6 B, Figure 30 B), within a region deemed to be area 9, extending into areas 9/46d, 8Ad, and 8B. No effects of condition survived correction, but there was a significant simple effect within the elderly experimental condition which potentially drove the interaction.
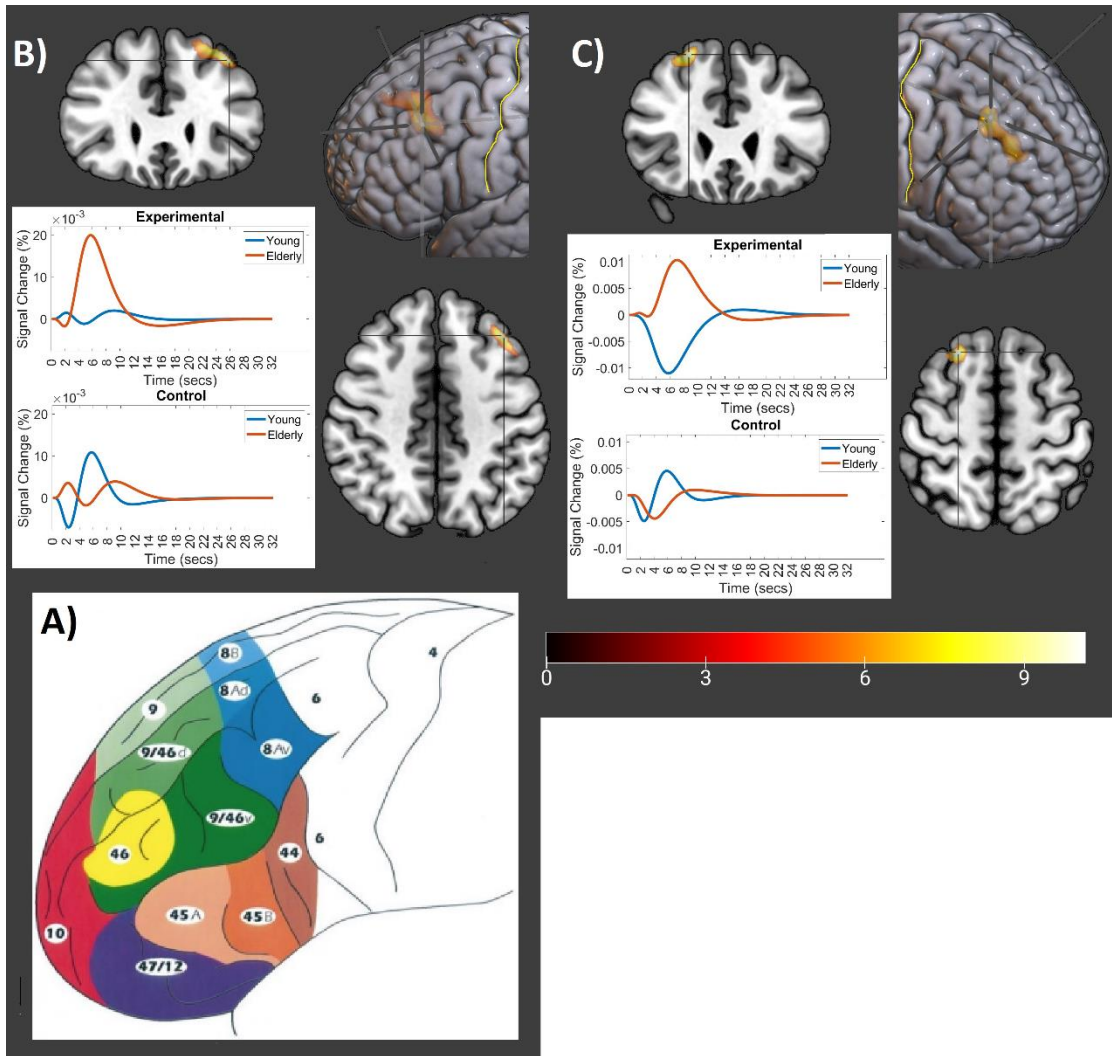
Figure 30. Coordinates with a significant age x condition interaction, within the frontal lobe analysis (central sulcus highlighted in yellow). Section A is copied from Petrides & Pandya (1999) with permission. Plots show estimated BOLD responses for each level of condition and age group. Colour-bar denotes F values.

Table 6. Coordinates with a significant age x condition interaction, within the frontal lobe analysis.

Gross Anatomical Region	Cytoarchitectonic Region	Prob.	Coordinates	Peak F/Z	Peak P (FWE)	Cluster P (FWE)	K
A) L MFG	N/A	N/A	-39,28.5,45	12.57/5.20	<.002	<.02	744
Effect				Explanation			
Simple effect (elderly experimental)				+			
Effect of condition (elderly)				Experimental > Control			
B) R SFG	N/A	N/A	22.5,25.5,57	10.24/4.60	<.02	<.03	612
Effect				Explanation			
Simple effect (elderly experimental)				+			

5.2.2.3. Condition x Practise Conjunction: Pertaining to Hypothesis 5, there were no interactions between condition and practise across both age groups within either the frontal lobe or the cerebellum.

5.3.2.4. Age x Condition x Practise: Pertaining to Hypothesis 6, there were no interactions between age, condition, and practise within either the frontal lobe or the cerebellum.

5.3.2.5. Whole Brain Analysis: An exploratory whole brain analysis was conducted with FWE whole brain correction (α = .05), looking for activity beyond pre-specified regions of interest. There were no additional interactions beyond the two frontal lobe clusters reported, nor any age x condition x practise interactions, or condition x practise interactions across both age groups. There were however six additional regions where there was an effect of condition in both age groups, see Table 7.

Table 7. All additional significant coordinates in a whole brain analysis with FWE correction
(α = .05).

Region	Cytoarchitectonic	Coordinate	F	Z	K	p (FWE) peak
Left Superior Parietal Gyrus extending into the angular gyrus and intraparietal sulcus.	7A (47.3%) extending into hIP3, hIP6, 7P, and 7PC.	-21, -61.5, 58.5	17.4	6.23	2036	<.001
Right Superior Parietal Gyrus extending into the angular gyrus and intraparietal sulcus.	7A (67.5%) extending into hIP3, and 7P.	22.5, -58.5, 60	16.74	6.10	1518	<.001
Left caudate, extending into the anterior internal capsule and genu, and the anterior thalamic nucleus.	N/A	-15, 6, 9	10.75	4.74	76	<.03
Bilateral medial Superior Parietal Gyrus (Precuneous) including the intraparietal sulcus.	7P (7.4%).	-3, -55.5, 49.5	10.44	4.66	18	<.04
Left Lingual Gyrus bordering on the calcarine sulcus.	hOc1 (79.2%) extending into hOc2.	-9, -88.5, -1.5	10.28	4.61	7	<.04
Right caudate extending into the internal Capsule.	N/A	13.5, 3, 10.5	10.24	4.60	7	<.04

All regions showed the same trends of positive BOLD responses in the experimental

condition, which exceeded the magnitude of those in the control condition. In the lingual

gyrus and right caudate the young experimental condition did not have a significant effect

when the number of trials covariate was included. Activations extended into the internal

capsule, with it considered that as a white matter tract it may not reliably produce enough

signal to be picked up using fMRI, however some studies at 4T have found signal here

(Frizzell et al., 2020; Gawryluk et al., 2011; Mazerolle et al., 2013). This could also be a result

of the 8mm smoothing kernel. See Figure 31 for an overview of significant regions.
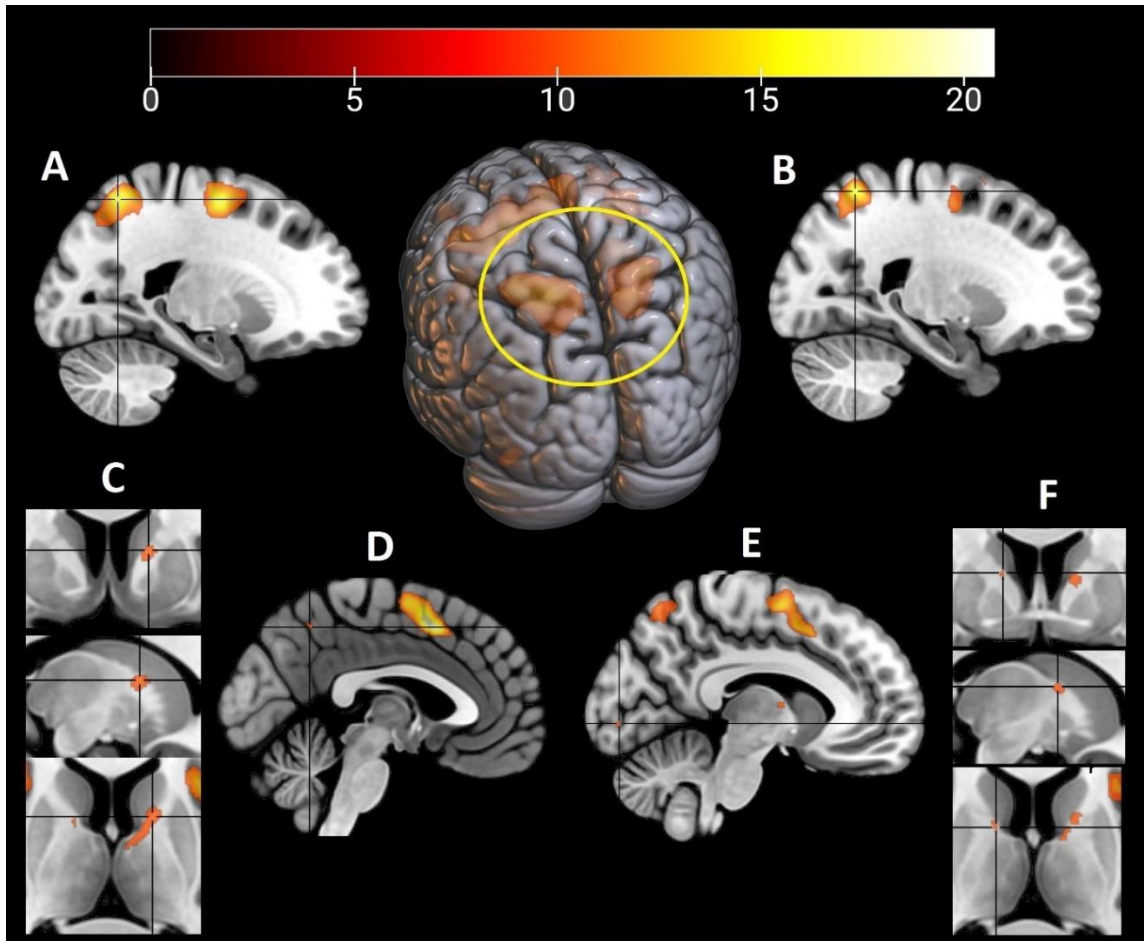
Figure 31. Results of a whole brain analysis (FWE corrected; α = .05) showing clusters with significant peaks pertaining to an effect of condition in; A) left superior parietal gyrus, B) right superior parietal gyrus, C) left caudate, D) bilateral medial superior parietal gyrus, E) left lingual gyrus, F) right caudate. Colour bar denotes F values.

5.4. Discussion

5.4.1. Overview: The primary aims of this study were to establish whether brain regions consistent with a prefronto-cerebellar network would be active upon presentation of a symbolic cue informing an oculomotor response, and whether there was evidence of age-related differences alongside any corresponding changes in functional brain activity. Behavioural data established that the elderly participants learnt more slowly, showed less evidence of automaticity, and tended to persevere with incorrect responding. Functional

data provided evidence of brain activity in candidate regions such as the mid dlPFC, cerebellar CRUS I, and the eye fields. This differed specifically in the dlPFC, the elderly demonstrating more activations within regions just dorsal and caudal to the area 46 cluster which was commonly active across both age cohorts.

5.4.2. Hypotheses

When considering performance and Hypothesis 1, the null Hypothesis can be rejected as there was a significant main effect of age driven by greater percentage accuracy in the young cohort, the difference significant in blocks two to five (see section **5.3.1.1. Percentage Accuracy**). This confirmed that age groups were performing equally at the start, when they had little to no information to base their choices upon, but both reached a comparable level of performance by block six. However, this is tentative as with outliers removed the young cohort still outperformed the elderly in this final block. Critically the younger cohort learned faster, reaching asymptote by block three compared to block four in the elderly cohort. This was consistent with the literature describing impairments to cognition as being part of the normal ageing process (Ferguson et al., 2021; Hedden & Gabrieli, 2004; Rajeshkumar & Trewartha, 2019; Salthouse, 2004).

A further breakdown of the age effect found a trend of elderly participants making more errors, with evidence of perseveration, seen both before and after finding the correct response within a rule (see section **5.3.1.2. Errors**). It could be that the elderly are forgetting information presented to them, however this assumes learning has taken place. It is also plausible that the elderly are slower at processing feedback to be used in determining future decisions, consistent with hypothesised prefronto-cerebellar network impairments. It was considered whether the processing speed hypothesis (Salthouse, 1994) may have contributed to these age effects. This theory suggests that global impairments in aspects

such as conduction speed, synaptic density, and both white and grey matter density (Dickstein et al., 2007; Price et al., 2017; Xi et al., 1999) mean memory traces are encoded more slowly in the elderly, resulting in more disruption and less available information. Reaction times during the control trials were used to index processing speed, representing both perceptual processing (locating the target) and oculomotor processing (initiating a saccade), this approach similar to that employed by Albinet et al. (2012). However age remained a significant predictor of performance even when including median reaction time as a covariate (see section **5.3.1.2. Processing Speed**). It was also checked whether incorrect responses were biased by either the immediately previous reinforced response or the most recently reinforced experimental response (potentially linked to proactive interference, see section **5.3.1.2. Errors**). This effect has been found to be stronger in the elderly (Levine et al., 1997) which may indicate a failure to inhibit incorrect response strategies. However there were no differences found between age groups, and so it cannot be concluded that performance differences were due to a failure of inhibition.

In relation to Hypothesis 2, there was no significant interaction between age group, condition, and block when looking at reaction times within correct trials (see section **5.3.1.1. Reaction Times**). However this was found in the pupillometry data, with a significant condition x block interaction specific to the younger cohort (see section **5.3.1.1. Pupillometry**). This was driven by pupil area being larger in experimental trials relative to control trials within the first pair of blocks, but with no significant difference across the middle or final pairs of blocks. In the elderly cohort there were main effects of condition and block but no interaction, implying that only the young adults demonstrated a reduction in cognitive demand over time, specific to the experimental condition (Alnæs et al., 2014; Beatty & Kahneman, 1966; Bradshaw, 1967; Gavas et al, 2017; Hosseini et al., 2017; Hess &

Polt, 1964; Huh et al., 2019; Kahneman & Beatty, 1966, 1967; Kahneman & Peavler, 1969).

This suggested automation to a greater degree than seen within elderly participants and

justified rejection of the null Hypothesis. It remains possible that the main effect of block

within the elderly cohort may be attributable to cognitive overload, as this has been

associated with constriction of the pupil (Granholm et al., 1996).

In relation to Hypothesis 3, a conjunction analysis was run looking for effects of

condition across both age groups. There was significant positive experimental BOLD activity

seen in left-lateralised CRUS I extending into lobule HVI (see section **5.3.2.1. Cerebellum**).

Within the frontal lobe (see section **5.3.2.1. Frontal Lobe**) significant activations were found

in multiple locations typified by positive BOLD responses in the experimental condition with

the magnitude exceeding that of the control. Activity included the dlPFC as predicted

(deemed to be within bilateral areas 46, 9/46v, and right 9/46d, see Figures 27 and 28).

There was also a large cluster crossing bilaterally including aspects of the medial wall (see

Figure 19) deemed to include the SEFs and CEFs (see Figure 24), and caudo-lateral PFC such

as area 6 (see Figure 23) and the FEFs (see Figures 20, 21, and 24). For this reason the null

hypothesis can be rejected. Finally although hypotheses were not made about this area,

there was a pair of clusters positioned bilaterally including the frontal operculum, insula, and

lateral orbital gyri, with overlap into the IFG (areas 44 and 45, stronger in the right

hemisphere, see Figures 25 and 26).

In relation to Hypothesis 4 there were trends of condition x age interactions in the

cerebellum (see section **5.3.2.2. Cerebellum**), however these did not survive small-volume

FWE correction meaning the null Hypothesis cannot be conclusively rejected. Uncorrected

activations straddled the left primary fissure, albeit with a small cluster in right CRUS I. In

both regions significant (uncorrected) positive BOLD responses were specific to the elderly

experimental condition. When investigating the frontal lobe for condition x age interactions (see section **5.3.2.2. Frontal Lobe**) there were two sites of activity located within the dlPFC. These extended bilaterally across areas 9, 9/46d, 8Ad and 8B, as well as left-lateralised 8Av. Therefore the null Hypothesis can be rejected regarding the mid dlPFC, with larger magnitude positive BOLD responses again seen in the elderly experimental condition

There was a failure to reject null Hypothesis 5, with no significant interactions between practise and condition across both age groups in either the cerebellum or frontal lobe. There was also a failure to reject null Hypothesis 6 due to no age x condition x practise interactions in either the cerebellum or frontal lobe.

5.4.3. Summary of Functional Results

The activations found within left CRUS I across cohorts was consistent with previous work supporting the role of this region in processing goal information pertaining to rules (Balsters & Ramnani, 2008, 2011; Balsters et al, 2013). Given that these studies used the hand as an effector (compared with the eye here) further suggests that CRUS I activity is not directly involved in preparation of the response, but in cognitive components. That activity spread into lobule HVI and was also found in more caudal frontal regions may be consistent with the work of O'Reilly et al. (2010) who used functional connectivity to demonstrate that cerebellar lobules VI and VIII show connectivity with both visual and premotor areas (not extending into caudal area 8 where the FEFs are thought to be located), and cerebellar lobule VIIa connects with rostral area 8. Additionally, recent work by Longley et al. (2021) has found evidence of a rostro-caudal gradient of connectivity between the frontal lobe and the cerebellum, whereby when travelling rostrally from the central sulcus connectivity with the cerebellum moves from anterior and posterolateral cerebellar lobules, converging on

lobule HVIIa. Therefore it is plausible that caudal frontal and other more posterior brain regions will contribute to patterns of cerebellar activity observed either side of lobule HVIIa.

Activity in the mid dlPFC was identified as predicted based upon it being associated with the prospective encoding of rules (Bunge, 2004; Mansouri et al., 2020; Passingham & Wise, 2012, pp. 157-194; Petrides, 2005; Sakai et al., 2002). That the right-lateralised cluster was larger was also consistent with expectations in the literature, as cognitive functions such as spatial working memory (seen in dorsolateral areas 46 and 9), episodic memory retrieval, perception, and inhibitory control tend to be right lateralised (Reuter-Lorenz et al., 2000). Furthermore, this lends tentative support to a prefronto-cerebellar network, as the mid dlPFC is know to reciprocally connect with lobule HVIIa (Balsters et al., 2014; Buckner et al., 2011; Kelly & Strick, 2003; Ramnani, 2006; Schmahmann & Pandya, 1995, 1997) predominately contralaterally (Morales & Tomsick, 2015; Palesi et al., 2017) with it expected that the mid dlPFC would elicit excitation of Purkinje cells. It was also seen that areas such as the FEFs and SEFs were similarly active at the time of the cue, which would be consistent with connectivity between both of these regions and the mid dlPFC (Huerta & Kaas, 1990; Hutchison et al., 2012) as well as the SEFs and FEFs themselves being connected (Hutchison et al., 2012; Schall et al., 1993).

It is therefore plausible that a rostro-caudal controller-plant relationship exists (Petrides, 2005; Ramnani, 2014) with the dlPFC encoding the goal (error correction taking place via cerebellar forward models), sending information on to the SEFs where an action to achieve the goal is formed, then prepared in the FEFs for execution via outputs to the striatum (active in the whole brain analysis, see section **5.3.2.5**) and superior colliculus (Gaymard et al., 1998; Jerde et al., 2012; Matsumoto et al., 2018; Parthasarathy et al., 1992; Purves et al., 2008, pp. 460-507; Rivaud et al., 1994; Segraves & Goldberg, 1987; Shook et

al., 1990; Wise & Murray, 2000), see Figure 32. Chen & Wise (1995a, 1995b) further support

the SEFs being involved in cue-related learning (and the suggested comparison to the PMC)

acting as an intermediate node between the mid dlPFC and the FEFs. There is also evidence

that the SEFs encode the goal in craniotopic space, with this then transformed into

retinotopic space within the FEFs ready for execution (Schall et al., 1993), consistent with

the SEFs not being associated with gross execution but timing, sequencing, learning, and

value-based decisions (Abzug & Sommer, 2017). That the FEFs were still active at the time of

the cue also suggests a role beyond simple execution, with evidence that they are implicated

in aspects of response preparation (Armstrong et al., 2009; Blanke et al., 1999; Bourgeois et

al., 2021; Curtis & Connolly, 2008; Rivaud et al., 1994; Segraves & Goldberg, 1987). The role

of the CEFs is less clear, however in humans voluntary eye movements may be elicited

within the cingulate cortex in response to conditional visual cues (Paus et al., 1993),

consistent with cingulate motor areas projecting to both the FEFs and SEFs (Amiez &

Petrides, 2009).
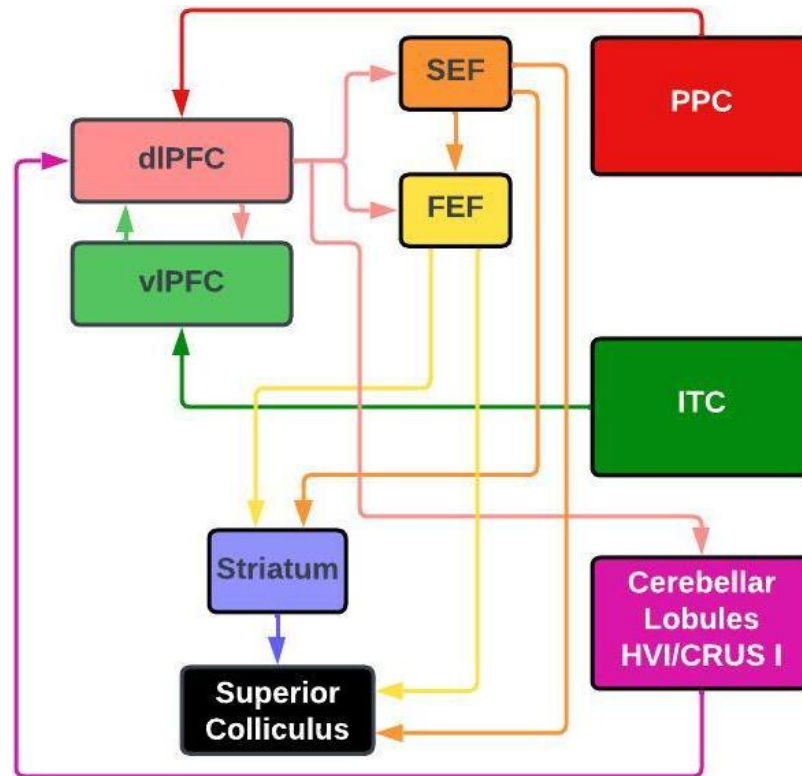
Figure 32. A simplified schematic of the core brain errors expected to form the prefronto-cerebellar network (omitting structures such as the thalamus, substantia nigra pars reticulata, and cerebellar nuclei).

Regarding age differences in functional data, increased evidence of bilateral dlPFC activations were consistent with the prefrontal-executive theory (West, 1996, 2000) suggesting the PFC (especially the dlPFC) is more susceptible to age-related impairment. This is potentially driven by a drop in volume (attributed to neuron size) and synaptic density (Haug & Eggers, 1991; Huttenlocher, 1979; Raz et al., 1997), and supported by tasks requiring the dlPFC showing impairment in the elderly (MacPherson et al., 2002). It is possible that these localised age-related impairments are compensated for by a phenomenon called hemispheric asymmetry reduction (Cabeza, 2002), as activity pertaining to cognitive functions (such as spatial working memory) which tend to be right lateralised become increasingly bilateral in the elderly (Reuter-Lorenz et al., 2000), supported in this study by interactions producing a larger cluster in the left hemisphere. This may represent

67

either an alternative behavioural strategy or recruitment of additional neural resources to compensate for deficits in attention, processing speed, memory or inhibitory control (Cabeza, 2002). That this is compensatory is supported by evidence that the elderly recruit left-lateralised areas 8 and 9 when dealing with interference (Hinault et al., 2019), and that when investigated specifically within the elderly, increased bilaterality associates with improved performance (Reuter-Lorenz et al., 2000). This process may be attributable to dedifferentiation, whereby functions undergo neural differentiation over early development (Garrett, 1946) but become increasingly dedifferentiated in the elderly, with correlations between cognitive measures, and between cognitive and sensory measures increasing (Baltes & Lindenberger, 1997).

A compensatory role of additional dlPFC activity within this study and specific to the elderly is further supported, as activations were in plausible regions involved in the prospective encoding of goals (Passingham & Wise, 2012, pp. 157-194) as well as extending into area 9 which shows connectivity with both the hippocampus and precerebellar nuclei (Petrides & Pandya, 1999; Petrides, 2005; Schmahmann & Pandya, 1995, 1997), and is implicated in inhibition of cognitive sets (Mansouri et al., 2020). Also, interactions remained significant when a metric of performance was included as a covariate (mean number of trials included per learned cue, which was not a direct measure of overall performance but did correlate highly with it; $r(46) = .946$, $p<.001$). This suggested that changes in the BOLD response were not linearly related to performance, tentatively supporting a more complex interaction whereby increased functional activations may compensate specifically within the elderly. These patterns of dlPFC activity were also consistent with the sub-threshold interactions found bilaterally in the cerebellum, the cluster falling into CRUS I being specific to the right hemisphere, and mid dlPFC interactions being more prevalent in the left

hemisphere. These would require replication to form firm conclusions, but even when considering the trends the potential causal factor remains unclear. As there was no parametrically modulated change over trials (and incorrect trials were not analysed for comparison) it cannot be inferred that the mid dlPFC-HVIIa mechanism is impaired and potentially causing increased functional dlPFC activity. Instead these interactions could be compensating for changes in another network, or for more general age-related differences, with this study not placed to make a causal inference.

5.4.4. Additional Functional Results

Activations in the frontal operculum, insula, orbital, and inferior frontal regions were also plausible (see section **5.3.2.1. Frontal Lobe;** Figures 25 and 26). For example the orbital cortex is associated with goal choice in relation to actions and reward expectation, associating choices and outcomes, grey matter volume associating with IQ (Burke et al., 2008; Bussey et al., 2001; Frank & Claus, 2006; Groman et al., 2019; Mansouri et al., 2020; Murray & Rudebeck, 2013; Nestor et al., 2015; Passingham & Wise, 2012, p. 97, pp. 157-194; Wallis et al., 2001; Schoenbaum et al., 1998, 2003; Schoenbaum & Roesch, 2005; Takahashi et al., 2009), and the frontal operculum implicated in cognitive control when guiding attention to stimuli held in memory (Higo et al., 2011). Finally overlap into the IFG included areas 44 and 45, arguably strongest in the right hemisphere, these regions connected with temporal gyral areas and associated with controlled memory retrieval (Petrides et al., 2012). This was consistent with the work of Passingham & Lau (2022) who suggest that the vlPFC guides future choices based upon object information. However given an 8mm smoothing kernel and activations sitting on the border of all regions it is unclear which represent true signal and which are noise.

When looking at the whole brain analysis (see section **5.3.2.5. Whole Brain Analysis**) it was also evidenced that superior-posterior regions of the parietal cortex were active, consistent with a role in context dependent rules (Mansouri et al., 2020), encoding spatial components of rules (Passingham & Wise, 2012, pp.157-194; Rao et al., 1997), and bidirectional associations between the PFC and temporoparietal areas linking 'thought' to models of the external world (Ito, 2005). The PPC has also shown functional connectivity with lobule HVIIa (O'Reilly et al., 2010), however this was deemed unlikely to cause cerebellar activity in this study. This was justified as O'Reilly et al. (2010) found that parietal connections specifically to CRUS I were weaker, and parietal activity in this study did not overlap with peaks in the work of O'Reilly, whereas bilateral conjunction and left lateralised interaction effects in the dlPFC did. As parietal activity implies a visuospatial component (rather than object recognition) and was more active in the experimental condition, activations here but not in the temporal lobe still suggest processing of the goal/location, rather than the cue object. This was further supported by temporo-occipital and both inferior and middle temporal gyral activations when looking at a conjunction across both age groups and both conditions (not reported above), suggesting object-related information processing not specific to the experimental condition. Finally there were also activations within visual regions and the striatum (specifically the caudate) extending into the internal capsule and anterior thalamic nucleus. This is consistent with suggestions by Gaymard et al. (1998) of a parietal-tectal pathway through the posterior limb of the internal capsule, but also a route from the visual to parietal cortex (where a spatial map is formed), on to the dlPFC where information is stored. The dlPFC then sends information to the FEFs where it sits in a 'memorization loop' (FEF > caudate nucleus > substantia nigra pars reticulata > thalamus > FEF) until called upon for action execution. At this point it travels through the internal capsule to regions such as the pontine nucleus and superior colliculus. Apart from its

omission of the cerebellum and SEFs, this model is consistent with that suggested in this paper.

5.4.5. Limitations and Future Research

Interpretation: It is not entirely clear to what degree the BOLD response is influenced by parallel fiber versus Purkinje cell versus climbing fiber activation, albeit with evidence that climbing fibers make a significant contribution (Yang et al., 2003). Crucially, no claims can be made as to whether parallel fiber-Purkinje connectivity is comparable between age groups, nor whether cerebellar outputs back to cortical sources via the cerebello-thalamo-cortical pathway, or connections from pre-cerebellar nuclei such as the inferior olive and VTA (Ikai et al., 1992; Sasaki et al., 1977; Suzuki et al., 2012; Swenson et al., 1989; Watson et al., 2009) are affected by age. Future research could investigate this further using paradigms which provide a greater number of error trials, enabling a separate analysis of error and correct trials and potentially exploring how an error affects activity on the subsequent trial during visuo-oculomotor learning (as per Medina & Lisberger, 2008).

There is also a question of whether the measured haemodynamic activity is representative of differences at the neural level, or just indicative of differences between age groups in neurovascular coupling (Csipo et al., 2019). Importantly, evidence generally suggests an age-related decline in magnitude of the BOLD signal (Ances et al., 2009; Balbi et al., 2015; Morsheddost et al., 2015; Ross et al., 1997; Tekes et al., 2005; West et al., 2019), which is opposite to the effects seen. Additionally, the conjunction analysis found similar effects across age groups, and within the frontal lobe interactions were typified by the young having either no BOLD response, or a negative BOLD response. This suggests that any effect of age-related differences in neurovascular coupling were unlikely to account for the interactions found.

Methodology: The 2nd-level analysis employed a summary statistic approach

looking at between-subject variability in parameter estimates (Mumford & Nichols, 2006)

found to be robust even when 1st-level design matrices are unbalanced (Penny & Holmes,

2007). This is relevant as the number of regressors was equal, but the number of events

differed (see section **5.3.1.2. Number of Trials**) as did the length of the scan (as some

participants took longer to calibrate than others). There was therefore a risk that

correlations within the 1st-level design matrices would differ systematically between age

groups (see section **5.3.1.2. Multicollinearity**). For example, the experimental unmodulated

regressor pertaining to the cue events showed greater multicollinearity within the young

cohort, and the experimental parametrically modulated regressor pertaining to cue events

showed greater multicollinearity within the elderly cohort. As these correlations still sat

below r=.30, and age group differences in mean r values (unmodulated analysis) was just

.032, they were deemed unlikely to drive the magnitude of differences seen, which

remained consistent with the ageing literature (Baltes & Lindenberger, 1997; Cabeza, 2002).

Finally, that conjunction analyses showed much comparable activity without significant

interaction supports the claim that these correlations did not introduce a measurable

systematic bias.

Regarding the parametric analysis, as a basic linear modulation was used other

modelling approaches such as Rescorla-Wagner may find different results, supported by no

experience-related change found within the frontal lobe despite evidence in the literature

(Jenkins et al., 1994; Jueptner et al., 1997; Passingham,1996; Raichle et al., 1994). However

this approach did find significant cerebellar effects when applied by Balsters & Ramnani

(2011) albeit with pre-training. This suggested that learning being less established may have

contributed to the non-significant results reported here. Future research may benefit from

applying different modelling techniques and including a greater number of trials. Unfortunately this was not possible in this study due to a combination of time constraints (meaning multiple scanning sessions were not practical) and a desire to prioritise participant comfort by keeping the study duration to under an hour. Again it may be of benefit to look at both incorrect and correct trials in order to establish any gross difference between the two, as it remains possible that the age differences are driven by changes during the error trials, whereby perhaps the younger cohort narrow down to a set of active internal models within the cerebellum more effectively, also resulting in less distributed prefrontal activity. This would be consistent with the ideas of Imamizu et al. (2000) who suggested that initially multiple internal models were active, but refined and reduced in number over experience.

When comparing two age groups in a cross-sectional design there was a risk of other extraneous factors impacting the results, potentially exacerbated by the young cohort being drawn from the student body at Royal Holloway University. Therefore a number of checks were put in place. Firstly, due to known differences in optimum time of day for testing the MEQ was used to determine approximately when a participant would be scanned (Intons-Peterson et al., 1998; Mecacci et al., 1986; Roveda et al., 2017; Park & Schwarz, 1999, pp. 153-154). No interaction found between age and MEQ score (regarding time tested) implied that the scanning slots were allocated in a comparable manner between age groups (see section **5.3.1.2. Time of Day**). IQ was also measured with no significant difference found between age groups (see section **5.3.1.2. IQ)**. However associations between IQ and the dependent variable in the parametric analysis prompted its inclusion as a covariate. There was also a difference in gender ratios between age groups (predominately male in the elderly cohort and female in the young cohort). As there was an association with the dependent variable gender was included as a covariate in all fMRI analyses.

73

Furthermore, due to recruitment drives there was a tendency to test different age groups in batches, however order of testing did not impact performance in a manner that differed systematically between age groups (see section **5.3.1.2. Order of Testing)**. There was also no significant difference between age groups regarding the number of missed trials (where the eye-tracker failed to detect a selection) which confirmed that percentage accuracy scores were not differentially affected (see section **5.3.1.2. Missed Trials)**. However as the younger cohort performed better there was a significant increase in the number of trials included in the fMRI analysis (see section **5.3.1.2. Number of Trials)**. This was deemed unlikely to influence the results given a trend of less activity found within the better sampled younger cohort. Finally evidence exists of memory impairment when in an MRI scanner, with a greater impact on the elderly during high load memory tasks, especially those drawing on the dlPFC (Gutchess & Park, 2006). Though this still relates to a performance deficit in the elderly, it suggests distraction may have exaggerated age-related differences.

A further complication within the analysis was that two age groups known to have haemodynamic response functions differing in shape, were compared. Previous work in our lab has indeed found that the commonly used canonical HRF was more similar in shape to the BOLD response of an elderly cohort, and so biases towards finding activations within this group. Addition of the temporal and dispersion derivatives was shown to model the baseline variability between age groups in a more unbiased manner, hence its application. Additionally, the experimental condition was always compared to a control condition in which no learning took place, meaning baseline differences were accounted for. When significant coordinates were identified the BOLD response was then plotted and comments were made on magnitude differences. It is not necessarily the case that magnitude drove the

74

significant differences seen, as magnitude and temporal parameters of the response cannot be meaningfully differentiated. Consequently, these comments should be viewed as observations rather than causal inferences.

5.4.6. Conclusion

In conclusion, the pattern of BOLD activity observed in the cerebellar cortex, dlPFC, and eye fields was theoretically plausible (Balsters et al., 2010, 2014; Buckner et al., 2011; Diedrichsen et al., 2009; Kelly & Strick, 2003; Matano, 2001; Morales & Tomsick, 2015; Palesi et al., 2017; Schmahmann & Pandya, 1995, 1997) given an experimental condition requiring working memory, a suggested hierarchical structure (Ramnani, 2014), and a mid dlPFC-Lobule HVIIa network (Balsters et al., 2014; Buckner et al., 2011; Kelly & Strick, 2003; Ramnani, 2006; Schmahmann & Pandya, 1995, 1997) mediating prefrontal activity during a visuo-oculomotor learning task. These networks appeared to be employed by both age groups, however behaviourally the elderly showed evidence of slower learning and perseveration (whereas the young were closer to learning from single events), accompanied by an increased cognitive load, based upon automaticity being evidenced only in the younger cohort. Functional activations were identified in the dlPFC, lateral cerebellum, ventral prefrontal/opercular/orbital cortex, temporal and parietal lobes, the striatum, caudal PFC, the FEFs/SEFs/CEFs, and both the cingulate and paracingulate cortex. That age x condition interactions only survived correction in mid, caudal, and dorsal dlPFC supports an impairment in working memory, inhibition, and/or prospective encoding, with no evidence of age differences in object/visuo-spatial processing in posterior regions, or saccade preparation/execution (consistent with no age-differences in control condition reaction times). Although it is possible the dlPFC is compensating for non-dlPFC deficits, it is deemed unlikely based on both the literature implicating this region (de Chastelaine et al., 2015;

Gutchess & Park, 2006; Haug & Eggers, 1991; Huttenlocher, 1979; Levine et al., 1997; Raz et al., 1997; MacPherson et al., 2002; West, 1996, 2000; Winocur, 1991, 1992) and it being the sole region in which an interaction was found. In summary, during the task the healthy elderly cohort had to work harder at a neural level, yet still underperformed relative to the young cohort. This may be attributable to differences in how active cerebellar internal models are formed (Imamizu et al., 2000) during error trials, the elderly potentially working their prefrontal cortex harder to compensate for an impairment in this process, however cerebellar interactions did not survive correction and so this would require replication. These results support the prefrontal-executive theory suggesting that processes reliant upon the dlPFC are specifically sensitive to age-related impairment (West, 1996, 2000), and align with findings of age-related hemispheric asymmetry (Cabeza, 2002; Hinault et al., 2019; Reuter-Lorenz et al., 2000).

5.5. References

Abzug, Z. M., & Sommer, M. A. (2017). Supplementary eye fields. *Reference module in neuroscience and biobehavioral psychology*. http://dx.doi.org/10.1016/B978-0-12-809324-5.02941-2

Albinet, C. T., Boucard, G., Bouquet, C. A., & Audiffren, M. (2012). Processing speed and executive functions in cognitive aging: How to disentangle their mutual relationship?. *Brain and cognition*, *79*(1), 1-11. https://doi.org/10.1016/j.bandc.2012.02.001

Albus, J. S. (1971). A theory of cerebellar function. *Mathematical Biosciences*, *10*(1-2), 25-61. https://doi.org/10.1016/0025-5564(71)90051-4

Albus, J. S. (1989). The Marr and Albus Theories of the Cerebellum: Two Early Models of Associative Memory. *Research Inst. for Advanced Computer Science, Cerebellar Models of Associative Memory: Three Papers from IEEE COMPCON Spring 1989*. https://doi.org/10.1109/CMPCON.1989.301996

Alnæs, D., Sneve, M. H., Espeseth, T., Endestad, T., van de Pavert, S. H. P., & Laeng, B. (2014). Pupil size signals mental effort deployed during multiple object tracking and predicts brain activity in the dorsal attention network and the locus coeruleus. *Journal of vision*, *14*(4), 1-1. https://doi.org/10.1167/14.4.1

Amiez, C., & Petrides, M. (2009). Anatomical organization of the eye fields in the human and non-human primate frontal cortex. *Progress in neurobiology*, *89*(2), 220-230. https://doi.org/10.1016/j.pneurobio.2009.07.010

Ances, B. M., Liang, C. L., Leontiev, O., Perthen, J. E., Fleisher, A. S., Lansing, A. E., & Buxton, R. B. (2009). Effects of ageing on cerebral blood flow, oxygen metabolism, and blood

oxygenation level dependent responses to visual stimulation. *Human brain
mapping*, *30*(4), 1120-1132. https://doi.org/10.1002/hbm.20574

Armstrong, K. M., Chang, M. H., & Moore, T. (2009). Selection and maintenance of spatial
information by frontal eye field neurons. *Journal of Neuroscience*, *29*(50), 15621-
15629. https://doi.org/10.1523/JNEUROSCI.4465-09.2009

Arsalidou, M., Duerden, E. G., & Taylor, M. J. (2013). The centre of the brain: topographical
model of motor, cognitive, affective, and somatosensory functions of the basal
ganglia. *Human brain mapping*, *34*(11), 3031-3054.
https://doi.org/10.1002/hbm.22124

Balbi, M., Ghosh, M., Longden, T. A., Vega, M. J., Gesierich, B., Hellal, F., ... & Plesnila, N.
(2015). Dysfunction of mouse cerebral arteries during early aging. *Journal of
Cerebral Blood Flow & Metabolism*, *35*(9), 1445-1453.
https://doi.org/10.1038/jcbfm.2015.107

Balsters, J. H., & Ramnani, N. (2008). Symbolic representations of action in the human
cerebellum. *Neuroimage*, *43*(2), 388-398.
https://doi.org/10.1016/j.neuroimage.2008.07.010

Balsters, J. H., Cussans, E., Diedrichsen, J., Phillips, K. A., Preuss, T. M., Rilling, J. K., &
Ramnani, N. (2010). Evolution of the cerebellar cortex: the selective expansion of
prefrontal-projecting cerebellar lobules. *Neuroimage*, *49*(3), 2045-2052.
https://doi.org/10.1016/j.neuroimage.2009.10.045

Balsters, J. H., & Ramnani, N. (2011). Cerebellar plasticity and the automation of first-order
rules. *Journal of Neuroscience*, *31*(6), 2305-2312.
https://doi.org/10.1523/JNEUROSCI.4358-10.2011

Balsters, J. H., Whelan, C. D., Robertson, I. H., & Ramnani, N. (2013). Cerebellum and

cognition: evidence for the encoding of higher order rules. *Cerebral Cortex*, *23*(6),

1433-1443. https://doi.org/10.1093/cercor/bhs127

Balsters, J. H., Laird, A. R., Fox, P. T., & Eickhoff, S. B. (2014). Bridging the gap between

functional and anatomical features of cortico-cerebellar circuits using meta-analytic

connectivity modeling. *Human brain mapping*, *35*(7), 3152-3169.

https://doi.org/10.1002/hbm.22392

Baltes, P. B., & Lindenberger, U. (1997). Emergence of a powerful connection between

sensory and cognitive functions across the adult life span: a new window to the

study of cognitive aging?. *Psychology and aging*, *12*(1), 12-21.

https://psycnet.apa.org/doi/10.1037/0882-7974.12.1.12

Beatty, J., & Kahneman, D. (1966). Pupillary changes in two memory tasks. *Psychonomic

Science*, *5*(10), 371-372. https://psycnet.apa.org/doi/10.3758/BF03328444

Bellebaum, C., & Daum, I. (2004). Effects of age and awareness on eyeblink conditional

discrimination learning. *Behavioral neuroscience*, *118*(6), 1157-1165.

https://psycnet.apa.org/doi/10.1037/0735-7044.118.6.1157

Blanke, O., Morand, S., Thut, G., Michel, C. M., Spinelli, L., Landis, T., & Seeck, M. (1999).

Visual activity in the human frontal eye field. *Neuroreport*, *10*(5), 925-930.

https://psycnet.apa.org/doi/10.1097/00001756-199904060-00006

Bloedel, J. R., Ebner, T. J., & Wise, S. P. (Eds.). (1996). *The acquisition of motor behavior in

vertebrates*. MIT Press.

Borson, S., Scanlan, J., Brush, M., Vitaliano, P., & Dokmak, A. (2000). The mini-cog: a

cognitive 'vital signs' measure for dementia screening in multi-lingual

elderly. *International journal of geriatric psychiatry*, *15*(11), 1021-1027.

https://doi.org/10.1002/1099-1166(200011)15:11%3C1021::AID-GPS234%3E3.0.CO;2-6

Borson, S., Scanlan, J. M., Chen, P., & Ganguli, M. (2003). The Mini-Cog as a screen for dementia: validation in a population-based sample. *Journal of the American Geriatrics Society*, *51*(10), 1451-1454. https://doi.org/10.1046/j.1532-5415.2003.51465.x

Borson, S., Scanlan, J. M., Watanabe, J., Tu, S. P., & Lessig, M. (2005). Simplifying detection of cognitive impairment: comparison of the Mini-Cog and Mini-Mental State Examination in a multiethnic sample. *Journal of the American Geriatrics Society*, *53*(5), 871-874. https://doi.org/10.1111/j.1532-5415.2005.53269.x

Bourgeois, A., Sterpenich, V., Iannotti, G. R., & Vuilleumier, P. (2021). Reward-driven modulation of spatial attention in the human frontal eye-field. *NeuroImage*, *247*, 118846. https://doi.org/10.1016/j.neuroimage.2021.118846

Bracha, V., Zhao, L., Irwin, K. B., & Bloedel, J. R. (2000). The human cerebellum and associative learning: dissociation between the acquisition, retention and extinction of conditioned eyeblinks. *Brain research*, *860*(1-2), 87-94. https://doi.org/10.1016/S0006-8993(00)01995-8

Bradshaw, J. (1967). Pupil size as a measure of arousal during information processing. *Nature*, *216*(5114), 515-516. https://doi.org/10.1038/216515a0

Bright, P., & van der Linde, I. (2020). Comparison of methods for estimating premorbid intelligence. *Neuropsychological Rehabilitation*, *30*(1), 1-14. https://doi.org/10.1080/09602011.2018.1445650

Brodaty, H., Low, L. F., Gibson, L., & Burns, K. (2006). What is the best dementia screening instrument for general practitioners to use?. *The American Journal of Geriatric Psychiatry*, *14*(5), 391-400. https://doi.org/10.1097/01.JGP.0000216181.20416.b2

Browning, P. G., & Gaffan, D. (2008). Prefrontal cortex function in the representation of

temporally complex events. *Journal of Neuroscience*, *28*(15), 3934-3940.

https://doi.org/10.1523/JNEUROSCI.0633-08.2008

Buckner, R. L., Krienen, F. M., Castellanos, A., Diaz, J. C., & Yeo, B. T. (2011). The organization

of the human cerebellum estimated by intrinsic functional connectivity. *Journal of*

neurophysiology, *106*(5), 2322-2345. https://doi.org/10.1152/jn.00339.2011

Budisavljevic, S., & Ramnani, N. (2012). Cognitive deficits from a cerebellar tumour: A

historical case report from Luria's laboratory. *Cortex*, *48*(1), 26-35.

https://doi.org/10.1016/j.cortex.2011.07.001

Bunge, S. A. (2004). How we use rules to select actions: a review of evidence from cognitive

neuroscience. *Cognitive, Affective, & Behavioral Neuroscience*, *4*(4), 564-579.

https://psycnet.apa.org/doi/10.3758/CABN.4.4.564

Burke, K. A., Franz, T. M., Miller, D. N., & Schoenbaum, G. (2008). The role of the

orbitofrontal cortex in the pursuit of happiness and more specific

rewards. *Nature*, *454*(7202), 340-344. https://doi.org/10.1038/nature06993

Bussey, T. J., Wise, S. P., & Murray, E. A. (2001). The role of ventral and orbital prefrontal

cortex in conditional visuomotor learning and strategy use in rhesus monkeys

(Macaca mulatta). *Behavioral neuroscience*, *115*(5), 971-982.

https://psycnet.apa.org/doi/10.1037/0735-7044.115.5.971

Cabeza, R. (2002). Hemispheric asymmetry reduction in older adults: the HAROLD

model. *Psychology and ageing*, *17*(1), 85-100. https://doi.org/10.1037//0882-

7974.17.1.85

Campbell, K. L., Lustig, C., & Hasher, L. (2020). Aging and inhibition: Introduction to the

    special issue. *Psychology and Aging*, *35*(5), 605-613.

    https://doi.org/10.1037/pag0000564

Chapman, P. F., Steinmetz, J. E., & Thompson, R. F. (1988). Classical conditioning does not

    occur when direct stimulation of the red nucleus or cerebellar nuclei is the

    unconditioned stimulus. *Brain research*, *442*(1), 97-104.

    https://doi.org/10.1016/0006-8993(88)91436-9

Chen, L. L., & Wise, S. P. (1995a). Neuronal activity in the supplementary eye field during

    acquisition of conditional oculomotor associations. *Journal of*

    Neurophysiology, *73*(3), 1101-1121. https://doi.org/10.1152/jn.1995.73.3.1101

Chen, L. L., & Wise, S. P. (1995b). Supplementary eye field contrasted with the frontal eye

    field during acquisition of conditional oculomotor associations. *Journal of*

    Neurophysiology, 73(3), 1122-1134. https://doi.org/10.1152/jn.1995.73.3.1122

Christophel, T. B., Klink, P. C., Spitzer, B., Roelfsema, P. R., & Haynes, J. D. (2017). The

    distributed nature of working memory. *Trends in cognitive sciences*, *21*(2), 111-124.

    https://doi.org/10.1016/j.tics.2016.12.007

Cromer, J. A., Roy, J. E., & Miller, E. K. (2010). Representation of multiple, independent

    categories in the primate prefrontal cortex. *Neuro l66*(5), 796-807.

    https://doi.org/10.1016/j.neuron.2010.05.005

Csipo, T., Mukli, P., Lipecz, A., Tarantini, S., Bahadli, D., Abdulhussein, O., ... & Hand, R. A.

    (2019). Assessment of age-related decline of neurovascular coupling responses by

    functional near-infrared spectroscopy (fNIRS) in humans. *Geroscience*, *41*(5), 495-

    509. https://doi.org/10.1007/s11357-019-00122-x

Curtis, C. E., & Connolly, J. D. (2008). Saccade preparation signals in the human frontal and

parietal cortices. *Journal of Neurophysiology*, *99*(1), 133-145.

https://doi.org/10.1152/jn.00899.2007

de Chastelaine, M., Mattson, J. T., Wang, T. H., Donley, B. E., & Rugg, M. D. (2015).

Sensitivity of negative subsequent memory and task-negative effects to age and

associative memory performance. *Brain research*, *1612*, 16-29.

https://doi.org/10.1016/j.brainres.2014.09.045

Dickstein, D. L., Kabaso, D., Rocher, A. B., Luebke, J. I., Wearne, S. L., & Hof, P. R. (2007).

Changes in the structural complexity of the aged brain. *Aging cell*, *6*(3), 275-284.

https://doi.org/10.1111/j.1474-9726.2007.00289.x

Diedrichsen, J., Balsters, J. H., Flavell, J., Cussans, E., & Ramnani, N. (2009). A probabilistic

MR atlas of the human cerebellum. *Neuroimage*, *46*(1), 39-46.

https://doi.org/10.1016/j.neuroimage.2009.01.045

Duvernoy, H. M. (1999). *The human brain: surface, three-dimensional sectional anatomy*

with MRI, and blood supply. Springer Science & Business Media.

Ferguson, H. J., Brunsdon, V. E., & Bradford, E. E. (2021). The developmental trajectories of

executive function from adolescence to old age. *Scientific reports*, *11*(1), 1-17.

https://doi.org/10.1038%2Fs41598-020-80866-1

Field, A. (2009). *Discovering statistics using IBM SPSS statistics*. Sage.

Frank, M. J., & Claus, E. D. (2006). Anatomy of a decision: striato-orbitofrontal interactions in

reinforcement learning, decision making, and reversal. *Psychological review*, *113*(2),

300. https://doi.org/10.1037/0033-295X.113.2.300

Frizzell, T. O., Grajauskas, L. A., Liu, C. C., Ghosh Hajra, S., Song, X., & D'Arcy, R. C. (2020).

White matter neuroplasticity: Motor learning activates the internal capsule and

reduces hemodynamic response variability. *Frontiers in Human Neuroscience*, *14*, 509258. https://doi.org/10.3389/fnhum.2020.509258

Gaffan, D., & Wilson, C. R. (2008). Medial temporal and prefrontal function: recent behavioural disconnection studies in the macaque monkey. *Cortex*, *44*(8), 928-935. https://doi.org/10.1016/j.cortex.2008.03.005

Gajewski, P. D., Hanisch, E., Falkenstein, M., Thönes, S., & Wascher, E. (2018). What does the n-back task measure as we get older? Relations between working-memory measures and other cognitive functions across the lifespan. *Frontiers in psychology*, *9*, 2208. https://doi.org/10.3389/fpsyg.2018.02208

Garrett, H. E. (1946). A developmental theory of intelligence. *American Psychologist*, *1*(9), 372-378. https://psycnet.apa.org/doi/10.1037/h0056380

Gavas, R., Chatterjee, D., & Sinha, A. (2017, October). Estimation of cognitive load based on the pupil size dilation. In *2017 IEEE International Conference on Systems, Man, and C'bernetics (SMC)* (pp. 1499-1504). IEEE. https://doi.org/10.1109/SMC.2017.8122826

Gawryluk, J. R., Mazerolle, E. L., Brewer, K. D., Beyea, S. D., & D'Arcy, R. C. (2011). Investigation of fMRI activation in the internal capsule. *BMC neuroscience*, *12*(1), 1-7. https://doi.org/10.1186/1471-2202-12-56

Gaymard, B., Ploner, C. J., Rivaud, S., Vermersch, A. I., & Pierrot-Deseilligny, C. (1998). Cortical control of saccades. *Experimental brain research*, *123*(1), 159-163. https://doi.org/10.1007/s002210050557

Gellersen, H. M., Guell, X., & Sami, S. (2021). Differential vulnerability of the cerebellum in healthy ageing and Alzheimer's disease. *NeuroImage: Clinical*, *30*, 102605. https://doi.org/10.1016/j.nicl.2021.102605

Genovesio, A., Wise, S. P., & Passingham, R. E. (2014). Prefrontal–parietal function: from

foraging to foresight. *Trends in cognitive sciences*, *18*(2), 72-81.

https://doi.org/10.1016/j.tics.2013.11.007

Granholm, E., Asarnow, R. F., Sarkin, A. J., & Dykes, K. L. (1996). Pupillary responses index

cognitive resource limitations. *Psychophysiology*, *33*(4), 457-461.

https://doi.org/10.1111/j.1469-8986.1996.tb01071.x

Groman, S. M., Keistler, C., Keip, A. J., Hammarlund, E., DiLeone, R. J., Pittenger, C., ... &

Taylor, J. R. (2019). Orbitofrontal circuits control multiple reinforcement-learning

processes. *Neuron*, *103*(4), 734-746. https://doi.org/10.1016/j.neuron.2019.05.042

Gutchess, A. H., & Park, D. C. (2006). fMRI environment can impair memory performance in

young and elderly adults. *Brain research*, *1099*(1), 133-140.

https://doi.org/10.1016/j.brainres.2006.04.102

Haug, H., & Eggers, R. (1991). Morphometry of the human cortex cerebri and corpus

striatum during aging. *Neurobiology of aging*, *12*(4), 336-338.

https://doi.org/10.1016/0197-4580(91)90013-A

Hedden, T., & Gabrieli, J. D. (2004). Insights into the ageing mind: a view from cognitive

neuroscience. *Nature reviews neuroscience*, *5*(2), 87-96.

https://doi.org/10.1038/nrn1323

Heiney, S. A., Kim, J., Augustine, G. J., & Medina, J. F. (2014). Precise control of movement

kinematics by optogenetic inhibition of Purkinje cell activity. *Journal of

Neuroscience*, *34*(6), 2321-2330. https://doi.org/10.1523/JNEUROSCI.4547-13.2014

Henson, R. N. A., Buechel, C., Josephs, O., & Friston, K. J. (1999). The slice-timing problem in

event-related fMRI. *NeuroImage*, *9*, 125. https://www.mrc-

cbu.cam.ac.uk/personal/rik.henson/personal/HensonEtAl_HBM_Abstract_99.pdf

Hess, E. H., & Polt, J. M. (1964). Pupil size in relation to mental activity during simple

problem-solving. *Science*, *143*(3611), 1190-1192.

https://doi.org/10.1126/science.143.3611.1190

Higo, T., Mars, R. B., Boorman, E. D., Buch, E. R., & Rushworth, M. F. (2011). Distributed and

causal influence of frontal operculum in task control. *Proceedings of the National

Academy of Sciences*, *108*(10), 4230-4235.

https://doi.org/10.1073/pnas.1013361108

Hinault, T., Larcher, K., Bherer, L., Courtney, S. M., & Dagher, A. (2019). Age-related

differences in the structural and effective connectivity of cognitive control: a

combined fMRI and DTI study of mental arithmetic. *Neurobiology of aging*, *82*, 30-

39. https://doi.org/10.1016/j.neurobiolaging.2019.06.013

Hirano, T. (2018). Regulation and interaction of multiple types of synaptic plasticity in a

Purkinje neuron and their contribution to motor learning. *The Cerebellum*, *17*(6),

756-765. https://doi.org/10.1007/s12311-018-0963-0

Horne, J. A., & Ostberg, O. (1976). A self-assessment questionnaire to determine

morningness-eveningness in human circadian rhythms. *International Journal of

Chronobiology, 4(2),* 97-110. https://psycnet.apa.org/record/2015-49334-001

Hosseini, S. H., Bruno, J. L., Baker, J. M., Gundran, A., Harbott, L. K., Gerdes, J. C., & Reiss, A.

L. (2017). Neural, physiological, and behavioral correlates of visuomotor cognitive

load. *Scientific reports*, *7*(1), 1-9. https://doi.org/10.1038%2Fs41598-017-07897-z

Huerta, M. F., & Kaas, J. H. (1990). Supplementary eye field as defined by intracortical

microstimulation: connections in macaques. *Journal of Comparative

Neurology*, *293*(2), 299-330. https://doi.org/10.1002/cne.902930211

Huh, D., Kim, J. H., & Jo, I. H. (2019). A novel method to monitoring changes in cognitive load in video-based learning. *Journal of Computer Assisted Learning*, *35*(6), 721-730. https://doi.org/10.1111/jcal.12378

Hutchison, R. M., Gallivan, J. P., Culham, J. C., Gati, J. S., Menon, R. S., & Everling, S. (2012). Functional connectivity of the frontal eye fields in humans and macaque monkeys investigated with resting-state fMRI. *Journal of neurophysiology*, *107*(9), 2463-2474. https://doi.org/10.1152/jn.00891.2011

Huttenlocher, P. R. (1979). Synaptic density in human frontal cortex-developmental changes and effects of aging. *Brain Res*, *163*(2), 195-205. https://doi.org/10.1016/0006-8993(79)90349-4

Ikai, Y., Takada, M., Shinonaga, Y., & Mizuno, N. (1992). Dopaminergic and non-dopaminergic neurons in the ventral tegmental area of the rat project, respectively, to the cerebellar cortex and deep cerebellar nuclei. *Neuroscience*, *51*(3), 719-728. https://doi.org/10.1016/0306-4522(92)90310-X

Imamizu, H., Miyauchi, S., Tamada, T., Sasaki, Y., Takino, R., PuÈtz, B., ... & Kawato, M. (2000). Human cerebellar activity reflecting an acquired internal model of a new tool. *Nature*, *403*(6766), 192-195. https://www.nature.com/articles/35003194

Intons-Peterson, M. J., Rocchi, P., West, T., McLellan, K., & Hackney, A. (1998). Aging, optimal testing times, and negative priming. *Journal of Experimental Psychology: Learning, Memory, and Cognition, 24(2),* 362-376. https://psycnet.apa.org/doi/10.1037/0278-7393.24.2.362

Ito, M. (2005). Bases and implications of learning in the cerebellum—adaptive control and internal model mechanism. *Progress in brain research*, *148*, 95-109. https://doi.org/10.1016/S0079-6123(04)48009-1

Ito, M., Yamaguchi, K., Nagao, S., & Yamazaki, T. (2014). Long-term depression as a model of

cerebellar plasticity. *Progress in brain research 210*, 1-30.

https://doi.org/10.1016/B978-0-444-63356-9.00001-7

Jenkins, I. H., Brooks, D. J., Nixon, P. D., Frackowiak, R. S., & Passingham, R. E. (1994). Motor

sequence learning: a study with positron emission tomography. *Journal of*

Neuroscience, *14*(6), 3775-3790. https://doi.org/10.1523/JNEUROSCI.14-06-

03775.1994

Jirenhed, D. A., & Hesslow, G. (2016). Are Purkinje cell pauses drivers of classically

conditioned blink responses?. *The Cerebellum*, *15*(4), 526-534.

https://doi.org/10.1007%2Fs12311-015-0722-4

Johansson, F., Jirenhed, D. A., Rasmussen, A., Zucca, R., & Hesslow, G. (2014). Memory trace

and timing mechanism localized to cerebellar Purkinje cells. *Proceedings of the*

National Academy of Sciences, *111*(41), 14930-14934.

https://doi.org/10.1073/pnas.1415371111

Jueptner, M., Stephan, K. M., Frith, C. D., Brooks, D. J., Frackowiak, R. S., & Passingham, R. E.

(1997). Anatomy of motor learning. I. Frontal cortex and attention to action. *Journal*

of neurophysiology, *77*(3), 1313-1324. https://doi.org/10.1152/jn.1997.77.3.1313

Kahneman, D., & Beatty, J. (1966). Pupil diameter and load on memory. *Science*, *154*(3756),

1583-1585. https://doi.org/10.1126/science.154.3756.1583

Kahneman, D., & Beatty, J. (1967). Pupillary responses in a pitch-discrimination

task. *Perception & Psychophysics*, *2*(3), 101-105.

https://doi.org/10.3758/BF03210302

Kahneman, D., & Peavler, W. S. (1969). Incentive effects and pupillary changes in association

learning. *Journal of Experimental Psychology*, *79*(2), 312-318.

https://psycnet.apa.org/doi/10.1037/h0026912

Kelly, R. M., & Strick, P. L. (2003). Cerebellar loops with motor cortex and prefrontal cortex of a nonhuman primate. *Journal of neuroscience*, *23*(23), 8432-8444. https://doi.org/10.1523/JNEUROSCI.23-23-08432.2003

Larner, A. J. (2020). Mini-Cog versus Codex (cognitive disorders examination) Is there a difference?. *Dementia & Neuropsychologia*, *14*(2), 128-133. https://doi.org/10.1590/1980-57642020dn14-020005

Levine, B., Stuss, D. T., & Milberg, W. P. (1997). Effects of aging on conditional associative learning: process analyses and comparison with focal frontal lesions. *Neuropsychology*, *11*(3), 367-381. https://psycnet.apa.org/doi/10.1037/0894-4105.11.3.367

Longley, M., Danvers, M., & Ramnani. (2021, November 8-11). *Topographically organised frontal cortex maps in the human cerebellar cortex.* [Poster Presentation]. SFN 2021, virtual.

MacPherson, S. E., Phillips, L. H., & Della Sala, S. (2002). Age, executive function and social decision making: a dorsolateral prefrontal theory of cognitive aging. *Psychology and aging*, *17*(4), 598. https://psycnet.apa.org/doi/10.1037/0882-7974.17.4.598

Mansouri, F. A., Freedman, D. J., & Buckley, M. J. (2020). Emergence of abstract rules in the primate brain. *Nature Reviews Neuroscience*, 1-16. https://doi.org/10.1038/s41583-020-0364-5

Marr, D. (1969). A theory of cerebellar cortex. *Journal of Physiology, 202*, 437-470.

MarsBaR FAQ — MarsBaR 0.45 documentation. (n.d.). Retrieved October 11, 2022, from https://marsbar-toolbox.github.io/faq.html

Matano, S. (2001). Brief communication: proportions of the ventral half of the cerebellar dentate nucleus in humans and great apes. *American Journal of Physical Anthropology: The Official Publication of the American Association of Physical*

Anthropologists, *114*(2), 163-165. https://doi.org/10.1002/1096-8644(200102)114:2%3C163::AID-AJPA1016%3E3.0.CO;2-F

Matsumoto, M., Inoue, K. I., & Takada, M. (2018). Causal role of neural signals transmitted from the frontal eye field to the superior colliculus in saccade generation. *Frontiers in neural circuits. 12*, 69. https://doi.org/10.3389/fncir.2018.00069

Mazerolle, E. L., Gawryluk, J. R., Dillen, K. N., Patterson, S. A., Feindel, K. W., Beyea, S. D., ... & D'Arcy, R. C. (2013). Sensitivity to white matter FMRI activation increases with field strength. *PloS one*, *8*(3), e58130. https://doi.org/10.1371/journal.pone.0058130

Mecacci, L., Zani, A., Rocchetti, G., & Lucioli, R. (1986). The relationships between morningness-eveningness, ageing and personality. *Personality and Individual Differences, 7(6),* 911-913. https://doi.org/10.1016/0191-8869(86)90094-2

Medina, J. F., & Lisberger, S. G. (2008). Links from complex spikes to local plasticity and motor learning in the cerebellum of awake-behaving monkeys. *Nature neuroscience*, *11*(10), 1185-1192. https://doi.org/10.1038/nn.2197

Miller, E. K., & Cohen, J. D. (2001). An integrative theory of prefrontal cortex function. *Annual review of neuroscience*, *24*(1), 167-202. https://doi.org/10.1146/annurev.neuro.24.1.167

Mittleman, G. U. Y., Goldowitz, D., Heck, D. H., & Blaha, C. D. (2008). Cerebellar modulation of frontal cortex dopamine efflux in mice: relevance to autism and schizophrenia. *Synapse*, *62*(7), 544-550. https://doi.org/10.1002/syn.20525

Morales, H., & Tomsick, T. (2015). Middle cerebellar peduncles: Magnetic resonance imaging and pathophysiologic correlate. *World journal of radiology*, *7*(12), 438-447. https://doi.org/10.4329%2Fwjr.v7.i12.438

Morsheddost, H., Asemani, D., & Shalchy, M. A. (2015). Evaluation of hemodynamic

response function in vision and motor brain regions for the young and elderly

adults. *Basic and Clinical Neuroscience*, *6*(1), 58-68.

https://www.ncbi.nlm.nih.gov/pmc/articles/PMC4741271/

Muhammad, R., Wallis, J. D., & Miller, E. K. (2006). A comparison of abstract rules in the

prefrontal cortex, premotor cortex, inferior temporal cortex, and striatum. *Journal of*

cognitive neuroscience, *18*(6), 974-989. https://doi.org/10.1162/jocn.2006.18.6.974

Mumford, J. A., & Nichols, T. (2006). Modeling and inference of multisubject fMRI data. *IEEE*

Engineering in Medicine and Biology Magazine, *25*(2), 42-51.

https://doi.org/10.1109/MEMB.2006.1607668

Murray, E. A., & Rudebeck, P. H. (2013). The drive to strive: goal generation based on current

needs. *Frontiers in neuroscience*, *7*, 112. https://doi.org/10.3389/fnins.2013.00112

Nelson, H. E., & Willison, J. (1982). National adult reading test (NART) manual. *Windsor,*

Bershire, UK: NFER-Nelson.

Nestor, P. G., Nakamura, M., Niznikiewicz, M., Levitt, J. J., Newell, D. T., Shenton, M. E., &

McCarley, R. W. (2015). Attentional control and intelligence: MRI orbital frontal gray

matter and neuropsychological correlates. *Behavioural neurology*, *2015*.

https://doi.org/10.1155/2015/354186

O'Reilly, J. X., Beckmann, C. F., Tomassini, V., Ramnani, N., & Johansen-Berg, H. (2010).

Distinct and overlapping functional zones in the cerebellum defined by resting state

functional connectivity. *Cerebral cortex*, *20*(4), 953-965.

https://doi.org/10.1093/cercor/bhp157

Palesi, F., De Rinaldis, A., Castellazzi, G., Calamante, F., Muhlert, N., Chard, D., ... & Gandini

Wheeler-Kingshott, C. A. (2017). Contralateral cortico-ponto-cerebellar pathways

reconstruction in humans in vivo: implications for reciprocal cerebro-cerebellar

structural connectivity in motor and non-motor areas. *Scientific reports*, *7*(1), 1-13.

https://doi.org/10.1038/s41598-017-13079-8

Park, D., & Schwarz, N. (1999). *Cognitive ageing: A primer*. Psychology Press.

Parthasarathy, H. B., Schall, J. D., & Graybiel, A. M. (1992). Distributed but convergent

ordering of corticostriatal projections: analysis of the frontal eye field and the

supplementary eye field in the macaque monkey. *Journal of Neuroscience*, *12*(11),

4468-4488. https://doi.org/10.1523/JNEUROSCI.12-11-04468.1992

Passingham, R. E. (1996). Attention to action. *Philosophical Transactions of the Royal Society

of London. Series B: Biological Sciences*, *351*(1346), 1473-1479.

https://doi.org/10.1098/rstb.1996.0132

Passingham, R. E., & Wise, S. P. (2012). *The neurobiology of the prefrontal cortex: anatomy,

evolution, and the origin of insight* (No. 50). Oxford University Press.

Passingham, R. E., & Lau, H. (2022). Do we understand the prefrontal cortex?. *Brain

Structure and Function*, 1-11. https://doi.org/10.1007/s00429-022-02587-7

Paus, T., Petrides, M., Evans, A. C., & Meyer, E. (1993). Role of the human anterior cingulate

cortex in the control of oculomotor, manual, and speech responses: a positron

emission tomography study. *Journal of neurophysiology*, *70*(2), 453-469.

https://doi.org/10.1152/jn.1993.70.2.453

Peavler, W. S. (1974). Pupil size, information overload, and performance differences.

Psychophysiology, *11*(5), 559-566. https://doi.org/10.1111/j.1469-

8986.1974.tb01114.x

Penny, W., & Holmes, A. (2007). Random effects analysis. *Statistical parametric mapping:

The analysis of functional brain images*, *156*, 165.

https://citeseerx.ist.psu.edu/document?repid=rep1&type=pdf&doi=6ed105062770d089d86e9bcc7827f54487a22017

Petrides, M., & Pandya, D. N. (1999). Dorsolateral prefrontal cortex: comparative cytoarchitectonic analysis in the human and the macaque brain and corticocortical connection patterns. *European Journal of Neuroscience*, *11*(3), 1011-1036. https://doi.org/10.1046/j.1460-9568.1999.00518.x

Petrides, M. (2000). The role of the mid-dorsolateral prefrontal cortex in working memory. *Experimental brain research*, *133*, 44-54. https://doi.org/10.1007/s002210000399

Petrides, M. (2005). Lateral prefrontal cortex: architectonic and functional organization. *Philosophical Transactions of the Royal Society B: Biological Sciences*, *360*(1456), 781-795. https://doi.org/10.1098/rstb.2005.1631

Petrides, M., Tomaiuolo, F., Yeterian, E. H., & Pandya, D. N. (2012). The prefrontal cortex: comparative architectonic organization in the human and the macaque monkey brains. *Cortex*, *48*(1), 46-57. https://doi.org/10.1016/j.cortex.2011.07.002

Poldrack, R. A., Mumford, J. A., & Nichols, T. E. (2011). *Handbook of functional MRI data analysis*. Cambridge University Press.

Price, D., Tyler, L. K., Henriques, R. N., Campbell, K. L., Williams, N., Treder, M. S., ... & Henson, R. N. A. (2017). Age-related delay in visual and auditory evoked responses is mediated by white-and grey-matter differences. *Nature communications*, *8*(1), 1-12. https://doi.org/10.1038/ncomms15671

Raichle, M. E., Fiez, J. A., Videen, T. O., MacLeod, A. M. K., Pardo, J. V., Fox, P. T., & Petersen, S. E. (1994). Practice-related changes in human brain functional anatomy during nonmotor learning. *Cerebral cortex*, *4*(1), 8-26. https://doi.org/10.1093/cercor/4.1.8

Rajeshkumar, L., & Trewartha, K. M. (2019). Advanced spatial knowledge of target location eliminates age-related differences in early sensorimotor learning. *Experimental brain research*, *237*(7), 1781-1791. https://doi.org/10.1007/s00221-019-05551-w

Ramnani, N., Toni, I., Josephs, O., Ashburner, J., & Passingham, R. E. (2000). Learning-and expectation-related changes in the human brain during motor learning. *Journal of Neurophysiology*, *84*(6), 3026-3035. https://doi.org/10.1152/jn.2000.84.6.3026

Ramnani, N. (2006). The primate cortico-cerebellar system: anatomy and function. *Nature reviews neuroscience*, *7*(7), 511-522. https://doi.org/10.1038/nrn1953

Ramnani, N. (2014). Automatic and controlled processing in the corticocerebellar system. *Progress in Brain Research*, *210*, 255-285. https://doi.org/10.1016/B978-0-444-63356-9.00010-8

Rao, S. C., Rainer, G., & Miller, E. K. (1997). Integration of what and where in the primate prefrontal cortex. *Science*, *276*(5313), 821-824. https://doi.org/10.1126/science.276.5313.821

Raz, N., Gunning, F. M., Head, D., Dupuis, J. H., McQuain, J., Briggs, S. D., ... & Acker, J. D. (1997). Selective aging of the human cerebral cortex observed in vivo: differential vulnerability of the prefrontal gray matter. *Cerebral cortex (New York, NY: 1991)*, *7*(3), 268-282. https://doi.org/10.1093/cercor/7.3.268

Reuter-Lorenz, P. A., Jonides, J., Smith, E. E., Hartley, A., Miller, A., Marshuetz, C., & Koeppe, R. A. (2000). Age differences in the frontal lateralization of verbal and spatial working memory revealed by PET. *Journal of cognitive neuroscience*, *12*(1), 174-187. https://doi.org/10.1162/089892900561814

Rhodes, R. E., & Katz, B. (2017). Working memory plasticity and aging. *Psychology and aging*, *32*(1), 51-59. https://psycnet.apa.org/doi/10.1037/pag0000135

Rivaud, S., Müri, R. M., Gaymard, B., Vermersch, A. I., & Pierrot-Deseilligny, C. (1994). Eye movement disorders after frontal eye field lesions in humans. *Experimental Brain Research*, *102*(1), 110-120. https://doi.org/10.1007/BF00232443

Rogers, T. D., Dickson, P. E., Heck, D. H., Goldowitz, D., Mittleman, G., & Blaha, C. D. (2011). Connecting the dots of the cerebro-cerebellar role in cognitive function: Neuronal pathways for cerebellar modulation of dopamine release in the prefrontal cortex. *Synapse*, *65*(11), 1204-1212. https://doi.org/10.1002/syn.20960

Ross, M. H., Yurgelun-Todd, D. A., Renshaw, P. F., Maas, L. C., Mendelson, J. H., Mello, N. K., ... & Levin, J. M. (1997). Age-related reduction in functional MRI response to photic stimulation. *Neurology*, *48*(1), 173-176. https://doi.org/10.1212/WNL.48.1.173

Roveda, E., Vitale, J., Montaruli, A., Galasso, L., Carandente, F., & Caumo, A. (2017). Predicting the actigraphy-based acrophase using the Morningness–Eveningness Questionnaire (MEQ) in college students of North Italy. *Chronobiology international*, *34*(5), 551-562. https://doi.org/10.1080/07420528.2016.1276928

Sakai, K., Rowe, J. B., & Passingham, R. E. (2002). Active maintenance in prefrontal area 46 creates distractor-resistant memory. *Nature neuroscience*, *5*(5), 479-484. https://doi.org/10.1038/nn846

Salthouse, T. A. (1993). Speed mediation of adult age differences in cognition. *Developmental psychology*, *29*(4), 722-738. https://psycnet.apa.org/doi/10.1037/0012-1649.29.4.722

Salthouse, T. A. (1994). Aging associations: influence of speed on adult age differences in associative learning. *Journal of experimental psychology: learning, memory, and cognition*, *20*(6), 1486-1503. https://psycnet.apa.org/doi/10.1037/0278-7393.20.6.1486

Salthouse, T. A. (2000). Pressing issues in cognitive aging. In D. C. Park & N. Schwarz

(Eds.), *Cognitive aging: A primer* (pp. 43–54). Psychology Press.

Salthouse, T. A. (2004). What and when of cognitive aging. *Current directions in*

psychological science, *13*(4), 140-144. https://psycnet.apa.org/doi/10.1111/j.0963-

7214.2004.00293.x

Salthouse, T. A. (2010). Selective review of cognitive aging. *Journal of the International*

Neuropsychological Society: JINS, *16*(5), 754-760.

https://doi.org/10.1017/S1355617710000706

Sasaki, K., Oka, H., Kawaguchi, S., Jinnai, K., & Yasuda, T. (1977). Mossy fibre and climbing

fibre responses produced in the cerebellar cortex by stimulation of the cerebral

cortex in monkeys. *Experimental Brain Research*, *29*(3), 419-428.

https://doi.org/10.1007/BF00236180

Schall, J. D., Morel, A., & Kaas, J. H. (1993). Topography of supplementary eye field afferents

to frontal eye field in macaque: implications for mapping between saccade

coordinate systems. *Visual neuroscience*, *10*(2), 385-393.

https://doi.org/10.1017/S0952523800003771

Schmahmann, J. D., & Pandya, D. N. (1995). Prefrontal cortex projections to the basilar pons

in rhesus monkey: implications for the cerebellar contribution to higher

function. *Neuroscience letters*, *199*(3), 175-178. https://doi.org/10.1016/0304-

3940(95)12056-A

Schmahmann, J. D., & Pandya, D. N. (1997). Anatomic organization of the basilar pontine

projections from prefrontal cortices in rhesus monkey. *Journal of*

Neuroscience, *17*(1), 438-458. https://doi.org/10.1523/JNEUROSCI.17-01-

00438.1997

Schmahmann, J. D., Doyon, J., Petrides, M., Evans, A. C., & Toga, A. W. (2000). *MRI atlas of the human cerebellum*. Academic press.

Schoenbaum, G., Chiba, A. A., & Gallagher, M. (1998). Orbitofrontal cortex and basolateral amygdala encode expected outcomes during learning. *Nature neuroscience*, *1*(2), 155-159. https://doi.org/10.1038/407

Schoenbaum, G., Setlow, B., Saddoris, M. P., & Gallagher, M. (2003). Encoding predicted outcome and acquired value in orbitofrontal cortex during cue sampling depends upon input from basolateral amygdala. *Neuron*, *39*(5), 855-867. https://doi.org/10.1016/S0896-6273(03)00474-4

Schoenbaum, G., & Roesch, M. (2005). Orbitofrontal cortex, associative learning, and expectancies. *Neuron*, *47*(5), 633-636. https://doi.org/10.1016/j.neuron.2005.07.018

Segraves, M. A., & Goldberg, M. E. (1987). Functional properties of corticotectal neurons in the monkey's frontal eye field. *Journal of neurophysiology*, *58*(6), 1387-1419. https://doi.org/10.1152/jn.1987.58.6.1387

Sendhilnathan, N., & Goldberg, M. E. (2020). The mid-lateral cerebellum is necessary for reinforcement learning. *BioRxiv*, 2020-03. https://doi.org/10.1101/2020.03.20.000190

Shook, B. L., Schlag-Rey, M., & Schlag, J. (1990). Primate supplementary eye field: I. Comparative aspects of mesencephalic and pontine connections. *Journal of Comparative Neurology*, *301*(4), 618-642. https://doi.org/10.1002/cne.903010410

Sladky, R., Friston, K. J., Tröstl, J., Cunnington, R., Moser, E., & Windischberger, C. (2011). Slice-timing effects and their correction in functional MRI. *Neuroimage*, *58*(2), 588-594. https://doi.org/10.1016/j.neuroimage.2011.06.078

Steele, C. J., Anwander, A., Bazin, P. L., Trampel, R., Schäfer, A., Turner, R., ... & Villringer, A.

    (2017). Human cerebellar sub-millimeter diffusion imaging reveals the motor and

    non-motor topography of the dentate nucleus. *Cerebral Cortex*, *27*(9), 4537-4548.

    https://doi.org/10.1093/cercor/bhw258

Suzuki, L., Coulon, P., Sabel-Goedknegt, E. H., & Ruigrok, T. J. (2012). Organization of

    cerebral projections to identified cerebellar zones in the posterior cerebellum of the

    rat. *Journal of Neuroscience*, *32*(32), 10854-10869.

    https://doi.org/10.1523/JNEUROSCI.0857-12.2012

Swenson, R. S., Sievert, C. F., Terreberry, R. R., Neafsey, E. J., & Castro, A. J. (1989).

    Organization of cerebral cortico-olivary projections in the rat. *Neuroscience*

    research, *7*(1), 43-54. https://doi.org/10.1016/0168-0102(89)90036-9

Takahashi, Y. K., Roesch, M. R., Stalnaker, T. A., Haney, R. Z., Calu, D. J., Taylor, A. R., ... &

    Schoenbaum, G. (2009). The Orbitofrontal Cortex and Ventral Tegmental Area Are

    Necessary for Learning from Unexpected Outcomes. *Neuron*, *62*, 269-280.

    https://doi.org/10.1016/j.neuron.2009.03.005

Tekes, A., Mohamed, M. A., Browner, N. M., Calhoun, V. D., & Yousem, D. M. (2005). Effect

    of age on visuomotor functional MR imaging1. *Academic radiology*, *12*(6), 739-745.

    https://doi.org/10.1016/j.acra.2004.08.015

Tsujimoto, S., Genovesio, A., & Wise, S. P. (2010). Evaluating self-generated decisions in

    frontal pole cortex of monkeys. *Nature neuroscience*, *13*(1), 120.

    https://doi.org/10.1038/nn.2453

van Schouwenburg, M., Aarts, E., & Cools, R. (2010). Dopaminergic modulation of cognitive

    control: distinct roles for the prefrontal cortex and the basal ganglia. *Current*

    pharmaceutical design, *16*(18), 2026-2032.

    https://doi.org/10.2174/138161210791293097

Walker, A. E. (1940). A cytoarchitectural study of the prefrontal area of the macaque

   monkey. *Journal of Comparative Neurology*, *73*(1), 59-86.

   https://doi.org/10.1002/cne.900730106

Wallis, J. D., Anderson, K. C., & Miller, E. K. (2001). Single neurons in prefrontal cortex

   encode abstract rules. *Nature*, *411*(6840), 953-956.

   https://doi.org/10.1038/35082081

Watson, T. C., Jones, M. W., & Apps, R. (2009). Electrophysiological mapping of novel

   prefrontal-cerebellar pathways. *Frontiers in inteltive neuroscience*, *3*, 18.

   https://doi.org/10.3389/neuro.07.018.2009

West, R. L. (1996). An application of prefrontal cortex function theory to cognitive

   aging. *Psychological bulletin*, *120*(2), 272. https://doi.org/10.1037/0033-

   2909.120.2.272

West, R. (2000). In defense of the frontal lobe hypothesis of cognitive aging. *Journal of the*

   International Neuropsychological Society, *6*(6), 727-729.

   https://doi.org/10.1017/S1355617700666109

West, K. L., Zuppichini, M. D., Turner, M. P., Sivakolundu, D. K., Zhao, Y., Abdelkarim, D., ... &

   Rypma, B. (2019). BOLD hemodynamic response function changes significantly with

   healthy ageing. *Neuroimage*, *188*, 198-207.

   https://doi.org/10.1016/j.neuroimage.2018.12.012

Winocur, G. (1991). Functional dissociation of the hippocampus and prefrontal cortex in

   learning and memory. *Psychobiology*, *19*(1), 11-20.

   https://doi.org/10.1007/BF03337952

Winocur, G. (1992). Conditional learning in aged rats: evidence of hippocampal and

prefrontal cortex impairment. *Neurobiology of Aging*, *13*(1), 131-135.

https://doi.org/10.1016/0197-4580(92)90020-X

Wise, S. P., & Murray, E. A. (2000). Arbitrary associations between antecedents and

actions. *TrendIn neurosciences*, *23*(6), 271-276. https://doi.org/10.1016/S0166-

2236(00)01570-8

Woodruff-Pak, D. S., Papka, M., & Ivry, R. B. (1996). Cerebellar involvement in eyeblink

classical conditioning in humans. *Neuropsychology*, *10*(4), 443-458.

https://psycnet.apa.org/doi/10.1037/0894-4105.10.4.443

Woodruff-Pak, D. S., Foy, M. R., Akopian, G. G., Lee, K. H., Zach, J., Nguyen, K. P. T., ... &

Thompson, R. F. (2010). Differential effects and rates of normal aging in cerebellum

and hippocampus. *Proceedings of the National Academy of Sciences*, *107*(4), 1624-

1629. https://doi.org/10.1073/pnas.0914207107

World Health Organization. (2018). *Integrated care for older people: realigning primary*

health care to respond to population aging (No. WHO/HIS/SDS/2018.44). World

Health Organization.

Xi, M. C., Liu, R. H., Engelhardt, J. K., Morales, F. R., & Chase, M. H. (1999). Changes in the

axonal conduction velocity of pyramidal tract neurons in the aged

cat. *Neuroscience*, *92*(1), 219-225. https://doi.org/10.1016/S0306-4522(98)00754-4

Yang, G., Zhang, Y., Ross, M. E., & Iadecola, C. (2003). Attenuation of activity-induced

increases in cerebellar blood flow in mice lacking neuronal nitric oxide

synthase. *American Journal of Physiology-Heart and Circulatory Physiology*, *285*(1),

H298-H304. https://doi.org/10.1152/ajpheart.00043.2003

Yang, L., Yan, J., Jin, X., Jin, Y., Yu, W., Xu, S., & Wu, H. (2016). Screening for dementia in

older adults: comparison of Mini-Mental State Examination, Mini-Cog, Clock Drawing

test and AD8. *PloS one*, *11*(12), e0168949.

https://doi.org/10.1371/journal.pone.0168949

Chapter 6

Elucidating cortico-cortical and corticocerebellar circuitry in conditional visuo-oculomotor learning using ultra-high field imaging

Matthew Danvers
Narender Ramnani
In preparation for publication

Word count: 12,814 excluding references

Abstract

When studying conditional learning there is evidence of contributions from a network of brain regions. Three key components are the visual perception of instrumental cues, the encoding of goals based upon previous feedback, and the subsequent execution of an appropriate response. This was investigated in nine 21-29 year-olds who partook in a conditional visuo-oculomotor learning study, all participants demonstrating increasing accuracy over the course of learning. Ultra-high field functional imaging was employed in an effort to boost signal-noise ratios and increase spatial resolution, to identify regions active at different stages within a trial, and also different stages of learning. This demonstrated that regions such as the frontopolar, middle frontal, superior frontal, paracingulate, posterior orbital, and insular gyri contributed, as well as cerebellar lobules HVI-CRUS I and OMV, the striatum, eye fields, and both parietal and temporo-occipital cortices. Findings further support previous work carried out in our lab, which suggested a network involving dorsolateral regions of the prefrontal cortex and cerebellar lobules HVI-CRUS I. There was also an effect of learning status, with greater magnitude blood oxygen level dependent (BOLD) responses typically seen during incorrect trials at the time of the cue. In conclusion, dorsolateral prefrontal areas and connected cerebellar lobules appeared to encode goals prior to a response being made, potentially receiving feedback information via orbital gyri and the striatum.

6.1. Introduction

Conditional visuo-motor learning, also known as conditional discrimination or arbitrary visuo-motor mapping (Wise & Murray, 2000), involves an arbitrary instrumental cue being associated with an action in order to achieve a goal. As a form of associative learning this falls withing the realms of instrumental or operant conditioning and is a core example of flexible intelligent behaviour (Wise & Murray, 2000). The study described below utilised conditional visuo-oculomotor learning using the eyes as an effector, choices indicated via saccadic eye movements. This was run whilst participants partook in a whole-brain ultra-high field functional magnetic resonance imaging (fMRI) scan. It was hoped that the boost in signal-to-noise would facilitate the finding of potentially more subtle effects especially when considering trial-to-trial excitability changes, alongside an increase in spatial resolution to aid anatomical localisation. The task involved presentation of an arbitrary non-spatial visual cue. Participants then had to form and execute a visuo-spatially defined goal (selecting and saccading to one of three identical but spatially differentiated targets). Feedback as to whether the correct target had been selected was given, with this informing future encoding of goals.

Brain regions likely to be involved in the conditional learning process include the hippocampus, basal ganglia, temporal cortex, parietal cortex, cerebellum, orbitofrontal cortex (OFC), cingulate cortex, and prefrontal cortex (PFC) (Balsters & Ramnani, 2008, 2011; Balsters et al., 2013; Hadj-Bouziane et al., 2003; Wise & Murray, 2000; Yahya, 2021). Starting in the temporal lobe, regions such as the inferior temporal cortex (ITC) are evidenced as providing non-spatial visual information to the PFC (Muhammad et al., 2006). This is both direct via the uncinate fascicle, and indirect via connections to the putamen and caudate. These output via the globus pallidus to the thalamus, which relays information to both the

prefrontal and premotor cortices (Wise & Murray, 2000). Looking at specific regions of the

PFC the dorsolateral prefrontal cortex (dlPFC) is considered. Petrides (2000) defined this

functionally as being in both the middle frontal gyrus (MFG) and superior frontal gyrus (SFG),

encompassing areas 46, 9, 9/46, 8, some of area 10, and the rostral portion of area 6.

Petrides (2005) report that areas 9, 46, and 9/46 of the dlPFC (mid dlPFC) connect with the

multimodal superior temporal sulcus (STS) and the rostral superior temporal gyrus (STG).

More caudally area 8 connects with posterior visual temporal areas, and more ventrally the

ventrolateral prefrontal cortex (vlPFC; specifically areas 45 and 47/12) is connected with the

auditory STG and multimodal STS, with area 47/12 specifically connecting with the rostral

inferotemporal visual association cortex.

This explains the first step in the network whereby information about visual objects

(cues) can reach the PFC. Importance of the dlPFC specifically is demonstrated by evidence

that lesions result in associative learning (areas 8 and rostral 6; Levine et al., 1997) and

memory (areas 8, 9, 9/46, and 46; Moore et al., 2012) impairments. A role in maintaining the

memory trace between cue presentation and action execution has been suggested (Bunge,

2004; Mansouri et al., 2020; Sakai et al., 2002), with links to prospective encoding of visuo-

spatially defined goals (Passingham & Wise, 2012, pp. 157-194). Also the vlPFC is seen to

play a role (Mansouri et al., 2020) with a 2.3 fold increase in errors when pathways between

ITC and vlPFC are cut (Bloedel et al., 1996, pp. 266-267). This is supported by Passingham &

Lau (2022) who suggest the vlPFC uses object information to guide the future choices of

objects. Work in our lab has supported this, with dlPFC activity time-locked to cue

presentation, within area 46 and extending into the more ventral sub-region area 9/46v,

which is itself connected to the ventral PFC (Petrides & Pandya, 2002). Therefore it is

reasonable to assert that both vlPFC and dlPFC play a role in conditional visuo-motor

learning, with both 'what' and 'where' information converging (Rao et al., 1997), consistent

with the two regions being connected (Petrides & Pandya, 2002; Petrides, 2005). However in order to understand their roles more fully, other areas need to be considered.

Firstly there is the parietal cortex, with relevance to visuo-spatially defined goals as it processes information pertaining to number, distance, and crucially location (Burr et al., 2010; Merritt et al., 2010). In the case of visuo-motor learning, in order to select the appropriate response one first needs to encode the goal, in this case the location of the target (characterised visuo-spatially). It is known that regions within the intraparietal sulcus (IPS) show functional activity that is associated with dorsolateral areas 8 and 46 (Sakai et al., 2002), and that the posterior parietal cortex (PPC) is connected to both the FEFs (Rivaud et al., 1994) and dorsolateral area 46 (Passingham & Wise, 2012, pp. 157-194) with further connectivity found between FEFs and dorsolateral area 9/46 (Hutchison et al., 2012). The visuo-spatial inferior parietal cortex is also connected to area 8 (Petrides, 2005), with area 8A outputting to area 9/46 (Passingham & Lau, 2022). All this supports the role of the dlPFC in encoding goals in terms of location in visual space, with outputs to regions involved in oculomotor control (e.g. the FEFs). Given that this is crucial to sequence learning, it is perhaps not surprising there are suggestions this is the function of the dlPFC (Passingham & Lau, 2022). However work in our lab suggests the dlPFC is involved in encoding locations as goals whether in a sequence or not.

As dorsolateral areas 8, 9, 9/46, and 46 may have a role in maintaining a memory trace (Mansouri et al., 2020; Moore et al., 2012), the hippocampus is next considered. The dlPFC is know to connect with hippocampal regions (Petrides, 2005), and so it is reasonable to suggest some shared role in memory processes. Lesion studies suggest the hippocampus' role is in the learning of new information, rather than recollection of learnt associations, with activity reducing over learning (Murray & Wise, 1996; Petrides, 1985; Wise & Murray, 2000). If so, hippocampal activity may contribute more to early error trials than later correct

trials. Hippocampal connectivity therefore reinforces the idea that the PFC not only encodes object and spatial information to generate and maintain a spatial goal, but that the hippocampus assists in this process by aiding retention during the early stages of learning. One suggestion is that this region assists in associating events or items that are discontiguous either in time or space (Wallenstein et al., 1998), important in conditional learning as both cue and feedback can be separated temporally. This is consistent with lesion studies in rats finding greater impairment of conditional learning as the inter-stimulus interval is increased (Winocur, 1991).

Next the formation and execution of an appropriate action is required, based upon location of the goal, position in space, and the desired effector. The caudally located dorsal premotor cortex has been implicated here, lesions specifically disrupting learning of cue-action associations rather than the subject's baseline ability to recognise cues or perform actions (Wise & Murray, 2000). However, when the response is oculomotor there is evidence that the supplementary eye fields (SEF) may play a role (Bloedel et al., 1996, pp. 266-275; Chen & Wise, 1995a; Petrides, 2019, pp. 91-108). This region is shown to represent saccades based on final positioning of the eye in space (unlike the FEFs which represent saccades based on retinal position; Schall et al, 1993) and are not necessarily implicated in saccade production specifically, but in timing, sequencing, learning, and decisions based upon value (Abzug & Sommer, 2017). Activity pertains to population vector tuning (akin to work in the motor cortex for hand movement; Georgopoulos et al., 1982, 1983; Scott, 2000) found to represent net directional signal with increasing accuracy over trials, and evidence of both learning selectivity (reducing over learning) and learning dependency (increasing over learning; Chen & Wise, 1995a). The SEFs connect with the FEFs, dlPFC (principal and arcuate sulci), and superior colliculus (Huerta & Kaas, 1990; Hutchison et al., 2012; Schall et al., 1993; Shook et al., 1990), and so are well placed to fulfil a role akin to the premotor

cortex (Chen & Wise, 1995b). Regions such as the FEFs may then generate the oculomotor response via projections to the paramedian pontine reticular formation, either direct or through the superior colliculus (Purves et al., 2008, pp. 460-507). In this way the SEFs could be converting the spatial goal into an appropriate retinotopically guided action elicited by the FEFs. It is also suggested that the oculomotor vermis (OMV; vermal lobules VI-VIII) may be active, as it is implicated in saccadic adaptation (Kojima & Soetedjo, 2018; Lefevre et al., 1998; Quaia et al., 1999). Furthermore the superior colliculus shows potential OMV connectivity via pre-cerebellar nuclei (Brodal & Brodal, 1981; Frankfurter et al., 1976; Yamada & Noda, 1987), with a suggested similar pattern seen from the FEFs and SEFs (Voogd et al., 2012), supported by tracer studies finding connections to the pontine nucleus from the FEFs (Stanton et al., 1988) and SEFs (Shook et al., 1990) in NHPs.

This explains the process from cue presentation to action execution, but missing is the critical role of feedback to guide future choices. The first region considered in relation to this is the frontopolar cortex (FPC). It has been shown in monkeys (performing tasks whereby visual cues guide oculomotor responses) that the FPC encodes the chosen goal (e.g. left hand target) at the time of feedback via response-specific (saccade to left or right target) neural activity (Tsujimoto et al., 2011a). This is not however seen at the time of cue presentation or during the subsequent delay period (Tsujimoto et al., 2012). Termed retrospective monitoring, it is considered that the FPC may be re-representing goals at the time of reward, meaning the goal can be reinforced when paired with positive feedback. This may, like the hippocampus, partly address the issue of discontiguity between cue and feedback events. Activity has been seen to be greater on correct trials than on incorrect, likely driven by the FPC specifically signalling correct responses (Tsujimoto et al., 2012). The OFC is also relevant, connected with limbic and inferior temporal regions and thought to generate expectations to inform actions based on the outcomes of past cue-associated

choices (Passingham & Wise, 2012, pp. 128-129; Saleem et al., 2008; Schoenbaum et al., 1998, 2003; Schoenbaum & Roesch, 2005). Like the FPC, the OFC shows response specific activity at the time of feedback but does not discriminate between correct and incorrect trials (Tsujimoto et al., 2010, 2011a). However this region also demonstrated strategy specific activity (stay with or shift from previous saccade target) at the time of the cue (Tsujimoto et al., 2012), and attempted to encode the correct strategy even when not employed, with activity seen even within incorrect trials (Tsujimoto et al., 2011b). Finally dorsolateral area 46 was considered within the circuit, with cue-locked activity pertaining to both strategy and response (Tsujimoto et al., 2011b, 2012), and feedback-locked activity encoding the response with greater activity on correct than on error trials (Tsujimotor et al., 2011a, 2012). As a result Tsuijimoto et al. (2011b, 2012) concluded that area 46 has a role generating responses based on decisions and strategies, the OFC assigns outcomes to the decisions which informed the response, and the FPC assigns outcomes to the cognitive processes which underpinned these decisions. This is somewhat consistent with the work of Ramnani & Owens (2004) who suggested that frontopolar area 10 is implicated in integrating outcomes of multiple cognitive processes and coordinating information processing across supramodal cortical areas.

Following on from this statement and based upon previous work in our lab, the cerebellum is considered next as a region implicated in conditional learning (Balsters & Ramnani, 2008, 2011; Balsters et al., 2013). This is made possible by evidence of connectivity between dorsolateral areas in the MFG such as 46 and 9/46, and cerebellar lobule HVIIa (Balsters et al., 2014; Kelly & Strick, 2003), projections from the dlPFC (including frontopolar area 10) to pre-cerebellar nuclei (Schmahmann & Pandya, 1995, 1997), and those with cerebellar damage showing pseudo-frontal symptoms (Budisavljevic & Ramnani, 2012). Furthermore, it is suggested by Ramnani (2014) that the role of the cerebellum can be

described in control theoretic terms, with the PFC arranged in a hierarchical fashion, rostral 'controllers' acting on caudal 'plants'. This is thought to facilitate information pertaining to rules being converted into visuo-spatially defined goals which can be achieved with relevant actions. Within this description the cerebellum acts as a forward model (a form of internal model) which receives efference copies of projections from controllers to plants via the pontine nucleus. Additionally the cerebellum is thought to receive information about both sensory consequences (via the inferior olive which acts as a comparator looking for discrepancy between actual and ideal) and reward consequences (via the inferior olive and ventral tegmental area (VTA)). The purpose of the internal model is to represent input-output pairings, Imamizu et al. (2000) suggesting multiple are active initially but narrowed down with experience to a subset of accurate models. Therefore over the course of learning it is expected that models are refined until context-specific responses can occur intuitively and relatively independently of feedback, thus reducing the load on the PFC. Ito (2005) suggested that a similar internal model could be used to regulate connections between 'thinking' in the PFC and mental models of the external world held in temporoparietal cortices. It is considered that this may explain previous findings by our lab of parietal activity time locked to cue presentation, specific to the experimental condition, potentially representing a visuo-spatially defined goal.

Consequently the study below looked at BOLD responses time-locked to both presentation of the cue, and presentation of feedback. The purpose of this was to ascertain what brain regions were involved in prospective encoding of rules and/or processing of feedback, whilst regressing out and separately investigating areas involved in oculomotor response execution. A sub-division was also included based upon error-status, in an attempt to ascertain which regions differentially encoded error versus correct trials. As a result the following hypotheses were formed.

8

6.1.1. Hypotheses

1. There will be a main effect of condition driven by BOLD responses in the experimental condition. This will be tested in the frontal lobe (with a focus upon the dlPFC, frontal pole, OFC, and eye fields) and cerebellum (with a focus upon lobule HVIIa).

2. There will a condition x event interaction driven by BOLD responses in the experimental condition differing between cue and feedback events. This will be tested in the frontal lobe (with a focus upon the dlPFC, frontal pole, OFC, and eye fields) and cerebellum (with a focus upon lobule HVIIa).

3. There will a condition x error-status interaction driven by BOLD responses in the experimental condition differing between correct and incorrect trials. This will be tested in the frontal lobe (with a focus upon the dlPFC, frontal pole, OFC, and eye fields) and cerebellum (with a focus upon lobule HVIIa).

4. There will be a condition x error-status x event interaction, driven by interactions between condition and error-status differing at the time of cue and feedback events. This will be tested in the frontal lobe (with a focus upon the dlPFC, frontal pole, OFC, and eye fields) and cerebellum (with a focus upon lobule HVIIa).

5. There will be activity across eye fields and within the OMV at the time of target presentation.

6.2. Methods

All scripts are available on https://github.com/mdanve01/Project4

6.2.1. Participants

The opportunity sample was comprised of nine adults aged 21-29 (M = 23.33 years, SD = 2.45 years, 100% female) with 23 participants originally booked. Of the 14 participants

removed from the analysis one was a technical pilot and resulting changes to the design meant they could not be included, but their anatomical scan was still used to create a template. Two were lost due to head size meaning their eyes could not be tracked. One was lost due to scanner failure. Three were lost due to the illuminator on the eye-tracker malfunctioning, two of which had usable anatomical scans. One was removed due to excessive translational head motion with a range of 5.45mm in the z dimension and inter-scan jumps up to 3.08mm, but with a usable anatomical scan. Six were removed due to a missed trial rate greater than 33% in the experimental condition (caused by the eye-tracker failing to record a response), but all had usable anatomical scans. Participants were offered a £50 Amazon voucher in return for participation. All participants were right-handed, had normal or corrected to normal vision, reported no diagnosis of a psychiatric, developmental, neurological or sensory disorder, or any specific learning difficulties such as dyslexia, dyspraxia or ADHD, and had no history of seizures or epilepsy. Ethical approval was provided by Ethics Committees of both Royal Holloway University of London, and Oxford University. Participants were contacted via Microsoft Teams where the study was explained and eligibility checked, including Oxford University's MRI Volunteer Screening Form used to identify MRI contraindications. If eligible a scanning session was arranged.

6.2.2. Apparatus

An MRI compatible Eyelink 1000 eyetracker provided by SR research (sampling at 1000hz) recorded left eye movements, with standard 7T adaptations. Custom calibration points were used due to a limited field of view. A 50mm MRI compatible lens and an MRI compatible illuminator were affixed to a mount strapped to the scanner bed, with a custom support to reduce vibration. A 'hot mirror' provided participants visual access to the projector screen through a two-way mirror which facilitated recording of the eye. The distance from center of screen to 'hot mirror' was ~685mm, from 'hot mirror' to eye was

~50mm, from camera to two-way mirror was 80mm, and from hot mirror to two-way mirror was ~510mm (variability due to participant-specific adjustments). The study was run using Experiment Builder (resolution = 1024 x 768) and the experiment was presented to participants via an Eiki LC-XL100 projector (resolution = 1024 x 768).

To monitor and manage event timings TTL pulses from the scanner were sent to a custom parallel port connected to a Windows 'stimulus' PC from which the experiment was run. A TTL input trigger was used to initiate the start of each trial, and TTL pulses were recorded using a CED 1401 via Spike2 software on a Windows laptop. All events were recorded using a CED 1401 with Spike2 software (sampling at 5000hz) using TTL outputs from experiment builder to the parallel port. These were used to verify that data held by Eyelink's own software Dataviewer (sampling at 1000hz) was accurate. All processing of fMRI data was carried out on a Dell laptop with an 11th Gen Intel® Core™ i7-1165G7 processor running Matlab 2022a, and SPM12 (7771). Analysis of behavioural data was carried out using IBM SPSS statistics version 25.

6.2.3. Behavioural Task

Experimental Design: The conditional visuo-oculomotor task involved learning a set of associations (which remained constant over the study) whereby ten different shapes (cues; see Figure 1) were each arbitrarily paired with one of three spatially defined targets. Therefore the rule might be "if shown a square, look at the left-hand target", see Figure 2.

Experimental		Control	
Square	103w x 103h = 10609	Circle	116w x 116h = 10568
Hexagon	Rectangle = 118w x 59h Right-Angled Triangles = 2 x (117w x 30h) Total = 10472	Rhombus	146w x 146h = 10658
Equilateral Triangle	157w x 136h = 10676	Rectangle	126w x 84h = 10584
Rectangle	84w x 126h = 10584	Parallelogram	Rectangle = 60w x 119h Right-Angled Triangles = 2 x (30w x 119h) Total = 10710
Trapezium	Rectangle = 60w x 119h Right-Angled Triangles = 2 x (30w x 119h) Total = 10710	Hourglass	Isoceles Triangles = 2 x (205w x 51h) = 10455
Semi-Circle	164w x 82h = 10562	Pentagon	Square = 92w x 92h Isoceles Triangle = 92w x 46h Total = 10580
Quarter-Circle	116w x 116h = 10568	Double Isoceles Triangle	2 x (103w x 103h) = 10609
Double Circle	2 x (82w x 82h) = 10562	Double Right-Angled Triangle	2 x (103w x 103h) = 10609
Double Isoceles Triangle	2 x (103w x 103h) = 10609	Double Circle	2 x (82w x 82h) = 10562
Double Quarter-Circle	2 x (82w x 82h) = 10562	Semi-Circle	82w x 164h = 10562

Figure 1. Cue shapes and sizes
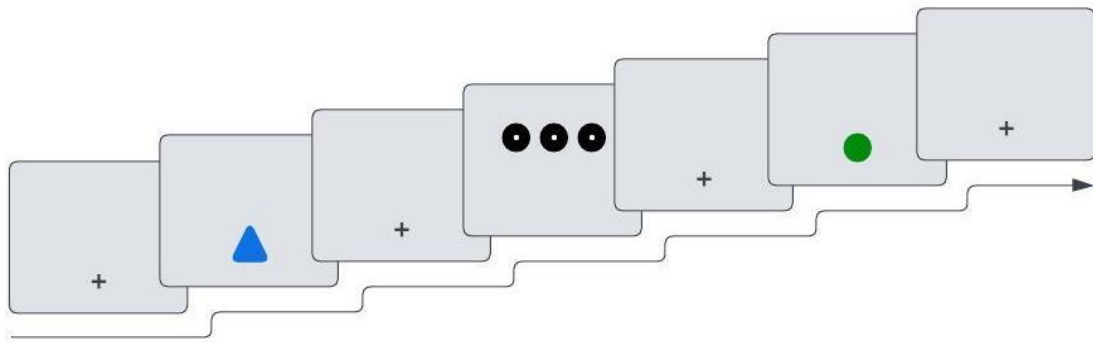
Figure 2. Standard trial structure demonstrating presentation of a cue (blue triangle), three targets to choose from (black circles), and feedback (green circle).

The number of cues exceeded the number of targets to ensure that any target could be associated with more than one cue, preventing participants using information about one rule to inform deductions about another. After making their selection feedback was given. Participants were aware of the task structure, but acquired cue-target pairings via trial and error. Consequently there were a total of three event types (cue onset, target onset, and feedback onset) across two levels of condition (experimental and control), and two levels of error-status (correct and incorrect). These were arranged into a design matrix of regressors using the general linear model (GLM), see **section 6.2.8. GLM Design** below. Correct trials were only modelled as such when the preceding trial within the same rule was also correct. This ensured correct trials represented cases of established learning, rather than guesses made during active learning. That target events were modelled independently facilitated a check that expected oculomotor structures were active at the time of target presentation, as per hypothesis 5. Hypotheses 1-4 relied on the full three-factor design as it was investigated where BOLD responses were significant specific to the experimental condition, whilst also examining differences between cue and feedback events, as well as correct and incorrect trials.

For the above reason control trials involved presentation of a single target randomly positioned within one of the three target locations. Control cue-target pairings changed pseudorandomly over the course of the study, each cue paired with each target an equal number of times, but never having the same association more than twice in a row. This meant control and experimental conditions were matched in terms of a cue being presented, followed by a target and consequent saccade, followed by feedback presentation, but differed in that no association could be learnt in the control condition. In order to match the experience between conditions, each of the 10 cue shapes in the control condition was arbitrarily yoked to a specific cue shape in the experimental condition. Whatever feedback was received in relation to a given experimental cue was mirrored in the yoked control cue. For example, if over the first six trials an experimental cue received the feedback; red, red, green, red, green, green, this was also the feedback given for the first six trials of the yoked control cue. Participants were made explicitly aware that control condition feedback was just for matching purposes and carried no meaningful information. As feedback in the control trials had to match the experimental condition this required an offset whereby control trials consistently lagged behind experimental. In total there were 150 trials at each level of condition, with the study split into five blocks of 60 (30 experimental and 30 control).

Trial Structure: When stimuli were not on the screen a fixation cross was presented to keep participant gaze focused at the screen-coordinate where cues and feedback were presented. Within a trial there was a variable delay after which a cue was presented. If blue this indicated an experimental trial, if black this indicated a control trial. Post cue offset there was a variable delay followed by target presentation (these were positioned in a horizontal formation), see Figure 3. Presentation of targets acted as a 'GO' signal, indicating the participant was to select one by fixating it. Selection was registered when participants

fixated within an area of interest for at least 200ms (see **6.2.3.4. Areas of Interest** below).

Due to minor processing delays in Experiment Builder and a 1250ms target presentation

time, participant fixation onsets had to occur within approximately 1010ms of target onset.

Post target offset there was another variable delay followed by presentation of feedback.

This was either green if correct, red if incorrect, or yellow if no fixation was detected. Due to

the 60Hz refresh rate of the projector actual event durations had a fluctuating +/-~16.67ms

error (as presentation or removal of a stimulus from the screen had to wait for a refresh).
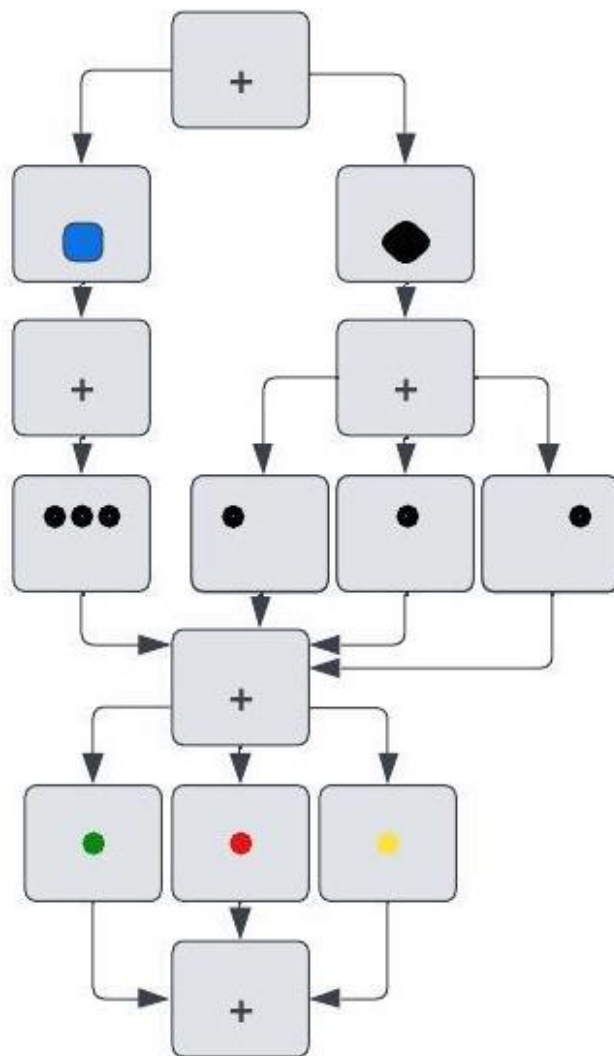
Figure 3. Schematic of task structure showing branches for the experimental (blue square)
and control (black rhombus) conditions on the left and right respectively. The sequence of
events was cue presentation, followed by targets, followed by feedback.

15

Stimuli: All stimulus sizes reported below are in number of pixels. All fixation, cue, and feedback stimuli were presented at position x = 512, y = 435 on a light grey background. The fixation cross comprised two black intersecting 50 pixel lines with a thickness of 5 pixels. Targets were black circles with a 50-pixel diameter and a centrally located 10-pixel diameter white circle to aid fixation. Due to a limited field of view and a need to separate the targets adequately they were not spaced equidistantly from the fixation cross. Instead they were positioned in a horizontal line 135 pixels above the fixation, each 300 pixels apart. Therefore the central target was positioned at x = 512, y = 300, the leftward at position x = 212, y = 300, and the rightward at position x = 812, y = 300.

Areas of Interest: As areas of interest had a diameter of 200 pixels even if the participant was delayed in disengaging from their centralised fixation the system should not register the closest central target as being selected. However if head motion resulted in a higher fixation point than intended, this could overlap into the area of interest surrounding the central target. To ensure this did not happen three adjustments were made. Firstly the fixation cross disappeared when the targets appeared, to help with visual disengagement. Secondly the participant had to make a fixation with a minimum duration of 200ms before a target was declared selected. Although it was deemed unlikely that participants would continue to fixate steadily with no visible fixation cross, if an artificially long fixation lasting 200ms or more fell into one of the areas of interest and continued even briefly upon presentation of the targets, the area of interest could be triggered. To ensure this did not happen a delay period was introduced, whereby the system would not register fixations within the first 250ms, but would register any fixation event exceeding 200ms (regardless of when it started) detected within any area of interest 250ms after target onset. This was found to give participants enough time to initiate their first saccade, and functioned well in pilot runs.

16

Timings: Within a trial the cue was presented for 250ms (uniformly jittered between 0 and 1760ms from trial start), the targets presented for 1250ms (uniformly jittered between 2110 and 4030ms), and feedback presented for 250ms (uniformly jittered between 5280 and 7800ms). Total trial length was 8800ms and there was always at least 750ms between offset of feedback and trial end, allowing the system to prepare the next trial, see Figure 4.
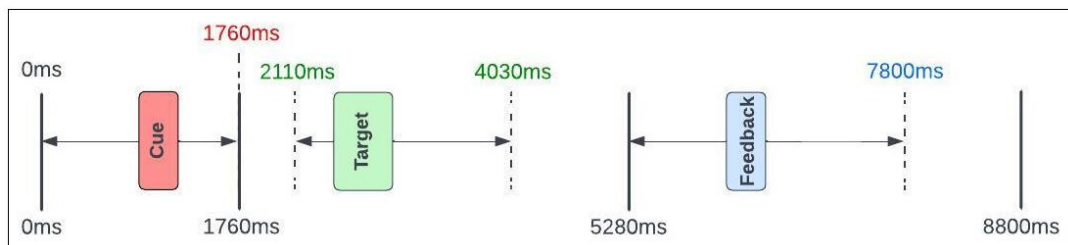
Figure 4. Event timings with temporal jitter. Solid black lines separate the blocks of time within which each event was jittered, each pertaining to a set number of scans.

Where the onset of an event occurred across more than one scan (each scan with a repetition time (TR) of 1760ms) the jitter was manipulated to prevent overlap regarding onset times within the 1760ms peristimulus period, ensuring maximal sampling. This was applicable to target and feedback events (see Figure 5).
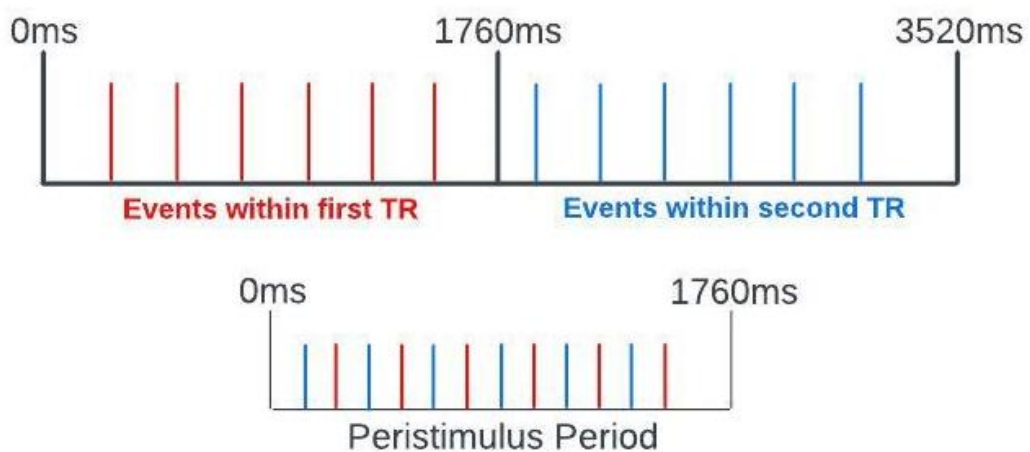
Figure 5. A visual theoretical representation of how events were uniformly spread across two scans.

17

The jittered onset times for each event were then randomised iteratively to reduce the correlation across event types (run separately within each condition) to minimise multicollinearity in the design matrix.

6.2.4. Procedure

On the day of the scan, where mandated by the Department a Covid screening call was made prior to visit. Participants changed into scrubs provided and completed screening forms in the presence of the experimenter. The task and procedure was explained with it made clear that the participant could end the study at any time. The participant then read the information sheet and filled out consent forms. One of the department radiographers double-checked for any contraindications. When ready ear plugs were inserted and the participant lay on the scanner bed with cushions either side of their head (minimising motion, attenuating noise, and securing ear plugs). The eye-tracker was focused, the participant entered the scanner, calibration was carried out, and then eight practise trials were completed. These comprised seven experimental and one control trial. One experimental cue was repeated five times to facilitate learning of at least one rule. If learning was not achieved the experimenter would speak with the participant and if necessary practise trials were repeated. The main task used a different set of cues to ensure there was no carry-over effect from the practise trials. MRI localizers were run, followed by MRI calibration, anatomical scans, and field-mapping. The eye-tracker was then calibrated/validated and the echo planar imaging (EPI) sequence commenced, triggering the main task. Calibration and validation checks were run after each break period to minimise drift and ensure accurate target selection. Upon task completion the EPI sequence was stopped and participants debriefed.

6.2.5. Behavioural Data Acquisition

Both Experiment Builder and a CED 1401 collected data on the timings of all events within the study, and these were classified into the relevant conditions based on outputs from Experiment Builder and Dataviewer. This provided all data required to construct 1st-level fMRI regressors.

6.2.6. MRI Data Acquisition

Scanning utilised a 7T Siemens Magnetom scanner located at the FMRIB Centre within the John Radcliffe Hospital in Oxford, with a 32-channel head array coil (one transmit channel). Localizers used a voxel size of 1.0x1.0x3.0mm and 1.4x1.4x1.4mm, and lasted 8.8 and 23 seconds respectively, TR = 4.5ms, TE = 2.15ms. Calibration used a voxel size of 3.0x3.0x5.0mm, and lasted 11 seconds, TR = 100ms, TE = 12ms. Anatomical scans used a voxel size of 0.7x0.7x0.7mm and lasted 6 minutes and 35 seconds, phase encoding direction = A>>P, TR = 2200ms, TE = 3.02ms, flip angle = 7 degrees, PAT mode = GRAPPA, Accelerating factor PE = 2, ascending series, and FoV read = 224mm. Field mapping lasted 2 minutes and 2 seconds, voxel size = 2.0x2.0x2.0mm, phase encoding direction = A>>P, TR = 620ms, TE1 = 4.08ms, TE2 = 5.10ms, and flip angle = 39 degrees. The EPI sequence used isotropic 1.5x1.5x1.5mm voxels and ran for a maximum of 1 hour (due to calibration periods the length of the experiment was variable but averaged ~50 minutes), phase encoding direction = A>>P, TR = 1760ms, TE = 18.4ms, multi-band acceleration factor = 3, slices = 96, slice thickness = 1.5mm, interleaved acquisition, flip angle = 60 degrees, and EPI factor = 128.

6.2.7. Pre-Processing Methods

DICOM Conversion, Field Mapping, and Realignment: For each participant the fMRI data was then converted from DICOM to nifti format using the SPM12-r7771 batch editor in Matlab 2022a. A voxel displacement map (VDM) was created using phase and magnitude files, TE = [4.08 5.10], blip direction = -1, EPI readout time = 46.08ms. The EPI images were

realigned to the mean and unwarped using the VDM. Outputs during this process allowed for a manual check that unwarping of EPI images functioned as expected.

Co-registration and Segmentation: The anatomical image was co-registered to the mean EPI image (estimation only) with outputs during this process allowing for a manual check that co-registration had proceeded accurately. The anatomical image was then segmented using MNI tissue probability maps. Slice timing correction was omitted due to risks of aliasing and interactions with head motion (Henson et al., 1999; Poldrack et al., 2011, pp. 41-42; Sladky et al., 2011).

Normalisation and Smoothing: A Shoot template was created using Dartel imported grey and white matter tissue class images. This step used all 19 participants with an anatomical scan (ages ranging 21-33, 78.95% female) in order to create a well sampled average template. Realigned and unwarped EPI images were then normalised (using the Shoot template) with a 4mm full-width-half-maximum gaussian smoothing kernel. Accuracy was checked using SPM's check-reg function as well as MRIcroGL, comparing EPI images to the MNI brain. The smoothed and normalised EPI images then underwent 1st-level fixed effects analyses with con images produced for all events.

Quality Control: At this stage checks were made for abnormal signal variation across both slices of the brain and across scans, as well as evidence of periodicity across scans. Head motion was also examined, looking for instances of abnormally high variability across participants.

6.2.8. GLM Design

fMRI 1st-level Experimental Design: The canonical model with temporal and dispersion derivatives was employed to account for variability in the shape of the haemodynamic response function (HRF), based upon previous work by Danvers et al. (2021).

At the 1st-level of analysis a GLM was constructed using the following event-related

regressors, with con images derived for each (see Table 1, and Figure 6).

Table 1. Event-related regressors for the 1st-level GLM with summary statistics regarding the number of trials for each.

Regressor	Explanation	Median	Range
1-3	Experimental Correct Cue Event (preceded by a correct trial within the same rule)	73	18-109
4-6	Control Correct Cue Event	73	18-109
7-9	Experimental Incorrect Cue Event	39	26-53
10-12	Control Incorrect Cue Event	39	26-53
13-15	Experimental Junk (missed event/ cue and feedback events not preceded by a correct trial within the same rule)	59	31-151
16-18	Control Junk (missed target event/cue and feedback events with yellow feedback/cue and feedback events not preceded by a correct trial within the same rule)	59	31-160
19-21	Target Event (target 1 selected)	89	24-111
22-24	Target Event (target 2 selected)	93	49-105
25-27	Target Event (target 3 selected)	82	44-95
28-30	Experimental Correct Feedback Event (preceded by a correct trial within the same rule)	73	18-109
31-33	Control Correct Feedback Event	73	18-109
34-36	Experimental Incorrect Feedback Event	39	26-53
37-39	Control Incorrect Feedback Event	39	26-53
40-42	Rest/Calibration (block design)	N/A	N/A
43-48	Head Motion Parameters	N/A	N/A
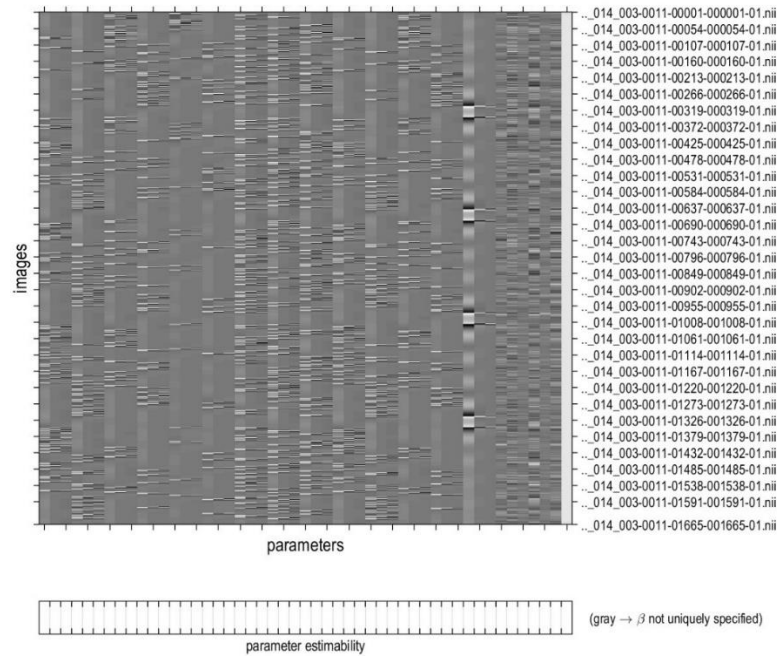
Figure 6. The 1st-level design matrix pertaining to a randomly chosen participant.

fMRI 2nd-level Experimental Design: Two analyses were run at the 2nd-level, the first looking at cue and feedback events, the second at target events, each using a full factorial design.

Cue/Feedback Analysis: The design had four categorical factors; event (two levels; cue vs feedback, independence = no, variance = unequal), error-status (two levels; correct vs incorrect, independence = no, variance = unequal), condition (two levels; experimental versus control, independence = no, variance = unequal), and basis set function (three levels; canonical function vs temporal derivative vs dispersion derivative, independence = no, variance = unequal), see Figure 7.
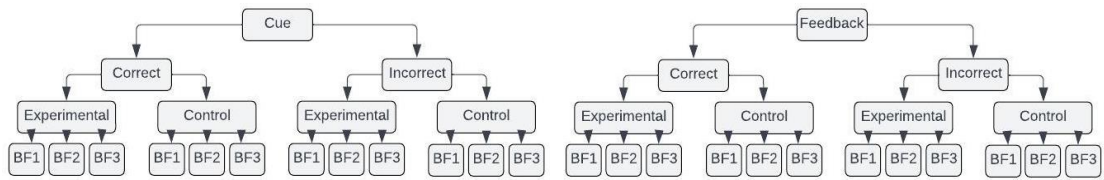
Figure 7. A schematic of the experimental design, denoting factors representing event type, error-status, condition, and basis function (BF).

To analyse hypotheses 1-4, the contrasts outlined in Figure 8 were run at the 2nd-level of analysis, with the 3 basis functions linearly combined for each of the eight conditions of interest. These enabled an investigation into effects of condition (to help establish functional activity specific to experimental conditions), narrowing down to test whether regions show different effects of condition either between cue and feedback events, or between correct and incorrect trials. Finally it was investigated whether effects of condition varied both across levels of event and error-status, e.g. were there regions where functional activity in the experimental condition was only found at the time of the cue, during incorrect trials.

Main Effect of Condition

Cue												Feedback											
Correct						Incorrect						Correct						Incorrect					
Exp			Con			Exp			Con			Exp			Con			Exp			Con		
1			-1			1			-1			1			-1			1			-1		
	1			-1			1			-1			1			-1			1			-1	
		1			-1			1			-1			1			-1			1			-1

Event x Condition Interaction

Cue												Feedback											
Correct						Incorrect						Correct						Incorrect					
Exp			Con			Exp			Con			Exp			Con			Exp			Con		
1			-1			1			-1			-1			1			-1			1		
	1			-1			1			-1			-1			1			-1			1	
		1			-1			1			-1			-1			1			-1			1

Error-Status x Condition Interaction

Cue												Feedback											
Correct						Incorrect						Correct						Incorrect					
Exp			Con			Exp			Con			Exp			Con			Exp			Con		
1			-1			-1			1			1			-1			-1			1		
	1			-1			-1			1			1			-1			-1			1	
		1			-1			-1			1			1			-1			-1			1

Error-Status x Event x Condition Interaction

Cue												Feedback											
Correct						Incorrect						Correct						Incorrect					
Exp			Con			Exp			Con			Exp			Con			Exp			Con		
1			-1			-1			1			-1			1			1			-1		
	1			-1			-1			1			-1			1			1			-1	
		1			-1			-1			1			-1			1			1			-1

Figure 8. Weightings applied to contrast images to investigate main effects and interactions at the 2nd-level of analysis.

Target Analysis: The design had two categorical factors; target saccaded to (three levels; left vs up vs right, independence = no, variance = unequal), and basis set function (three levels; canonical function vs temporal derivative vs dispersion derivative, independence = no, variance = unequal). The analysis focused on whether there was evidence of significance in any of the directions saccaded to (see Figure 9).

Leftward Saccade			Upward Saccade			Rightward Saccade		
1			1			1		
	1			1			1	
		1			1			1

Figure 9. Weightings applied to contrast images when investigating target events at the 2nd-level of analysis.

6.2.9. Statistical Analysis

Within significant coordinates the estimated haemodynamic response function was calculated and plotted by multiplying each basis function by its respective beta value and summing across the three. This was then divided by the mean baseline signal across participants at that voxel (based on the beta value from the final column of each participant's 1st-level design matrix), and multiplied by 100 to create percentage signal change (as per MarsBaR FAQ — MarsBaR 0.45 documentation, n.d). In order to differentiate positive from negative peaks the percentage weighting of the canonical regressor's absolute beta value (relative to the absolute sum of all 3 functions) was ascertained. If the weighting of the canonical function represented more than 33%, its valence (positive or negative) determined whether a BOLD response was interpreted as positive or negative (a positively weighted canonical function indicating a positive BOLD response). If under 33%, maximum and minimum magnitudes were calculated and the greatest absolute value determined whether a BOLD response was positive or negative.

Accuracy was measured as the percentage of correct experimental trials across the entire experimental run, relative to the total number of experimental trials in which a target was successfully fixated. As experimental missed trials could represent either a failure to choose a target in time (performance relevant) or a system failure (performance irrelevant) these were modelled separately in the GLM analysis (mean percentage of missed experimental trials across participants = 9.31%, SD = 10.95). As hypotheses were made specifically about the frontal lobe and cerebellum small volume FWE corrections were applied (α = .05). To do this a cerebellar mask was generated using SPM's anatomy toolbox version 2.2b, containing bilateral lobules I-X (including vermal regions VI-X). A binary bilateral grey matter mask of the frontal lobe (central sulcus to frontal pole) was also

25

constructed manually. Due to technical problems, of the nine participants included three did not have data across all five blocks (the final block was removed for one participant, the two last blocks were removed for the other two), and one participant had some limited prior experience of the task.

6.2.10. Anatomical Classification

The anatomical locations of all significant peak coordinates were superimposed on the MNI152 brain and their anatomical locations were verified using the atlas of Duvernoy (1999) for the frontal lobe, and Schmahmann (2000) for the cerebellum. The FEFs were defined based upon the work of Amiez & Petrides (2009) who split these into 4 regions; the FEFs located in the ventral branch of the superior precentral sulcus (vsPCS), the supplementary eye fields (SEF) located rostral to the medial precentral sulcus at the junction of the medial and lateral cortical surface, the cingulate eye fields (CEF) located in the vertical branch of the cingulate sulcus, and the premotor eye fields (PrEF) in the dorsal branch of the inferior precentral sulcus (diPCS). It should be noted that Amiez & Petrides (2009) warn the PrEF may overlap with a region within area 6 involved in blinking, and so serves as a potentially less reliable candidate for the FEFs. This was based on both inter-species comparisons (using gross anatomy and functional classification) and an fMRI study in humans in which saccadic movement was compared against ocular fixation. Previous cytoarchitectonic studies were used to differentiate structures within the frontal lobe (Petrides & Pandya, 1999; Petrides, 2005; Petrides et al., 2012).

6.3. Results

Firstly behavioural data is discussed in **section 6.3.1**, examining percentage accuracy across blocks. Then functional activity is investigated using the *cue/feedback analysis* GLM design matrix, looking for main effects of condition in section **6.3.2.1**, event x condition interactions in section **6.3.2.2**, error-status x condition interactions in section **6.3.2.3**, and

three-way event x error-status x condition interactions in section **6.3.2.4**. Using the same design matrix two post-hoc analyses were run. The first was a conjunction analysis looking for activity across all levels of error-status and condition, but time-locked to the cue (section **6.3.2.5**) and the second a whole brain analysis investigating the four effects in sections **6.3.2.1-4** (see section **6.3.2.6**). Finally functional activity at the time of target presentation was investigated using the *target analysis* GLM design matrix (section **6.3.2.7**).

6.3.1. Behavioural

Percentage correct values were calculated for each block, in each participant, see Figure 10. All participants showed evidence of practise-related improvement, with final block performance always exceeding that of the first block. Additionally, it was only ever the first block that sat on or just below chance.
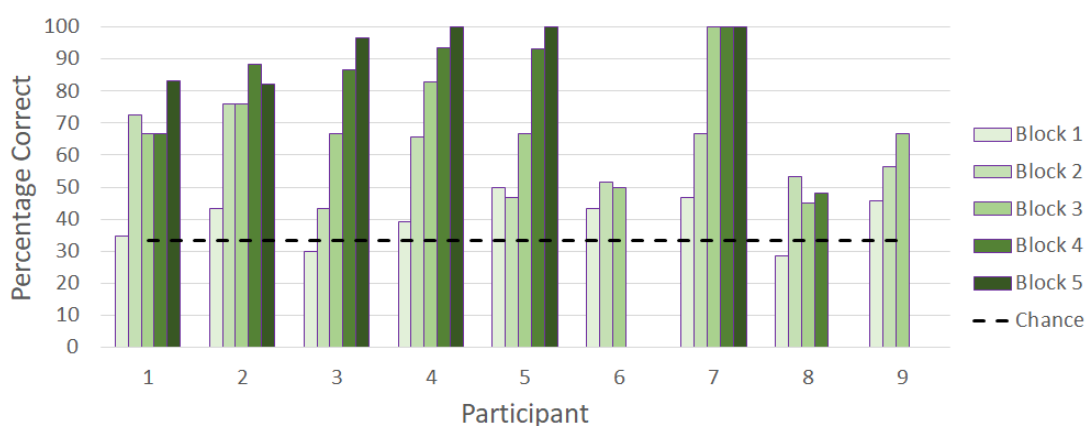
Figure 10. Percentage correct values for each block, across all participants. Dotted line denotes chance performance of 33.33%.

As mentioned in **section 6.2.9**, three of the nine participants did not have data across all six blocks. Consequently a 1x5 repeated-measures ANOVA was run on the six participants for whom all five blocks of data were available. A Kolmogorov-Smirnov test found no evidence of significant skew, and sphericity was assumed (W = .098, p = .590). There was a significant main effect of block; $F_{(4,20)} = 28.834$, p<.001, with a large effect size

27

(partial η^2 = .852). Bonferroni corrected post-hoc tests found that the first block differed

from blocks 3-5. See Figure 11.
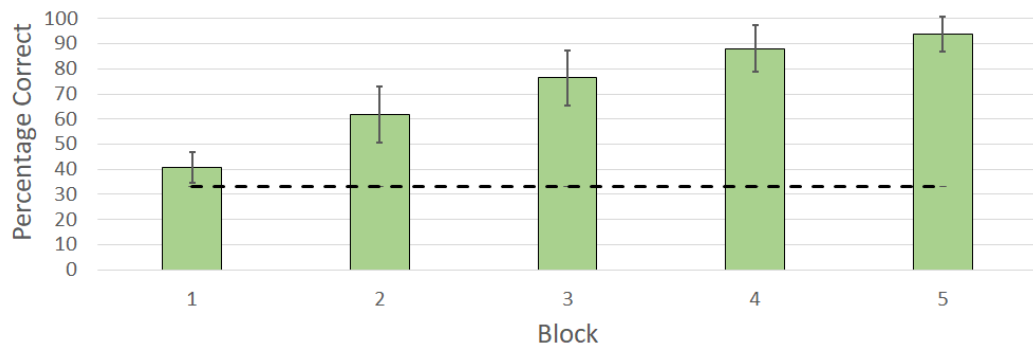
Figure 11. Mean percentage correct values across all blocks within the six participants for

whom data was available. The dotted line denotes chance performance (33.33%) and error

bars show two standard errors.

As data was available for all nine participants over the first three blocks, a second

repeated-measures ANOVA was run. There was no evidence of skew, the assumption of

sphericity was met (W = .973, p = .908), and a significant main effect of block was found;

$F(2,16)$ = 19.254, p<.001, with a large effect size (partial η^2 = .706). Bonferroni corrected

post-hoc tests found that the first block differed from blocks two and three. See Figure 12.
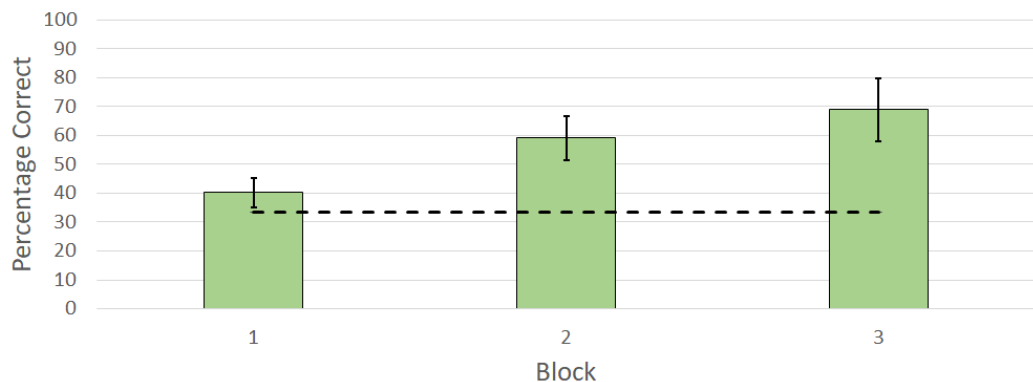
Figure 12. Mean percentage correct values across the first three blocks within all nine

participants. The dotted line denotes chance performance (33.33%) and error bars show two

standard errors.

6.3.2. fMRI

6.3.2.1. Main Effect of Condition

Effects of condition included a cluster peaking in the paracingulate gyrus which arguably extended into preSMA and the vertical cingulate sulcus, putatively where the CEFs are located (see Table 2A, and Figure 13A). There was also a peak in the left lateral frontopolar gyrus, extending into the SFG, and bilaterally onto the medial surface (see Table 2B, and Figure 13B), and another in the medial precentral gyrus (see Table 2I, and Figure 13C), including the SMA and overlapping into the medial caudal SFG.
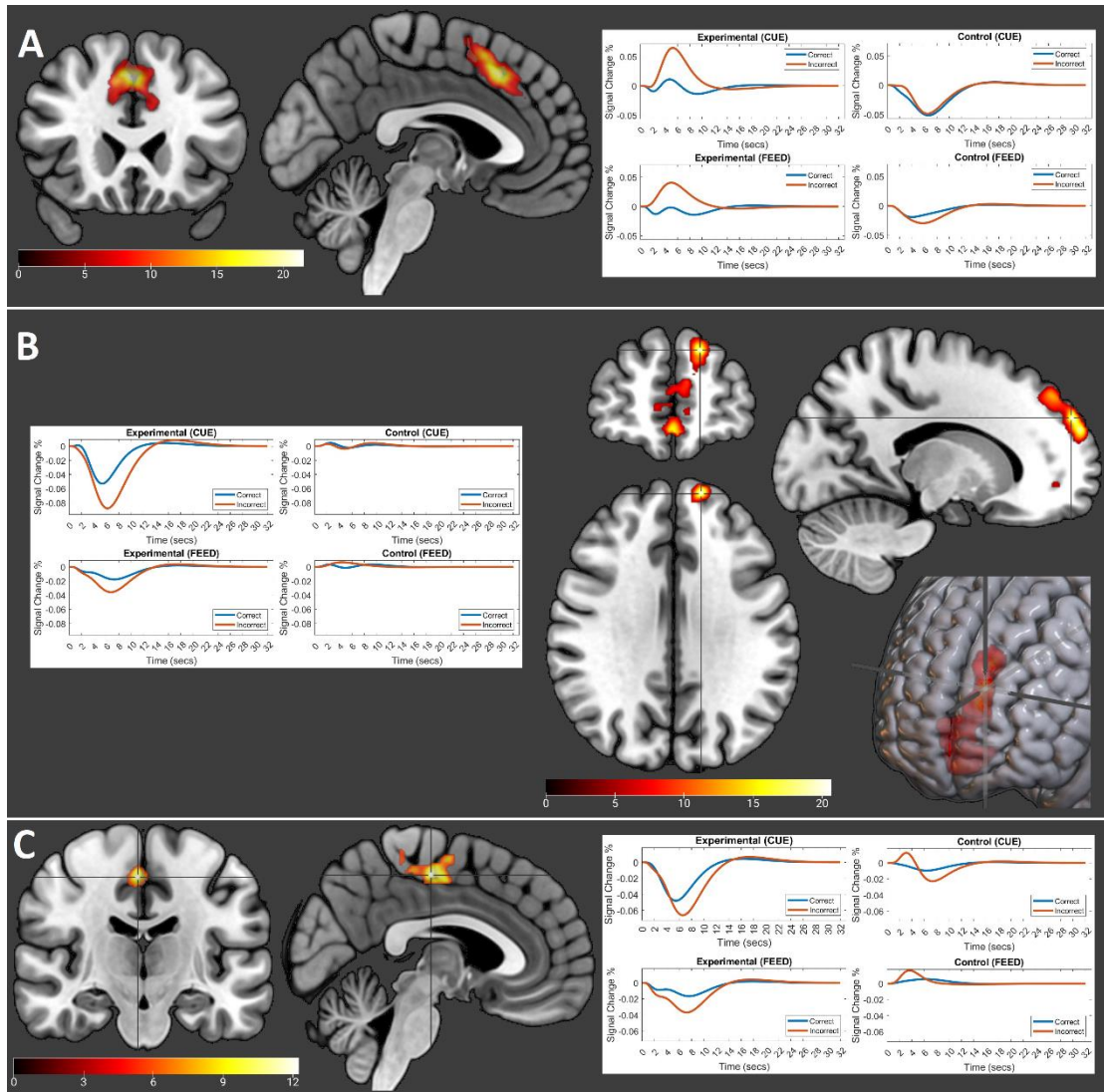
Figure 13. Clusters and peaks pertaining to main effects in the medial and frontopolar cortex. Colourbars indicate F values.

Within middle and superior frontal gyri there was a coordinate in the left MFG (see Table 2D, and Figure 14A), mainly sat in the SFS overlapping into areas 9/46d and 9. Coordinates were also identified in the SFG, the first (see Table 2H, and Figure 14B) in the right hemisphere (arguably within area 9), the second and third located bilaterally in the caudal SFG (area 6d1, see Table 2J-K, and Figure 14C-D).
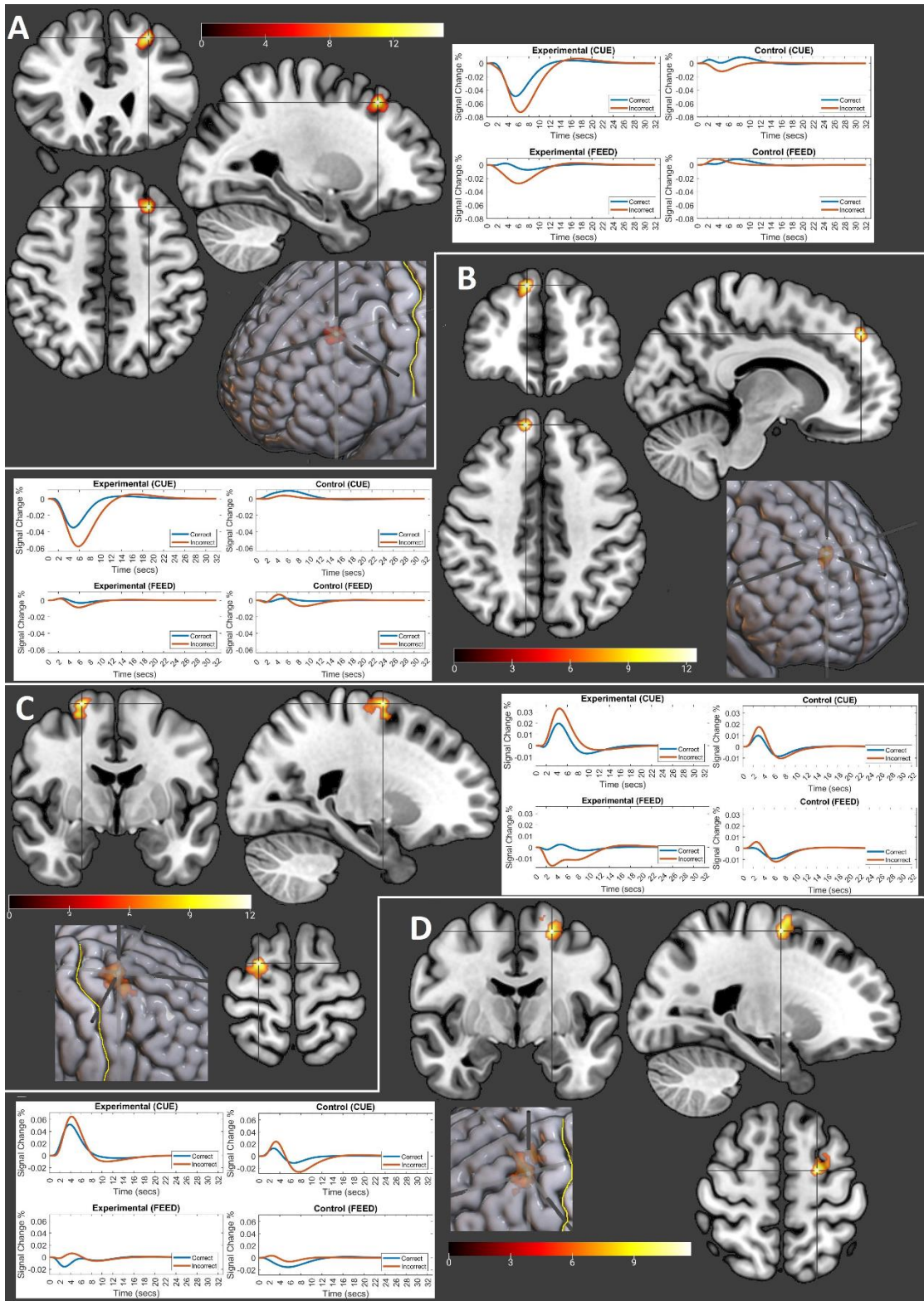
Figure 14. Clusters and peaks pertaining to main effects in the MFG and SFG. Colourbars indicate F values. The central sulcus is outlined in yellow.

Peaks were also identified in the right central operculum (see Table 2L, and Figure 15A), and the insular cortex (extending into the orbital gyrus and central operculum, and occasionally the inferior frontal gyrus (IFG)), see Table 2C, E and G, and Figure 15B-D. Another peak was identified in the subcallosal cortex (see Table 2F, and Figure 15E).
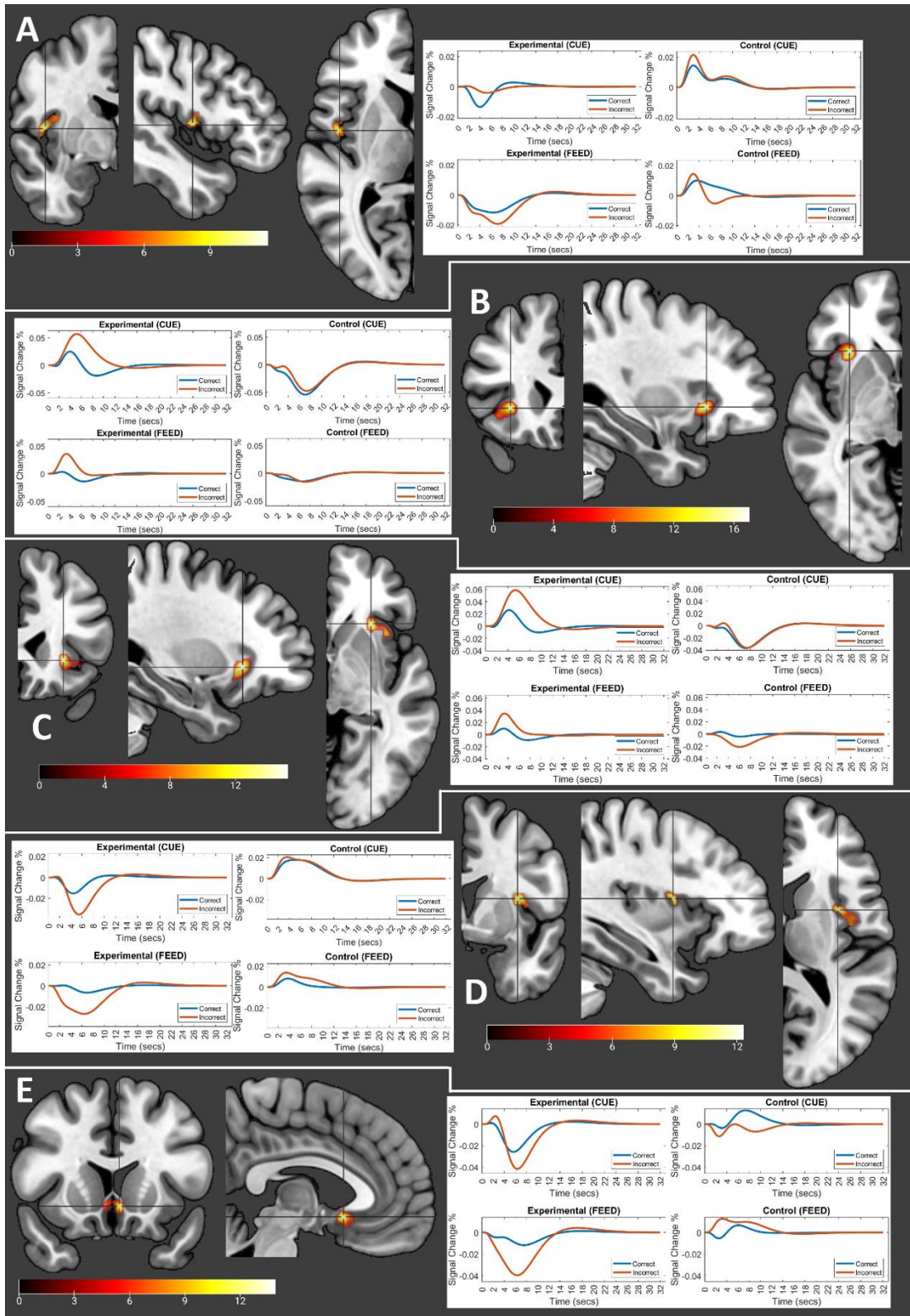
Figure 15. Clusters and peaks pertaining to main effects in insular, opercular, and sub callosal regions. Colourbars indicate F values.

Within the cerebellum there were a pair of peaks within cerebellar lobule HVI with clusters extending into CRUS I (see Table 2M-N, and Figure 16A-B). The left lateralised peak was only marginally significant (p = .053) but the cluster remained highly significant, and at the peak there was a significant effect of condition within incorrect trials at the time of the cue.
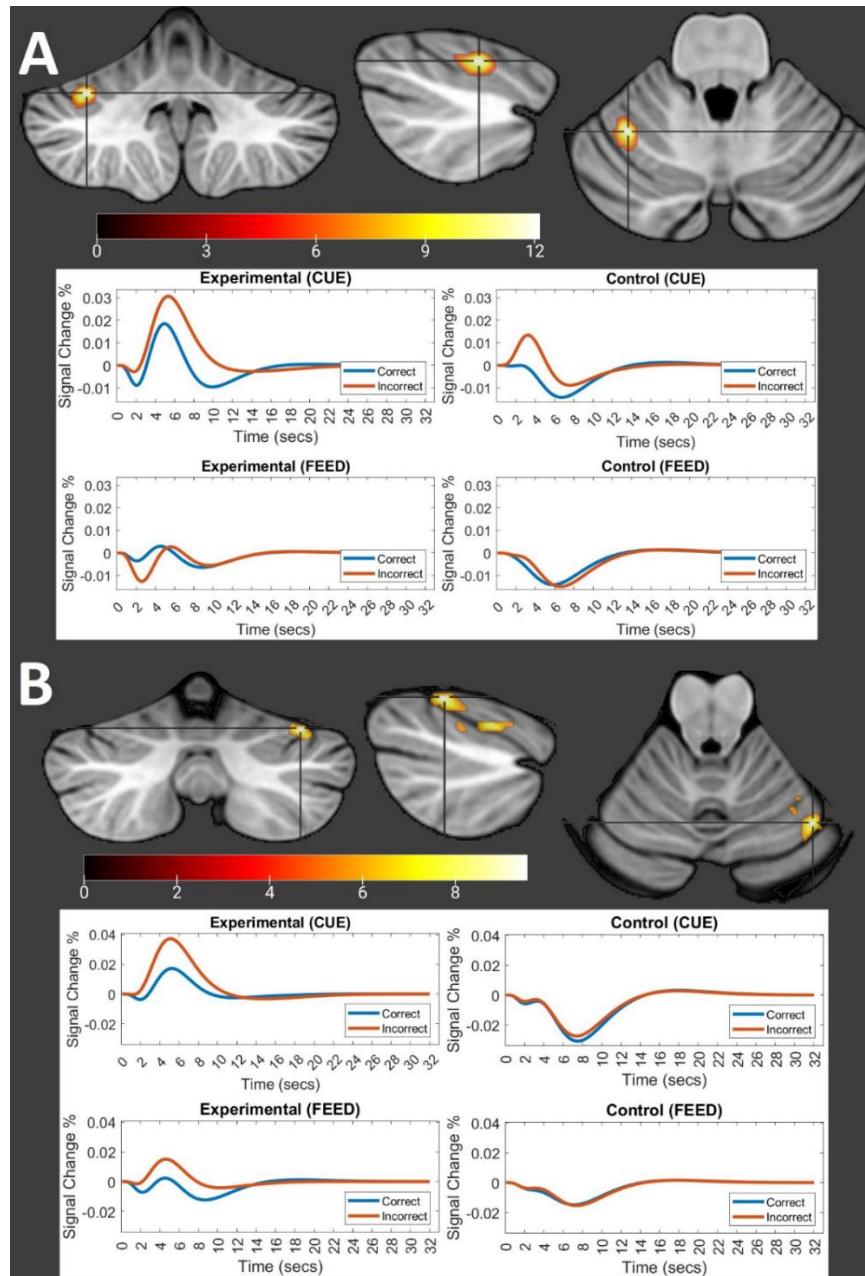
Figure 16. Clusters and peaks pertaining to main effects in the cerebellum. Colourbars indicate F values.

Table 2. Peak coordinates pertaining to significant main effects. All main effects and follow up analyses underwent small volume FWE correction using the frontal lobe and cerebellar mask respectively.

Gross Anatomical Region	Cytoarchitectonic Region	Prob.	Coordinates	Peak F/Z	Peak P (FWE)	Cluster P (FWE)	K
Frontal Lobe							
A) Paracingulate Gyrus	Extends into preSMA	N/A	0, 22.5, 43.5	22.13/6.91	<.001	<.001	2332
Effect				Explanation			
Error Status x Condition interaction				Stronger within incorrect trials			
Error-Status x Condition interaction specifically at time of the cue				Stronger within incorrect trials			
Effect of Condition specific to Incorrect trials at time of the cue				Experimental (+) > Control (-)			
Simple effect (incorrect experimental cue)				+			
Simple effect (incorrect control cue)				-			
B) L Frontopolar Gyrus	Extends into Fp1 and Fp2	N/A	-15, 57, 31.5	21.59/6.83	<.001	<.001	2646
Effect				Explanation			
Effect of Condition specific to Incorrect trials at time of the cue				Experimental Significant			
Simple effect (incorrect experimental cue)				-			
C) R Insular Cortex	Id7	.101	31.5, 24, -3	17.55/6.14	<.001	<.001	289
Effect				Explanation			
Event x Condition interaction				Stronger effect at the time of the cue			
Effect of Condition specific to Incorrect trials at time of the cue				Experimental (+) > Control (-)			
D) L MFG	N/A	N/A	-27, 25.5, 48	15.62/5.77	<.002	<.001	282
Effect				Explanation			
Effect of Condition within incorrect trials at the time of the cue				Experimental significant			
Effect of Condition within correct trials at the time of the cue				Experimental significant			
Simple effect (incorrect experimental cue)				-			
Simple effect (correct experimental cue)				-			
E) L Insular Cortex	Id7	.044	-28,5, 22.5, -3	15.52/5.75	<.002	<.001	449
Effect				Explanation			
Event x Condition interaction				Stronger effect at the time of the cue			
Effect of Condition within Incorrect trials at the time of the cue				Experimental (+) > Control (-)			
F) L Subcallosal Cortex	25	.595	-4.5, 15, -7.5	15.15/5.68	<.002	<.002	141
Effect				Explanation			
Effect of Condition within Incorrect trials at the time of the cue				Experimental (-) < Control (-)			
G) L Insular Cortex	Id6	.428	-34.5, 3, 12	13.12/5.24	<.02	<.002	147
Effect				Explanation			
N/A				N/A			

H) R SFG	N/A	N/A	10.5, 48, 42	12.73/5.15	<.02	<.002	139
Effect				Explanation			
Effect of Condition within Incorrect trials at the time of the cue				Experimental significant			
Simple effect (incorrect experimental cue)				-			
I) R Medial Precentral Gyrus	6mc/SMA	.432	3, -18, 51	12.61/5.13	<.02	<.001	1018
Effect				Explanation			
N/A				N/A			
J) R Caudal SFG	6d1	.420	22.5, -3, 67.5	12.47/5.10	<.03	<.001	445
Effect				Explanation			
N/A				N/A			
K) L Caudal SFG	6d1	.340	-22.5, -6, 58.5	12.01/4.99	<.04	<.001	520
Effect				Explanation			
N/A				N/A			
L) R Central Operculum	Id4	.124	45, -1.5, 7.5	11.8/4.94	<.05	<.001	160
Effect				Explanation			
N/A				N/A			
Cerebellum							
M) R HVI	N/A	N/A	33, -54, -28.5	12.57/5.12	<.005	<.001	136
Effect				Explanation			
N/A				N/A			
N) L HVI	N/A	N/A	-36, -66, -22.5	10.5/4.61	.053	<.001	291
Effect				Explanation			
Effect of Condition within Incorrect trials at the time of the cue				Experimental (+) > Control (-)			

6.3.2.2. Condition x Event Interaction

There were two significant bilaterally located clusters peaking in the posterior
orbital gyrus, which extended bilaterally into the frontal operculum and insular cortex, and
within the right hemisphere into the frontopolar gyrus (see Table 3A-B, and Figure 17A-B).
There was also a significant peak in the medial SFG, the cluster extending onto the
dorsolateral surface (see Table 3C, and Figure 17C).
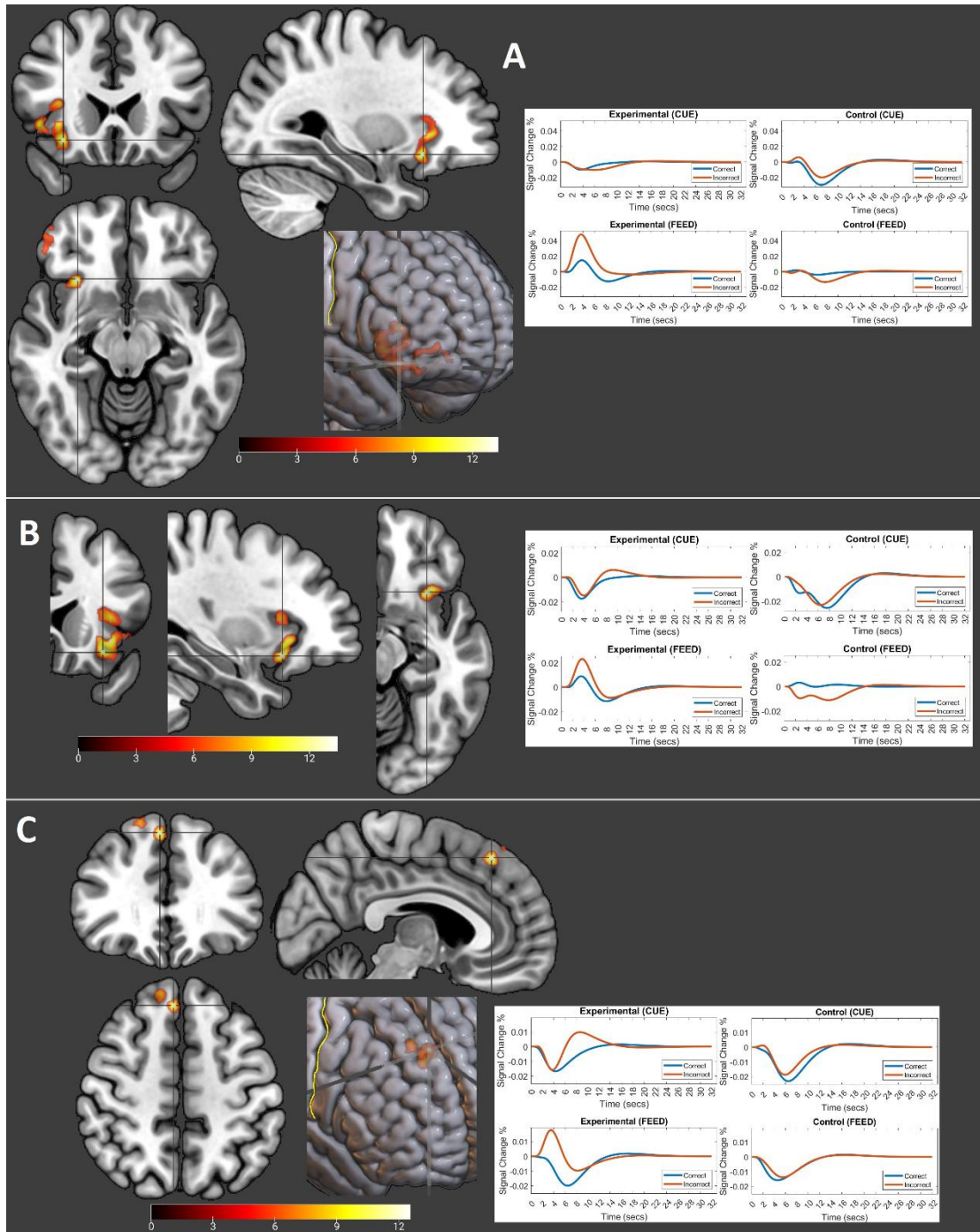
Figure 17. Clusters and peaks pertaining to significant Event x Condition interactions.

Colourbars indicate F values. The central sulcus is outlined in yellow.

Table 3. Peak coordinates pertaining to significant Event x Condition interactions. All interactions and follow up analyses underwent small volume FWE correction using the frontal lobe mask.

Gross Anatomical Region	Cytoarchitectonic Region	Prob.	Coordinates	Peak F/Z	Peak P (FWE)	Cluster P (FWE)	K
Frontal Lobe							
A) R Posterior Orbital Gyrus	Extends into ID7, ID6, OP8, and Fo6	N/A	30, 21, -12	13.95/5.42	<.005	<.001	987
Effect				Explanation			
Effect of condition within incorrect trials at the time of feedback				Experimental significant			
Simple effect (incorrect experimental feedback)				+			
B) L Posterior Orbital Gyrus	Extends into Id7, Id6, OP8, and	N/A	-31.5, 18, -13.5	13.82/5.4	<.01	<.001	720
Effect				Explanation			
Simple effect (incorrect experimental feedback)				+			
C) R Medial SFG	N/A	N/A	4.5, 33, 51	12.77/5.16	<.02	<.001	350
Effect				Explanation			
N/A				N/A			

6.3.2.3. Condition x Error-Status Interaction

There was a significant peak in the left medial SFG (overlapping the main effect in Table 2A), the cluster extending into the paracingulate gyrus (see Table 4A, and Figure 18A). A second cluster was located in the right MFG (see Table 4B, and Figure 18B). The peak did not survive FWE correction, but did survive FDR correction (q = .05).
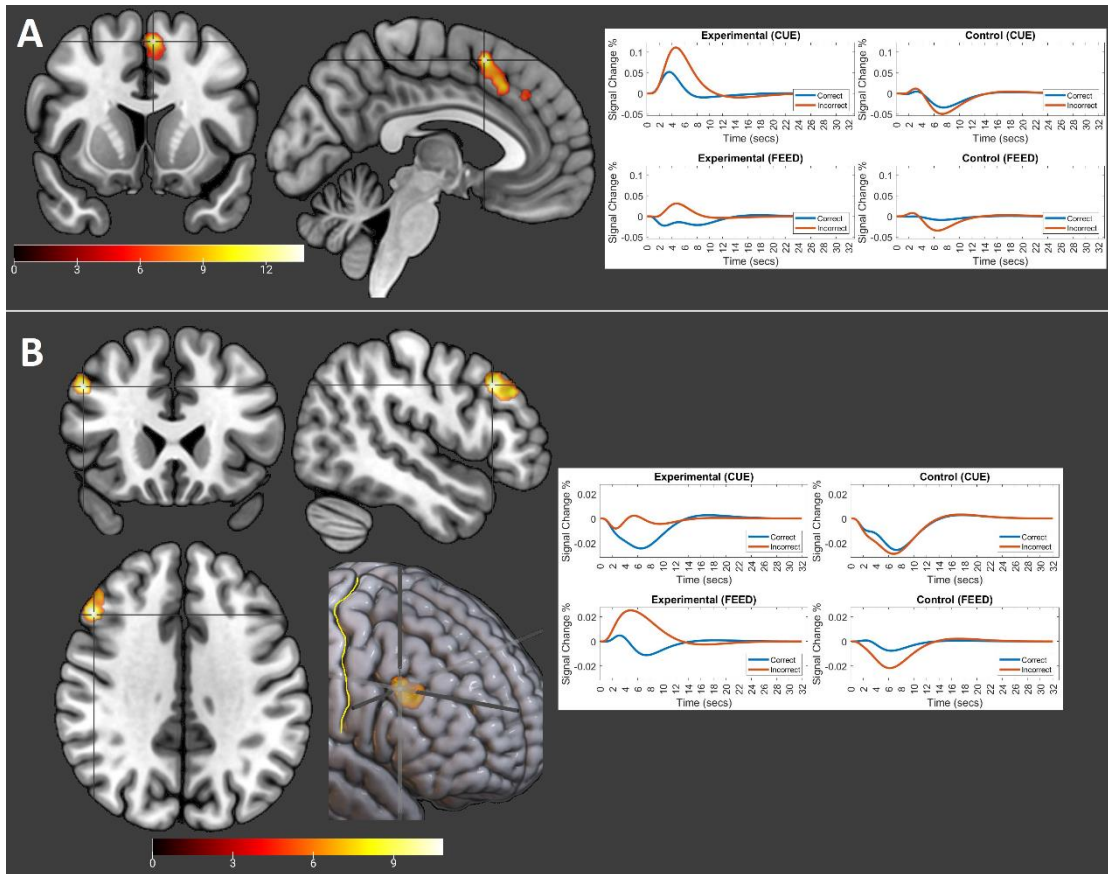
Figure 18. Clusters and peaks pertaining to significant Error-Status x Condition interactions.

Colourbars indicate F values. The central sulcus is outlined in yellow.

Table 4. Peak coordinates pertaining to significant Error-Status x Condition interactions. All interactions and follow up analyses underwent small volume FWE correction using the frontal lobe mask.

Gross Anatomical Region	Cytoarchitectonic Region	Prob.	Coordinates	Peak F/Z	Peak P (FWE)	Cluster P (FWE)	K
Frontal Lobe							
A) L Medial SFG	6mr/preSMA	.839	-4.5, 12, 55.5	14.37/5.52	<.005	<.001	1066
Effect				Explanation			
Main effect of condition				Stronger effect in experimental condition			
Condition x error-status interaction at the time of the cue				Stronger within incorrect trials			
Effect of condition within incorrect trials at the time of the cue				Experimental significant			
Simple effect (incorrect experimental cue)				+			
B) R MFG	N/A	N/A	48, 22.5, 36	10.94/4.72	.115	<.001	411
Effect				Explanation			
N/A				N/A			

6.3.2.4. Condition X Error-Status x Event Interaction

There were no coordinates with a significant three-way interaction.

6.3.2.5. Conjunction Analysis

Finally a conjunction analysis was run to confirm which brain regions were active in both experimental and control conditions, across correct and incorrect trial types, time-locked to the cue event. Clusters were predominately temporo-occipital, including the inferior lateral occipital gyrus (bilateral h0c41a and right h0c41p), superior lateral occipital gyrus (right hIP5 and left hIP7 and 8, both within the IPS), temporal occipital fusiform gyrus (bilateral FG3, left FG1), and the inferior temporal gyrus (right FG3). See Figure 19.
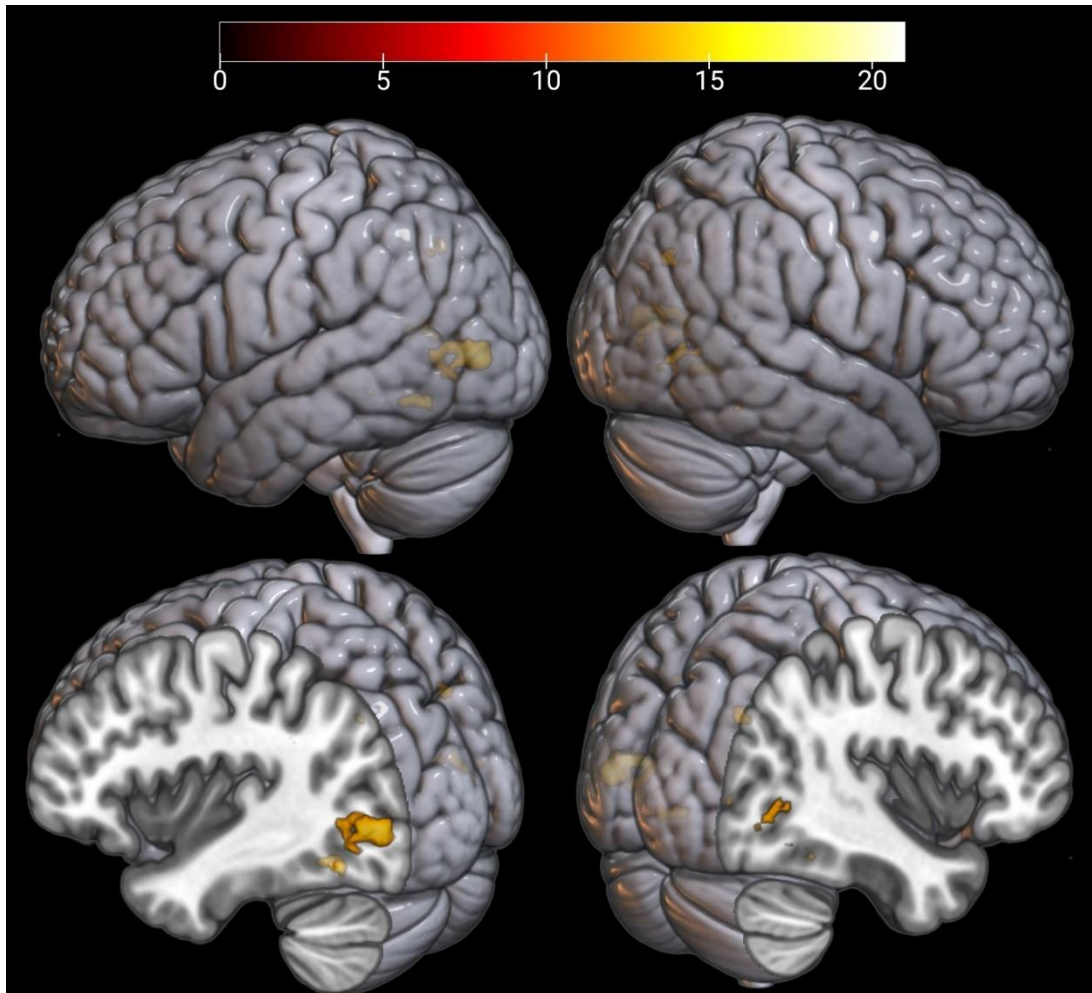
Figure 19. Coordinates in which significant activations were cue-locked, across levels of condition and error-status, with a whole-brain FWE correction (α = .05). Colour bar denotes F values.

6.3.2.6. Whole Brain Analysis

A whole brain FWE correction was also applied to investigate additional regions. There were significant main effects of condition bilaterally within the caudate nucleus (Figure 20A), extending into the putamen. A peak was also identified in the left middle temporal gyrus (Figure 20B) in area TE5 (probability = 82.8%), and a further two in the left precuneus (Figure 20C). The dorsal peak was in area 7P of the superior parietal lobule (probability = .675). There were additional coordinates with an event x condition interaction

(Figure 20A) identified bilaterally within the caudate (overlapping the internal capsule) and

in the left putamen.
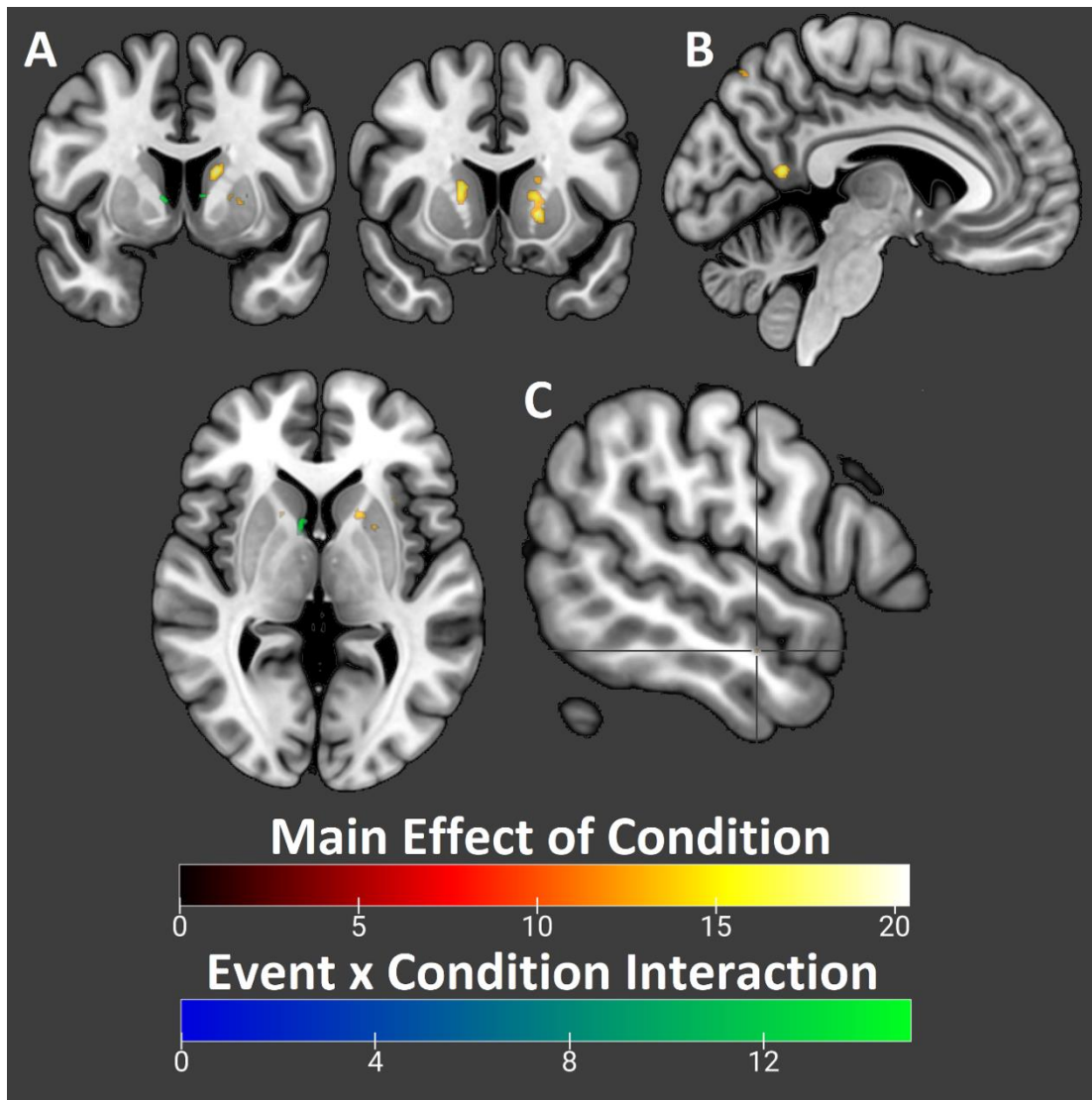
Figure 20. Selected clusters with significant peaks within the striatum (A), the precuneus (B), and the MTG (C). Colourbars denote F values.

6.3.2.7. Target Analysis

When looking at significant regions at the time of the saccade there was a large

volume of activations despite whole brain FWE correction, likely caused by the lack of a

control condition. Crucially however, significant activity was found in areas pertaining to the

FEF, SEF, PrEF, and CEF, as well as cerebellar vermal lobule VI (oculomotor vermis). See

Figure 21.
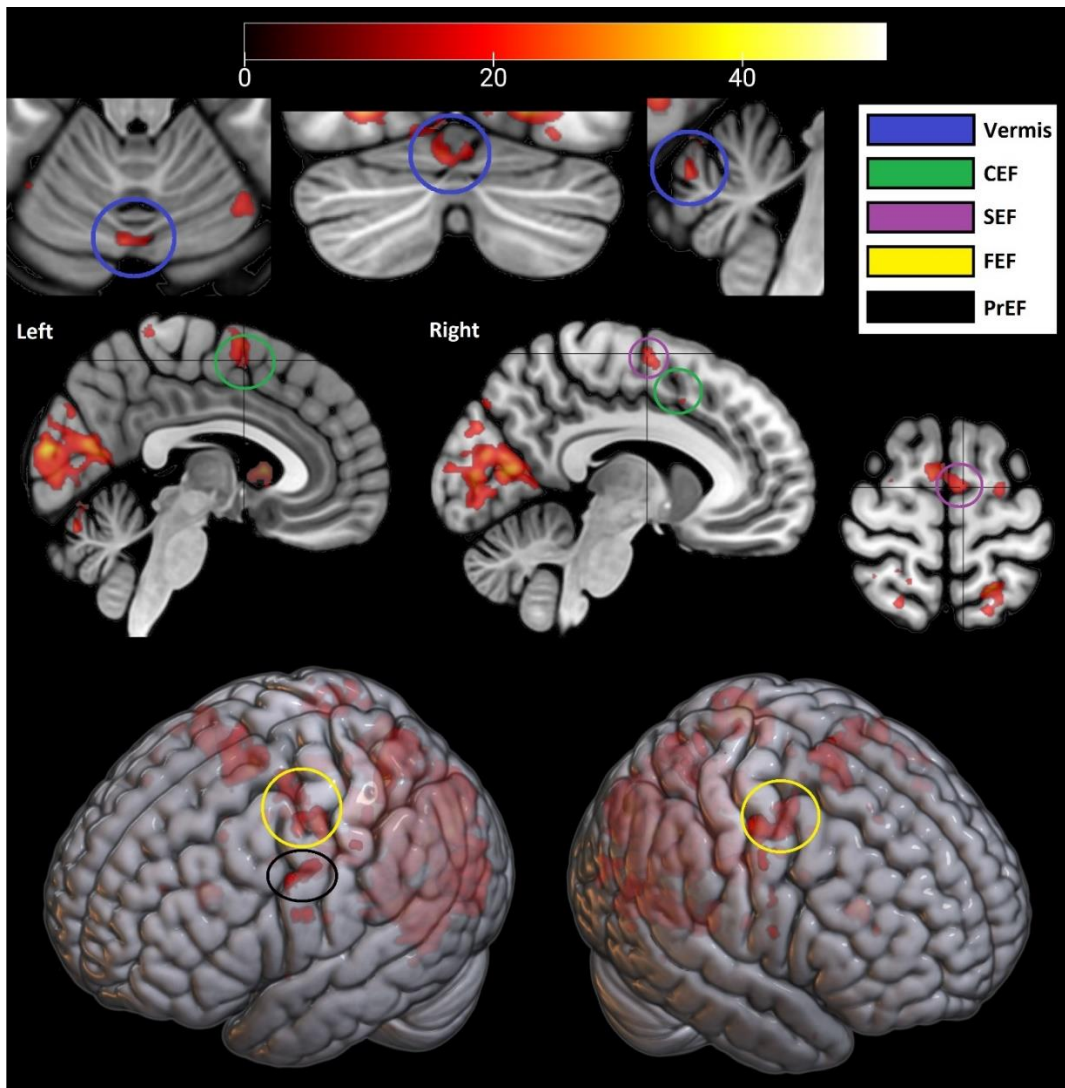
Figure 21. Coordinates in which significant activations were found at the time of target

presentation, with an FWE correction (.05). Colour bar denotes F values.

6.4. Discussion

6.4.1. Overview

Participants demonstrated evidence of learning across blocks, and so an

investigation of functional activity was carried out, with an aim to identify which brain

regions were active during a conditional visuo-oculomotor task. Main effects of condition

were identified within the frontal lobe and cerebellum, including the dlPFC, frontopolar

gyrus, medial wall, caudal SFG, and cerebellar lobules HVI-CRUS I. There was also evidence

within the orbital gyri and SFG that the effect of condition varied significantly between cue

and feedback events, alongside evidence on the medial wall and caudal MFG that effects of

condition differed between correct and incorrect trials. Furthermore, whole brain analyses

identified main effects of condition in the more medial posterior parietal lobe, and in the

striatum both effects of condition and interactions with event were found. Finally, all four

eye fields were deemed active at the time of target presentation, as well as the OMV. These

results are discussed in more detail below, informing understanding of the roles played by

specific regions which may form a conditional learning network.

6.4.2. Hypotheses

Hypothesis 1 predicted a main effect of condition whereby functional activity in

experimental and control trials differed, suggesting an involvement in the learning aspect of

the task (see **section 6.2.3.1**). The strongest activation was identified in the paracingulate

gyrus but extended into the vertical cingulate sulcus (an area deemed to be the CEFs as per

Amiez & Petrides, 2009), with a more caudal peak also identified in the medial precentral

gyrus within area 6mc/SMA. There was also a single cluster peaking in the frontopolar gyrus,

which was mainly left-lateralised and extended into cytoarchitectonic areas Fp1 and Fp2,

and into the SFG (area 9). Looking at the lateral surface a peak was identified in the left MFG

within area 9/46d (as per Petrides & Pandya, 1999) with a further three in the SFG. The first

was positioned more rostrally in area 9 of the right hemisphere, and the remaining two

positioned bilaterally and caudally, within area 6d1. These were just rostral to the dorsal

aspect of the vsPCS, and could be argued as including the FEFs (as per Amiez & Petrides,

2009). Main effects were also identified in the bilateral insular cortex, but overlapping into

opercular and orbital regions. Typically follow up effects identified that effects of condition were generally driven by incorrect trials at the time of cue presentation.

Within the cerebellum there was a pair of peaks within lobule HVI but the clusters extended into CRUS I (more strongly in the left hemisphere). The left peak did not quite meet significance but the cluster did, and at the peak there was both a significant effect of condition within incorrect trials at the time of the cue, and a positive BOLD response of greater magnitude in the experimental condition (the right peak showing the same pattern, but with no significant follow up effects). As a result null hypothesis 1 can be rejected as regions including the frontopolar gyrus, dlPFC, and CEFs showed significant main effects of condition, as did clusters bordering the FEFs and overlapping into CRUS I. There was a pattern of follow up effects generally being driven by cue-locked activity, mainly in incorrect experimental trials, however most peaks did not show event x condition interactions (except in the insular cortex) or error-status x condition interactions (except in the paracingulate gyrus).

Hypothesis 2 predicted an event x condition interaction whereby differences in functional activity between conditions would vary between cue and feedback events, suggesting regions specifically involved in one event or the other (see **section 6.2.3.2**). Peaks were identified bilaterally in the posterior orbital gyri, with some extension into opercular, insular, and right-lateralised frontopolar regions. Follow up analyses indicated that the effect was mainly driven by feedback-related activity, and simple effects were only significant within incorrect experimental trials. There was also a peak in right-lateralised dorsomedial area 9 of the SFG, the cluster extending onto the dorsolateral surface. No follow up effects were significant, however a similar pattern was seen whereby experimental BOLD responses were of greater magnitude during feedback events in incorrect trials. For this reason null

hypothesis 2 can be rejected as regions within the OFC and SFG demonstrated effects of condition which differentiated between cue and feedback events.

Hypothesis 3 predicted an error-status x condition interaction whereby differences in functional activity between conditions would vary between correct and incorrect trials (see **section 6.2.3.3**). This was identified in two regions, the first within the left medial SFG (extending into and overlapping with the main effect in the paracingulate gyrus, but slightly rostral to the CEFs) with follow up effects finding that significant simple effects were specific to the cue-locked incorrect experimental trials. The second was in the right MFG, an area arguably located in lobule 8Av (as per Petrides & Pandya, 1999), the peak surviving FDR correction but not FWE. There were no follow up effects, however the pattern was of BOLD responses being of greater positive magnitude within incorrect experimental trials. For this reason null hypothesis 3 can be rejected as these regions demonstrated effects of condition which differentiated between correct and incorrect trials.

There was a failure to reject null hypothesis 4 as no event x error-status x condition interactions survived correction, however this may have been attributable to the small sample size (discussed below). However null hypothesis 5 can be rejected as there were significant effects at the time of target presentation located within all four eye fields and the OMV (see **section 6.2.3.7**). As per work by Amiez & Petrides (2009) these were specifically in the left ventral aspect of the diPCS (PrEFs), bilaterally in the vsPCS (FEFs), and medially within the vertical cingulate sulcus (CEFs) and the precentral sulcus (SEFs). The cerebellar cluster was deemed to be within the OMV as it was located in medial lobule VI. This confirmed utilisation of the expected circuitry when executing a voluntary saccade (Amiez & Petrides, 2009; Kojima & Soetedjo, 2018; Lefevre et al., 1998; Matsumoto et al., 2018; Petrides, 2005; Quaia et al., 1999; Schall et al., 1993; Shook et al., 1990).

6.4.3. Whole Brain Analysis

The whole brain analysis applied the same four analyses to regions outside of the

cerebellar and frontal lobe masks, but with whole brain FWE correction (see **section 6.2.3.6**).

Despite this conservative method there were significant effects of condition. These included

two peaks in the left precuneus, one dorsal (within area 7P of the superior parietal lobule)

and another ventral with a simple effect specific to cue-linked incorrect experimental trials.

This activity is reported as there is evidence the precuneus processes goal directed action,

episodic memory retrieval, and visuo-spatial imagery (Cavanna & Trimble, 2006), and that

the inferior parietal cortex is connected to dorsolateral area 8 (Petrides, 2005), especially

relevant as area 8A outputs to mid-dorsolateral area 9/46 (Passingham & Lau, 2022). Further

effects of condition were also identified in the middle temporal gyrus (no follow up effects),

and bilaterally in the striatum (peaking in the caudate), the right peak showing a significant

effect of condition specifically within incorrect cue-locked trials (with a positive BOLD

response in the experimental condition). Within the striatum there were also event x

condition interactions, peaking bilaterally in the caudate (with a significant simple effect

within feedback-linked incorrect experimental trials in the right peak), and left lateralised in

the putamen (with a significant simple effect in cue-linked incorrect experimental trials,

showing a negative BOLD response).

6.4.4. Summary of Functional Results

The main focus of this paper was to investigate how regions such as the dlPFC

prospectively encode visuo-spatially defined goals based on non-spatial visual cues, the

contribution of frontopolar and orbital areas relating to feedback and re-representation of

goals, and the role of the cerebellum in the formation of internal models of cognition.

Furthermore, effects of error-status were investigated as these may imply that functional

activity was differentiated by progression through learning. The purpose was to better

understand how this putative network operates when perceiving a cue and using this information to inform future action choices based upon past and ongoing feedback. Going back to the introduction (**section 6.1**) it was suggested that the ITC provides non-spatial visual information to prefrontal and premotor regions via the striatum, with specific projections to the vlPFC (Muhammad et al., 2005; Passingham & Lau, 2022; Petrides, 2005; Wise & Murray, 2000), consistent with lesion studies (Bloedel et al., 1996, pp. 266-267). This was supported in the results as inferotemporal regions were among those active at the time of the cue (irrespective of condition, see **section 6.3.2.5**), and striatal activity was identified time-locked to the cue. This suggested processing of cue-related visual information accessible to relevant dorsolateral circuitry via connections between ventral and dorsolateral PFC (Petrides & Pandya, 2002; Petrides, 2005). It was further expected that regions of the parietal cortex would contribute visuo-spatial information (Burr et al., 2010; Merritt et al., 2010) informing both prospective encoding via connectivity with the dlPFC (Passingham & Wise, 2012, pp. 157-194; Petrides, 2005) and oculomotor responses via connectivity with the FEFs (Rivaud et al., 1994). This was also supported in results as main effects of condition were identified in the precuneus, with support for this being driven predominately by cue-linked experimental trials. Therefore as suggested by Rao et al. (1997) it is plausible that the dlPFC receives necessary what/where information when using visual cues to inform visuo-spatially defined goals.

Given a putative role prospectively encoding the goal (e.g. saccade to left-hand target) it was anticipated the dlPFC would be active during experimental trials (more so during cue presentation) transforming object and spatial data into a plan of action and maintaining this until execution (Bunge, 2004; Levine et al., 1997; Mansouri et al., 2020; Moore et al., 2012; Passingham & Wise, 2012, pp. 157-194; Sakai et al., 2002; Tsuijimoto et al., 2011b, 2012). This role was supported by main effects of condition found in bilateral

area 9 (typified by cue-locked activity within incorrect experimental trials) and left area 9/46d (again effects typically cue-locked). Furthermore, evidence of interactions with error status in left dorsomedial area 9 and right dorsolateral area 8Av were typified by increased magnitude within incorrect trials. This suggests that over the course of learning functional BOLD responses in the PFC reduce in magnitude, potentially associated with automation of function (Jenkins et al., 1994; Jueptner et al., 1997; Passingham,1996; Raichle et al., 1994).

In order for the dlPFC to inform oculomotor responses, outputs to regions such as the SEFs and FEFs were anticipated, as these project on to the superior colliculus where saccades can be initiated (Bloedel et al., 1996, pp. 266-275; Chen & Wise, 1995a; Huerta & Kaas, 1990; Hutchison et al., 2012; Petrides, 2019, pp. 91-108; Purves et al., 2008, pp. 460-507; Schall et al., 1993; Shook et al., 1990). In the target analysis (**section 6.3.2.7**) there was activity identified both within the FEFs and SEFs, supporting this. As suggested in the introduction, the SEFs may fulfil a 'premotor role' (Chen & Wise 1995b) as they are implicated more in saccade preparation/decisions/timing (Abzug & Sommer, 2017) whereas the FEFs code for retinally defined saccades (Schall et al., 1993), potentially based on information from the dlPFC. The CEFs may also contribute, connecting to both FEFs and SEFs, and being implicated in saccadic control in the face of conditional cues (Amiez & Petrides, 2009; Paus et al., 1993). This was supported by significant effects in the CEFs identified at the time of target presentation, as well as effects of condition predominately time-locked to presentation of the conditional cue, with BOLD responses of greater magnitude within incorrect trials. At this juncture it is considered that effects within the paracingulate gyrus may also be associated with response inhibition (Congdon et al., 2010; Zhang et al., 2017), supported by effects being strongest within incorrect trials, suggesting when a cue is learned there is a reduced requirement to inhibit incorrect responses. Finally at the time of target presentation there was also a significant effect in the OMV (cerebellar vermal lobule VI),

consistent with a purported role in saccadic adaptation (Kojima & Soetedjo, 2018; Lefevre et al., 1998; Quaia et al., 1999). This may be achieved through the formation of forward models, consistent with connectivity between pre-cerebellar nuclei and the FEF, SEF, and superior colliculus (Brodal & Brodal, 1981; Frankfurter et al., 1976; Shook et al., 1990; Stanton et al., 1988; Voogd et al., 2012; Yamada & Noda, 1987), the OMV perhaps reducing error in the oculomotor components of the response.

It was also predicted that cerebellar lobule HVIIa would be involved in conditional learning at the time of the cue, forming increasingly accurate forward models of prefrontal functions based upon feedback from the VTA and inferior olive (Ramnani, 2006, 2014). This would be consistent with past evidence (Balsters & Ramnani, 2008, 2011; Balsters et al., 2013) and lobule HVIIa connecting with the dlPFC and FPC (Balsters et al., 2014; Kelly & Strick, 2003; Schmahmann & Pandya, 1995, 1997). This was supported by significant effects bilaterally in lobule HVI/CRUS I, typically time locked to the cue and specific to incorrect trials, consistent with work by Imamizu et al. (2000) who identified that BOLD responses in the cerebellum reduce as learning progresses. This is also consistent with effects of cerebellar long term depression at the parallel fiber-Purkinje synapse (Albus, 1971; Hirano, 2018; Ito et al., 2014) and evidence of BOLD responses reducing in magnitude with increasing automation (Balsters et al., 2011). That cerebellar clusters peaked in lobule HVI was considered, this being a key site for learning (Thompson & Kim, 1996) but typically associated with classical conditioning of motor reflexes (Longley & Yeo, 2014; Ramnani & Yeo, 1996; Thompson & Steinmetz, 2009; Yeo et al., 1985). However functional connectivity studies have shown that cerebellar lobules VI and VIII connect with visual and premotor areas (O'Reilly et al., 2010) supported by a rostro-caudal gradient of connectivity between the frontal lobe and cerebellum, more caudal frontal regions connecting with anterior and posterolateral cerebellar lobules, but connectivity with increasingly rostral frontal regions

converging on lobule HVIIa (Longley et al., 2021). Furthermore lobules HVI and CRUS I have been implicated in working memory functions pertaining to preparing complex motor responses (not pertaining to execution), word recall, and covert speech (Kansal et al., 2017; Marvel & Desmond, 2010).

Next to consider is the role feedback may play in guiding prospective encoding within the dlPFC, and in providing the cerebellum with error information. There is deemed potential for neural activity in frontopolar area 10 to represent response-specific information specifically at the time of feedback and in correct trials, potentially re-representing the correct goal to facilitate the formation of goal-feedback associations (Tsujimoto et al., 2011a, 2012). This was not identified in the results above, as the frontopolar peak which extended into area 10 (cytoarchitectonic areas fp1 and fp2) showed an effect of condition primarily driven by incorrect trials at the time of the cue. This may support a supervisory role coordinating cognitive processes which inform decisions (Petrides, 2005; Ramnani & Owen, 2004), potentially functioning as a controller projecting to plants within the dlPFC (Ramnani, 2014).

An alternative region expected to be active at the time of feedback was the OFC, with evidence of a role assigning outcomes to decisions (Tsuijimoto et al., 2011b, 2012). This was supported by the data, with evidence of posterior orbital gyri showing an effect of condition that interacted with levels of event, driven by significant BOLD responses during incorrect experimental feedback. Of interest, these clusters overlapped with those in the insula where peaks relating to a main effect of condition were identified, which also showed this event x condition interaction (typically driven by significant effects specific to incorrect trials). However in insula-located peaks there was evidence of BOLD responses being cue-locked, rather than feedback-locked. This is consistent with a potential role in guiding attention to novel stimuli (Uddin et al., 2017) and a meta-analysis implicating the anterior-

dorsal insula (overlapping with significant peaks in results) in task updating and multimodal integration (Kurth et al., 2010). Of interest, homologues of human orbital and insula cortex (as well as cingulate areas 25 and 32) show connectivity with the inferior olive, identified using tracer studies in rats (Swenson et al., 1989; Wise, 2008). Therefore the OFC (as well as the insula and cingulate regions) has the potential to assist in provision of a teaching signal to the cerebellum, using errors to guide the formation of forward models (Ramnani, 2006). Differentiation between effects specific to the OFC and the insula remained difficult however, as they neighbour each other and significant clusters sat on the border. Furthermore, insula activations were only identified as smoothing of the frontal lobe mask allowed for these to intrude into the analysis.

It was considered that the striatum may also play a role in feedback, given evidence in conditional learning based upon convergence of sensory/motor/reward information (Graybiel, 2008; Hadj-Bouziane et al., 2003; Yahya, 2021; Yin and Knowlton, 2006), connections with the OFC (Passingham & Wise, 2012, pp. 35-36) and connectivity with relevant oculomotor areas such as the FEFs and SEFs (Parthasarathy et al., 1992). That effects were identified at both time of cue and feedback presentation (predominately within incorrect experimental trials) supported a role combining multimodal information to inform action, with the potential to provide error-information in the form of a teaching signal to the cerebellar lobule HVII via the ventral tegmental area (VTA) and inferior olive (Chowdhury et al., 2013; Ikai et al., 1992, 1994; Loopuijt & Van der Kooy, 1985; Oades & Halliday, 1987; Ramnani, 2014). In this way it is possible that the striatum not only sends feedback data to the cerebellum (potentially influencing encoding of cue-linked rules) but further applies this to subsequent oculomotor decisions when presented with a conditional cue.

6.4.5. Limitations and Future Research

Initially there was also an issue pertaining to eye-tracking in an ultra-high field MRI environment. This included electrical interference and physical vibration, both of which contributed to the high failure rate and reduced sample size. It is suggested that future research applying eye-tracking should take these issues into consideration during experimental design. For example, a fixation trigger was used, requiring a 200ms long fixation upon a target before it was marked as 'selected'. This failed in the face of vibration as the camera motion was mistaken for saccadic activity, breaking up the fixation into multiple smaller fixations. Instead an invisible boundary trigger may be more appropriate, based on the total duration that gaze remains in a region of interest irrespective of fixation and saccade. Originally the intention was to investigate the effect of error trials upon subsequent correct trials, looking for trial-trial changes in the cerebellum which correspond to learning (in a manner theoretically comparable to work by Medina & Lisberger, 2008), but this was rendered impractical due to reduced trial numbers (ranging between 0-12, median = 3). It is the opinion of the author that future research would benefit from running this investigation, helping inform the literature about how the cerebellum is contributing to the encoding of goals. The investigation discussed in this paper was a previously devised backup analysis, taking advantage of the large number of incorrect trials and the yoked control condition.

As a result of the small sample size and reduction in power a lack of significant effects cannot be meaningfully interpreted. For example, that there was no significant three-way interaction between event, error-status, and condition does not mean this effect does not exist. On the contrary, there was evidence within significant coordinates that would suggest bias towards one event type or another, and a tendency for significant follow-up effects to be found only in incorrect trials. That a large number of clusters with significant

53

peaks were identified was deemed evidence that the sample size was large enough to justify a random effects analysis, as well as ultra-high field being deemed to have sufficient signal-to-noise to justify interpretation even of single-subject data (Viessmann & Polimeni, 2021; Vu et al., 2017). That these coordinates survived FWE correction also lends support for the analysis being justifiable, especially considering the increased number of voxels as a result of improved spatial resolution. The risk of false negatives was potentially further increased due to multicollinearity within the 1st-level GLM, whereby the canonical function pertaining to feedback events was correlated with the dispersion derivative of cue events. If the canonical function more strongly contributed to the model then it is plausible that feedback-locked signal was less likely to be found than cue-locked signal. However, there were still significant effects at the time of feedback, suggesting this was not always the case. Labs looking to replicate this work may benefit from using partial reinforcement, as this would allow for instances where cue and target presentation take place without feedback, helping reduce multicollinearity between cue and feedback events.

6.4.6. Conclusion

In conclusion, the results outlined above are consistent with the ITC and PPC providing information to the dlPFC where a goal can be encoded, which outputs down a rostro-caudal axis to the eye fields where a saccade is prepared to achieve the goal, and sent on to the superior colliculus for execution via the paramedian pontine reticular formation (Purves et al., 2008, pp. 460-507). There was also evidence that the frontopolar gyrus was active, potentially coordinating cognitive processing in the PFC (Petrides, 2005; Ramnani & Owen, 2004). Significant effects within cerebellar lobules HVI-CRUS I at the time of the cue and within the OMV at the time of target presentation support a cerebellar contribution to both cognitive processing of goals, and execution of oculomotor responses, consistent with patterns of connectivity (Balsters et al., 2014; Brodal & Brodal, 1981; Frankfurter et al., 1976;

Kelly & Strick, 2003; Longley et al., 2021; O'Reilly et al., 2010; Schmahmann & Pandya, 1995, 1997; Shook et al., 1990; Stanton et al., 1988; Voogd et al., 2012; Yamada & Noda, 1987) and theoretical work by Ramnani (2006, 2014). That effects were typically strongest within incorrect trials was also considered, potentially indicating that a spatial location is being encoded, and as the rule is as yet unlearnt there is a greater cognitive load in prefrontal regions, and more error feedback being provided to the cerebellum. Finally there was evidence that the OFC and striatum may contribute to provision of error feedback to guide future responses (supported by connectivity between the two; Passingham & Wise, 2012, pp. 35-36), with significant effects identified at both the presentation of the cue (striatum) and feedback (OFC and striatum). These regions therefore may at least partially address the temporal discontiguity between cue and feedback events.

6.5. References

Abzug, Z. M., & Sommer, M. A. (2017). Supplementary eye fields. *Reference module in neuroscience and biobehavioral psychology*. http://dx.doi.org/10.1016/B978-0-12-809324-5.02941-2

Albus, J. S. (1971). A theory of cerebellar function. *Mathematical Biosciences*, *10*(1-2), 25-61. https://doi.org/10.1016/0025-5564(71)90051-4

Amiez, C., & Petrides, M. (2009). Anatomical organization of the eye fields in the human and non-human primate frontal cortex. *Progress in neurobiology*, *89*(2), 220-230. https://doi.org/10.1016/j.pneurobio.2009.07.010

Balsters, J. H., & Ramnani, N. (2008). Symbolic representations of action in the human cerebellum. *Neuroimage*, *43*(2), 388-398. https://doi.org/10.1016/j.neuroimage.2008.07.010

Balsters, J. H., & Ramnani, N. (2011). Cerebellar plasticity and the automation of first-order rules. *Journal of Neuroscience*, *31*(6), 2305-2312. https://doi.org/10.1523/JNEUROSCI.4358-10.2011

Balsters, J. H., Whelan, C. D., Robertson, I. H., & Ramnani, N. (2013). Cerebellum and cognition: evidence for the encoding of higher order rules. *Cerebral Cortex*, *23*(6), 1433-1443. https://doi.org/10.1093/cercor/bhs127

Balsters, J. H., Laird, A. R., Fox, P. T., & Eickhoff, S. B. (2014). Bridging the gap between functional and anatomical features of cortico-cerebellar circuits using meta-analytic connectivity modeling. *Human brain mapping*, *35*(7), 3152-3169. https://doi.org/10.1002/hbm.22392

Bloedel, J. R., Ebner, T. J., & Wise, S. P. (Eds.). (1996). *The acquisition of motor behavior in vertebrates*. MIT Press.

Brodal, P., & Brodal, A. (1981). The olivocerebellar projection in the monkey. Experimental

studies with the method of retrograde tracing of horseradish peroxidase. *Journal of*

Comparative Neurology, *201*(3), 375-393. https://doi.org/10.1002/cne.902010306

Budisavljevic, S., & Ramnani, N. (2012). Cognitive deficits from a cerebellar tumour: A

historical case report from Luria's laboratory. *Cortex*, *48*(1), 26-35.

https://doi.org/10.1016/j.cortex.2011.07.001

Bunge, S. A. (2004). How we use rules to select actions: a review of evidence from cognitive

neuroscience. *Cognitive, Affective, & Behavioral Neuroscience*, *4*(4), 564-579.

https://psycnet.apa.org/doi/10.3758/CABN.4.4.564

Burr, D. C., Ross, J., Binda, P., & Morrone, M. C. (2010). Saccades compress space, time and

number. *Trends in cognitive sciences*, *14*(12), 528-533.

https://doi.org/10.1016/j.tics.2010.09.005

Cavanna, A. E., & Trimble, M. R. (2006). The precuneus: a review of its functional anatomy

and behavioural correlates. *Brain*, *129*(3), 564-583.

https://doi.org/10.1093/brain/awl004

Chen, L. L., & Wise, S. P. (1995a). Neuronal activity in the supplementary eye field during

acquisition of conditional oculomotor associations. *Journal of*

Neurophysiology, *73*(3), 1101-1121. https://doi.org/10.1152/jn.1995.73.3.1101

Chen, L. L., & Wise, S. P. (1995b). Supplementary eye field contrasted with the frontal eye

field during acquisition of conditional oculomotor associations. Journal of

Neurophysiology, 73(3), 1122-1134. https://doi.org/10.1152/jn.1995.73.3.1122

Chowdhury, R., Lambert, C., Dolan, R. J., & Düzel, E. (2013). Parcellation of the human

substantia nigra based on anatomical connectivity to the striatum. Neuroimage, 81,

191-198. https://doi.org/10.1016/j.neuroimage.2013.05.043

Congdon, E., Mumford, J. A., Cohen, J. R., Galvan, A., Aron, A. R., Xue, G., ... & Poldrack, R. A. (2010). Engagement of large-scale networks is related to individual differences in inhibitory control. *Neuroimage*, *53*(2), 653-663. https://doi.org/10.1016/j.neuroimage.2010.06.062

Danvers, M., Longley, M., & Ramnani. (2021, November 8-11). *Modelling the BOLD response: On the insufficiency of conventional modelling approaches.* [Poster Presentation]. SFN 2021, virtual.

Duvernoy, H. M. (1999). *The human brain: surface, three-dimensional sectional anatomy with MRI, and blood supply*. Springer Science & Business Media.

Frankfurter, A., Weber, J. T., Royce, G. J., Strominger, N. L., & Harting, J. K. (1976). An autoradiographic analysis of the tecto-olivary projection in primates. *Brain research*, *118*(2), 245-257. https://doi.org/10.1016/0006-8993(76)90710-1

Georgopoulos, A. P., Kalaska, J. F., Caminiti, R., & Massey, J. T. (1982). On the relations between the direction of two-dimensional arm movements and cell discharge in primate motor cortex. *Journal of Neuroscience*, *2*(11), 1527-1537. https://doi.org/10.1523/JNEUROSCI.02-11-01527.1982

Georgopoulos, A. P., Caminiti, R., Kalaska, J. F., & Massey, J. T. (1983). Spatial coding of movement: a hypothesis concerning the coding of movement direction by motor cortical populations. *Experimental Brain Research*, *49*(Suppl. 7), 327-336. https://doi.org/10.1007/978-3-642-68915-4_34

Graybiel, A. M. (2008). Habits, rituals, and the evaluative brain. *Annual review of neuroscience*, *31*(1), 359-387. https://doi.org/10.1146/annurev.neuro.29.051605.112851

Hadj-Bouziane, F., Meunier, M., & Boussaoud, D. (2003). Conditional visuo-motor learning in

primates: a key role for the basal ganglia. *Journal of Physiology-Paris*, *97*(4-6), 567-

579. https://doi.org/10.1016/j.jphysparis.2004.01.014

Henson, R., Büchel, C., Josephs, O., & Friston, K. (1999). The slice-timing problem in event-

related fMRI. *NeuroImage*, *9*, 125. https://www.mrc-

cbu.cam.ac.uk/personal/rik.henson/personal/HensonEtAl_HBM_Abstract_99.pdf

Hirano, T. (2018). Regulation and interaction of multiple types of synaptic plasticity in a

Purkinje neuron and their contribution to motor learning. *The Cerebellum*, *17*(6),

756-765. https://doi.org/10.1007/s12311-018-0963-0

Huerta, M. F., & Kaas, J. H. (1990). Supplementary eye field as defined by intracortical

microstimulation: connections in macaques. *Journal of Comparative

Neurology*, *293*(2), 299-330. https://doi.org/10.1002/cne.902930211

Hutchison, R. M., Gallivan, J. P., Culham, J. C., Gati, J. S., Menon, R. S., & Everling, S. (2012).

Functional connectivity of the frontal eye fields in humans and macaque monkeys

investigated with resting-state fMRI. *Journal of neurophysiology*, *107*(9), 2463-2474.

https://doi.org/10.1152/jn.00891.2011

Ikai, Y., Takada, M., Shinonaga, Y., & Mizuno, N. (1992). Dopaminergic and non-

dopaminergic neurons in the ventral tegmental area of the rat project, respectively,

to the cerebellar cortex and deep cerebellar nuclei. *Neuroscience*, *51*(3), 719-728.

https://doi.org/10.1016/0306-4522(92)90310-X

Ikai, Y., Takada, M., & Mizuno, N. (1994). Single neurons in the ventral tegmental area that

project to both the cerebral and cerebellar cortical areas by way of axon

collaterals. *Neuroscience*, *61*(4), 925-934. https://doi.org/10.1016/0306-

4522(94)90413-8

Imamizu, H., Miyauchi, S., Tamada, T., Sasaki, Y., Takino, R., PuÈtz, B., ... & Kawato, M.

    (2000). Human cerebellar activity reflecting an acquired internal model of a new

    tool. *Nature*, *403*(6766), 192-195. https://www.nature.com/articles/35003194

Ito, M. (2005). Bases and implications of learning in the cerebellum—adaptive control and

    internal model mechanism. *Progress in brain research*, *148*, 95-109.

    https://doi.org/10.1016/S0079-6123(04)48009-1

Ito, M., Yamaguchi, K., Nagao, S., & Yamazaki, T. (2014). Long-term depression as a model of

    cerebellar plasticity. *Progress in brain research 210*, 1-30.

    https://doi.org/10.1016/B978-0-444-63356-9.00001-7

Jenkins, I. H., Brooks, D. J., Nixon, P. D., Frackowiak, R. S., & Passingham, R. E. (1994). Motor

    sequence learning: a study with positron emission tomography. *Journal of

    Neuroscience*, *14*(6), 3775-3790. https://doi.org/10.1523/JNEUROSCI.14-06-

    03775.1994

Jueptner, M., Stephan, K. M., Frith, C. D., Brooks, D. J., Frackowiak, R. S., & Passingham, R. E.

    (1997). Anatomy of motor learning. I. Frontal cortex and attention to action. *Journal

    of neurophysiology*, *77*(3), 1313-1324. https://doi.org/10.1152/jn.1997.77.3.1313

Kansal, K., Yang, Z., Fishman, A. M., Sair, H. I., Ying, S. H., Jedynak, B. M., ... & Onyike, C. U.

    (2017). Structural cerebellar correlates of cognitive and motor dysfunctions in

    cerebellar degeneration. *Brain*, *140*(3), 707-720.

    https://doi.org/10.1093/brain/aww327

Kelly, R. M., & Strick, P. L. (2003). Cerebellar loops with motor cortex and prefrontal cortex

    of a nonhuman primate. *Journal of neuroscience*, *23*(23), 8432-8444.

    https://doi.org/10.1523/JNEUROSCI.23-23-08432.2003

Kojima, Y., & Soetedjo, R. (2018). Elimination of the error signal in the superior colliculus

impairs saccade motor learning. *Proceedings of the National Academy of*

Sciences, *115*(38), E8987-E8995. https://doi.org/10.1073/pnas.1806215115

Kurth, F., Zilles, K., Fox, P. T., Laird, A. R., & Eickhoff, S. B. (2010). A link between the systems:

functional differentiation and integration within the human insula revealed by meta-

analysis. *Brain Struct Funct*, *214*, 519-534. https://doi.org/10.1007/s00429-010-

0255-z

Lefevre, P., Quaia, C., & Optican, L. M. (1998). Distributed model of control of saccades by

superior colliculus and cerebellum. *Neural networks*, *11*(7-8), 1175-1190.

https://doi.org/10.1016/S0893-6080(98)00071-9

Levine, B., Stuss, D. T., & Milberg, W. P. (1997). Effects of aging on conditional associative

learning: process analyses and comparison with focal frontal

lesions. *Neuropsychology*, *11*(3), 367-381.

https://psycnet.apa.org/doi/10.1037/0894-4105.11.3.367

Longley, M., & Yeo, C. H. (2014). Distribution of neural plasticity in cerebellum-dependent

motor learning. *Progress in brain research*, *210*, 79-101.

https://doi.org/10.1016/B978-0-444-63356-9.00004-2

Longley, M., Danvers, M., & Ramnani. (2021, November 8-11). *Topographically organised*

frontal cortex maps in the human cerebellar cortex. [Poster Presentation]. SFN 2021,

virtual.

Loopuijt, L. D., & Van der Kooy, D. (1985). Organization of the striatum: collateralization of

its efferent axons. Brain research, 348(1), 86-99. https://doi.org/10.1016/0006-

8993(85)90363-4

Mansouri, F. A., Freedman, D. J., & Buckley, M. J. (2020). Emergence of abstract rules in the

primate brain. *Nature Reviews Neuroscience*, 1-16. https://doi.org/10.1038/s41583-

020-0364-5

MarsBaR FAQ — MarsBaR 0.45 documentation. (n.d.). Retrieved October 11, 2022,

from https://marsbar-toolbox.github.io/faq.html

Marvel, C. L., & Desmond, J. E. (2010). Functional topography of the cerebellum in verbal

working memory. *Neuropsychology review*, *20*(3), 271-279.

https://doi.org/10.1007/s11065-010-9137-7

Matsumoto, M., Inoue, K. I., & Takada, M. (2018). Causal role of neural signals transmitted

from the frontal eye field to the superior colliculus in saccade generation. *Frontiers

in neural circuits. 12*, 69. https://doi.org/10.3389/fncir.2018.00069

Medina, J. F., & Lisberger, S. G. (2008). Links from complex spikes to local plasticity and

motor learning in the cerebellum of awake-behaving monkeys. *Nature

neuroscience*, *11*(10), 1185-1192. https://doi.org/10.1038/nn.2197

Merritt, D. J., Casasanto, D., & Brannon, E. M. (2010). Do monkeys think in metaphors?

Representations of space and time in monkeys and humans. *Cognition*, *117*(2), 191-

202. https://doi.org/10.1016/j.cognition.2010.08.011

Moore, T. L., Schettler, S. P., Killiany, R. J., Rosene, D. L., & Moss, M. B. (2012). Impairment in

delayed nonmatching to sample following lesions of dorsal prefrontal cortex.

Behavioral neuroscience, *126*(6), 772-780.

https://psycnet.apa.org/doi/10.1037/a0030493

Muhammad, R., Wallis, J. D., & Miller, E. K. (2006). A comparison of abstract rules in the

prefrontal cortex, premotor cortex, inferior temporal cortex, and striatum. *Journal of

cognitive neuroscience*, *18*(6), 974-989. https://doi.org/10.1162/jocn.2006.18.6.974

Murray, E. A., & Wise, S. P. (1996). Role of the hippocampus plus subjacent cortex but not amygdala in visuomotor conditional learning in rhesus monkeys. *Behavioral neuroscience*, *110*(6), 1261-1270. https://psycnet.apa.org/doi/10.1037/0735-7044.110.6.1261

Oades, R. D., & Halliday, G. M. (1987). Ventral tegmental (A10) system: neurobiology. 1. Anatomy and connectivity. *Brain Research Reviews*, *12*(2), 117-165. https://doi.org/10.1016/0165-0173(87)90011-7

O'Reilly, J. X., Beckmann, C. F., Tomassini, V., Ramnani, N., & Johansen-Berg, H. (2010). Distinct and overlapping functional zones in the cerebellum defined by resting state functional connectivity. *Cerebral cortex*, *20*(4), 953-965. https://doi.org/10.1093/cercor/bhp157

Parthasarathy, H. B., Schall, J. D., & Graybiel, A. M. (1992). Distributed but convergent ordering of corticostriatal projections: analysis of the frontal eye field and the supplementary eye field in the macaque monkey. *Journal of Neuroscience*, *12*(11), 4468-4488. https://doi.org/10.1523/JNEUROSCI.12-11-04468.1992

Passingham, R. E. (1996). Attention to action. *Philosophical Transactions of the Royal Society of London. Series B: Biological Sciences*, *351*(1346), 1473-1479. https://doi.org/10.1098/rstb.1996.0132

Passingham, R. E., & Wise, S. P. (2012). *The neurobiology of the prefrontal cortex: anatomy, evolution, and the origin of insight* (No. 50). Oxford University Press.

Passingham, R. E., & Lau, H. (2022). Do we understand the prefrontal cortex?. *Brain Structure and Function*, 1-11. https://doi.org/10.1007/s00429-022-02587-7

Paus, T., Petrides, M., Evans, A. C., & Meyer, E. (1993). Role of the human anterior cingulate cortex in the control of oculomotor, manual, and speech responses: a positron

emission tomography study. *Journal of neurophysiology*, *70*(2), 453-469.

https://doi.org/10.1152/jn.1993.70.2.453

Petrides, M. (1985). Deficits on conditional associative-learning tasks after frontal-and

temporal-lobe lesions in man. *Neuropsychologia*, *23*(5), 601-614.

https://doi.org/10.1016/0028-3932(85)90062-4

Petrides, M., & Pandya, D. N. (1999). Dorsolateral prefrontal cortex: comparative

cytoarchitectonic analysis in the human and the macaque brain and corticocortical

connection patterns. *European Journal of Neuroscience*, *11*(3), 1011-1036.

https://doi.org/10.1046/j.1460-9568.1999.00518.x

Petrides, M. (2000). The role of the mid-dorsolateral prefrontal cortex in working

memory. *Experimental brain research*, *133*, 44-54.

https://doi.org/10.1007/s002210000399

Petrides, M., & Pandya, D. N. (2002). Comparative cytoarchitectonic analysis of the human

and the macaque ventrolateral prefrontal cortex and corticocortical connection

patterns in the monkey. *European Journal of Neuroscience*, *16*(2), 291-310.

https://doi.org/10.1046/j.1460-9568.2001.02090.x

Petrides, M. (2005). Lateral prefrontal cortex: architectonic and functional

organization. *Philosophical Transactions of the Royal Society B: Biological

Sciences*, *360*(1456), 781-795. https://doi.org/10.1098/rstb.2005.1631

Petrides, M., Tomaiuolo, F., Yeterian, E. H., & Pandya, D. N. (2012). The prefrontal cortex:

comparative architectonic organization in the human and the macaque monkey

brains. *Cortex*, *48*(1), 46-57. https://doi.org/10.1016/j.cortex.2011.07.002

Petrides, M. (2019). *The frontal lobes revisited*. Psychology Press.

Poldrack, R. A., Mumford, J. A., & Nichols, T. E. (2011). *Handbook of functional MRI data

analysis*. Cambridge University Press.

Purves, D., Augustine, G. J., Fitzpatrick, D., Hall, W. C., LaMantia, A. S., McNamara, J. O., …

    (2008). *Neuroscience.* Sinauer Associates, Inc.

Quaia, C., Lefèvre, P., & Optican, L. M. (1999). Model of the control of saccades by superior

    colliculus and cerebellum. *Journal of neurophysiology*, *82*(2), 999-1018.

    https://doi.org/10.1152/jn.1999.82.2.999

Raichle, M. E., Fiez, J. A., Videen, T. O., MacLeod, A. M. K., Pardo, J. V., Fox, P. T., & Petersen,

    S. E. (1994). Practice-related changes in human brain functional anatomy during

    nonmotor learning. *Cerebral cortex*, *4*(1), 8-26. https://doi.org/10.1093/cercor/4.1.8

Ramnani, N., & Yeo, C. H. (1996). Reversible inactivations of the cerebellum prevent the

    extinction of conditioned nictitating membrane responses in rabbits. *The Journal of*

    Physiology, *495*(1), 159-168. https://doi.org/10.1113/jphysiol.1996.sp021581

Ramnani, N., & Owen, A. M. (2004). Anterior prefrontal cortex: insights into function from

    anatomy and neuroimaging. *Nature reviews neuroscience*, *5*(3), 184-194.

    https://doi.org/10.1038/nrn1343

Ramnani, N. (2006). The primate cortico-cerebellar system: anatomy and function. *Nature*

    reviews neuroscience, *7*(7), 511-522. https://doi.org/10.1038/nrn1953

Ramnani, N. (2014). Automatic and controlled processing in the corticocerebellar system.

    Progress in Brain Research, *210*, 255-285. https://doi.org/10.1016/B978-0-444-

    63356-9.00010-8

Rao, S. C., Rainer, G., & Miller, E. K. (1997). Integration of what and where in the primate

    prefrontal cortex. *Science*, *276*(5313), 821-824.

    https://doi.org/10.1126/science.276.5313.821

Rivaud, S., Müri, R. M., Gaymard, B., Vermersch, A. I., & Pierrot-Deseilligny, C. (1994). Eye movement disorders after frontal eye field lesions in humans. *Experimental Brain Research*, *102*(1), 110-120. https://doi.org/10.1007/BF00232443

Sakai, K., Rowe, J. B., & Passingham, R. E. (2002). Active maintenance in prefrontal area 46 creates distractor-resistant memory. *Nature neuroscience*, *5*(5), 479-484. https://doi.org/10.1038/nn846

Saleem, K. S., Kondo, H., & Price, J. L. (2008). Complementary circuits connecting the orbital and medial prefrontal networks with the temporal, insular, and opercular cortex in the macaque monkey. *Journal of Comparative Neurology*, *506*(4), 659-693. https://doi.org/10.1002/cne.21577

Schall, J. D., Morel, A., & Kaas, J. H. (1993). Topography of supplementary eye field afferents to frontal eye field in macaque: implications for mapping between saccade coordinate systems. *Visual neuroscience*, *10*(2), 385-393. https://doi.org/10.1017/S0952523800003771

Schmahmann, J. D., & Pandya, D. N. (1995). Prefrontal cortex projections to the basilar pons in rhesus monkey: implications for the cerebellar contribution to higher function. *Neuroscience letters*, *199*(3), 175-178. https://doi.org/10.1016/0304-3940(95)12056-A

Schmahmann, J. D., & Pandya, D. N. (1997). Anatomic organization of the basilar pontine projections from prefrontal cortices in rhesus monkey. *Journal of Neuroscience*, *17*(1), 438-458. https://doi.org/10.1523/JNEUROSCI.17-01-00438.1997

Schmahmann, J. D., Doyon, J., Petrides, M., Evans, A. C., & Toga, A. W. (2000). *MRI atlas of the human cerebellum*. Academic press.

Schoenbaum, G., Chiba, A. A., & Gallagher, M. (1998). Orbitofrontal cortex and basolateral amygdala encode expected outcomes during learning. *Nature neuroscience*, *1*(2), 155-159. https://doi.org/10.1038/407

Schoenbaum, G., Setlow, B., Saddoris, M. P., & Gallagher, M. (2003). Encoding predicted outcome and acquired value in orbitofrontal cortex during cue sampling depends upon input from basolateral amygdala. *Neuron*, *39*(5), 855-867. https://doi.org/10.1016/S0896-6273(03)00474-4

Schoenbaum, G., & Roesch, M. (2005). Orbitofrontal cortex, associative learning, and expectancies. *Neuron*, *47*(5), 633-636. https://doi.org/10.1016/j.neuron.2005.07.018

Scott, S. H. (2000). Population vectors and motor cortex: neural coding or epiphenomenon?. *Nature neuroscience*, *3*(4), 307-308. https://doi.org/10.1038/73859

Shook, B. L., Schlag-Rey, M., & Schlag, J. (1990). Primate supplementary eye field: I. Comparative aspects of mesencephalic and pontine connections. *Journal of Comparative Neurology*, *301*(4), 618-642. https://doi.org/10.1002/cne.903010410

Sladky, R., Friston, K. J., Tröstl, J., Cunnington, R., Moser, E., & Windischberger, C. (2011). Slice-timing effects and their correction in functional MRI. *Neuroimage*, *58*(2), 588-594. https://doi.org/10.1016/j.neuroimage.2011.06.078

Stanton, G. B., Goldberg, M. E., & Bruce, C. J. (1988). Frontal eye field efferents in the macaque monkey: II. Topography of terminal fields in midbrain and pons. *Journal of Comparative Neurology*, *271*(4), 493-506. https://doi.org/10.1002/cne.902710403

Swenson, R. S., Sievert, C. F., Terreberry, R. R., Neafsey, E. J., & Castro, A. J. (1989).

Organization of cerebral cortico-olivary projections in the rat. *Neuroscience*

research, *7*(1), 43-54. https://doi.org/10.1016/0168-0102(89)90036-9

Thompson, R. F., & Kim, J. J. (1996). Memory systems in the brain and localization of a

memory. *Proceedings of the national academy of sciences*, *93*(24), 13438-13444.

https://doi.org/10.1073/pnas.93.24.13438

Thompson, R. F., & Steinmetz, J. E. (2009). The role of the cerebellum in classical

conditioning of discrete behavioral responses. *Neuroscience*, *162*(3), 732-755.

https://doi.org/10.1016/j.neuroscience.2009.01.041

Tsujimoto, S., Genovesio, A., & Wise, S. P. (2011a). Frontal pole cortex: encoding ends at the

end of the endbrain. *Trends in cognitive sciences*, *15*(4), 169-176.

https://doi.org/10.1016/j.tics.2011.02.001

Tsujimoto, S., Genovesio, A., & Wise, S. P. (2011b). Comparison of strategy signals in the

dorsolateral and orbital prefrontal cortex. *Journal of Neuroscience*, *31*(12), 4583-

4592. https://doi.org/10.1523/JNEUROSCI.5816-10.2011

Tsujimoto, S., Genovesio, A., & Wise, S. P. (2012). Neuronal activity during a cued strategy

task: comparison of dorsolateral, orbital, and polar prefrontal cortex. *Journal of*

Neuroscience, *32*(32), 11017-11031. https://doi.org/10.1523/JNEUROSCI.1230-

12.2012

Uddin, L. Q., Nomi, J. S., Hébert-Seropian, B., Ghaziri, J., & Boucher, O. (2017). Structure and

function of the human insula. *Journal of clinical neurophysiology: official publication*

of the American Electroencephalographic Society, *34*(4), 300-306.

https://doi.org/10.1097%2FWNP.0000000000000377

Viessmann, O., & Polimeni, J. R. (2021). High-resolution fMRI at 7 Tesla: challenges, promises and recent developments for individual-focused fMRI studies. *Current Opinion in Behavioral Sciences*, *40*, 96-104. https://doi.org/10.1016/j.cobeha.2021.01.011

Voogd, J., Schraa-Tam, C. K., van der Geest, J. N., & De Zeeuw, C. I. (2012). Visuomotor cerebellum in human and nonhuman primates. The Cerebellum, 11, 392-410. https://doi.org/10.1007/s12311-010-0204-7

Vu, A. T., Jamison, K., Glasser, M. F., Smith, S. M., Coalson, T., Moeller, S., ... & Yacoub, E. (2017). Tradeoffs in pushing the spatial resolution of fMRI for the 7T Human Connectome Project. *Neuroimage*, *154*, 23-32. https://doi.org/10.1016/j.neuroimage.2016.11.049

Wallenstein, G. V., Hasselmo, M. E., & Eichenbaum, H. (1998). The hippocampus as an associator of discontiguous events. *Trends in neurosciences*, *21*(8), 317-323. https://doi.org/10.1016/S0166-2236(97)01220-4

Winocur, G. (1991). Functional dissociation of the hippocampus and prefrontal cortex in learning and memory. *Psychobiology*, *19*(1), 11-20. https://doi.org/10.1007/BF03337952

Wise, S. P., & Murray, E. A. (2000). Arbitrary associations between antecedents and actions. *Trends in neurosciences*, *23*(6), 271-276. https://doi.org/10.1016/S0166-2236(00)01570-8

Wise, S. P. (2008). Forward frontal fields: phylogeny and fundamental function. *Trends in neurosciences*, *31*(12), 599-608. https://doi.org/10.1016/j.tins.2008.08.008

Yahya, K. (2021). The basal ganglia corticostriatal loops and conditional learning. *Reviews in the Neurosciences*, *32*(2), 181-190. https://doi.org/10.1515/revneuro-2020-0047

Yamada, J., & Noda, H. (1987). Afferent and efferent connections of the oculomotor

cerebellar vermis in the macaque monkey. *Journal of comparative neurology*, *265*(2),

224-241. https://doi.org/10.1002/cne.902650207

Yeo, C. H., Hardiman, M. J., & Glickstein, M. (1985). Classical conditioning of the nictitating

membrane response of the rabbit. *Experimental brain research*, *60*(1), 114-126.

https://doi.org/10.1007/BF00237022

Yin, H. H., & Knowlton, B. J. (2006). The role of the basal ganglia in habit formation. *Nature*

Reviews Neuroscience, *7*(6), 464-476. https://doi.org/10.1038/nrn1919

Zhang, R., Geng, X., & Lee, T. (2017). Large-scale functional neural network correlates of

response inhibition: an fMRI meta-analysis. *Brain Structure and Function*, *222*(9),

3973-3990. https://doi.org/10.1007/s00429-017-1443-x

Chapter 7
General Discussion

Matthew Danvers

Word count: 9,681 excluding references

7.1. Thesis Overview

This thesis served to understand optimal modelling of the BOLD response, with consideration given to age-related differences in the time-course of the haemodynamic response function (HRF), the results of which were reported in chapters 3-4 and summarised below in section **7.1.1. Methodological Overview**. This informed an investigation of the systems engaged in visuo-oculomotor learning carried out across both young end elderly cognitively healthy adults, the results of which were reported in chapters 5-6 and summarised below in section **7.1.3. Functional Application Overview.** These results are then considered holistically in section **7.2. General Conclusion.**

7.1.1. Methodological Overview

In chapter 3, consistent with predictions it was identified that flexible modelling approaches resulted in a greater number of significant voxels being found in a random-effects analysis, consistent with the literature (Henson et al., 1999, 2001; Lindquist et al., 2009; Lindquist & Wager, 2007; Ramnani & Henson, 2005; Steffener et al., 2010). This must be interpreted cautiously regarding improvement over the fixed canonical (HRFc) model, as slice-timing correction was not applied and so results are likely biased in favour of flexible models, however the primary focus was a comparison of these flexible approaches. Both the HRFtd (HRFc with derivatives) and the Fourier basis sets were chosen as common flexible modelling-methods, whilst also following up on work by Ramnani & Henson (2005). To improve sensitivity an extra set of design matrices were formed looking for additional variance captured when regressing out the opposing model. There was little difference in the number of voxels captured by each of the flexible models, but there was evidence that the Fourier basis set captured additional variance beyond that captured using the HRFtd model, within all regions of interest (ROI). This was in line with predictions based upon the Fourier set making fewer assumptions about the time-course of the estimated HRF (Friston

et al., 1998b; Josephs et al., 1997). However the HRFtd model also captured additional

variance beyond that modelled using the Fourier approach, with evidence of this being the

case in a greater number of voxels within four of the five ROIs (M1, A1, V1 and the

cerebellum). Within these ROIs there was much overlap as each flexible model commonly

captured additional signal within the same voxel, however in these shared voxels the HRFtd

model still showed evidence of superiority. It was only in the anterior prefrontal cortex

(aPFC) specifically area Fp1 of the frontopolar cortex (FPC) that the Fourier set captured

additional variance in more voxels than the HRFtd model, attributed to estimated

haemodynamic response functions (HRF) in this ROI typically having a much-increased peak

latency and dispersion. In general across grey matter it was seen that the estimated HRF

typically had a lower peak latency and dispersion than predicted by the HRFc model, and

that the Fourier set tended to underestimate these reductions relative to the HRFtd model.

In order to understand why the Fourier set would capture more variance within

estimated HRFs with delayed timing properties (such as peak latency and dispersion)

simulations were run. These identified that the HRFtd model was fairly resilient to

reductions in timing properties, but with a marked drop in performance when they were

increased. Consistent with it making fewer assumptions, the Fourier set was less variable

over simulated HRF shapes, and so better dealt with increased timing properties, yet still

underperformed relative to the HRFtd model when both peak latency and dispersion were

low. This was attributed to the Fourier set being comprised of multiple functions which

oscillate at different frequencies. To model a peak with low latency and dispersion, higher

frequency functions are weighted (evidenced in chapter 3 simulations), which leads to a

poorer fit later in the estimated HRF when signal returns to baseline. This could theoretically

result in high within-subject variance at the 1st-level of analysis. At the 2nd-level of analysis

there is also an issue relating to the bias-variance trade off (Poldrack et al., 2011, pp. 76-77),

with a greater risk of variability in the parameter estimates drawn from the 1st-level

analysis. This was evidenced in chapter 3 using simulations, finding the greatest variability in

signal across simulated participants when using the Fourier set, a potential example of

overfitting. Therefore although the Fourier set has the least bias, the HRFtd model may have

struck a better balance in the bias-variance trade-off.

Next in chapter 4 this investigation was applied to an analysis of the impact of age

upon timing properties of the estimated HRF, and the capacity of modelling approaches to

capture these time-courses. Here predictions were made about peak latency and dispersion

based upon both previous evidence (Richter & Richter, 2003; Stefanova et al., 2013; Taoka et

al., 1998; West et al., 2019) and as a means of following up on chapter 3, looking across a

selection of grey matter coordinates. A post-hoc analysis was also run looking at the

magnitude of the undershoot relative to positive peak, based on observed differences in the

dataset and following up on past observations by Ramnani & Henson (2005). As

hypothesised, both peak latency and dispersion increased with increasing age, but remained

below that predicted by the HRFc model. This was seen across multiple brain regions, with a

subjectively viewed trend of strong age-related change in the cerebellum. There was

evidence of heteroscedasticity in the form of greater variability within the older age groups,

however peak latency was still higher in the oldest relative to youngest group in more than

99% of voxels (more than 85% for dispersion). There was also an age x modelling-approach

interaction in both timing properties, with change over age groups seen to be statistically

stronger when using the HRFtd model, and statistical differences between flexible models

stronger in younger age groups (with low timing properties) than older age groups. This was

consistent with work in chapter 3, as the HRFtd model was typically better at capturing

reductions in timing properties, and so may better model activity in the younger cohorts.

Regarding the undershoot amplitude, there was an interaction driven by a general decrease

3

with increasing age using the HRFtd approach, but an increase using the Fourier approach. This highlighted a potential weakness of the HRFtd model, in that the reduced number of functions may contribute to an exaggeration of the undershoot when derivatives are heavily weighted (more common in the younger age groups).

Looking across grey matter it was also identified that the HRFtd model captured the greatest number of significant voxels, followed by the Fourier set, then the HRFc model. Comparisons were run between the three oldest and the three youngest age groups, finding that when using the HRFc model more significant voxels were identified in the elderly cohort, but when using flexible models more were captured in the younger cohort. This was consistent with predictions made, as the elderly group demonstrated estimated HRFs more similar in timing properties to the HRFc model, increasing the likelihood that this approach was biased towards capturing signal in this cohort. Further evidence of this was found in that the canonical function showed greater relative weighting in the HRFtd model, as a function of age. In application therefore, using the HRFc model could lead to biased data when investigating issues such as hemispheric asymmetry reduction (Cabeza, 2002; Reuter-Lorenz et al., 2000) wherein greater bilateral activity is identified in the elderly. It should be noted regarding the ratio of significant voxels (young:elderly) there was only a marginal difference between flexible models, in favour of the Fourier set. In total this proved that flexible modelling is crucial when running age comparisons to minimise biasing of results towards any one group, and that in terms of application there was little separating the two flexible models tested.

7.1.2. Methodological Conclusion

Based on these findings, it was concluded that the time-course of the estimated HRF rarely conformed to that assumed by the HRFc model, consistent with evidence of variability across people, age-groups, tasks, and brain regions (Aguirre et al., 1998; Fabiani et al., 2014;

Handwerker et al., 2004; Hillman, 2014; Hutchison et al., 2013; Miezin et al., 2000; Ramnani & Henson, 2005; Sloan et al., 2010; Tarantini et al., 2017; Taylor et al., 2018; Ward et al., 2015). This supported a shift towards less biased flexible modelling approaches which are deemed better able to capture variable estimated HRF time-courses (Henson et al., 2001; Lindquist et al., 2009; Lindquist & Wager, 2007; Liu et al., 2017; Ramnani & Henson, 2005; Steffener et al., 2010) consistent with the data discussed in chapter 3. This carries an additional benefit in that it reduces the requirement for slice-timing correction (Josephs & Henson, 1999; Ramnani & Henson, 2005), which carries risks due to potential aliasing and interactions with head motion (Henson et al., 1999; Poldrack et al., 2011, pp. 41-42; Sladky et al., 2011). The results further caution against application of the HRFc model when running age comparisons, given evidence that with increasing age comes increasing conformity to the HRFc-modelled time-course. This was to such a degree that chapter 4 demonstrated a reversal of the effect of age regarding number of voxels, between flexible and inflexible modelling approaches. When choosing between flexible models it was considered that the Fourier set may be appropriate, being the least biased of the two, and with prefrontal regions such as the FPC (including the area defined as aPFC in chapter 3) and parts of the dlPFC showing a bias towards delayed timing properties (supported by Schacter et al., 1997) which may be better modelled via this approach. However, the cerebellum was also a crucial ROI and demonstrated greater capture of additional variance using the HRFtd model. Furthermore, given evidence that the HRFtd model better captured typical estimated HRF shapes, showed the least bias between age groups in chapter 4, captured the most significant voxels, and arguably represents a better balance of the bias-variance trade-off, it was selected for application.

7.1.3. Functional Application Overview

Chapter 5 identified not only that the elderly show a slower learning curve, but they also perseverate with previously attempted incorrect responses, and show a failure to implement positively reinforced responses (termed 'forgetting') consistent with (Levine et al., 1997; Salthouse, 1993; Salthouse & Kersten, 1993). It is important to state at this juncture that a failure to implement the correct response may actually be a failure to convert knowledge into the appropriate action, rather than forgetting of the association. Furthermore, the young but not the elderly demonstrated automation based upon change in pupil size, implying that the elderly cohort were under a greater cognitive load (Alnæs et al., 2014; Beatty & Kahneman, 1966; Bradshaw, 1967; Gavas et al, 2017; Hess & Polt, 1964; Hosseini et al., 2017; Huh et al., 2019; Kahneman & Beatty, 1966, 1967; Kahneman & Peavler, 1969). In terms of functional activity, looking specifically at correct trials it was identified that a candidate cerebellar region within CRUS I showed a significant positive BOLD response at presentation of the cue (consistent with Balsters & Ramnani, 2008, 2011 and Balsters et al., 2013) within the left hemisphere. There were also positive BOLD responses in dorsolateral areas 46 and 9/46, extending caudally into the frontal eye fields (FEFs), and with further evidence in the supplementary eye fields (SEFs). Mid dorsolateral prefrontal cortex (mid dlPFC) clusters were larger in the right hemisphere, consistent with a predominately contralateral connection to the left cerebellum (Kelly & Strick, 2003; Morales & Tomsick, 2015; Palesi et al., 2017). There were also interactions in the dlPFC driven by larger positive BOLD responses in the elderly. These were typically located more dorsally (area 9) and caudally (area 8), but did extend into area 9/46. This pattern of activity was consistent with the literature, as clusters were larger in the left hemisphere (Reuter-Lorenz et al., 2000) with areas 8 and 9 suggested as playing a compensatory role (Hinault et al., 2019). That the role was compensatory was further supported by effects surviving even

when a performance measure was included as a covariate. Age group x condition interaction trends were also identified in the cerebellum (including right CRUS I) which would be consistent with increased left lateralised activity in the mid dlPFC, however these did not survive FWE correction.

Critically, comparable effects of condition were identified across both age groups in multiple brain regions, including the caudo-lateral and medial superior frontal gyrus (SFG), paracingulate gyrus, cingulate gyrus (processing abstract rules; Mansouri et al., 2020), operculum (with a role in cognitive control; Higo et al., 2011), orbitofrontal cortex (OFC; goal choice and rewards; Burke et al., 2008; Bussey et al., 2001; Frank & Claus, 2006; Groman et al., 2019; Mansouri et al., 2020; Murray & Rudebeck, 2013; Passingham & Wise, 2012, pp. 97, 157-194; Schoenbaum et al., 1998, 2003; Schoenbaum & Roesch, 2005; Takahashi et al., 2009; Wallis et al., 2001), ventrolateral PFC (vlPFC; object processing; Passingham & Lau, 2022), superior-posterior parietal lobe (encoding visuo-spatial rules; Passingham & Wise, 2012, pp.157-194; Rao et al., 1997), and the striatum (linked to reward, saccade execution, and the decision to move; Gaymard et al., 1998; Graybiel, 2008; Hadj-Bouziane et al., 2003; Purves et al., 2008, pp. 460-474; Yin and Knowlton, 2006). This suggested that differences identified in dorsolateral regions were the exception, rather than the rule. A parametrically modulated analysis however found no evidence of a continuous reduction in magnitude over the course of learning (as in Balsters & Ramnani, 2011) within either the cerebellum or dlPFC (nor any other brain regions). As a result it cannot be inferred directly that the differences in magnitude between young and elderly groups were the result of a learning process which progresses more slowly in the elderly. It can however be stated that the elderly participants learned more slowly, showed less evidence of automaticity, and had evidence of potentially compensatory activity in the mid, caudal, and dorsal dlPFC, consistent with the literature.

7

Finally chapter 6 carried out a further investigation of the conditional visuo-oculomotor learning task using ultra-high field 7T fMRI. Learning was considered in two stages, firstly 'active learning' when the rule is not known and a trial-and-error approach is implemented (incorrect trials). Secondly there was 'established learning', deemed the period after a cue has been paired with the appropriate target and correct feedback has been given, with the association being 'stamped in' (correct trials preceded by a correct trial within the same rule). Therefore the analysis separated trials into these correct/incorrect conditions facilitating an analysis of differences between these two stages of learning, rather than the more refined parametric investigation applied in chapter 5, which was limited to correct trials only. Furthermore, each event within a learning trial was investigated, looking at the delivery of a cue, the execution of a response, and the receipt of feedback. Learning progressed approximately as anticipated, participants performing above chance and with performance improving across blocks. There were significant effects of condition in the cerebellum at the time of the cue, sat bilaterally and including both lobules HVI and CRUS I. These demonstrated positive BOLD responses generally linked to incorrect experimental trials, suggesting that in the early stages of learning there is greater cerebellar activity. This was consistent with Sendhilnathan & Goldberg (2020) who found cerebellar inactivation only impaired new learning, and Imamizu et al. (2000) who suggested multiple cerebellar internal models are narrowed down over learning, until only a select few accurate models remain. There was also dlPFC activity within experimental trials (typically at the time of the cue) including left mid dlPFC (area 9/46d), and bilateral SFG (area 9, activity specific to incorrect trials). This indicated a trend consistent with greater prefrontal activity early in active learning, thought to reduce as learning progresses (Jenkins et al., 1994; Jueptner et al., 1997; Passingham,1996; Raichle et al., 1994). There was further evidence of condition interacting

with error-status in the right dorsolateral area 8Av, and with event in the right dorsomedial SFG, extending onto the lateral surface (area 9).

It was anticipated that the frontopolar gyrus would be active at the time of feedback during correct trials, re-representing correct goals during reward (retrospective monitoring; Tsujimoto et al., 2012). However only cue-locked activity was found with effects of condition specific to incorrect trials, the cluster peaking in the left SFG but extending into Fp1 and Fp2. It was considered then that activity in the FPC may hold a role monitoring processing in downstream regions such as the dlPFC (Petrides, 2005; Ramnani & Owens, 2004; Ramnani, 2006, 2014). At the time of the cue there was also some posterior parietal activity, generally strongest within incorrect experimental trials (potentially forming a model representing targets in the external world; Ito, 2005), and occipito-temporal activity across trial types (putatively representing object information). There was also striatal activity related to main effects of condition and condition x event interactions, with some peaks having a role at the time of the cue and others at feedback. Also seen active at the time of the cue was the insular cortex, and at the time of feedback the posterior orbital gyrus. The implications of these findings are discussed in more detail below. At the time of the saccade (target presentation) there was much expected activity, extending across all four eye fields (Abzug & Sommer, 2017; Amiez & Petrides, 2009; Chen & Wise, 1995a; Schall et al., 1993) and the oculomotor vermis (OMV; Kojima & Soetedjo, 2018; Lefevre et al., 1998; Quaia et al., 1999). Additionally the main effect of condition did identify activity bordering on both the cingulate eye fields (CEFs) and FEFs, with evidence to support these being cue-locked.

7.1.4. Functional Application Conclusion

In summary, the regions seen to be active were consistent with a rostro-caudal gradient (Koechlin & Summerfield, 2007; Ramnani, 2006, 2014) whereby the frontal pole monitors activity in the dlPFC which corresponds to prospective encoding of goals

(Passingham & Wise, 2012, p. 157-194; Petrides, 2005). The dlPFC can communicate with both the vlPFC and occipito-temporal regions (Petrides & Pandya, 2002; Petrides, 2005) to access object information about the cue (object-processing evidenced in chapters 5-6), and also with parietal regions encoding visuo-spatial information regarding the target (Passingham & Wise, 2012, pp. 157-194). The mid dlPFC further communicates with the caudal dlPFC (area 8) which is itself connected to visuo-spatial parietal regions (Passingham & Lau, 2022; Petrides, 2005). Continuing with the rostro-caudal gradient it is suggested that the dlPFC encodes goals to inform a suitable response, supported by known outputs to the FEFs (Hutchison et al., 2012) which were active in chapters 5-6 and are known to connect with both the parietal lobe (Rivaud et al., 1994) and the superior colliculus (Purves et al., 2008, p. 460-507). Furthermore the SEFs were also active in chapters 5-6, and connect with the dlPFC, FEFs, and superior colliculus (Huerta & Kaas, 1990; Hutchison et al., 2012; Schall et al., 1993; Shook et al., 1990). See Figure 1 for an overview of eye field activity across chapters 5-6.
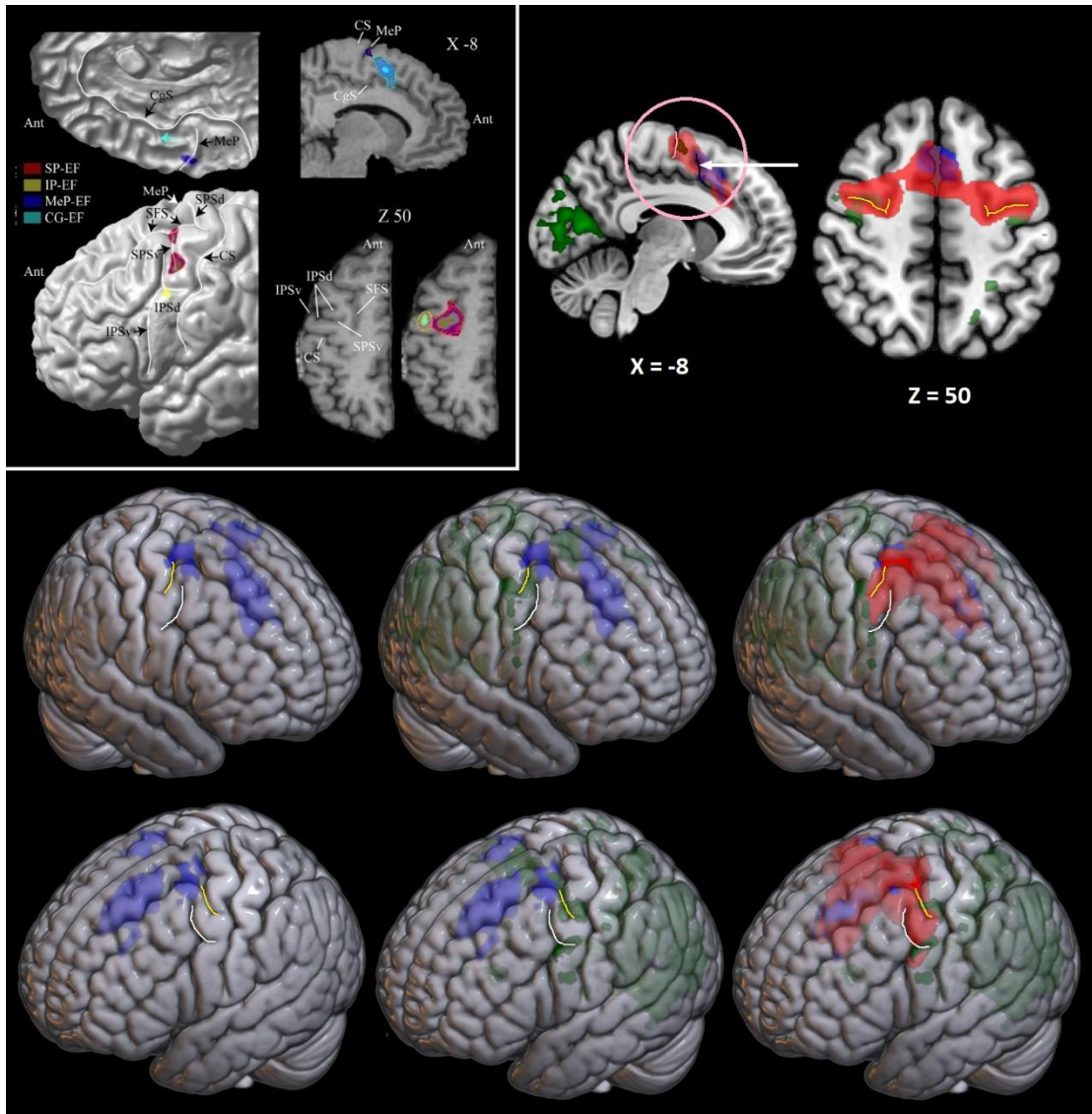
Figure 1. Activations from the effect of condition (cue-linked) in chapter 5 (**red**), the main effect of condition (cue and feedback events) in chapter 6 (**blue**), and at the time of target presentation in chapter 6 (**green**). The precentral sulcus is outlined in pink medially (sagittal plot), and on the lateral surface the ventral branch of the superior precentral sulcus is in yellow, and the dorsal branch of the inferior precentral sulcus is in white. The vertical branch of the cingulate sulcus is emphasised in black (sagittal plot) and indicated with a white arrow. In the top left is a figure copied from Amiez & Petrides (2009) with permission, identifying locations of the FEFs (SP-EF), PrEFs (IP-EF), SEFs (MeP-EF) and CEFS (CG-EF).

It is suggested that the SEFs process target information based on the position of the eye in space rather than eliciting the saccade (Abzug & Sommer, 2017; Schall et al., 1993),

determining a goal-oriented retinotopic coordinate which can be encoded in the FEFs where the response is initiated via the gaze centers (PPRF and rostral interstitial nucleus). This can be done either directly or via the superior colliculus (Jerde et al., 2012; Purves et al., 2008, p. 460-507; Segraves & Goldberg, 1987) and suggests that the SEF may play a role similar to the premotor cortex (PMC) in standard conditional visuo-motor learning (Chen & Wise, 1995b), with a hierarchy comprised of dlPFC > SEF > FEF (see Figure 2).
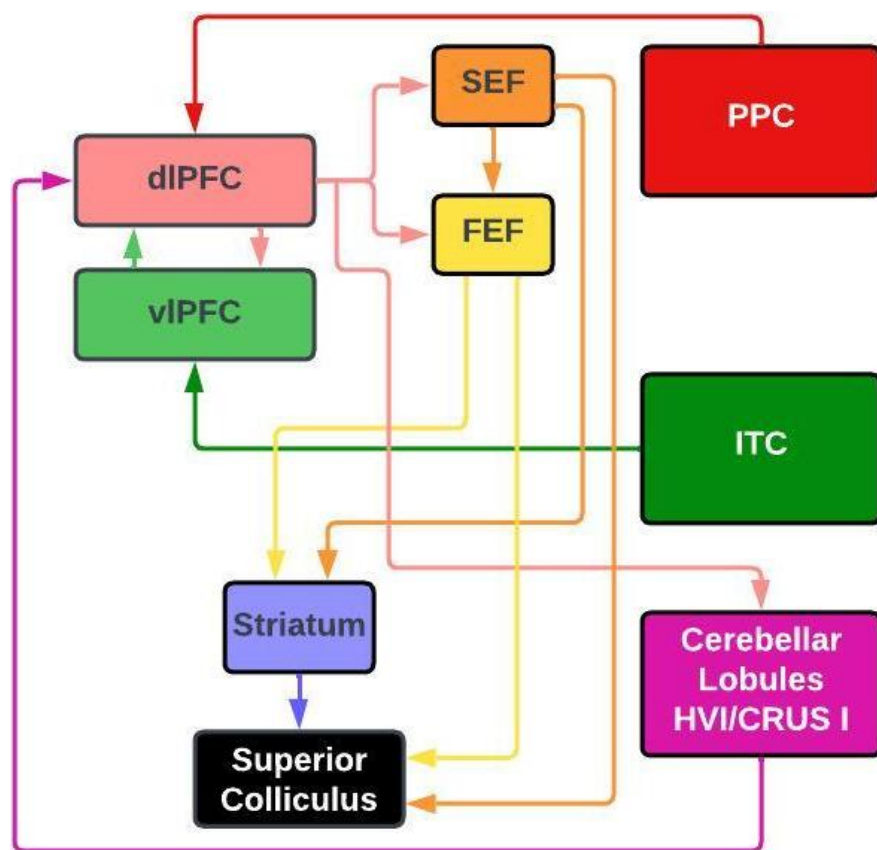
Figure 2. A simplified schematic taken from chapter 5. This represents the expected prefronto-cerebellar network (omitting structures such as the thalamus, substantia nigra pars reticulata, and cerebellar nuclei).

As discussed in chapter 5, clusters in the dlPFC which were commonly active across age groups (Figure 3 in red) peaked in area 46 (extending into 9/46) and were larger in the right hemisphere, consistent with the literature (Reuter-Lorenz et al., 2000). However

interactions extended both dorsally and caudally into area 9/46, 8, and 9 with larger clusters

generally seen in the left hemisphere, and greater magnitude positive BOLD responses in the

elderly participants (Figure 3 in green) consistent with Hinault et al. (2019). Activations in

chapter 6 pertaining to a main effect of condition (Figure 3 in dark blue) included the

frontopolar gyrus and SFG. As the effect of condition was strongest within incorrect trials

this activity could imply a role in the 'active learning' of novel unknown rules, which may

diminish as rules are further stamped in. There was also a main effect in left 9/46d (Figure 3

in dark blue, overlapping heavily with the left lateralised chapter 5 interaction), an event x

condition interaction in the SFG (Figure 3 in light blue, with a trend of being associated with

feedback), and an error-status x condition interaction in right area 8Av (Figure 3 in yellow,

with a trend of increased magnitude in incorrect trials). In total, there was much evidence of

more dorsal and caudally located activations in chapter 6 (areas 8, 9, and 9/46d). This may

be consistent with chapter 6 employing a more difficult task based on the number of rules

(ten versus four) and with trial durations more than halved (requiring faster responding).

Furthermore interactions in the elderly (chapter 5) typically extended into similar areas,

Hinault et al. (2019) suggesting recruitment of left lateralised areas 8 and 9 within the

elderly compensates in the face of distraction. This may indicate the elderly are continuing

to utilise circuitry involved in active learning of novel information, rather than circuitry

involved in encoding a learned response (established learning). This would be consistent

with the reduced learning rate and evidence of perseveration found within the elderly in

chapter 5. It was noted that chapter 6 did not identify peaks in area 46 proper, despite this

being seen across age groups in chapter 5 (Figure 1 in red). It remains possible that these

effects in chapter 5 were specific to established learning (consistent with Sakai et al., 2002),

and due to the increased task difficulty in chapter 6 it may be that no participants reached

the same level of established learning. Furthermore chapter 6 had a reduced sample size,

and if effects of condition during correct trials were more subtle the lack of activity specific to correct trials may be the result of a type 2 error.
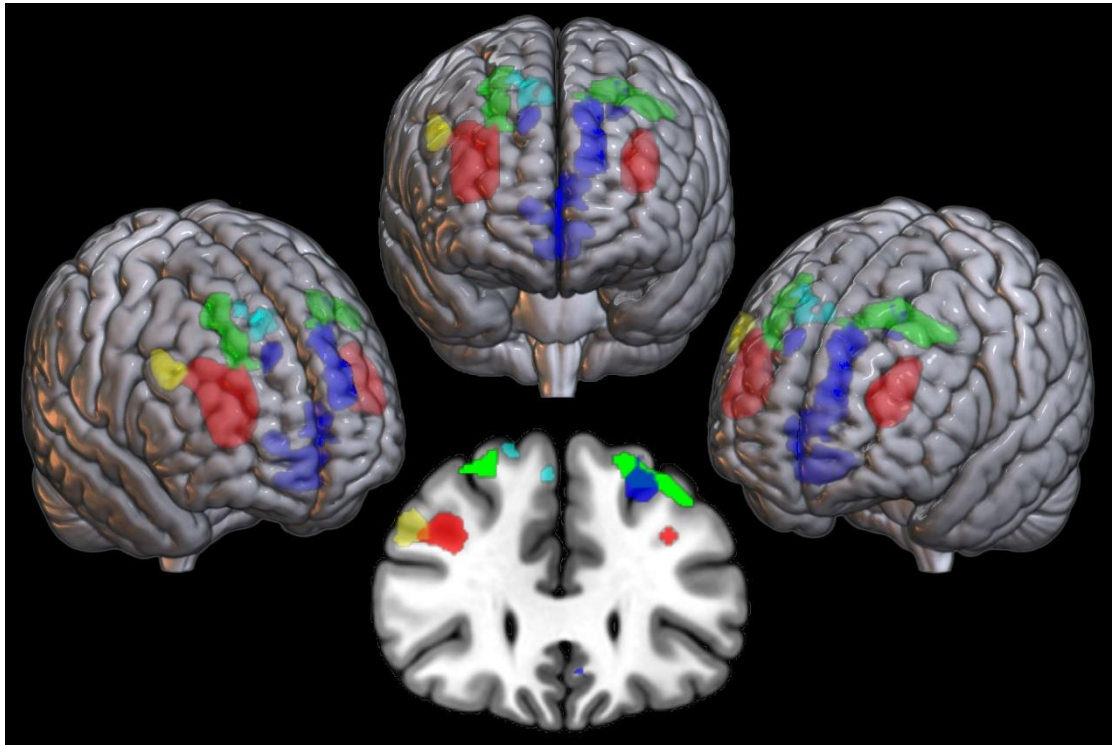
Figure 3. Activations surviving small volume FWE correction from chapters 5 and 6, centered around the dlPFC and overlayed upon the MNI brain. Activations from chapter 5 pertaining to the conjunction effect of condition across age groups are in **red**, and those pertaining to the age x condition interaction are in **green**. Activations from chapter 6 pertaining to the main effect of condition are in **dark blue**, the event x condition interaction in **light blue**, and the error-status x condition interaction in **yellow**.

As suggested in chapter 1, the cerebellum may also contribute to this learning process via the formation of internal models (Ramnani, 2006, 2014), with known connectivity between the mid dlPFC and lobule HVIIa, strongest in CRUS II in non-human primates (NHPs; Kelly & Strick, 2003) but dorsolateral connectivity stronger with CRUS I within humans (Buckner et al., 2011). Interestingly there is also evidence that when moving rostrally from the central sulcus there is a pattern of connectivity with anterior and posterolateral cerebellar lobules, converging on lobule HVIIa when the mid dlPFC is reached

(Longley et al., 2021) supported by O'Reilly et al. (2010). Therefore internal models in the

cerebellum have the capacity to represent prospective encoding in the dlPFC, but with

possible further representations at each stage of the suggested rostro-caudal axis. This is

supported by projections to the pontine nucleus from area 9 (Schmahmann & Pandya, 1995,

1997), and putatively from both the FEF and SEF (Huerta & Harting, 1984; Shook et al., 1990;

Stanton et al., 1988; Voogd et al., 2012). In this way the FEF and SEF may communicate with

the OMV (Voogd et al., 2012), with further projections evidenced from the superior

colliculus to the OMV (Brodal & Brodal, 1981; Frankfurter et al., 1976; Yamada & Noda,

1987). Therefore cerebellar internal models of SEF/FEF activity may be contributing more to

the saccadic response itself, than the goal underpinning it, supported by the OMV being

associated with oculomotor adaptation (Kojima & Soetedjo, 2018; Lefevre et al., 1998; Quaia

et al., 1999) and significant BOLD responses being limited to the time of target-presentation

in chapter 6. That different prefrontal and frontal regions can communicate with the

cerebellum may also explain why cerebellar activity at the time of the cue in chapters 5-6

was typically within lobules HVI and CRUS I, rather than sitting directly within HVIIa. It could

be that a bias towards activity within more caudal regions of the dlPFC is altering the

location of purported internal models in the cerebellum. Interestingly cerebellar lobules HVI

and HVIIa are also seen to be active in classical eyeblink conditioning within humans

(Ramnani et al., 2000), a separate behavioural model yet still within the realms of cerebellar-

dependent associative learning.

As mentioned above, that in chapter 5 the cluster identified in CRUS I was left

lateralised (Figure 4 in red) was consistent with greater right lateralised activity in the dlPFC

(evidenced in chapter 5 and the literature; Reuter-Lorenz et al., 2000), given the

predominately contralateral connection between these structures (Morales & Tomsick,

2015; Palesi et al., 2017). Cerebellar functional activity in chapter 5 was further supported by

overlap with left lateralised activations pertaining to main effects of condition in chapter 6
(Figure 4 in blue). However in chapter 6 there was also a right lateralised cluster which
tallied with the work of Imamizu et al. (2000), who suggests that in the early stages of active
learning (incorrect trials in chapter 6) there is a strong bilateral cerebellar effect, potentially
representing multiple internal models being recruited. However later in established learning
this is potentially reduced to a more specific lateralised cluster indicating a smaller set of
more accurate internal models. This is consistent with cerebellar activity in chapter 6
generally being associated with effects of condition within incorrect trials, as well as the
literature suggesting a trend of reduced activity with learning, across prefrontal and
cerebellar regions (Balsters & Ramnani, 2011; Imamizu et al., 2000; Jenkins et al., 1994;
Jueptner et al., 1997; Passingham, 1996; Raichle et al., 1994; Sendhilnathan & Goldberg,
2020). There was admittedly no parametrically modulated evidence of long term depression
(LTD) in chapter 5, but this was potentially due to the resulting Purkinje cell pause being
slow to develop (Johansson, 2019) or the linear model used being too simplistic. Any actual
change in signal may have been too subtle to survive thresholding, unlike the categorical
change between incorrect and correct trials in chapter 6. Furthermore, that the trends of
cerebellar interactions included slightly different lobules was consistent with dlPFC
interactions being more dorsally and caudally located, as per the rostro-caudal axis of
corticocerebellar connectivity discussed above. For example, right-lateralised dlPFC
interactions within area 9 may be consistent with the left-lateralised cerebellar cluster
(crossing the primary fissure into both lobules HV and HVI) showing a trend of greater
magnitude in the elderly. Interactions in the cerebellum must be cautiously interpreted
though, as they did not survive FWE correction.

Figure 4. Activations within the cerebellum from chapters 5 and 6 overlayed upon the MNI brain. Activations from chapter 5 pertaining to the conjunction effect of condition across age groups are in **red**, and those pertaining to the age x condition interaction (not surviving correction) are in **green**. Activations from chapter 6 pertaining to the main effect of condition are in **blue**.

In order for the cerebellum to function as an internal model a teaching signal is also required (Ramnani, 2006, 2014). There is theoretical potential for just such a signal to reach the cerebellum, with the VTA known to project to lobule HVII (Ikai et al., 1992, 1994) potentially via the inferior olive (Oades & Halliday, 1987), relevant as the VTA processes outcomes (Chowdhury et al., 2013; Ramnani, 2014). The OFC may contribute here as it connects with the VTA (Takahashi et al., 2009), projects to lobule VII (Suzuki et al., 2012), was active in chapter 5 at the time of the cue, and has a purported role in feedback and reward processing (Burke et al., 2008; Frank & Claus, 2006; Groman et al., 2019; Murray & Rudebeck, 2013; Takahashi et al., 2009). A role in feedback further aligned with posterior OFC activity in chapter 6 being associated with incorrect experimental trials during feedback. The OFC may therefore be generating expectations relating to subsequent behaviours (Schoenbaum et al., 1998, 2003; Schoenbaum & Roesch, 2005) and associating outcomes and decisions in such a way as to facilitate prospective encoding in the dlPFC (Passingham & Wise, 2012, pp. 157-194) supported by evidence of activity both at the cue and at feedback (consistent with; Tsujimoto et al., 2010, 2011a, 2011b, 2012). The insular cortex may also be relevant as it was active predominately at the time of the cue in chapter 6, with it possible that this region provides cue-locked feedback to the cerebellum via connectivity with the inferior olive (Swenson et al., 1989; Wise, 2008), further supported by effects in the insula being associated with incorrect trials. However this remains speculation, an alternative explanation being that the insula may be contributing to task updating and the guidance of attention to novel stimuli (Kurth et al., 2010; Uddin et al., 2017).

Further considering the VTA, this region is known to reciprocally connect with the striatum (Chowdhury et al., 2013; Loopuijt & Van der Kooy, 1985; Ramnani, 2014) the striatum also connecting with the superior colliculus (Purves et al., 2008, pp. 460-474) and receiving inputs from the FEF and SEF, which were both active in chapters 5-6 (Parthasarathy

et al., 1992). The striatum may still contribute to the reward components of learning

(Graybiel, 2008; Hadj-Bouziane et al., 2003; Yin and Knowlton, 2006), as well as holding a

potential role as part of a memorization loop mentioned in chapter 5. The aforementioned

loop purportedly functions whereby information from the dlPFC loops through the FEF,

caudate nucleus, substantia nigra pars reticulata (SNPR), thalamus, and back to the FEF, until

the response is called for (Gaymard et al., 1998) consistent with a striatal role in the decision

to saccade rather than execution of the saccade itself (Purves et al., 2008, pp. 460-474). It

was seen that in chapter 5 the caudate showed a significant effect of condition at the time of

the cue within correct trials (Figure 5 in red). This did not differ between age groups, and as

striatal outputs disinhibit both thalamic outputs and the superior colliculus (Purves et al.,

2008, pp. 460-474) it may be that the striatum is actively facilitating the output of

information, potentially pertaining to eye movements and/or reward. It was also seen in

chapter 6 that striatal activity was time locked to both the cue and feedback (Figure 5 in blue

and green respectively), with follow up tests suggesting this was predominately driven by

effects of condition within incorrect trials. This implied that the striatum contributed to

both cue and feedback processing, with stronger activation in the earlier stages of active

learning. This supports a role in providing a teaching signal in the form of error signals

transmitted to the cerebellum via the VTA (and potentially the inferior olive; Oades &

Halliday, 1987), consistent with striatal function (Hull, 2020; Kostadinov et al., 2019; Schultz,
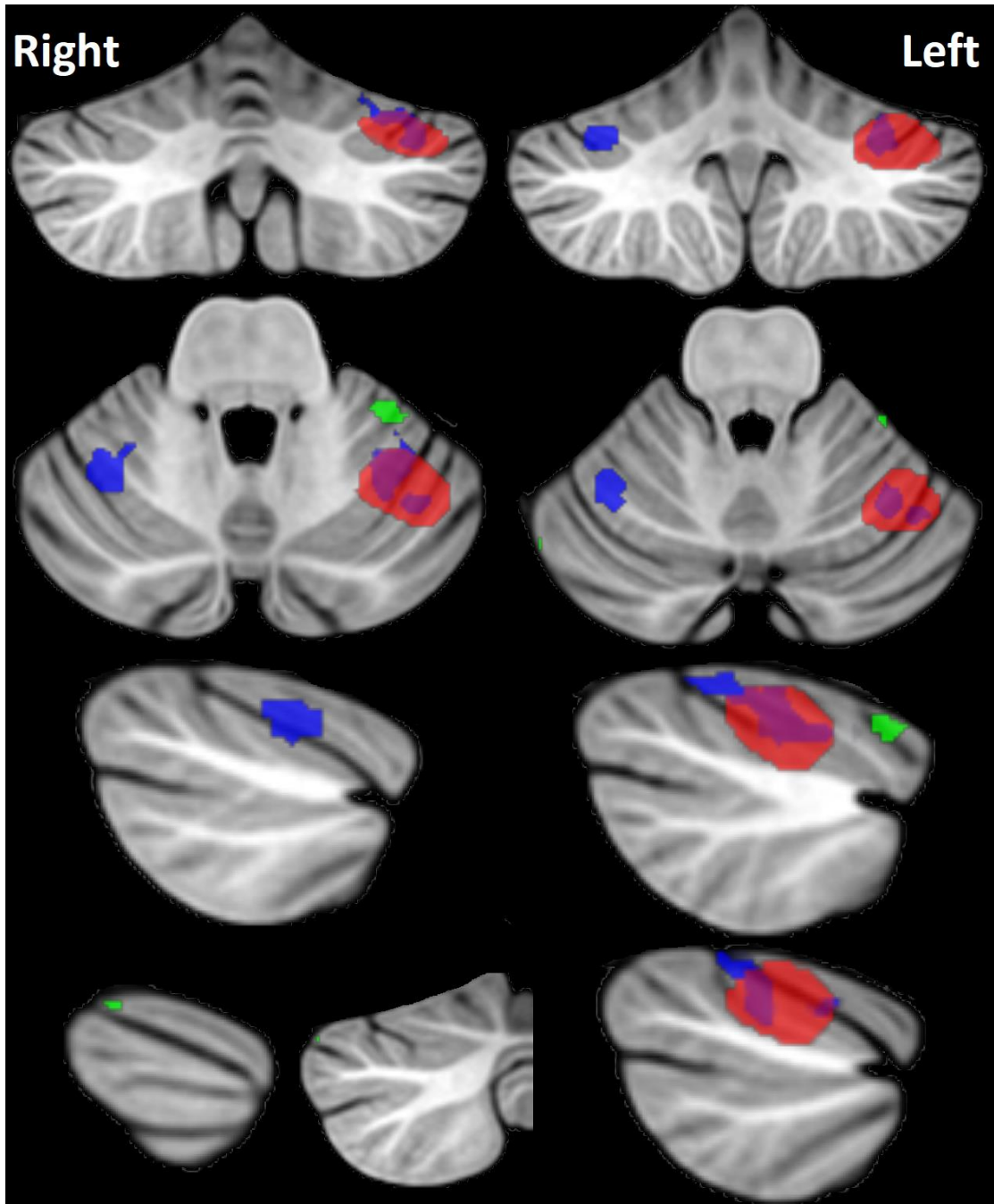
2013).
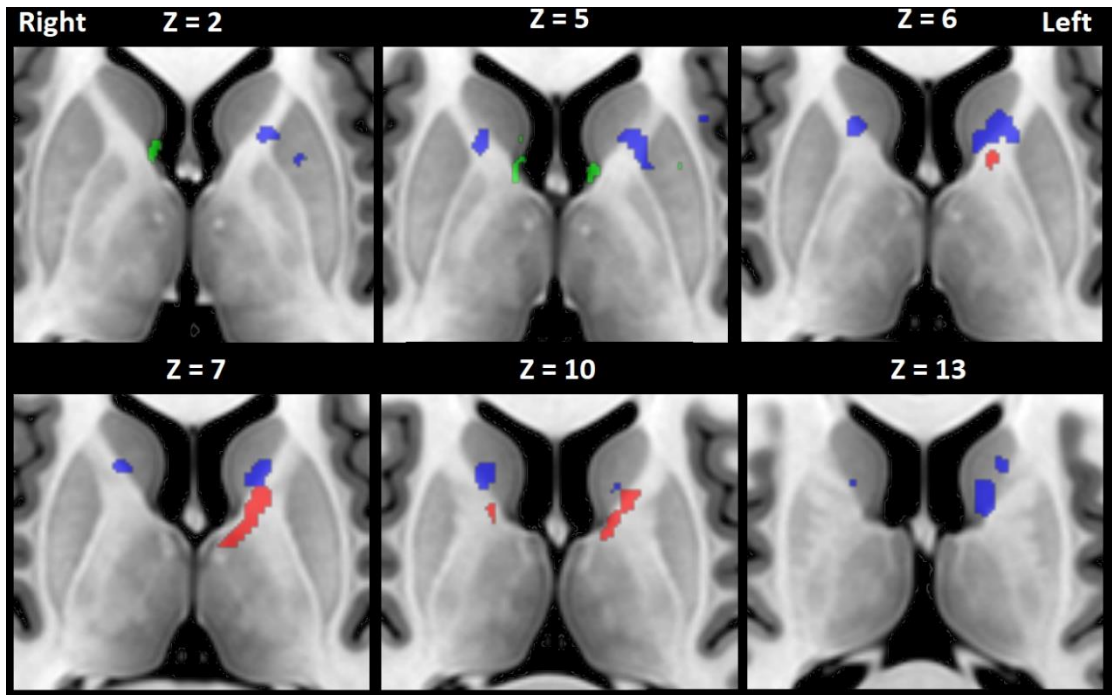
Figure 5. Activations surviving FWE correction within the striatum from chapters 5 and 6 overlayed upon the MNI brain. Activations from chapter 5 pertaining to the conjunction effect of condition across age groups are in **red**. Activations from chapter 6 pertaining to the main effect of condition are in **blue**, and event x condition interactions are in **green**.

7.2. General Conclusion

In conclusion then, it can be stated that there is support for a rostro-caudal axis of activity in the PFC pertaining to conditional visuo-oculomotor learning, based on functional activity in chapters 5-6, and evidence of relevant connectivity in the literature. There is also support for a dlPFC-Lobule HVIIa network given concurrent activation of regions evidenced as being connected. That it was the dlPFC projecting to CRUS I (rather than the similarly connected posterior parietal cortex (PPC); Buckner et al., 2011; O'Reilly, et al., 2010) was supported by peak coordinates from the O'Reilly study being located near the left CRUS I cluster in chapters 5-6, and either within or neighbouring the dlPFC clusters in chapter 5 (interaction and conjunction analyses), see Figure 6. Additionally the parietal cortex has weaker connections to CRUS I (O'Reilly et al., 2010), and the peak parietal coordinates did

not overlap with those in the conjunction analysis in chapter 5 or main effects in the

precuneus within chapter 6.
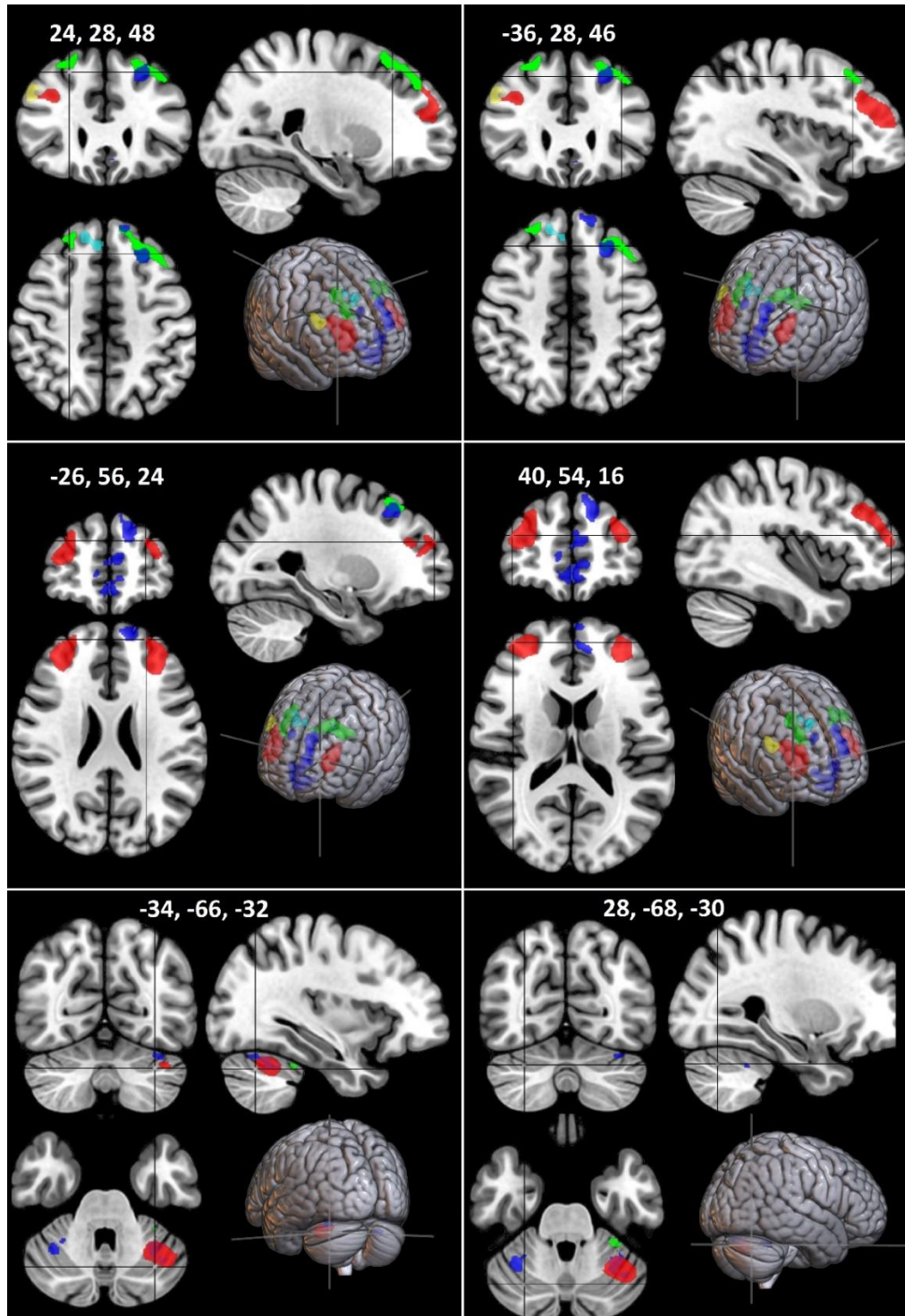
Figure 6. Effects of condition (chapter 5 in **red**, chapter 6 in **blue**), age x condition interactions from chapter 5 (**green**), event x condition interactions from chapter 6 (**light blue**) and error-status x condition interactions in chapter 6 (yellow). Cross-hairs indicate location of peak MNI coordinates regarding prefronto-cerebellar connectivity, as per O'Reilly et al. (2010).

Returning to the core focus of the thesis (namely cognitive ageing) the *ABC* triangle of factors (Raz & Lindenberger, 2011) and the, **where**, **what**, and **how** questions asked at the beginning of chapter 1 are considered. It can be inferred that **A***ge* differences in performance were found between an 18-30 year old cohort and a 65-80 year old cohort. Considering which *Brain Structures* these were associated with (also addressing the question of **where** age differences can be traced to), interactions were only identified in the dlPFC, specifically areas 9, 9/46, and 8. As discussed above and in chapter 5, these are consistent with compensatory activity in the face of distraction (Hinault et al., 2019). Although this was not a distraction study, it is likely that the MRI environment could be deemed distracting, supported by an effect of memory performance reduction when in the scanner (Gutchess & Park, 2006). Regarding *Cognition* and answering the question of **what** age differences exist, the elderly were impaired in terms of conditional visuo-oculomotor learning, showing a slower learning rate. This could have been consistent with the processing speed theory of cognitive ageing which suggests greater repetition is required (Salthouse, 1993, 1996), however there was no observed effect of processing speed accounting for the age-related decline in performance. That processing speed did not mediate performance goes against the common cause hypothesis too, in that sensory functioning did not predict cognitive functioning (Lindenberger & Baltes, 1994; Park & Schwarz, 1999, p. 17), consistent with suggestions that effects of cognitive ageing are likely to be context-dependent (Baudouin et al., 2019). Upon investigation, performance impairments within the elderly appeared to be caused by both perseveration and a failure to provide the correct response post reinforcement (as per; Levine et al., 1997; Salthouse, 1993; Salthouse & Kersten, 1993).

Regarding what differential dlPFC activity means in terms of the cause of cognitive ageing (answering the question of **how**), it is considered that the finding aligns with

hemispheric asymmetry reduction, whereby lateralised activity becomes increasingly bilateral in the elderly (Baltes & Lindenberger, 1997; Cabeza, 2002; Garrett, 1946; Reuter-Lorenz et al., 2000; Hinault et al., 2019). It is suggested that this is compensatory, supported by the literature (Hinault et al., 2019; Reuter-Lorenz et al., 2000) and evidence in chapter 6 that dorsal and caudal dlPFC activity is generally more prevalent in early active learning. Further support comes from additional elderly-specific functional activity in chapter 5 being within regions that are, a) known to connect with the hippocampus via the retrosplenial cortex and so potentially involved in memory (Petrides & Pandya, 1999; Petrides, 2005), b) have a role in cognitive inhibition (Mansouri et al., 2020; West, 1996), and c) contribute to prospective encoding (Passingham & Wise, 2012, pp. 157-194). This suggests persistence of an active rather than an established learning process, and potentially a failure of response inhibition (potentially contributing to the elderly tending to learn a smaller number of rules to a relatively greater degree) perhaps necessitating increased neural recruitment (Levine et al., 1997). Although failed response inhibition is suggested based on functional data and perseveration, responses were not differentially biased between age groups based upon previous/other positively reinforced responses (pre-potent responses as per West, 1996). It remains possible that additional dorsolateral activity may reduce the impact of impaired inhibitory control, however these mixed findings at the behavioural level mean this thesis cannot draw firm conclusions regarding the inhibition theory of cognitive ageing (Campbell et al., 2020). It is also relevant to consider that in the PFC Genovesio, Brasted & Wise (2006) found that past and future goals are represented by independent neurons, helping differentiate the two (e.g. separating a goal linked to the previous trial from a goal linked to the current trial). Therefore additional activity in some prefrontal regions could still lead to perseveration if increasing the risk of past cue-linked goals being confused with the current cue-linked goal at a neural level. If so this could be an incidental by-product of additional

dorsolateral activity (potentially still resulting in a net gain) or it could be that regions such as the dlPFC actively compensate for this effect in other brain areas. However, evidence in chapter 5 suggests that increased activity/magnitude in the elderly may not be directly implicated in reduced performance.

Interestingly age x condition interactions were not seen in many of the regions that were nonetheless active in chapters 5-6 at the time of the cue, and therefore likely to contribute to cognitive components of the task. These include areas potentially corresponding to reward/feedback (such as the insula, OFC, and striatum; Mansouri et al., 2020; Passingham & Wise, 2012, pp. 97, 157-194; Schoenbaum et al., 1998, 2003; Schoenbaum & Roesch, 2005; Swenson et al., 1989; Tsujimoto et al., 2011b, 2012), retrospective monitoring and coordination of cognitive processes (such as the FPC; Petrides, 2005; Ramnani & Owen, 2004; Tsujimoto et al., 2011a, 2012), response preparation (such as the SEFs and FEFs; Armstrong et al., 2009; Blanke et al., 1999; Bloedel et al., 1996, p. 266-275; Chen & Wise, 1995a; Curtis & Connolly, 2008; Rivaud et al., 1994; Schall et al., 1993; Segraves & Goldberg, 1987), and visuo-spatial information processing (such as regions of the parietal cortex; Burr et al., 2010; Merritt et al., 2010; Passingham & Wise, 2012, pp.157-194; Rao et al., 1997). This functional data suggests that processing of visual information and oculomotor execution are relatively unaffected, supported by control condition reaction times also being comparable between age groups. Therefore, the evidence of age x condition interactions specifically within the dlPFC implicates processes such as inhibition, attention, and spatial working memory, which inform prospective encoding (Cabeza, 2000; Hinault et al., 2019; Mansouri et al., 2020; Passingham & Wise, 2012, pp. 157-194; Reuter-Lorenz et al., 2000). Based on the performance deficit, this interaction may indicate an impairment within one or more of these functions, which is potentially improved when compensated by increased bilateral activity in the relevant brain areas. Working memory is

specifically considered, as it is a key role of the dlPFC (Goldman & Rosvold, 1970; Mansouri et al., 2020; Passingham & Wise, 2012, p. 157-194; Sakai et al., 2002) helping to guide focussed attention by prospectively encoding the spatial target (Rainer et al., 1998). This is in accordance with fluid intelligence declining over the adult lifespan (Gajewski et al., 2018; Park & Schwarz, 1999, pp. 43-54; Salthouse, 2010) which includes both working memory and inhibition (Diamond, 2013; Ferguson et al., 2021; Roca et al., 2010). Given the localised nature of age-differential activity in the brain this thesis primarily finds support for the prefrontal-executive theory, which suggests the PFC shows greater age-related decline than other structures (West, 1996, 2000), supported by the anatomical findings of past studies which isolate this to dorsolateral regions (Huttenlocher, 1979; MacPherson et al., 2002; Raz et al., 1997). This is also consistent with West (1996) suggesting that the dlPFC has a specific role in prospective memory, their description of which aligns with prospective encoding as discussed in this thesis.

Further considering the question of **how,** it is plausible that this suggested deficit in prospective encoding may be partially attributable to an impairment in the proposed dlPFC-Lobule HVIIa mechanism, with trends of cerebellar interactions (see Figure 4 in green) being consistent with impaired LTD over increasing age. This aligns with the non-human literature (Woodruff-Pak et al., 2010), impaired cerebellar-dependent eye-blink conditioning in humans (Bellebaum & Daum, 2004), age-related atrophy in lobules HVI-HVIII and the OMV (associated with working memory, attention, and visual processing via frontoparietal networks; Gellersen et al., 2021), and general age-effects of reduced white matter density, synaptic density, and soma size across the brain (Dickstein et al., 2007; Price et al., 2017). It is also consistent with cerebellar activity being identified on earlier incorrect trials in chapter 6, suggesting the elderly show a trend during supposedly established learning (correct responding) that is functionally similar to activity expected in earlier incorrect responding (as

per Imamizu et al., 2000). Trend remains the operative word here, as these cerebellar

interactions in chapter 5 did not survive FWE correction, and so require replication. This

means it cannot be definitively concluded that the cerebellar mechanism is impaired, only

that the dlPFC shows age-differentiated activity, consistent with reduced evidence of

automaticity in the elderly (chapter 5) and increased functional activity generally being

associated with incorrect trials (chapter 6).

Putatively compensatory dlPFC activity in the elderly may therefore be attributable

to this cohort 'working harder' at a neural level to maintain attention towards a visuo-spatial

target and prospectively encode the goal. However although activations in chapter 6 suggest

this, it cannot be directly claimed that differences between age groups are the result of

neural activity in the young cohort reducing more rapidly between incorrect and correct

trials (which would suggest the same mechanism is used but progresses more slowly in the

elderly). The alternative is that greater functional activity during correct trials within the

elderly was the result of elderly-specific activations (potential compensation for the

mechanism), however there was overlap with activations in chapter 6, suggesting that these

are not just seen within older age groups. That said, the chapters are not directly

comparable due to increased difficulty in the chapter 6 task. This may be responsible for

these additional activations, forcing even young adults to work harder to maintain attention

to and prospectively encode the goal, in a manner comparable to the elderly cohort during

the less complex task in chapter 5. This could not be investigated directly in chapter 5 as

there were not enough incorrect trials for modelling, and chapter 6 comprised only a young

cohort, but would form an important area of future research. In order to consider all

options, and based upon evidence in the literature of impaired connectivity and reduced

conduction speed (Deary et al., 2009; Dickstein et al., 2007; Price et al., 2017; Rabbitt &

Lowe, 2000; Xi et al., 1999), potentially compensatory dlPFC activity (based on chapters 5-6

27

and with similar cerebellar trends), and a general effect of delayed haemodynamic activity across a range of grey matter structures in chapter 4 (whether neural in origin or not), may support a core-biological age-related change also contributing to age-related deficits in learning (as discussed in chapter 1). However, that age x condition interactions were so localised to the dlPFC primarily supports the prefrontal-executive theory of cognitive ageing.

7.3. Strengths, Implications, Limitations, and Future Research

A key strength of this thesis is deemed to be the systematic manner in which modelling approaches were investigated in chapter 3, helping inform a further investigation of age-related differences in the timing properties of the estimated HRF in chapter 4. This made use of the CamCAN dataset (comprising more than 500 healthy adults aged 18-87; Shafto et al., 2014; Taylor et al., 2017) and highlighted that the canonical model was biased in favour of capturing variance within HRFs that show a time-course typical of the elderly. As a result all subsequent choices made in chapters 5-6 utilised flexible modelling approaches. Furthermore these results have the potential to inform the functional study of cognitive ageing generally, with the conclusion that the HRFtd formed the best compromise regarding the bias-variance trade-off. The application of this could also extend across users of functional neuroimaging generally, when considering different estimated HRF time-courses across people, age-groups, tasks, and brain regions (Aguirre et al., 1998; Fabiani et al., 2014; Handwerker et al., 2004; Hillman, 2014; Hutchison et al., 2013; Miezin et al., 2000; Ramnani & Henson, 2005; Sloan et al., 2010; Tarantini et al., 2017; Taylor et al., 2018; Ward et al., 2015). There are of course limitations, one being that only the three models were investigated, and so it cannot be said that the HRFtd approach is the best on the market. This was a trade-off and so forms both a strength and a limitation, given that a whole brain investigation was carried out, rather than comparing a large number of models at a set of peak coordinates. Finally, as electrophysiological measures were not taken, the study could

not differentiate between altered neuronal activity and altered neurovascular coupling in chapter 4, nor could it confirm whether additional activity found across chapters 3-4 was meaningful or just noise introduced by flexible models having fewer assumptions (Friston et al., 1998b; Josephs et al., 1997). In general this was not deemed critical, as the purpose was to investigate whether age-related differences exist irrespective of their cause. However future research could still benefit from investigating across the brain to determine how much age-related differences are attributable to neuronal activity versus differential neurovascular coupling, alongside further comparisons between modelling approaches (such as the inverse logit function and FLOBS; Lindquist & Wager, 2007; Woolrich et al., 2004). This is all with an aim to best harness the power of fMRI.

Given the current ageing population (World Health Organisation, 2018), that the thesis investigated cognitive ageing is also deemed a core strength. It is important to understand how and why age-related deficits present, to best tailor social structures to accommodate them, with this pertaining to issues such as driving, making informed choices regarding health, will-writing, and upskilling at work (Park & Schwarz, 1999, pp. 217-232). Considering the driving example, statistics pertaining to road traffic accidents show that the elderly have greater rates of crashing relative to distance travelled, with this especially prominent in complex situations (Wood, 2002) such as turning against oncoming traffic (Chandraratna & Stamatiadis, 2003). Although not directly related, driving involves visuo-spatial processing, and the conversion of visual information into goal-oriented actions in a way comparable to both visuo-motor and visuo-visual tasks. As it was identified in chapter 5 that the elderly struggled to learn saccadic eye movements conditional upon novel visual cues, it is reasonable to suggest that when driving in novel, complex, or dynamic situations a similar deficit could contribute. For this reason it would be of interest to extend the work in chapters 5-6 to include both eye-tracking studies in a driving simulator (to ascertain if gross

oculomotor errors are presenting in the elderly) and also to study driving scenarios in fMRI to confirm, a) whether the same errors present, and b) whether functional brain activity differs between age groups in a way that may shed light upon the purported mechanism. Through this it may be possible to inform how new junctions are constructed, how signage is arranged, or how navigation services deliver instructions, in an effort to reduce crash statistics and maintain the independence of the elderly.

A further strength of the thesis was that functional activity pertaining to conditional learning was gathered across age groups in a 3T MRI scanner (chapter 5), and across both trial types and intra-trial events in a 7T MRI scanner (chapter 6), with well adapted control conditions (chapter 6 using a control providing feedback yoked to the experimental condition). This meant conclusions were better informed than would be possible from either study alone, as both the mechanism in general, and the mechanism in relation to ageing were relevant. It also meant findings could be replicated, as seen in the left cerebellar lobules HVI and CRUS I. This highlights a limitation however, as it would have been preferable to investigate all trial types and events across age groups. This was not feasible as the study duration in chapter 5 was shortened to ensure participants (especially the elderly) did not get uncomfortable in the scanner, and the task was simplified to ensure both age groups would provide a sufficient number of correct trials for analysis. For example, in chapter 5 there were four rules to learn, and three potential targets, with the task lasting ~30 minutes. In chapter 6 where only a young cohort was tested there were still three targets, but ten rules to learn, and the protocol lasted approximately twice as long. Based on the feedback from elderly participants it was unlikely they would have been comfortable remaining in the scanner beyond 45 minutes (including anatomical scans and field mapping), and given reduced performance the ten rule task would likely prove overwhelming. Some of these issues could be avoided in future research by inviting participants back in and running

the learning paradigm over multiple sessions, however this incurs a risk of differences

between age groups in terms of retention over the delay between visits, and was not

possible due to time and budgetary constraints. Investigation of all events could more easily

be carried out whilst comparing age groups, and was only omitted due to, a) insufficient

time, and b) the thesis being primarily interested in cognitive (and so cue-locked) rather than

oculomotor impairments. Future studies may also benefit from recruiting larger samples of

each age cohort, so that both can be split into high and low performers. This would facilitate

investigation of an age x performance interaction, which may shed greater light on whether

additional activity in the elderly truly was compensatory. A median split based upon

performance was attempted with the elderly cohort in chapter 5, however there were no

significant results, potentially due to the small sample size.

That eye-tracking was applied in both chapters 5 and 6 further provided novel

information such as pupillometry data, and enabled investigation of the learning of an

oculomotor response which is well characterised functionally and neuroanatomically (Amiez

& Petrides, 2009; Brodal & Brodal, 1981; Frankfurter et al., 1976; Jerde et al., 2012; Kojima &

Soetedjo, 2018; Lefevre et al., 1998; Purves et al., 2008, p. 460-507; Quaia et al., 1999;

Segraves & Goldberg, 1987; Sommer & Wurtz, 2004; Voogd et al., 2012; Yamada & Noda,

1987). This also meant comparisons could be drawn between this thesis and studies carried

out using the hand as an effector (Balsters & Ramnani, 2008, 2011; Balsters et al., 2013),

with similar regions of the cerebellum found to be active, further supporting the role of this

region in the encoding of the goal, rather than the action itself. Use of eye-tracking when

carrying out ultra-high field 7T fMRI however did present with difficulties (discussed in

chapter 6). Consequently due to the small sample size, an absence of significant effects in

chapter 6 cannot be meaningfully interpreted, as the risk of type II errors was heightened.

On the other hand, that significant results were found in this small sample, surviving FWE

correction, some of which replicated the work in chapter 5, supports these being genuine, strong effects. Eye-tracking complications in chapter 6 also meant that an originally planned analysis looking at how error trials impact subsequent correct trials (akin to work by Medina & Lisberger, 2008) could not be carried out, due to very low numbers of events in the regressors. It is the opinion of the author that this would be the next step to investigate how the cerebellar mechanism operates during conditional visuo-oculomotor learning, with comparisons between age groups potentially yielding further illuminating results.

Although the results of the studies in chapters 5-6 do support a rostro-caudal axis in the PFC (Petrides, 2005; Ramnani, 2006, 2014) as well as a role of dlPFC-Lobule HVIIa connectivity (Balsters et al., 2010, 2014; Buckner et al., 2011; Diedrichsen et al., 2009; Kelly & Strick, 2003; O'Reilly et al., 2010) pertaining to prospective encoding (Goldman & Rosvold, 1970; Passingham & Wise, 2012, pp. 157-194; Petrides, 2005; Sakai et al., 2002), and potentially connectivity between the eye fields and the OMV (Lynch et al., 1994; Shook et al., 1990; Stanton et al., 1988; Voogd et al., 2012), these all have the potential to be incidental. A strength is that the relevant connectivity has been proven based upon the literature and is in accordance with the functional activity described here. However future work may benefit from running dynamic causal modelling to ascertain if the proposed directions of effect are supported. This could even be applied to the existing datasets collected as part of this thesis, and has only been omitted due to time constraints. It is also worth noting a further limitation pertaining to chapter 5 and attribution of causation. Here differences between age groups regarding behavioural performance cannot be causally attributed to differences in functional activity. For example, the dlPFC could be more active in the elderly cohort as a direct result of a localised impairment, or it could be more active because participants progressed less far through learning due to a separate/global impairment. Specifically, the trends of cerebellar activity being of greater magnitude in the

elderly (chapter 5) may be caused by an impaired dlPFC-Lobule HVIIa mechanism, but could similarly be caused by an impaired useful field of view (Dunterman et al., 2019; Edwards et al., 2006; Sekuler et al., 2000). This may result in active learning of new information progressing more slowly, and so learning is less entrenched by the dlPFC-Lobule HVIIa mechanism due to fewer correct trials being present. It could be that the putative dlPFC-Lobule HVIIa mechanism works and will entrench learned information well once the impaired active learning phase is over. To check for this, in chapter 5 the average number of included correct trials per rule was included as a covariate. As main effects and interactions remained significant, the suggested differences seen between age groups transcended different levels of progression through the entrenching process. This also implied that the additional activity seen in the elderly (consistent with hemispheric asymmetry reduction; Baltes & Lindenberger, 1997; Cabeza, 2002; Garrett, 1946; Reuter-Lorenz et al., 2000; Hinault et al., 2019) was not linearly associated with performance. Therefore this additional check leant support to a compensatory role specifically within the elderly, in line with the literature (Hinault et al., 2019; Reuter-Lorenz et al., 2000).

7.4. Discussion Summary

In summary, this thesis identified that the blood oxygen level dependent (BOLD) response typically had timing properties that differed from those assumed when using the HRFc model, supporting the use of flexible modelling. This was even more relevant when comparing age groups, as older participants typically showed a time-course more comparable to the HRFc model, meaning fixed modelling was more likely to identify significant haemodynamic activity within this demographic. Flexible modelling however was not a simple fix, as flexible approaches had differing strengths and weaknesses. The HRFtd model was deemed to produce the best compromise for general modelling across the brain, and comparisons between age groups. With this taken into consideration, the thesis next

identified that during a conditional visuo-oculomotor learning task there was support for the role of a hierarchically organised frontal network of brain regions. This is thought to utilise working memory to convert visual inputs into spatially guided oculomotor responses, tailored to the context. Furthermore, the role of a prefronto-cerebellar network within the corticocerebellar system was supported, given activity within lobule HVIIa and the dlPFC. There was additional evidence of elderly participants showing reduced performance and slower learning rates, as well as additional recruitment of dorsolateral prefrontal regions thought to be associated with compensation of age-related dysfunction. Trends of age x condition effects in the cerebellum were also found, but as these did not survive correction firm conclusions regarding age-related impairment of the prefronto-cerebellar network cannot be made, pending further investigation. That differences in timing properties of the BOLD response occurred over a range of brain regions lends tentative support to a core biological deficit in cognitive ageing, however as associations were not made with performance in chapters 3-4 this cannot be confirmed as a causal factor in age-related deficits. Fundamentally, the results do strongly support the prefrontal-executive theory (West, 1996, 2000) as differential brain activity was not only specific to the PFC, but to dorsolateral regions deemed to be involved in converting knowledge into the appropriate action, supported by known neural degeneration in this region. These conclusions were made possible by use of cutting-edge eye-tracking and imaging methods, making this thesis uniquely placed to investigate **where** in the brain effects of cognitive ageing can be localised to, whilst also considering **how** these lead to age-related deficits. This utilised merging of data pertaining to differences in the time-course of the HRF, the contribution of processing speed, evidence supporting the prefrontal executive theory, and an expanding literature regarding the role of the cerebellum in cognition.

References

Abrams, R. A., Meyer, D. E., & Kornblum, S. (1989). Speed and accuracy of saccadic eye movements: characteristics of impulse variability in the oculomotor system. Journal of Experimental Psychology: Human Perception and Performance, 15(3), 529-543. https://psycnet.apa.org/doi/10.1037/0096-1523.15.3.529

Abzug, Z. M., & Sommer, M. A. (2017). Supplementary eye fields. *Reference module in neuroscience and biobehavioral psychology*. http://dx.doi.org/10.1016/B978-0-12-809324-5.02941-2

Acquiring and using field maps — LCNI. (n.d.). Retrieved October 17, 2022, from https://lcni.uoregon.edu/kb-articles/kb-0003

Aguirre, G. K., Zarahn, E., & D'Esposito, M. (1998). The variability of human, BOLD hemodynamic responses. *Neuroimage*, *8*(4), 360-369. https://doi.org/10.1006/nimg.1998.0369

Albinet, C. T., Boucard, G., Bouquet, C. A., & Audiffren, M. (2012). Processing speed and executive functions in cognitive aging: How to disentangle their mutual relationship?. *Brain and cognition*, *79*(1), 1-11. https://doi.org/10.1016/j.bandc.2012.02.001

Albus, J. S. (1971). A theory of cerebellar function. *Mathematical Biosciences*, *10*(1-2), 25-61. https://doi.org/10.1016/0025-5564(71)90051-4

Albus, J. S. (1989). The Marr and Albus Theories of the Cerebellum: Two Early Models of Associative Memory. *Research Inst. for Advanced Computer Science, Cerebellar Models of Associative Memory: Three Papers from IEEE COMPCON Spring 1989*. https://doi.org/10.1109/CMPCON.1989.301996

Alnæs, D., Sneve, M. H., Espeseth, T., Endestad, T., van de Pavert, S. H. P., & Laeng, B. (2014).

Pupil size signals mental effort deployed during multiple object tracking and predicts

brain activity in the dorsal attention network and the locus coeruleus. *Journal of*

vision, *14*(4), 1-20. https://doi.org/10.1167/14.4.1

Amiez, C., & Petrides, M. (2009). Anatomical organization of the eye fields in the human and

non-human primate frontal cortex. *Progress in neurobiology*, *89*(2), 220-230.

https://doi.org/10.1016/j.pneurobio.2009.07.010

Armstrong, K. M., Chang, M. H., & Moore, T. (2009). Selection and maintenance of spatial

information by frontal eye field neurons. *Journal of Neuroscience*, *29*(50), 15621-

15629. https://doi.org/10.1523/JNEUROSCI.4465-09.2009

Arthurs, O. J., & Boniface, S. J. (2003). What aspect of the fMRI BOLD signal best reflects the

underlying electrophysiology in human somatosensory cortex?. *Clinical*

Neurophysiology, *114*(7), 1203-1209. https://doi.org/10.1016/S1388-

2457(03)00080-4

Ashburner, J., & Friston, K. J. (2011). Diffeomorphic registration using geodesic shooting and

Gauss–Newton optimisation. *NeuroImage*, *55*(3), 954-967.

https://doi.org/10.1016/j.neuroimage.2010.12.049

Ashburner, J., Barnes, G., Chen, C., Daunizeau, J., Flandin, G., Friston, K., ... & Phillips, C.

(2020). SPM12 manual. *Wellcome Centre for Human Neuroimaging, London, UK*.

https://www.fil.ion.ucl.ac.uk/spm/

Balsters, J. H., & Ramnani, N. (2008). Symbolic representations of action in the human

cerebellum. *Neuroimage*, *43*(2), 388-398.

https://doi.org/10.1016/j.neuroimage.2008.07.010

Balsters, J. H., Cussans, E., Diedrichsen, J., Phillips, K. A., Preuss, T. M., Rilling, J. K., & Ramnani, N. (2010). Evolution of the cerebellar cortex: the selective expansion of prefrontal-projecting cerebellar lobules. *Neuroimage*, *49*(3), 2045-2052. https://doi.org/10.1016/j.neuroimage.2009.10.045

Balsters, J. H., & Ramnani, N. (2011). Cerebellar plasticity and the automation of first-order rules. *Journal of Neuroscience*, *31*(6), 2305-2312. https://doi.org/10.1523/JNEUROSCI.4358-10.2011

Balsters, J. H., Whelan, C. D., Robertson, I. H., & Ramnani, N. (2013). Cerebellum and cognition: evidence for the encoding of higher order rules. *Cerebral Cortex*, *23*(6), 1433-1443. https://doi.org/10.1093/cercor/bhs127

Balsters, J. H., Laird, A. R., Fox, P. T., & Eickhoff, S. B. (2014). Bridging the gap between functional and anatomical features of cortico-cerebellar circuits using meta-analytic connectivity modeling. *Human brain mapping*, *35*(7), 3152-3169. https://doi.org/10.1002/hbm.22392

Baltes, P. B., & Lindenberger, U. (1997). Emergence of a powerful connection between sensory and cognitive functions across the adult life span: a new window to the study of cognitive aging?. *Psychology and aging*, *12*(1), 12-21. https://psycnet.apa.org/doi/10.1037/0882-7974.12.1.12

Bandettini, P. A. (2002). *Neuropsychopharmacology – 5th Generation of Progress*: *The spatial, temporal, and interpretive limits of functional MRI.* Lippincott Williams and Wilkins.

Bandettini, P. A. (2020). *fMRI.* MIT Press.

Barber, S. J. (2017). An examination of age-based stereotype threat about cognitive decline: Implications for stereotype-threat research and theory development. *Perspectives on Psychological Science*, *12*(1), 62-90. https://doi.org/10.1177/1745691616656345

Barber, S. J. (2020). The applied implications of age-based stereotype threat for older adults. *Journal of Applied Research in Memory and Cognition*. https://doi.org/10.1016/j.jarmac.2020.05.002

Baudouin, A., Isingrini, M., & Vanneste, S. (2019). Executive functioning and processing speed in age-related differences in time estimation: a comparison of young, old, and very old adults. *Aging, Neuropsychology, and Cognition*, *26*(2), 264-281. https://doi.org/10.1080/13825585.2018.1426715

Beatty, J., & Kahneman, D. (1966). Pupillary changes in two memory tasks. *Psychonomic Science*, *5*(10), 371-372. https://psycnet.apa.org/doi/10.3758/BF03328444

Bellebaum, C., & Daum, I. (2004). Effects of age and awareness on eyeblink conditional discrimination learning. *Behavioral neuroscience*, *118*(6), 1157-1165. https://psycnet.apa.org/doi/10.1037/0735-7044.118.6.1157

Benarroch, E. E. (2009). The locus ceruleus norepinephrine system: functional organization and potential clinical significance. *Neurology*, *73*(20), 1699-1704. https://doi.org/10.1212/WNL.0b013e3181c2937c

Bernard, J. A., Seidler, R. D., Hassevoort, K. M., Benson, B. L., Welsh, R. C., Wiggins, J. L., ... & Peltier, S. J. (2012). Resting state cortico-cerebellar functional connectivity networks: a comparison of anatomical and self-organizing map approaches. *Frontiers in neuroanatomy*, *6*, 31. https://doi.org/10.3389/fnana.2012.00031

Birren, J. E., Casperson, R. C., & Botwinick, J. (1950). Age changes in pupil size. *Journal of Gerontology, 5*(3), 216-221. https://doi.org/10.1093/geronj/5.3.216

Blanke, O., Morand, S., Thut, G., Michel, C. M., Spinelli, L., Landis, T., & Seeck, M. (1999). Visual activity in the human frontal eye field. *Neuroreport*, *10*(5), 925-930. https://psycnet.apa.org/doi/10.1097/00001756-199904060-00006

Blanke, O., Spinelli, L., Thut, G., Michel, C. M., Perrig, S., Landis, T., & Seeck, M. (2000). Location of the human frontal eye field as defined by electrical cortical stimulation: anatomical, functional and electrophysiological characteristics. *Neuroreport*, *11*(9), 1907-1913. https://doi.org/10.1097/00001756-200006260-00021

Blanke, O., & Seeck, M. (2003). Direction of saccadic and smooth eye movements induced by electrical stimulation of the human frontal eye field: effect of orbital position. *Experimental brain research*, *150*(2), 174-183. https://doi.org/10.1007/s00221-003-1395-7

Bloedel, J. R., Ebner, T. J., & Wise, S. P. (Eds.). (1996). *The acquisition of motor behavior in vertebrates*. MIT Press.

Boele, H. J., Peter, S., Ten Brinke, M. M., Verdonschot, L., IJpelaar, A. C., Rizopoulos, D., ... & De Zeeuw, C. I. (2018). Impact of parallel fiber to Purkinje cell long-term depression is unmasked in absence of inhibitory input. *Science advances*, *4*(10), 1-8. https://doi.org/10.1126/sciadv.aas9426

Borson, S., Scanlan, J., Brush, M., Vitaliano, P., & Dokmak, A. (2000). The mini-cog: a cognitive 'vital signs' measure for dementia screening in multi-lingual elderly. *International journal of geriatric psychiatry*, *15*(11), 1021-1027.

https://doi.org/10.1002/1099-1166(200011)15:11%3C1021::AID-GPS234%3E3.0.CO;2-6

Borson, S., Scanlan, J. M., Chen, P., & Ganguli, M. (2003). The Mini-Cog as a screen for dementia: validation in a population-based sample. *Journal of the American Geriatrics Society*, *51*(10), 1451-1454. https://doi.org/10.1046/j.1532-5415.2003.51465.x

Borson, S., Scanlan, J. M., Watanabe, J., Tu, S. P., & Lessig, M. (2005). Simplifying detection of cognitive impairment: comparison of the Mini-Cog and Mini-Mental State Examination in a multiethnic sample. *Journal of the American Geriatrics Society*, *53*(5), 871-874. https://doi.org/10.1111/j.1532-5415.2005.53269.x

Boschin, E. A., & Buckley, M. J. (2015). Differential contributions of dorsolateral and frontopolar cortices to working memory processes in the primate. *Frontiers in Systems Neuroscience*, *9(144)*, 22-29. https://doi.org/10.3389/fnsys.2015.00144

Bottiroli, S., Tassorelli, C., Lamonica, M., Zucchella, C., Cavallini, E., Bernini, S., ... & Sandrini, G. (2017). Smart aging platform for evaluating cognitive functions in aging: A comparison with the MoCA in a normal population. *Frontiers in aging neuroscience*, *9*(379), 1-14. https://doi.org/10.3389/fnagi.2017.00379

Bourgeois, A., Sterpenich, V., Iannotti, G. R., & Vuilleumier, P. (2021). Reward-driven modulation of spatial attention in the human frontal eye-field. *NeuroImage*, *247*, 118846. https://doi.org/10.1016/j.neuroimage.2021.118846

Boynton, G. M., Engel, S. A., Glover, G. H., & Heeger, D. J. (1996). Linear systems analysis of functional magnetic resonance imaging in human V1. *Journal of*

Neuroscience, *16*(13), 4207-4221. https://doi.org/10.1523/JNEUROSCI.16-13-04207.1996

Bracke-Tolkmitt, R., Linden, A., Canavan, A. G. M., Rockstroh, B., Scholz, E., Wessel, K. D. H. C., & Diener, H. C. (1989). The cerebellum contributes to mental skills. *Behavioral Neuroscience*, *103*(2), 442-446. https://psycnet.apa.org/doi/10.1037/0735-7044.103.2.442

Bradshaw, J. (1967). Pupil size as a measure of arousal during information processing. *Nature*, *216*(5114), 515-516. https://doi.org/10.1038/216515a0

Brodal, P., & Brodal, A. (1981). The olivocerebellar projection in the monkey. Experimental studies with the method of retrograde tracing of horseradish peroxidase. *Journal of Comparative Neurology*, *201*(3), 375-393. https://doi.org/10.1002/cne.902010306

Brodaty, H., Low, L. F., Gibson, L., & Burns, K. (2006). What is the best dementia screening instrument for general practitioners to use?. *The American Journal of Geriatric Psychiatry*, *14*(5), 391-400. https://doi.org/10.1097/01.JGP.0000216181.20416.b2

Browning, P. G., & Gaffan, D. (2008). Prefrontal cortex function in the representation of temporally complex events. *Journal of Neuroscience*, *28*(15), 3934-3940. https://doi.org/10.1523/JNEUROSCI.0633-08.2008

Buckner, R. L., Krienen, F. M., Castellanos, A., Diaz, J. C., & Yeo, B. T. (2011). The organization of the human cerebellum estimated by intrinsic functional connectivity. *Journal of neurophysiology*, *106*(5), 2322-2345. https://doi.org/10.1152/jn.00339.2011

Budisavljevic, S., & Ramnani, N. (2012). Cognitive deficits from a cerebellar tumour: A historical case report from Luria's laboratory. *Cortex*, *48*(1), 26-35. https://doi.org/10.1016/j.cortex.2011.07.001

Bunge, S. A. (2004). How we use rules to select actions: a review of evidence from cognitive

neuroscience. *Cognitive, Affective, & Behavioral Neuroscience*, *4*(4), 564-579.

https://psycnet.apa.org/doi/10.3758/CABN.4.4.564

Burke, K. A., Franz, T. M., Miller, D. N., & Schoenbaum, G. (2008). The role of the

orbitofrontal cortex in the pursuit of happiness and more specific

rewards. *Nature*, *454*(7202), 340-344. https://doi.org/10.1038/nature06993

Burr, D. C., Ross, J., Binda, P., & Morrone, M. C. (2010). Saccades compress space, time and

number. *Trends in cognitive sciences*, *14*(12), 528-533.

https://doi.org/10.1016/j.tics.2010.09.005

Bussey, T. J., Wise, S. P., & Murray, E. A. (2001). The role of ventral and orbital prefrontal

cortex in conditional visuomotor learning and strategy use in rhesus monkeys

(Macaca mulatta). *Behavioral neuroscience*, *115*(5), 971-982.

https://psycnet.apa.org/doi/10.1037/0735-7044.115.5.971

Buxton, R. B., Uludağ, K., Dubowitz, D. J., & Liu, T. T. (2004). Modeling the hemodynamic

response to brain activation. *Neuroimage*, *23*, 220-233.

https://doi.org/10.1016/j.neuroimage.2004.07.013

Cabeza, R. (2002). Hemispheric asymmetry reduction in older adults: the HAROLD

model. *Psychology and aging*, *17*(1), 85-100. https://doi.org/10.1037//0882-

7974.17.1.85

Campbell, K. L., Lustig, C., & Hasher, L. (2020). Aging and inhibition: Introduction to the

special issue. *Psychology and Aging*, *35*(5), 605-613.

https://doi.org/10.1037/pag0000564

Canavan, A. G. M., Springelmeyer, R., Diener, H. C., & Hömberg, V. (1994). Conditional associative learning is impaired in cerebellar disease in humans. *Behavioral neuroscience*, *108*(3), 475-485. https://psycnet.apa.org/doi/10.1037/0735-7044.108.3.475

Carson, N., Leach, L., & Murphy, K. J. (2018). A re-examination of Montreal Cognitive Assessment (MoCA) cutoff scores. *International journal of geriatric psychiatry*, *33*(2), 379-388. https://doi.org/10.1002/gps.4756

Carter, B. T., & Luke, S. G. (2020). Best practices in eye-tracking research. *International Journal of Psychophysiology*, *155*, 49-62. https://doi.org/10.1016/j.ijpsycho.2020.05.010

Chandraratna, S., & Stamatiadis, N. (2003). Problem driving maneuvers of elderly drivers. *Transportation Research Record, 1843*(1), 89-95. https://doi.org/10.3141/1843-11

Chen, L. L., & Wise, S. P. (1995a). Neuronal activity in the supplementary eye field during acquisition of conditional oculomotor associations. *Journal of Neurophysiology*, *73*(3), 1101-1121. https://doi.org/10.1152/jn.1995.73.3.1101

Chen, L. L., & Wise, S. P. (1995b). Supplementary eye field contrasted with the frontal eye field during acquisition of conditional oculomotor associations. Journal of Neurophysiology, 73(3), 1122-1134. https://doi.org/10.1152/jn.1995.73.3.1122

Chowdhury, R., Lambert, C., Dolan, R. J., & Düzel, E. (2013). Parcellation of the human substantia nigra based on anatomical connectivity to the striatum. Neuroimage, 81, 191-198. https://doi.org/10.1016/j.neuroimage.2013.05.043

Christophel, T. B., Klink, P. C., Spitzer, B., Roelfsema, P. R., & Haynes, J. D. (2017). The distributed nature of working memory. *Trends in cognitive sciences*, *21*(2), 111-124. https://doi.org/10.1016/j.tics.2016.12.007

Crepel, F., Hemart, N., Jaillard, D., & Daniel, H. (1996). Cellular mechanisms of long-term depression in the cerebellum. *Behavioral and Brain Sciences*, *19*(3), 347-353. https://doi.org/10.1017/S0140525X00081449

Cromer, J. A., Roy, J. E., & Miller, E. K. (2010). Representation of multiple, independent categories in the primate prefrontal cortex. *Neuron*, *66*(5), 796-807. https://doi.org/10.1016/j.neuron.2010.05.005

Csipo, T., Mukli, P., Lipecz, A., Tarantini, S., Bahadli, D., Abdulhussein, O., ... & Hand, R. A. (2019). Assessment of age-related decline of neurovascular coupling responses by functional near-infrared spectroscopy (fNIRS) in humans. *Geroscience*, *41*(5), 495-509. https://doi.org/10.1007/s11357-019-00122-x

Curtis, C. E., & Connolly, J. D. (2008). Saccade preparation signals in the human frontal and parietal cortices. *Journal of Neurophysiology*, *99*(1), 133-145. https://doi.org/10.1152/jn.00899.2007

Daneault, V., Vandewalle, G., Hébert, M., Teikari, P., Mure, L. S., Doyon, J., ... & Carrier, J. (2012). Does pupil constriction under blue and green monochromatic light exposure change with age?. Journal of biological rhythms, 27(3), 257-264. https://dx.doi.org/10.1177/0748730412441172

D'Angelo, E. (2014). The organization of plasticity in the cerebellar cortex: from synapses to control. *Progress in brain research*, *210*, 31-58. https://doi.org/10.1016/B978-0-444-63356-9.00002-9

Deary, I. J., Corley, J., Gow, A. J., Harris, S. E., Houlihan, L. M., Marioni, R. E., ... & Starr, J. M.

(2009). Age-associated cognitive decline. *British medical bulletin*, *92*(1), 135-152.

https://doi.org/10.1093/bmb/ldp033

Demer, J. L., Echelman, D. A., & Robinson, D. A. (1985). Effects of electrical stimulation and

reversible lesions of the olivocerebellar pathway on Purkinje cell activity in the

flocculus of the cat. *Brain research*, *346*(1), 22-31. https://doi.org/10.1016/0006-

8993(85)91090-X

D'esposito, M., Zarahn, E., Aguirre, G. K., & Rypma, B. (1999). The effect of normal aging on

the coupling of neural activity to the bold hemodynamic

response. *Neuroimage*, *10*(1), 6-14. https://doi.org/10.1006/nimg.1999.0444

D'esposito, M., Deouell, L. Y., & Gazzaley, A. (2003). Alterations in the BOLD fMRI signal with

aging and disease: a challenge for neuroimaging. *Nature Reviews*

Neuroscience, *4*(11), 863-872. https://doi.org/10.1038/nrn1246

Diamond, A. (2013). Executive functions. *Annual review of psychology*, *64*, 135-168.

https://doi.org/10.1146/annurev-psych-113011-143750

Dickstein, D. L., Kabaso, D., Rocher, A. B., Luebke, J. I., Wearne, S. L., & Hof, P. R. (2007).

Changes in the structural complexity of the aged brain. *Aging cell*, *6*(3), 275-284.

https://doi.org/10.1111/j.1474-9726.2007.00289.x

Diedrichsen, J., Balsters, J. H., Flavell, J., Cussans, E., & Ramnani, N. (2009). A probabilistic

MR atlas of the human cerebellum. *Neuroimage*, *46*(1), 39-46.

https://doi.org/10.1016/j.neuroimage.2009.01.045

D'Mello, A. M., & Gabrieli, J. D. (2018). Cognitive neuroscience of dyslexia. *Language, speech, and hearing services in schools*, *49*(4), 798-809. https://doi.org/10.1044/2018_LSHSS-DYSLC-18-0020

Dow, R. S. (1942). Cerebellar action potentials in response to stimulation of the cerebral cortex in monkeys and cats. *Journal of Neurophysiology*, *5*(2), 121-136. https://doi.org/10.1152/jn.1942.5.5.363

Drepper, J., Timmann, D., Kolb, F. P., & Diener, H. C. (1999). Non-motor associative learning in patients with isolated degenerative cerebellar disease. *Brain*, *122*(1), 87-97. https://doi.org/10.1093/brain/122.1.87

Dunterman, R. A., Intrieri, R. C., & Guernsey, M. (2019). Useful field of view and driving simulation across two age groups. *Innovation in Aging*, *3*(Suppl 1), 968-969. https://doi.org/10.1093%2Fgeroni%2Figz038.3511

Duyn, J. H. (2012). The future of ultra-high field MRI and fMRI for study of the human brain. *Neuroimage*, *62*(2), 1241-1248. https://doi.org/10.1016/j.neuroimage.2011.10.065

Eden, G. F., VanMeter, J. W., Rumsey, J. M., Maisog, J. M., Woods, R. P., & Zeffiro, T. A. (1996). Abnormal processing of visual motion in dyslexia revealed by functional brain imaging. *Nature*, *382*(6586), 66-69. https://doi.org/10.1038/382066a0

Edwards, J. D., Ross, L. A., Wadley, V. G., Clay, O. J., Crowe, M., Roenker, D. L., & Ball, K. K. (2006). The useful field of view test: normative data for older adults. *Archives of Clinical Neuropsychology*, *21*(4), 275-286. https://psycnet.apa.org/doi/10.1016/j.acn.2006.03.001

Evans, A. C., Collins, D. L., Mills, S. R., Brown, E. D., Kelly, R. L., & Peters, T. M. (1993,

    October). 3D statistical neuroanatomical models from 305 MRI volumes. In *1993*

    IEEE conference record nuclear science symposium and medical imaging

    conference (pp. 1813-1817). IEEE. https://doi.org/10.1109/NSSMIC.1993.373602

Evarts, E. V., & Thach, W. T. (1969). Motor mechanisms of the CNS: cerebrocerebellar

    interrelations. *Annual review of physiology*, *31*(1), 451-498.

    https://doi.org/10.1146/annurev.ph.31.030169.002315

Fabiani, M., Gordon, B. A., Maclin, E. L., Pearson, M. A., Brumback-Peltz, C. R., Low, K. A., ...

    & Gratton, G. (2014). Neurovascular coupling in normal aging: a combined optical,

    ERP and fMRI study. *Neuroimage*, *85*(1), 592-607.

    https://dx.doi.org/10.1016/j.neuroimage.2013.04.113

Faßl, C., Quante, M., Mariani, S., & Randler, C. (2019). Preliminary findings for the validity of

    the Morningness–Eveningness-Stability Scale improved (MESSi): Correlations with

    activity levels and personality. *Chronobiology international*, *36*(1), 135-142.

    https://doi.org/10.1080/07420528.2018.1519570

Ferguson, H. J., Brunsdon, V. E., & Bradford, E. E. (2021). The developmental trajectories of

    executive function from adolescence to old age. *Scientific reports*, *11*(1), 1-17.

    https://doi.org/10.1038%2Fs41598-020-80866-1

Francis, S., & Panchuelo, R. S. (2014). Physiological measurements using ultra-high field

    fMRI: a review. *Physiological measurement*, *35*(9), R167.

    https://doi.org/10.1088/0967-3334/35/9/R167

Frankfurter, A., Weber, J. T., Royce, G. J., Strominger, N. L., & Harting, J. K. (1976). An autoradiographic analysis of the tecto-olivary projection in primates. *Brain research*, *118*(2), 245-257. https://doi.org/10.1016/0006-8993(76)90710-1

Frank, M. J., & Claus, E. D. (2006). Anatomy of a decision: striato-orbitofrontal interactions in reinforcement learning, decision making, and reversal. *Psychological review*, *113*(2), 300. https://doi.org/10.1037/0033-295X.113.2.300

Friston, K. J., Williams, S., Howard, R., Frackowiak, R. S., & Turner, R. (1996). Movement-related effects in fMRI time-series. *Magnetic resonance in medicine*, *35*(3), 346-355. https://doi.org/10.1002/mrm.1910350312

Friston, K. J., Fletcher, P., Josephs, O., Holmes, A., Rugg, M. D., & Turner, R. (1998a). Event-related fMRI: characterizing differential responses. *Neuroimage*, *7*(1), 30-40. https://doi.org/10.1006/nimg.1997.0306

Friston, K. J., Josephs, O., Rees, G., & Turner, R. (1998b). Nonlinear event-related responses in fMRI. *Magnetic resonance in medicine*, *39*(1), 41-52. https://doi.org/10.1002/mrm.1910390109

Frostig, R. D., Lieke, E. E., Ts'o, D. Y., & Grinvald, A. (1990). Cortical functional architecture and local coupling between neuronal activity and the microcirculation revealed by in vivo high-resolution optical imaging of intrinsic signals. *Proceedings of the National Academy of Sciences*, *87*(16), 6082-6086. https://doi.org/10.1073/pnas.87.16.6082

Gaffan, D., & Wilson, C. R. (2008). Medial temporal and prefrontal function: recent behavioural disconnection studies in the macaque monkey. *Cortex*, *44*(8), 928-935. https://doi.org/10.1016/j.cortex.2008.03.005

Gajewski, P. D., Hanisch, E., Falkenstein, M., Thönes, S., & Wascher, E. (2018). What does the n-back task measure as we get older? Relations between working-memory measures and other cognitive functions across the lifespan. *Frontiers in psychology*, *9*, 2208. https://doi.org/10.3389/fpsyg.2018.02208

Gao, Y., Barreto, A., Zhai, J., & Rishe, N. (2007). Digital filtering of pupil diameter variations for the detection of stress in computer users. In *Proc 11th world multi-conference on systemics, cybernetics and informatics, Orlando* (pp. 30-35).

Garrett, H. E. (1946). A developmental theory of intelligence. *American Psychologist*, *1*(9), 372-378. https://psycnet.apa.org/doi/10.1037/h0056380

Gavas, R., Chatterjee, D., & Sinha, A. (2017, October). Estimation of cognitive load based on the pupil size dilation. In *2017 IEEE International Conference on Systems, Man, and Cybernetics (SMC)* (pp. 1499-1504). IEEE.

Gaymard, B., Ploner, C. J., Rivaud, S., Vermersch, A. I., & Pierrot-Deseilligny, C. (1998). Cortical control of saccades. *Experimental brain research*, *123*(1), 159-163. https://doi.org/10.1007/s002210050557

Geisler, S., & Wise, R. A. (2008). Functional implications of glutamatergic projections to the ventral tegmental area. *Reviews in the neurosciences, 19*(4-5), 227-244. https://doi.org/10.1515/REVNEURO.2008.19.4-5.227

Gellersen, H. M., Guell, X., & Sami, S. (2021). Differential vulnerability of the cerebellum in healthy ageing and Alzheimer's disease. *NeuroImage: Clinical*, *30*, 102605. https://doi.org/10.1016/j.nicl.2021.102605

Genovesio, A., Brasted, P. J., Mitz, A. R., & Wise, S. P. (2005). Prefrontal cortex activity

related to abstract response strategies. *Neuron*, *47*(2), 307-320.

https://doi.org/10.1016/j.neuron.2005.06.006

Genovesio, A., Brasted, P. J., & Wise, S. P. (2006). Representation of future and previous

spatial goals by separate neural populations in prefrontal cortex. *Journal of

Neuroscience*, *26*(27), 7305-7316. https://doi.org/10.1523/JNEUROSCI.0699-06.2006

Genovesio, A., Tsujimoto, S., & Wise, S. P. (2006). Neuronal activity related to elapsed time

in prefrontal cortex. *Journal of Neurophysiology*, *95*(5), 3281-3285.

https://doi.org/10.1152/jn.01011.2005

Genovesio, A., Wise, S. P., & Passingham, R. E. (2014). Prefrontal–parietal function: from

foraging to foresight. *Trends in cognitive sciences*, *18*(2), 72-81.

https://doi.org/10.1016/j.tics.2013.11.007

Glickstein, M., May III, J. G., & Mercier, B. E. (1985). Corticopontine projection in the

macaque: the distribution of labelled cortical cells after large injections of

horseradish peroxidase in the pontine nuclei. *Journal of Comparative

Neurology*, *235*(3), 343-359. https://doi.org/10.1002/cne.902350306

Goldman, P. S., & Rosvold, H. E. (1970). Localization of function within the dorsolateral

prefrontal cortex of the rhesus monkey. *Experimental neurology*, *27*(2), 291-304.

https://doi.org/10.1016/0014-4886(70)90222-0

Gormezano, I., Schneiderman, N., Deaux, E., & Fuentes, I. (1962). Nictitating membrane:

Classical conditioning and extinction in the albino rabbit. *Science*, *138*(3536), 33-34.

https://doi.org/10.1126/science.138.3536.33

Granholm, E., Asarnow, R. F., Sarkin, A. J., & Dykes, K. L. (1996). Pupillary responses index

cognitive resource limitations. *Psychophysiology*, *33*(4), 457-461.

https://doi.org/10.1111/j.1469-8986.1996.tb01071.x

Graybiel, A. M. (2008). Habits, rituals, and the evaluative brain. *Annual review of*

neuroscience, *31*(1), 359-387.

https://doi.org/10.1146/annurev.neuro.29.051605.112851

Greger, B., Norris, S. A., & Thach, W. T. (2004). Spike firing in the lateral cerebellar cortex

correlated with movement and motor parameters irrespective of the effector

limb. *Journal of neurophysiology*, *91*(1), 576-582.

https://doi.org/10.1152/jn.00535.2003

Groman, S. M., Keistler, C., Keip, A. J., Hammarlund, E., DiLeone, R. J., Pittenger, C., ... &

Taylor, J. R. (2019). Orbitofrontal circuits control multiple reinforcement-learning

processes. *Neuron*, *103*(4), 734-746. https://doi.org/10.1016/j.neuron.2019.05.042

Gutchess, A. H., & Park, D. C. (2006). fMRI environment can impair memory performance in

young and elderly adults. *Brain research*, *1099*(1), 133-140.

https://doi.org/10.1016/j.brainres.2006.04.102

Hadj-Bouziane, F., Meunier, M., & Boussaoud, D. (2003). Conditional visuo-motor learning in

primates: a key role for the basal ganglia. *Journal of Physiology-Paris*, *97*(4-6), 567-

579. https://doi.org/10.1016/j.jphysparis.2004.01.014

Halsband, U., & Passingham, R. (1982). The role of premotor and parietal cortex in the

direction of action. *Brain research*, *240*(2), 368-372. https://doi.org/10.1016/0006-

8993(82)90239-6

Handwerker, D. A., Ollinger, J. M., & D'Esposito, M. (2004). Variation of BOLD hemodynamic responses across participants and brain regions and their effects on statistical analyses. *Neuroimage*, *21*(4), 1639-1651. https://doi.org/10.1016/j.neuroimage.2003.11.029

Harel, N. (2012). Ultra high resolution fMRI at ultra-high field. *Neuroimage*, *62*(2), 1024-1028. https://doi.org/10.1016/j.neuroimage.2012.01.018

Haug, H., & Eggers, R. (1991). Morphometry of the human cortex cerebri and corpus striatum during aging. *Neurobiology of aging*, *12*(4), 336-338. https://doi.org/10.1016/0197-4580(91)90013-A

Hebb, D. (1949). *The Organization of Behavior*. Wiley: New York.

Heiney, S. A., Kim, J., Augustine, G. J., & Medina, J. F. (2014). Precise control of movement kinematics by optogenetic inhibition of Purkinje cell activity. *Journal of Neuroscience*, *34*(6), 2321-2330. https://doi.org/10.1523/JNEUROSCI.4547-13.2014

Henson, R., Büchel, C., Josephs, O., & Friston, K. (1999). The slice-timing problem in event-related fMRI. *NeuroImage*, *9*, 125. https://www.mrc-cbu.cam.ac.uk/personal/rik.henson/personal/HensonEtAl_HBM_Abstract_99.pdf

Henson, R., Rugg, M. D., & Friston, K. J. (2001). The choice of basis functions in event-related fMRI. *NeuroImage*, *13*(6), 149. https://doi.org/10.1016/S1053-8119(01)91492-2

Hess, E. H., & Polt, J. M. (1964). Pupil size in relation to mental activity during simple problem-solving. *Science*, *143*(3611), 1190-1192. https://doi.org/10.1126/science.143.3611.1190

Higo, T., Mars, R. B., Boorman, E. D., Buch, E. R., & Rushworth, M. F. (2011). Distributed and causal influence of frontal operculum in task control. *Proceedings of the National Academy of Sciences*, *108*(10), 4230-4235. https://doi.org/10.1073/pnas.1013361108

Hillman, E. M. (2014). Coupling mechanism and significance of the BOLD signal: a status report. *Annual review of neuroscience*, *37*, 161-181. https://doi.org/10.1146/annurev-neuro-071013-014111

Hinault, T., Larcher, K., Bherer, L., Courtney, S. M., & Dagher, A. (2019). Age-related differences in the structural and effective connectivity of cognitive control: a combined fMRI and DTI study of mental arithmetic. *Neurobiology of aging*, *82*, 30-39. https://doi.org/10.1016/j.neurobiolaging.2019.06.013

Hirano, T. (2018). Regulation and interaction of multiple types of synaptic plasticity in a Purkinje neuron and their contribution to motor learning. *The Cerebellum*, *17*(6), 756-765. https://doi.org/10.1007/s12311-018-0963-0

Hoang, H., Tsutsumi, S., Matsuzaki, M., Kano, M., Toyama, K., Kitamura, K., & Kawato, M. (2023). *Negative reward-prediction errors of climbing fiber inputs for cerebellar reinforcement learning algorithm*. BioRxiv. https://doi.org/10.1101/2023.03.13.532374

Hofer, S. M., Sliwinski, M. J., & Flaherty, B. P. (2002). Understanding ageing: Further commentary on the limitations of cross-sectional designs for ageing research. *Gerontology*, *48*(1), 22-29. https://doi.org/10.1159/000048920

Horne, J. A., & Ostberg, O. (1976). A self-assessment questionnaire to determine morningness-eveningness in human circadian rhythms. *International Journal of Chronobiology*, *4*(2), 97-110. https://psycnet.apa.org/record/2015-49334-001

Hosseini, S. H., Bruno, J. L., Baker, J. M., Gundran, A., Harbott, L. K., Gerdes, J. C., & Reiss, A. L. (2017). Neural, physiological, and behavioral correlates of visuomotor cognitive load. *Scientific reports*, *7*(1), 1-9. https://doi.org/10.1038%2Fs41598-017-07897-z

Huerta, M. F., & Harting, J. K. (1984). Connectional organization of the superior colliculus. *Trends in Neurosciences*, *7*(8), 286-289. https://doi.org/10.1016/S0166-2236(84)80197-6

Huerta, M. F., & Kaas, J. H. (1990). Supplementary eye field as defined by intracortical microstimulation: connections in macaques. *Journal of Comparative Neurology*, *293*(2), 299-330. https://doi.org/10.1002/cne.902930211

Huh, D., Kim, J. H., & Jo, I. H. (2019). A novel method to monitoring changes in cognitive load in video-based learning. *Journal of Computer Assisted Learning*, *35*(6), 721-730. https://doi.org/10.1111/jcal.12378

Hull, C. (2020). Prediction signals in the cerebellum: beyond supervised motor learning. *elife*, *9*, e54073. https://doi.org/10.7554/eLife.54073

Hutchison, J. L., Lu, H., & Rypma, B. (2013). Neural mechanisms of age-related slowing: the ΔCBF/ΔCMRO2 ratio mediates age-differences in BOLD signal and human performance. *Cerebral Cortex*, *23*(10), 2337-2346. https://doi.org/10.1093/cercor/bhs233

Hutchison, R. M., Gallivan, J. P., Culham, J. C., Gati, J. S., Menon, R. S., & Everling, S. (2012). Functional connectivity of the frontal eye fields in humans and macaque monkeys

investigated with resting-state fMRI. *Journal of neurophysiology*, *107*(9), 2463-2474. https://doi.org/10.1152/jn.00891.2011

Huttenlocher, P. R. (1979). Synaptic density in human frontal cortex-developmental changes and effects of aging. *Brain Res*, *163*(2), 195-205. https://doi.org/10.1016/0006-8993(79)90349-4

Ikai, Y., Takada, M., Shinonaga, Y., & Mizuno, N. (1992). Dopaminergic and non-dopaminergic neurons in the ventral tegmental area of the rat project, respectively, to the cerebellar cortex and deep cerebellar nuclei. *Neuroscience*, *51*(3), 719-728. https://doi.org/10.1016/0306-4522(92)90310-X

Ikai, Y., Takada, M., & Mizuno, N. (1994). Single neurons in the ventral tegmental area that project to both the cerebral and cerebellar cortical areas by way of axon collaterals. *Neuroscience*, *61*(4), 925-934. https://doi.org/10.1016/0306-4522(94)90413-8

Imamizu, H., Miyauchi, S., Tamada, T., Sasaki, Y., Takino, R., PuÈtz, B., ... & Kawato, M. (2000). Human cerebellar activity reflecting an acquired internal model of a new tool. *Nature*, *403*(6766), 192-195. https://www.nature.com/articles/35003194

Intons-Peterson, M. J., Rocchi, P., West, T., McLellan, K., & Hackney, A. (1998). Aging, optimal testing times, and negative priming. *Journal of Experimental Psychology: Learning, Memory, and Cognition, 24(2),* 362-376. https://psycnet.apa.org/doi/10.1037/0278-7393.24.2.362

Ito, M., Shiida, T., Yagi, N., & Yamamoto, M. (1974). The cerebellar modification of rabbit's horizontal vestibulo-ocular reflex induced by sustained head rotation combined with visual stimulation. *Proceedings of the Japan Academy*, *50*(1), 85-89. https://doi.org/10.2183/pjab1945.50.85

Ito, M. (2005). Bases and implications of learning in the cerebellum—adaptive control and internal model mechanism. *Progress in brain research*, *148*, 95-109. https://doi.org/10.1016/S0079-6123(04)48009-1

Ito, M. (2008). Control of mental activities by internal models in the cerebellum. *Nature Reviews Neuroscience*, *9*(4), 304-313. https://doi.org/10.1038/nrn2332

Ito, M., Yamaguchi, K., Nagao, S., & Yamazaki, T. (2014). Long-term depression as a model of cerebellar plasticity. *Progress in brain research 210*, 1-30. https://doi.org/10.1016/B978-0-444-63356-9.00001-7

James, W., Burkhardt, F., Bowers, F., & Skrupskelis, I. K. (1890). *The principles of psychology* (Vol. 1, No. 2). London: Macmillan.

Jenkins, I. H., Brooks, D. J., Nixon, P. D., Frackowiak, R. S., & Passingham, R. E. (1994). Motor sequence learning: a study with positron emission tomography. *Journal of Neuroscience*, *14*(6), 3775-3790. https://doi.org/10.1523/JNEUROSCI.14-06-03775.1994

Jerde, T. A., Merriam, E. P., Riggall, A. C., Hedges, J. H., & Curtis, C. E. (2012). Prioritized maps of space in human frontoparietal cortex. *Journal of Neuroscience*, *32*(48), 17382-17390. https://doi.org/10.1523/JNEUROSCI.3810-12.2012

Jha, A., Tabet, N., & Orrell, M. (2001). To tell or not to tell—comparison of older patients' reaction to their diagnosis of dementia and depression. *International journal of geriatric psychiatry*, *16*(9), 879-885. https://doi.org/10.1002/gps.412

Jirenhed, D. A., Bengtsson, F., & Hesslow, G. (2007). Acquisition, extinction, and reacquisition of a cerebellar cortical memory trace. *Journal of Neuroscience*, *27*(10), 2493-2502. https://doi.org/10.1523/JNEUROSCI.4202-06.2007

Jirenhed, D. A., & Hesslow, G. (2016). Are Purkinje cell pauses drivers of classically

conditioned blink responses?. *The Cerebellum*, *15*(4), 526-534.

https://doi.org/10.1007%2Fs12311-015-0722-4

Johansson, F., Jirenhed, D. A., Rasmussen, A., Zucca, R., & Hesslow, G. (2014). Memory trace

and timing mechanism localized to cerebellar Purkinje cells. *Proceedings of the*

National Academy of Sciences, *111*(41), 14930-14934.

https://doi.org/10.1073/pnas.1415371111

Johansson, F., Carlsson, H. A., Rasmussen, A., Yeo, C. H., & Hesslow, G. (2015). Activation of a

temporal memory in Purkinje cells by the mGluR7 receptor. *Cell reports*, *13*(9), 1741-

1746. https://doi.org/10.1016/j.celrep.2015.10.047

Johansson, F., Hesslow, G., & Medina, J. F. (2016). Mechanisms for motor timing in the

cerebellar cortex. *Current opinion in behavioral sciences*, *8*, 53-59.

https://doi.org/10.1016/j.cobeha.2016.01.013

Johansson, F., Jirenhed, D. A., Rasmussen, A., Zucca, R., & Hesslow, G. (2018). Absence of

parallel fibre to Purkinje cell LTD during eyeblink conditioning. *Scientific*

reports, *8*(1), 1-5. https://doi.org/10.1038/s41598-018-32791-7

Johansson, F. (2019). Intrinsic memory of temporal intervals in cerebellar Purkinje

cells. *Neurobiology of learning and memory*, *166*, 107103.

https://doi.org/10.1016/j.nlm.2019.107103

Johansson, F., & Hesslow, G. (2020). Kir3 channel blockade in the cerebellar cortex

suppresses performance of classically conditioned Purkinje cell responses. *Scientific*

Reports, *10*(1), 1-8. https://doi.org/10.1038/s41598-020-72581-8

Josephs, O., Turner, R., & Friston, K. (1997). Event-related f MRI. Human brain mapping, 5(4), 243-248. https://doi.org/10.1002/(SICI)1097-0193(1997)5:4%3C243::AID-HBM7%3E3.0.CO;2-3

Josephs, O., & Henson, R. N. (1999). Event-related functional magnetic resonance imaging: modelling, inference and optimization. *Philosophical transactions of the royal society of london. series b: biological sciences*, *354*(1387), 1215-1228. https://doi.org/10.1098/rstb.1999.0475

Jueptner, M., Stephan, K. M., Frith, C. D., Brooks, D. J., Frackowiak, R. S., & Passingham, R. E. (1997). Anatomy of motor learning. I. Frontal cortex and attention to action. *Journal of neurophysiology*, *77*(3), 1313-1324. https://doi.org/10.1152/jn.1997.77.3.1313

Kahneman, D., & Beatty, J. (1966). Pupil diameter and load on memory. *Science*, *154*(3756), 1583-1585. https://doi.org/10.1126/science.154.3756.1583

Kahneman, D., & Beatty, J. (1967). Pupillary responses in a pitch-discrimination task. *Perception & Psychophysics*, *2*(3), 101-105. https://doi.org/10.3758/BF03210302

Kahneman, D., & Peavler, W. S. (1969). Incentive effects and pupillary changes in association learning. *Journal of Experimental Psychology*, *79*(2), 312-318. https://psycnet.apa.org/doi/10.1037/h0026912

Kahneman, D. (2011). *Thinking Fast and Slow*. New York.

Katz, M. J., Wang, C., Nester, C. O., Derby, C. A., Zimmerman, M. E., Lipton, R. B., ... & Rabin, L. A. (2021). T-MoCA: A valid phone screen for cognitive impairment in diverse community samples. *Alzheimer's & Dementia: Diagnosis, Assessment & Disease Monitoring*, *13*(1), e12144. https://doi.org/10.1002/dad2.12144

Kelly, R. M., & Strick, P. L. (2003). Cerebellar loops with motor cortex and prefrontal cortex of a nonhuman primate. *Journal of neuroscience*, *23*(23), 8432-8444. https://doi.org/10.1523/JNEUROSCI.23-23-08432.2003

Klein, A., Andersson, J., Ardekani, B. A., Ashburner, J., Avants, B., Chiang, M. C., ... & Song, J. H. (2009). Evaluation of 14 nonlinear deformation algorithms applied to human brain MRI registration. *Neuroimage*, *46*(3), 786-802. https://doi.org/10.1016/j.neuroimage.2008.12.037

Koechlin, E., & Summerfield, C. (2007). An information theoretical approach to prefrontal executive function. *Trends in cognitive sciences*, *11*(6), 229-235. https://doi.org/10.1016/j.tics.2007.04.005

Kojima, Y., & Soetedjo, R. (2018). Elimination of the error signal in the superior colliculus impairs saccade motor learning. *Proceedings of the National Academy of Sciences*, *115*(38), E8987-E8995. https://doi.org/10.1073/pnas.1806215115

Kostadinov, D., Beau, M., Blanco-Pozo, M., & Häusser, M. (2019). Predictive and reactive reward signals conveyed by climbing fiber inputs to cerebellar Purkinje cells. *Nature Neuroscience*, *22*(6), 950-962. https://doi.org/10.1038/s41593-019-0381-8

Kumar, S., Rao, S. L., Chandramouli, B. A., & Pillai, S. V. (2009). Reduction of functional brain connectivity in mild traumatic brain injury during working memory. *Journal of Neurotrauma*, *26*(5), 665-675. https://doi.org/10.1089/neu.2008.0644

Kurth, F., Zilles, K., Fox, P. T., Laird, A. R., & Eickhoff, S. B. (2010). A link between the systems: functional differentiation and integration within the human insula revealed by meta-analysis. *Brain Struct Funct*, *214*, 519-534. https://doi.org/10.1007/s00429-010-0255-z

Lamont, R. A., Swift, H. J., & Abrams, D. (2015). A review and meta-analysis of age-based stereotype threat: negative stereotypes, not facts, do the damage. *Psychology and aging*, *30*(1), 180. https://psycnet.apa.org/doi/10.1037/a0038586

Larner, A. J. (2020). Mini-Cog versus Codex (cognitive disorders examination) Is there a difference?. *Dementia & Neuropsychologia*, *14*(2), 128-133. https://doi.org/10.1590/1980-57642020dn14-020005

Lefevre, P., Quaia, C., & Optican, L. M. (1998). Distributed model of control of saccades by superior colliculus and cerebellum. *Neural networks*, *11*(7-8), 1175-1190. https://doi.org/10.1016/S0893-6080(98)00071-9

Levine, B., Stuss, D. T., & Milberg, W. P. (1997). Effects of aging on conditional associative learning: process analyses and comparison with focal frontal lesions. *Neuropsychology*, *11*(3), 367-381. https://psycnet.apa.org/doi/10.1037/0894-4105.11.3.367

Lindenberger, U., & Baltes, P. B. (1994). Sensory functioning and intelligence in old age: a strong connection. *Psychology and aging*, *9*(3), 339-355. https://psycnet.apa.org/doi/10.1037/0882-7974.9.3.339

Lindquist, M. A., & Wager, T. D. (2007). Validity and power in hemodynamic response modeling: a comparison study and a new approach. *Human brain mapping*, *28*(8), 764-784. https://doi.org/10.1002/hbm.20310

Lindquist, M. A., Loh, J. M., Atlas, L. Y., & Wager, T. D. (2009). Modeling the hemodynamic response function in fMRI: efficiency, bias and mis-modeling. *Neuroimage*, *45*(1), 187-198. https://doi.org/10.1016/j.neuroimage.2008.10.065

Linke, A. C., Olson, L., Gao, Y., Fishman, I., & Müller, R. A. (2017). Psychotropic medication

use in autism spectrum disorders may affect functional brain connectivity. *Biological

Psychiatry: Cognitive Neuroscience and Neuroimaging*, *2*(6), 518-527.

https://doi.org/10.1016/j.bpsc.2017.06.008

Liu, J., Duffy, B. A., Bernal-Casas, D., Fang, Z., & Lee, J. H. (2017). Comparison of fMRI analysis

methods for heterogeneous BOLD responses in block design

studies. *Neuroimage*, *147*, 390-408.

https://doi.org/10.1016/j.neuroimage.2016.12.045

Logothetis, N. K., Pauls, J., Augath, M., Trinath, T., & Oeltermann, A. (2001).

Neurophysiological investigation of the basis of the fMRI signal. *nature*, *412*(6843),

150-157. https://doi.org/10.1038/35084005

Logothetis, N. K. (2003). The underpinnings of the BOLD functional magnetic resonance

imaging signal. *Journal of Neuroscience*, *23*(10), 3963-3971.

https://doi.org/10.1523/JNEUROSCI.23-10-03963.2003

Longley, M., Danvers, M., & Ramnani. (2021, November 8-11). *Topographically organised

frontal cortex maps in the human cerebellar cortex.* [Poster Presentation]. SFN 2021,

virtual.

Loopuijt, L. D., & Van der Kooy, D. (1985). Organization of the striatum: collateralization of

its efferent axons. Brain research, 348(1), 86-99. https://doi.org/10.1016/0006-

8993(85)90363-4

Lu, Y., Grova, C., Kobayashi, E., Dubeau, F., & Gotman, J. (2007). Using voxel-specific

hemodynamic response function in EEG-fMRI data analysis: An estimation and

detection model. *Neuroimage*, *34*(1), 195-203.

https://doi.org/10.1016/j.neuroimage.2006.08.023

Lynch, J. C., Hoover, J. E., & Strick, P. L. (1994). Input to the primate frontal eye field from the

substantia nigra, superior colliculus, and dentate nucleus demonstrated by

transneuronal transport. *Experimental brain research, 100*(1), 181-186.

https://doi.org/10.1007/BF00227293

MacPherson, S. E., Phillips, L. H., & Della Sala, S. (2002). Age, executive function and social

decision making: a dorsolateral prefrontal theory of cognitive aging. *Psychology and*

aging, *17*(4), 598. https://psycnet.apa.org/doi/10.1037/0882-7974.17.4.598

Mansouri, F. A., Rosa, M. G., & Atapour, N. (2015). Working memory in the service of

executive control functions. *Frontiers in Systems Neuroscience*, *9(166)*, 30-37.

https://doi.org/10.3389/fnsys.2015.00166

Mansouri, F. A., Freedman, D. J., & Buckley, M. J. (2020). Emergence of abstract rules in the

primate brain. *Nature Reviews Neuroscience*, 1-16. https://doi.org/10.1038/s41583-

020-0364-5

Marr, D. (1969). A theory of cerebellar cortex. *Journal of Physiology, 202*, 437-470.

https://physoc.onlinelibrary.wiley.com/doi/epdf/10.1113/jphysiol.1969.sp008820?s

rc=getftr

MarsBaR FAQ — MarsBaR 0.45 documentation. (n.d.). Retrieved October 11, 2022,

from https://marsbar-toolbox.github.io/faq.html

Matano, S. (2001). Brief communication: proportions of the ventral half of the cerebellar

dentate nucleus in humans and great apes. *American Journal of Physical*

Anthropology: The Official Publication of the American Association of Physical

Anthropologists, *114*(2), 163-165. https://doi.org/10.1002/1096-8644(200102)114:2%3C163::AID-AJPA1016%3E3.0.CO;2-F

Mecacci, L., Zani, A., Rocchetti, G., & Lucioli, R. (1986). The relationships between morningness-eveningness, ageing and personality. *Personality and Individual Differences, 7(6),* 911-913. https://doi.org/10.1016/0191-8869(86)90094-2

Medina, J. F., & Lisberger, S. G. (2008). Links from complex spikes to local plasticity and motor learning in the cerebellum of awake-behaving monkeys. *Nature neuroscience*, *11*(10), 1185-1192. https://doi.org/10.1038/nn.2197

Merritt, D. J., Casasanto, D., & Brannon, E. M. (2010). Do monkeys think in metaphors? Representations of space and time in monkeys and humans. *Cognition*, *117*(2), 191-202. https://doi.org/10.1016/j.cognition.2010.08.011

Miezin, F. M., Maccotta, L., Ollinger, J. M., Petersen, S. E., & Buckner, R. L. (2000). Characterizing the hemodynamic response: effects of presentation rate, sampling procedure, and the possibility of ordering brain activity based on relative timing. *Neuroimage*, *11*(6), 735-759. https://doi.org/10.1006/nimg.2000.0568

Mikl, M., Mareček, R., Hluštík, P., Pavlicová, M., Drastich, A., Chlebus, P., ... & Krupa, P. (2008). Effects of spatial smoothing on fMRI group inferences. *Magnetic resonance imaging*, *26*(4), 490-503. https://doi.org/10.1016/j.mri.2007.08.006

Miller, E. K., & Cohen, J. D. (2001). An integrative theory of prefrontal cortex function. *Annual review of neuroscience*, *24*(1), 167-202. https://doi.org/10.1146/annurev.neuro.24.1.167

Mittleman, G. U. Y., Goldowitz, D., Heck, D. H., & Blaha, C. D. (2008). Cerebellar modulation of frontal cortex dopamine efflux in mice: relevance to autism and schizophrenia. *Synapse*, *62*(7), 544-550. https://doi.org/10.1002/syn.20525

Moore, T. L., Schettler, S. P., Killiany, R. J., Rosene, D. L., & Moss, M. B. (2012). Impairment in

    delayed nonmatching to sample following lesions of dorsal prefrontal cortex.

    Behavioral neuroscience, *126*(6), 772-780.

    https://psycnet.apa.org/doi/10.1037/a0030493

Morales, H., & Tomsick, T. (2015). Middle cerebellar peduncles: Magnetic resonance imaging

    and pathophysiologic correlate. *World journal of radiology*, *7*(12), 438-447.

    https://doi.org/10.4329%2Fwjr.v7.i12.438

Muhammad, R., Wallis, J. D., & Miller, E. K. (2006). A comparison of abstract rules in the

    prefrontal cortex, premotor cortex, inferior temporal cortex, and striatum. *Journal of*

    cognitive neuroscience, *18*(6), 974-989. https://doi.org/10.1162/jocn.2006.18.6.974

Murphy, P. R., O'connell, R. G., O'sullivan, M., Robertson, I. H., & Balsters, J. H. (2014). Pupil

    diameter covaries with BOLD activity in human locus coeruleus. *Human brain*

    mapping, *35*(8), 4140-4154. https://doi.org/10.1002/hbm.22466

Murray, E. A., & Rudebeck, P. H. (2013). The drive to strive: goal generation based on current

    needs. *Frontiers in neuroscience*, *7*, 112. https://doi.org/10.3389/fnins.2013.00112

Nasreddine, Z. S., Phillips, N. A., Bédirian, V., Charbonneau, S., Whitehead, V., Collin, I., ... &

    Chertkow, H. (2005). The Montreal Cognitive Assessment, MoCA: a brief screening

    tool for mild cognitive impairment. *Journal of the American Geriatrics Society*, *53*(4),

    695-699. https://doi.org/10.1111/j.1532-5415.2005.53221.x

Nutt, D. J., & Malizia, A. L. (2004). Structural and functional brain changes in posttraumatic

    stress disorder. *Journal of Clinical Psychiatry*, *65*, 11-17.

    https://www.psychiatrist.com/read-pdf/20094/

Oades, R. D., & Halliday, G. M. (1987). Ventral tegmental (A10) system: neurobiology. 1. Anatomy and connectivity. *Brain Research Reviews*, *12*(2), 117-165. https://doi.org/10.1016/0165-0173(87)90011-7

Ogawa, S., Lee, T. M., Kay, A. R., & Tank, D. W. (1990). Brain magnetic resonance imaging with contrast dependent on blood oxygenation. *proceedings of the National Academy of Sciences*, *87*(24), 9868-9872. https://doi.org/10.1073/pnas.87.24.9868

O'Reilly, J. X., Beckmann, C. F., Tomassini, V., Ramnani, N., & Johansen-Berg, H. (2010). Distinct and overlapping functional zones in the cerebellum defined by resting state functional connectivity. *Cerebral cortex*, *20*(4), 953-965. https://doi.org/10.1093/cercor/bhp157

Orr, J. M., Jackson, T. B., Imburgio, M. J., & Bernard, J. A. (2019). Dissociable Cerebellar-Prefrontal Networks Underlying Executive Function: Evidence from the Human Connectome Project. *bioRxiv*, 431593. https://doi.org/10.1101/431593

Palesi, F., De Rinaldis, A., Castellazzi, G., Calamante, F., Muhlert, N., Chard, D., ... & Gandini Wheeler-Kingshott, C. A. (2017). Contralateral cortico-ponto-cerebellar pathways reconstruction in humans in vivo: implications for reciprocal cerebro-cerebellar structural connectivity in motor and non-motor areas. *Scientific reports*, *7*(1), 1-13. https://doi.org/10.1038/s41598-017-13079-8

Park, D., & Schwarz, N. (1999). *Cognitive aging: A primer*. Psychology Press.

Parthasarathy, H. B., Schall, J. D., & Graybiel, A. M. (1992). Distributed but convergent ordering of corticostriatal projections: analysis of the frontal eye field and the supplementary eye field in the macaque monkey. *Journal of Neuroscience*, *12*(11), 4468-4488. https://doi.org/10.1523/JNEUROSCI.12-11-04468.1992

Passingham, R. E. (1985). Cortical mechanisms and cues for action. *Philosophical Transactions of the Royal Society of London. B, Biological Sciences*, *308*(1135), 101-111. https://doi.org/10.1098/rstb.1985.0013

Passingham, R. E. (1996). Attention to action. *Philosophical Transactions of the Royal Society of London. Series B: Biological Sciences*, *351*(1346), 1473-1479. https://doi.org/10.1098/rstb.1996.0132

Passingham, R. E., & Wise, S. P. (2012). *The neurobiology of the prefrontal cortex: anatomy, evolution, and the origin of insight* (No. 50). Oxford University Press.

Passingham, R. E., & Lau, H. (2022). Do we understand the prefrontal cortex?. *Brain Structure and Function*, 1-11. https://doi.org/10.1007/s00429-022-02587-7

Paus, T., Petrides, M., Evans, A. C., & Meyer, E. (1993). Role of the human anterior cingulate cortex in the control of oculomotor, manual, and speech responses: a positron emission tomography study. *Journal of neurophysiology*, *70*(2), 453-469. https://doi.org/10.1152/jn.1993.70.2.453

Peavler, W. S. (1974). Pupil size, information overload, and performance differences. *Psychophysiology*, *11*(5), 559-566. https://doi.org/10.1111/j.1469-8986.1974.tb01114.x

Penny, W., & Holmes, A. (2007). Random effects analysis. *Statistical parametric mapping: The analysis of functional brain images*, *156*, 165-186. https://citeseerx.ist.psu.edu/document?repid=rep1&type=pdf&doi=6ed105062770d089d86e9bcc7827f54487a22017

Penny, W. D., Friston, K. J., Ashburner, J. T., Kiebel, S. J., & Nichols, T. E. (Eds.). (2011). *Statistical parametric mapping: the analysis of functional brain images*. Elsevier.

Petrides, M. (1982). Motor conditional associative-learning after selective prefrontal lesions in the monkey. *Behavioural brain research*, *5*(4), 407-413. https://doi.org/10.1016/0166-4328(82)90044-4

Petrides, M. (1985). Deficits in non-spatial conditional associative learning after periarcuate lesions in the monkey. *Behavioural brain research*, *16*(2-3), 95-101. https://doi.org/10.1016/0166-4328(85)90085-3

Petrides, M., & Pandya, D. N. (1999). Dorsolateral prefrontal cortex: comparative cytoarchitectonic analysis in the human and the macaque brain and corticocortical connection patterns. *European Journal of Neuroscience*, *11*(3), 1011-1036. https://doi.org/10.1046/j.1460-9568.1999.00518.x

Petrides, M. (2000). The role of the mid-dorsolateral prefrontal cortex in working memory. *Experimental brain research*, *133*, 44-54. https://doi.org/10.1007/s002210000399

Petrides, M., & Pandya, D. N. (2002). Comparative cytoarchitectonic analysis of the human and the macaque ventrolateral prefrontal cortex and corticocortical connection patterns in the monkey. *European Journal of Neuroscience*, *16*(2), 291-310. https://doi.org/10.1046/j.1460-9568.2001.02090.x

Petrides, M. (2005). Lateral prefrontal cortex: architectonic and functional organization. *Philosophical Transactions of the Royal Society B: Biological Sciences*, *360*(1456), 781-795. https://doi.org/10.1098/rstb.2005.1631

Petrides, M., Tomaiuolo, F., Yeterian, E. H., & Pandya, D. N. (2012). The prefrontal cortex: comparative architectonic organization in the human and the macaque monkey brains. *Cortex*, *48*(1), 46-57. https://doi.org/10.1016/j.cortex.2011.07.002

Petrides, M. (2019). *The frontal lobes revisited*. Psychology Press.

Petzold, G. C., & Murthy, V. N. (2011). Role of astrocytes in neurovascular coupling. *Neuron*, *71*(5), 782-797. https://doi.org/10.1016/j.neuron.2011.08.009

Poldrack, R. A., Mumford, J. A., & Nichols, T. E. (2011). *Handbook of functional MRI data analysis*. Cambridge University Press.

Price, D., Tyler, L. K., Henriques, R. N., Campbell, K. L., Williams, N., Treder, M. S., ... & Henson, R. N. A. (2017). Age-related delay in visual and auditory evoked responses is mediated by white-and grey-matter differences. *Nature communications*, *8*(1), 1-12. https://doi.org/10.1038/ncomms15671

Purves, D., Augustine, G. J., Fitzpatrick, D., Hall, W. C., LaMantia, A. S., McNamara, J. O., ... (2008). *Neuroscience.* Sinauer Associates, Inc.

Quaia, C., Lefèvre, P., & Optican, L. M. (1999). Model of the control of saccades by superior colliculus and cerebellum. *Journal of neurophysiology*, *82*(2), 999-1018. https://doi.org/10.1152/jn.1999.82.2.999

Rabbitt, P., & Lowe, C. (2000). Patterns of cognitive aging. *Psychological Research*, *63*(3-4), 308-316. https://doi.org/10.1007/s004269900009

Raichle, M. E., Fiez, J. A., Videen, T. O., MacLeod, A. M. K., Pardo, J. V., Fox, P. T., & Petersen, S. E. (1994). Practice-related changes in human brain functional anatomy during nonmotor learning. *Cerebral cortex*, *4*(1), 8-26. https://doi.org/10.1093/cercor/4.1.8

Rainer, G., Asaad, W. F., & Miller, E. K. (1998). Selective representation of relevant information by neurons in the primate prefrontal cortex. *Nature*, *393*(6685), 577-579. https://psycnet.apa.org/doi/10.1038/31235

Ramnani, N., Toni, I., Josephs, O., Ashburner, J., & Passingham, R. E. (2000). Learning-and expectation-related changes in the human brain during motor learning. *Journal of Neurophysiology*, *84*(6), 3026-3035. https://doi.org/10.1152/jn.2000.84.6.3026

Ramnani, N., & Miall, R. C. (2003). Instructed delay activity in the human prefrontal cortex is modulated by monetary reward expectation. *Cerebral Cortex*, *13*(3), 318-327. https://doi.org/10.1093/cercor/13.3.318

Ramnani, N., & Owen, A. M. (2004). Anterior prefrontal cortex: insights into function from anatomy and neuroimaging. *Nature reviews neuroscience*, *5*(3), 184-194. https://doi.org/10.1038/nrn1343

Ramnani, N., & Henson, R. (2005). "Modelling the BOLD impulse response: Insufficiency of canonical basis functions", Abstracts of the 11th Annual Meeting of the Organization for Human Brain Mapping (2005), *NeuroImage*, Volume 26, Supplement 1, Abstract No. 622.

Ramnani, N. (2006). The primate cortico-cerebellar system: anatomy and function. *Nature reviews neuroscience*, *7*(7), 511-522. https://doi.org/10.1038/nrn1953

Ramnani, N. (2014). Automatic and controlled processing in the corticocerebellar system. *Progress in Brain Research*, *210*, 255-285. https://doi.org/10.1016/B978-0-444-63356-9.00010-8

Rao, S. C., Rainer, G., & Miller, E. K. (1997). Integration of what and where in the primate prefrontal cortex. *Science*, *276*(5313), 821-824. https://doi.org/10.1126/science.276.5313.821

Rasmussen, A., Zucca, R., Johansson, F., Jirenhed, D. A., & Hesslow, G. (2015). Purkinje cell activity during classical conditioning with different conditional stimuli explains

central tenet of Rescorla–Wagner model. *Proceedings of the National Academy of Sciences*, *112*(45), 14060-14065. https://doi.org/10.1073/pnas.1516986112

Rayner, K. (2009). The 35th Sir Frederick Bartlett Lecture: Eye movements and attention in reading, scene perception, and visual search. *Quarterly journal of experimental psychology*, *62*(8), 1457-1506. https://doi.org/10.1080/17470210902816461

Raz, N., Gunning, F. M., Head, D., Dupuis, J. H., McQuain, J., Briggs, S. D., ... & Acker, J. D. (1997). Selective aging of the human cerebral cortex observed in vivo: differential vulnerability of the prefrontal gray matter. *Cerebral cortex (New York, NY: 1991)*, *7*(3), 268-282. https://doi.org/10.1093/cercor/7.3.268

Raz, N., & Lindenberger, U. (2011). Only time will tell: Cross-sectional studies offer no solution to the age–brain–cognition triangle: Comment on Salthouse (2011). *Neuroscience Research*, *148*, 1-8. https://psycnet.apa.org/doi/10.1037/a0024503

Ress, D., Thompson, J. K., Rokers, B., Khan, R., & Huk, A. C. (2009). A model for transient oxygen delivery in cerebral cortex. *Frontiers in neuroenergetics*, *1*(3), 1-12. https://doi.org/10.3389/neuro.14.003.2009

Reuter-Lorenz, P. A., Jonides, J., Smith, E. E., Hartley, A., Miller, A., Marshuetz, C., & Koeppe, R. A. (2000). Age differences in the frontal lateralization of verbal and spatial working memory revealed by PET. *Journal of cognitive neuroscience*, *12*(1), 174-187. https://doi.org/10.1162/089892900561814

Rhodes, R. E., & Katz, B. (2017). Working memory plasticity and aging. *Psychology and aging*, *32*(1), 51-59. https://psycnet.apa.org/doi/10.1037/pag0000135

Richter, W., & Richter, M. (2003). The shape of the fMRI BOLD response in children and

adults changes systematically with age. *NeuroImage*, *20*(2), 1122-1131.

https://doi.org/10.1016/S1053-8119(03)00347-1

Rivaud, S., Müri, R. M., Gaymard, B., Vermersch, A. I., & Pierrot-Deseilligny, C. (1994). Eye

movement disorders after frontal eye field lesions in humans. *Experimental Brain

Research*, *102*(1), 110-120. https://doi.org/10.1007/BF00232443

Roca, M., Parr, A., Thompson, R., Woolgar, A., Torralva, T., Antoun, N., ... & Duncan, J.

(2010). Executive function and fluid intelligence after frontal lobe

lesions. *Brain*, *133*(1), 234-247. https://doi.org/10.1093/brain/awp269

Rogers, T. D., Dickson, P. E., Heck, D. H., Goldowitz, D., Mittleman, G., & Blaha, C. D. (2011).

Connecting the dots of the cerebro-cerebellar role in cognitive function: Neuronal

pathways for cerebellar modulation of dopamine release in the prefrontal

cortex. *Synapse*, *65*(11), 1204-1212. https://doi.org/10.1002/syn.20960

Rogers, W. A., Hertzog, C., & Fisk, A. D. (2000). An individual differences analysis of ability

and strategy influences: age-related differences in associative learning. *Journal of

Experimental Psychology: Learning, Memory, and Cognition*, *26*(2), 359-394.

https://psycnet.apa.org/doi/10.1037/0278-7393.26.2.359

Roldán, M., & Reinoso-Suárez, F. (1981). Cerebellar projections to the superior colliculus in

the cat. *Journal of Neuroscience*, *1*(8), 827-834.

https://doi.org/10.1523/JNEUROSCI.01-08-00827.1981

Rupniak, N. M., & Gaffan, D. (1987). Monkey hippocampus and learning about spatially

directed movements. *Journal of Neuroscience*, *7*(8), 2331-2337.

https://web.archive.org/web/20170815134202id_/http://www.jneurosci.org/content/jneuro/7/8/2331.full.pdf

Sakai, K., Rowe, J. B., & Passingham, R. E. (2002). Active maintenance in prefrontal area 46 creates distractor-resistant memory. *Nature neuroscience*, *5*(5), 479-484. https://doi.org/10.1038/nn846

Salthouse, T. A., & Kersten, A. W. (1993). Decomposing adult age differences in symbol arithmetic. *Memory & Cognition*, *21*(5), 699-710. https://doi.org/10.3758/BF03197200

Salthouse, T. A. (1993). Speed mediation of adult age differences in cognition. *Developmental psychology*, *29*(4), 722-738. https://psycnet.apa.org/doi/10.1037/0012-1649.29.4.722

Salthouse, T. A. (1996). The processing-speed theory of adult age differences in cognition. *Psychological review*, *103*(3), 403. https://psycnet.apa.org/doi/10.1037/0033-295X.103.3.403

Salthouse, T. A. (2004). What and when of cognitive aging. *Current directions in psychological science*, *13*(4), 140-144. https://psycnet.apa.org/doi/10.1111/j.0963-7214.2004.00293.x

Salthouse, T. A. (2010). Selective review of cognitive aging. *Journal of the International Neuropsychological Society: JINS*, *16*(5), 754-760. https://doi.org/10.1017/S1355617710000706

Salthouse, T. A. (2016). Aging cognition unconfounded by prior test experience. *Journals of Gerontology Series B: Psychological Sciences and Social Sciences*, *71*(1), 49-58. https://doi.org/10.1093/geronb/gbu063

Salthouse, T. A. (2019). Trajectories of normal cognitive aging. *Psychology and aging*, *34*(1), 17-24. http://dx.doi.org/10.1037/pag0000288

Sasaki, K., Oka, H., Kawaguchi, S., Jinnai, K., & Yasuda, T. (1977). Mossy fibre and climbing fibre responses produced in the cerebellar cortex by stimulation of the cerebral cortex in monkeys. *Experimental Brain Research*, *29*(3), 419-428. https://doi.org/10.1007/BF00236180

Schacter, D. L., Buckner, R. L., Koutstaal, W., Dale, A. M., & Rosen, B. R. (1997). Late onset of anterior prefrontal activity during true and false recognition: an event-related fMRI study. *Neuroimage*, *6*(4), 259-269. https://doi.org/10.1006/nimg.1997.0305

Schall, J. D., Morel, A., & Kaas, J. H. (1993). Topography of supplementary eye field afferents to frontal eye field in macaque: implications for mapping between saccade coordinate systems. Visual neuroscience, 10(2), 385-393. https://doi.org/10.1017/S0952523800003771

Schmahmann, J. D., & Pandya, D. N. (1995). Prefrontal cortex projections to the basilar pons in rhesus monkey: implications for the cerebellar contribution to higher function. *Neuroscience letters*, *199*(3), 175-178. https://doi.org/10.1016/0304-3940(95)12056-A

Schmahmann, J. D., & Pandya, D. N. (1997). Anatomic organization of the basilar pontine projections from prefrontal cortices in rhesus monkey. *Journal of Neuroscience*, *17*(1), 438-458. https://doi.org/10.1523/JNEUROSCI.17-01-00438.1997

Schoenbaum, G., Chiba, A. A., & Gallagher, M. (1998). Orbitofrontal cortex and basolateral

amygdala encode expected outcomes during learning. *Nature neuroscience*, *1*(2),

155-159. https://doi.org/10.1038/407

Schoenbaum, G., Setlow, B., Saddoris, M. P., & Gallagher, M. (2003). Encoding predicted

outcome and acquired value in orbitofrontal cortex during cue sampling depends

upon input from basolateral amygdala. *Neuron*, *39*(5), 855-867.

https://doi.org/10.1016/S0896-6273(03)00474-4

Schoenbaum, G., & Roesch, M. (2005). Orbitofrontal cortex, associative learning, and

expectancies. *Neuron*, *47*(5), 633-636.

https://doi.org/10.1016/j.neuron.2005.07.018

Schonewille, M., Gao, Z., Boele, H. J., Veloz, M. F. V., Amerika, W. E., Šimek, A. A., ... & De

Zeeuw, C. I. (2011). Reevaluating the role of LTD in cerebellar motor

learning. *Neuron*, *70*(1), 43-50. https://doi.org/10.1016/j.neuron.2011.02.044

Schultz, W. (2013). Updating dopamine reward signals. *Current opinion in*

neurobiology, *23*(2), 229-238. https://doi.org/10.1016/j.conb.2012.11.012

Segraves, M. A., & Goldberg, M. E. (1987). Functional properties of corticotectal neurons in

the monkey's frontal eye field. *Journal of neurophysiology*, *58*(6), 1387-1419.

https://doi.org/10.1152/jn.1987.58.6.1387

Sekuler, A. B., Bennett, P. J., & Mamelak, M. (2000). Effects of Aging on the Useful Field of

View. *Experimental Aging Research*, *26*(2), 103-120.

https://doi.org/10.1080/036107300243588

Sendhilnathan, N., & Goldberg, M. E. (2020). The mid-lateral cerebellum is necessary for

reinforcement learning. *BioRxiv*, 2020-03.

https://doi.org/10.1101/2020.03.20.000190

Shafto, M. A., Tyler, L. K., Dixon, M., Taylor, J. R., Rowe, J. B., Cusack, R., ... & Henson, R. N.

(2014). The Cambridge Centre for Ageing and Neuroscience (Cam-CAN) study

protocol: a cross-sectional, lifespan, multidisciplinary examination of healthy

cognitive ageing. *BMC neurology*, *14*(204), 1-25. https://doi.org/10.1186/s12883-

014-0204-1

Shook, B. L., Schlag-Rey, M., & Schlag, J. (1990). Primate supplementary eye field: I.

Comparative aspects of mesencephalic and pontine connections. *Journal of

Comparative Neurology*, *301*(4), 618-642. https://doi.org/10.1002/cne.903010410

Sladek, J. R., & Bowman, J. P. (1975). The distribution of catecholamines within the inferior

olivary complex of the cat and rhesus monkey. *Journal of Comparative

Neurology*, *163*(2), 203-213. https://doi.org/10.1002/cne.901630206

Sladky, R., Friston, K. J., Tröstl, J., Cunnington, R., Moser, E., & Windischberger, C. (2011).

Slice-timing effects and their correction in functional MRI. *Neuroimage*, *58*(2), 588-

594. https://doi.org/10.1016/j.neuroimage.2011.06.078

Sloan, H. L., Austin, V. C., Blamire, A. M., Schnupp, J. W., Lowe, A. S., Allers, K. A., ... & Sibson,

N. R. (2010). Regional differences in neurovascular coupling in rat brain as

determined by fMRI and electrophysiology. *Neuroimage*, *53*(2), 399-411.

https://doi.org/10.1016/j.neuroimage.2010.07.014

Sommer, M. A., & Wurtz, R. H. (2004). What the brain stem tells the frontal cortex. I.

Oculomotor signals sent from superior colliculus to frontal eye field via mediodorsal

thalamus. *Journal of neurophysiology, 91*(3), 1381-1402.

https://doi.org/10.1152/jn.00738.2003

SR Research Experiment Builder 2.1.140 [Computer software]. (2017). Mississauga, Ontario, Canada: SR Research Ltd

SR Research Ltd. (2022a, June 29). *About Eye-tracking*. Fast, Accurate, Reliable Eye-tracking. Retrieved October 11, 2022, from https://www.sr-research.com/about-eye-tracking/

SR Research Ltd. (2022b, June 24). *EyeLink 1000 Plus - The Most Flexible Eye-tracker - SR Research*. Fast, Accurate, Reliable Eye-tracking. Retrieved October 11, 2022, from https://www.sr-research.com/eyelink-1000-plus/

Stanton, G. B., Goldberg, M. E., & Bruce, C. J. (1988). Frontal eye field efferents in the macaque monkey: II. Topography of terminal fields in midbrain and pons. *Journal of Comparative Neurology*, *271*(4), 493-506. https://doi.org/10.1002/cne.902710403

Steele, C. J., Anwander, A., Bazin, P. L., Trampel, R., Schäfer, A., Turner, R., ... & Villringer, A. (2017). Human cerebellar sub-millimeter diffusion imaging reveals the motor and non-motor topography of the dentate nucleus. *Cerebral Cortex*, *27*(9), 4537-4548. https://doi.org/10.1093/cercor/bhw258

Steenland, N. K., Auman, C. M., Patel, P. M., Bartell, S. M., Goldstein, F. C., Levey, A. I., & Lah, J. J. (2008). Development of a rapid screening instrument for mild cognitive impairment and undiagnosed dementia. *Journal of Alzheimer's disease*, *15*(3), 419-427. https://doi.org/10.3233/JAD-2008-15308

Stefanova, I., Stephan, T., Becker-Bense, S., Dera, T., Brandt, T., & Dieterich, M. (2013). Age-related changes of blood-oxygen-level–dependent signal dynamics during

optokinetic stimulation. *Neurobiology of aging*, *34*(10), 2277-2286.

https://doi.org/10.1016/j.neurobiolaging.2013.03.031

Steffener, J., Tabert, M., Reuben, A., & Stern, Y. (2010). Investigating hemodynamic response

variability at the group level using basis functions. *Neuroimage*, *49*(3), 2113-2122.

https://doi.org/ 10.1016/j.neuroimage.2009.11.014

Sundermann, B., & Pfleiderer, B. (2012). Functional connectivity profile of the human

inferior frontal junction: involvement in a cognitive control network. *BMC*

neuroscience, *13*(1), 1-13. https://doi.org/10.1186/1471-2202-13-119

Suzuki, L., Coulon, P., Sabel-Goedknegt, E. H., & Ruigrok, T. J. (2012). Organization of

cerebral projections to identified cerebellar zones in the posterior cerebellum of the

rat. *Journal of Neuroscience*, *32*(32), 10854-10869.

https://doi.org/10.1523/JNEUROSCI.0857-12.2012

Swenson, R. S., Sievert, C. F., Terreberry, R. R., Neafsey, E. J., & Castro, A. J. (1989).

Organization of cerebral cortico-olivary projections in the rat. *Neuroscience*

research, *7*(1), 43-54. https://doi.org/10.1016/0168-0102(89)90036-9

Takahashi, Y. K., Roesch, M. R., Stalnaker, T. A., Haney, R. Z., Calu, D. J., Taylor, A. R., ... &

Schoenbaum, G. (2009). The Orbitofrontal Cortex and Ventral Tegmental Area Are

Necessary for Learning from Unexpected Outcomes. *Neuron*, *62*, 269-280.

https://doi.org/10.1016/j.neuron.2009.03.005

Takano, T., Tian, G. F., Peng, W., Lou, N., Libionka, W., Han, X., & Nedergaard, M. (2006).

Astrocyte-mediated control of cerebral blood flow. *Nature neuroscience*, *9*(2), 260-

267. https://doi.org/10.1038/nn1623

Taoka, T., Iwasaki, S., Uchida, H., Fukusumi, A., Nakagawa, H., Kichikawa, K., ... & Ohishi, H.

 (1998). Age correlation of the time peak latency in signal change on EPI-

 fMRI. *Journal of computer assisted tomography*, *22*(4), 514-517.

 https://doi.org/10.1097/00004728-199807000-00002

Tarantini, S., Tran, C. H. T., Gordon, G. R., Ungvari, Z., & Csiszar, A. (2017). Impaired

 neurovascular coupling in aging and Alzheimer's disease: contribution of astrocyte

 dysfunction and endothelial impairment to cognitive decline. *Experimental*

 gerontology, *94*, 52-58. https://doi.org/10.1016/j.exger.2016.11.004

Taylor, A. J., Kim, J. H., & Ress, D. (2018). Characterization of the hemodynamic response

 function across the majority of human cerebral cortex. *NeuroImage*, *173*, 322-331.

 https://doi.org/10.1016/j.neuroimage.2018.02.061

Taylor, J. R., Williams, N., Cusack, R., Auer, T., Shafto, M. A., Dixon, M., ... & Henson, R. N.

 (2017). The Cambridge Centre for Ageing and Neuroscience (Cam-CAN) data

 repository: structural and functional MRI, MEG, and cognitive data from a cross-

 sectional adult lifespan sample. *Neuroimage*, *144*, 262-269.

 https://dx.doi.org/10.1016/j.neuroimage.2015.09.018

Thompson, R. F., & Kim, J. J. (1996). Memory systems in the brain and localization of a

 memory. *Proceedings of the national academy of sciences*, *93*(24), 13438-13444.

 https://doi.org/10.1073/pnas.93.24.13438

Timmann, D., Drepper, J., Maschke, M., Kolb, F. P., Böring, D., Thilmann, A. F., & Diener, H. C.

 (2002). Motor deficits cannot explain impaired cognitive associative learning in

 cerebellar patients. *Neuropsychologia*, *40*(7), 788-800.

 https://doi.org/10.1016/S0028-3932(01)00181-6

Toonen, M., van Dijken, H., Holstege, J. C., Ruigrok, T. J., Koekkoek, S. K., Hawkins, R. K., ... & De Zeeuw, C. I. (1998). Light microscopic and ultrastructural investigation of the dopaminergic innervation of the ventrolateral outgrowth of the rat inferior olive. *Brain research*, *802*(1-2), 267-273. https://doi.org/10.1016/S0006-8993(98)00593-9

Tsujimoto, S., Genovesio, A., & Wise, S. P. (2010). Evaluating self-generated decisions in frontal pole cortex of monkeys. *Nature neuroscience*, *13*(1), 120. https://doi.org/10.1038/nn.2453

Tsujimoto, S., Genovesio, A., & Wise, S. P. (2011a). Frontal pole cortex: encoding ends at the end of the endbrain. *Trends in cognitive sciences*, *15*(4), 169-176. https://doi.org/10.1016/j.tics.2011.02.001

Tsujimoto, S., Genovesio, A., & Wise, S. P. (2011b). Comparison of strategy signals in the dorsolateral and orbital prefrontal cortex. *Journal of Neuroscience*, *31*(12), 4583-4592. https://doi.org/10.1523/JNEUROSCI.5816-10.2011

Tsujimoto, S., Genovesio, A., & Wise, S. P. (2012). Neuronal activity during a cued strategy task: comparison of dorsolateral, orbital, and polar prefrontal cortex. *Journal of Neuroscience*, *32*(32), 11017-11031. https://doi.org/10.1523/JNEUROSCI.1230-12.2012

Tucker, J., Harding, A. E., Jahanshahi, M., Nixon, P. D., Rushworth, M., Quinn, N. P., ... & Passingham, R. E. (1996). Associative learning in patients with cerebellar ataxia. *Behavioral neuroscience*, *110*(6), 1229-1234. https://psycnet.apa.org/doi/10.1037/0735-7044.110.6.1229

Uddin, L. Q., Nomi, J. S., Hébert-Seropian, B., Ghaziri, J., & Boucher, O. (2017). Structure and

function of the human insula. *Journal of clinical neurophysiology: official publication

of the American Electroencephalographic Society*, *34*(4), 300-306.

https://doi.org/10.1097%2FWNP.0000000000000377

Uddin, L. Q. (2021). Cognitive and behavioural flexibility: neural mechanisms and clinical

considerations. *Nature Reviews Neuroscience*, *22*(3), 167-179.

https://doi.org/10.1038/s41583-021-00428-w

Uğurbil, K. (2012). The road to functional imaging and ultrahigh fields. *Neuroimage*, *62*(2),

726-735. https://doi.org/10.1016/j.neuroimage.2012.01.134

van der Zwaag, W., Francis, S., Head, K., Peters, A., Gowland, P., Morris, P., & Bowtell, R.

(2009). fMRI at 1.5, 3 and 7 T: characterising BOLD signal

changes. *Neuroimage*, *47*(4), 1425-1434.

https://doi.org/10.1016/j.neuroimage.2009.05.015

Viessmann, O., & Polimeni, J. R. (2021). High-resolution fMRI at 7 Tesla: challenges, promises

and recent developments for individual-focused fMRI studies. *Current Opinion in

Behavioral Sciences*, *40*, 96-104. https://doi.org/10.1016/j.cobeha.2021.01.011

Voogd, J., Schraa-Tam, C. K., van der Geest, J. N., & De Zeeuw, C. I. (2012). Visuomotor

cerebellum in human and nonhuman primates. The Cerebellum, 11, 392-410.

https://doi.org/10.1007/s12311-010-0204-7

Vu, A. T., Jamison, K., Glasser, M. F., Smith, S. M., Coalson, T., Moeller, S., ... & Yacoub, E.

(2017). Tradeoffs in pushing the spatial resolution of fMRI for the 7T Human

Connectome Project. *Neuroimage*, *154*, 23-32.

https://doi.org/10.1016/j.neuroimage.2016.11.049

Walford, E. (2011). Age differences in associative and strategic processes in human

conditional learning. *Journal of Cognitive Psychology*, *23*(7), 783-794.

https://doi.org/10.1080/20445911.2011.567190

Walker, A. E. (1940). A cytoarchitectural study of the prefrontal area of the macaque

monkey. *Journal of Comparative Neurology*, *73*(1), 59-86.

https://doi.org/10.1002/cne.900730106

Walker, S. (1987). *Animal learning: Introductions to Modern Psychology*. New York, NY:

Routledge & Kegan Paul.

Wallis, J. D., Anderson, K. C., & Miller, E. K. (2001). Single neurons in prefrontal cortex

encode abstract rules. *Nature*, *411*(6840), 953-956.

https://doi.org/10.1038/35082081

Ward, L. M., Aitchison, R. T., Tawse, M., Simmers, A. J., & Shahani, U. (2015). Reduced

Haemodynamic Response in the Ageing Visual Cortex Measured by Absolute

fNIRS. *PLoS ONE*, *10*(4), e0125012. https://doi.org/10.1371/journal.pone.0125012

Watson, T. C., Jones, M. W., & Apps, R. (2009). Electrophysiological mapping of novel

prefrontal-cerebellar pathways. *Frontiers in integrative neuroscience*, *3*, 18.

https://doi.org/10.3389/neuro.07.018.2009

Welsh, J. P., Yamaguchi, H., Zeng, X. H., Kojo, M., Nakada, Y., Takagi, A., ... & Llinás, R. R.

(2005). Normal motor learning during pharmacological prevention of Purkinje cell

long-term depression. *Proceedings of the National Academy of Sciences*, *102*(47),

17166-17171. https://doi.org/10.1073%2Fpnas.0508191102

West, R. L. (1996). An application of prefrontal cortex function theory to cognitive aging. *Psychological bulletin*, *120*(2), 272. https://doi.org/10.1037/0033-2909.120.2.272

West, R. (2000). In defense of the frontal lobe hypothesis of cognitive aging. *Journal of the International Neuropsychological Society*, *6*(6), 727-729. https://doi.org/10.1017/S1355617700666109

West, K. L., Zuppichini, M. D., Turner, M. P., Sivakolundu, D. K., Zhao, Y., Abdelkarim, D., ... & Rypma, B. (2019). BOLD hemodynamic response function changes significantly with healthy aging. *Neuroimage*, *188*, 198-207. https://doi.org/10.1016/j.neuroimage.2018.12.012

Willstrand, T. D., Broberg, T., & Selander, H. (2017). Driving characteristics of older drivers and their relationship to the useful field of view test. *Gerontology*, *63*(2), 180-188. https://doi.org/10.1159/000448281

Winocur, G. (1991). Functional dissociation of the hippocampus and prefrontal cortex in learning and memory. *Psychobiology*, *19*(1), 11-20. https://doi.org/10.1007/BF03337952

Winocur, G. (1992). Conditional learning in aged rats: evidence of hippocampal and prefrontal cortex impairment. *Neurobiology of Aging*, *13*(1), 131-135. https://doi.org/10.1016/0197-4580(92)90020-X

Wise, S. P., & Murray, E. A. (2000). Arbitrary associations between antecedents and actions. *Trends in neurosciences*, *23*(6), 271-276. https://doi.org/10.1016/S0166-2236(00)01570-8

Wise, S. P. (2008). Forward frontal fields: phylogeny and fundamental function. *Trends in neurosciences*, *31*(12), 599-608. https://doi.org/10.1016/j.tins.2008.08.008

Wood, J. M. (2002). Aging, driving and vision. *Clinical and experimental optometry, 85*(4), 214-220. https://doi.org/10.1111/j.1444-0938.2002.tb03040.x

Woodruff-Pak, D. S., Foy, M. R., Akopian, G. G., Lee, K. H., Zach, J., Nguyen, K. P. T., ... & Thompson, R. F. (2010). Differential effects and rates of normal aging in cerebellum and hippocampus. *Proceedings of the National Academy of Sciences*, *107*(4), 1624-1629. https://doi.org/10.1073/pnas.0914207107

Woolrich, M. W., Behrens, T. E., & Smith, S. M. (2004). Constrained linear basis sets for HRF modelling using Variational Bayes. *NeuroImage*, *21*(4), 1748-1761. https://doi.org/10.1016/j.neuroimage.2003.12.024

World Health Organization. (2018). *Integrated care for older people: realigning primary health care to respond to population aging* (No. WHO/HIS/SDS/2018.44). World Health Organization.

Worsley, K. J., Liao, C. H., Aston, J., Petre, V., Duncan, G. H., Morales, F., & Evans, A. C. (2002). A general statistical analysis for fMRI data. *Neuroimage*, *15*(1), 1-15. http://www.math.mcgill.ca/keith

Woutersen, K., Guadron, L., van den Berg, A. V., Boonstra, F. N., Theelen, T., & Goossens, J. (2017). A meta-analysis of perceptual and cognitive functions involved in useful-field-of-view test performance. *Journal of vision*, *17*(14), 11-11. https://doi.org/10.1167/17.14.11

Woutersen, K., van den Berg, A. V., Boonstra, F. N., Theelen, T., & Goossens, J. (2018). Useful field of view test performance throughout adulthood in subjects without ocular disorders. *PloS one*, *13*(5), e0196534. https://doi.org/10.1371/journal.pone.0196534

Xi, M. C., Liu, R. H., Engelhardt, J. K., Morales, F. R., & Chase, M. H. (1999). Changes in the axonal conduction velocity of pyramidal tract neurons in the aged cat. *Neuroscience*, *92*(1), 219-225. https://doi.org/10.1016/S0306-4522(98)00754-4

Yaffe, K., Fiocco, A. J., Lindquist, K., Vittinghoff, E., Simonsick, E. M., Newman, A. B., ... & Harris, T. B. (2009). Predictors of maintaining cognitive function in older adults: the Health ABC study. *Neurology*, *72*(23), 2029-2035. https://doi.org/10.1212/WNL.0b013e3181a92c36

Yamada, J., & Noda, H. (1987). Afferent and efferent connections of the oculomotor cerebellar vermis in the macaque monkey. *Journal of comparative neurology*, *265*(2), 224-241. https://doi.org/10.1002/cne.902650207

Yang, G., Zhang, Y., Ross, M. E., & Iadecola, C. (2003). Attenuation of activity-induced increases in cerebellar blood flow in mice lacking neuronal nitric oxide synthase. *American Journal of Physiology-Heart and Circulatory Physiology*, *285*(1), H298-H304. https://doi.org/10.1152/ajpheart.00043.2003

Yang, L., Yan, J., Jin, X., Jin, Y., Yu, W., Xu, S., & Wu, H. (2016). Screening for dementia in older adults: comparison of Mini-Mental State Examination, Mini-Cog, Clock Drawing test and AD8. *PloS one*, *11*(12), e0168949. https://doi.org/10.1371/journal.pone.0168949

Yarrow, K. (2010). *Attention and time*. New York, NY: Oxford University press.

Yin, H. H., & Knowlton, B. J. (2006). The role of the basal ganglia in habit formation. *Nature Reviews Neuroscience*, *7*(6), 464-476. https://doi.org/10.1038/nrn1919

Zagermann, J., Pfeil, U., & Reiterer, H. (2018, April). Studying eye movements as a basis for measuring cognitive load. In *Extended Abstracts of the 2018 CHI Conference on Human Factors in Computing Systems* (pp. 1-6). https://doi.org/10.1145/3170427.3188628

Zaval, L., Li, Y., Johnson, E. J., & Weber, E. U. (2015). Complementary contributions of fluid and crystallized intelligence to decision making across the life span. In *Aging and decision making* (pp. 149-168). Academic Press. https://doi.org/10.1016/B978-0-12-417148-0.00008-X